CIVIL ENGINEERING STUDIES

STRUCTURAL RESEARCH SERIES NO. 227

DYNAMIC STUDIES OF BRIDGES ON THE AASHO TEST ROAD

by

S. J. FENVES

A. S. VELETSOS

C. P. SIESS

Final Report

to

AASHO ROAD TEST

HIGHWAY RESEARCH BOARD

NATIONAL ACADEMY OF SCIENCES — NATIONAL RESEARCH COUNCIL

UNIVERSITY OF ILLINOIS

URBANA, ILLINOIS

FEBRUARY 1962

DYNAMIC STUDIES OF BRIDGES ON THE AASHO TEST ROAD

by

S. J. Fenves
A. S. Veletsos
C. P. Siess

Final Report

to

AASHO ROAD TEST
HIGHWAY RESEARCH BOARD
NATIONAL ACADEMY OF SCIENCES - NATIONAL RESEARCH COUNCIL

University of Illinois
Urbana, Illinois
February 1962

TABLE OF CONTENTS

TABLE OF CONTENTS (Cont'd)

TABLE OF CONTENTS (Cont'd)

LIST OF TABLES

LIST OF FIGURES

LIST OF FIGURES (Cont'd)

LIST OF FIGURES (Cont'd)

LIST OF FIGURES (Cont'd)

I. INTRODUCTION

1. General Objectives

This report deals with the program of dynamic tests conducted on the bridges of the AASHO Road Test at Ottawa, Illinois, and the analysis and interpretation of the results obtained.

For a description of the overall Road Test project, the reader is referred to the final reports on the AASHO Road Test[1]*. There were 18 bridges included in the Test Road, specifically designed to study their behavior under repeated applications of high overstress. Each bridge was a simple-span structure, consisting of three beams and a reinforced concrete slab. The beams, spanning 50 feet, were steel wide-flange sections, prestressed concrete I-beams, or reinforced concrete T-beams. Each bridge provided one lane of test traffic.

The broad objective of the program described herein was to study the dynamic effects produced in the test bridges under moving vehicles, and to relate the observed behavior to the results predicted by theory. It was also hoped that, based on the knowledge obtained from this investigation, directions for further studies on the subject might be indicated. A special effort was made to obtain reliable, carefully controlled data on the behavior of the test bridges under actual field conditions.

The scope of the program was limited by the fact that the test bridges were simplified structures and were not directly representative of those designed for more conservative stress level. Furthermore, no consideration was given in the design of the bridges to any particular requirements of the dynamic studies. Because of these limitations, no attempt has been made to derive an "impact formula" for the bridges tested, much less for a general

---

* Numbers in parentheses refer to items listed in the Bibliography.

class of bridges. Instead, emphasis has been placed on understanding the dynamic behavior of the bridges and vehicles.

It should be emphasized that the results obtained are limited to the structures tested, and are not necessarily applicable beyond the range of variables considered. However, the results provided valuable information about the dynamic behavior of vehicles and bridges in general.

The significance of the present investigation to the general problem of the dynamic behavior of bridges can be best seen by placing it in the perspective of the current knowledge. Available experimental information on the dynamic behavior of simple-span highway bridges comes from two sources:

(a) laboratory experiments on scale models, using idealized bridge and vehicle models[2,3,4], and

(b) full-scale field tests, employing actual vehicles and bridges[4,5,6].

Many laboratory test results have been successfully correlated with theoretical analyses, especially where the bridge and vehicle models were relatively simple[2]. Although under some conditions excellent correlation has been obtained between field tests and theoretical solutions[4], the field tests generally have not been comprehensive.

The experimental setup at the AASHO Test Road consisted of actual heavy vehicles and full-scale bridges, although the latter were to an extent simplified models. Together with these, instrumentation and experimental control facilities normally found only in the best laboratory experiments were available. Furthermore, the opportunity existed to perform additional tests to determine the characteristics of both vehicles and bridges and obtain experimental data not commonly available.

Thus, the present program serves as a transition between the simplified laboratory tests on one hand, and the full-scale field tests on the other hand.

2. Scope of Program

The investigation reported herein can conveniently be classified into the following three parts:

(a) study of the static and dynamic properties of the bridges;

(b) study of the characteristics of the vehicles under static and dynamic conditions; and

(c) study of the dynamic behavior of the bridge-vehicle system.

The first two parts of the investigation, although not as extensive as the third part, were as important as the latter. It was felt that before the behavior of the bridges under moving vehicles could be adequately understood and analyzed, the properties of the bridges and vehicles had to be accurately determined and interpreted.

The various parts of the study are briefly described in the following sections.

2.1 Study of the Characteristics of Bridges. Loading tests were made on the bridges both with stationary and slowly moving vehicles. The objectives of these tests were: first, to determine the stiffness of the bridges at various stages of the test program; and second, to study the lateral distribution of effects in order to determine to what extent the test bridges behaved as a beam, which was an assumption involved in the theoretical solutions used in this project to predict the dynamic behavior.

The natural frequencies of the bridges were determined at various stages of the test program, and the results compared with the computed values. Studies were made to ascertain whether the frequencies in the free-vibration era were representative of the natural frequencies while the vehicle was on the bridge. The damping characteristics of the bridges were determined from the rate of decay of the motion of the bridges after the vehicle had left the span. For certain bridges, these results were related to those obtained from steady-state forced vibration tests.

The profiles of the approach pavements and the bridge surfaces were recorded at regular intervals, and an attempt was made to relate the major surface irregularities to the oscillations of the vehicles.

2.2 Study of the Characteristics of Vehicles. Static loading tests were performed on the vehicles, to determine their load-deformation characteristics, and to study the effect of friction in the suspension system.

A large number of dynamic tests were performed in which vehicles were driven at different speeds over various pavements and obstructions. In some tests, the suspension springs of the vehicle were blocked. The objectives of these tests were: first, to determine directly the natural frequencies of the vehicles; second, to evaluate the damping characteristics of the tires and of the suspension system under dynamic conditions, and to relate these to the results of static tests; and third, to determine the magnitude of the vertical oscillations of the vehicle.

2.3 Dynamic Studies on the Bridges. The program of dynamic tests consisted of approximately 1900 test runs, and involved composite and non-composite steel bridges, prestressed and reinforced concrete bridges, as well as 14 different vehicles. Speeds ranged from 10 to 50 mph.

Tests were made for a large number of combinations of bridges and vehicles, in order to get data on the effect of all pertinent parameters. Additional tests were made to determine any variation in the dynamic behavior of the bridges due to changes in their characteristics with increased cycles of overstress.

In several tests, the vehicle springs were blocked, so that the results could be more readily compared with the theoretical solutions. A study was made of the effect of friction in the vehicle suspension system on the bridge response.

In the above tests, no attempt was made to excite either the bridge or the vehicle prior to the entrance of the vehicle on the span. In general, however, oscillations were always present in the vehicle. Tests were also conducted with induced initial oscillations in the vehicle. In a few tests, attempts were made to simulate continuous traffic, by operating two vehicles on the bridge, and adjusting the distance between them so that the second vehicle entered the span while the bridge was still in motion.

In addition to the tests where the vehicle moved along the center-line of the bridge, tests were made with the vehicle located eccentrically.

Finally, one set of tests was intended to study the effect of braking the vehicle on the bridge.

The results of these tests were analyzed and interpreted in the light of the available theoretical background. In addition, experimental data have been compared with theoretical predictions, using the theoretical model originally developed as part of the Cooperative Highway Bridge Impact Investigation at the University of Illinois.

Comparisons were first made on the basis of history curves of measured and computed responses as the vehicle moved across the span. Such comparisons were made for a number of tests involving different bridges and vehicles. The effect of the experimental uncertainties was studied by varying the parameters in the theoretical solutions. On the basis of the history curves, the maximum values of the measured and computed effects were compared over the range of speeds involved.

The outline of this report follows the scope described above. In the last section of this chapter the planning of the tests is described. Chapter II deals with the test program and describes the data obtained. The characteristics of the bridges and vehicles are dealt with in Chapter III and IV, respectively. Chapters V through VII deal with the dynamic tests on the bridges. In Chapter V, a representative number of dynamic tests are described, to illustrate the detailed characteristics of the behavior. The results of the dynamic tests are analyzed and interpreted in Chapters VI and VII. The comparison of experimental data with theory is presented in Chapter VIII. In Chapter IX the major findings are summarized, and conclusions and suggestions for further work are presented.

3. Planning and Conduct of Tests

The tests described herein were performed between October 1958 and October 1960, and were divided into five major series. Throughout the duration of the project, the program of tests was closely coordinated with the analysis and interpretation of the experimental data, and it was kept flexible so that changes and additions could be made in the light of the results obtained. The planning of the tests was guided by the results of theoretical analyses. Some of the observed trends were anticipated on

the basis of available knowledge, and tests were incorporated in the program specifically in an attempt to confirm the theoretical results. In other cases, specific tests were proposed to obtain data on conditions not accounted for by the available theory.

The procedure of planning and executing the tests was as follows. For each major series of tests, a tentative outline was prepared, describing the objectives and outlining a set of specific proposals for their implementation. At a meeting of the Special Committee on Dynamic Behavior of the Test Bridges, appointed by the Highway Research Board, a final program was formulated and its execution was assigned to the Bridge Research Branch of the AASHO Road Test. After completion of the tests and preliminary reduction work, the test data were forwarded to the University of Illinois for further reduction and analysis. Throughout the duration of the project, the closest cooperation was maintained with the Road Test staff.

Due to limitations in time, not all of the experimental data obtained could be studied in detail. Similarly, because of space limitations, some of the test results are discussed only in general terms in this report. In particular, the analytical studies reported deal with a small proportion of the tests, and in many cases are essentially exploratory in character.

It should be noted that the planning of the tests was not governed solely by the analysis and interpretation of the results in the present investigation. It was realized that not all data could be reduced and thoroughly interpreted within the time limits of this investigation. Thus the tests were designed to provide, after the completion of the present study, information valuable for further work in the field.

4. Notation

The symbols used in this report are defined in the text where they are first introduced. For convenience, the important symbols are summarized here in alphabetical order.

a_1 = horizontal distance from front axle to the center of gravity of the vehicle

a_2 = $s - a_1$

AF = amplification factor-ratio of maximum dynamic effect to corresponding maximum crawl effect

AF_D = amplification factor for deflection

AF_M = amplification factor for moment (computed) or strain (measured)

b = width of bridge slab

C_1, C_2 = constants defined by equation (3)

D = rigidity of slab per unit width

DI = dynamic increment - difference between dynamic effect at an instant and the corresponding crawl effect, in terms of the maximum crawl effect

DI_D = dynamic increment for deflection

DI_M = dynamic increment for moment (computed) or strain (measured)

EI = flexural rigidity of beams

E_s = modulus of elasticity of the material of the slab

F_i = limiting frictional force in the suspension springs of the i^{th} axle

f_b = fundamental natural frequency of the bridge

$f_{1,2}$ = natural frequencies of the vehicle

$\bar{f}_{t,i}$ = frequency of the i^{th} axle vibrating on its tires

$\bar{f}_{ts,i}$ = frequency of the i^{th} axle vibrating on the combined springs and tires

g = acceleration of gravity

h = height of obstruction

I = impact factor

i_1, i_2 = dynamic indexes of tractor and trailer, respectively

k_e = effective stiffness

$k_{s,i}$ = stiffness of suspension springs for the i^{th} axle

$k_{t,i}$ = stiffness of tires for the i^{th} axle

$k_{ts,i}$ = stiffness of combined tires and suspension springs for the i^{th} axle

L = length of span

ℓ = length of obstruction

P_i = interaction force on the i^{th} axle

P_o = initial axle load for static tests (section 15 only)

$P_{o,i}$ = initial interaction force on the i^{th} axle

P_s = component of axle load carried by suspension spring

$P_{st,i}$ = static load on the i^{th} axle

$R = \frac{W}{W_b}$, a weight ratio

r = radius of gyration of sprung mass of vehicle

s_1, s_2 = wheelbase of tractor and trailer, respectively

T_b = fundamental period of vibration of bridge

T_v = natural period of vibration of vehicle axle

t = elapsed time measured from instant of entry of rear axle of vehicle on the span

t' = time of transit over the bridge

t_d = time of transit over an obstruction

v = speed of vehicle

W = total weight of vehicle

W_b = total weight of bridge

w = unsprung weight of axle

w_b = weight of bridge per unit of length

x = distance from the position of rear axle of vehicle to the left support

y_o = initial deflection for static tests (section 15 only)

y_i = deflection of i^{th} axle

$y_{st,i}$ = static deflection of i^{th} axle

$\alpha = \frac{vT_b}{2L}$, a speed parameter

β_b = damping coefficient for bridge

$\Delta = \frac{\Delta_c}{y_{st,i}}$, a profile variation parameter

Δ_c = deviation of bridge profile at midspan from a line through the supports

δ_{st} = dead-load deflection of bridge at midspan

θ = phase angle

μ_i = coefficient of interleaf friction for the i^{th} axle

$\varphi = \frac{f_i}{f_b}$, a frequency ratio

5. Acknowledgments

The investigation reported herein was conducted as a cooperative research project between the University of Illinois and the Highway Research Board of the National Academy of Sciences - National Research Council, and was sponsored by the latter agency. This report constitutes the final report on the project by the University of Illinois to the sponsors.

The program described was conducted under the general supervision of the Special Committee on Dynamic Behavior of the Test Bridges, appointed by the Highway Research Board. The members of the Special Committee were:

G. S. Paxson, Chairman	Oregon Highway Department
W. N. Carey, Jr.	AASHO Road Test
I. M. Viest	AASHO Road Test
C. P. Siess	University of Illinois
A. S. Veletsos	University of Illinois

The dynamic tests were performed by the AASHO Road Test Bridge Branch under the direction of Ivan M. Viest, Bridge Research Engineer, and John W. Fisher, Assistant Bridge Research Engineer.

At the University of Illinois, the project was under the general direction of C. P. Siess and A. S. Veletsos, Professors of Civil Engineering. The immediate supervision was the responsibility of R. K. L. Wen, formerly Assistant Professor of Civil Engineering, from February 1958 to February 1959, and of S. J. Fenves, Instructor in Civil Engineering, since that date. The project personnel consisted of E. G. Endebrock, N. L. Hickerson, A. Korn, W. P. Moore and R. L. Rolfe, Research Assistants in Civil Engineering. The computer program used to obtain the theoretical solutions reported herein was developed by Tseng Huang, formerly Assistant Professor of Civil Engineering. This program is a modification of the one for continuous beams reported in Ref. (16).

This report also constitutes the doctoral dissertation of S. J. Fenves prepared under the direction of Professor Veletsos. The authors wish to acknowledge the cooperation and assistance of all the persons listed above, and particularly of Messrs. Carey, Viest, and Fisher from the AASHO Road Test staff.

II. DESCRIPTION OF TEST PROGRAM

The purpose of this chapter is to describe the experimental setup for this investigation and to summarize the tests performed and the data obtained. The various tests are described in relation to the scope of the project discussed earlier, rather than in the order in which they were performed.

For administrative purposes, the dynamic tests were divided into five series, with each series further subdivided into a number of subseries. Generally, a subseries involved one bridge and one vehicle, the only variable being the speed of the vehicle. Throughout this report, the test subseries will be referred to by the subseries numbers assigned by the AASHO Road Test. Similarly, the bridge and vehicle designations will be those used on the Road Test.

6. Tests to Determine Characteristics of Bridges

6.1 Description of Test Bridges. The detailed description of the test bridges may be found in the appropriate parts of Ref. 1, and is beyond the scope of this report. In this section, a brief description is given, primarily to make the report self-contained.

The test bridges were located in the test loops subject to the heaviest trucks in the regular tests. They were placed in four groups of four bridges each. Each bridge provided one traffic lane, and each traffic lane crossed two bridges in tandem. At both ends of each bridge site there were heavily reinforced concrete approach pavement slabs 20 feet long. All test bridges were built on a 0.2 percent slope.

Early in the course of tests two of the bridges (4A and 4B) failed and were replaced by bridges 9A and 9B. Thus, altogether 18 test bridges were available, as follows:

Composite steel - Bridges 2B and 3B.
Noncomposite steel - Bridges 1A, 1B, 2A, 3A, 4A, 4B, 9A and 9B.
Prestressed concrete - Bridges 5A, 5B, 6A, and 6B.
Reinforced concrete - Bridges 7A, 7B, 8A, and 8B.

The above bridge designations, used in the Road Test Reports, will be used throughout this report. The dimensions of the bridges are presented in Section 9.1.

6.2 Crawl tests. As part of every subseries of dynamic tests, from two to six additional tests were performed, with a vehicle speed of approximately 3 mph. These will be referred to as crawl tests. Static tests, with the drive axle of the vehicle placed at midspan, were also performed in the first two series of tests. The test methods and measurements obtained were the same as those used in the dynamic tests described below. The crawl and static measurements were always taken preceding and following the dynamic tests. This procedure provided an additional check on the instrumentation, and, in a few cases, the comparison of "before" and "after" crawl tests was helpful in isolating defective records. In addition to the above tests, one subseries (No. 5451-18) consisted entirely of crawl and static tests on Bridges 2B, 5A, 7A and 9B.

6.3 Measurements of Profiles of Bridges and Approaches. The longitudinal and transverse profiles of all bridges were determined. In the longitudinal direction measurements were taken at one foot intervals along two concentric wheelpaths on 100 feet of pavement preceding the bridges and on the bridges themselves. The transverse profiles of the bridges were obtained by measurements at the supports and quarter-points

along five lines, namely the three beam lines and the two edges of the bridge slab. All of the measurements were taken with a conventional rod and level, and were expressed as deviations from the design grade.

Longitudinal profile data were obtained on the following four dates: Sept. 24, 1958; Oct. 10, 1959; March 25, 1960; and Nov. 22, 1960. Lateral profiles were obtained approximately every three months during a three-year period.

6.4 Forced Vibration Tests. Forced vibration tests were conducted on five bridges (3B, 6A, 6B, 8A and 9B) after the completion of the regular test traffic (February 1961). The test method for each bridge was the same. The only weight placed on the bridge was the weight of the mechanical oscillator which was 2,000 pounds. The oscillator was placed transversely at midspan of each bridge and bolted to the deck. The vibrator was run at a constant frequency, and a continuous oscillograph record of the strains at midspan of the three beams was obtained.

The frequencies were changed a small amount, and each time a corresponding response record was taken. Several series of tests were made on each bridge to obtain replication of results. The frequencies varied from low frequencies up to the resonant frequency of the bridge and from high frequencies down to the resonant frequency. The vibrator produced a maximum frequency of 5.8 cps. On the prestressed concrete bridges, the resonant frequency could not be attained, and response records were obtained only up to the maximum frequency of the vibrator.

7. Tests to Determine Characteristics of the Vehicles

7.1 Description of Test Vehicles. The vehicles available for the dynamic tests included all test vehicles used on the Road Test, as

well as two-axle maintenance trucks. The only limitation placed on the choice of vehicles was that the regular test vehicles assigned to the loop on which a particular bridge was located, or any heavier vehicles, could not be used in the dynamic tests. This limitation was made to insure that the bridges would not be overloaded beyond their design load.

The vehicles used in the dynamic tests included two-axle, three-axle (truck-semitrailer), and five-axle (truck-semitrailer with tandem drive and rear axles) vehicles, as follows:

Two-axle maintenance (dump) trucks - No's. 91 and 94.
Two-axle test vehicle - No. 221.
Three-axle test vehicles - No's. 315, 415, 417, 511, 513, and 517.
Five-axle test vehicles - No's. 324, 325, and 327.

The numerical designation of the test vehicles used in this report is the same as that used in all Test Road reports. All the test vehicles used were taken directly from the regular test traffic operations, with the exception of Vehicle No. 511, which was specially loaded for the dynamic tests.

7.2 Static Loading Tests. A total of 43 static loading tests were performed on seven vehicles used in the dynamic tests. One test pertained to one axle of the test vehicle. The table below lists the number of tests for each of the vehicles considered.

Vehicle No.	Number of Tests		
	Front Axle	Drive Axle	Rear Axle
91	2	2	-
94	3	3	-
315	-	3	2
415	1	3	5
417	1	1	1
511	2	4	5
513	1	2	2

In these tests, the vehicle was loaded in approximately 1000 lb. increments from its empty weight to beyond its rated load, and then unloaded. In several tests, intermediate level unloading and reloading were also performed. The data obtained were the deflection of the two tires and two springs of the axle and the corresponding axle load, for each increment or decrement of loading.

7.3 Dynamic Tests on Pavements. A total of 24 subseries of tests were performed in which the vehicles were run over various pavements and obstructions. Four vehicles were involved: two two-axle vehicles (No's. 91 and 94), and two three-axle vehicles (No's. 513 and 417). Speeds ranged from 10 to 40 mph, approximately. The two major test variables were the condition of the vehicle suspension system and the type of pavement or obstruction.

Two types of vehicle suspension systems were considered:

(a) springs in normal operating condition; and

(b) springs blocked.

For the two-axle vehicle No. 91, the springs on both axles were blocked, while for the three-axle vehicle No. 513 only the drive and rear axle springs were blocked. No tests with blocked springs were made on Vehicles No. 94 and 417.

Six types of pavements or obstructions were involved:

(a) "smooth" pavement;

(b) "rough" pavement;

(c) obstruction consisting of a 1" x 12" board placed across the wheelpaths on a smooth pavement;

(d) obstruction consisting of a 2" x 6" board placed across the wheelpaths on a smooth pavement;

(e) long obstruction, consisting of a 1 inch high by 24 inch wide ramp, 18 feet long, placed under each wheelpath on a smooth pavement. The first foot of the ramp was planed down to afford a gradual transition.

(f) long obstruction placed under one wheelpath only.

The "smooth" and "rough" pavements were selected on the basis of the Present Serviceability Index (PSI) used on the Road Test to rate the performance of the pavements[7]. The PSI ratings for the two pavements involved were 4.4 and 2.0, respectively, based on a scale of 5 for "very good" and 0 for "very poor".

The vehicle instrumentation was the same as for the dynamic tests described below. In addition, the roadway profile for all pavement sections was recorded.

Table 1 summarizes the dynamic tests on pavements. Figure 1b shows Vehicle No. 513 approaching the ramp described in (f) above.

8. Dynamic Tests on Bridges

8.1 Test Variables. Of the 18 bridges on the Test Road, 15 were tested on the dynamic studies reported herein. These bridges covered all four types of construction used, namely; noncomposite steel (2A, 4A, 4B, 9A and 9B), composite steel (2B and 3B), prestressed concrete (5A, 5B, 6A and 6B), and reinforced concrete (7A, 7B, 8A and 8B). Three noncomposite steel bridges (1A, 1B and 3A) were not tested.

Twelve vehicles were used in the tests. Of these, nine were standard test vehicles used in the regular tests, two were maintenance trucks and one was a standard vehicle (No. 511) with special loading. The latter was used with three different loads, designated as A, B and C.

All others were regular test vehicles loaded with the weights used in the regular test traffic operations. Thus, altogether fourteen different load combinations were used, as follows:

4 two-axle vehicles (A, No's. 91, 94, 221)

7 three-axle vehicles (B, C, No's. 315, 415, 417, 513, 517)

3 five-axle (tandem) vehicles (No's. 324, 325, 327)

Nominal speeds normally ranged from 20 to 50 mph, with a few isolated values up to 56 mph. Increments of speed ranged from 2 to 10 mph, depending on the number of test runs in the subseries.

In the addition to bridge type, vehicle type, and speed, several other variables were involved in the dynamic tests. These include: the lateral position of the vehicle on the bridge, the condition of the vehicle springs (acting or blocked), the initial conditions of the vehicle, simulation of continuous traffic, and sudden braking of the vehicle on the bridge. These variables are further described in Section 8.3.

Table 2 summarizes the dynamic tests on the bridges by subseries. Column (2) of the table is a classification code number, which designates the type of tests. The legend for the code number is given in Table 3a. Columns (3) and (5) show the bridges, and Column (7) the vehicle involved in each subseries. Column (10) gives the number of test runs for each subseries, including crawl and static tests. Column (11) gives the date of the tests. As a further aid in evaluating the scope of the dynamic tests, Table 4 shows the subseries numbers for all bridge-vehicle combinations involved.

8.2 Test Methods. The setup for the dynamic and crawl tests was the same for all subseries. The tests were normally performed during the four-hour rest period in the regular test traffic. The dynamic test

runs were randomized with respect to speed. In all dynamic tests, the direction of travel of the test vehicles was opposite to that of the regular test traffic; that is, the vehicles approached the bridges from the straight (tangent) section, and continued to move onto the turnaround provided at the end of the test loops.

The measurements obtained included the bridge response, vehicle response and data on the position and speed of the vehicle.

Bridge instrumentation consisted of permanently mounted strain and deflection gages. The number of gage responses recorded varied from one subseries to another, depending on the objectives of the particular tests. In most cases, the response at the bottom strain and deflection gages at midspan of all three beams of a bridge was recorded. In some subseries additional strain gage responses were also measured, while in others, certain gage responses were not recorded, or the deflection gages were placed at points other than midspan. Columns (4) and (6) of Table 2 show an instrumentation code number for all bridges. The legend for this code number, showing the number and type of active gages, is given in Table 3b. The response of the active gages was recorded by oscillograph equipment. Figure 2 shows a group of four test bridges with the trailer housing the recording equipment, and a closeup of the deflection gages on one of the bridges. A further description of the bridge instrumentation is given in Reference (1a).

Vehicle instrumentation consisted of spring deflection gages, tire pressure gages, or both. Tire pressure measurements were obtained only in one series of tests. The type of instrumentation used in each subseries is indicated by a code number in Column (9) of Table 2, and explained in Table 3c. The spring deflections were measured by linear potentiometers

between the axles and the body of the test vehicle, and recorded by direct-writing recorders carried on the vehicle. Tire pressures were measured by differential pressure gages connected to the tires, and recorded by recorders mounted on a light instrument van pulled by the test vehicle. This equipment was developed by the AASHO Road Test Staff and is described in detail in Reference (8). Figure 1a shows one of the instrumented test vehicles and the instrument van.

For the purpose of recording vehicle position and speed on the bridge records, two rubber hoses connected to pressure transducers were laid perpendicular to the bridge axis, either on the bridge bearings or on the pavement near the ends of the bridges being tested. The position of the vehicle was identified by marker "pips" recorded on the bridge record whenever an axle passed over these hoses. In all but the first series, vehicle speed was also measured by an electronic timer activated by the passage of the axles over these hoses. In order to record the same information on the vehicle records, small obstructions were placed between the wheel lines of the truck near the hoses. These obstructions engaged a "kicker arm" on the vehicle and activated a contact switch, exactly at the instant an axle passed over one of the hoses, producing a "pip" on the vehicle record. The position of the vehicle was also indicated on the vehicle record by means of a revolution counter pulled by the test vehicle. The instrumentation described is shown schematically in Fig. 3.

Vehicle speeds were normally held to within 1 mph of the desired nominal speeds. The lateral position of the vehicle on the bridge was observed by a person standing at the far end of the test bridges and was held to within 4 inches of the desired position. Runs in which either of these tolerances were exceeded, or in which the recording equipment malfunctioned, were repeated.

8.3 Regular and Special Tests. In the majority of the dynamic tests, the bridge was at rest when the vehicle entered, there were no induced initial oscillations in the vehicle, the vehicle suspension system was in its normal operating condition (i.e. the springs were free to deflect) and the vehicle followed a path centered over the center beam of the bridge, producing a concentric loading. These tests will be referred to as regular tests throughout this report, and are identified by Test Classification Code 1 in Tables 2 and 4.

In addition, in several subseries, the testing procedures were changed by modifying one or more of the conditions described above. All of the latter tests will be referred to as special tests. Because of the specific nature of these tests, the test methods used for each group of tests are described in Chapter VII preceding the discussion of the results, and are only summarized here. Seven types of special tests were performed, as follows:

(a) Vehicle springs blocked, concentric loading;

(b) Induced initial oscillations in the vehicle by means of the ramp described in Section 7.2;

(c) Induced initial oscillations, vehicle springs blocked;

(d) Simulation of continuous traffic by two closely spaced test vehicles;

(e) Eccentric loading with two wheellines on the bridge;

(f) Eccentric loading with one line of wheels on the bridge, the other line of wheels travelling on the adjacent bridge;

(g) Sudden braking on the bridge.

Finally, two groups of tests were performed specifically for the purpose of obtaining data for the statistical analysis of certain variables.

One group, subseries 5451-18 has been discussed in connection with the crawl tests. The second group, involving subseries 5452-5 through 16 and 5452-21 through 24, consisted of replicate subseries in which two groups of three vehicles each were run on three sets of bridges at three speed levels. The test methods were identical to those for regular tests.

III. PROPERTIES OF BRIDGES

9. Static Properties and Computed Frequencies

This section summarizes the data obtained from static measurements on the bridges and the properties computed on the basis of these measurements.

9.1 Dimensions, Weights and Stiffnesses. All test bridges had a span of 50'-0" center to center of bearings, and consisted of a reinforced concrete slab 15'-0" wide supported by three identical longitudinal beams. The beams were steel wide-flange sections, prestressed concrete I-beams, or reinforced concrete T-beams. The spacing of the beams was 5'-0" for the steel bridges and 4'-8" for the concrete bridges. The slab was placed unsymmetrically with respect to the center beam, so as to provide 1'-0" overhang on the outside of the bridges. This overhang supported a 12" x 12" timber guardrail. The plan, elevation and cross-section of a typical test bridge are shown in Fig. 3. A schematic layout of all the test bridges is given in Fig. 4. A more detailed description of the bridges, including the dimensions of the beams and slabs, is given in Reference (1b).

The weights of the bridges were computed from the dimensions and unit weights given in Ref. (1c), and are tabulated in Column (2) of Table 5. The computed weights range from 73 kips for the composite steel bridges to 103 kips for the reinforced concrete bridges. No direct measurements of the weights were made.

In the computation of stiffnesses, the moduli of elasticity of concrete cylinders at the beginning of the test traffic (October 1958) were used. These values are shown in Columns (3) and (4) of Table 5. The values of the corresponding moduli at 28 days and at the end of the test traffic

(November 1960) are given in Ref. (1d). The mean measured modulus of elasticity of the bridge slabs at the end of the test traffic was 5.6×10^6 psi, or less than 10 percent higher than the values used. The effect of this change on the computed properties was not considered.

The moments of inertia of the individual beams were computed by the conventional elastic analysis. For the concrete and composite steel bridges, the tributary slab for the center beam was taken to be equal to the beam spacing, whereas for the edge beams it was assumed to include the slab overhang plus one-half of the beam spacing. The moments of inertia for the prestressed concrete bridges were evaluated for an uncracked section, and those for the reinforced concrete bridges were based on a cracked section. Columns (5), (6) and (7) of Table 5 show the moments of inertia of the individual beams. For steel bridges with cover plates, the values shown are those for the cover-plated section.

In Column (8) of Table 5 is given the flexural rigidity, EI, of the entire cross section of the bridges. For the composite steel bridges and the concrete bridges, this quantity was taken equal to the sum of the effective EI's of the three beams considering their tributary slabs. For the noncomposite bridges it was taken equal to the sum of the EI's of the three beams plus the rigidity of the slab, Db, where

$$Db = \frac{E_s t^3}{12(1-\mu^2)} \qquad (1)$$

E_s = the modulus of elasticity of the material of the slab

t = the average thickness of the slab

μ = Poisson's ratio (assumed as 0.1)

b = the total width of the slab

For the four noncomposite bridges studied, the quantity Db contributes approximately from 10 to 17 percent of the total stiffness. The computed rigidities, EI, of all the bridges studied range from $221 \cdot 10^6$ to $1,130 \cdot 10^6$ kips-in^2.

In Column (9) of Table 5 are given the values of the dead-load deflection of the bridges at midspan, computed on the assumption that the entire bridge acts as a single beam. These results are based on the weights and stiffnesses presented above. These quantities represent only a measure of the stiffness of the bridges, and do not necessarily represent the actual deflections from zero load. Since the computations were made on the basis of the final composite EI's, no attempt was made to separate the effects of the loads applied directly to the beams from those applied to the composite section.

9.2 Computed Frequencies. The natural frequencies of the test bridges were computed on the assumption that each bridge behaved as a single beam. With the exception of the steel bridges with cover plates, the frequencies in cycles per second, f_b, were computed from the equation:

$$f_b = \frac{\pi}{2L^2}\sqrt{\frac{EIg}{w_b}} = \frac{\pi}{2}\sqrt{\frac{5}{384}\frac{g}{\delta_{st}}} \qquad (2)$$

where L = span length

EI = flexural rigidity of the cross section of the bridge

g = acceleration of gravity

w_b = weight of bridge per unit length

δ_{st} = computed static dead-load deflection at midspan, as given in Column (9) of Table 5

For the steel bridges with cover plates, Stodola's iterative method was used[9a]. For the bridges considered, the length of the cover-plates

varied from 29 to 36 percent of the span, and the ratio of the moments of inertia of the base section to the cover-plated section varied from 0.75 to 0.86. It may be interesting to note that for these bridges, the difference between the frequency corresponding to the actual variation of EI and the frequency for a prismatic beam with the EI of the coverplated section never exceeded 8 percent.

The results of the computations are shown in Column (10) of Table 6. The computed frequencies range from 2.64 cps for Bridge 4A (noncomposite steel) to 7.00 cps for Bridge 5A (prestressed concrete).

As mentioned earlier, the frequency of the reinforced concrete bridges was computed for a cracked section. Frequencies higher than those tabulated could be expected if, in the earlier tests, the concrete in tension were not completely cracked. On the other hand, any cracking in the prestressed concrete beams would considerably lower their stiffness and the resulting frequencies. Finally, any friction between the slab and the beams in the noncomposite steel bridges would tend to increase the natural frequencies.

10. Representation of Maximum Static Effects

10.1 Selection of Base for Computation of Dynamic Effects.

Throughout this report, the dynamic effects produced in the bridges under the influence of moving vehicles are expressed in terms of the corresponding effects produced at crawl speeds.

In all of the crawl records obtained, small dynamic effects, amounting to several percent of the maximum response, were clearly visible, even at the low vehicle speed involved. Because of the presence of these

small disturbances, in the process of reduction a mean curve was drawn through the actual records for all the crawl curves studied, and the mean curve was taken to represent the crawl effects. In the early stages of the program, a study was made to determine whether the maximum ordinate of the mean crawl curve was a reliable measure of the maximum static effect. Several crawl records were studied and the results correlated with the effects produced by vehicles standing on the bridges. In this study, the following quantities were measured and compared:

(a) the maximum ordinates of the mean crawl curves;

(b) the maximum crawl ordinates, including the minor vibrations;

(c) the static response; and

(d) the ordinates of the mean crawl curve measured at the instant when the vehicle was in the same position as in the static tests.

It was found that the maximum ordinates of the mean crawl curves were uniformly the most reproducible. A subsequent statistical analysis of the static and crawl effects[10] substantiated the above conclusion.

In the remainder of this report, the terms maximum crawl value or simply crawl value will refer to the maximum ordinate of the mean crawl curve, and all crawl curves reported will be the mean curves drawn through the actual records.

10.2 Reliability of Measured Crawl Effects. Table 6 shows the maximum crawl values of strains and deflections at midspan of the individual beams for a selected number of runs corresponding to five different subseries. Included are the corresponding average values for each subseries. These results are typical of approximately 400 crawl tests studied. It can

be seen that, for a given series, there is in general good agreement in the magnitude of duplicate crawl values. When there is an obvious discrepancy, such as for Bridge 5A, Subseries 5451-4, it can generally be traced to malfunctionings of the instrumentation or recording system. The type of discrepancy shown in the table occurred only on 19 out of the 267 different gages involved in these tests.

Table 7 presents the average values of the maximum crawl strains and deflections at midspan for all the subseries studied in this report. The values shown are averages of two to six measurements. As an indication of the reproducibility of the data presented, the maximum percentage deviation of any individual measurement from the average values for the center beam is given in Columns (5) and (7). It can be seen that, for concentric runs, this deviation is always less than 10 percent for strains, and in only three cases does it exceed 10 percent for deflections. The majority of the deviations are less than 3 percent. The deviations for the edge beams, not reported herein, and for all three beams in the eccentric runs were generally larger; this is to be expected since these values are influenced by changes in the lateral position of the vehicles. It is apparent that discrepancies between individual crawl values are of the same order of magnitude as the tolerance involved in recording these effects. The errors introduced in the reduction process are estimated to be of the same order of magnitude.

The average values shown in Table 7 have been used in all subsequent computations as the base values for computing dynamic effects. It is important, however, that this spread in the crawl values be kept in mind in the interpretation of the dynamic effects, and in particular, in the comparison of measured effects with those predicted by theory.

11. Comparison of Measured and Computed Effects

11.1 Maximum Effects. Table 8 shows a comparison between measured and computed crawl moments and deflections. The data shown refer to one vehicle (No. 415) and seven bridges. Crawl measurements were available at three different dates approximately eight months apart. The measured moment in each beam was obtained as the measured strain in the beam times the corresponding section modulus times the modulus of elasticity of the beam material. The measured moment shown is the sum of the moments in the three beams. The measured deflection is the average of the deflections of the three beams. The computed moment in the three beams equals the computed external static moment, except for the noncomposite bridges, where it was modified by the factor $\frac{EI \text{ of } 3 \text{ beams}}{EI \text{ of } 3 \text{ beams} + Db}$ to account for the moment carried by the slab. The computed deflection is based on the same value of EI as that used in the frequency computations.

The following conclusions can be drawn from the information presented in Table 8:

(a) for the composite and noncomposite steel bridges, there is substantial agreement (within 10%) between measured and computed values.

(b) for the prestressed and reinforced concrete bridges, the measured moments and deflections are consistently higher than the computed values. As mentioned in Section 9.2, any cracking in the beam concrete beyond that assumed in the analysis of the sections results in reduced stiffnesses and section moduli, and would explain the high ratios obtained. In connection with the prestressed concrete bridges,

it should be noted that the section moduli used did not take into account the reduction due to the presence of access holes to the strain gages in the bottom flange of the beams.

The effect of repeated load applications resulted primarily in additional cracking in the concrete, further reducing the actual stiffnesses. This trend is definitely noticeable in the deflections of Bridges 5B, 7A, and 7B.

The table below shows the longitudinal distribution of measured strains in the middle third of the center beam of Bridges 3B and 5A, together with the ordinates of the computed curve of maximum moments. All three curves have been normalized so as to make the midspan effect equal to unity.

Quantity	Ratio of Effect to Midspan Effect				
	Gage Location, x/L				
	$\frac{1}{3}$	$\frac{5}{12}$	$\frac{1}{2}$	$\frac{7}{12}$	$\frac{2}{3}$
Computed curve of maximum moments	0.924	0.994	1.000	0.942	0.820
Measured strains, Bridge 3B	0.88	1.01	1.00	0.97	0.85
Measured strains, Bridge 5A	0.83	0.84	1.00	0.64	0.62

It can be seen that for the composite bridge 3B the agreement between measured computed curves is very good. On the other hand, the prestressed concrete bridge 5A shows a very erratic behavior, undoubtedly caused by cracking in the beam near the midspan.

11.2 Crawl History Curves. The vertical ordinates of the crawl curves presented in this article have been normalized with respect to the maximum crawl value, since only the shape of the curves is of interest. The horizontal scale is given in terms of the position parameter x/L, where x is the distance from the left support to the position of the rear axle of the vehicle, and L is the span of the bridge.

Figures 5a and 5b show the degree of replication achieved in two crawl curves involving the same bridge and the same vehicle. It can be seen that the replication for all three midspan strain and deflection gages is excellent. The maximum discrepancy between the two sets of records is of the order of a few percent of the maximum crawl value, and usually occurs away from the point of maximum crawl response. This figure is typical of a large number of replicate plots studied. The discrepancies may be attributed to the presence of minor irregularities in the records when the axles pass near the gage locations, or to the fact that the speed of the vehicle is not constant over the entire run.

Figure 6 shows crawl curves for the three midspan strain gages for the vehicle moving (a) in the normal direction (from tangent to turn-around) and (b) in the reverse direction (used in the regular test traffic). The agreement between the two sets of curves shows that the bridge is symmetrical, and that the direction of travel is of no importance. The slight shift in the position of the point of maximum response is again probably due to slight changes in speed while the vehicle is on the bridge.

The lateral distribution of strains and deflections for a typical crawl record is shown in Fig. 7, where the crawl curves for strain in three beams are plotted against the mean of the maximum crawl ordinates of the three beams. It can be seen that the exterior beam, having the largest

stiffness, has larger strains and deflections than the other two beams. It is also apparent that while the deflection of the center beam is somewhat less than the average of the two edge beams, exactly the reverse is true for strains. The difference in the maximum ordinates of the three curves is generally less than indicated by the particular test shown, as can be verified by comparing the maximum crawl values for the three beams shown in Table 7.

In Fig. 8, the crawl curves presented in the previous figure are shown with each curve normalized with respect to the maximum ordinate for that curve. It can be seen that the three beam responses coincide quite closely, indicating no basic difference in behavior of the three beams. This conclusion could have been anticipated from the knowledge that the test bridges are relatively narrow, so that for concentric loading there is no significant difference in the behavior of the three beams. A large number of comparisons between crawl curves for the center beam responses and the average curves of the responses of the three beams have shown that the two types of curves coincide for all practical purposes, and therefore can be used interchangeably to represent the crawl behavior. A typical comparison is shown in Fig. 9.

The experimental crawl curves have been compared to theoretical curves for a simple prismatic beam, and to curves obtained by considering the bridge as a slab on flexible beams. In the latter solutions, the effect of the variable EI of the steel beams with cover plates was included. From the discussion of the previous paragraph, no significant differences can be expected between the two theories. This is indeed the case, as in all the comparisons involving concentric loading there were no differences between the plots of the two theoretical solutions, including the cover-plated steel beams. Therefore, in the remainder of this report, theoretical crawl curves

will refer to solutions based on the assumption of a simply supported prismatic beam.

Figure 10 compares the average responses of the three beams to the corresponding theoretical solutions. For deflection, the agreement is very good, except for a slight change in phase. In the bottom of the figure, the average measured strain is compared to the computed moment curve. While the agreement is good, it should be noted that the computed curve comes to a sharp point when the drive axle is at midspan, while the measured curve shows a slight rounding. The agreement could be considerably improved if the experimental curve were extrapolated to a point, and this point matched up with the peak of the computed curve. Equally good agreement was obtained when the theoretical and experimental curves were compared at the third-points.

The general conclusion of this section is that computed and measured crawl responses are in reasonable agreement. However, the reduction error in all the ordinates of the crawl curves is of the same order as the error in the maximum values discussed in the preceding section. At points away from midspan, the relative error can thus be appreciable. This fact should be kept in mind for the discussion of dynamic effects, which involve the difference in the ordinates of the dynamic and crawl response curves.

12. Dynamic Properties

The purpose of this section is to present data on the frequency and damping characteristics of the test bridges, and to correlate the measured frequencies with the computed values presented previously.

12.1 Measured Frequencies. Bridge frequencies were normally obtained from the free-vibration portions of the dynamic records. The average frequency of the bridge over five cycles of oscillation immediately after the passage of the test vehicle was computed. This procedure was repeated for at least four records from every subseries, and the results averaged. The scatter between individual values was generally of the order of a few percent.

The characteristics of the free-vibration records merit some discussion. As was pointed out in Section 9.1, the projection of the slab over the exterior beam was one foot larger than that over the interior beam. Furthermore, in the concentric tests, the vehicle was centered over the middle beam, but lateral deviations up to four inches were allowed. As a consequence, the longitudinal axes of the center of mass of the bridge, the center of stiffness (point of load application to produce symmetric deflections), and the center of the applied vehicle mass did not necessarily coincide. A detailed examination of a number of free-vibration records showed that, even for the concentric runs, there was a component of motion due to the first torsional mode of vibration. The amplitude of this component was found to be quite erratic. For the records studied, its largest value was approximately 20 percent of that for the corresponding symmetric component[14a]. In the subsequent discussion the participation of the torsional mode will be neglected.

The average measured frequencies of the bridges are shown in Column (2) of Table 9. All data shown are from Series 5452 (February 1960), except for Bridges 4A, 4B, 6A and 6B, which were not tested in that series and for which data from Series 5450 (October 1958) were used. Thus the

values presented correspond to different numbers of vehicle trips for the different bridges. The effect of the number of vehicle trips on the measured frequencies is discussed below. The computed frequencies are reproduced in Column (3), and the ratios of measured to computed frequencies are given in Column (4). The following observations are made:

(a) for the composite steel bridges and the prestressed concrete bridges the agreement between measured and computed values is good;

(b) for the noncomposite steel bridges, the measured frequencies are considerably greater than those computed on the assumption of noncomposite behavior. The ratios of frequencies computed on the assumption of composite to noncomposite action are 1.71 for Bridges 4A and 4B, and 1.58 for Bridges 9A and 9B. It should be recalled that as the degree of composite action increases from zero to full composite action, the computed frequency first increases very rapidly, and then tapers off gradually. Thus, the ratios shown in Column (4) of the table indicate that in the free-vibration era these bridges have almost complete composite action;

(c) for the reinforced concrete bridges, the measured frequencies are somewhat higher than the computed values, indicating that in the free-vibration era these bridges were somewhat stiffer than predicted by an analysis based on a cracked section.

Table 11 shows the change in the values of the bridge frequencies for seven of the bridges studied in approximately two years of test traffic. The data shown substantiate essentially the predictions made in Section 9.2 regarding computed frequencies:

(a) the frequencies of the composite steel bridges and prestressed concrete bridges remained essentially unchanged. It should be noted that Bridge 5A, which was cracked, shows a slight loss in stiffness;

(b) for the noncomposite steel bridges, the measured frequencies decreased gradually from those approaching full composite action to those corresponding essentially to no composite action. This change may be due either to loss of friction due to "working" between the slab and the beams, or to loss of slab stiffness due to cracking, or to a combination of these factors;

(c) for the reinforced concrete bridges, the frequencies decreased appreciably between the first two series of tests, and from then on gradually approached the values predicted by the cracked-section analysis. This trend is in agreement with that observed in connection with changes in live-load deflections.

12.2 Comparison of Properties of Loaded and Unloaded Bridges. The discussions relative to the live-load deflections in Section 11.1 and the measured frequencies in the preceding section may appear to be contradictory. For example it has been noted that for the noncomposite bridges the measured live-load deflections essentially agree with the computed values based on non-composite action, whereas the measured frequencies in the free-vibration era show almost 100 percent composite action. This apparent discrepancy arises from the fact that the properties of the bridge while the test vehicle is on the span are different from those in the free-vibration era immediately after the passage of the vehicle. This is illustrated by the data given in Table 11.

In Column (2) of this table are given the ratios of the measured effective flexural rigidity EI of the bridges in their loaded condition to the computed values reported previously. Since deflection is inversely proportional to EI, these ratios can be obtained from the live-load deflection

measurements, and are in fact the inverse of those given in Column (7) of Table 8. In Column (3) are given the ratio of measured to computed EI for the free-vibration era. Since the natural frequency is proportional to the square root of EI, these ratios are obtained by squaring the ratios based on the frequency measurements given in Column (4) of Table 9. Now, since the same values of EI were used for both the deflection and frequency calculations, the ratio of Column (3) to Column (2) shows the ratio of measured EI of the unloaded to the loaded bridges. This value is shown in Column (4), and its square root, which gives the ratio of measured frequencies, is shown in Column (5). It is important to note that the frequency of the loaded bridge does not include the effect of the weight of the vehicle. The difference is due exclusively to changes in the properties of the bridge itself. In this connection, it may be noted that, in general, the amplitude of free vibration was less than 20 percent of the live-load deflection.

Examination of Columns (4) and (5) explains the contradictions referred to above:

(a) for the composite steel bridge, the ratios are close to unity, indicating that the properties of the bridge in the loaded and unloaded eras are essentially the same;

(b) for the noncomposite bridges the frequencies are 28 to 33 percent higher in the free-vibration era than in the period while the test vehicle is on the span. This is attributed to the fact that the application of the vehicle overcomes the friction between slab and beams, making the bridge behave essentially as noncomposite, but that as soon as the applied load is removed, the frictional force is sufficient to make the bridge act close to fully composite;

(c) the prestressed concrete and reinforced concrete bridges are from 16 to 37 percent stiffer in the free-vibration era, indicating that some cracks which open under the application of the vehicle load tend to close up after the passage of the vehicle. Bridge 5B, which was uncracked, shows a smaller change than Bridge 5A, in which all beams were cracked early in the tests.

No comparisons have been made for the other bridges tested. However, since their construction is similar to the bridges discussed, the conclusions reached may be considered to apply for all bridges tested.

The above observations have important implications on the analytical comparisons to be presented later, since the bridge frequency is one of the basic parameters controlling the dynamic response of the bridge. In what follows, the frequencies used are those obtained from the free-vibration era, since these were the only values which could be measured with any reliability. It should be kept in mind, however, that the true frequencies of the bridges corresponding to the conditions of the bridges while the vehicle is on the span may be less than these values by as much as 30 percent for the noncomposite steel bridges and 15 percent for the concrete bridges. Furthermore, this difference is obviously a function of the position of the vehicle and therefore varies as the vehicle moves across the span.

12.3 Bridge Damping. The damping of the bridge was determined primarily from the free-vibration portions of the dynamic records. The interpretation of these records was made difficult by the presence of a somewhat systematic low-frequency oscillation superimposed on the main oscillations.[11a] This oscillation was possibly due to a "beating"

effect between the motion of the bridge in the funadmental mode and the torsional mode which, as previously noted, was excited in several of the tests. The data reported here were obtained after the records were "smoothed" out to eliminate the effect of "beating" and should be considered as approximate.

It was found that the damping of the bridge was neither purely of the viscous nor of the frictional type, but probably some combination of both. However, it is felt that logarithmic decrements[9b] computed on the assumption of viscous damping provide some measure of the amount of damping present. Therefore, for the records used to measure the frequencies reported in Section 12.1 logarithmic decrements were computed based on five cycles of oscillation immediately after the passage of the test vehicle. The average values obtained from the records studied are shown in Column (5) of Table 9. While there was considerable scatter in the data, the average values reported in the table exhibit a degree of consistency for each bridge type. The composite steel bridges had the lowest values (5 to 7 percent); these were followed by the prestressed concrete (4 to 11 percent), reinforced concrete (9 to 13 percent) and the noncomposite steel bridges (19 to 29 percent). It is particularly noteworthy that the cracked prestressed concrete Bridges 5A and 6A have higher damping characteristics than the uncracked Bridges 5B and 6B. The damping factors of the bridges, β_b, in percent of critical damping, are given in Column (6) of Table 9.

The high damping in the noncomposite steel bridges is attributed to the mobilization of the frictional force between slab and beams discussed earlier. This is further substantiated by the fact that, in general, the largest scatter in damping factors was observed for these bridges, indicating that the change from noncomposite to composite behavior took place in

a highly unpredictable fashion. The relatively small damping in the reinforced concrete bridges, coupled with their low frequency, accounts for the persistence of visible vibrations for a long time after the passage of the test vehicles, a fact observed by many visitors to the test site.

On the basis of a limited number of additional records studied for Bridges 3B and 7A, it appears that there was no significant change in the magnitude of the logarithmic decrements with time.

The vibrator tests described in Section 6.3, provided data for the comparison between the damping characteristics of the loaded and unloaded bridges. In these tests, the amplitude of the bridge response, at least near the resonant frequency, was of the same order of magnitude as that caused by the passage of a test vehicle. Thus the characteristics of the bridges in these tests may be considered to be comparable to those of the loaded bridges.

Figure 11 shows the measured stress at midspan of the center beam as a function of the oscillator frequency for Bridge 3B. From this plot, the damping coefficient, β_b, was evaluated as approximately four percent. This value should be compared with the value of one percent obtained from the free-vibration records. This increase in the damping coefficient appears to be due to the fact that in these tests the amplitude of the oscillations was large enough to mobilize the bridge bearings, which are the principal source of bridge damping, while in the free-vibration era the bearings probably did not move. The measured resonant frequency of approximately 4.0 cps is 11 percent lower than the natural frequency measured from the free-vibration records. It should be recalled, however, that the vibration tests were executed after the completion of the regular

tests. Bridge 3B had at that stage developed a fatigue crack in the lower flange of the center beam. Furthermore, the data obtained refer to the double-amplitude of forced vibrations of the unloaded bridge. Near the resonant frequency the bridge slab may have been in tension, thus introducing additional sources of damping.

The results of the vibrator tests are summarized in the table below, together with the approximate resonant frequencies. For comparison, the measured damping coefficients and frequencies obtained from the free-vibration records are reproduced from Table 10.

Bridge No. and Type	β_b, percent critical		Frequency, cps	
	Vibrator tests	Free-vibration records	Vibrator tests	Free-vibration records
3B - Composite steel	3.5	0.8	4.00	4.39
9A - Noncomposite steel	6.0	3.3	2.92	4.15
6B - Prestressed concrete	-	0.6	5.30	6.78
8A - Reinforced concrete	3.9	2.0	3.12	3.48

It should be noted that a large uncertainty exists in the resonant frequencies, and that the damping coefficients were obtained in some cases on the basis of only two or three points on the frequency-response curve. These values should thus be considered only as a qualitative measure of the damping characteristics of the bridges under conditions comparable to those produced by the test vehicles.

13. Profiles of Approaches and Bridges

13.1 Profiles of Approaches. In Figs. 12a through 12c are shown the longitudinal profiles of the approach pavements to Bridges 2B, 3B, 5A,

and 7A, for a length of 80 feet immediately preceding the bridges. The quantitites shown are the average values of the measurements along two concentric wheel paths. The differences between the values for the two wheel paths were small, usually amounting to 2 or 3 hundredths of a foot. The four sets of profiles presented apply to one bridge at each of the four test locations. The approaches to the bridges adjacent to those shown are essentially similar in their major features. The ordinates shown represent the deviations of the actual profile from the design grade (0.2 percent slope) passing through a point on the intersection of the outside pavement edge and the bridge abutment.

The high frequency irregularities, two or three feet long, in these plots are believed to be due to the highly exaggerated scale of the figures in comparison with the accuracy of the original measurements. It can be seen that the approaches for Bridges 2B and 3B are considerably smoother than those for Bridges 5A and 7A, although some major irregularities are also present in the first two sets of plots, especially at the later dates. The major changes in the ordinates for the approaches to Bridges 2B, 5A, and 7A at the later dates are due to overlays (patches) placed on pavement sections that have failed.

In comparing the profile measurements at successive dates, it can be seen that, except for the overlays, the major irregularities are reproduced from one date to the next, and that in most cases they become more pronounced with time. In particular, on the approaches to Bridges 2B and 3B, the rise in the profile near the abutment becomes progressively more noticeable. This change is undoubtedly due to settlement of the approach fill.

To assess the importance of the effects of various irregularities on the response of the vehicle, it must be kept in mind that this response depends not only on the length and amplitude of the different "waves" of the profile, but also on the speed and natural period of the vehicle. Specifically, for a particular configuration of the irregularity, the response of an axle is a function of the ratio t_d/T_v, where t_d = time of transit of the axle over the irregularity, and T_v = natural period of the axle. For a single "wave" of practically any shape, the effects are maximum when t_d/T_v is of the order of 0.5 to 1.0. For values of this ratio less than 0.1 or greater than approximately 3.0, the effect of the irregularity on the response of the vehicle may be negligible. It is shown later that for the test vehicles used, T_v ranges approximately from 0.25 to 0.5 seconds. For speeds in the range of 30 to 40 mph, the lengths of "waves" corresponding to the critical values of t_d/T_v given above are from 6 to 30 feet. Irregularities within these lengths may be expected to influence significantly the response of the vehicle.

It should be noted in the figures that the lengths of the irregularities on the approaches are within the range given above. For example, while the approaches to Bridges 2B and 3B show no major irregularities at the earlier dates, the effect of the settlement at the later dates can be approximated by triangles 20 and 10 feet in length, respectively. Similarly, irregularities roughly in the shape of half-sine waves and of lengths of 20, 30, and 60 feet are discernible on the approaches to Bridges 3B, 5A, and 7A, respectively. In the sense of this discussion, only the approaches to Bridges 2B and 3B in the early tests can be considered as "smooth", and the approaches to Bridges 5A and 7A are quite irregular. For the latter

bridges, the condition of the vehicle at the entrance is highly uncertain, and may be quite sensitive to changes in the vehicle characteristics or the speed.

Finally, it should be noted that the closer the irregularity is to the bridge, the more important is its effect on the bridge response, because of the effect of frictional damping in the vehicle. For a speed of 30 mph, the test vehicles executed approximately four to eight cycles of oscillations while traveling 80 feet. It will be shown later that the friction in the vehicle suspension system acts to reduce oscillations of any magnitude to a very small fraction of their original value in a few cycles of oscillations. Thus, the portions of the approach profile shown represent a sufficient length to evaluate the effect of the irregularities.

13.2 Longitudinal Bridge Profiles. The profiles along the decks of Bridges 2B, 3B, 5A, and 7A are shown in Figs. 13a and 13b. As before, the ordinates represents deviations from the design grade and therefore the curves presented include the effect of the settlement of the bridge supports. For clarity, only the first and last set of measurements have been plotted. The comments concerning local irregularities made earlier also apply here. However, distinct irregularities, undoubtedly due to poor leveling during construction, are evident in practically all plots. The curves presented are again averages of the measurements along the two wheelpaths. The differences between the minor irregularities between the two wheelpaths are negligible. However, there is a consistent trend in the transverse profiles, which is discussed in the next section.

In order to examine the deviations of the bridge deck from a straight line through the supports, one set of profiles for the bridges

considered in detail in this section have been replotted in Fig. 14 by "smoothing" out the original measurements and correcting for any deviations of the supports. For comparison, the figures include a second degree parabola passing through the midspan ordinate of the measured profile. It can be seen that major irregularities still exist on the "smoothed" curves, and that the lengths of these irregularities are of the order of 10 to 20 feet. Thus the irregularities of the bridge deck itself may contribute to the response of the vehicle, as discussed in the previous section. However, the ordinates of the deviations from the parabola are generally small, of the order of 0.1 inches, except for Bridge 7A.

The permanent deflections of all bridges increased with time. Figure 15 shows plots of the permanent midspan deflections at the center of the four bridges considered, measured from a straight line through the supports. It can be seen that there is some scatter in the data, but that the general pattern is consistent.

The table below shows the permanent midspan deflections of the center beam after construction and at the end of the test traffic for all the bridges tested. For any intermediate date, the deflection can be approximated with sufficient accuracy by straight-line interpolation between the values shown.

13.3 Transverse Bridge Profiles. Because of the unsymmetrical nature of the dead load of the bridges, the transverse profile of several bridges was not horizontal after construction, with the exterior beam (beam under the timber guardrail) having the largest sag or least camber. Bridges 5A, 5B, 7B, 8A, 8B, 9A, and 9B were approximately level at the beginning of the tests.

Bridge Type and Number	Midspan Deflection, in. After Construction	Midspan Deflection, in. End of Traffic
Composite steel		
2B	-0.39 (sag)	-1.23
3B	-0.30	-0.90
Noncomposite steel		
9A	0	-0.70
9B	+0.05 (camber)	-0.72
Prestressed concrete		
5A	+0.12	-0.46
5B	-0.30	-0.44
6A	+0.27	-0.13
6B	-0.33	-0.18
Reinforced concrete		
7A	+1.06	+0.33
7B	+0.82	+0.09
8A	+1.22	+0.41
8B	+1.06	+0.31

Figures 16a and 16b present the lateral profiles of Bridges 2B, 3B, 5A, and 7A at several dates. The deflections for the dates not shown fall between those presented. These figures are typical of all the bridges examined. It can be seen that while deflections increase with time, the relative position of the three beams remains essentially unchanged. For example, on Bridge 3B, the outside edge had a sag of approximately 0.8 inches at the beginning of the tests, while the inside edge was level. At the end of the tests, the inside edge had deflection approximately 0.65 inches, but the outside edge deflection 1.40 inches so that the difference in levels was 0.75 inches, or essentially the same as at the beginning of tests. A similar pattern can be seen for Bridge 7A. Bridge 5A, which was essentially level at the beginning of tests, remained so throughout the entire test period.

While the lateral profiles of the bridge decks at the quarter points differ somewhat from those at midspan, the slopes are, in general, roughly proportional to those at midspan. Thus, it is felt that the lateral profile at midspan, in conjunction with the longitudinal profile described above, presents an accurate picture of the permanent bridge deflections.

It is apparent from Fig. 16 that the two wheel lines of the test vehicle traverse the bridge at different elevations. The possible effects of this condition on the vehicle and bridge responses will be discussed in later sections.

IV. PROPERTIES OF VEHICLES

This chapter summarizes the information relating to the characteristics of the vehicles used in the test program. This information includes the dimensions and weights of the vehicles, the results of static loading tests, and the results of measurements obtained on the vehicles while moving over pavements and various obstructions.

The number of vehicles used in the various tests and the scope of the measurements have been described in Section 7.

14. Dimensions and Weights of Test Vehicles

Several typical vehicles used in the tests are shown in Fig. 17. Figure 18 shows schematic diagrams of the vehicles, and the dimensions of all the vehicles used in the tests. Three of the test vehicles, designated as A, B, and C, were loaded specifically for the dynamic tests; all other vehicles carried the same loads as in the regular tests on the Test Road. A detailed description of all test vehicles may be found in Reference (1e).

The weights of the vehicles are listed in Table 12. The weights were determined by means of an electronic scale, which weighed one axle at a time. Generally, the test vehicles were weighed several times. The values given in the table are the averages of all the measurements taken. The last column of the table shows the number of weighings for each vehicle.

In the comparison of the results of replicate weighings, it was found that day-to-day variations existed not only in the individual axle loads, but also in the total weight. The table below shows the weights obtained for vehicle 5131-32, together with the date of each weighing.

Test No.	Axle weights (kips) Front	Drive	Rear	Total weight (kips)	Date
1	4.2	22.1	22.1	48.4	8/12/59
2	5.0	23.1	23.2	51.3	11/10/59
3	4.9	22.6	22.5	50.0	8/30/60
4	4.4	22.5	22.6	49.5	8/31/60
5	4.7	22.1	22.5	49.3	9/1/60
6	4.7	22.5	22.8	50.0	9/6/60
7	4.6	22.2	23.9	50.7	1/6/61
8	5.0	22.7	23.9	51.6	1/13/61
9	5.0	22.1	23.4	50.9	1/20/61
10	4.6	23.4	23.5	51.5	1/24/61
Average	4.8	22.5	23.0	50.3	

It can be seen that differences in total weights between two measurements made in the same week are of the same order of magnitude as those between two weighings performed a year apart. The variation in the moisture contents of the concrete blocks used for loading may be responsible for the above differences.

15. Static Load-Deflection Characteristics of Axles

15.1 Vehicle Tires. When examined critically, the data obtained from the loading tests show that the load-deflection characteristics of the tires can be represented by a bilinear diagram. The reasons for this relationship can be described as follows. When a vehicle is loaded statically, the friction between the roadway surface and the tire prevents the lateral spreading of the tire with the result that the effective stiffness of the tires is somewhat greater than that which would be exhibited on a frictionless surface.

As the load is increased, the frictional resistance is overcome, the tire spreads out laterally, and the effective stiffness of the tire is reduced. During unloading, the above process is reversed, so that when the applied load reaches its starting value, there is a net residual deflection. This process is illustrated graphically in Fig. 19a, where P_o and y_o denote the starting load and the corresponding deflection, respectively.

Figure 19b shows the experimental load-deflection diagram for the drive axle tires of Vehicle No. 91. The ordinates of this plot represent the axle load. The abscissas represent the average deflection of the two sets of tires on the axle, measured from the equilibrium position at the beginning of the loading test. Thus, at zero deflection the axle load recorded is that of the unloaded vehicle. The figure clearly shows the behavior described above; however, it is noted that the difference in stiffness for the regions with and without lateral slippage is extremely small. In fact, for several of the tests this difference could not be distinguished, but the spread between the loading and unloading portions was always noticeable. On the diagram, the "break" due to partial unloading and reloading is clearly noticeable. In general, the above diagram is typical of all 43 tire loading tests.

Figure 19c shows the results of duplicate tests. Replication is excellent in this case. In general, the differences in the slope of duplicate diagrams were of the same order of magnitude as those determined from the loading and unloading portions of the diagram for a particular test. In view of this, no attempt was made to isolate the two cases discussed above, and the tires were considered to behave as linearly elastic springs. The spring constants were determined as the average slope of the load-deflection

diagrams at the static load level. It may be noted that under dynamic conditions, with the tire rolling over the pavement, the spread discussed above can be expected to be smaller than under static conditions.

Column (5) of Table 13 shows the average spring constants of the tires studied, in kips of axle load per inch of average deflection of the axle. The values shown are the averages of all individual tests. It can be seen that the values obtained are reasonably uniform, the grand average values being 10.8 kips/in. for the front axles (two tires) and 24.0 kips/in. for the drive and rear axles (four tires). Column (7) of Table 13 lists the average static deflections of the tires. The static deflection is defined as the ratio of the static axle load to the average spring constant. As mentioned earlier in connection with the static deflection of the bridges, this value may not equal the true deformation of the tire from zero to the static load if the initial portion of the load-deflection curve is not linear, and serves only as a measure of the tire stiffness. The average values shown range from 0.5 to 1.1 inches.

15.2 Suspension Springs. The leaf-type vehicle suspension spring exhibits a bi-linear behavior of a somewhat different nature from that described above for the tires. The suspension spring can be thought of as a linear spring of stiffness k_s, connected in parallel with a frictional damper. Denoting by P the total load on the suspension system and by P_s the component of the load carried by the spring, the maximum or limiting frictional force in the damper may be expressed as $F = \mu P_s$. The coefficient of interleaf friction, μ, is considered to be constant. If the loading were to start from zero, the spring would immediately engage, and the force carried by the frictional damper would have its limiting value of μP_s at all times.

The total force on the suspension system would be $P = (1 + \mu)P_s$, and the effective stiffness of the system would be $(1 + \mu)k_s$ as shown by the uppermost line on Fig. 20a. If the loading were now reversed, the change in load would be resisted solely by the damper until the load were reduced by $2\mu P_s$, namely until the frictional force would change direction and attain its limiting value in the opposite direction. In this interval, the suspension spring would remain "locked", and there would be no change in deflection. In reality, the spring would deflect in this period as a single beam. However, the beam stiffness is very large in comparison to the sum of the stiffnesses of the individual leaves, so that the assumption of no deflection is reasonable. If the load were further reduced, the spring would again engage and carry a load P_s, but the frictional force would act in the opposite direction so that the total load carried by the system would be $P = (1 - \mu)P_s$ and the effective stiffness would become $(1 - \mu)k_s$. In actual tests, the loading does not start from zero, but from some initial value P_o corresponding to a deflection y_o. In this case, the frictional force may have any value between $\pm \mu P_s$ and, as the load is increased, no deflection is produced until the frictional force reaches its limiting value and the springs engage. The behavior described is illustrated graphically in Fig. 20a.

In the analytical solutions presented in Chapter VIII, it is assumed that the limiting frictional force in the suspension system of the vehicle has a constant value of $F = \mu P_{st}$, where P_{st} is the static axle load. This is equivalent to assuming that the loading and unloading portions of the load-deflection diagram are parallel and are $2F = 2\mu P_{st}$ apart vertically, as shown by the dashed lines on Fig. 20a. This assumption is justified by the fact that the variation of the dynamic loads from the static load is

usually small (of the order of 20 percent), so that the true value of the limiting frictional force varies little from the assumed constant value. The same assumption was used in the reduction of the test data. The spring constant of the spring suspension system, k_s, was obtained as the average of the slopes of the loading and unloading portions of the experimental diagrams at the static load level, and the coefficient of interleaf friction was determined as one-half the vertical distance between the loading and unloading portions, measured at the point where this distance is bisected by the horizontal line representing the static axle load.

Figure 20b shows the results of two duplicate tests on the drive axle of vehicle No. 415. Again, the abscissas represent the average deflection of the suspension system, measured from the position at the beginning of the loading. The figure shows clearly the high initial friction in the springs, the slight convergence of the loading and unloading portions of the diagram when the springs are engaged, and the near-vertical unloading when the springs are locked.

Figure 20c shows the results of duplicate tests involving partial unloading and reloading. The behavior of the suspension system is in essential agreement with that discussed earlier. These two figures are typical of the data obtained for the tests on the drive axles of the vehicles. In general, the agreement between duplicate tests was reasonable. Additional plots are given in Ref. (11b).

The results for the loading tests on the front axle show a behavior similar to that described above, but the amount of friction in the coil springs is considerably smaller than in the leaf springs. The replication was again good for all tests.

Figures 20d and 20e show typical results for the rear (semitrailer) axles. In general, the results for the semitrailer suspension systems showed a gradual transition between the vertical and sloping portions of the diagram, and in many cases no distinct spring constant could be obtained. The interleaf friction was generally higher and replication was considerably poorer than for the tractor axles. As an example, Fig. 20e shows a 100 percent change in the spring constant for two tests performed on the same day. By comparison with other tests, the higher value was rejected.

The average values of the spring stiffnesses for all the vehicles tested are summarized in Column (6) of Table 13, and the corresponding static deflections are given in Column (8). The values shown are averages of all test data. In general, from two to four loading tests were performed on each axle. The differences between individual measured spring constants and the averages reported are of the order of 5 to 15 percent for the front and drive axles, and up to 50 percent for the rear axles. For Vehicle No. 94, two sets of values are shown, since the two groups of tests a year apart showed reductions in spring stiffness of 40 and 50 percent for the front and rear springs, respectively. The spring constants range from 7.6 to 16.7 kips/in. for the drive axle springs, and from 12.3 to 24.0 kips/in. for the rear axle springs. The average values of coefficients of interleaf friction given in Column (9) range from 4 to 11 percent for the front axle, from 11 to 17 percent for the drive axle, and from 18 to 20 percent for the rear axle. However, the results of duplicate tests differed in some cases by as much as 25 percent from the average values reported. The frictional force at the beginning of the loading tests ranged from 6 to 25 percent of the static load, or 0.4 to 1.5 times the corresponding coefficients of interleaf friction.

15.3 Summary. It has been shown from the static load-deflection data that, for all practical purposes, the behavior of the tires may be considered to be linearly elastic. Similarly, the load-deflection characteristics of the front and drive axle springs may be represented with sufficient accuracy by the bilinear diagram illustrated in Fig. 20a. Although the replication of the results is generally good, there may be appreciable differences in the detailed features of the diagrams, particularly in the tests with partial unloading and reloading. On the rear axle springs, the replication was in general erratic and in many cases the observed load-deflection characteristics were at considerable variance with the idealized behavior assumed in the reduction.

It must also be emphasized that the results presented are given in terms of the average deflection of the two tires or two springs of an axle. The data showed that the deflections of the two tires or springs were in general not equal. However, since only the total axle load was measured, it is not known whether the stiffnesses of the two tires or springs on an axle were actually different.

All of the above uncertainties enter in the evaluation of the dynamic results to be presented in the succeeding chapters.

16. Computed Frequencies of Axles and Vehicles

As used in this report, the term axle of frequency represents the frequency of vibration of a single-degree-of-freedom system having the same stiffness as the effective stiffness of a vehicle axle, consisting of the tires and the suspension springs, and a mass corresponding to the static axle load. These frequencies were computed from the load-deflection data presented in the preceding sections, based on the following assumptions:

(a) the springs are blocked - in this case the effective stiffness, k_e, equals the stiffness of the tires, k_t; and

(b) the springs are free - in this case the springs act in series with the tires, and the effective stiffness of the system is

$$k_e = k_{ts} = \frac{1}{\frac{1}{k_t} + \frac{1}{k_s}}$$

These assumptions represent the two extreme possibilities of behavior of the test vehicle. In any time period during which the dynamic axle load varies by less than 2 μP_{st}, the springs remain locked, and there is no change in the force carried by the suspension spring. Whenever the frictional force is exceeded, the springs engage, the effective stiffness is reduced, and the change in the force carried by the suspension spring is equal to the variation in the axle load. If the direction of movement is reversed, the vehicle springs become locked until the frictional force is again exceeded. Thus, the actual frequency of the vehicle is a continuously varying quantity which depends on the change in axle load.

The axle frequencies computed for the two assumptions are shown in Columns (4), (5) and (6) of Table 14. The effective mass in both cases is assumed to be that corresponding to the total axle load, even though the unsprung mass, representing the mass of the axle and frame, is supported by the tires only. In subsequent chapters, the axle frequency of the i^{th} axle will be designated as $\bar{f}_{t,i}$ when computed on the assumption of blocked springs, and as $\bar{f}_{ts,i}$ when computed for springs free to act.

While the axle frequency is a convenient measure of the dynamic characteristics of an individual axle, for purposes of comparison with experimental data the actual frequencies of the vehicles must be known.

For a two-axle vehicle, the natural frequencies, f_1 and f_2, can be related to the axle frequencies, $\bar{f}_1$ and $\bar{f}_2$, as follows:

$$(f_{1,2})^2 = \frac{1}{2}\left(C_1 \pm \sqrt{C_1^2 - 4C_2}\right) \qquad (3)$$

where $C_1 = \bar{f}_1^{\,2} + \bar{f}_2^{\,2} + \frac{1-i}{i}\left(\frac{a_1}{s}\bar{f}_1^{\,2} + \frac{a_2}{s}\bar{f}_2^{\,2}\right)$

$$C_2 = \frac{\bar{f}_1^{\,2}\,\bar{f}_2^{\,2}}{i}$$

s = wheelbase

a_1 = horizontal distance from front axle to center of gravity of the sprung mass

$a_2 = s - a_1$

The quantity i is known as the dynamic index, and is a measure of the longitudinal distribution of the vehicle mass. It is given by the equation

$$i = \frac{r^2}{a_1 a_2} \qquad (4)$$

where r = the radius of gyration of the sprung mass.

The smaller value of f, f_1, represents the bounce frequency and the larger value, f_2, the pitching frequency of the vehicle.

It can be seen that if the two-axle frequencies are equal, the bounce frequency equals the axle frequency, and the pitch frequency equals $\frac{1}{\sqrt{1}}$ times the axle frequency. Furthermore, for i = 1.0 the bounce and pitch frequencies are identical. In the computation of i, the distances a_1, a_2 can be found by statics from the axle loads. However, the values of the radii of gyration of the test vehicles are not known. This quantity is extremely difficult to evaluate[15], and no attempt was made to measure it

in the field. Based on published data pertaining to vehicles similar in size and weight to the test vehicles, a value of i = 0.8 has been assumed for all two-axle vehicles and tractors of the tractor-semitrailer combinations.

The natural frequencies of a three-axle truck-semitrailer combination depend on the dynamic indexes of both the tractor and the trailer, as well as the position of the junction between the tractor and trailer, the so-called "fifth wheel" support. The expressions for computing the three natural frequencies of such a vehicle are given in Ref. (16a). On the semitrailers used in the dynamic tests, the loading consists essentially of two large masses placed almost exactly over the "fifth wheel" and the rear axle. For this loading, it can be assumed that i = 1.0 and this value was used in all computations. It can be shown that for this value of i, the motion of the rear axle is independent of that of the tractor, and the frequency of the rear axle is a true natural frequency for the system. However, the other two natural frequencies cannot be obtained by equation (3), since the motion of the tractor is still influenced by the dynamic reaction at the "fifth wheel". In the computation of frequencies, the expressions given in Reference (16a) were used. For the value of i used, the modal shapes associated with the vibration of a three-axle vehicle correspond to the bounce and pitch motions of the tractor while the rear axle remains stationary; and the vertical motion of the rear axle with the tractor in a stationary position. It should be noted that Ref. (1a) assumes that there are no horizontal components of inertia forces due to angular rotations transmitted at the "fifth wheel", i.e., that the centers of gravity of the truck and semitrailer are on a horizontal line passing through the "fifth wheel".

Columns (7) and (8) of Table 14 show the natural bounce and pitch frequencies of the two-axle vehicles and tractors of three-axle vehicles. It can be seen that the bounce frequencies of all vehicles are remarkably uniform, ranging from 3.1 to 4.2 cps when the suspension springs are considered to be blocked, and from 1.7 to 2.7 cps when the springs are considered to act in series with the tires. The frequency of the drive axle is very close to the bounce frequency of the vehicle, the two quantities actually being identical for 9 out of the 18 sets of results shown. Finally, the pitch frequencies of all vehicles are from 30 to 40 percent higher than the corresponding bounce frequencies.

One additional frequency is of interest for comparison with experimental data. This is the so-called "tire-hop frequency" of the axle, which corresponds to the frequency of the unsprung mass of the axle vibrating between the roadway and the body of the vehicle. This frequency is given by the expression:

$$f_h = \frac{1}{2\pi}\sqrt{\frac{(k_t + k_s)g}{w}} \qquad (5)$$

where w is the unsprung weight of the axle.

For vehicle No. 91, the computed tire-hop frequencies of the front and rear axles are 12.5 and 13.2 cps, respectively. If there is any play in the spring suspension system, the unsprung mass may be vibrating on the tires only without engaging the springs; in this case the value of the tire-hop frequency would be approximately 10 cps for both axles.

17. Dynamic Response of Vehicles in Tests on Pavements

17.1 General. This section deals with the analysis and interpretation of the data obtained from the dynamic tests on the vehicles and the

correlation of the observed response with that predicted on the basis of the static tests reported in the previous section. As described in Section 7.2 the available data include the measurements of the variation of the force in the tires and springs of the vehicles, both for vehicles with blocked springs and with normal suspension.

The quantities of interest in this study are the observed frequencies of the vehicles, the damping characteristics of the tires and the suspension system, and the magnitude of the variation of the interaction force.

The natural frequencies and damping characteristics of the vehicles can best be determined by means of an oscillator, in a manner similar to the one used on the bridges, or, more conveniently, by dropping the vehicle from a ramp and recording the free-vibration of the stationary vehicle. There was no equipment available to perform the first type of tests, and due to an oversight, the latter tests were not conducted after the tire pressure gages were perfected. Therefore, the frequencies can only be inferred from the data obtained for a moving vehicle. In this connection, it should be remembered from the discussion of the previous article that the test vehicle is not a simple linear system of two or three degrees of freedom, but that it is a complex system, including additional degrees of freedom associated with the unsprung axle masses. Thus, the test data obtained represent the response of a complex dynamic system to the irregular excitation provided by the roadway unevenness, and one can only distinguish and discuss the predominant components of the response, with their associated frequencies, amplitudes, and damping characteristics.

In connection with the observed magnitudes, it must be emphasized that all of the experimental data show only variations in tire or spring

forces with respect to an unknown base value, which is not necessarily equal to the static axle load. The tire pressure measurements give variations with respect to the ambient tire pressure at the instant the bypass valve around the pressure transducer is closed (Ref. 8). Since the vehicle is in motion at that instant, the actual pressure and the corresponding wheel load are unknown. Similarly, the spring records show the deformations of the springs from their equilibrium position at the beginning of the particular test run. As described in the previous article and shown in Fig. 20a, the actual force corresponding to this position cannot be determined. Concerning the accuracy of the experimental data, the correlation of tire pressures to wheel loads was found to be linear but with considerable scatter of individual points,(8) so that loads computed from the experimental data may be in error by as much as ten percent. Also, on most records, drifting due to loss of air pressure was noticeable, but no attempt has been made to correct for this effect in reducing the records. Similarly, the spring forces obtained with the aid of the spring constants presented in the previous article can only be considered as approximate, due to the variations in spring constants discussed earlier. The smallest change in spring displacement that could be observed on the records is of the order of five percent of the static load. Finally, the time scale on the records could be obtained only from the paper speed of the oscillograph records. These oscillographs were driven by small unregulated generators. In the cases where comparisons could be made with the electronic timer used on the bridge tests, the time scales on the tire and spring records were found to be in error by as much as 25 percent.

The results presented in this section pertain to two of the four vehicles tested: the two-axle vehicle No. 91 and the three-acle vehicle

No. 513. The results are representative of the data obtained, and bring out the important findings relevant to the overall scope of the project.

17.2 Behavior of Vehicles with Blocked Springs

(a) Drop Tests. Figure 21a shows the results of a drop test involving the two-axle vehicle, for a speed of approximately 20 mph, with the springs blocked on both axles. The origin of the abcissas was chosen arbitrarily, but it is the same for the two wheel responses shown. The ordinates are given as variations in the interaction force in terms of the static load on the axle. As mentioned above, the horizontal base line is not known. For this record, the base line was arbitrarily selected so as to bisect approximately the amplitude of the response. This method of presentation is used in all figures of this section. A slight drift is noticeable on the records, however, as discussed above, no correction was applied. The responses of the two remaining wheels are not shown; they are essentially in agreement with the curves presented.

In observing the characteristics of the records at the obstruction, it is noted that there is an increase in the interaction force as an axle enters the ramp, as expected. Usually, there is a sudden decrease in the force as the axle leaves the ramp; however, because the motion at this point is influenced by the motion on the ramp, and because the motions of the two axles are interrelated, this decrease is not always noticeable. The double-amplitudes of oscillation immediately after the exit are the same for the front and rear axles. After the vehicle leaves the ramp, the motion of the two axles are essentially in phase, but the rate of decay is different, with the front axle motion damping out rapidly. This fact is due to the interference of the rear axle; since the center of oscillation for the pitching mode is

located close to the rear axle, the effect of any component of the pitching mode is more pronounced on the front axle response than on that of the rear axle.

The measured frequency based on the paper speed of the record is of the order of 3.1 cps, or approximately 82 percent of the value of 3.8 cps presented in the previous section on the basis of the static measurements. In attempting to explain this difference, it should be kept in mind that discrepancies in the paper speed of the same order as above were observed. Furthermore, as discussed previously, the static measurements yielded only the deflection of the axles, and not that of the point of application of the load. Thus, beside the tires additional sources of flexibility may be present in the vehicle. Because of these two independent factors, the discrepancy between measured and computed frequencies cannot be ascertained from the pavement tests above. However, in the bridge tests to be presented later, frequencies of the order of 2.9 to 3.5 cps were measured using the more exact electronic timer. Therefore, it appears that the frequency based on the static measurements may be somewhat higher than the true frequency of the vehicle.

The response of the rear axle was used to determine the damping characteristics of the tires. Figure 22 shows a plot of the amplitude of vibration versus the number of cycles of oscillations after the rear axle has dropped from the ramp for the record shown in Fig. 21a. For comparison, an exponential curve of "best fit" is shown as a dashed line. The observed decay corresponds to an equivalent viscous damping coefficient of the order of 0.8 percent. The significant difference between the amplitudes of the left and right wheels cannot be explained; however, the average of the maximum

amplitudes of the two wheels is in reasonable agreement with the computed value for the entire axle, based on a 7/8" drop. The observed damping coefficient for the front axle based on the first cycle of oscillation is comparable to the value presented for the rear axle.

A typical drop test for the three-axle vehicle, with a speed of 20 mph, is shown in Fig. 21b. The front axle, which was not blocked, shows distinctly the tire-hop response at the end of the ramp. The measured tire-hop frequency of 13 cps agrees with the value presented in the previous section. This motion is damped out rapidly by the suspension springs, as will be discussed in the next section.

Concerning the responses of the drive and rear axles, if the dynamic index, i_2, of the semitrailer were equal to one, and the horizontal force on the fifth wheel was negligible, the motions of the two axles would be uncoupled, as discussed previously. However, the responses of the two axles are in phase. Furthermore, the rear axle motion is increased when the drive axle is on the ramp, and conversely, the drive axle response shows a buildup coincident with the entry of the rear axle on the ramp. Thus it can be concluded that there is a coupling between the axles in addition to that used in the computation of the vehicle frequencies. Because of this coupling, damping cannot be determined from the records, and the observed frequencies cannot be compared with those presented in the previous section on the assumption of no coupling. It is observed, however, that the measured value of 3.4 cps is in reasonable agreement with the computed bounce frequency of 3.1 cps, and semitrailer axle frequency of 3.4 cps.

The maximum double-amplitude is 1.2 P_{st} on the rear axle, as compared to a value of 2.0 P_{st} for the two-axle vehicle. This reduction is

to be expected, since the amplitude of response to a given excitation is generally smaller for a system with more degrees of freedom.

(b) Tests on pavements. Figures 21c and 21d present typical responses on a smooth pavement for the two- and three-axle vehicles, respectively. It can be seen that the double-amplitudes of oscillation are low, and are of the order of 0.4 to 0.5 P_{st} for both vehicles. The vehicles perform essentially a bounce motion, but the response is influenced by the details of the irregularities of the pavements.

Figures 21e and 21f show the responses of the same two vehicles on a rough pavement. The double-amplitudes of approximately 1.2 P_{st} for both vehicles are much larger than on the smooth pavement, and approach those recorded for the drop tests. The beating effect on the front axle of Vehicle No. 91 is very noticeable. The responses of the drive and rear axles of Vehicle No. 513 are generally in phase, again indicating some coupling between the axles. However, in certain regions of the records the two responses are out of phase, and show higher frequencies and lower amplitudes than in the former regions. This phenomenon seems to indicate that under certain types of excitation, there may be interference created between the responses of the two axles. The observed frequencies for both vehicles are of the order of magnitude presented for the drop tests, but because of the uncertainties discussed previously, no numerical values are presented.

17.3 Behavior of Vehicles with Normal Suspension

(a) Drop tests. Figure 23a shows the results of a typical drop test performed at 10 mph with the two-axle vehicle. The ordinates

obtained from the tire pressure measurements are given in terms of the static load, as before. The results of the spring deflection measurements give the force in the springs in terms of the static load. The equilibrium position of the springs is taken as the base line, and a value of 1.0 P_{st} is assigned to it, although, as discussed in connection with Fig. 20a, the actual force in the springs may be anywhere between the limits $P_{st}\ (1 \pm \mu)$, where μ is the coefficient of interleaf friction.

It can be seen that the tire-hop motion is predominant in the response of both axles, but that this motion is rapidly damped out. On both axles, the springs are compressed immediately upon the entrance on the ramp, and remain engaged while the vehicle is on the ramp. At the exit, the first noticeable feature is the large increase in the interaction force and spring response as the vehicle "bottoms" after leaving the ramp. The magnitude of the double-amplitude at the first half-cycle is approximately 1.1 P_{st}, or almost the same as that for the blocked springs.

After the drop, the springs of the front and rear axles return essentially to their equilibrium position in one-half and one-and-a-half cycles, respectively. In this interval, the double-amplitude of the interaction force is reduced to approximately 0.2 P_{st}, as compared to the slight reduction for the vehicle with blocked springs.

The frictional force in the springs was determined quantitatively by comparing the amplitudes of the tire pressure and spring displacement records. On the basis of the idealized model presented in the previous section, the response measured from the spring record was taken to be $(1 - 2\mu)\Delta P$, whenever the double-amplitude of force variation from the tire pressure record was ΔP. This relationship was applied to successive half-cycles of oscillation, measured from peak to peak. For the rear axle response shown, the values of μ obtained are as follows:

first half cycle	$\mu = 0.10$
second half cycle	$\mu = 0.08$
third half cycle	$\mu = 0.05$
succeeding cycles	$\mu > 0.10$ (i.e. no spring response for double-amplitudes of the order of $0.2\ P_{st}$)

The value of μ measured from the static loading tests was 0.11. It can be seen that μ is not a constant quantity as assumed, but appears to be decreasing with each oscillation. This phenomenon was observed on several records for both vehicles. A possible explanation may be that there is a certain amount of play between the leaves of the springs, so that as the excitation builds up, the normal force between the spring leaves is reduced, and the frictional force decreases in proportion. When the severity of the excitation is reduced, the coefficient of friction seems to return essentially to its static value.

Figure 23b shows the results for a drop test with the three-axle vehicle. The amplitudes of response are of the order of $0.3\ P_{st}$. On the ramp and immediately after the drop, the coefficient of friction in the drive axle springs appears to be reduced to zero; that is, the vehicle appears to be oscillating continuously on the combined springs and tires. For later portions of the record, however, the springs remain locked whenever the variation in the interaction force is less than the frictional force, exactly as predicted by the assumed bilinear model.

(b) Tests on pavements. Figures 23c and 23d present typical responses of the two vehicles studied on smooth pavements. The spring records show no discernible displacements, and are not presented. The

double-amplitudes of force variation for both vehicles are of the order of 0.2 P_{st}, or one-half the values recorded for the same vehicles with springs blocked. Thus, it is apparent that some mechanism of damping does exist. Considering that the resolution of the spring records is of the order of 0.05 P_{st}, and since the measured amplitudes in general do not exceed the statically determined limiting frictional force by more than this amount, it is probable that small changes in the spring displacement do occur, but cannot be distinguished on the records. The measured frequencies agree substantially with those for blocked springs. This is to be expected, since the spring deflections, if any, would be of such short duration as not to affect materially the observed "frequencies".

For the tests on rough pavements presented in Figs. 23e and 23f, it can be seen from the records that the excitation of the vehicle is not continuous, but consists of occasional impulses strong enough to produce changes in the spring deformation. The springs return to their original position, within the margin discernible on the record, in a time corresponding to from one-half to several cycles of oscillation. For the two-axle vehicle, the values of the coefficient of friction, μ, measured on the records range from 10 to 12 percent on the front spring and 13 to 15 percent on the rear spring. These values are only slightly higher than the values of 8 and 11 percent, respectively, reported in Table 14 on the basis of the static tests.

For the three-axle vehicle (Fig. 23d) the spring excitations described last for several cycles of oscillation. On the left rear springs of the record shown, values of μ of 18 and 16 percent were obtained. Similar values were measured on the right rear spring. On the drive axle, however,

a phenomenon similar to that described for the drop tests was observed; namely, for the excitations lasting several cycles, the apparent friction gradually reduced to zero, and then built up again.

The double-amplitudes of force variation for both vehicles range up to 0.4 P_{st}, or approximately one-third of the values observed for the case of blocked springs. Larger amplitudes are always accompanied by the deflection of the springs. No values of measured frequencies are given, because in addition to the experimental uncertainties discussed, the periodic engagement of the springs results in "frequencies" that vary with the excitation. However, in the regions where the springs are engaged continuously over several cycles of oscillations, the measured frequencies are somewhat lower than in the portions where the springs are locked, as expected.

The major conclusion of this section is that the coefficient of interleaf friction is not a constant quantity, but appears to depend on the severity of the excitation. If the excitation is very strong, the suspension system may act as if there was no interleaf friction at all. This observation has serious implications on the prediction of the interaction force from the spring records alone. On the basis of the assumed vehicle behavior presented in the previous section, a reasonable estimate of the double-amplitude of the interaction force could be obtained as the sum of the measured variation in the spring force and twice the static limiting frictional force. Judging from the records examined this estimate may be considerably higher than the true value.

V. REPRESENTATIVE DATA ON BRIDGE-VEHICLE BEHAVIOR

18. General

This chapter contains a qualitative discussion of the behavior of bridges and vehicles in the dynamic tests. Data are presented from a selected number of tests to illustrate the detailed characteristics of the response of one test bridge under the passage of a two-axle vehicle, and of the response of the vehicle itself. The results presented are representative of those obtained for a large number of test runs examined, involving essentially all of the bridges and vehicles used in the tests.

The response of the vehicle and the bridge is presented in terms of history curves. A history curve is a plot of the variation of a quantity, such as interaction force, deflection, or strain, as a function of time.

The experimental data obtained consist of oscillograph records of the dynamic forces exerted by the vehicle tires on the bridge, the deformations of the vehicle springs, and the deflections and strains at various gage locations on the bridge. Figures 24a and 24b show typical field records for a dynamic test run on Bridge 3B using the two-axle vehicle No. 91. The tire pressure and bridge records have been reproduced photographically, while the spring deformation record was retraced full scale. The active gages and the various markers identifying the paper speed of the records and the position of the vehicle are identified on the figures.

The abcissas of all history curves represent the ratio x/L, where x is the distance between the entrance to the bridge and the position of the last axle of the vehicle (drive axle of a two-axle vehicle or semitrailer axle of a three-axle vehicle), and L is the span length. It should be noted that

$$\frac{x}{L} = \frac{vt}{L} = \frac{t}{t'} \qquad (6)$$

where v = the speed of the vehicle

t = elapsed time measured from the instant of entry

t' = time of transit

Thus the abcissas may be interpreted either as position coordinates or as time coordinates. Negative values of x/L correspond to times prior to the entrance of the last axle. In particular, the point of entry of the front axle of a two-axle vehicle is at $-s_1/L$, where s_1 is the wheelbase. Values of x/L greater than one correspond to the free-vibration era following the exit of the vehicle.

19. Results for a Regular Test

19.1 Response Curves. As described in Section 8.3, in the regular tests the bridge was initially at rest, there were no induced initial oscillations in the vehicle, the vehicle suspension system was in its normal operating condition, and the vehicle followed a path centered over the center beam of the bridge, producing a concentric loading. The particular run selected, for which the original field data were presented above, is from Subseries 5453-1, involving the composite bridge 3B and the two-axle vehicle No. 91. The speed of the vehicle was 44.5 mph. The pertinent properties of the bridge and vehicle were presented in the previous two chapters. The results are shown in Figs. 25a through 25f.

Figure 25a presents history curves of the interaction forces for the four wheels of the vehicle. The ordinates represent the dynamic interaction forces in terms of their static value, as before. Increases in force are shown downward in the figure, to conform with the sign convention chosen for the bridge response. The comments made previously concerning the uncertainty in

the base line and the drift in the records are applicable to all history curves of interaction forces presented in this and succeeding chapters.

It can be seen that both axles have a vertical component of motion prior to entering the bridge. This fact has been observed on all the records obtained. While the motion of the front axle is small, the double-amplitude of oscillation of the rear axle is of the order of 0.3 P_{st}, or somewhat higher than the results obtained from the tests on smooth pavements. The magnitude of initial oscillations is studied in detail in Section 24.3. The variation of the interaction forces while the vehicle is on the bridge is generally small for the front axle. For the rear axle, however, there is a large reduction in these forces immediately after the entrance, caused partially by the sudden change in the curvature of the profile at that point, and to some extent by the deflection of the bridge itself. The ensuing motion of the rear axle has a frequency of the order of 2.2 cps. At the exit, the forces are again reduced as the axles pass onto Bridge 3A.

The responses of the vehicle springs for the same test are shown in Fig. 25b. As before, the horizontal base line is taken as the equilibrium position at the beginning of the record. It should be noted that the springs engage only for a small fraction of the time of transit, so that generally the vehicle vibrates on its tires only.

History curves for the dynamic effects on the bridge are shown in Fig. 25c, with the corresponding crawl curves superimposed. The responses shown are for deflection and strain at midspan of the center beam. Each effect is expressed in terms of the maximum static value of that effect. The static values used were discussed in Section 10.1 and are given in

Table 7. In Fig. 25d, the above history curves for total dynamic effects have been reproduced, together with the corresponding history curves of dynamic increments. The term dynamic increment denotes the difference between the dynamic response at a given instant and the corresponding static response at the same instant, expressed in terms of the maximum static effect. A history curve of dynamic increments is thus a time-wise plot of the difference between the history curve for total response at a particular location and the corresponding crawl curve.

The characteristics of the dynamic bridge behavior can best be seen on the dynamic increment curves. In particular, it can be seen that the frequency of oscillation throughout the test run is essentially that of the bridge. It is not possible to distinguish on the records oscillations corresponding to the frequency of the interaction force.

19.2 Correlation of Dynamic Increment Curves. It can be seen from Figs. 25c and 25d that the total dynamic responses for deflection and strain at midspan of the center beam are different, due to differences in the shapes of the corresponding crawl curves. However, when the history curves of dynamic increments for the two responses are compared, it is noted that the shapes of the two curves are identical for all practical purposes. The amplitude of the dynamic increment curve for deflection is generally somewhat larger than that for the strain. This result is in agreement with theoretical knowledge[16b]. Thus, knowing the dynamic increments for one response, the corresponding values for the other can be estimated.

Extending the comparison to effects at different sections, the bottom portion of Fig. 25e shows history curves of total response for three successive strain gages on the center beam, located at the third point,

midspan, and the two-thirds point, respectively. As in the previous figure, each of the responses has been normalized with respect to the maximum static value of the particular effect at the section considered. At the top of the figure are shown history curves for dynamic increment for the same three gage locations. Comparison of the total response and dynamic increment curves again shows that differences in the total response are due only to differences in the shape of the crawl curves and that the dynamic increments are essentially equal in both phase and magnitude. Only the response of the first mode of vibration can be detected on the dynamic increment curves, and the contribution of the second mode is negligible even at the third-points.

In Fig. 25f, the dynamic increment curves for deflection and strain at midspan of the center beam are compared to the corresponding curves for the edge beams. In the figure, the dynamic increment curve for each gage location has been normalized with respect to the maximum static value at the location considered. Thus, if the dynamic increments were proportional to the static effects, the curves for the three beams would coincide. It can be seen that this condition is not exactly satisfied. Although the responses of the three beams are in phase showing that the bridge behaves essentially as a single beam, there are slight differences in magnitude. The lateral distribution of dynamic effects is discussed in greater detail in Section 32.2. However, two general observations can be made at this point:

(a) The trend in the relative magnitudes of the responses in the three beams seems to be related to the relative magnitudes of the interaction forces on the two wheel lines of the vehicle. Comparing Figs. 25a and 25f, it can be seen that the maximum dynamic increment in the outside beam, which is located closest to the right wheelpath, is less than that of the other two

beams. This lower value of the response appears to correspond to the lower value of the interaction force on the right rear wheel shown in Fig. 25a; however, as discussed above, the drift in the tire pressure records is such as to make a direct correlation impossible.

(b) In the free-vibration era, the responses of the three beams are not equal, with the relative positions of the three beam responses remaining essentially constant. This is due to the fact that, as mentioned in Section 9.1, the bridges are not symmetrical about the longitudinal center line, and as a consequence, the cross-section of the bridge at a natural mode of vibration is not a horizontal line, but a curve with different ordinates at the exterior beams.

It can be concluded from the above comparisons that for all practical purposes, the bridge behaves as a beam. Thus the response of a single gage, when expressed as a history curve of dynamic increments in the form presented, reflects with sufficient accuracy the dynamic behavior of the entire bridge. This conclusion applies to all test bridges. In the following chapters, emphasis is placed primarily on the dynamic effects at midspan of the center beam.

It must be emphasized, however, that the above conclusion is limited to the test bridges considered subjected to concentric loads, and should not be generalized for wider bridges, for which it may represent a considerable oversimplification of the true behavior[3,17]. The conclusion does not apply to the tests with eccentric loads on the bridges considered.

A detailed study of the results of the regular tests is presented in Chapter VI.

20. Results for a Test with Induced Vehicle Oscillations

Figures 26a through 26c show the results for a representative run with induced vehicle oscillations. The test run selected is from Subseries 5453-10, which involved the same bridge (3B) and vehicle (No. 91) as the test run presented in the previous section. The speed of the vehicle was 31.0 mph. The end of the ramp designed to induce the initial oscillations in the vehicle, and described in Section 7.3, was placed directly on the bridge abutment, as shown in Fig. 26a.

History curves for the interaction forces and response of the vehicle springs for the four wheels are shown in Figs. 26a and 26b, respectively. The history curves for the interaction forces are essentially similar to the ones presented for the pavement runs in Section 17.3, and as in the pavement runs, in the region immediately following the drop the measured interleaf friction approaches zero. In comparing the interaction force curves with the corresponding curves for the regular test run, it can be seen that while the presence of the ramp changes the initial phase of the interaction force, the average magnitude of variation of the interaction forces while the vehicle is on the bridge is essentially the same for the two cases.

The top curves in Fig. 26c show the history curves for dynamic increment for strain at midspan of the three beams. The corresponding curves for deflection are essentially identical to those for strain and are not reported. It can be seen that the curves for the three beams are practically the same, thus confirming the conclusion made earlier that the bridge behaves as a single beam. As before, the dynamic increments reflect both the contribution of the intertia of the bridge and of the variation in the interaction force. However, in contrast to the regular runs, the contribution of the

variation of the interaction force is more pronounced. Upon close examination, components of the response in phase with both the front and rear axle force variation may be detected. Finally, at several places on the records, the curves for the edge beams oscillate about the center beam curve, indicating the presence of a slight contribution of the torsional mode of vibration.

History curves of dynamic increments for strain at the third points of the center beam are shown at the bottom of Fig. 26c. The high-frequency oscillations observed at the third points correspond to the second natural (first antisymmetrical) frequency of the bridge, as can be seen from the fact that the third-point responses are 180° out of phase, and have a frequency approximately four times the natural frequency of the bridge. This contribution of the second mode is always most pronounced in the early stages of the response, and tends to decrease at later stages. This is to be expected, since damping in the bridge tends to decrease the high-frequency oscillations faster than those of the lower frequencies. When compared to the regular tests, the contribution of the second mode is more pronounced, due to the greater initial disturbance applied to the bridge. However, in all the records studied, the contribution of the second mode at the third points (measured as the amplitude of the deviation of the actual curve from an "average" curve) is only of the order of 10 percent or less of the maximum static response, as compared to dynamic increments ranging up to 75 percent. Thus it is apparent that the high-frequency oscillations contribute a relatively small amount to the total bridge response. In general, the correlation between the "mean" dynamic increment curves at the third points and midspan is good.

It can be concluded that the dynamic increment curve for the center beam midspan response is still a reasonable measure of the total bridge response,

and that, except for the high-frequency components, the correlation between the various dynamic increment curves is satisfactory. In this connection, it must be noted that the theoretical correlation presented in the previous section is based on the assumption that only the contribution of the fundamental mode of the bridge is important. Tests with induced initial oscillations are further discussed in Section 30.

21. Effect of Speed on Bridge and Vehicle Response

In this section, the qualitative discussion of behavior presented in the previous articles for two typical dynamic runs is extended to the results of several additional tests, in order to illustrate the effect of speed on the response.

In Fig. 27a, the response of the bridge and vehicle for the regular dynamic test run presented in Section 19 is compared to two other test runs from the same subseries. The vehicle speeds for the three runs are 24.7, 33.7, and 44.5 mph. The top curves show the interaction forces for the right rear wheel for the three runs considered. As mentioned earlier in connection with Fig. 25a, there are differences in magnitude between the responses of the two wheels. However, since this discussion is concerned with trends only, the response of one wheel can be taken as representative of that of the entire vehicle.

The frequency of the force variation is the same for all three curves, and, at least on the approach pavement, corresponds essentially to the frequency of the axle vibrating on its tires. However, since the abcissas represent position coordinates, these curves are not in phase. There is, however, one important exception. Approximately five feet prior to entrance to the bridge (i.e. at $x/L = -0.1$), the motion for all three records becomes essentially

the same, and the three records show similar initial conditions when the vehicle enters the bridge. This indicates that for the bridge considered, the profile of the approach appears to determine to a great extent the initial condition of the vehicle entering on the bridge, regardless of the nature of its prior motion. In Fig. 12a a pronounced upward slope of the approach slab can be detected in this region, and is in all probability the cause of this observed effect.

In general, the double-amplitude of the force variation increases with increasing speed. This is true both when the vehicle is on the approach pavement and when it is on the bridge.

The response of the bridge for the two faster runs considered is shown on the bottom of Fig. 27a in terms of the dynamic increment curves for midspan deflection of the center beam. For the slower run, only the portion of the record near the maximum dynamic increment is shown. As the vehicle speed increases, the number of oscillations that the bridge undergoes during the passage of the vehicle decreases. Consequently, the number of waves in the response curve decreases, and successive peaks shift to the right. It can be seen that the peak dynamic increments increase with speed. This fact is representative of all the tests. Furthermore, for the particular runs considered, the peaks move closer to midspan, so that the maximum total response increases faster than the peak dynamic increment.

In general, however, an increase in speed is not always associated with in an increase in total response at a section, since the peak dynamic increment may combine with a low crawl ordinate. The dynamic increment of most significance is the "critical" dynamic increment, that is, the one corresponding to the maximum total response. Depending on the number of

bridge oscillations, the "critical" dynamic increment may be one of several relative maxima. For this reason, a plot of maximum total response at a section as a function of speed is quite sensitive to variations in the speed.

In Fig. 27b, the responses of the bridge and vehicle for the test run with induced initial vehicle oscillations presented in the previous article is compared to a second run from the same subseries, but with a vehicle speed of 37.1 mph. As before, the vehicle behavior is represented by the history curves for interaction force of the right rear wheel. It can be seen that for the two runs the initial conditions of the vehicle as it enters the bridge are similar, even though the variation of the force on the ramp is somewhat different for the two runs, due to the difference in time of transit over the obstruction. It can be seen that the initial vehicle conditions are better controlled, i.e. more uniform, than in the regular tests.

The response of the bridge, measured by the dynamic increment curves for strain at midspan of the center beam, is shown on the bottom of Fig. 27b. As before, the number of waves is reduced with the increased speed, and consequently the dynamic increment curve shifts to the right. There is a slight increase in the maximum increment with speed. It may be noted that for similar speeds, the magnitude of effects is comparable to that for the regular tests. These curves further illustrate the dependence of the maximum total effect on both the magnitude and position of the "critical" dynamic increment. For the slower run, peak dynamic increments occur at $x/L = 0.24$ and $x/L = 0.62$. The second of these peaks combines with a crawl value of 0.80, giving a total maximum response of 1.02. On the other hand, for the faster run, peak dynamic increments occur at $x/L = 0.32$ and $x/L = 0.80$, and it is the first peak which

combines with a larger crawl ordinate to produce a maximum total response. In the two runs presented, the maximum dynamic increment happens to be the "critical" one; however, in many cases a smaller peak dynamic increment closer to the maximum crawl value may be "critical".

In summary, both the vehicle and bridge responses show increased effects with speed. The dynamic increment curves show almost a linear increase in magnitude with speed, and the position of the maximum ordinate also varies with speed. The total bridge response, which is the sum of the crawl and dynamic effects, reflects both the magnitude and position of the "critical" dynamic increment, and is thus sensitive to changes in speed. Furthermore, since both of the above factors can be affected by minor experimental variations, notably in the initial conditions of the vehicle when it enters the bridge, a considerable scatter in the maximum total response can be expected, as discussed in the next section.

22. Representative Spectrum Curves

In the preceding sections, the bridge response was studied in terms of history curves for particular test runs. While this type of presentation gives the most complete picture of the behavior, and will be continued in later sections, the large volume of data obtained precludes the presentation and study of dynamic effects in terms of history curves alone. Furthermore, from a design point of view the quantity of primary interest is the maximum value of a given dynamic response.

As an introduction to the comprehensive study presented in Chapter VI, the results of the two subseries discussed in the previous two sections will be presented in terms of the maximum effects observed in the individual test

runs. The results obtained are presented as spectrum curves. A spectrum curve, as used in this report, represents a plot of the maximum dynamic values of a selected response as a function of vehicle speed. Thus, for each dynamic test run, only the maximum response for the run is plotted, regardless of the position of the vehicle for which the maximum effect occurred.

Spectrum curves for the two subseries considered are shown in Figs. 28a and 28b. In these curves, the ordinates have been normalized with respect to the corresponding maximum static values. The ratio of the maximum total dynamic response to the corresponding static value is defined as the amplification factor, A.F. In the presentation of spectrum curves, the symbols AF_D and AF_M will be used to designate amplification factors for deflection and strain, respectively. The static values used in computing the amplification factors are given in Table 7. The abcissas of the spectrum curves are given in terms of the speed parameter, α, defined as

$$\alpha = \frac{vT_b}{2L} \tag{7}$$

where T_b is the fundamental natural period of the bridge, determined from the free-vibration records from the subseries considered, as discussed in Section 12.1. The engineering significance of this parameter will be discussed in the next chapter.

The spectrum curves presented refer to amplification factors for deflection and strain at midspan of the center beam. As discussed previously, these two responses reflect with sufficient accuracy the dynamic behavior of the entire bridge. Each spectrum plot shows all the experimental points and a line representing an "average" of these points. The "average" curves,

drawn somewhat arbitrarily, serve mainly for the subsequent comparison of different spectrum curves.

Figure 28a shows the spectrum curves for the regular test runs, Subseries 5453-1. The points corresponding to the history curves previously discussed are shown by vertical arrows. It can be seen that amplification factors generally increase with speed, and range from 1.08 to 1.34 for deflection and 1.01 to 1.22 for strains. The scatter between individual points, anticipated in the previous section, is evident. The significance and range of the scatter will be explored more fully in Section 25.2. The magnitude of the scatter makes it impossible to distinguish between the shapes of the two spectrum curves. However, there is a pronounced difference between the magnitudes of the spectrum curves for deflection and strain. This difference can be explained by reference to the history curves for total response, Fig. 25c. It has been shown previously that the dynamic increment curves for deflection and strain are essentially the same both with regard to phase and magnitude, but that the shape of the crawl curves for the two effects is different. Thus differences in the curves for the total deflection or strain reflect primarily the differences between the shapes of the two crawl curves. Since the crawl curve for deflection is relatively flat in the middle third of the record, a given maximum dynamic increment occurring anywhere in this region will yield essentially the same total response. On the other hand, for a two-axle vehicle the crawl curve for strain comes to a sharp peak, and the total response is more sensitive to variations in the position of the maximum dynamic increment. A dynamic increment occurring farther away from midspan produces a considerably smaller total response. The same reasoning accounts for the dip in the spectrum curve for strain at approximately $\alpha = 0.10$. For the slower speeds, the "critical" dynamic increment occurs at a point

corresponding to approximately two full cycles of oscillations after the entrance of the rear axle. As the speed is increased, (i.e. the time of transit, t', is decreased), eventually the first maximum becomes the "critical" dynamic increment. It therefore follows that for intermediate speeds, both of these maxima combine with low ordinates of the crawl curves, and that, conversely, the peak crawl ordinate is combined with a negative dynamic increment. Because of the flat crawl curve for deflection, this transition is hardly noticeable on the spectrum curve for deflection.

The spectrum curves for the dynamic tests with initial vehicle oscillations, Subseries 5453-10, are shown in Fig. 28b. In comparison with the spectrum curves presented above for regular tests, two features are worth noting. The first is the relatively smaller scatter in the individual points. This fact has been observed in all tests in which the initial conditions of either the vehicle or the bridge were controlled, and substantiates the observation made previously, that the uncontrolled variation in the initial conditions affects both the magnitude and phase of the dynamic increments. The other observation to be made is that the amplification factors are considerably more sensitive to variations in speed than for the regular runs. This fact follows from the previous discussion, since for these tests, there are two components of the response (one due to the inertia of the bridge, and one to the variation in the interaction force), both of which can change the magnitude and position of the "critical" dynamic increment. In particular, several values of amplification factor for strain less than unity are noted. These correspond to the speeds for which the rear axle interaction forces, have a minimum value when the rear axle is near midspan (see Fig. 26a). The above observations are in agreement with the theoretical predictions made in Ref.[16b].

Finally, it should be noted that the amplification factors for deflection are essentially of the same magnitude as those for the regular tests, while the amplification factors for strain are actually lower than the corresponding values for the regular tests. Referring again to Fig. 26a, it can be seen that for that particular test, (and actually for the majority of the tests in the subseries), the interaction force had a minimum value near midspan. It can be expected that for different vehicle or bridge frequencies, speeds, or bridge spans, the vehicle could have "bottomed" at midspan, producing much higher amplification factors.

VI. RESULTS OF REGULAR TESTS

23. General

This chapter presents the results of the regular dynamic tests, together with the analysis and interpretation of these tests in the light of available theoretical knowledge. Regular tests have been previously defined as those in which the bridge was initially at rest, there were no induced initial oscillations in the vehicle, the suspension system was in its normal operating condition, and the vehicle was centered over the middle beam of the bridge. As can be seen from Table 4, 37 test subseries, involving 14 bridges and 7 vehicles, fall in the category of regular tests. Of these 37 subseries, five yielded insufficient or erroneous data which could not be properly reduced. Furthermore, as shown in Fig. 4, 12 of the 14 bridges were placed in pairs, with the test vehicle crossing both bridges on each test run. This chapter will deal primarily with the bridges located first in the line of travel, since the response of the bridges located second in the line of travel was found to be influenced by the vertical oscillations in the vehicle induced by its passage over the first bridges. The responses of the bridges located first and second in the line of travel are compared in Section 27.1.

This chapter deals mainly with 32 subseries involving 6 bridges and 6 vehicles, as follows:

Bridges: 2 composite steel (2B and 3B)
1 noncomposite steel (9B)
2 prestressed concrete (5A and 6A)
1 reinforced concrete (7A)

Vehicles: 2 two-axle vehicles (A and No. 91)
4 three-axle vehicles (C, Nos. 315, 415 and 513).

The combination of bridges and vehicles for each subseries is listed in Columns (1) and (2) of Table 15. Additional bridges and subseries are discussed briefly in Sections 27.1 and 27.4.

The discussion on this chapter will be based principally on spectrum curves for maximum total response (deflection or strain) at midspan of the center beam of the bridges considered. It has been shown in the previous chapter that the center beam midspan gages reflect with sufficient accuracy the response of the entire bridge. History curves of dynamic increments will be introduced wherever additional explanation of the behavior is required.

It should be emphasized that in this chapter the results will be interpreted in the light of theoretical predictions in general terms only. Actual comparisons between measured and predicted response are presented and discussed in Chapter VIII.

24. Bridge-Vehicle Parameters

24.1 Definition of Basic Parameters. The dynamic response of the bridge-vehicle system depends on the vehicle speed and the combination of the pertinent bridge and vehicle parameters. The significant bridge parameters, namely span, weight, frequency, and permanent deflection, have been presented and discussed in Chapter III. The vehicle parameters, including axle spacing, total weight, weight distribution to the axles, frequencies of the axles, natural frequencies, limiting frictional forces in the springs, and dynamic indices, have been presented in Chapter IV. In the analysis of the problem these parameters enter as dimensionless ratios. From previous studies[18], it is known that the most significant of the dimensionless ratios are:

a. Speed Parameter. Denoted by α, the speed parameter is defined by equation (7). From the definition of α it follows that the bridge undergoes approximately $\frac{1}{2\alpha}$ cycles of oscillation during the passage of an axle over the span (the reason that this later relationship is only approximate is that the frequency of the bridge-vehicle system is a function of the position of the vehicle on the bridge). Since it has been shown in Chapter V that the frequency of the dynamic increments is important in determining the ordinate of the crawl response combines which with a peak dynamic increment to produce the maximum total response, it can be seen that the parameter α is a more significant measure of the effect of speed than the vehicle speed alone.

b. Weight Ratio. Denoted by R in this report, this ratio is defined as:

$$R = \frac{\text{Total weight of the vehicle}}{\text{Total weight of the bridge}}$$

c. Frequency Ratio. Associated with each axle of the vehicle there is a frequency ratio, φ, defined as:

$$\varphi = \frac{\text{Frequency of axle}}{\text{Natural frequency of the bridge}}$$

It should be recalled that the axle frequency is the natural frequency of a single-degree-of-freedom system, the mass of which corresponds to the axle load and the stiffness of which equals the effective spring stiffness of the axle. In this study, the axle frequency used will be that of the drive axle of the vehicle, since it corresponds closely to the computed natural frequency of the vehicle (see Table 14). The frequency ratio, φ, will be denoted by φ_t if the axle frequency is computed for blocked springs ($\overline{f}_t$), and by φ_{ts} if the axle frequency refers to the combined springs and tires ($\overline{f}_{ts}$).

d. Profile Variation Parameter. Also associated with each axle, there is a ratio denoted by Δ, defined as:

$$\Delta = \frac{\text{Deflection of the unloaded bridge at midspan}}{\text{Static deflection of the axle}}$$

The numerator of this ratio, and therefore the sign of Δ, may be positive or negative, depending on whether the bridge deflection is downward (sag) or upward (camber). The static deflection of the axle used in computing Δ is taken to be that of the drive axle of the vehicle, assuming blocked springs. The deflection of the unloaded bridge is taken to be deflection at midspan of the center beam, measured from a straight line through the supports, and interpolated from plots such as Fig. 15 for the date of each subseries. In this connection, it should be recalled from Section 13 that the lateral deflection of the bridges was not uniform, and that the longitudinal profile may deviate considerably from the parabola assumed in the theoretical analysis. Thus the parameter Δ must be taken as an approximation only. The profile variation parameter has a simple physical interpretation: it represents the change in the interaction force, in terms of the static axle load, due to a vertical movement equal to the deflection of the unloaded bridge at midspan, assuming that the vehicle springs do not engage.

Several parameters of minor importance have not been discussed above, either because their effect is known to be small from theoretical considerations, or because their range was restricted in the tests. In the latter category belongs the axle spacing ratio, s/L, which was essentially constant for all three-axle vehicles used (see Fig. 18).

24.2 Ranges of Parameters. The principal bridge-vehicle parameters for the 32 subseries involved in the regular tests are shown in Columns (4) through (8) of Table 15. For the speed parameter, α, only the maximum value

for each subseries is shown. The ranges of the parameters R, φ_t, φ_{ts} and Δ, and the maximum values of α are listed in Table 16 for each group of tests involving the same types of bridge and vehicle.

It can be seen from Table 16 that values of α range up to 0.22. For normal bridges of the same span, this value of the speed parameter corresponds to higher vehicle speeds than those considered in this program. This difference is due to the fact that the test bridges were designed for high stress levels, and their natural periods were higher than those of bridges designed on the basis of more conservative stress levels. It can also be seen that the parameters R, φ_t, φ_{ts} vary approximately by a factor of two between minimum and maximum values. The maximum values of the weight ratio (R = 0.66) and of the frequency ratios (φ_t = 1.23 and φ_{ts} = 0.76) are high for 50 foot simple-span bridges, but the ranges of α, R, and φ obtained are representative of normal bridges of a range of spans[19].

Finally, it should be recalled that the bridges were not specifically designed for the dynamic tests, and that the test vehicles were in general standard trucks used in the regular tests. Thus, the significant parameters could not be varied continuously and independently of each other throughout their respective ranges. For example, the ranges of α obtained for the prestressed and reinforced concrete bridges are different, due to the large difference in the periods for the two bridge types. Similarly, the bridge-vehicle parameters R, φ and Δ occur in predetermined combinations; interchanging two vehicles or two bridges changes all three of the parameters. For this reason, the effects of the parameters will, in general, have to be considered in groups.

24.3 Initial Oscillations. In addition to the parameters described above, the behavior of the bridge-vehicle system depends on the conditions of

the bridge and vehicle at the instant the vehicle enters the span. In all of the regular tests, the bridge was initially at rest. The vehicle, however, generally performed a vertical motion on its suspension system prior to its entrance on the bridge. The magnitude of this oscillation was uncontrolled.

Initial vehicle oscillations are caused by the unevenness of the approach pavement, including any discontinuity between the approach pavement and the bridge deck. For the majority of the regular tests, the nature and magnitude of the initial vehicle oscillations were unknown, as these tests were conducted before the tire pressure recording equipment became available. However, in the fourth series of tests, the tire pressure data provided information for a detailed study of the initial vehicle oscillations.

Figures 29a and 29b show typical curves of the variation in the interaction force on the approach pavement in terms of the static load. As before, the right rear wheel is taken to be representative of the entire vehicle. The curves show clearly the vertical motion of the vehicle at approximately the natural frequency of the vehicle with springs blocked, as well as the "tire-hop" motion caused by the sudden discontinuity between the approach slab and the bridge deck. It can be seen that, in general, the initial conditions of the vehicle at the entrance to the bridge are uncontrolled and may vary from an almost true smoothly rolling condition to high values of initial variations in the interaction force and of the vertical velocity.

The magnitude of the initial oscillations was studied by computing (a) the double-amplitude of the oscillation for the cycle of oscillation immediately preceding the entrance to the bridge, and (b) the average double-amplitude over five cycles of oscillations preceding the entrance. Table 17

shows the values obtained for two subseries, involving Vehicle No. 91 and the approach pavements to Bridges 3B and 7A. Both the double-amplitude at the entrance and the average double-amplitudes generally increase with speed. For the higher speeds, the double-amplitude at the entrance is roughly twice the average value.

The effect of speed on the magnitude of initial oscillations is further examined in Figs. 30a and 30b, which show the amplitude of initial oscillation (expressed as one-half of the double amplitude immediately preceding the entrance) as a function of speed, for all regular tests for which tire pressure measurements were available. It can be seen that for both Vehicles No. 91 and No. 513, the largest amplitudes of the initial oscillation occur on the approaches to Bridges 3B and 7A, and that the amplitudes increase with speed, reaching values as high as 25 to 30 percent of the static load. On the other hand, the initial oscillations on the approaches to Bridges 9B and 6A seldom exceed 15 percent of the static load and seem to be independent of speed. It is noteworthy to observe that the scatter of the points is not very large.

The mean amplitudes of the force variation in terms of the static load for the seven subseries considered are as follows:

Vehicle	Mean Amplitude of Force Variation, P_{st}			
	Approach to Bridge			
	3B	7A	9B	6A
No. 91, Drive axle	0.14	0.16	0.08	0.09
No. 513, Rear axle	0.16	0.16	0.08	--

It should be noted that the mean amplitudes of oscillations for two entirely different vehicles on the same approach are remarkably uniform.

In Fig. 31, the variation in the interaction force for a selected number of runs on Bridges 3B and 7A are replotted with the profile of the approaches to these bridges. It can be seen that the beginning of the high-frequency "tire-hop" oscillations, as well as certain aspects of the lower-frequency components, can generally be related to the profile of the approach pavement. Of particular interest is the sharp rise in the profile starting approximately five feet from the entrance to Bridge 3B (i.e. at $x/L = -0.1$). This rise appears to induce a large impact in the axle of the vehicle. The tire pressure records for all the test runs on this bridge show essentially the same phase angle when the axle enters the bridge, as discussed in Section 21. The sharp curvature of the bridge deck immediately after the entrance is noticeable in the figure. In contrast to Bridge 3B, the phase angle of the interaction force curve at the instant of entry is completely arbitrary for all the other bridges.

In an attempt to estimate the magnitude of the initial vehicle oscillations from the characteristics of the approaches, the major profile deviations for the approaches shown in Fig. 31 were approximated by half-sine waves with lengths, ℓ, of 60 and 30 feet, and amplitudes, y, of 0.6 and 0.5 inches, respectively, as shown by the dashed lines in the figure. Using the axle frequency and the static deflection of the vehicle given in Tables 14 and 15, and assuming that the springs do not engage, the following results are obtained:

Quantity	Approach to Bridge 3B		Approach to Bridge 7A	
	Run 11	Run 14	Run 12	Run 7
Speed, v, f_{ps}	64.6	49.4	66.2	50.8
Time of Transit, $t_d = \ell/v$	0.93	1.21	0.45	0.59
Ratio t_d/T_v	2.23	2.92	1.09	1.42
Dynamic amplification factor	0.30	0.30	1.10	0.50
Static change in force, $(y/y_{st}) \cdot P_{st}$	0.38	0.38	0.31	0.31
Computed dynamic amplitude, P_{st}	0.14	0.14	0.34	0.16
Measured dynamic amplitude, P_{st}	0.18	0.18	0.27	0.18

In the above table, the dynamic amplification factor refers to the ratio of the distortion in the spring of a simple linear oscillator, subject to a ground displacement in the form of a half-sine wave with the value of t_d/T_v shown, to the static displacement equal to the height of the distortion[9c]. The static change in the interaction force, in terms of the static load, is obtained as the ratio of the height of the obstruction to the static deflection of the axle. The product of the amplification factor and the static change in the force yields the computed dynamic amplitude. For Bridge 3B, the amplification factors used were those occurring during the excitation.

For comparison, the measured amplitudes are included in the table. It is apparent that this simple approximation of the roadway unevenness gives computed amplitudes of force variation which are in reasonable agreement with the measured values.

An attempt has been made to correlate the magnitude of the initial oscillations of the vehicle with the value of the Present Serviceability Index (PSI), described previously, for the corresponding approach pavements.

The table below shows the mean amplitudes of force variation on the approach pavements for the drive axle of Vehicle No. 91, together with the PSI values for the pavements, evaluated approximately at the time of the tests:

	Approach to Bridge			
	3B	7A	9B	6A
Force Variation	$0.14\ P_{st}$	$0.16\ P_{st}$	$0.08\ P_{st}$	$0.09\ P_{st}$
PSI	3.8	2.2	3.8	2.0

It can be seen that there is no correlation. This disagreement is undoubtedly due to the fact that the longitudinal slope variance, which is the major quantity entering in the determination of the PSI value, is based on slope measurements at 1-ft. intervals. At the vehicle speeds used (30 to 70 fps), these variations in slope correspond to very high-frequency components, which do not excite the vehicle appreciably. It is felt that a power-spectrum density analysis of the approach profile, which shows the contribution of all frequencies, may provide more meaningful correlation with the magnitude of vehicle oscillation.

24.4 Theoretical Predictions. In order to provide a frame of reference for the presentation of the extensive data obtained in the regular tests, a brief review of the major effects expected on the basis of theoretical studies is given in this section.

It is known[16c] that for vehicles that may be considered "smoothly rolling", the speed parameter α is the most important single parameter affecting the bridge response. A plot of amplification factors versus α for fixed values of the other parameters gives an undulating curve for which the magnitudes of successive peaks generally increase with α. The weight and frequency ratios are relatively secondary parameters. The variation of these

ratios affects the detailed characteristics of the response, but has a relatively small effect on the maximum response. By varying the weight ratio and frequency ratio within reasonable limits, a family of spectrum curves is obtained. The envelope to these curves is essentially a straight line the ordinates of which increase with α. The effect of the deviation of the bridge profile from a straight line is generally to increase the amplification factor due to the increased variation in the interaction force.

Finally, the initial oscillations of the vehicle again increase the amplification factors. The amplification factors generally increase with increasing amplitudes of initial oscillation, all other factors being equal. In addition, initial vehicle oscillations change the frequency of the dynamic increments, so that the critical dynamic increments occur at different points. On the spectrum curves, this change corresponds to a shift of the abcissas of the peak amplification factors.

From the discussion of initial oscillations in the preceding section, it can be expected that the effects of the initial oscillations of the vehicle will be most pronounced on Bridge 7A. On Bridge 3B where the magnitude of the initial oscillations is of the same order as on Bridge 7A, the effects should be of the same order of magnitude, but because the somewhat more consistent phase angle of the interaction force at the entrance, a smaller scatter may be expected than on Bridge 7A. For Bridges 9B and 6A, the effect of the initial oscillations can be expected to be small. For the other bridges in the tests, for which no tire pressure data are available, it is difficult to estimate the relative significance of the effect of initial oscillations. However, on the basis of the correlation with the longitudinal profile, relatively small effects should be expected on Bridge 2B, the

approach of which is relatively smooth, (Fig. 13a), except for a discontinuity near the abutment, which is similar to, but somewhat flatter than, the one discussed in connection with Bridge 3B. On the other hand, the unevenness of the approach to Bridge 5A is even more pronounced than that of Bridge 7A, and resembles a versed sine curve approximately 80 feet long and 2 inches high. For the rear axle of Vehicle No. 415, and a speed of 60 fps, the computed amplitude of force variation, neglecting the effect of friction in the suspension, is 0.30 P_{st}. Thus, for this bridge, the effects of initial vehicle oscillations may be considerable. In this connection, it should be recalled that the unevenness of the approach profile generally increased with time. Thus, the effect of the initial oscillations on all bridges can be expected to be less in the earlier tests than in later tests. In particular, the effect of initial vehicle oscillations on Bridge 2B at the early dates can be expected to be negligible.

25. Reliability of Data

The purpose of this section is to discuss the reliability of the experimentally determined spectrum curves.

25.1 Experimental and Reduction Errors. The errors that have a bearing on the reliability of the results may be caused by the experimental setup, the recording equipment, and the method of reduction. These possible sources of error will be discussed in the following paragraphs.

Errors due to the experimental setup may be due primarily to errors in vehicle speed or lateral position. The speed of the vehicle was obtained by timing the passage over two hoses 50 to 100 feet apart, using the assumption that the speed was constant over this interval. In a few cases, where detailed checks were made, it was found that occasionally the vehicle tended

to slow down, the difference between the speeds at the entrance and the exit being of the order of five percent or less. Thus the recorded average speed may in some cases be less than the actual speed in the portion of the record that is of prime interest. As pointed out earlier, small lateral deviations from the center line have negligible effect on the response of the middle beam.

Errors in the recording instruments are primarily caused by drift and by calibration errors. Drifting of the recording equipment was observed in a few records, but was usually very small and was controlled by frequent adjustments. No attempt was made to correct for drifting in the individual records; thus the values of the recorded response may in some cases be slightly lower than the true values. Discrepancies of the order of five percent were observed both in the gain (amplification) and the time scale of the recording instruments. Errors due to these differences were minimized by always using the crawl responses and bridge periods from the same subseries as the dynamic tests.

Finally, the reduction errors are related to the accuracy with which the recorded responses could be measured. It is estimated that this accuracy was held to within five percent both as to the vehicle speed and the magnitude of the maximum response.

25.2 Replication of Experimental Results. The reliability of the experimental data will be further investigated by examining the replication of the test results. The two comparisons that are of prime interest are the replication of individual results within one subseries, and the replication of the trends in behavior between subseries involving the same bridge and vehicle.

Figure 32 shows the spectrum curves for total response (deflection and strain) at midspan of the center beam for subseries 5452-26, involving Bridge 3B (composite steel) and Vehicle No. 415. It can be seen that the test data are scattered in bands the width of which is approximately 20 percent of the maximum static response for deflection, and about 10 percent for strain. The scatter is reduced by averaging the three beam responses, as shown in Fig. 33, but it is still appreciable for deflection. Thus the center beam response is only slightly affected by discrepancies in the lateral position of the vehicle.

In order to examine further the possible causes of the experimental scatter, dynamic increment curves for several test runs from the subseries considered, for two values of the speed parameter α, are shown in Fig. 34. For the higher value of α, it can be seen that the bridge behavior is for all practical purposes identical for the two replicate runs, but that there is a consistent difference in the magnitudes of the two responses. For the slower speed, the agreement for the three curves is reasonably good up to the value of $x/L = 0.3$, after which one of the records shows a superimposed high-frequency wave. In all of these records, the major differences begin shortly after the drive axle enters the span. There are no tire pressure measurements available to study quantitatively the variation in interaction forces; however, it appears that the observed discrepancies are due mainly to different initial conditions of the vehicle. This assumption is further substantiated by the fact that in the earlier subseries, when the approach pavements were considerably smoother, much better replication was obtained (see Fig. 16, Ref. 11).

The relatively larger scatter in the spectrum curve for deflection as compared to that for strain may be tentatively explained by two factors.

First, the difference may be due to the difference in the shapes of the crawl curves. For the three-axle vehicle, in the region near the maximum static response (i.e. $0.1 < x/L < 0.5$), the crawl response for deflection is a smooth curve the ordinates of which vary from 0.90 to 1.00 times the maximum response, while the strain response is essentially a straight line between 1.00 at $x/L = 0.1$ and 0.96 at $x/L = 0.5$ (see Fig. 5). Thus a change in the position of the critical dynamic increment corresponds to a larger change in the maximum effect for deflection than for strain. Exactly the reverse relationship is true for the two-axle vehicles, because of the sharply "peaked" crawl curve for strain for the latter vehicles (see Fig. 8). Secondly, it should be noted from Table 7, that for regular runs on the bridge considered (3B), the scatter in the maximum crawl values for deflection was generally somewhat higher than for strain. For the particular subseries considered (5452-26), the maximum deviation in the center beam crawl values from the averages used in computing the amplification factors were 5.2 and 0.6 percent, respectively, for deflection and strain.

The response spectrum curves for two other subseries (Nos. 5452-27 and 28) involving Bridge 3B and Vehicle No. 415 are shown in Fig. 35. The two subseries were performed 3 and 4 days, respectively, after subseries 5452-25 shown in Fig. 32. It can be seen that the shapes of the spectrum curves agree very well. It is noted that the scatter on the spectrum curve for deflection is not as large as in the previously presented figure, even though the number of test runs is greater.

The measured bridge periods for the three subseries considered in Figs. 32 and 35 differed by approximately four percent. These discrepancies

may be due either to differences in the frequency of the power supply or to unavoidable scaling errors in the reduction of the records. Discrepancies of similar magnitude also occurred in the ordinates of the crawl curve (see Table 7). In general, it may be stated that the overall pattern of the spectrum curves is adequately replicated.

It is concluded that a single point on the spectrum curve has little meaning, because of unavoidable errors in recording and reduction, and because of the experimental scatter introduced by uncontrollable test conditions. However, the aggregate of the points describes adequately the general trends in the maximum dynamic response.

26. General Summary of Experimental Results

In this section a summary is given of all the experimental results in the form of spectrum curves for total response, and certain general trends are discussed. In this and succeeding sections, only the midspan response (deflection and strain) of the center beam will be considered.

26.1 Presentation of Data and Major Trends. Space does not permit the presentation of separate spectrum curves for all 32 subseries of the regular tests. Figures 36a through 36e show the combined spectrum curves for Bridges 2B, 3B, 9B, 5A and 7A, respectively, for all subseries involving regular tests with three-axle vehicles. The results shown for Bridge 3B do not include the data from the three subseries presented in the previous section.

It can be seen that, with one exception, the spectrum curves for deflection show a general increase of effects with increasing α. This increase with α is apparent both for the points defining the bounds and for

the "averages" of all points, even though, as discussed in the preceding article, the other bridge-vehicle parameters (R and φ) vary by as much as a factor of two for any given bridge. The "peaks" of the individual spectrum curves are not readily distinguishable, because of the initial vehicle oscillations and the experimental scatter previously discussed.

The only exception to the above statement is provided by the results for Bridge 3B, which are shown in Fig. 36b. For the subseries shown in the figure, it can be seen that the experimental points generally follow a broad curve, with maximum values occurring roughly between $\alpha = 0.10$ to 0.14. However, it should be noted that the subseries shown cover a relatively small range of α, and that in Figs. 32 and 35 presented previously there ia a general increase in the amplification factors with increasing values of α. For the range of α covered by the spectrum curves shown in Fig. 36b, the amplification factors are in excellent agreement with those shown in Figs. 32 and 35.

The spectrum curves for strain follow the same general pattern as those for deflection, but the amplification factors are smaller, as is expected from theoretical considerations. The very large scatter in the strains of Bridge 5A (Fig. 36d) is noteworthy. Variations of this order have been observed in the repeated load studies on this bridge, and appear to be due to bond failures in the vicinity of the strain gage locations.

The largest amplification factors observed were those on Bridge 7A, corresponding to the largest values of α. However, a consistent pattern of differences between the spectrum curves for the various bridges is apparent. Thus, for the values of α that are common to Bridges 5A and 7A, the lowest recorded amplification factors for Bridge 5A are consistently higher than the highest values obtained on Bridge 7A. The amplification factors for

Bridges 2B and 9B generally fall between the above two extremes. It is therefore apparent that while α is a controlling parameter, the cumulative effect of the other parameters precludes a direct comparison of results for different bridges. The effects of these parameters are discussed in Section 27.

Figures 37a through 37c show the spectrum curves for regular tests with two-axle vehicles on the composite steel, noncomposite steel, and concrete bridges, respectively. The amplification factors for deflection generally increase with α, with two exceptions: in Subseries 5450-1 on Bridge 2B (Fig. 37a) the measured effects are consistently low, and in Subseries 5453-3 on Bridge 7A, (Fig. 37c), the amplification factors actually decrease with α. These discrepancies from the general pattern are investigated in Chapter VIII in connection with the theoretical comparisons.

The amplification factors for strain are generally small, and, except for the tests on Bridges 3B and 9B, show only a slight increase with α. This fact is to be expected, since the critical dynamic increments must occur very close to midspan and combine with the sharp "peak" of the crawl curve to produce any sizeable total dynamic effects.

26.2 Summary of Data. The distributions of the amplification factors for deflection and strain for all 533 regular test runs involved in the 27 subseries with three-axle vehicle are shown in Fig. 38. The cumulative percentages are shown in Fig. 39.

Concerning deflections, it can be seen that for only five percent of the test runs were the amplification factors higher than 1.40, and that for 88 percent of the runs the amplification factors were between 1.10 and 1.40. The maximum single amplification factor was 1.63. On the other hand,

the maximum amplification factor for strain was 1.41, with only two percent of the runs exceeding 1.30, and 90 percent of the runs giving amplification factors between 1.05 and 1.30. The relationship between amplification factors for deflection and strain demonstrates two facts known from theoretical considerations:

(a) that dynamic increments, and therefore amplification factors, are higher for deflection than for strain, and

(b) that for three-axle vehicles the spread of the amplification factors is larger for deflection than for strain. This latter observation is again related to the difference in the crawl curves for the two responses. If the critical dynamic increment occurs in the region $0.1 < x/L < 0.5$, it will result in essentially the same amplification factors for deflection and strain, as discussed previously. However, outside of this region the crawl curve for strain drops off more rapidly than that for deflection. Thus, critical dynamic increments located outside of the above range correspond to low amplification factors for strain.

In connection with Fig. 39 it is worthwhile to compare the distribution of amplification factors for strain with the formula for impact given by the AASHO Standard Specifications[20]

$$I = \frac{50}{L + 125}$$

where I denotes the impact factor.

For the test bridges, this formula yields an impact factor of 28.5 percent, or an amplification factor of 1.285. Of the 533 tests reported, only 24 tests, or 4.4 percent of the total, gave amplification factors for strain which exceeded this value.

Because of the large experimental scatter, and the effects of the bridge-vehicle parameters to be discussed, it is not possible to draw a reasonable curve of maximum amplification factors as a function of the speed parameter α. As an indication of the magnitude of effects and their variation with α, Fig. 40 shows all amplification factors for deflection exceeding 1.30, and all amplification factors for strain exceeding 1.20, as a function of α. It can be seen that the majority of experimental points in this category result from tests on the composite steel Bridges 2B and 3B, which comprised 64 percent of all regular tests. It is to be expected that if a similar number of tests were run on Bridge 7A, a proportionately larger number of points with high amplification factors would have been obtained. It is apparent that the maximum single effects do not increase noticeably with α, and that for values of α up to approximately 0.18, amplification factors of 1.4 and 1.3 for deflection and strain, respectively, can be considered reasonable absolute maximum values. It should be recalled that the figure includes all tests with three-axle vehicles, and thus reflects the effect of the additional parameters, to be discussed in the next section.

27. Detailed Study of Effects

In the preceding section, it has been shown that for a given bridge, there are large variations in the response caused by different vehicles, and that there are consistent differences between the spectrum curves for different bridges. In this section, the effects of the bridge-vehicles parameters will be examined in an attempt to explain the above differences.

It should be recalled that the spectrum curves are generally undulatory in nature, reflecting the effect of successive "critical" dynamic

increments as α increases. The detailed features of the spectrum curves, particularly the abscissas corresponding to the peak amplification factors, are affected by variations in the bridge-vehicle parameters and the unavoidable experimental scatter. However, the details of the spectrum curves are of little significance, and from a design standpoint only the peak amplification factors are of interest. Thus, in the comparisons to be presented, emphasis will be placed primarily on the level of the peak amplification factors.

27.1 Isolation of Effects of Bridge-Vehicle Parameters. The effect of the various bridge-parameters will be investigated by comparing spectrum curves for which all but one of the dimensionless parameters listed in Section 24.1 are nearly identical. As pointed out earlier, the data available for such comparisons are limited. Furthermore, the presence of initial vehicle oscillations introduces an unknown and uncontrollable parameter. The comparisons presented in this section are restricted to the composite steel bridges 2B and 3B and the noncomposite bridge 9B.

In Fig. 41, the effect of the speed parameter α is examined. Spectrum curves are presented for four subseries of tests, involving three bridges and three vehicles, with values of R, φ_t, and Δ kept nearly constant. It can be seen that the increase in the peak amplification factors with increasing α is more clearly pronounced than in the composite spectrum curves presented earlier. In connection with the spectrum curves for deflection, it should be noted that the peak values for the two curves involving Bridge 3B are essentially identical, while there is a spread of approximately 15 percent between the spectrum curves for Vehicle No. 415 on Bridges 3B and 9B. It should be recalled, however, that this spread is of the order of that

observed for a single subseries. The differences between the spectrum curves may be attributed to the effect of initial oscillations, since the approach pavement to Bridge 2B was relatively smooth at the time of the tests considered, while for Bridge 9B the observed initial oscillations were found to be smaller than for Bridge 3B. The smaller scatter in the amplification factors for strain is consistent with the results reported earlier.

In order to investigate the effect of the weight ratio R, spectrum curves for deflection involving two subseries of tests on Bridges 3B and 9B are shown in Fig. 42. For each bridge, results are shown for the two-axle Vehicle No. 91 and the three-axle Vehicle No. 415. The frequency ratio φ_t and the profile variation parameter Δ are approximately the same, but the weight ratio R differs by a factor of two. It can be seen that even this wide variation in R has little effect on the peak value of the amplification factors.

The large difference in the ordinates of the two spectrum curves for Bridge 3B near $\alpha = 0.10$ is noteworthy. History curves for dynamic increments corresponding to the above value of α are shown on the top of Fig. 43 for the two vehicles. It can be seen that the differences in amplification factors are not due solely to the differences in the shape of the crawl curves, but that the peak dynamic increment for the three-axle vehicle is greater. The characteristics of the curves suggest that the differences in the dynamic increments are due to different initial conditions in the vehicle. For the higher speeds the peak dynamic increments shown in the bottom of Fig. 43 are comparable in magnitude, and occur approximately at the same point, resulting in essentially identical total effects. This trend has been generally observed, so that, for deflections, the peak values of amplification factors (which usually occur at higher speeds) are comparable for two- and three-axle vehicles.

Returning to Fig. 42, it can be seen that on Bridge 9B, for which the approach conditions were smoother, the spectrum curves for the two subseries are in much better agreement.

The effect of the frequency ratio φ was difficult to isolate, because the range of variation of this parameter was small for the steel bridges. The only valid comparison that could be made (Subseries 5451-14 on Bridge 3B vs. Subseries 5454-4 on Bridge 9B) involved a change in φ of the order of 25 percent, and any possible effect of this parameter was completely obscured by the different initial conditions for the two bridges, and the unusually large scatter in the test data for Bridge 9B.

The effect of the profile parameter Δ is demonstrated by the spectrum curves for the two test subseries shown in Fig. 44, for which the variation of Δ was the largest, and the initial oscillations were expected or known to be small. On the spectrum curves for deflection, it can be seen that doubling Δ increases the amplification factors by approximately 15 percent. However, the spectrum curves for strain show a much less pronounced trend. This seems to indicate that the effect of Δ on the peak dynamic increments is not very pronounced, and that the increase of the amplification factors for deflection is primarily due to a shift in the position of the critical dynamic increments.

The effect of initial oscillations cannot be isolated since this parameter was not controlled. The overall effect of initial vehicle oscillation, as has already been discussed in connection with the spectrum curves presented, is to increase the peak ordinates of the spectrum curves. In this connection, it is of interest to compare the responses of the bridge pairs which are identical in construction, and where the vehicle enters the second

bridge after oscillations have been induced by its passage over the first bridge in the line of travel. Two such comparisons are presented in Fig. 45.

In the top plot of Fig. 45 the responses of Bridges 9B (first in line of travel) and 9A (second) are compared for one subseries of tests. All bridge-vehicle parameters are the same, since the weights, frequencies, and permanent deflections of the two bridges are essentially the same. It can be seen that the responses of the two bridges are indistinguishable for all practical purposes. In examining the amplitudes of the interaction forces it was found that the oscillations on the approach pavement and on Bridge 9A (the latter acting as the initial oscillations for Bridge 9B) are essentially of the same magnitude, averaging 7 to 8 percent of the static load. For these small amplitudes, the phase of the initial motion of the vehicle is unimportant, suggesting that the effects may be comparable to a smoothly rolling load.

At the bottom of Fig. 45, a similar comparison is shown for Bridges 7A (first) and 7B (second). The major difference between the two spectrum curves is obvious. In this case, the amplitude of the initial oscillation of the vehicle prior to entrance on Bridge 7A was of the order of 18 percent of the static load. By the time of exit from the first bridge, the amplitude was generally reduced to approximately 10 percent of the static load. However, this reduction in the amplitude of initial oscillations above does not account for the observed differences, as it will be shown later that the irregularities of the bridge profile on Bridge 7A are responsible for the large effects at $\alpha = 0.20$. No detailed study was made of the records for Bridge 7B.

27.2 Comparisons of Dynamic Effects on Individual Bridges. The type of comparisons presented above cannot be extended to other subseries

because the ranges of most of the parameters for different bridges in general do not overlap. In order to extend the comparisons to all tests, the dimensionless parameters R, φ_t, and Δ must be allowed to vary simultaneously.

As a first comparison, the effect of three different three-axle vehicles on the same bridge are investigated. The available test data pertain to Bridges 3B and 7A, and three standard three-axle test vehicles (No.'s 315, 415, and 513).

The results for Bridge 3B are shown on the top of Fig. 46. It can be seen that the peak amplification factors for the three vehicles are essentially the same. It appears from this comparison that the effect of the larger profile parameter is counter-balanced by that of a smaller weight ratio. The important conclusion to be drawn is that for a fixed range of speeds, the maximum amplification factors produced by heavy vehicles carrying their rated loads are essentially the same.

On the bottom of Fig. 46, similar comparisons are made for Bridge 7A. It can be seen that the effects of the same vehicles are much larger than on Bridge 3B, the maximum amplification factor being 1.63 for Bridge 7A vs. a value of 1.43 for Bridge 3B. The three spectrum curves shown are similar in shape, but there is a difference of 20 percent of the static value between the peak amplification factors caused by Vehicles No. 315 and No. 415. As a further evidence of the similarity, history curves of dynamic increments for midspan deflection corresponding to $\alpha = 0.19$ for the three subseries discussed are shown in Fig. 47. It can be seen that the three curves are exactly in phase. The critical dynamic increments occur almost exactly at the value of x/L for which the crawl curve is a maximum, and are much larger than any of the other peak ordinates. The trend of the magnitudes of the three critical dynamic increments is the same as that of the corresponding spectrum curves.

There were no tire pressure measurements available for the above subseries. The spring deformation records, however, show that the drive axle springs engaged approximately 30 feet from the entrance, corresponding to the position of the rear axle of $x/L = 0.1$ in Fig. 47. This point corresponds to the end of the pronounced irregularity of the bridge surface discussed in connection with Figs. 13b and 14. Approximating the major irregularity of the bridge profile by a half-sine "wave" with $\ell = 18$ feet and $y = 0.2$ inches, and assuming that the vehicles vibrate on the combined tires and springs, the computed amplitudes of the interaction force variation range from $0.15\ P_{st}$ for Vehicle No. 315 to $0.10\ P_{st}$ for Vehicle No. 415. These values by themselves are too low to account for the high dynamic increments observed. However, it appears that the above variations in the interaction force, occurring exactly at the point of maximum static response, and combined with frequency ratios close to unity, can account for the large increase of the critical dynamic increments. Furthermore, the trend in the observed magnitudes of the dynamic increments and spectrum curve ordinates for the three vehicles is the same as that of the computed interaction force variations.

The second class of comparisons that can be made for all subseries is to keep the vehicle parameters constant and vary the bridge parameters, that is, examine the responses of different bridges under the passage of the same vehicle. Four vehicles (No's 315, 415, 513, and 91) were involved in identical tests subseries on three or more bridges. The results of the tests with the above vehicles are shown in Figs. 48a and 48b.

It should be noted in connection with the bridge-vehicle parameters shown on the above figures that, while for each comparison the range of the

weight and frequency ratios is roughly the same as that used in the previous comparisons, the variation in the profile parameter is much larger, and that the comparisons shown include the results for Bridge 7A, for which Δ was negative. It should also be remembered that the approach pavements of all the bridges were different, so that the effect of initial vehicle oscillations should be expected to be different for each bridge. Finally, while the top speeds of the vehicles in all tests were essentially the same, the maximum values of α are different, due to the large range in the bridge frequencies.

It can be seen from the figures that in general there is no agreement between the spectrum curves for the different bridges. In particular, the results for Bridge 7A stand out from the general pattern; this is due partly to the difference in the profile parameter Δ, and partly to the irregularity of the bridge deck discussed previously. With the exception of Bridge 7A, the general effect of the variation in the bridge parameters and the initial vehicle oscillations is to shift the position of the peak ordinates of the spectrum curves.

27.3 Effect of Number of Load Applications. One of the objectives of the test program was to determine the effect of time (i.e. number of load applications) on the response of the test bridges. Four of the test bridges (2B, 9B, 5A and 7A) were tested in identical subseries approximately eight months apart. The same vehicle (No. 415) was used in all tests. The cumulative number of load applications on the bridges at the time of each test subseries, rounded to the nearest hundred, were as follows:

Test Series	Cumulative Number of Load Applications			
	Bridge			
	2B	9B	5A	7A
5451	75,000	7,900	85,500	77,300
5452	230,900	150,200	239,700	242,000
5454	525,200	441,500	523,500	518,400

The primary changes that occurred in all bridges between the successive tests were:

(a) a progressive decrease in stiffness, as indicated by a reduction in the bridge frequency (Table 10);

(b) a consistent increase in the permanent sag, or, in the case of Bridge 7A, a decrease in camber (Fig. 15);

(c) an increase in the magnitude of the unevenness of the approach pavements, as evidenced both by the decrease of the Present Serviceability Index of the approach pavements and by observation of the profile deviation measurements (Figs. 12a through 12c).

The change in the bridge frequency results in a change of α for the same speed, and in change of the frequency ratio. The dimensionless parameters were computed on the basis of constant values of the vehicle parameters, since there were no data available to determine any changes in the properties of the test vehicle in the period corresponding to the tests described.

Spectrum curves for the center beam midspan deflection for the four bridges considered in this study are shown in Figs. 49a and 49b. For Bridge 2B, there is no noticeable change in the response with time. This is to be expected, since both the frequency and the permanent deflection of the bridge changed very little, and the approach pavement remained relatively smooth.

For Bridge 9B, the change in the bridge-vehicle parameters with time was of the same order as for Bridge 2B, and therefore no significant changes in the response would be expected. As can be seen from Fig. 49a, there was in fact essentially no change in the response between the first and second series of tests. The majority of the results of the third series are higher than those for the previous two sets, and form a well-defined curve. However, it should be noted that there are points on the latter spectrum curve which are actually below those for the first two curves, and that the scatter of points is larger than that observed in any of the subseries presented thus far. To understand the bridge behavior in the latter subseries, and in particular to explain the reason for the large scatter, it would be necessary to examine in detail the history curves of bridge response. Within the available time, this study could not be made, and the differences in response are tentatively attributed to the reduction of friction between the beams and the slab of the bridge. In this connection, it should be noted that the repeated application of loads caused a longitudinal displacement of the slabs of Bridges 9A and 9B, until the slabs became tightly wedged against the abutment. At several dates, the slabs were jacked back to their original position. This movement of the slabs could have materially affected the initial oscillations induced in the vehicles, as well as the frequency and damping characteristics of the bridges.

For Bridge 5A, the changes in the frequency ratio and the profile parameter are given in Fig. 49b. The irregularities of the approach pavement became progressively worse with time, as shown in Fig. 12b. It can be seen from Fig. 49b that the peak amplification factors increased from 1.3 to 1.4 between the second and third set of tests. It is not possible to attribute this increase to any one of the parameters, since, as will be

shown in the next chapter, the details of the response are influenced by the degree of cracking in the prestressed concrete beams. It should be noted, however, that the above difference in amplification factors is of the order of the scatter within one subseries for the bridge considered.

Finally, on Bridge 7A, while the change in bridge frequency was negligible, the profile parameter decreased by a factor of two within the time considered. Furthermore, the profile of the approach pavement was changed radically between the times of the second and third sets of tests, when an asphaltic overlay was placed on the approach pavement (see Fig. 12c), thereby eliminating the largest irregularity. The major irregularity on the bridge deck also appears to have become less pronounced (see Fig. 13b). It can be seen in Fig. 49b that while the spectrum curves for the first two sets of series are similar in shape, there is a large difference in shape between the second and third curves, with a corresponding reduction of peak amplification factors from 1.4 to 1.2. This difference can be attributed to the combination of changes in the initial oscillations, the bridge camber, and the irregularities of the bridge profile, all of which influence the location of the "critical" dynamic increment.

The general comment to be made concerning the results presented in this and the previous section is that, due to the simultaneous variation of a number of bridge-vehicle parameters, analytical studies are necessary to account for the observed trends and to isolate the important parameters. Exploratory studies in this direction are presented in Chapter VIII.

27.4 Statistical Study of Effects. In addition to the 37 subseries of regular tests discussed previously, a limited number of test runs were conducted on five bridges with a total of seven vehicles of three

different types. These tests constituted Subseries 5452-5 through 15 and 5452-21 through 24, and have been summarized in Table 4. The purpose of these tests was to determine the order of magnitude of the dynamic effects in the bridges considered, and to insure that no condition producing severe effects was overlooked in the test program.

The bridges selected for this study included: Bridge 3B (composite steel) which had been studied in detail previously; Bridges 6A (prestressed concrete) and 8A (reinforced concrete) which had not been tested previously; and Bridges 6B and 8B, which were second in line of travel. The vehicles included: two three-axle vehicles from loop 4, two three-axle vehicles from loop 5, and three five-axle (tandem axle)vehicles from loop 3. The different vehicles from the same loop had essentially similar dimensions (Fig. 18) and weights (Table 12), but were of different manufacture.

Test runs were made at vehicle speeds from 25 to 45 mph in increments of 5 mph, so that only from four to eight runs per subseries were obtained. The conduct of the tests and the bridge instrumentation were the same as for the regular tests; however, the vehicles were not instrumented. All of the tests were performed within approximately two months.

The table below shows the maximum amplification factors for each bridge. The values shown are the peak values for all the vehicles considered and all the tests performed, including duplicate tests. Also included in the table are the maximum values of the speed parameter for all the bridges considered.

Quantity	Bridge				
	3B	6A	6B	8A	8B
a. Maximum Amplification Factors					
Deflection	1.39	1.44	1.36	1.42	1.28
Strain	1.28	1.27	1.28	1.38	1.23
b. Maximum Values of Speed Parameter					
α_{max}	0.16	0.12	0.12	0.25	0.25

Because of the large increments of speeds used, the above amplification factors may not represent the true maximum effects within the range of speeds considered. However, it is unlikely that any major effects have been overlooked in this comparison.

In comparing the above maximum values with the results of the regular tests, it can be seen that for Bridge 3B, the values are within the experimental scatter for the other tests (Fig. 32). The results for Bridge 6A are essentially in agreement with those for the other prestressed bridge tested (Bridge 5A, Fig. 36d). The results for Bridge 8A, however, are somewhat lower than the corresponding values for Bridge 7A (Fig. 36e), even though the maximum value of α obtained is actually larger than that for Bridge 7A. This difference is undoubtedly due to the absence of pronounced surface irregularities on the slab of Bridge 8A. The maximum amplification factors for the second bridges in the lines of travel (6B and 8B) are consistently lower than the corresponding values for the first bridges (6A and 8A).

The results of these tests were used by the AASHO Road Test Staff to make a statistical evaluation of the effects of the various factors influencing the bridge response. For each bridge-vehicle combination, amplification factors for deflection and strain at midspan of the three beams corresponding

to vehicle speeds of 30, 35, and 40 mph were computed. These values were then used to evaluate the degree of replication, the response of the individual beams in a bridge, and the effects of vehicle speed, vehicle characteristics, and bridge type. The results of this study were reported in Ref. (21), and the major conclusions are briefly reviewed in the following paragraphs:

(a) "The deflection amplification factors for the three beams of the same bridge generally did not differ significantly. On the other hand, the stress amplification factors for the center beams were generally lower than for the outside beams." This finding substantiates the data presented in Section 19.2 and is further discussed in the next chapter. However, the differences in amplification factors for strain are generally small.

(b) "The difference between the amplification factors for the same group of vehicles run at different times was generally significant.* As a rule, this finding was homogeneous over all bridges for both stress and deflection." These differences under seemingly identical conditions, as previously noted, arise from unavoidable errors in recording and reducing the experimental data, as well as from the differences in the initial conditions of the vehicle at the entrance. This finding substantiates the discussion of the reliability of experimental data presented in Section 25.

(c) "The differences between (amplification factors for) a three-axle vehicle at different times was as great as the differences between two three-axle vehicles of different types." This finding is in agreement with the conclusion of Section 27.2 that the response of the bridges is not sensitive to variations in the vehicle parameters within the range considered.

---

* In the Reference cited, "significant indicates that the hypothesis of no effect was rejected at the five percent level of risk; highly significant indicates that the hypothesis of no effect was rejected at the one percent level of risk."

(d) "The effect of speed was generally found to be significant for the three levels studied. The same general trend with regard to speed was noted for both stress and deflection." This finding substantiates the effect of the speed parameter α discussed in Section 27.1. It is noteworthy that the statistical significance of the effect of speed is directly related to the change in α corresponding to the change in vehicle speed.

VII. RESULTS OF SPECIAL TESTS

28. General

This chapter is devoted to the presentation and analysis of the special dynamic tests which include all tests other than those presented in the previous chapter. The objectives of these tests were:

(a) to place the regular tests in proper perspective by studying the effects of certain parameters over a wider range of values than was possible in the regular tests, and

(b) to obtain information on the effect of certain unusual conditions of bridge-vehicle behavior.

The special tests comprised two subseries with blocked vehicle springs, nine subseries with induced vehicle oscillations, and two subseries simulating continuous traffic. For these tests the vehicle was centered about the longitudinal center line of the bridge. In addition, five subseries were run with eccentrically placed vehicles, to study the lateral distribution of dynamic effects.

Finally, one subseries (5451-17) was intended to determine the effect of sudden braking while the vehicle was on the bridge. It was anticipated that the effect of braking would be to increase the force on the front axle and thereby produce increased dynamic effects on the bridge. However, these tests proved inconclusive because the braking force applied to the vehicle was too small to produce discernible effects. The results were reported in Ref. (13a) and are not discussed here.

29. Tests with Blocked Vehicle Springs

The objective of these tests was to study the effect of large variations in the interaction force resulting from the absence of damping in the vehicle springs. The tests involved two subseries, as follows:

Subseries No.	Bridge	Vehicle No.	Number of axles
5453-5	3B	91	2
5453-35	3B	513	3

For the two-axle vehicle, the springs on both axles were blocked, and instrumentation consisted of tire pressure gages on all four tires. For the three-axle vehicle, the springs were blocked on the drive and rear axles only, and tire pressure gages were installed on the left front, left drive, and both rear tires. The bridge instrumentation and the details of the tests were identical to those used in the regular tests.

29.1 Presentation and Analysis of Data. Figures 50a and 50b show typical vehicle and bridge response curves for the two subseries considered. The vehicle response is depicted in terms of the interaction force and the bridge response in terms of dynamic increments for deflection at midspan of the center beam.

As would be expected from the data obtained from the test runs on pavements, the behavior of the vehicle in these tests is characterized by large variations in the interaction force. With the suspension springs blocked, the only damping mechanism in the vehicle is that provided by the tires. Because of the severity of the variation of the interaction forces, the bridge responds predominantly at the frequency of these forces.

For the two-axle vehicle considered in Fig. 50a the bridge response reflects almost exclusively the frequency of the force variation for the rear axle. For the three-axle vehicle considered in Fig. 50b, for which the amplitude of variation of the interaction forces is smaller, the major component of the bridge response is still at the frequency of the interaction forces, but the bridge frequency is also noticeable throughout the record. It may be

noted that for the two-axle vehicle the frequency of the interaction force variation which should correspond closely to the natural frequency of the vehicle is about 3.0 cps or 80 percent of the computed value. The reason for this discrepancy has been discussed in Section 17.

29.2 Relationship to Regular Tests. In the two subseries considered the amplitudes of initial oscillation of the vehicle were found to vary over a wide range. The double-amplitude of force variation at the entrance for the drive axle of Vehicle No. 91 ranged from almost zero to 1.5 P_{st}, and for the drive and rear axles of Vehicle No. 513 from 0.2 to 1.0 P_{st}. The corresponding values for the same vehicles with normal suspension used in the regular tests varied from 0.2 to 0.4 P_{st} for Vehicle No. 91 and from 0.2 to 0.5 P_{st} for Vehicle No. 513. For the vehicles with blocked springs, the magnitude of the interaction force at the entrance was considerably more sensitive to variations in speed than for the same vehicles with normal suspension. This is due to the fact that for the vehicles with blocked springs, the ratio of the time of transit over the major irregularity of the approach pavement to the period of the vehicle ranges from 0.5 to 0.8, and the dynamic amplification corresponding to this range is very sensitive to small variations in the time transit.

In Figs. 51a and 51b two sets of typical history curves for interaction forces and dynamic increments for deflection are compared with the corresponding curves obtained from regular tests with comparable values of α. The significant increase in the amplitude of the force variation as compared to the regular tests and the corresponding increase in the amplitude of the dynamic increments are noteworthy. The detailed characteristics of the dynamic increment curves are changed, as previously noted.

For the runs presented in Fig. 51a, the peak dynamic increments for deflection are increased from 0.16 for the vehicle with normal suspension to 0.48 for the vehicle with springs blocked. The corresponding increase in amplification factors is from 1.12 to 1.45, showing that for both cases the peak dynamic increments occur in the region of the maximum crawl response. For the three-axle vehicle considered in Fig. 51b, the increase in the peak dynamic increment is only from 0.31 to 0.50, and again corresponds to essentially a linear increase in total amplification factors (1.27 to 1.49).

Figures 52a and 52b show comparisons of spectrum curves for the two subseries with blocked vehicle springs and the corresponding regular tests. It can be seen that the characteristics of the curves, particularly the values of α corresponding to the peak amplification factors, are considerably changed. This shift reflects the change in the position of the critical dynamic increments. There is a noticeable increase in the magnitude of the peak amplification factors; for the two-axle vehicle, the increase is approximately 20 percent of the maximum static value for both strain and deflection, while for the three-axle vehicle the increase amounts to approximately 15 percent for deflection and 25 percent for strain.

In summary, blocking the vehicle springs increased the variation in the interaction forces and the resulting dynamic effects on the bridge. The magnitude of the peak dynamic increments was approximately twice that produced by the same vehicles with normal suspension. For the tests considered, the maximum amplification factor for deflection was 1.54, as compared to a value of 1.37 for the corresponding vehicle with normal suspension.

30. Tests with Initial Vehicle Oscillations

The objective of this study was to determine the effect of controlled initial oscillations in the test vehicles with both normal suspension and blocked springs. Two groups of tests were performed: in two subseries (5451-7 and 8) an attempt was made to obtain maximum dynamic effects at midspan; in the remaining seven subseries, the vehicle oscillations were induced at the bridge entrance. The subseries involved in these tests were as follows:

Subseries	Bridge		Vehicle	
	Number	Type	No. of axles	Number
5451-7	3B	Comp. Steel	2	94
5451-8	5A	Prestr. Concrete	2	94
5453-10	3B	Comp. Steel	2	91
5453-6	3B	Comp. Steel	2	91 (springs blocked)
5453-11	7A	Reinf. Concrete	2	91
5453-13	9B	Noncomp. Steel	3	513
5453-36	9B	Noncomp. Steel	3	513 (springs blocked)
5453-14	7A	Reinf. Concrete	3	513
5453-37	7A	Reinf. Concrete	3	513 (springs blocked)

Initial oscillations in the vehicle were induced by allowing the vehicle to drop from a ramp. Original plans called for a long triangular ramp producing a smooth transition from the approach pavement and a sudden drop. Due to difficulties in fabricating such a ramp, the actual obstruction used consisted of two boards, as described in Section 7.3 and shown in Fig. 1a. Ref. (13b) describes the planning of the experiment and the ramp as well as the selection of ramp position and speeds to produce the desired effects in subseries 5451-7 and 8. In the remaining subseries, the end of the ramp was placed directly over the bridge abutment, (approximately 10 inches from the bridge bearing). Except for the presence of the ramp, the tests were executed in the same manner as the regular tests. The crawl runs were performed without the ramps.

30.1 Vehicle Response. The solid line curves of Fig. 53a through 53c show typical history curves of the interaction force variation in the vehicles. The location of the ramp is indicated in the figures. The first two plots are for the drive axle of Vehicle No. 91 for tests on Bridges 3B and 7A respectively, the third for the same vehicle with blocked springs, and the fourth for the rear axle of Vehicle No. 513.

Comparing the solid line curves, it can be seen that the largest variations in the interaction forces occur for the vehicle with blocked springs, as would be expected from the discussion of the previous section. The smallest variations exist for the three-axle vehicle, as was also found true in the pavement tests. This reduction in amplitude can be attributed to the large amount of coupling between the tractor and semitrailer.

Except for the presence of high-frequency oscillations at the beginning of the record, the response curves for Vehicle No. 91 on Bridge 3B and 7A are similar in shape, but it should be noted that the amplitudes on Bridge 7A are three times as large as on Bridge 3B. This difference is not due to differences in the bridge response, but reflects the different initial conditions in the vehicle prior to the entrance on the ramp. It can be seen from the figures that the ramp was not sufficiently long to block out the effects of the vehicle oscillation prior to entrance on the ramp. It should be recalled from Section 13.1 that while for Bridge 7A the major irregularity on the approach terminated approximately 20 feet from the bridge and was thus in front of the ramp, for Bridge 3B the most pronounced discontinuity was immediately prior to the entrance and was therefore covered by the ramp.

The fact that the vehicle response is essentially independent of the bridge response is further substantiated by comparing the results with those obtained from the drop tests on rigid pavements. This comparison is

hampered by two difficulties; first, as discussed in Section 17, the time scale for the records in the pavement tests was uncertain; and second, since the profile of the pavement in front of the ramp for the two sets of tests was not the same, the initial conditions of the axles at the entrance on the ramp were different. Thus, even if the effect of the bridge were disregarded, the two sets of tests are, strictly speaking not directly comparable.

The dashed curves in Figs. 53a and 53b show the interaction force history curves for drop tests on rigid pavement, with the time scales adjusted to correspond to those for the bridge tests. The excellent agreement between the solid and dashed curves for the test run on Bridge 7A is noteworthy. For the run on Bridge 3B, the agreement in phase is equally good, however, the difference in amplitudes after the drop is undoubtedly due to the different initial conditions of the vehicle prior to the entrance on the ramp.

For the vehicle with blocked springs, the record for the pavement run is not shown because of the large apparent discrepancy on the time scales, however, the amplitudes and damping in the interaction force curves are in excellent agreement with the values obtained in the dynamic test shown. For the three-axle vehicle, the magnitudes of the interaction force variation are comparable, but no agreement in the details can be expected, due to the small amplitude of the interaction force history curves.

The major conclusions to be drawn concerning the vehicle behavior in the tests with initial oscillations, based on the records for all the subseries considered, are: first, that the vehicle behavior on the bridge is essentially the same as on the rigid pavements; and, second, that the interaction force variation for the three-axle vehicle is small. The first

conclusion is in agreement with the theoretical studies reported in Ref. (22), where it has been shown that for low frequency ratios and large initial oscillations, the computed vehicle behavior on the bridge may be reliably predicted by an analysis assuming a rigid surface.

The effect of speed on the vehicle response was discussed in Chapter V in connection with Fig. 27. Increasing the vehicle speed consistently increases the magnitude of the interaction forces. The effect of speed, however, cannot be accounted for solely by the difference in horizontal scales due to the different speeds. For all vehicles with normal suspension, at faster speeds the vehicle springs are engaged throughout most of the duration of travel on the bridge, showing that the variation in interaction force exceeds the limiting frictional force. At slower speeds (30 mph or less), the spring motion is damped out in a short time. This observation again shows that the oscillation induced in the vehicle does not correspond simply to a sudden change in displacement corresponding to the drop from the ramp, but is also influenced by the vehicle motion preceding the drop.

Finally, it was shown in Ref. (13c) that moving the ramp with respect to the bridge results essentially in a shift of the history curve. This corresponds approximately to the shift in the point of release, indicating again that the vehicle behavior is to a great extent independent of the bridge behavior.

30.2 Bridge Response. The solid line curves in Fig. 54a show dynamic increment curves for deflection at midspan of the center beam for the two tests for which interaction force curves have been presented in Fig. 53a. For comparison, the dashed curves in the figures shows the corresponding response for regular tests with comparable values of α. It can be

seen that the induced vehicle oscillations produce increased dynamic increments, and that the predominant frequency of the dynamic increment curves, particularly at the early stages of record, is that of the interaction force. However, because of the large damping in the vehicle suspension system, only the first bottoming of the vehicle, which occurs early in the record, produces large variations in the interaction force and large dynamic increments. Thus, the critical dynamic increments are either associated with low crawl ordinates, or correspond to the second bottoming of the vehicle, which is associated with a change in the interaction force of the same order of magnitude as in the regular tests. Consequently the maximum effects at midspan are not significantly larger than those obtained in the regular tests.

In Fig. 54b, the history curve of dynamic increments for deflection corresponding to the interaction force curve of Fig. 53b is presented. In this case, with the vehicle springs blocked, the variation in the interaction force is large throughout the run, and the dynamic increments are in phase with the interaction force for the entire record. The extremely large ordinates of dynamic increments (from -1.36 to 1.10) are noteworthy; these values are more than twice as large as those for comparable runs with blocked vehicle springs, but without induced oscillations (see Fig. 50a). These values are, of course, much larger than those obtained for tests with normal vehicle suspension.

It has been shown in Ref. (13d) that moving the point of release of the vehicle results in a proportionate shift in the dynamic increment curve, without significant changes in the magnitude of the peak values. The effect of speed on the bridge response has been discussed in Section 21 in connection with Fig. 27b. Here again, as discussed in the previous section for the interaction forces, the effect of increased speed is to shift the

position of the peak dynamic increments corresponding to the successive bottomings of the vehicle, as well as to increase slightly their magnitude.

Spectrum curves for total effects at midspan of the center beams are shown in Figs. 55a through 55f for six subseries with induced vehicle oscillations. The amplification factors for Subseries 5451-7 and 5451-8 have been tabulated in Ref. (13e). For comparison, the corresponding curves for regular tests are shown in the figures.

In comparing the two sets of spectrum curves involving the same vehicle-bridge combinations, the curves corresponding to the tests with induced oscillations are distinguished by more sharply defined peaks and valleys, especially for the two-axle vehicles, and by considerably smaller experimental scatter. Both of these observations could be predicted on the basis of the vehicle behavior discussed previously. First, it has been shown that maximum dynamic increments correspond to successive "bottomings" of the vehicle. Thus, as the vehicle speed is increased, the critical dynamic increment combining with the maximum static effect changes from that associated with the second bottoming of the vehicle to that corresponding to the first bottoming. In between these two, a large negative dynamic increment occurs at midspan, and the total dynamic effect is reduced. Concerning the second observation, it has been shown in Section 25 that the major cause of the experimental scatter was the initial oscillation of the vehicle. The obstruction used to induce the initial oscillations tends to control the condition of the vehicles at the entrance, and thus reduce the influence of a major cause of scatter.

The table below shows the maximum amplification factors obtained in the tests with induced initial vehicle oscillations, and the corresponding values for the tests without induced oscillations.

Bridge	Vehicle	Maximum Amplification Factors			
		Tests with Induced Oscillations		Tests without Induced Oscillations	
		AF_D	AF_M	AF_D	AF_M
	a. Vehicles with Normal Suspension				
3B	91	1.23	1.11	1.34	1.22
	94	1.37	1.15	--	--
5A	94	1.63	1.53	--	--
7A	91	1.42	1.19	1.36	1.15
	513	1.51	1.50	1.35	1.35
9B	513	1.35	1.14	1.29	1.23
	b. Vehicles with Blocked Springs				
3B	91	2.10	1.89	1.44	1.38
7A	513	2.24	2.27	--	--
9B	513	1.57	1.43	--	--

It can be seen that for vehicles with normal suspension, the maximum effects occur on Bridge 7A. This fact is attributed to the combined effect of the initial oscillations and the unevenness of the bridge profile. With the above exception, the maximum amplification factors in the tests with normal suspension and a one-inch drop are of the same order of magnitude as those obtained in the regular tests. The tests with initial oscillations and blocked vehicle springs yield amplification factors in excess of 2.0.

30.3 Longitudinal Distribution of Effects in Regular Tests and Tests with Initial Vehicle Oscillations. In the preceding sections only the effects at midspan of the center beam were investigated. It has been shown in Chapter V, in connection with both regular tests and tests with initial vehicle oscillations, that while the history curves for total response at the third points are different from those at midspan, the general trends of the dynamic increments curves for the three locations are on the average

the same. The curves presented in Chapter V were given in terms of local amplification factors, that is, in terms of the maximum crawl response for each gage. From a design standpoint, the quantities of interest are the amplification factors in terms of the design, or maximum static, moment. These quantities will be designated as absolute amplification factors, and are obtained as the ratio of the dynamic gage response to the maximum crawl response at midspan. It has been shown in Section 11 that, for Bridge 3B, the maximum crawl responses for the various gage lines are in substantial agreement with the computed curve of maximum moments.

Figure 56 shows absolute amplification factors for speeds of approximately 44 mph, for three positions of the obstruction, obtained in Subseries 5451-7, involving Bridge 3B and Vehicle No. 94. It can be seen that high absolute amplification factors were obtained at considerable distances from midspan, the largest values usually being observed at 5/12 of the span from the support (gage 4L). Total moments in excess of that recorded at midspan occurred throughout the middle third of the span.

The comparison of absolute amplification factors is extended to spectrum curves in Fig. 57. Unfortunately, due to changes in bridge instrumentation, only on Bridge 9B were the same gages instrumented for both regular tests and tests with initial oscillations. The gages at the third-points (gage lines 3 and 7) were close to the cover plate cutoff points and showed considerable deviations from the computed curve of maximum moments, therefore the dynamic effects measured at these gages are not presented. Thus the comparison is inconclusive in itself, but is presented to illustrate the effect of speed on the absolute amplification factors. For the regular tests (top plot of Fig. 57), it can be seen that for low speeds, the gage 50 inches past midspan shows the largest effects, since the critical dynamic

increment corresponds to two bridge oscillations after the entrance of the rear axle, and occurs past midspan. As the speed increases, the critical dynamic increment eventually corresponds to the first cycle of oscillation and consequently larger effects are measured ahead of midspan. In the tests with initial oscillations (bottom plot), the critical dynamic increment is always associated with the first bottoming of the vehicle, and consequently the gage nearest the entrance consistently shows higher effects.

Thus it is apparent that in both types of tests, the absolute amplification factors in the entire middle third of the beams may be of the same order of magnitude.

31. Tests with Initial Bridge Oscillations

The objective of these tests was to obtain information on the bridge behavior under conditions simulating continuous traffic. The tests consisted of two subseries, as follows:

Subseries	Bridge	Vehicles
5452-19	3B	417 followed by 415
5452-20	7A	417 followed by 415

The tests were conducted by having two trucks follow one another over the bridge within a short time so that the bridge was still in motion when the second truck entered. A continuous record of the bridge response was obtained from the time the first vehicle entered the bridge till after the second vehicle left the span. In the initial planning, an attempt was made to choose combinations of speed and spacing between vehicles which were estimated to produce maximum effects. In the actual tests, however, due to

the dangerous driving conditions caused by the proximity of the turnarounds, the vehicle speeds were kept low, and, furthermore, the distance between vehicles could not be controlled. Vehicle speeds varied from 19 to 31 mph, and the distance from the rear axle of the first vehicle to the front axle of the second varied from 51 to 143 feet.

The two vehicles involved had the same weights and dimensions. Although no detailed measurements were available for Vehicle No. 417, the two vehicles can be considered essentially the same.

The following discussion is based on the results for Bridge 3B only, since the comparison for Bridge 7A is made difficult by the presence of profile irregularities discussed previously.

On the top of Fig. 58 are shown two typical curves of dynamic increments for deflection at midspan of the center beam. The curves show only the portion of the record that is of interest in this study, namely from the time the rear axle of the first vehicle leaves the bridge until the second vehicle is part of the way across the bridge. The curves of dynamic increments corresponding to the passage of the first vehicle are similar to those presented previously. It can be seen that even small changes in the speed of the first vehicle produce large variations in the amplitude of the residual free-vibrations. For the records examined, the amplitudes of the free-vibration portions ranged from practically zero to approximately 20 percent of the maximum static response, and a small amount of damping was observable. For comparison, the bottom plot of Fig. 58 shows the corresponding portion of a history curve of dynamic increments for a regular test using the same vehicle. It can be seen that after the entrance of the rear axle, the bridge behavior is the same in the two types of tests.

In general, the amplitude of free-vibration, the number of cycles of free-vibration between the exit of the first vehicle and the entrance of the second, and the phase angle of the bridge motion the instant the second vehicle entered, all influenced the response of the bridge under the second vehicle, but only up to the time the rear axle of the second vehicle entered the bridge. After this time, the bridge behavior for all records examined was essentially the same. Since the critical dynamic increment, and the maximum total effect, occurred after the entrance of the rear axle, the initial bridge oscillations were found to have no effect on the maximum response.

The table below shows the range of amplification factors for deflection due to the passage of the second vehicle. For comparison, the corresponding range of values for the same vehicle in a regular test subseries (No. 5452-26) is also included.

Speed, mph	α	Range of Amplification Factors	
		Tests with Initial Bridge Oscillations	Regular Tests
20	0.064	1.05-1.06	1.04-1.16
26	0.085	1.09-1.14	1.09-1.28
30	0.096	1.17-1.18	1.14-1.32

It can be seen that the amplification factors for the tests with initial bridge oscillations fall within the range of experimental scatter for the regular tests. In comparing the bridge response due to the first and second vehicles, it was found that the amplification factors due to the first vehicle were generally somewhat higher than those due to the second vehicle, the difference in magnitudes being of the order of 10 percent of the maximum static value. This difference is of the same order as that observed for the same two vehicles in the tests described in Section 27.4. Furthermore, the amplification

for the first vehicle showed a larger scatter than those for the second vehicle.

32. Tests with Eccentric Loading

The objective of these tests was to study the dynamic effects caused by eccentrically applied loads, and to obtain additional data for the study of the lateral distribution of dynamic effects. The eccentric loading was applied to the bridges by having the test vehicle follow a different path from that used in the regular tests. Two lateral positions were considered: the test bridge was either loaded with one line of wheels along the interior beam producing an eccentricity of 60 inches, the other line of wheels traveling on the bridge adjacent to the one being tested; or the test bridge was loaded with two lines of wheels, one along the interior beam and the other between the center and exterior beam, producing an eccentricity of approximately 24 inches. The eccentric tests consisted of six subseries, as follows:

Subseries Number	Bridge	Vehicle	Number of wheel lines on bridge
5450-8	4B	C	1
5451-9	3B	94	1 and 2
5451-10	5A	94	1 and 2
5452-17	3B	415	2
5452-18	7A	415	2
5453-12	3B	91	2

In Subseries 5451-9 and 5451-10, tests with both one and two wheel lines on the bridge were performed. Except for the vehicle position, the conduct of the tests was identical to that presented earlier. The crawl curves for these tests were obtained for the same lateral position of the vehicle as for the dynamic tests.

32.1 Presentation and Analysis of Data. The top plot of Fig. 59a shows typical history curves of vehicle response for an eccentric test with two lines of wheels, expressed as variations of the interaction force in the two drive axle wheels. On the top of Fig. 59b are shown the dynamic increment curves for midspan deflection for the three beams of the bridge corresponding to the same run. In this and succeeding figures, the dynamic increment curve for each beam is expressed in terms of the maximum crawl value for the beam considered. On the top of Fig. 59c, similar curves are shown for an eccentric test using a three-axle vehicle. For comparison, the results of corresponding tests with concentric loading are shown on the bottom of Figs. 59a through 59c.

It can be seen that, in the form in which the results are expressed, the dynamic response of the three beams in the eccentric tests is essentially the same as in the concentric tests. In particular, it should be noted that the eccentric loading used is the one which produces the maximum effect in the interior edge beam, and that the dynamic increments for that beam are essentially the same as those for the center beam in the tests with concentric loading.

In Fig. 60, the results for a test run with one line of wheels on the bridge are shown. While the "critical" dynamic increments (at $x/L = 0.4$), expressed in terms of the respective maximum crawl values of the three beams, are essentially the same, there is a major difference in the response of the bridge as compared to the test presented previously. The position of the three curves indicate in this case a pronounced contribution of the torsional mode of vibration of the bridge. The very large dynamic increments in the outside edge beam are of no practical significance, since the maximum crawl values for deflection and strain of that beam equal only 54 and 58 percent, respectively, of the corresponding values for the beam directly under the load.

The results for the remaining tests with one line of wheels on the bridge have not been studied in detail.

From a design standpoint, only the maximum effect in the loaded beam for the tests with a 24 inch eccentricity is of interest. Spectrum curves for total response at midspan of the loaded beam are shown in Figs. 61a through 61c for Subseries 5453-12, 5452-17 and 5452-18, respectively. For comparison, the corresponding curves for the center beam in the concentric tests are also shown in the figures. The peak amplification factors for the two sets of tests are summarized below.

Bridge	Vehicle	Maximum Amplification Factors			
		Interior Beam, Eccentric Tests		Center Beam, Concentric Tests	
		AF_D	AF_M	AF_D	AF_M
3B	91	1.24	1.22	1.34	1.22
3B	415	1.34	1.23	1.39	1.28
7A	415	1.36	1.22	1.44	1.29

It can be seen from the figures and the above table that the two sets of values are essentially in agreement throughout the range of speeds considered, and that the maximum effects in the interior edge beam due to the eccentric loading are consistently from 5 to 10 percent lower than the corresponding values for the center beam due to a concentric loading. Even though this difference is less than the observed experimental scatter for the concentric test; it can be accounted for by the lateral distribution of dynamic effects, discussed in the following section.

32.2 Lateral Distribution of Effects in Regular and Eccentric Tests. Throughout this report, the observed response of one wheel was taken as representative of the behavior of both wheels on an axle. In this connection, it

should be recalled that the lateral profile of several of the bridges was not level, but showed a conssitent transverse slope, as discussed in Section 13.3. For the three bridges 3B, 7A, and 6A, the differences in elevation at midspan between the two wheel paths were approximately 0.2, 0.4, and 0.3 inches respectively. Recalling that the static deflection of the rear axle tires of Vehicle No. 91 is 0.7 inches, the above differences correspond to static changes in interaction force of the order of 0.3 to 0.6 P_{st}. Thus, as the vehicle crossed the bridge, one would expect that the above difference in elevation would either excite a rolling motion of the vehicle about its longitudinal axis, or, if the period corresponding to this motion was very low, it would result in a lateral redistribution of the wheel loads, with the wheel on the higher elevation producing the larger interaction force.

As discussed in Chapter V in connection with Fig. 25a, and as can be seen from the interaction force curves presented throughout this report, the drift in the tire pressure recording equipment, and the absence of a base line on the interaction force curves made it impossible to obtain reliable data on the lateral distribution of the applied loads.

With regard to the lateral distribution of the dynamic effects on the bridge, in Reference (3) it has been suggested that for multigirder bridges with a high stiffness in the transverse direction, the lateral distribution of dynamic increments may be thought of as consisting of two components: a uniform component corresponding to the inertia of the bridge itself, and a component proportional to the lateral distribution of the static effects produced by the vehicle.

For the concentric tests on the bridges considered, the above two extremes cannot be distinguished on the experimental records, since, as

discussed in Section 11, the lateral distribution of the static effects was itself practically uniform.

In short, all of the available data on concentric tests indicate that the bridges behaved as beams, and the observed differences in the lateral distribution of dynamic effects could not be separated from the experimental uncertainties involved.

Within the available time, no detailed study was made of the lateral distribution of dynamic effects for the eccentric tests. As an illustration of the order of magnitude involved, spectrum curves for strain at midspan of the three beams for Subseries 5453-12 and 5452-17 are presented in Fig. 62. It can be seen that in the latter subseries the amplification factors for the exterior edge beams, which is farthest from the point of application of the loads, expressed in terms of the maximum crawl value for that beam, are consistently higher than those for the two beams immediately under the load. This suggests the presence of a component of the dynamic response which is uniform for the three beams. For the subseries involving a two-axle vehicle, this trend becomes apparent only at the highest values of α. A more detailed understanding of the lateral distribution of effects could be obtained with the method of analysis recently published in Ref. (17).

VIII. COMPARISON BETWEEN EXPERIMENTAL AND ANALYTICAL RESULTS

33.1 General

In the previous chapters, the experimental results were analyzed and interpreted in terms of the available theoretical background on the subject. While in general many of the observed effects could be related to the theoretical knowledge, the validity of the theoretical analysis applied to the test data has not been as yet demonstrated. In this chapter, a detailed comparison is made between experimental results and the corresponding theoretical predictions.

The principal objectives of the work reported in this chapter are:

(a) to investigate the adequacy of the available method of analysis, and

(b) to account for any differences that may exist between the observed behavior and that predicted by the analysis.

The success in meeting the above objectives depends on two factors. One factor is the reliability of the experimental results forming the basis of the comparison, and the second is the ability to incorporate the conditions of the test in the analysis.

The uncertainties involved in the experimentally determined bridge-vehicle parameters have been discussed in the previous chapters, and are briefly summarized here. The speed of the vehicle was generally not exactly uniform throughout its passage over the bridge. It was found that the bridge properties, specifically the frequency and damping characteristics, determined from the free-vibration records are not necessarily representative of the true properties for the loaded bridges. For certain bridges, these properties can vary with the position of the load. The surface conditions of the bridges, while known, could not be faithfully reproduced in the analysis. Similarly,

uncertainties exist regarding the behavior of the vehicle suspension system. It was found that under both static and dynamic conditions the significant parameters defining the vehicle behavior could be measured only approximately, and that the replication of tests was far from perfect. Furthermore, the dynamically determined properties varied considerably from those computed on the basis of static measurements. Specifically, the observed frequencies and coefficients of interleaf friction were generally lower than the computed values.

One of the greatest uncertainties in the experimental results was the initial condition of the vehicle at the instant it entered the bridge. In order to define properly the initial conditions, not only the vertical deflection and velocity of each axle of the vehicle is required, but also the value of the interaction force in the suspension system at the instant of entry. In the majority of the dynamic tests, no measure of the initial conditions was available. In the relatively few tests where tire pressure measurements were available, the data obtained yielded only a rough order of magnitude of these conditions, due to the difficulty in locating the exact position of the vehicle from the records, and the approximation involved in eliminating the components of the response caused by the "tire-hop" motion of the axles.

In addition to the parameters defining the problem, the experimental curves used as the basis of comparison were subject to error. History curves for total effects in duplicate tests were generally not the same, reflecting, in addition to the experimental uncertainties, the unavoidable errors in reduction, as discussed in Section 11.2. History curves for dynamic increments showed even larger errors, since the dynamic increments were obtained as differences of two nearly identical experimental records. The relative errors were largest at the ends of the records, where both the dynamic and crawl ordinates

were low. Similarly, the experimental spectrum curves were affected by the scatter in the observed maximum crawl ordinates. Finally, the midspan response of the center beam, used in all comparisons, is not an absolute measure of the behavior of the entire bridge. In general, there were differences in the responses of the three beams.

Concerning the validity of the theory used in predicting the response, a distinction has to be made between the general method of analysis, and its specific application embodied in the available computer programs. The latter is by necessity more limited than the former. Thus, differences between measured and computed responses may be due simply to limitations of the computer program used, and do not necessarily reflect shortcomings in the theory.

In view of the above discussion, the degree of agreement that can be achieved between the measured and computed values must be examined. Ideally, the comparison between experimental and analytical results cannot be considered complete until all of the above uncertainties have been accounted for, or until the computer programs have been modified to include the effects of all parameters deemed necessary. In the solutions presented, such a complete comparison was not attempted. In a few cases, studies were made to ascertain the sensitivity of the computed results to the major uncertainties. However, in the majority of the cases, only a limited number of comparisons were made, and the differences between the predicted and observed behavior were evaluated in terms of the experimental uncertainties or the limitations of the computer programs.

The analytical investigation reported herein is far from being a complete study of the available data. An attempt has been made to achieve the objectives outlined above within the time limitations of the project, on the basis of a representative number of solutions. The comparisons presented

pertain to 10 subseries, involving four bridges and five test vehicles. The subseries selected were primarily those for which tire pressure measurements were available. The bridges considered were principally those for which the properties were subject to the least amount of uncertainties, namely the composite steel bridges. Additional studies, essentially exploratory in nature, were made for the bridges which exhibited the largest dynamic effects.

Comparisons were made both on the level of history curves and spectrum curves. The history curves afford a better basis for comparison, since discrepancies can be readily detected and the effect of uncertainties studied. On the basis of a limited number of history curve comparisons, the results were generalized to spectrum curves of maximum response.

34. Method of Analysis

34.1 Description of Method. The analytical solutions presented in this chapter were obtained by application of the method reported in Reference (13d). In this method of analysis, the bridge is represented by a massless beam of uniform rigidity and a series of concentrated point masses equally spaced along the span. The number of degrees of freedom of the beam is thus equal to the number of masses involved. The method is applicable both to simple-span and continuous beams, and can include the effect of bridge damping. The solutions given were obtained by considering a simply supported beam and five masses.

Each axle of the vehicle is represented by two springs in series. The bottom spring represents the tires, and the top spring represents the vehicle suspension spring. A damper representing the frictional resistance in the suspension system is considered to exist in parallel with the suspension spring. The limiting frictional force in the damper is assumed to be a constant.

As long as the change in the interacting force for an axle is less than the limiting frictional force, the suspension springs remain locked and the axle vibrates on its tires. When the limiting frictional force is overcome, the springs engage and the axle vibrates on the combined tire-spring suspension system. A three-axle vehicle is represented by two rigid masses, corresponding to the tractor and semi-trailer, interconnected at the "fifth wheel", and supported by the three axles. The unsprung masses corresponding to the weight of the axles and frame supported only by the tires are considered to be lumped with the sprung masses. Thus the number of degrees of freedom for the vehicle is equal to the number of axles. Both two and three axle vehicles can be considered.*

The solutions were obtained by means of a computer program for the ILLIAC, the high-speed computer at the University of Illinois. This program is a slight modification of the one described in Ref. (13e), in that the bridge considered is a simple-span beam.

In the early part of the study, solutions were also obtained by application of the theory reported in Ref. (18). In this method of analysis, the beam is considered to have a single degree of freedom. Specifically, the deflection configuration of the beam at any instant is considered to be proportional to the static deflection shape due to the static weight of the vehicle and the distributed weight of the beam itself. The significant limitation of the second method is that it does not consider the effect of friction in the vehicle suspension. Moreover, the program is applicable only to two-axle vehicles and does not consider the effect of bridge damping. On comparing the

---

* A recent modification of the computer program can include the effect of absolute damping for the vehicle oscillating on its tires. This version of the program was not used in the present study.

analytical solutions obtained by the two theories for identical parameters, they were generally found to be in excellent agreement (12a).

34.2 Problem Parameters. The principal dimensionless bridge-vehicle parameters entering in the analysis have been defined in Section 24, and the methods used to compute them were discussed in Chapters III and IV. For ease of reference, the parameters are briefly reviewed here.

The bridge properties of interest include the span, weight, natural frequency, and longitudinal profile. The span of all bridges was 50.0 feet, and the weights are given in Table 5. The natural frequency used was the average measured frequency from the free-vibration portion of the records for the particular subseries considered. The longitudinal profile of the bridges was approximated by a second-degree parabola with a midspan ordinate equal to the deviation of the actual bridge profile from a straight line through the supports, as shown in Fig. 14. The ordinates of the parabolas used were obtained from plots such as Fig. 15.

All of the tests reported in this chapter pertain to bridges which were first in the line of travel of the test vehicle. The presence of the second bridge in the line of travel was neglected. Unless otherwise noted, in all of the solutions presented the effect of damping in the bridge was neglected.

The vehicle properties of interest include the speed of the vehicle, its total weight, the axle loads, the axle spacing, the dynamic indexes of the tractor and semi-trailer defined in Eq. (14), the axle frequencies, and the coefficients of interleaf friction of each axle. The speed of the vehicle was computed from the measured time of passage over two marker hoses, on the assumption that this speed was constant throughout the run. The average total weights and axle loads shown in Table 12, and the axle spacings given in

Fig. 18 were used in all calculations. The dynamic indexes were assumed to be 0.8 for all two-axle vehicles and tractors of three-axle vehicles, and 1.0 for all trailers, as discussed in Section 15. In the first trial for each comparison, the axle frequencies and coefficients of interleaf friction used were those obtained from static loading tests, which are given in Tables 13 and 14. The effect of the instrument van, weighing 2.0 kips, was neglected in all solutions.

The values of the dimensionless parameters entering in the analytical solutions for all results presented in this chapter are given in Tables 19 and 20. These parameters include:

(a) For each subseries (Table 19):

(i) the profile parameter, Δ_c/δ_{st}, where Δ_c is the midspan ordinate of the assumed parabola and δ_{st} is the static deflection at midspan computed from the measured frequency by Equation (2).

(ii) the measured natural frequency of the bridge, f_b

(iii) the weight ratio, R

(iv) the frequency ratios, $\varphi_{t,i}$ and $\varphi_{ts,i}$, for each axle.

(v) the coefficient of interleaf friction, μ, for each axle.

(b) For each analytical solution (Table 20):

(i) the speed parameter, $\alpha = vT_b/2L$

(ii) the values of the frequency ratios, $\varphi_{t,i}$ and $\varphi_{ts,i}$, wherever these were different from the values obtained from the static loading tests.

(iii) the initial conditions of the axles at the instant they enter the span.

The initial oscillation of the vehicle axles is specified in terms of the interaction force, the vertical velocity, and the frictional force for each axle. In the present version of the computer program, initial oscillations can be specified only at the beginning of the problem, namely when the front axle enters the span. In cases where an attempt was made to consider the initial conditions of the drive and rear axles, a set of fictitious conditions was specified at the beginning of the problem, in such a manner that, when the axle in question entered the bridge, the computed magnitude and slope of the interaction force diagram would match the measured values, $P_{o,i}$ and $\dot{P}_{o,i}$, where $P_{o,i}$ and $\dot{P}_{o,i}$ are the magnitude and slope, respectively, of the interaction force diagram at the instant the i^{th} axle enters the bridge.

35. Comparisons for Tests with Blocked Vehicle Springs.

The comparison of experimental and analytical results will first be shown for the bridge and the vehicles for which the properties were known with the least amount of uncertainties. The bridge selected for this comparison is Bridge 3B (composite steel) and the vehicles are those with blocked springs.

35.1 Two-axle Vehicle. In Fig. 63, the experimentally determined history curves for interaction force for the rear axle and the dynamic increment for midspan deflection of the center beam are compared with the corresponding analytical solutions. The test selected is from subseries 5453-5, involving Bridge 3B and Vehicle No. 91 with springs blocked. The experimental interaction force diagram shown is the average of the two rear wheel responses, and has been corrected for the drift in the record. The individual responses of the two wheels are in good agreement, as can be seen by referring to Fig. 51a, showing the interaction force on the left wheel. The analytical solution represents the "first trial", using all parameters as determined from the static tests

on the bridge and vehicle. It should be noted that no initial oscillations were specified, and that damping was neglected for both the bridge and the vehicle.

It can be seen that the basic characteristics of the experimental curves have been reasonably duplicated. However, the magnitude of both the interaction force variation and the dynamic increments have been underestimated, and the computed response "leads" the measured response, the difference in phases becoming progressively worse with time. Furthermore, the initial conditions of the vehicle have not been matched, as expected. It may be of interest to note that the slight variation in the interaction force for $x/L < 0$ is due to the fact that for the value of $i = 0.8$ used, the motion of the rear axle is influenced by that of the front axle.

Figure 64 shows the results obtained on a later trial. The speed parameter α has been increased by 5%, in an attempt to account for the possible errors in the determination of this parameter, namely the uncertainties in the measured bridge frequency and vehicle speed, and the possible reduction errors involved in locating the points of entry and exit of the vehicle. Also, an attempt was made to match the initial vehicle conditions.

The agreement between experiment and theory is perfect for all practical purposes. The magnitude of the interaction force variation has been slightly overestimated, partly because the attempt to match the initial vehicle conditions was not exactly successful, and partly because the damping of the vehicle tires was neglected. As a consequence, the computed dynamic increments are slightly higher than the measured values. It is conceivable that by correcting the above factors or by including bridge damping still better agreement could be obtained. In view of the uncertainties involved, such refinements are believed to be unjustified.

In Fig. 65, the comparison is extended to another test run from the same subseries. The experimental history curve for the variation in the interaction force is again the average of the two wheel responses, with suitable correction for drift (the uncorrected response of the left wheel is shown in Fig. 50a). The analytical solutions represent the final result after several trials. The speed parameter has been increased by 5% over the computed value and the initial conditions have been provided, but with a reduced amplitude to compensate for the tire damping.

It can be seen that the frequency of the bridge response has been correctly predicted, but that the computed frequency of the interaction force is too low. It should be noted that on the experimental records, there is a phase difference between the interaction force and the dynamic increment curves. This apparent discrepancy is believed to be due to errors in locating accurately the points of entry and exit on the bridge or vehicle records, or both, and is an excellent illustration of the uncertainties involved in locating these points on the records. The error is substantiated by the fact that from this record it appears as if the observed vehicle frequency is higher than that computed from the static measurements, which contradicts all other experimental findings.

Concerning the comparison of the magnitudes, it can be seen that the discrepancy in the latter portions of the dynamic increment curve observed in the previous record is again present, and, because of the slower speed, is noticeable for a larger portion of the run. The large computed dynamic increments may be due to the combined effects of vehicle and bridge damping; however, the effect of these parameters was not investigated.

35.2 Three-axle Vehicle. The experimental history curves for the variation of the interaction force in the drive and rear axles and for the dynamic increment for deflection are compared with the corresponding analytical solutions in Figs. 66a and 66b for a test run from Subseries 5453-35, involving the composite steel bridge 3B and the three-axle vehicle No. 513. The springs on the drive and rear axle of the vehicle were blocked. Analytical results are presented both for a smoothly rolling solution (i.e. no initial oscillations), and for a solution which represents an attempt to use more realistic intial conditions.

While the agreement is reasonably good for the drive axle, the response of the rear axle is poorly predicted. In particular, the observed frequency of the rear axle is considerably lower than the computed value, so that the computed phase angle at the instant of entry is in error. For the rear axle, the region $x/L < 0$ is not to be compared, since the analytical solution in this region corresponds to a fictitious motion. The shift of the response in the remaining portion is due to the improper matching of the initial conditions. For $x/L \geq 0.59$, after the drive axle leaves the span, the measured and computed responses are again not directly comparable. The vehicle behavior in this region is further discussed below.

Notwithstanding the above differences in the vehicle response, the agreement in the bridge response is generally satisfactory, although there are some differences in the details. In particular, the computed peak dynamic increments bracket the measured value. After the rear axle passes midspan, the detailed differences are particularly noticeable; however, in this region, the response is extremely sensitive to variations in the parameters, as will be shown in the following section. No further attempts were made to improve the agreement by adjusting the frequency ratios or inserting more representative initial conditions.

The behavior of the vehicle after the drive axle leaves the span merits further discussion. In the analysis, it is assumed that after an axle leaves the span, it continues its motion on a smooth, rigid surface. For the particular value of i = 1.0 used for the semi-trailer, the motion of the rear axle is uncoupled from that of the tractor, and the above assumption has no effect. In the actual situation, the drive axle passed onto Bridge 3A, which at the time of the test was shored up, but had a midspan sag of the order of 3.5 inches. The discontinuity between the decks of the two bridges was very pronounced. The differences between the measured and computed responses of the rear axle in the region considered are larger than would be expected on the basis of the possible uncertainty in the value of the dynamic index. It would appear that the discrepancies are due to the fact that the computed results do not include the effect of the horizontal forces transmitted at the "fifth wheel", as discussed in Section 16. The resulting differences in the vehicle response appear to contribute to the discrepancy in the bridge response discussed above.

The above comparisons indicate that the theoretical analysis predicts satisfactorily the behavior of both the bridge and vehicle. The shortcomings detected, principally in the difficulty of specifying satisfactorily the motion of the vehicle before and after its passage over the bridge are related only to the computer program, and could be remedied by revising portions of the program. Even the coupling between the axles of a three-axle vehicle can be accounted for by suitably modifying the equations of motion of the vehicle, or possibly by specifying an "effective dynamic index" to account for the observed coupling.

On the other hand, in order to obtain the "best" agreement, each dynamic test run has to be considered individually, and different parameters

have to be varied over the range of the known uncertainties before a definite conclusion can be reached. However, such a procedure seems completely unwarranted in any practical application, because the detailed characteristics of the response are of little interest.

36. Comparisons for Regular Tests on Bridge 3B

In this section, comparisons are presented for three subseries of regular tests on the composite steel bridge 3B. The particular subseries selected include two subseries for which tire pressure measurements were available, and one involving the largest number of dynamic runs. The first two serve to illustrate the sensitivity of the response to known uncertainties in the parameters, while for the third an attempt is made to relate the observed experimental scatter to the effect of the initial vehicle oscillations.

36.1 Two-axle Vehicle. The results of subseries 5453-1 considered in this section were used in Chapter V to discuss the detailed characteristics of the dynamic behavior of the bridge and vehicle. The most extensive comparisons were made with the particular dynamic run presented in Section 19.1.

(a) History curves. The result of the first comparison is shown in Fig. 67. As before, the vehicle response is represented by the history curve of the interaction forces for the rear axle. The experimental curve shows the average of the responses of the rear wheels, which were presented separately in Fig. 25a. The analytical solution is based on a smoothly rolling condition. The initial frictional force at the entrance is assumed to be zero.

It can be seen that the computed and measured curves for the interaction curve are similar, except for a horizontal shift in the peak ordinates. This shift reflects the effect of different initial conditions, primarily in the frictional force at the entrance. It should be noted however, that the magnitudes of the interaction forces are in agreement.

Although the computed dynamic increment curve does not reproduce all the details of the experimental curve, the response near the peak value is reasonably predicted. It may be recalled in this connection that the reduction errors in the dynamic increments for the regions away from midspan are generally fairly large.

For the record presented, the sensitivity of the response to variations of several parameters was studied. It should be recalled from Chapter IV that the computed vehicle frequencies based on the static measurements were found to be high, and that, under certain conditions of excitation, the computed frictional force was also higher than the observed value. The variations considered included the reduction of the drive axle frequency, $\bar{f}_{t,2}$, by 10, 20 and 30 percent from the computed value, and a 50 percent reduction in the coefficient of interleaf friction, μ_2. The detailed characteristics of the response curves changed significantly with the above variations, but in general the peak response was not significantly affected. As an indication of the sensitivity of the response, Fig. 68 shows the results obtained by reducing the frequency of the rear axle on its tires by 10 and 30 percent, respectively, from the computed value. The results pertain to a smoothly rolling condition. It can be seen that reducing the axle frequency improves the phase agreement in the interaction force, as expected. Similar results were obtained by reducing the limiting frictional force in the rear axle springs, not reported here.

In general, it was found that the most reasonable agreement for several values of α could be obtained by reducing the rear axle frequency to 80% of its computed value. With this value, the smoothly rolling solutions appeared to best predict the magnitude of the peak dynamic increment, while the solutions with the proper magnitude of the initial oscillations gave the best agreement in the phase of the dynamic increment curve.

The results for the test considered are shown in Fig. 69, both for a smoothly rolling solution and one where an attempt was made to match the initial conditions of the vehicle. It can be seen in the latter solution that the initial magnitude and slope of the interaction force was properly matched, but that the assumed initial friction was considerably in error.

The above solution illustrates the difficulties in attempting to duplicate the observed initial conditions in the analytical solutions. This effort, in general, has been unsuccessful for two reasons. First, in order to specify the initial conditions, the vertical velocity of the axle and magnitudes of the interaction force and frictional force in the suspension system must be determined. None of these quantities can be directly measured from the available data. The vertical velocity can be inferred from the slope of the interaction force record only by assuming that the springs are not engaged. The actual interaction force is unknown, since, as mentioned earlier, only the variations in the force were recorded. Finally, the frictional force existing in the spring can only be approximated by comparing the amplitudes of the tire and spring records. The second difficulty comes about in introducing the above quantities in the numerical solution. While it is possible to specify a set of fictitious conditions such that the desired condition exists immediately prior to the entrance of the axle, it is not feasible to obtain the same for the instant immediately after the entrance, when the axle has already encountered the change in curvature of the bridge profile.

The effect of bridge damping was also studied, and was found to be negligible.

The parameters used in the solutions presented in Fig. 69 were found to give the best agreement for the three additional tests investigated. As an example, the comparison for a run with $\alpha = 0.124$ is shown in Fig. 70. The

excellent agreement in the peak values of the dynamic increment is particularly noteworthy. It should be noted, however, that there usually are unexplainable differences in the response near the end. These discrepancies start before the front axle leaves the span, and thus cannot be attributed to the discontinuity of the profile at the exit discussed earlier.

No comparisons are presented for dynamic increments for moment. In the cases where comparisons were made, the agreement was of the same order as for deflections. This conclusion could be expected on the basis of the relation between dynamic increment curves presented in Section 19.2, and the theoretical predictions presented in Reference (16b) and (17a).

(b) Spectrum curves. The extension of the above comparisons to the spectrum curves for total effects is shown in Fig. 71. The parameters for all the analytical solutions shown are the same as those for the two history curves presented, and include the reduced frequency of the rear axle on its tires. The curve identified as "initial oscillations" was obtained by matching the magnitude, but not necessarily the slope, of the initial oscillations, as described above.

It can be seen that the spectrum comparisons for deflection show an excellent agreement. It is particularly significant that the two sets of analytical solutions essentially bracket the experimental scatter. The agreement between the computed spectrum curves for moment, and the corresponding curves for measured strain at midspan of the center beam is equally good.

It should be noted in connection with Fig. 71 that the smoothly rolling condition does not necessarily imply a lower bound on the predicted response. The actual interaction force and frictional force may have any value at the entry, and the vertical velocity may be in either direction. Thus, it is possible for these effects to combine in such a manner as to produce smaller,

as well as larger response than smoothly rolling vehicle with zero frictional force at the instant of entry. For the particular subseries considered, several spring records show that the springs were already engaged at the instant of entry, indicating that the frictional force was at its limiting value.

As an additional comparison of dynamic effects, the spectrum curves of peak dynamic increments for deflection are shown in Fig. 72. The computed curve refers to the smoothly rolling assumption. It can be seen that for the runs considered, the measured dynamic increments are in excellent agreement with the computed values.

36.2 Three-axle Vehicles.

(a) History Curves. Subseries 5453-7 involved the same bridge and vehicle as the one discussed in Section 35.2 except that the vehicle springs were in their normal operating condition. The results of comparisons for two values of α are shown in Figs. 73a through 74b and can be discussed together. For both comparisons, analytical solutions are presented for a smoothly rolling condition, and for a case where the initial oscillations of the drive and rear axles were specified. No adjustments have been made to any of the parameters computed from the static measurements.

It can be seen that for both tests the agreement between computed and measured interaction force curves is good, especially for the drive axle. The minor differences that exist are due to a combination of the effects discussed in the previous two sections. First, as in the case of blocked springs, the computed axle frequencies are higher than the measured values, resulting in a phase difference at the instant of entry. Second, there is a definite discrepancy after the exit of the drive axle due to the coupling between the drive and rear axles, which is not predicted by the analytical solutions based on a

value of i = 1.0 for the trailer. Finally, as for the two-axle vehicle, the initial portions of the interaction force curves exaggerate the true conditions.

For both runs, the bridge behavior, except for minor details, is predicted with sufficient accuracy for values of x/L up to 0.6, namely the exit of the drive axle. As discussed earlier, the differences in the curves beyond this point are probably due to the combined effects of the discontinuity at the exit, the coupling between the axles, the sensitivity of the response to variations in the parameters, and the large uncertainty in the ordinates of the history curves.

(b) Spectrum Curves. The result of the comparison of spectrum curves for subseries 5453-7 is shown in Fig. 75. The analytical spectrum curve pertains to the smoothly rolling condition. It can be seen that the general agreement between predicted and measured values is very good. In comparing the spectrum curves for deflection and strain, it can be seen that while for deflection the measured values are higher than the computed values, generally the reverse is true for strain. The differences between the theoretical curves and the experimental data are of the order of the uncertainties in the maximum crawl values, and a slight change in the crawl ordinates could completely reverse the above trend. It should be noted, however, that changes in the initial conditions of the vehicle from those assumed in the analysis can also contribute to the discrepancy observed.

Subseries 5452-26, involving Vehicle No. 415, was discussed in Section 25 in connection with the reliability of the experimental spectrum curves. In Fig. 76, the experimental spectrum curves for midspan deflection and strain for the center beam are reproduced with the corresponding analytical spectrum curves obtained on the assumption of a smoothly rolling

condition. It should be recalled that no measurements of the vehicle response were made in this subseries. The history curve comparisons show differences in the details of the response similar to those discussed previously, and are not presented.

It can be seen that, as in all previous spectrum curve comparisons presented, the predicted curve based on a smoothly rolling condition essentially follows the lower edge of the band of experimental scatter. In Section 25, this scatter was attributed primarily to the uncertainties in the initial conditions of the axles at the entrance.

Figure 77 shows the results of an attempt to obtain a quantitative measure of the effect of variations in the initial conditions on the maximum response. For simplicity, a single-axle vehicle was used, which represents the rear axle of the three-axle vehicle involved. Because of this simplified representation of the vehicle, only the deflections of the bridge are considered, as the crawl curve for deflection is more nearly comparable to the actual crawl curve for the three-axle vehicle. The results pertain to a value of $\alpha = 0.15$.

In the top figure, the sensitivity of the maximum response to the phase angle of initial oscillations is studied. The equation of the interaction force curve prior to entry was assumed to be of the form

$$\frac{P_o}{P_{st}} = 1 + 0.15 \sin (2\pi \bar{f}_{t,3}\, t - \theta) \qquad (8)$$

and was evaluated at the entry ($t = 0$). Solutions were obtained by varying θ from $-\pi$ to π. For $\theta = 0$, the initial interaction force is equal to P_{st}, the frictional force is zero, and the vehicle has a maximum upward velocity. Simiarly, for $\theta = \pi/2$, the interaction force is $0.85\ P_{st}$, the frictional force is $-0.15\ P_{st}$ (i.e. the spring is about the engage in compression), and

the vertical velocity is zero. The amplitude of 0.15 P_{st} corresponds to the average amplitude of oscillation of Vehicles No. 91 and No. 513 on the approach pavement of the bridge considered (See Section 24.3). The curves show the variation of the maximum amplification factor for deflection as a function of θ. The corresponding result for a smoothly rolling solution is shown by a horizontal line.

For the bridge considered, the shape of the experimental interaction force curves at the bridge entrance was generally the same for all speeds, and showed an upward velocity. Thus the region of interest is the range of θ from $-\pi/2$ to $\pi/2$. It can be seen from the figure that for this range, the maximum amplification factors are consistently higher than those obtained by the smoothly rolling condition. The difference between computed amplifications factors for this range of θ is approximately 50 percent of the observed scatter on the spectrum curve of Fig. 76. The theoretical differences for maximum amplification factors for moment, using a crawl response similar to that produced by the actual vehicle, would be of comparable magnitude.

In addition to the phase angle, the magnitude of the interaction force at the entrance is unknown. At the bottom of Fig. 77, the change in amplification factors due to this uncertainty is investigated, using the same single-axle vehicle described above. The interaction force was assumed to be of the form

$$\frac{P_o}{P_{st}} = 1 + \frac{\Delta P_o}{P_{st}} \tag{9}$$

and $\Delta P_o/P_{st}$ was varied between the rather extreme limits of -0.2 to +0.2. The initial velocity, $\dot{P}_o/2\pi\,\bar{f}_t P_{st}$, was kept at a constant value of -0.15, corresponding to $\varphi = 0$ in the figure above. It can be seen that the maximum amplification factor for deflection is not sensitive to this uncertainty.

It should be remembered that the above comparisons have been made for an idealized case. Similar studies involving a three-axle vehicle, and different combinations of initial conditions for each axle, would be required to bound properly the experimental data.

37. Comparisons for Regular Tests on Bridge 2B

In this section, comparisons are presented for the results of three subseries of tests on the composite steel bridge 2B. These subseries (No's. 5450-1, 2, and 7) were part of the first series of tests, and were the first ones investigated in detail. There were no tire pressure measurements available, however, it should be recalled from Section 13.1 that the approaches to this bridge, especially at the time the tests considered were performed, could be considered reasonably smooth. Therefore, all solutions presented in this section are based on the assumption of a smoothly rolling vehicle.

37.1 Two-axle Vehicle. In Fig. 78 are given the results of a comparison for a test run from Subseries 5450-1, in terms of history curves of dynamic increments for deflection and strain at midspan. The vehicle used in this subseries was the tractor of a standard three-axle test vehicle (No. 511), modified for two-axle loading, and designated as Vehicle A.

The experimental record was selected at random, because of excellent replication with another test run with a similar value of α. It was the first record for which an extensive study was made to determine the effect of experimental uncertainties. This study has been reported in Ref. (12). The analytical solution presented in Fig. 78 represents the "best" agreement obtained. The coefficients of interleaf friction, μ, were taken as 2 and 18 percent for the front and drive axles, respectively, and differ slightly from the values of 5 and 16 percent determined from the static loading tests.

All other parameters were determined from the static tests, and are given in Table 19. The agreement between the theoretical and experimental records is excellent, especially for strain. In order to illustrate further the agreement obtained, the history curves for total response (deflection and strain) are shown in Fig. 79. It is important to note that no agreement could be obtained by neglecting the effect of interleaf friction in the suspension springs of the vehicle[12b].

In comparing total effects, the particular record discussed is represented by a single point on the theoretical spectrum curve. For several other records examined, major discrepancies in the maximum effects were observed, particularly for low speeds. A study of the history curves showed that for the higher speeds ($\alpha > 0.14$), the agreement in phase was consistently good, but that there were discrepancies in the magnitudes of the peak dynamic increments. For lower speeds, the agreement in phase was generally poor.

In an effort to investigate whether the above discrepancies were due solely to a possible shift in the location of the "critical" dynamic increments, such as may be caused by small errors in estimating the bridge frequency, α, or the exact entry and exit points on the experimental records, spectrum curves for peak dynamic increments were compared. The result of the comparisons is shown in Fig. 80. It can be seen that the computed values are consistently higher than the measured values, indicating that the discrepancy is not due to the shift discussed above.

The one parameter that may possibly account for the discrepancy at low values of α is the effect of bridge damping, but this factor was not investigated.

It should be noted that the dimensionless parameters for the subseries considered in this section are essentially the same as those for

Subseries 5453-1, discussed in Section 36.1 and that the theoretical solutions for the two subseries are in good agreement, yet the test data for the same two subseries are considerably different.

37.2 Three-axle Vehicles. In subseries 5450-2 and 5450-7, the same tractor (No. 511) was used as in the subseries just discussed, except that a semitrailer had been connected to it. Two different load levels, designated as B and C in this report, were used in the two subseries. No attempt was made to vary any of the vehicle parameters in the analytical solutions; for the tractor, the values used were those described in the previous section, while for the rear axle, the quantities determined from the static tests were used.

Figures 81 and 82 show comparisons of the spectrum curves for the two subseries considered. It can be seen that for both subseries, throughout the range of α considered, the agreement between measured and computed values is excellent. It is noteworthy that for the low values of α, the theoretical curves are more sensitive to variations in α than for the higher values. This fact is in line with the larger scatter in the experimental results at lower speeds.

History curve comparisons were made for several of the runs, but they are not reported here. In general, they show equally good correlation in all the major details of the response, except for occasional differences that can be attributed to the effects of slight initial oscillations in the vehicle.

38. Comparisons for Regular Tests on Bridges 6A and 7A

The comparisons presented in the previous sections dealt with the composite steel bridges, the properties of which were subject to relatively

small uncertainties. In this section, the results of exploratory comparisons are presented for a prestressed concrete and a reinforced concrete bridge, the properties of which were most uncertain.

38.1 Bridge 6A, Two-axle Vehicle. Subseries 5453-2, selected for this comparison, involved Vehicle No. 91 and the prestressed concrete bridge 6A. The measured natural frequency of the bridge, determined from the free-vibration records for the subseries considered, was 6.67 cps, or 98 percent of the computed frequency based on an uncracked gross section. However, at the time of the tests, the beams of the bridge had been severely cracked. Thus the measured frequencies may not be representative for the loaded bridge, as discussed in Section 12.2.

The experimental interaction force records were not directly usable, because the times of entrance and exit on the bridge were not properly recorded. However, the amplitude of the variation of the interaction forces on the approach pavement was low, of the order of 0.08 P_{st}, suggesting that the assumption of a smoothly rolling vehicle is realistic.

Figure 83 shows the results of the two comparisons attempted. The computed curves of dynamic increments pertain to a smoothly rolling condition. It can be seen that the agreement between measured and computed response is anything but satisfactory. It should be noted, however, that in the regions when the load is at a considerable distance from midspan the response is reasonably predicted, especially for the higher value of α. In the regions when the heavy axle of the vehicle is near midspan, the experimental records show an erratic behavior. It is of interest to note the high-frequency components in the measured response. Such components have been observed only on the records of the two prestressed concrete bridges tested (See also Fig. 17, Ref. (11)).

It is suspected that the discrepancy noted above is due to the change in bridge properties caused by cracking. The amount of opening of the cracks is related to the magnitude of the applied load, and thus to the position of the vehicle on the span. Thus, as discussed in Section 12.2, the frequency of the bridge depends on the position of the load. The largest changes in behavior from that predicted on the basis of the free-vibration frequency can be expected to occur when the difference between the actual frequency and the free-vibration frequency is the largest, namely when the vehicle is near midspan. This is clearly the case in the tests presented above.

Within the time available it did not prove possible to pursue these comparisons any further or to examine any additional records. While further studies would be necessary to clarify this discrepancy, it appears that because of the time-dependent frequency of the bridge, no overall satisfactory agreement may be obtained with a theoretical solution which assumes that the properties of the structure are constant.

In this connection, it should be noted that for the two tests considered, the maximum measured and computed amplification factors are as follows:

α	Max. Ampl. Factor for Deflection	
	Measured	Computed
0.096	1.15	1.12
0.102	1.15	1.14

This indicates that from a design standpoint the discrepancy may not be significant, but it also emphasizes the fact that if spectrum curve ordinates only had been compared, the agreement would have been termed excellent, and the basic discrepancy in behavior could have passed unnoticed.

38.2 Bridge 7A, Two-axle Vehicle. The solid line curves in Fig. 84 show measured dynamic increments for deflection at midspan for two test runs from Subseries 5453-3, involving the reinforced concrete bridge 7A and the two-axle vehicle No. 91. The dashed lines represent theoretical solutions assuming a smoothly rolling vehicle. The bridge profile in the theoretical solutions is assumed to be a second-degree parabola with a midspan ordinate equal to that of the actual bridge profile. It can be seen that the agreement between measured and computed responses is poor, although for both speeds the early portions of the curves agree in phase. However, as discussed earlier, the surface conditions corresponding to the two sets of curves are not comparable, and the results are included to emphasize the effect of the surface irregularities of the bridge.

In Fig. 85, the experimental interaction force curves for the two rear axle wheels are shown, corresponding to the high speed test run presented on the previous figure. Pronounced high-frequency "tire-hop" oscillations are evident throughout the record. These oscillations are typical for all test runs on this bridge, and are generally more pronounced than those for the other bridges tested. The presence of these oscillations indicates an increased degree of roughness of the bridge pavement. The figure also shows the deviation of the bridge profile from the parabola assumed in the analytical solution, the positive deviation denoting an increase in camber above that given by the assumed parabola. The presence of two "bumps", one near the third point and the other at the end of the bridge, is evident. While the latter cannot be expected to have large effects on the bridge-vehicle response, the first "bump" appears to account for the large dynamic effects observed on this bridge, as already discussed in Chapter VI.

Returning to Fig. 84, it can be seen that for both speeds, the measured dynamic increments increase rapidly in amplitude starting approximately at x/L = 0.4, corresponding to the end of the "bump". For the higher speed, the peak dynamic increment caused by the impact provided by the bump occurs at x/L = 0.85, and therefore produces a low total effect. However, for the slower speed, the peak dynamic increment occurs when the axle is still near midspan, and the resulting total amplification factor is very large. It is noteworthy that for the lower speed, as the oscillations produced by the "bump" are damped out, the measured response near the end of the record agrees reasonably well with the computed curve.

The fact that for the subseries considered the critical dynamic increment is always associated with the irregularity of the bridge deck explains the unusual spectrum curve, discussed in connection with Fig. 37c. For the lower speeds, the critical dynamic increment occurs near midspan, causing large amplification factors. As the speed increases, and thus the time of transit decreases with respect to the bridge period, the critical dynamic increments occur at larger values of x/L, and consequently combine with lower crawl ordinates. The net result is that amplification factors at large values of α are considerably lower than would be predicted for a smooth surface.

Because of the limitations of the available computer program, it was not possible to obtain solutions considering the effect of the profile irregularities. However, it should be noted that the above difference does not explain all of the discrepancies between the measured and computed response. In particular, there is a large apparent error in the base line of the measured dynamic increment curve for the record corresponding to $\alpha = 0.204$ shown in Fig. 84.

The findings of this section, however, can be used to explain quantitatively the very high amplification factors observed with the three-axle vehicles on Bridge 7A. For the three-axle vehicles used, the spacing of the two heavy axles is approximately 0.4L. Thus, when the rear axle enters the bridge, the drive axle encounters the "bump" described above. Therefore, the high oscillations induced by the excitation of the drive axle occur when the rear axle is close to midspan, namely when the static effects are maximum. This fact is illustrated in Fig. 86, where the measured dynamic increments for two- and three-axle vehicles are compared, with the points of entry of the drive axles lined up. It can be seen that the two responses are in phase until the drive axle leaves the span, and that the critical dynamic increments occur for the same position of the drive axle. It is noteworthy that for the three-axle vehicle, the motion of the bridge after the drive axle leaves the span is rapidly damped out. This is apparently caused by the "interference" of the two heavy axles, again indicating the presence of coupling between these axles.

39. Significance of the Comparisons Presented

The major conclusion to be drawn from the investigation presented in this chapter is that when the properties of the bridges and vehicles can be specified with a reasonable degree of accuracy, the theory used in this investigation can predict the behavior of the bridge-vehicle system with a surprising degree of accuracy. Thus, for the composite steel bridges, the behavior of which is subject to relatively few uncertainties, the predicted response agrees for all practical purposes with the measured behavior. This does not mean, of course, that perfect agreement was obtained for every

detail of every history curve studied. It does mean, however, that within the limitations of the experimental uncertainties and the available computer program, all major effects were accounted for. By varying the parameters within the limits of the experimental uncertainties, and by performing purely technical modifications on the computer programs, even better comparisons could be obtained. This, however, was not the purpose of the present investigation.

On the other hand, no agreement could be obtained for the prestressed concrete bridge using a theoretical model which assumes that the properties of the bridge are independent of the position of the load. It is suspected that this discrepancy is due to the cracked condition of the bridges, and further understanding of the behavior is necessary to provide a basis for interpreting the test data. Finally, for the reinforced concrete bridge the theoretical and experimental results could not be correlated, because of the limitations of the computer program. However, it was possible to account for the observed effects on the basis of theoretical considerations. By proper modifications of the computer program, the effect of the irregularities of the bridge profile could be further investigated if an agreement in the details of the response curves was desired.

The second significant result of the comparisons presented is that it was possible to determine what properties of the bridges and vehicles have the greatest influence on the agreement with theory, and thus helped in formulating suggestions for the conduct of future tests. These suggestions are included in the summary presented in the next chapter.

IX. SUMMARY AND CONCLUSIONS

40. Summary of Experimental Observations

In Chapters III through VII, the results of an extensive set of tests on the characteristics of bridges and vehicles and the results of approximately 1900 dynamic tests have been presented. In this study, primary emphasis has been placed on determining accurately the pertinent properties of the bridges and vehicles, and on understanding the dynamic behavior of the bridges under the passage of vehicles, and of the vehicles themselves.

The major conclusions drawn from this study are briefly as follows:

(1) For concentric loads, each test bridges acted essentially as a single simply supported beam. The differences between the magnitudes of the static response of the three beams were generally negligible. Both the magnitudes of the measured deflections and strains and the shape of the crawl history curves agreed with the corresponding values computed on the basis of a simply supported prismatic beam.

(2) For the noncomposite steel, prestressed concrete, and reinforced concrete bridges, the frequencies determined from the free-vibration era, after the vehicle had left the span, were not representative of the stiffness of the bridges while the vehicle was on the span. This difference is due to the different degrees of composite action or extent of openings of cracks under the two conditions. There appears to be a corresponding difference in the damping characteristics of the loaded and unloaded bridges.

(3) The effect of age (i.e. number of load applications) was manifested by increased permanent deflections of all bridges, and by reduced stiffness in all but the composite steel bridges.

(4) The static load-deflection characteristics of the vehicles could be acceptably represented by a linear spring for the tires, and by a

bi-linear model for the springs, which includes the effect of frictional damping in the suspension system. However, large differences were observed between the results of duplicate loading tests.

(5) Although there were uncertainties in the time scales of the experimental records, the frequencies of the vehicles under dynamic conditions appeared to be lower than predicted by the static measurements, reflecting the flexibility provided by the vehicle frame. The damping in the tires could be approximated on the basis of a viscous damping coefficient of the order of one percent. Under certain conditions of severe excitation of the vehicle, the frictional force in the suspension system was found to be less than the value obtained from the static tests and occasionally disappeared entirely.

(6) For comparable speeds and pavement irregularities, blocking of the vehicle springs was found to increase the amplitude of the interaction force variation by as much as a factor of three. The maximum observed double-amplitudes of variation in the interaction force in dynamic tests on rigid pavements were found to be as follows:

Drop tests using a 1-inch obstruction

Two-axle vehicle, springs blocked	2.0 P_{st}
Two-axle vehicle, springs normal	1.1 P_{st}
Three-axle vehicle, springs blocked	1.2 P_{st}
Three-axle vehicle, springs normal	0.3 P_{st}

Tests on smooth pavement

Two- and three-axle vehicles, springs blocked	0.5 P_{st}
Two- and three-axle vehicles, springs normal	0.2 P_{st}

For both blocked and normal suspension springs, the variation in the interaction force was found to be less for the three-axle vehicles than for the two-axle vehicles, due to the coupling between the tractor and semi-trailer.

(7) History curves of dynamic increments provided the best measure of the dynamic behavior of the bridges. Comparisons of history curves of bridge response confirmed the theoretical predictions that the dynamic increments for strain and deflection at a point, as well as those for the effects at different points on the same beam are essentially identical. Furthermore, for the bridges considered, the dynamic increments at midspan of the three beams were also found to be comparable so that the midspan response of the center beam, expressed in terms of dynamic increments, depicted with sufficient accuracy the dynamic behavior of the entire bridge.

(8) The peak dynamic increments generally increased with increased speed. The maximum amplification factors, which depend both on the magnitude and position of the critical dynamic increments (i.e., the peak dynamic increment which, superimposed on the corresponding crawl curve, produces the maximum total effect), were found to be sensitive to variations in vehicle speed.

(9) Initial vehicle oscillations of the vehicle were present in practically all tests, and introduced a large uncontrollable uncertainty in the dynamic response of the bridges. The amplitude of these oscillations could not be correlated with the PSI values used to rate the serviceability of the pavements. A qualitative measure of the trend in the amplitudes of the vehicle oscillations at the entrance to the bridge was obtained on the basis of simple approximations of the major surface irregularities of the approach pavements immediately preceding the bridge.

(10) Under seemingly identical conditions, the scatter in measured amplification factors was of the order of 20 percent for deflections and 10 percent for strains. This scatter is due to differences in the initial conditions of the vehicles, the variation in the characteristics of the vehicle, and the unavoidable errors in recording and reduction. For the setup and controls used, the above dispersion must be considered the normal experimental error, and does not imply a difference in bridge behavior or a lack of replication in the detailed characteristics of the response.

(11) In comparing the results of the regular tests (i.e. tests in which there were no induced initial oscillations in the vehicle or bridge, the vehicle suspension system was in its normal operating condition, and the vehicle followed a path centered along the center beam of the bridge), the maximum amplification factors generally increased with the speed parameter α. The differences in the amplification factors of the same bridge for different vehicles at different times, as well as between the responses of the different bridges were generally larger than the scatter of the data. The largest amplification factor for deflection in these tests was 1.63; however, only five percent of measured amplification factors for deflection exceeded 1.40, and only approximately five percent of the amplification factors for strain exceeded the value of 1.285 specified by the "impact formula" of the AASHO Standard Specifications. The largest effects were observed on a reinforced concrete bridge, but these results appeared to be influenced by the presence of a pronounced irregularity on the bridge surface.

(12) Where the effects of the individual bridge-vehicle parameters could be isolated, they were in general agreement with theoretical predictions. The presence of vehicle oscillations produced by irregularities both on the approach pavements and on the bridge itself made the comparisons of effects

difficult. In general, different vehicles on the same bridge produced comparable effects, while the same vehicle on different bridges produced markedly different effects, due to the relatively larger differences in the pertinent parameters, and to the differences in the profiles of the approaches and bridges.

(13) The increase of the number of load applications resulted in increased amplification factors only for those bridges for which the permanent sag and the approach profile roughness increased with time, and actually resulted in a decrease in effects when the bridge camber decreased and the approach profile was smoothed out by patching.

(14) Blocking of the vehicle springs resulted in approximately doubling the dynamic increments on the bridge, as well as imparting to the bridge response a noticeable component proportional to the variation in the interaction force.

(15) In the tests with induced vehicle oscillations, the vehicle behavior on the bridge was found to be essentially the same as on a rigid pavement. For vehicles with normal suspension, due to the large amount of frictional damping, only the first bottoming of the vehicle produced large changes in the interaction force. By the time the vehicle reached midspan, the variation in the interaction force was reduced to values comparable to those for the regular tests. Consequently, maximum amplification factors at midspan were generally only slightly larger than those produced without induced initial oscillations; however, the effects away from midspan were larger than those observed for the regular tests. On the other hand, initial bridge oscillations, similar to those produced by continuous traffic, were found to have no noticeable effect.

(16) Eccentricities of the vehicle of 24 inches were found to have no significant effect on the bridge behavior, but a single-wheel loading, at an eccentricity of 60 inches was responsible for exciting a large component of the torsional mode of vibration of the bridge.

41. Summary of Comparisons Between Experimental Results and Theoretical Predictions

Comparisons between experimental and theoretical results, both for history curves of bridge and vehicle response, and for spectrum curves of maximum effects have been presented in Chapter VIII. The study presented was based on a small proportion of the test data obtained, and was essentially exploratory in character. The comparisons were intended to study the reliability of the theoretical model used and the effect of the experimental uncertainties mentioned above, as well as the engineering significance of the observed effects. The following conclusions can be drawn from the results obtained:

(1) For those cases where there was little uncertainty about the properties of the bridges and vehicles, the theoretical solutions were found to be in excellent agreement with the experimental data. These cases comprised all the tests with blocked vehicle springs, and essentially all of the results studied for the regular tests on the composite steel bridges.

(2) In general, the exact agreement between theory and experiment was hampered by the large number of uncertainties involved in the experimentally determined parameters, the unavoidable errors in recording and reducing the experimental data forming the basis of comparisons, and by certain limitations of the computer program used to obtain the theoretical solutions.

(3) In the prestressed concrete bridge examined, the cracking of the beams appears to have changed significantly the properties of the bridge while the vehicle is on the span. Because of this, no agreement could be obtained using a theoretical model in which it is assumed that the properties of the bridge are independent of the position of the load.

42. Suggestions for Further Studies.

One of the prime objectives of this investigation was to evaluate critically the reliability of test data obtained from field tests on actual structures, and to formulate suggestions for further studies in the area. On the basis of the results of this study, it can be concluded that it is entirely possible to obtain highly reliable experimental data from field tests.

It appears from the results of the present investigation that two different types of field tests may be warranted in the future. One type of test would be aimed at providing the most reliable data on the dynamic behavior of bridges of various spans, widths, and types of construction under the passage of representative heavy vehicles. The principal purpose of these tests would be to provide data for further detailed comparisons with theoretical models for ranges of parameters exceeding those found in the tests reported herein. The second type would consist of tests on a very wide variety of bridge and vehicle types, with considerably less complete instrumentation and experimental control than for the first type. The objective of these tests would be to provide a wide range of experimentally determined bridge and vehicle parameters, which could be used in conjunction with theoretical studies of the type currently in progress[19], and to study analytically, and eventually statistically, the effect of these parameters on the bridge response.

In both types of tests, the characteristics of the bridges must be evaluated with the greatest care. The bridge properties of interest are the natural frequencies, the longitudinal profiles, and the damping characteristics. In view of the observed difference in behavior between the loaded and unloaded bridges, it may be advisable to obtain the frequencies and damping coefficients from forced vibration tests. However, if this is done, the variation in stresses near the resonant frequency should be representative of the actual variation produced by the passage of heavy vehicles. In this connection, stiffness and response data from fatigue tests on prestressed reinforced concrete beams may provide valuable data on the behavior of loaded bridges. The longitudinal profiles of the bridges and approaches should be evaluated more reliably than by conventional rod and level readings. Continuous profiles may be most valuable in this respect. In these measurements, care should be taken to measure accurately those components of the irregularities which may affect the vehicle oscillations at the speeds considered.

In a similar fashion, the properties of the vehicles under both static and dynamic conditions must be accurately known. Concerning static loading tests, it is important that the deflections measured pertain to a fixed point on the vehicle body over the axle, rather than to the incremental deflections in the tires and the suspension springs, in order to obtain the true load-deflection characteristics, including the effect of the flexibility of the vehicle frame. Unless the behavior is completely erratic, the bi-linear model used in this study can be depended upon to separate deflections of the tires from those of the combined tire-sprung suspension system. The most valuable dynamic measurements would probably be simple drop test on an electronic scale capable of producing a continuous record of the load. From the

results of theoretical results, there appears to be no need to evaluate experimentally the dynamic indexes of the vehicles, since the bridge response is not sensitive to variations of this parameter.

Because of the complexity of the equipment required, the instrumentation of the vehicles should be compatible with the objectives of the particular test program. If only a gross measure of effects id desired, nominal dynamic instrumentation would be adequate, provided that it is supplemented by the static loading tests referred to above. Specifically, the relatively simple instrumentation to measure spring deflections would make it possible to determine whether the variation in the interaction forces exceeded the limiting frictional force, and thus give an order of magnitude of the amplitude of force variation. On the other hand, if the objective of the test program is to yield data for detailed comparison with theory, it is imperative that the forces exerted by the vehicle be measured accurately. This information is needed for two reasons: first, to determine the initial conditions of the vehicle; and, second, to provide an intermediate level of comparison with analytical solutions.

The best method for measuring the dynamic interaction forces is an area worthy of further study. Regardless of the method used, whether it involves measurements of tire pressures, strain gages on the axles, displacement of the vehicle with respect to the roadway surface, lateral bulging of the tires, etc., there are three prime requirements which must be satisfied:

(a) the measurements must be referenced to a static base value, so that the actual forces, and not just their variation, can be obtained;

(b) the vertical displacement of the tires must be separated from that of the springs, so that an accurate measure of the frictional force at any instant can be obtained;

(c) there must be an accurate correlation between the time and position scales on the bridge and vehicle records.

Finally, concerning bridge instrumentation, one of the most important results of this study was to verify the theoretical predictions[16],[17] that the use of dynamic increments, rather than history curves of total effects, makes it possible to estimate reliably the response at any point of the bridge from a small number of actual records.

It must be emphasized that the bridges considered in this study were expected to, and actually did, behave essentially as beams. Further field tests, under carefully controlled conditions, are required on actual multigirder bridges to test the adequacy of the theory based on a beam, or of the more elaborate theory[17] which takes into account the actual transverse distribution of effects. The beam theory used in this study is quite general, but certain mechanical changes in the computer programs are warranted to account for conditions observed in the tests studied.

With regard to further field tests, special attention should be given to the effect of surface irregularities, which have been shown, both analytically and by the results of the tests described, to be of prime importance. In fact, it is conceivable that improved construction specifications for the control of the profile of the bridges and approach pavements may have a more far-reaching effect on the problem of bridge impact than any change in the impact formula now in use.

REFERENCES

1. "The AASHO Road Test", to be published by Highway Research Board.

   a. Report 4, Section 2.3
   b. Report 4, Section 2.1
   c. Report 4, Section 2.2
   d. Report 4, Section 2.2.2
   e. Report 3

2. Tung, T. P., Goodman, L. E., Chen, T. Y., and Newmark, N. M., "Highway Bridge Impact Problems," Highway Research Board, Bulletin 124, 1956, pp. 111-134.

3. Prince-Alfaro, J., and Veletsos, A. S., "Dynamic Behavior of an I-Beam Bridge Model Under a Smoothly Rolling Load," Civil Engineering Studies, Structural Research Series No. 168, University of Illinois, 1958.

4. Biggs, J. M., Suer, H. S., and Louw, J. M., "The Vibration of Simple Span Highway Bridges," ASCE Transactions, Vol. 124, 1959, pp. 291-318.

5. Von Eenam, N., "Live Load Stress Measurements of Fort Loudon Bridge," Proceedings, Highway Research Board, Vol. 31, 1952, p. 36.

6. Foster, G. M., and Oehler, L. T., "Vibrations and Deflection of Rolled-Beam and Plate-Girder Bridges," Highway Research Board Bulletin 124, 1956, pp. 79-110.

7. Carey, W. N. Jr., and Erick, P. E., "The Pavement Serviceability - Performance Concept," Highway Research Board Bulletin 250, 1960, pp. 40-58.

8. Fisher, J. W., "Development of Equipment and Methods Used to Determine Dynamic Loads of Vehicles at the AASHO Road Test," to be published by Highway Research Board.

9. Jacobsen, L. S., and Ayre, R. S., "Engineering Vibrations," McGraw-Hill, 1958.

   a. p. 439
   b. p. 201
   c. p. 163

10. Fisher, J. W., and Viest, I. M., "Comparison of Strains and Deflections from Static and Crawl Tests of Bridges," Field Office Report No. 24, AASHO Road Test, 1959.

11. Endebrock, E. G., Rolf, R. L., and Fenves, S. J., "Preliminary Report on First Series of Dynamic Tests," Progress Report No. 1, Dynamic Studies of Bridges on AASHO Road Test, University of Illinois, 1959.

    a. p. 11

12. Rolf, R. L., Fenves, S. J., and Veletsos, A. S., "Comparison of Experimental Data with Theoretical Solutions," Progress Report No. 2, Dynamic Studies of Bridges on AASHO Road Test, University of Illinois, 1960.

a. p. 17
b. p. 13

13. Korn, A., Fenves, S. J., and Veletsos, A. S., "Preliminary Report on the Second Series of Dynamic Tests," Progress Report No. 3, Dynamic Studies of Bridges on AASHO Road Test, University of Illinois, 1960.

a. p. 57
b. p. 35
c. p. 41
d. p. 48
e. p. 73-74

14. Endebrock, E. G., Fenves, S. J., and Veletsos, A. S., "A Study of Lateral Distribution of Dynamic Effects," Progress Report No. 4, Dynamic Studies of Bridges on AASHO Road Test, University of Illinois, 1960.

a. p. 9

15. Janeway, R. N., "A Better Truck Ride for Drive and Cargo," Special Report No. 154, Society of Automotive Engineers, 1958, p. I-5.

16. Huang, T. and Veletsos, A. S., "Dynamic Response of Three-Span Continuous Highway Bridges," Civil Engineering Studies, Structural Research Series No. 190, University of Illinois, 1960.

a. p. 14
b. p. 66
c. p. 76
d. p. 9
e. p. 36

17. Oran, C. and Veletsos, A. S., "Analysis of Static and Dynamic Response of Simple-Span, Multigirder Highway Bridges," Civil Engineering Studies, Structural Research Series No. 221, University of Illinois, 1961.

a. p. 56

18. Wen, R. K. L., "Dynamic Behavior of Simple Span Highway Bridges Traversed by Two-axle Vehicles," Civil Engineering Studies, Structural Research Series No. 142, University of Illinois, 1957.

19. Walker, W. H. and Veletsos, A. S., "A Method for Estimating the Dynamic Response of Simple-Span Highway Bridges," to be published in Civil Engineering Studies, Structural Research Series, University of Illinois, 1962.

20. "Standard Specifications for Highway Bridges," The American Association of State Highway Officials, 1957, p. 17.

21. Fisher, J. W., and Viest, I. M., "Effect of Vehicle Type of Dynamic Response of Test Bridges," Field Office Report No. 28, AASHO Road Test, 1961.

22. Nieto, J. A., "A Study of Effect of Interleaf Vehicle Friction on the Dynamic Response of Simple Span Highway Bridges," Tenth Progress Report, Highway Bridge Impact Investigation, University of Illinois, 1960, Part C.

TABLE 1 SUMMARY OF DYNAMIC TESTS ON PAVEMENTS

For explanation of instrumentation code see Table 3

Subseries Number	Vehicle			Condition of springs	Pavement Type	Obstruction Type	Number of runs
	Number	Number of axles	Instrumentation code				
5453-15	94	2	3	Normal	Smooth	--	9
16	94	2	3	Normal	Rough	--	8
17	94	2	3	Normal	Smooth	2 x 6	3
18	94	2	3	Normal	Smooth	1 x 12	4
19	91	2	3	Normal	Smooth	Two ramps	8
20	91	2	3	Normal	Smooth	One ramp	8
21	91	2	2	Blocked	Smooth	--	7
22	91	2	2	Blocked	Smooth	Two ramps	3
23	91	2	2	Blocked	Smooth	One ramp	4
24	91	2	2	Blocked	Rough	--	5
25	513	3	3	Normal	Smooth	--	7
26	513	3	3	Normal	Rough	--	10
27	513	3	3	Normal	Smooth	Two ramps	12
28	513	3	3	Normal	Smooth	One ramp	8
29	513	3	3	Normal	Smooth	1 x 12	8
30	513	3	2	Blocked	Smooth	--	8
31	513	3	2	Blocked	Rough	--	8
32	513	3	2	Blocked	Smooth	Two ramps	8
33	513	3	2	Blocked	Smooth	One ramp	8
34	513	3	2	Blocked	Smooth	1 x 12	8
39	417	3	3	Normal	Rough	--	10
40	417	3	3	Normal	Smooth	--	8
41	417	3	3	Normal	Smooth	Two ramps	12
42	417	3	3	Normal	Smooth	One ramp	11

TABLE 2 SUMMARY OF DYNAMIC TESTS ON BRIDGES

For explanation of columns (2), (4), (6) and (9) see Table 3

Subseries		Bridges				Vehicle			Number of Test Runs	Test Date
Number	Test Classification	First in Line Designation	First in Line Instrumentation	Second in line Designation	Second in line Instrumentation	Number	Number of Axles	Instrumentation		
(1)	(2)	(3)	(4)	(5)	(6)	(7)	(8)	(9)	(10)	(11)
5450-1	1	2B	1,3	2A	1,3	A	2	0	24	10/10/58
2	1	2B	1,3	2A	1,3	C	3	1	25	10/3/58
3	1	5A	1	5B	5	C	3	1	25	10/5/58
4	1	4B	2	4A	2	C	3	1	13	9/25/58
5	1	7A	1	7B	5	C	3	1	12	10/2/58
6	1	6A	1			B	3	1	25	10/8/58
7	1	2B	2	2A	2	B	3	1	24	10/9/58
8	5	4B	1	4A	1	C	3	1	12	9/30/58
5451-3	1	2B	1			415	3	1	27	6/17/59
4	1	5A	1	5B	1	415	3	1	28	7/6/59
5	1	7A	1	7B	1	415	3	1	23	6/18/59
6	1	9B	1	9A	1	415	3	1	24	7/7/59
7	3	3B	1,4			94	2	1	28	8/13/59
8	3	5A	1,4	5B	1,4	94	2	1	22	7/9/59
9	5	3B	1			94	2	1	22	7/8/59
10	5	5A	1	6B	1	94	2	1	18	7/9/59
11	1	3B	1			315	3	1	14	8/6/59
12	1	5A	1	5B	1	315	3	1	19	8/4/59
13	1	7A	1	7B	1	315	3	1	14	8/7/59
14	1	3B	1			415	3	1	20	5/14/59
15	1	3B	1			513	3	1	16	8/11/59
16	1	7A	1	7B	1	513	3	1	19	11/10/59
17	7	5A	1	5B	1	221	2	0	19	8/12/59
18	(see note 1)									

(Cont'd on next page)

TABLE 2 (cont'd)

Subseries Number	Test Classification	Bridges: First in Line Designation	First in Line Instrumentation	Second in Line Designation	Second in Line Instrumentation	Vehicle Number	Vehicle Number of Axles	Vehicle Instrumentation	Number of Test Runs	Test Date
(1)	(2)	(3)	(4)	(5)	(6)	(7)	(8)	(9)	(10)	(11)
5452-1	1	2B	1,7	1,7		415	3	3	18	2/2/60
2	1	7A	1,7	7B	1	415	3	1	20	2/17/60
3	1	9B	1,7	9A	1	415	3	1	16	2/3/60
4	1	5A	1,7	5B	1	415	3	1	17	2/9/60
5-16	(see note 2)									
17	6	3B	1,3			415	3	1	14	2/1/60
18	6	7A	1,3	7B	1,3	415	3	1	17	1/28/60
19	8	3B	1,7			415	3	0	79	3/6/7/60
						417	3	0		
20	8	7A	1,7			415	3	0	99	2/20/60
						417	3	0		
21-24	(see note 2)									
25	1	3B	1,6			415	3	0	60	4/7/60
26	1	3B	1,6,7			415	3	0	75	6/6/60
27	1	3B	1,6,7			415	3	0	57	6/9/60
28	1	3B	1,6,7			415	3	0	56	6/10/60
5453-1	1	3B	1,7			91	2	3	17	7/26/60
2	1	6A	1,7	6B	1	91	2	3	21	7/29/60
3	1	7A	1,7	7B	1	91	2	3	21	7/30/60
4	1	9B	1,7	9A	1	91	2	3	17	7/27/60
5	2	3B	1,7			91	2	2	14	8/16/60
6	4	3B	1,6			91	2	2	19	9/16/60
7	1	3B	1,7			513	3	3	17	9/1/60
8	1	9B	1,7	9A	1	513	3	3	17	9/2/60
9	1	7A	1,7	7B	1	513	3	3	14	9/6/60
10	3	3B	1,6			91	2	3	24	8/2/60
11	3	7A	1,6	7B	1	91	2	3	25	8/8/60
12	6	3B	1,8			91	2	3	17	8/1/60

(Cont'd on next page)

TABLE 2 (cont'd)

Subseries Number	Test Classification	Bridges: First in Line Designation	Bridges: First in Line Instrumentation	Bridges: Second in Line Designation	Bridges: Second in Line Instrumentation	Vehicle Number	Vehicle Number of Axles	Vehicle Instrumentation	Number of Test Runs	Test Date
(1)	(2)	(3)	(4)	(5)	(6)	(7)	(8)	(9)	(10)	(11)
5453-13	3	9B	1,6,7	9A	1,7	513	3	3	11	9/7/60
14	3	7A	1,7	7B	1	513	3	3	12	9/6/60
15-34	(see note 3)									
35	2	3B	1,9			513	3	2	16	9/10/60
36	4	9B	1,6,7	9A	1,7	513	3	2	14	9/11/60
37	9	7A	1,6,6	9B	1,7	513	3	2	20	9/11/60
38	1	3B	1,7			513	3	3	16	9/12/60
39-42	(see note 3)									
5454-1	1	2B	1,7			415	3	1	28	10/20/60
2	1	5A	1,7	5B	1,7	415	3	1	23	10/19/60
3	1	7A	1,7	7B	1,7	415	3	1	21	10/23/60
4	1	9B	1,7	9A	1,7	415	3	1	34	10/29/60

NOTES: 1. Subseries 5451-18 consisted of additional crawl and static tests on Bridges 2B, 5A, 7A, and 9B, using Vehicle No. 415 .

2. Subseries 5452-5 through 16 and 5452-21 through 24 were additional tests to study statistically the effects of various parameters. Three vehicles were used in each subseries (see Table 4 for bridge-vehicle combinations involved). The test codes for all subseries were as follows:

Test classification	1
Bridge instrumentation	1
Vehicle instrumentation	0

3. Subseries 5453-15 through 34 and 5453-39 through 42 were dynamic tests on pavements. See Table 1.

TABLE 3 EXPLANATION OF TEST CODES USED IN TABLES 1 AND 2

A. Test Classification (Column (2) of Table 2)

Code Number	Legend
1	Vehicle centered over middle beam of the bridge producing a concentric load.
2	Same as 1, except vehicle springs blocked.
3	Induced oscillations of vehicle produced by obstruction placed on approach pavement.
4	Same as 3, except vehicle springs blocked.
5	Vehicle following an eccentric path. Bridge loaded with one line of wheels.
6	Vehicle following an eccentric path with left line of wheels passing over interior beam. Bridge loaded with two lines of wheels.
7	Sudden braking applied at midspan.
8	Simulation of continuous traffic.

B. Bridge Instrumentation (Columns (4) and (6) of Table 2)

Code Number	Legend
1	Midspan strain and deflection gages on all three beams.
2	Midspan strain and deflection gages on center beam.
3	Strain gages on lines 3, 7 of center beam.
4	Strain gages on lines 3, 4, 6, 7 of center beam.
5	Deflection gages on lines 3, 5, 7 of center beam.
6	Strain gages on lines 3, 7 of all three beams
7	Strain gages on lines 4, 6 of center beam
8	Strain gages on lines 3, 7 of interior beam
9	Strain gages on lines 4, 6 of interior beam

C. Vehicle Instrumentation (Column (9) of Table 2)

Code Number	Legend
0	No vehicle instrumentation.
1	Spring deflection records.
2	Tire pressure records.
3	Spring deflection and tire pressure records.

TABLE 4 SUMMARY OF BRIDGE-VEHICLE COMBINATIONS IN DYNAMIC TESTS

Numbers indicate subseries for bridge-vehicle combinations shown
For test classification codes see Table 3

Vehicles		Bridges							
No. of Axles	Number	Composite Steel		Noncomp. Steel		Prestr. Concrete		Reinf. Concrete	
		2B	3B	4A, 4B	9A, 9B	5A, 5B	6A, 6B	7A, 7B	8A, 8B
1. REGULAR TESTS (Test Classification Code 1)									
2	A	5450-1							
2	91		5453-1		5453-4		5453-3	5453-2	
3	315		5451-11			5451-12		5451-13	
3	415	5451-3	5451-14		5451-6	5451-4		5451-5	
		5452-1	5452-25		5452-3	5452-4		5452-2	
		5454-1	5452-26		5454-4	5454-2		5454-3	
			5452-27						
			5452-28						
3	B	5450-7					5450-6		
3	C	5450-2		5450-4		5450-3		5450-5	
3	513		5451-15		5453-8			5451-16	
			5453-7					5453-9	
			5453-38						

(Cont'd on next page)

TABLE 4 (cont'd)

Vehicles		Bridges							
No. of Axles	Number	Composite Steel		Noncomp. Steel		Prestr. Concrete		Reinf. Concrete	
		2B	3B	4A, 4B	9A, 9B	5A, 5B	6A, 6B	7A, 7B	8A, 8B
2. SPECIAL TESTS									
a. Blocked Vehicle Springs (Test Classification Code 2)									
2	91		5453-5						
3	513		5453-35						
b. Induced Initial Oscillations (Test Classification Code 3)									
2	94		5451-7			5451-8			
2	91		5453-6					5453-11	
3	513				5451-13			5453-14	
c. Induced Initial Oscillations, Blocked Vehicle Springs (Test Classification Code 4)									
2	91		5453-10						
3	5131				5453-36			5453-37	
d. Simulation of Continuous Traffic (Test Classification Code 8)									
3	4151		5452-19					5452-20	
	4171								
e. Eccentric Loading (Test Classification Code 5 and 6)									
2	91		5453-12						
2	94		5451-9			5451-10			
3	C			5450-8					
3	4151		5452-17					5452-18	
f. Sudden Braking (Test Classification Code 7)									
2	221					5451-17			

(Cont'd on next page)

TABLE 4 (cont'd)

Vehicles		Bridges							
No. Of Axles	Number	Composite Steel		Noncomp. Steel		Prestr. Concrete		Reinf. Concrete	
		2B	3B	4A, 4B	9A, 9B	5A, 5B	6A, 6B	7A, 7B	8A, 8B
3. TESTS FOR STATISTICAL STUDIES (Test Classification Code 1)									
a. Crawl Tests									
3	415	5451-18		5451-18	5451-18		5451-18		
b. Statistical Study of Vehicle Types									
3	415		5452-5 5452-15				5452-7 5452-13		5452-8 5452-14
3	417		5452-10 5452-15 5452-24				5452-9 5452-11 5452-22		5452-6 5452-12
3	513		5452-10 5452-15 5452-24				5452-9 5452-11 5452-22 5452-23		5452-6 5452-12
3	517		5452-5 5452-15				5452-7 5452-13		5452-8 5452-14 5452-21
5	324		5452-5 5452-15				5452-7 5452-13		5452-8 5452-14 5452-21
5	325		5452-10 5452-15				5452-9 5452-11 5452-22		5452-6 5452-12
5	327		5452-24				5452-23		

TABLE 5 COMPUTED PROPERTIES OF BRIDGES

Bridge Type and Number	Total Weight, kips	Modulus of Elasticity, ksi · 10^3		Moment of Inertia*, $in^4 \cdot 10^3$			Total EI*, $kip\text{-}in^2 \cdot 10^6$	Dead-Load Deflection, inches	Computed Frequency, cps
		Beam	Slab	Beam 1	Beam 2	Beam 3			
(1)	(2)	(3)	(4)	(5)	(6)	(7)	(8)	(9)	(10)
Composite Steel									
2B	72.9	30.0	5.2	3.81	3.84	4.00	348.2	0.69	4.26
3B	76.2	30.0	5.2	4.36	4.29	4.16	384.3	0.61	4.52
Non-comp. Steel									
4A	75.8	30.0	5.2	1.17	1.17	1.18	126.5	1.76	2.64
4B	76.0	30.0	5.2	1.21	1.18	1.17	127.9	1.75	2.66
9A	84.4	30.0	5.2	2.10	2.12	2.13	214.2	1.20	3.21
9B	82.4	30.0	5.2	2.10	2.13	2.13	213.0	1.18	3.23
Prestr. Concrete									
5A	102.7	5.7	5.6	64.2	64.5	70.3	1,135.0	0.25	7.00
5B	102.8	5.7	5.6	62.4	63.4	69.1	1,111.0	0.26	6.91
6A	102.4	5.7	5.6	61.3	61.5	64.8	1,069.0	0.27	6.80
6B	103.8	5.7	5.6	61.1	60.6	65.8	1,069.0	0.27	6.75
Reinf. Concrete									
7A	102.2	5.0	5.0	14.8	14.8	15.0	220.5	1.31	3.08
7B	102.7	5.0	5.0	14.8	14.8	15.0	222.9	1.29	3.10
8A	103.4	5.0	5.0	15.9	15.8	15.3	235.1	1.24	3.16
8B	103.3	5.0	5.0	15.8	15.7	16.3	239.0	1.22	3.19

* For non-prismatic beams, values shown refer to cover-plated sections.

TABLE 6 TYPICAL MAXIMUM CRAWL MEASUREMENTS

Results are for a Section Across Midspan

Bridge and Subseries	Bottom Strain (μ in./in.)			Deflection (in.)		
	Beam 1	Beam 2	Beam 3	Beam 1	Beam 2	Beam 3
Composite Steel						
2B--5451-3	219	187	169	0.540	0.535	0.446
	195	187	192	0.486	0.537	0.500
	195	189	192	0.488	0.537	0.503
	193	187	196	0.484	0.535	0.498
	193	191	192	0.482	0.549	0.500
	196	187	192	0.482	0.537	0.496
	193	187	188	0.482	0.540	0.496
Average	198	188	189	0.492	0.539	0.491
Prestr. Concrete	154	147	222	0.177	0.208	0.173
5A--5451-4	150	142	224	0.172	0.193	0.166
	152	138	212	0.174	0.196	0.161
	108	105	169	0.151	0.143	0.156
	109	118	159	0.148	0.177	0.156
	116	107	162	0.152	0.177	0.143
Average	-	-	-	-	-	-
Prestr. Concrete	5.9	48	52	0.095	0.094	0.077
5B--5451-12	6.0	46	53	0.098	0.093	0.077
	5.9	47	50	0.093	0.091	0.074
	6.0	47	50	0.095	0.091	0.074
Average	6.0	47	51	0.095	0.092	0.076
Reinf. Concrete	348	339	338	0.514	0.556	0.641
7A--5451-5	340	337	337	0.509	0.562	0.585
	352	339	336	0.514	0.558	0.641
	352	345	338	0.518	0.558	0.648
	355	345	346	0.514	0.562	0.648
	359	347	338	0.523	0.576	0.645
Average	353	342	339	0.515	0.562	0.635
Non-Comp. Steel	139	175	169	0.820	0.785	0.770
9B--5451-6	162	167	163	0.807	0.770	0.767
	163	172	169	0.803	0.780	0.767
	161	169	163	0.810	0.760	0.743
	157	167	163	0.785	0.758	0.748
	157	167	167	0.768	0.758	0.757
Average	156	170	166	0.799	0.769	0.759

TABLE 7 SUMMARY OF AVERAGE CRAWL MEASUREMENTS

Bridge and Subseries	Average bottom strain (μ in/in)				Average Deflection (inches)			
	Beam 1	Beam 2	Beam 3	Beam 2 Max. % Deviation	Beam 1	Beam 2	Beam 3	Beam 2 Max. % Deviation
(1)	(2)	(3)	(4)	(5)	(6)	(7)	(8)	(9)
2B-Composite Steel								
5450-2	202	155	199	0.6	0.476	0.471	0.442	0.0
5451-3	198	188	189	1.6	0.492	0.539	0.491	1.9
5452-1	191	180	186	1.1	0.473	0.479	0.436	0.8
5454-1	185	183	178	1.1	0.516	0.480	0.445	1.0
3B-Composite Steel								
5451-7	124	125	124	5.6	0.260	0.310	0.290	3.2
(1)5451-9	21	56	113	5.5	0.056	0.152	0.235	2.0
(2)5451-9	88	124	165	2.4	0.208	0.310	0.359	0.3
5451-11	120	110	105	2.7	0.293	0.293	0.263	1.0
5451-14	179	173	163	2.3	-	0.386	0.398	3.1
5451-15	210	195	189	2.1	0.528	0.523	0.487	1.1
(2)5452-17	133	168	220	1.8	0.289	0.422	0.428	8.1
5452-25	181	180	171	2.2	0.426	0.409	0.390	3.7
5452-26	172	164	153	0.6	0.401	0.349	0.432	5.2
5452-27	174	169	156	6.5	0.470	0.430	0.470	4.7
5452-28	176	171	162	1.8	0.450	0.430	0.450	0.0
5453-1	131	121	115	0.8	0.276	0.270	0.268	1.9
5453-5	126	129	128	1.6	0.284	0.306	0.335	4.6
5453-6	135	134	129	1.5	0.306	0.302	0.282	3.6
5453-7	203	192	179	0.5	0.499	0.395	0.416	1.8
5453-10	131	130	122	1.5	0.267	0.270	0.274	1.1
(3)5453-10	126	127	126	1.6	0.254	0.256	0.277	3.9
(2)5453-12	85	124	166	1.6	0.184	0.273	0.507	0.7
5453-35	202	203	186	0.5	0.442	0.489	0.462	1.2
5453-38	205	211	191	1.4	0.517	0.487	0.434	3.1

(Contd on next page)

TABLE 7 (Cont'd)

Bridge and Subseries	Average bottom strain (μ in/in)				Average Deflection (inches)			
	Beam 1	Beam 2	Beam 3	Beam 2 Max. % Deviation	Beam 1	Beam 2	Beam 3	Beam 2 Max. % Deviation
(1)	(2)	(3)	(4)	(5)	(6)	(7)	(8)	(9)
9B-Non-Composite Steel								
5451-6	156	170	166	2.9	0.799	0.769	0.759	2.1
5452-3	164	163	161	3.7	0.737	0.664	0.694	3.8
5453-4	126	116	115	2.6	0.456	0.451	0.483	2.7
5453-8	198	194	194	2.1	0.880	0.777	0.772	1.2
(2)5453-13	197	196	194	1.0	0.896	0.744	0.754	4.6
5453-36	207	210	205	1.0	0.919	0.852	0.790	1.8
5454-4	169	178	161	3.9	0.726	0.703	0.733	11.4
9A-Non-Composite Steel								
5451-6	165	164	159	2.4	-	0.754	0.652	0.5
5452-3	164	160	170	3.1	0.776	0.810	0.701	3.2
5453-4	123	112	119	4.5	0.466	0.483	0.441	5.2
5453-8	193	189	195	3.2	0.935	0.951	0.865	2.9
(2)5453-13	194	188	194	12.2	0.931	0.925	0.866	2.2
5453-36	196	196	186	3.1	0.968	0.961	0.858	3.1
5454-4	170	175	168	4.0	0.748	0.755	0.795	6.1
5A-Prestr. Concrete								
5450-3	81	83	103	2.4	0.088	0.110	0.133	10.9
5451-8	98	97	-	6.3	0.100	0.104	0.108	3.8
(1)5451-10	80	36	18	8.8	0.081	0.047	0.021	4.3
(2)5451-10	117	85	86	5.0	0.124	0.098	0.077	4.1
5451-12	-	-	-	-	0.104	0.102	0.094	1.0
5452-4	177	139	221	3.6	0.169	0.187	0.206	2.1
5454-2	135	125	105	0.8	0.188	0.221	0.153	1.4

(Cont'd on next page)

TABLE 7 (Cont'd)

Bridge and Subseries	Average bottom strain (μ in/in)				Average Deflection (inches)			
	Beam 1	Beam 2	Beam 3	Beam 2 Max. % Deviation	Beam 1	Beam 2	Beam 3	Beam 2 Max. % Deviation
(1)	(2)	(3)	(4)	(5)	(6)	(7)	(8)	(9)
5B-Prestr. Concrete								
5450-3	-	-	-	-	-	0.115	-	10.4
5451-8	62	-	58	-	0.090	0.090	0.090	0.0
(1)5451-10	57	13	11	11.2	0.076	0.046	0.020	13.0
(2)5451-10	78	36	43	0.6	0.116	0.098	0.072	2.0
5451-12	60	47	51	1.3	0.095	0.092	0.076	2.2
5452-4	82	71	82	2.1	0.163	0.144	0.132	0.7
5454-2	84	71	69	2.7	0.173	0.152	0.140	5.3
6A-Prestr. Concrete								
5453-2	44	49	55	0.8	0.0933	0.0969	0.0900	2.5
6B-Prestr. Concrete								
5453-2	44	44	44	9.4	0.1097	0.0909	0.0851	2.5
7A-Reinf. Concrete								
5450-5	-	162	342	0.6	0.411	0.423	0.462	0.9
5451-5	353	342	339	1.5	0.515	0.562	0.635	2.5
5451-13	221	209	204	2.4	0.485	0.494	-	3.2
5451-16	400	392	399	0.5	0.983	0.966	1.013	1.1
(2)5452-18	368	344	314	1.2	0.742	0.679	0.595	1.0
5453-3	251	241	247	1.2	0.442	0.470	0.452	1.9
5453-9	404	377	389	1.1	0.885	0.816	0.770	0.2
5453-11	263	242	232	1.7	0.530	0.567	0.494	9.5
(3)5453-11	260	242	236	2.1	0.530	0.582	0.497	14.4
(2)5453-14	410	388	388	2.8	0.887	0.827	0.744	2.2
5453-37	404	392	382	2.0	0.770	0.787	0.790	2.4
5454-3	348	330	328	1.2	0.737	0.698	0.738	0.9

(Cont'd on next page)

TABLE 7 (Cont'd)

Bridge and Subseries	Average bottom strain (μ in/in)				Average Deflection (inches)			
	Beam 1	Beam 2	Beam 3	Beam 2 Max. % Deviation	Beam 1	Beam 2	Beam 3	Beam 2 Max. % Deviation
(1)	(2)	(3)	(4)	(5)	(6)	(7)	(8)	(9)
7B-Reinf. Concrete								
5450-5	-	-	-	-	-	0.646	-	2.3
5451-5	362	352	346	1.1	0.635	0.612	-	2.0
5451-13	232	229	217	1.3	0.424	0.510	0.419	0.6
5451-16	359	331	398	0.9	0.785	0.864	0.765	2.5
(2)5452-18	362	325	309	2.2	0.724	0.683	0.639	3.1
5453-3	252	267	258	4.1	0.478	0.472	0.475	1.5
5453-9	395	416	389	0.7	0.824	0.830	0.752	2.8
5453-11	261	264	257	1.5	0.493	0.463	0.440	3.0
(3)5453-11	260	263	260	2.7	0.480	0.463	0.442	3.0
(2)5453-14	402	412	394	1.9	0.840	0.832	0.767	1.2
5453-37	406	399	395	1.5	0.813	0.795	0.733	10.9
5454-3	338	346	326	2.0	0.693	0.678	0.699	0.7

Notes: (1) Eccentric crawl test - one line of wheels on bridge
(2) Eccentric crawl test - two lines of wheels on bridge
(3) Crawl test with vehicle moving in reverse direction

TABLE 8 COMPARISON OF MEASURED AND COMPUTED MOMENTS AND DEFLECTIONS

Results shown are for the three-axle vehicle No. 415

Bridge and Subseries		Sum of Moments in Three Beams			Aver. Deflection of Three Beams		
		Measured, in-kips	Computed, in-kips	Measured / Computed	Measured, in.	Computed, in.	Measured / Computed
(1)		(2)	(3)	(4)	(5)	(6)	(7)
Composite steel							
2B	5451-3	3,560	3,810	0.93	0.507		1.09
	5452-1	3,430		0.90	0.463	0.466	0.99
	5454-1	3,380		0.89	0.480		1.03
Non-comp. steel							
9A	5451-6	3,240	3,380	0.96	--		--
	5952-3	3,280		0.97	0.762	0.713	1.07
	5454-4	3,410		1.01	0.766		1.07
9B	5451-6	3,280	3,420	0.96	0.776		1.09
	5452-3	3,250		0.95	0.698	0.713	0.98
	5454-6	3,390		0.99	0.721		1.01
Prestr. concrete							
5A	5451-4	--		--	--		--
	5452-4	11,000	3,810	2.89	0.187	0.124	1.51
	5454-3	7,440		1.95	0.187		1.51
5B	5451-4	--	3,810	--	0.143		1.13
	5452-4	4,710		1.24	0.146	0.126	1.16
	5454-3	4,460		1.17	0.155		1.23
Reinf. concrete							
7A	5451-5	3,990	3,810	1.05	0.571		0.90
	5452-2	3,820		1.00	0.675	0.637	1.06
	5454-3	3,880		1.02	0.724		1.14
7B	5451-5	4,110	3,810	1.08	--		--
	5452-2	4,120		1.08	0.673	0.630	1.07
	5454-3	3,920		1.03	0.690		1.10

TABLE 9 AVERAGE MEASURED FREQUENCIES AND DAMPING OF BRIDGES

Measured Frequencies of Bridges Indicated with an Asterisk are from Series 5450; all Other Values are from Series 5452. Damping is Based on First to Fifth Maxima.

Bridge Type and Number	Frequency			Damping	
	Measured, cps	Computed, cps	Measured / Computed	Log Decrement	β_b Percent
(1)	(2)	(3)	(4)	(5)	(6)
Composite steel					
2B	4.17	4.26	0.98	0.07	1.1
3B	4.39	4.52	0.97	0.05	0.8
Non-Comp. steel					
4A	4.15	2.64	1.57	0.23	3.7
4B	4.46	2.66	1.68	0.29	4.6
9A	4.15	3.21	1.29	0.21	3.4
9B	4.00	3.23	1.24	0.19	3.0
Prestr. concrete					
5A	6.67	7.00	0.95	0.11	1.8
5B	6.89	6.91	1.00	0.08	1.3
6A	6.94	6.80	1.02	0.11	1.8
6B	6.78	6.75	1.01	0.04	0.6
Reinf. concrete					
7A	3.43	3.08	1.11	0.09	1.4
7B	3.21	3.10	1.04	0.10	1.6
8A	3.48	3.16	1.10	0.13	2.0
8B	3.59	3.19	1.12	0.12	1.9

TABLE 10

CHANGE IN MEASURED BRIDGE FREQUENCIES WITH TIME
Dates corresponding to tests shown are given in Table 2

Bridge Type and Number	Ratio of average measured frequency to computed frequency				
	Series 5450	Series 5451	Series 5452	Series 5453	Series 5454
Composite Steel					
2B	1.08	1.04	0.98	--	1.03
Non-Composite Steel					
9A	--	1.40	1.29	1.19	1.14
9B	--	1.40	1.24	1.19	1.05
Prestressed Concrete					
5A	1.00	0.97	0.95	--	0.97
5B	0.98	1.00	1.00	--	1.00
Reinforced Concrete					
7A	1.22	1.08	1.11	1.02	1.02
7B	1.18	1.04	1.04	1.00	1.01

TABLE 11

COMPARISON OF STIFFNESSES AND FREQUENCIES
OF "LOADED" AND UNLOADED BRIDGES

EI_L = Measured EI of "loaded" bridge

EI_U = Measured EI of unloaded bridge

EI_C = Computed EI

Bridge Type and Number	"Loaded" Bridge $\frac{EI_L}{EI_C}$	Unloaded Bridge $\frac{EI_U}{EI_C}$	Ratio $\frac{EI_U}{EI_L}$	Ratio $\frac{f_U}{f_L}$
(1)	(2)	(3)	(4)	(5)
Composite Steel				
2B	1.01	0.96	0.95	0.98
Non-Composite Steel				
9A	0.94	1.66	1.78	1.33
9B	0.94	1.54	1.64	1.28
Prestressed Concrete				
5A	0.66	0.90	1.37	1.16
5B	0.86	1.00	1.16	1.08
Reinforced Concrete				
7A	0.94	1.23	1.30	1.14
7B	0.94	1.08	1.16	1.08

TABLE 12 AVERAGE WEIGHTS OF TEST VEHICLES
For dimensions and typical plans and elevations see Figure 18

Vehicle		Average Axle Loads, kips			Total	Number
No. of Axles	Number	Front	Drive	Rear	Weight, kips	of Weighings
2	A	5.1	15.1	--	20.2	1
2	91	6.3	15.0	--	21.3	12
2	94	6.6	15.0	--	21.6	2
2	221	2.0	6.0	--	8.0	1
3	B	4.5	15.8	14.1	34.4	1
3	C	4.6	20.2	20.6	45.4	2
3	315	4.2	12.3	12.2	28.7	1
3	415	5.8	18.3	18.6	42.7	4
3	417	6.3	18.7	18.8	43.8	5
3	513	4.8	22.5	23.0	50.3	10
3	517	6.2	23.6	22.9	52.7	2
5	324	5.8	12.6-12.4	14.0-12.6	56.4	4
5	325	5.6	12.6-12.4	12.1-13.1	55.8	4

TABLE 13 SUMMARY OF LOAD-DEFLECTION CHARACTERISTICS OF VEHICLES
Values shown are averages of all available data

Vehicle No. of Axles	Vehicle Number	Axle	Static Axle Load, kips	Spring Constants, kips/in.		Deflection at Static Load, inches		Coeff. of Interleaf Friction, μ, percent
				Tires, k_t	Springs, k_s	Tires	Springs	
(1)	(2)	(3)	(4)	(5)	(6)	(7)	(8)	(9)
2	91	Front	6.3	10.3	4.0	0.6	1.6	8
		Drive	15.0	21.0	15.8	0.7	0.9	11
2	94 (7/59)	Front	6.6	13.5	9.4	0.5	0.7	8
		Drive	15.0	29.0	16.7	0.5	0.9	11
2	94 (6/60)	Front	6.6	9.5	5.8	0.7	1.1	--
		Drive	15.0	19.6	8.7	0.8	1.7	11
2	A	Front	5.1	8.9	3.6	0.6	1.4	--
		Drive	15.1	27.0	7.7	0.6	2.0	17
3	B	Front	4.5	8.9	3.6	0.5	1.7	--
		Drive	15.8	27.0	7.7	0.6	2.1	16
		Rear	14.1	26.1	15.8	0.5	0.9	20
3	C	Front	4.6	8.9	3.6	0.5	1.8	--
		Drive	20.1	24.7	8.3	0.8	2.4	17
		Rear	20.5	25.7	15.3	0.8	1.3	19
3	315	Front	--	--	--	--	--	--
		Drive	12.3	20.9	8.6	0.6	1.4	11
		Rear	12.2	19.9	12.3	0.6	1.0	18
3	415	Front	5.8	12.2	31.7	0.5	0.2	4
		Drive	18.4	26.8	7.6	0.7	2.4	13
		Rear	18.7	26.2	16.2	0.7	1.2	19
3	513	Front	4.7	9.8	1.6	0.5	2.9	11
		Drive	22.4	21.2	14.0	1.1	1.6	13
		Rear	22.6	26.1	24.0	0.9	0.9	--

TABLE 14 COMPUTED NATURAL FREQUENCIES OF AXLES AND VEHICLES

Vehicle		Condition of Springs	Axle Frequencies, cps			Vehicle Frequencies, cps	
No. of Axles	Number		Rear	Drive	Front	Bounce	Pitch
(1)	(2)	(3)	(4)	(5)	(6)	(7)	(8)
2	91	Blocked	--	3.7	4.0	3.8	4.4
		Free	--	2.4	2.1	2.3	2.6
2	94 (7/59)	Blocked	--	4.4	4.5	4.4	5.6
		Free	--	2.6	2.9	2.7	3.5
2	94 (6/60)	Blocked	--	3.6	3.8	3.6	4.2
		Free	--	2.5	2.3	2.4	2.7
2	A	Blocked	--	4.2	4.1	4.2	4.6
		Free	--	2.0	2.2	2.0	2.4
3	B	Blocked	4.3	4.1	4.4	4.1	4.5
		Free	2.6	1.9	2.4	2.0	2.4
3	C	Blocked	3.5	3.5	4.4	3.3	4.7
		Free	2.1	1.7	2.3	1.8	2.4
3	315	Blocked	4.0	4.1	--	--	--
		Free	2.5	2.2	--	--	--
3	415	Blocked	3.7	3.8	4.5	3.8	4.9
		Free	2.1	1.8	3.9	1.8	4.0
3	513	Blocked	3.4	3.0	4.6	3.1	4.6
		Free	2.3	1.9	1.7	1.7	2.0

TABLE 15

SUMMARY OF PARAMETERS FOR REGULAR TESTS

Bridge	Vehicle No.	Subseries No.	Max. speed parameter, α_{max}	Weight ratio, R	Frequency ratios: Springs blocked, φ_t	Frequency ratios: Springs free, φ_{ts}	Profile variation param.*, Δ
(1)	(2)	(3)	(4)	(5)	(6)	(7)	(8)
			(a) Three-Axle Vehicles				
Composite steel bridges							
2B	C	5450-2	0.15	0.62	0.76	0.37	0.9
2B	415	5451-3	0.17	0.59	0.86	0.41	1.3
2B	415	5452-1	0.15	0.59	0.91	0.43	1.4
2B	415	5454-1	0.15	0.59	0.87	0.41	1.7
3B	315	5451-11	0.15	0.38	0.87	0.47	1.2
3B	415	5451-14	0.15	0.56	0.81	0.39	1.0
3B	513	5451-15	0.16	0.66	0.64	0.41	0.6
3B	415	5452-25	0.17	0.56	0.88	0.42	1.2
3B	415	5452-26	0.17	0.56	0.85	0.40	1.2
3B	415	5452-27	0.17	0.56	0.86	0.41	1.2
3B	415	5452-28	0.18	0.56	0.87	0.41	1.2
3B	513	5453-7	0.13	0.66	0.66	0.42	0.8
Non-composite steel bridges							
9B	415	5451-6	0.16	0.52	0.84	0.40	0.7
9B	415	5452-3	0.17	0.52	0.95	0.45	0.9
9B	513	5453-8	0.18	0.61	0.84	0.54	0.6
9B	415	5454-4	0.19	0.52	1.04	0.49	1.0
Prestressed concrete bridges							
5A	C	5450-3	0.10	0.44	0.78	0.38	0.0
5A	315	5451-12	0.11	0.28	0.60	0.32	0.3
5A	415	5452-4	0.10	0.42	0.57	0.27	0.4
5A	415	5454-2	0.10	0.42	0.56	0.27	0.7
Reinforced concrete bridges							
7A	C	5450-5	0.17	0.44	0.94	0.45	-1.1
7A	315	5451-13	0.22	0.28	1.23	0.63	-1.3
7A	415	5451-5	0.22	0.42	1.15	0.54	-1.1
7A	513	5451-16	0.22	0.49	0.90	0.57	-0.7
7A	415	5452-2	0.20	0.42	1.11	0.53	-0.8
7A	513	5453-9	0.21	0.49	0.98	0.62	-0.4
7A	415	5454-3	0.21	0.42	1.21	0.57	-0.6

* Negative signs denote bridge cambered.

(Cont'd on next page)

TABLE 15 (Cont'd)

Bridge	Vehicle No.	Subseries No.	Max. speed parameter, α_{max}	Weight ratio, R	Frequency ratios: Springs blocked, Φ_t	Frequency ratios: Springs free, Φ_{ts}	Profile variation param.,* Δ
(1)	(2)	(3)	(4)	(5)	(6)	(7)	(8)
			(b) Two-Axle Vehicles				
Composite steel bridges							
2B	A	5450-1	0.18	0.28	0.91	0.43	1.3
3B	91	5453-1	0.14	0.28	0.78	0.51	1.3
Non-composite steel bridges							
9B	91	5453-4	0.17	0.26	0.97	0.63	0.9
Prestressed concrete bridges							
6A	91	5453-2	0.10	0.21	0.56	0.36	0.7
Reinforced concrete bridges							
7A	91	5453-3	0.21	0.21	1.18	0.76	-0.6

* Negative signs denote bridge cambered.

TABLE 16

RANGE OF BASIC BRIDGE-VEHICLE PARAMETERS FOR REGULAR TESTS

Parameters	Bridge Types			
	Composite Steel	Non-comp. Steel	Prestressed Concrete	Reinforced Concrete
(1)	(2)	(3)	(4)	(5)
Number of subseries				
2-axle vehicles	2	1	1	1
3-axle vehicles	12	4	4	7
Maximum value of speed parameter, α_{max}	0.18	0.19	0.11	0.22
Weight ratio, R				
2-axle vehicles	0.28	0.26	0.21	0.21
3-axle vehicles	0.38-0.66	0.52-0.61	0.28-0.44	0.28-0.49
Frequency ratios				
Springs blocked, φ_t				
2-axle vehicles	0.78-0.91	0.97	0.56	1.18
3-axle vehicles	0.64-0.91	0.84-1.04	0.56-0.78	0.90-1.23
Springs acting, φ_{ts}				
2-axle vehicles	0.43-0.51	0.63	0.36	0.76
3-axle vehicles	0.37-0.47	0.24-0.54	0.26-0.38	0.45-0.63
Profile variation parameter, Δ				
2-axle vehicles	1.3	0.9	0.7	(-0.6)*
3-axle vehicles	0.6-1.7	0.6-1.0	0.0-0.7	(-0.4)-(-1.3)

* Bridge cambered.

TABLE 17

TYPICAL AMPLITUDES OF INITIAL OSCILLATIONS IN REGULAR TESTS

Vehicle No. 91 - Right Drive Wheel

Bridge 3B - Subseries 5453-1				Bridge 7A - Subseries 5453-3			
Run Number	Speed, fps	Double-ampl. $2\Delta P_o/P_{st}$ At entrance	Average*	Run Number	Speed, fps	Double-ampl. $2\Delta P_o/P_{st}$ At entrance	Average*
15	36.2	0.22	0.17	17	34.9	0.13	0.15
7	43.5	0.29	0.14	6	35.2	0.13	0.14
10	45.9	0.31	0.15	14	35.7	0.18	0.16
14	49.4	0.36	0.18	10	40.6	0.20	0.17
3	51.6	0.31	0.16	5	43.4	0.20	0.14
13	58.4	0.40	0.17	13	50.0	0.40	0.20
9	59.0	0.40	0.20	15	55.5	0.44	0.23
4	61.0	0.44	0.25	9	55.8	0.53	0.24
11	64.6	0.36	0.25	16	61.5	0.58	0.29
12	65.3	0.36	0.25	12	64.2	0.49	0.30
	Mean	0.35	0.19	18	66.2	0.54	0.26
					Mean	0.36	0.21

* Averaged over five cycles of oscillation prior to entrance.

TABLE 18 PARAMETERS USED IN ANALYTICAL SOLUTIONS

Subseries Number	Bridge	Vehicle Number	$\frac{\Delta_c}{\delta_{st}}$	f_b, cps	$R = \frac{W}{W_b}$	Frequency Ratios						Coeff. of Interleaf Friction		
						$\varphi_{t,1}$	$\varphi_{t,2}$	$\varphi_{t,3}$	$\varphi_{ts,1}$	$\varphi_{ts,2}$	$\varphi_{ts,3}$	μ_1	μ_2	μ_3
5453-5	3B	91	1.79	4.37	0.277	0.868	0.762	-	-	-	-	-	-	-
5453-35	3B	513	1.79	4.44	0.652	0.975	0.636	0.721	-	-	-	-	-	-
5453-1	3B(1)	91	1.79	4.72	0.277	0.868	0.762	-	0.448	0.487	-	0.08	0.12	-
5453-7	3B	513	1.79	4.56	0.652	0.975	0.636	0.721	0.360	0.403	0.488	0.11	0.13	0.19
5452-25	3B	415	1.19	4.46	0.563	1.116	0.846	0.820	0.864	0.433	0.496	0.04	0.09	0.19
5452-25	3B	(2)	1.79	4.72	0.560	0.880	-	-	0.420	-	-	0.15	-	-
5450-1	2B	A	1.20	4.67	0.277	0.882	0.885	-	0.474	0.444	-	0.02	0.18	-
5450-2	2B	B	1.20	4.67	0.621	0.932	0.729	0.741	0.501	0.451	0.410	0.02	0.18	0.18
5450-7	2B	B	1.20	4.67	0.473	0.940	0.851	0.917	0.505	0.452	0.462	0.02	0.18	0.18
5453-2	6A	91	1.72	6.67	0.206	0.600	0.555	-	0.315	0.360	-	0.08	0.12	-
5453-3	7A	91	-0.40	3.14	0.206	1.272	1.177	-	0.668	0.763	-	0.08	0.12	-

Notes: (1) Spectrum curves obtained with $\varphi_{t,2} = 0.628$

$\varphi_{ts,2} = 0.463$

(2) Single-axle vehicle simulating effect of rear axle of Vehicle 415 $\alpha = 0.150$

TABLE 19 PARAMETERS USED IN ANALYTICAL HISTORY CURVES

All parameters, except as shown, are given in Table 18

Subseries Number	Bridge	Vehicle Number	Solution Number	$\alpha = \frac{vT_b}{2L}$	Variation in Frequency Ratio		Initial Vehicle Condition at Entrance			
					$\varphi_{t,2}$	$\varphi_{ts,2}$	$(P_o/P_{st})_2$	$(P_o/P_{st})_3$	$(\dot{P}_o/2\pi f_s P_{st})_2$	$(\dot{P}_o/2\pi \bar{f}_t P_{st})_3$
5453-5	3B	91	216	0.101	-	-	-	-	-	-
			248	0.106	-	-	0.920	-	-0.128	-
			245	0.091	-	-	0.750	-	-0.360	-
5453-35	3B	513	255	0.118	-	-	-	-	-	-
			254	0.118	-	-	1.000	0.850	-0.033	-0.171
5453-1	3B	91	203	0.138	-	-	-	-	-	-
			240	0.138	0.548	0.429	-	-	-	-
			241	0.138	0.706	0.492	-	-	-	-
			231	0.138	0.628	0.463	-	-	-	-
			229	0.138	0.628	0.463	1.160	-	-0.129	-
			232	0.128	0.628	0.463	-	-	-	-
			230	0.128	0.628	0.463	1.160	-	-0.129	-
5453-7	3B	513	251	0.120	-	-	-	-	-	-
			250	0.120	-	-	1.000	0.900	-0.108	-0.165
			253	0.130	-	-	-	-	-	-
			252	0.130	-	-	0.970	0.900	-0.051	-0.160
5450-1	2B	A	21	0.146	-	-	-	-	-	-
5453-2	6A	91	302	0.096	-	-	-	-	-	-
			308	0.102	-	-	-	-	-	-
5453-3	7A	91	300	0.204	-	-	-	-	-	-
			304	0.114	-	-	-	-	-	-

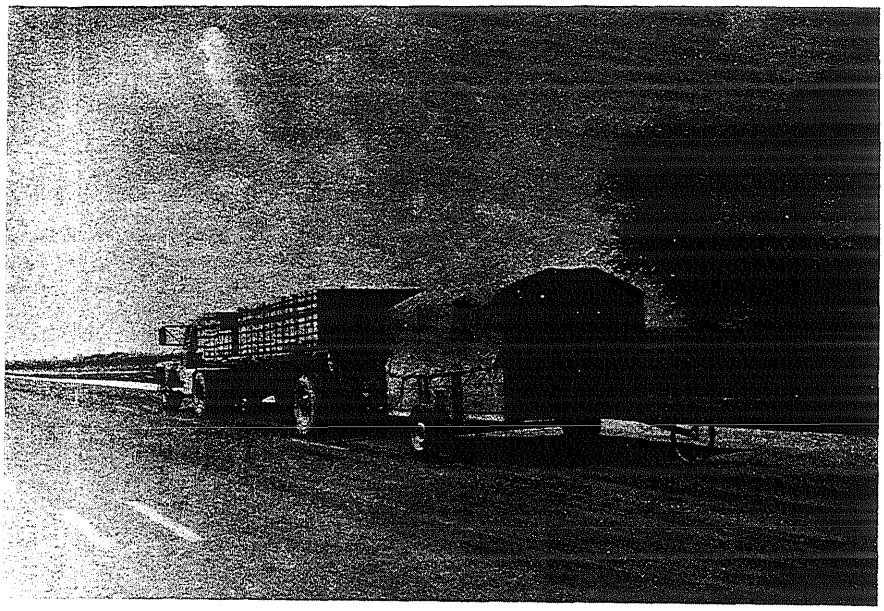

a. View of Vehicle No. 513 with Instrument Van

b. View of Vehicle Approaching Obstruction

FIG. 1 VIEWS OF TEST VEHICLES

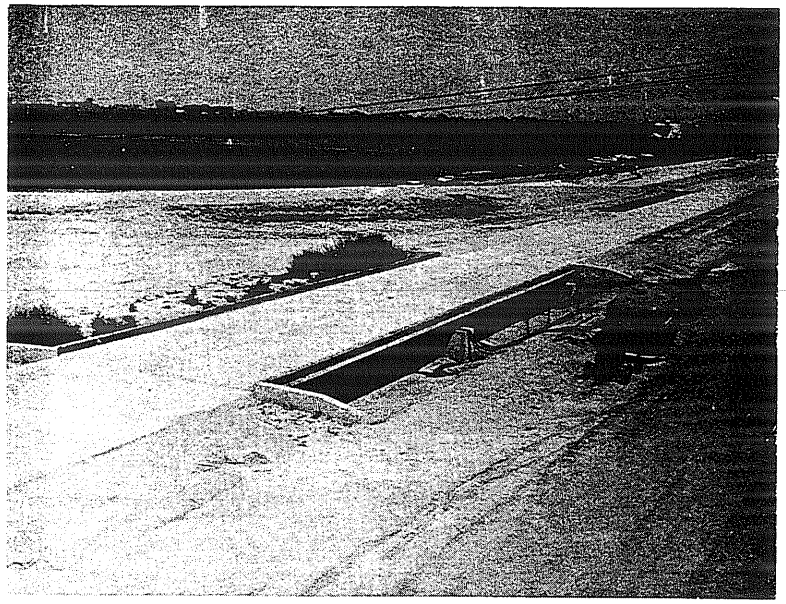

a. View of Bridges and Instrument Trailer

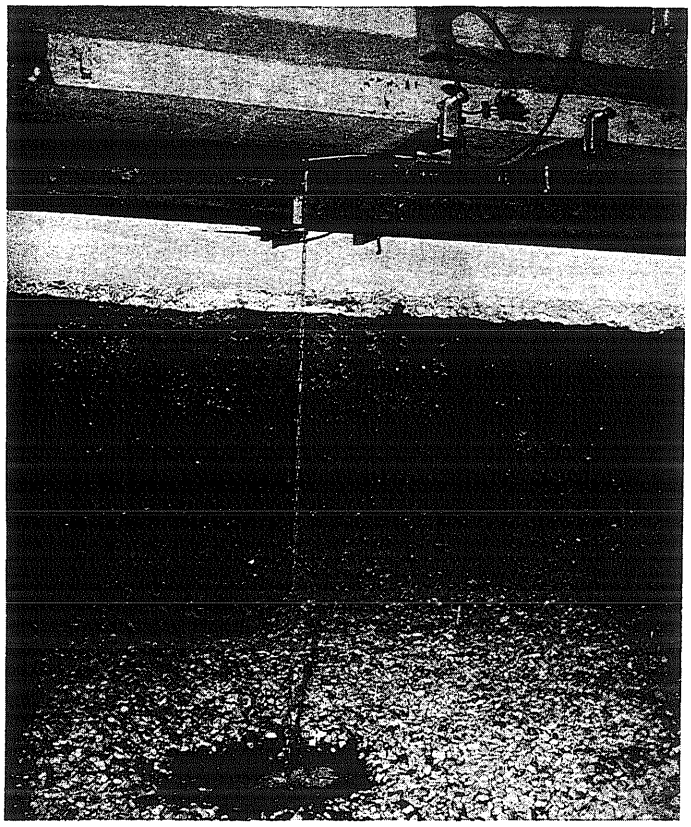

b. Closeup of Deflection Gage

FIG. 2 VIEWS OF TEST BRIDGES

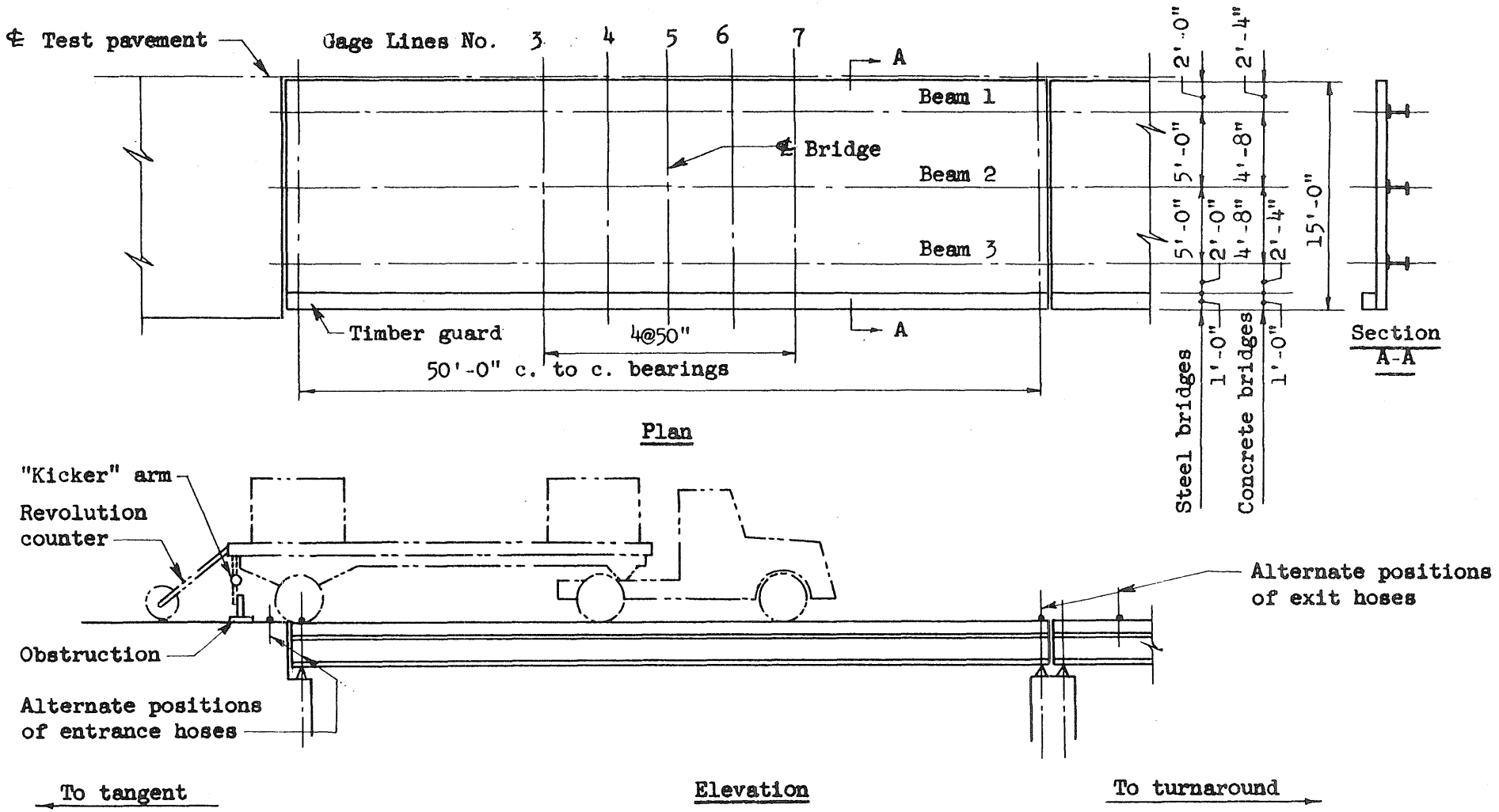

FIG. 3 TYPICAL BRIDGE LAYOUT FOR DYNAMIC TESTS

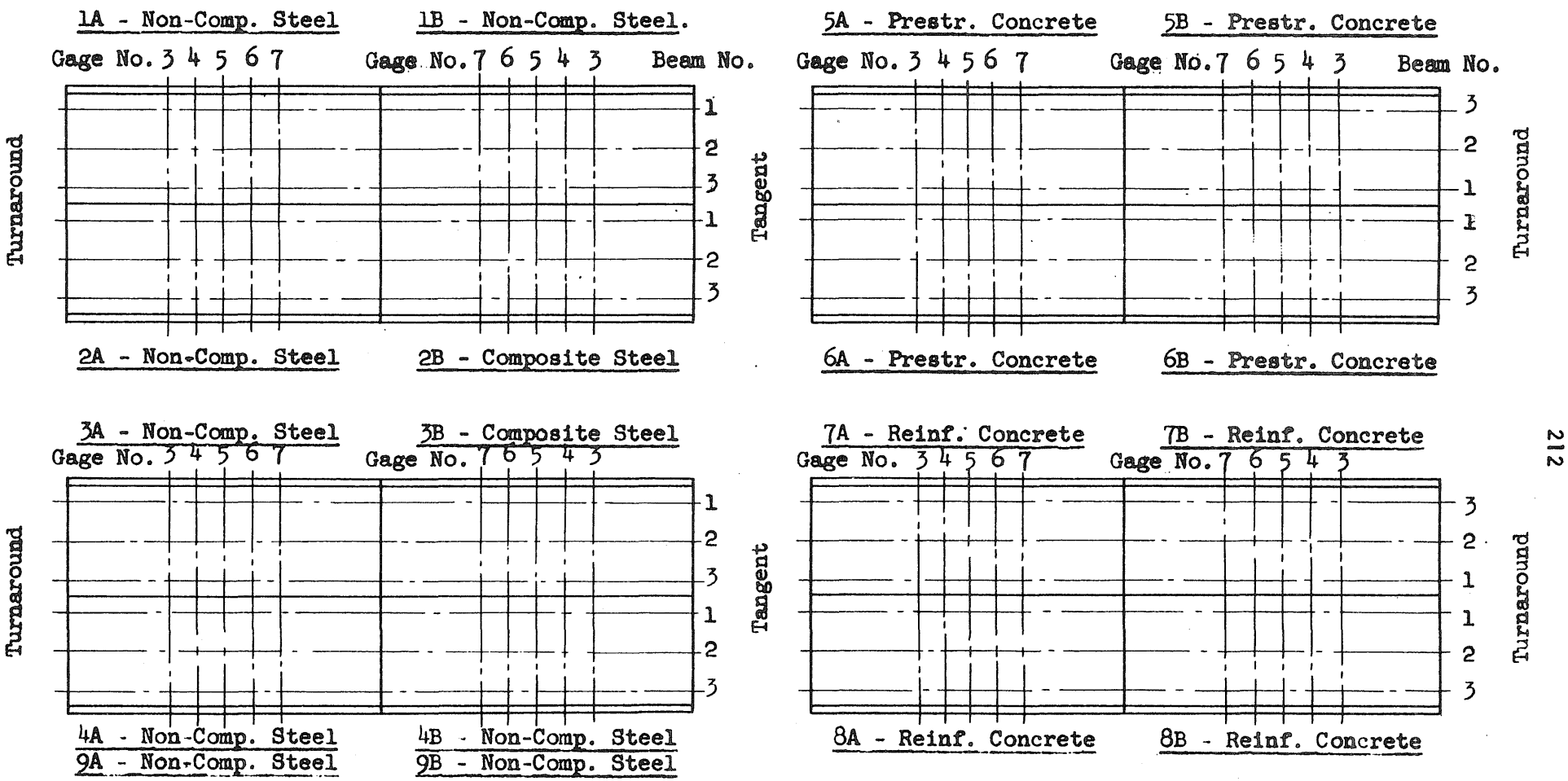

FIG. 4 LAYOUT OF TEST BRIDGES

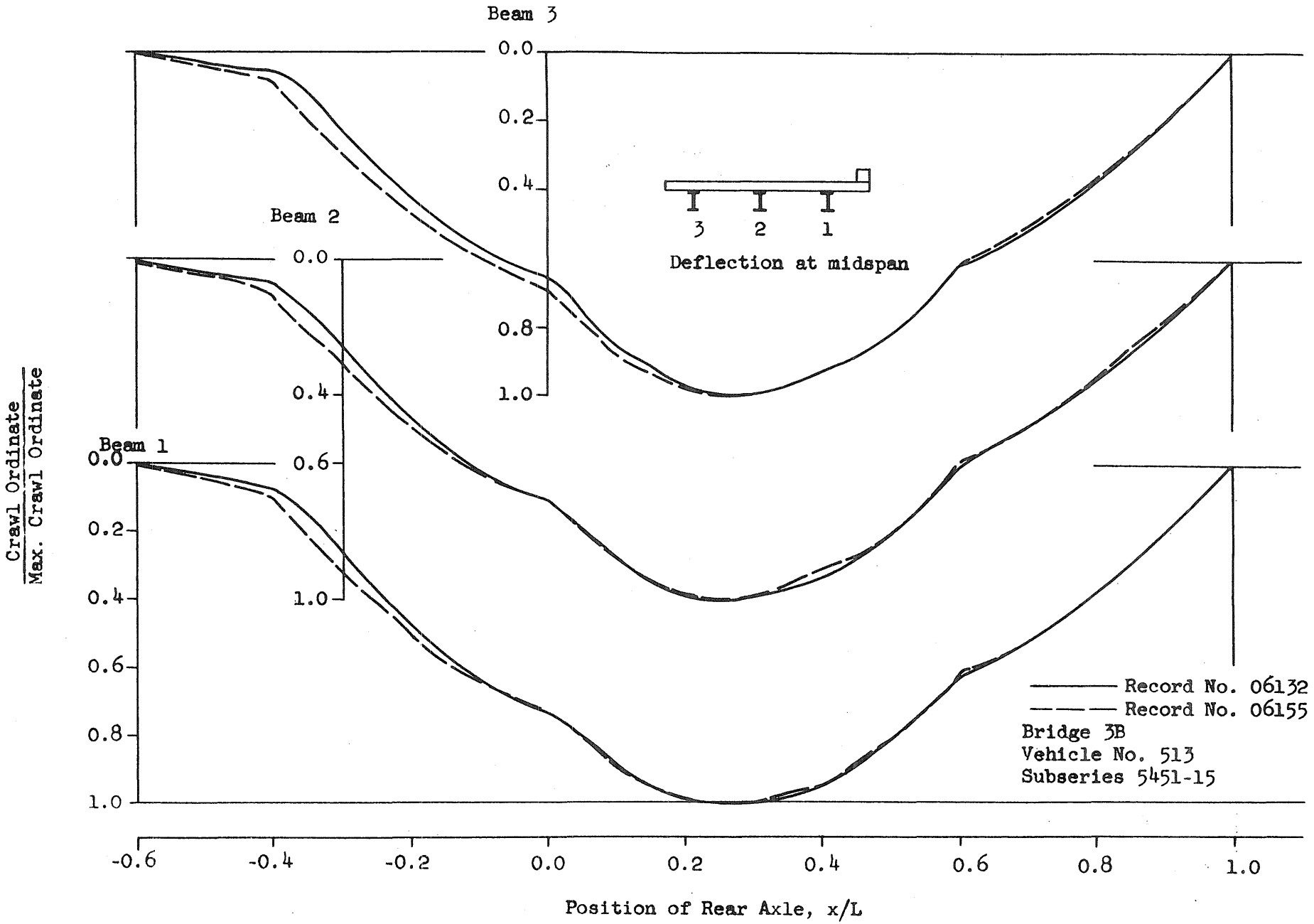

FIG. 5a REPLICATION OF CRAWL CURVES

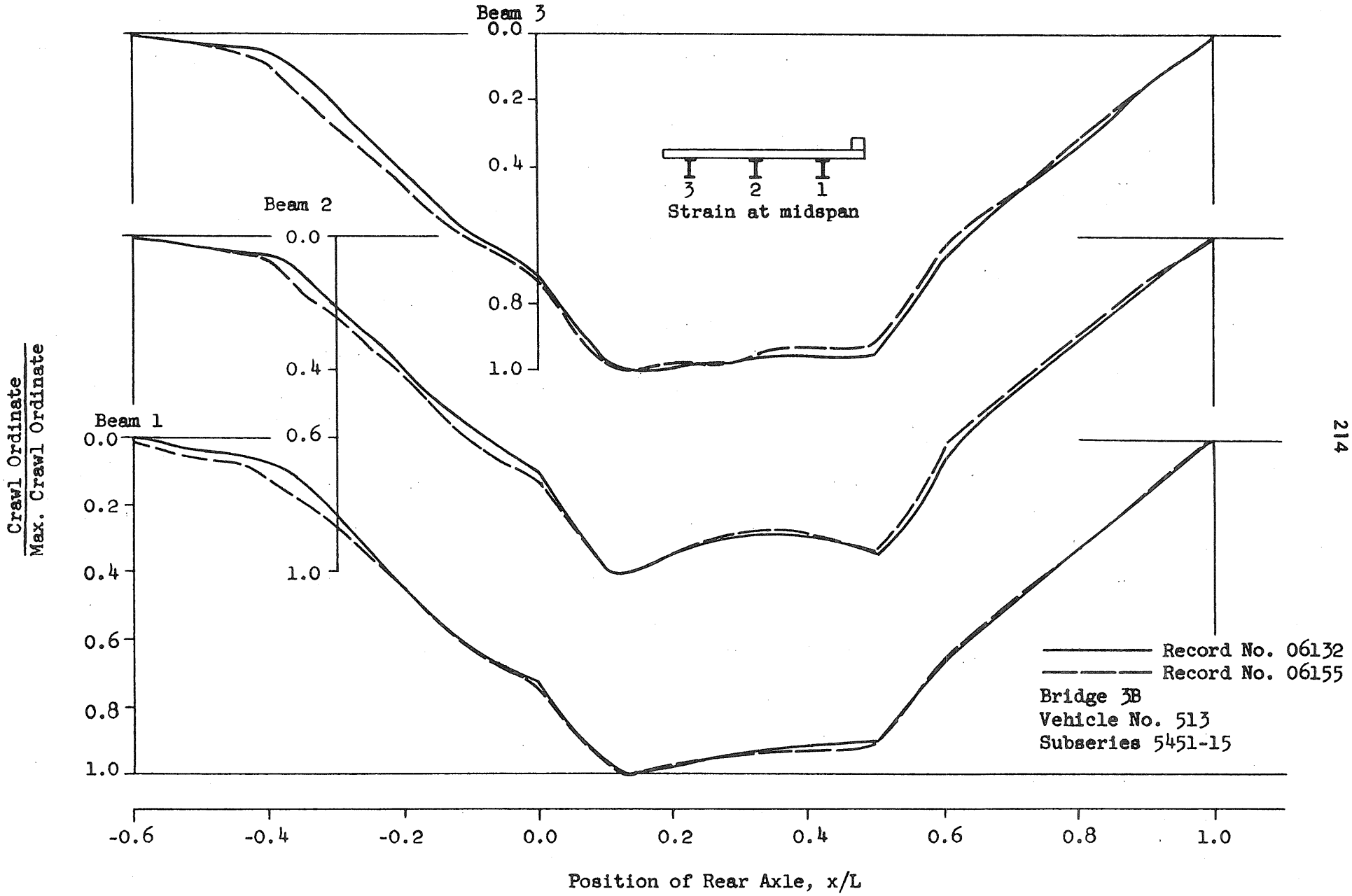

FIG. 5b REPLICATION OF CRAWL CURVES

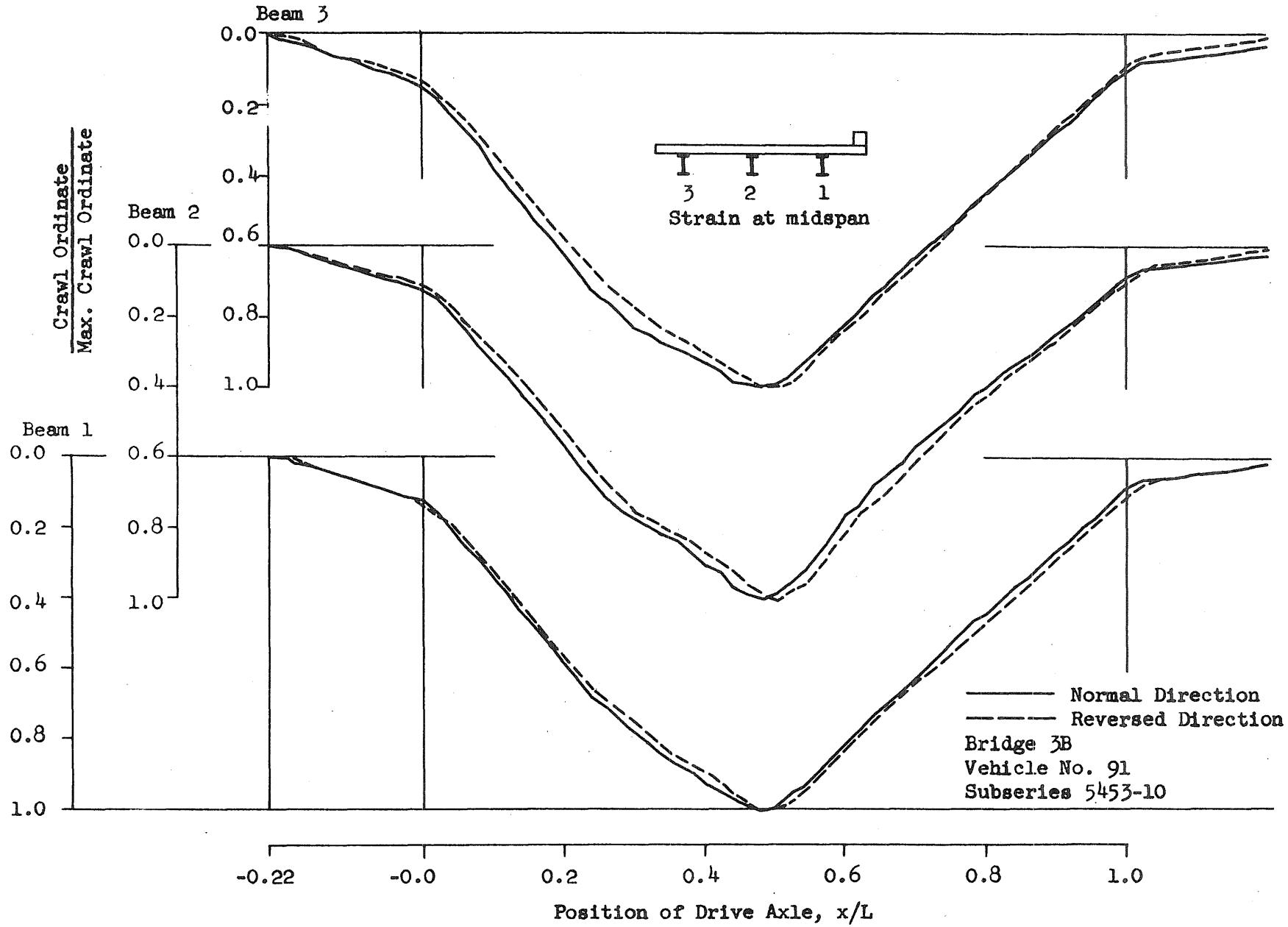

FIG. 6 SYMMETRY OF CRAWL CURVES

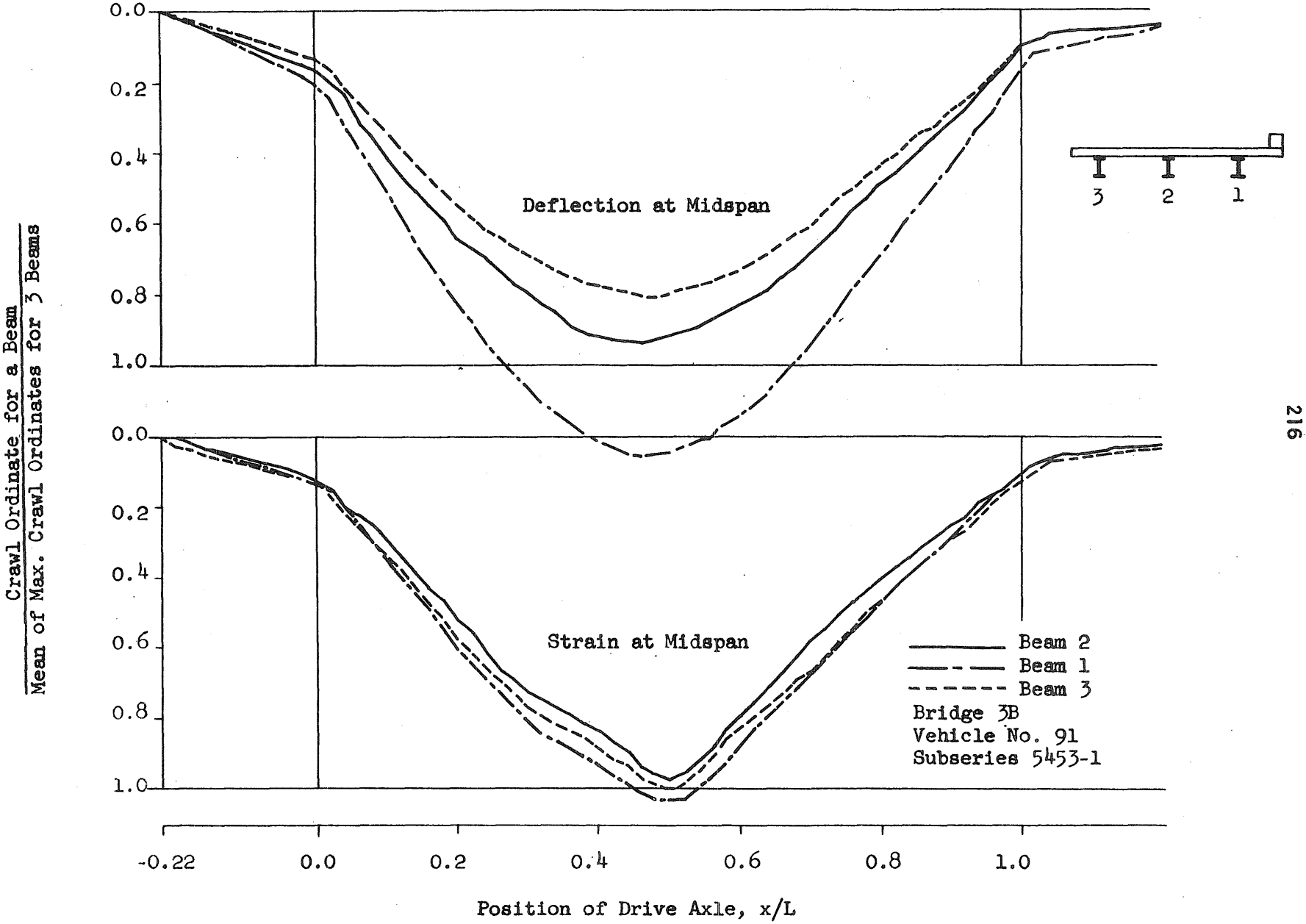

FIG. 7 RELATIVE MAGNITUDES OF CRAWL EFFECTS

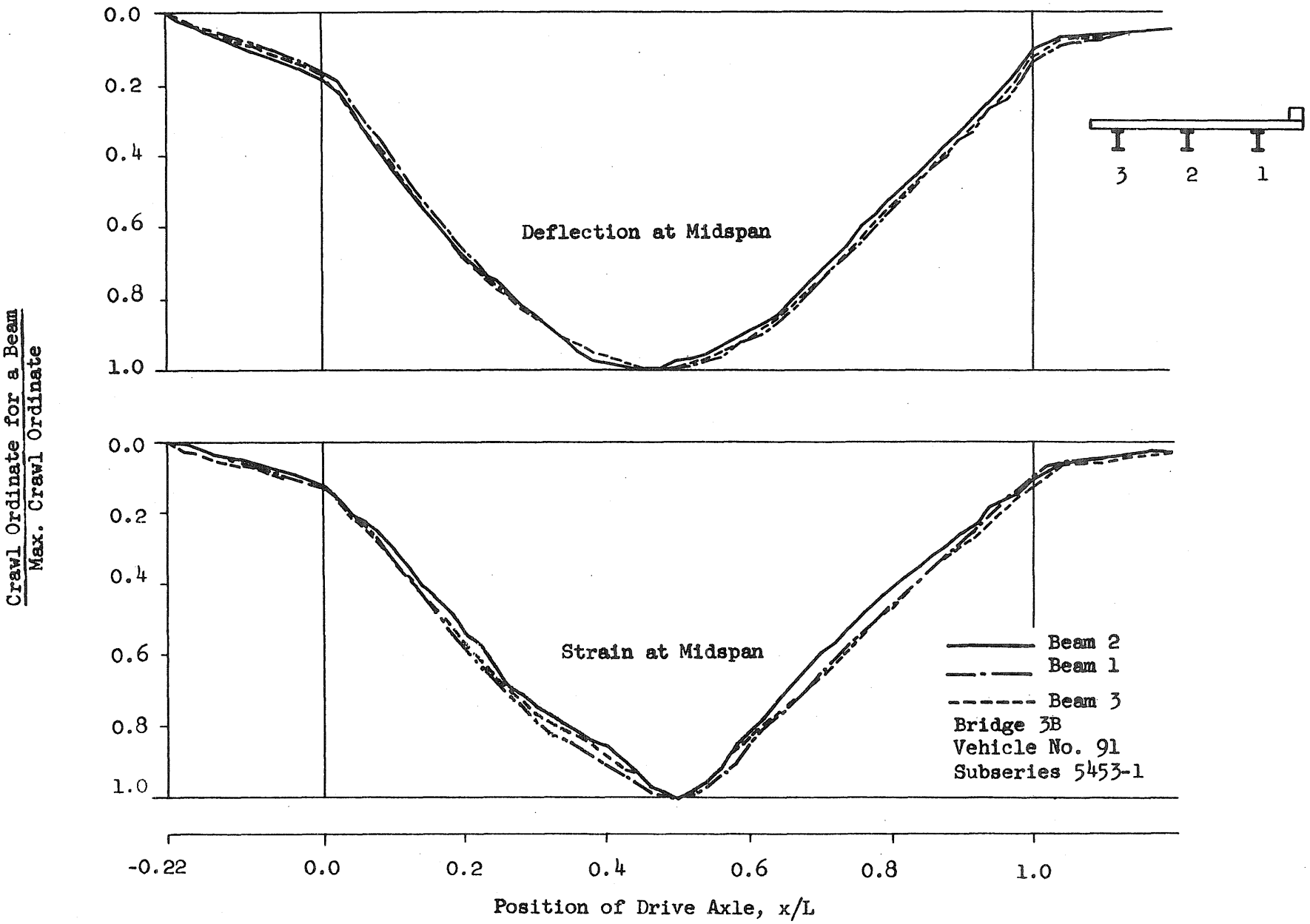

FIG. 8 COMPARISON OF SHAPES OF CRAWL CURVES

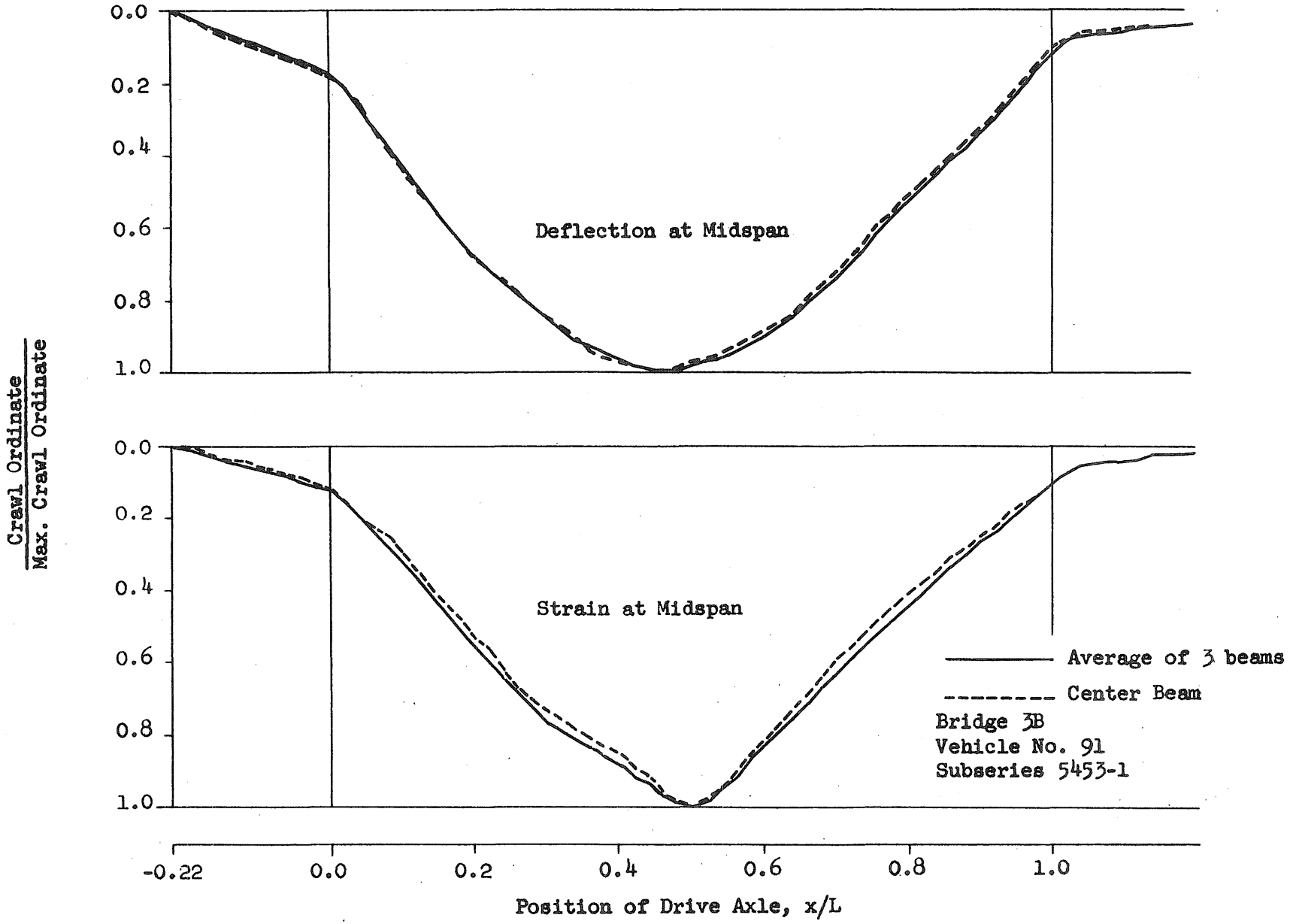

FIG. 9 COMPARISON OF AVERAGE AND CENTER BEAM CRAWL CURVES

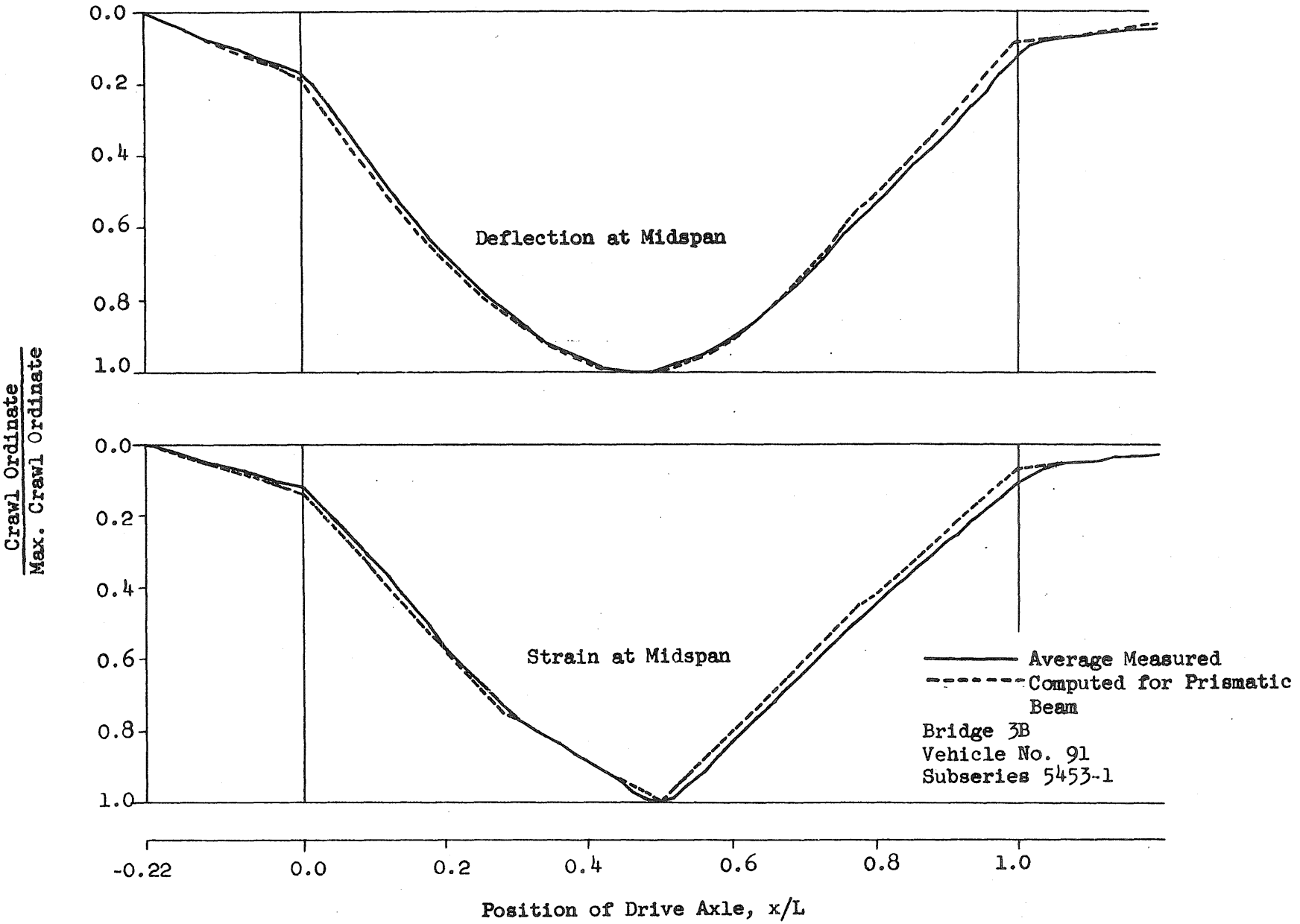

FIG. 10 COMPARISON OF MEASURED AND COMPUTED CRAWL CURVES

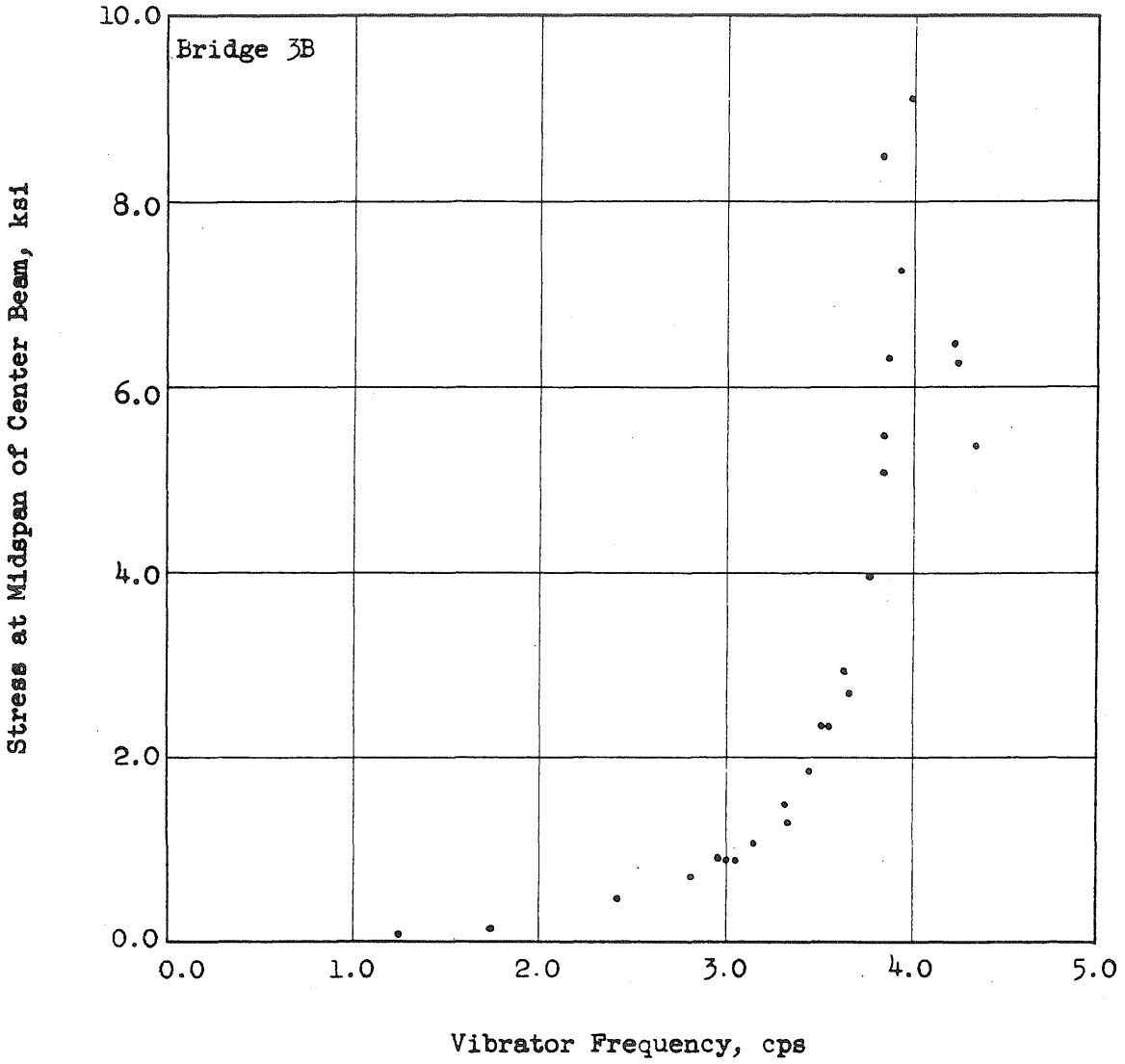

FIG. 11 TYPICAL FREQUENCY - RESPONSE CURVE

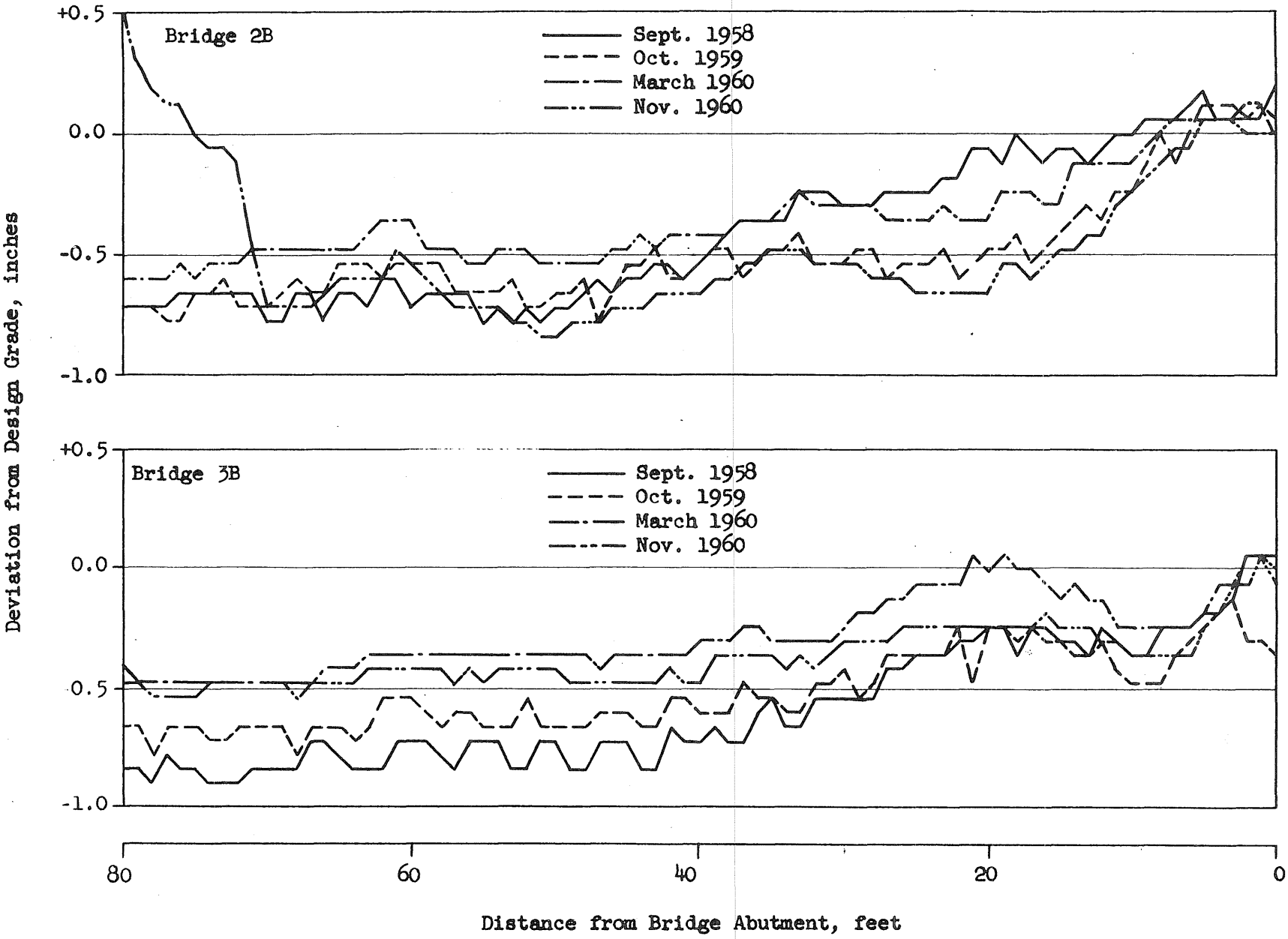

FIG. 12a LONGITUDINAL PROFILE OF APPROACH PAVEMENTS

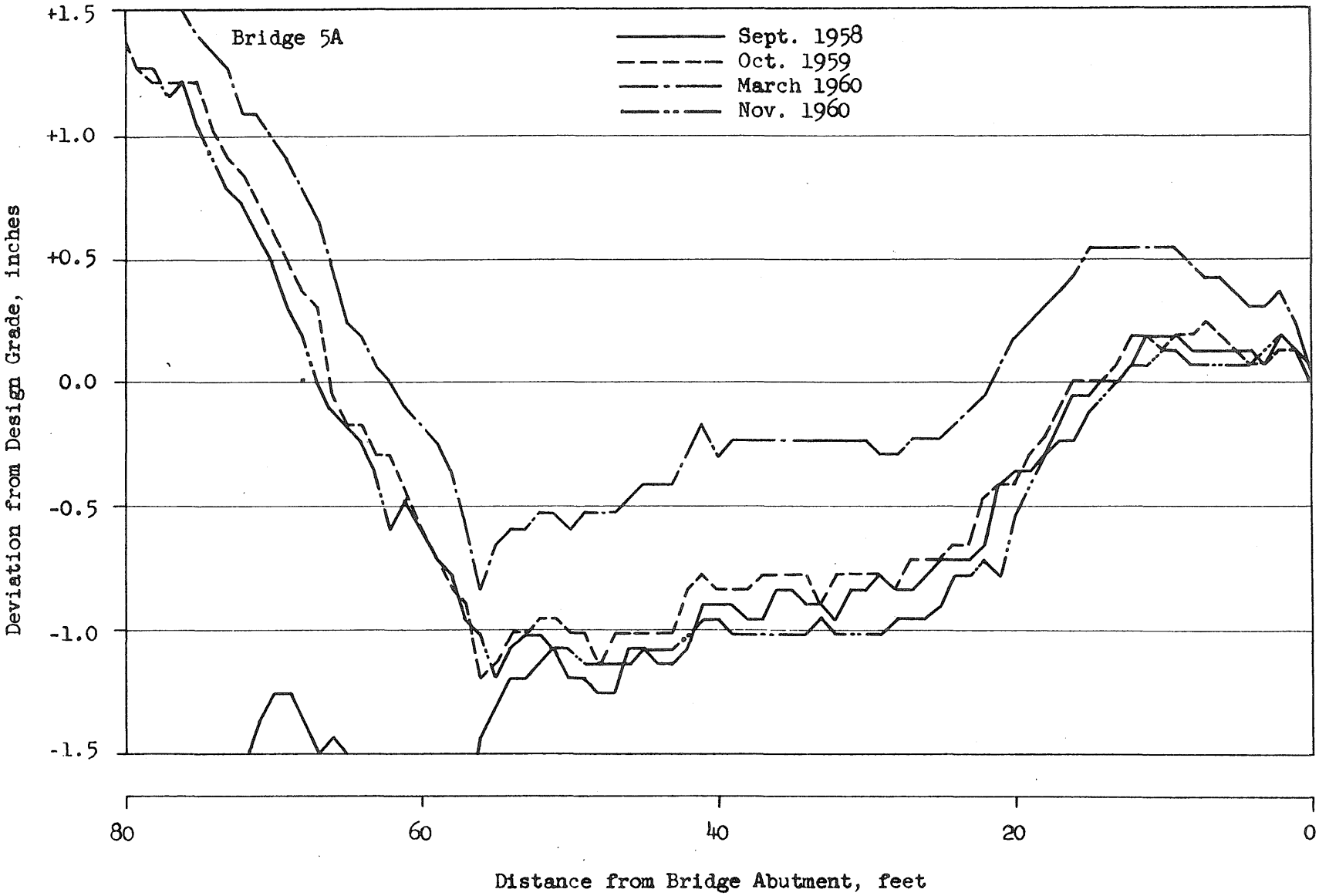

FIG. 12b LONGITUDINAL PROFILE OF APPROACH PAVEMENTS

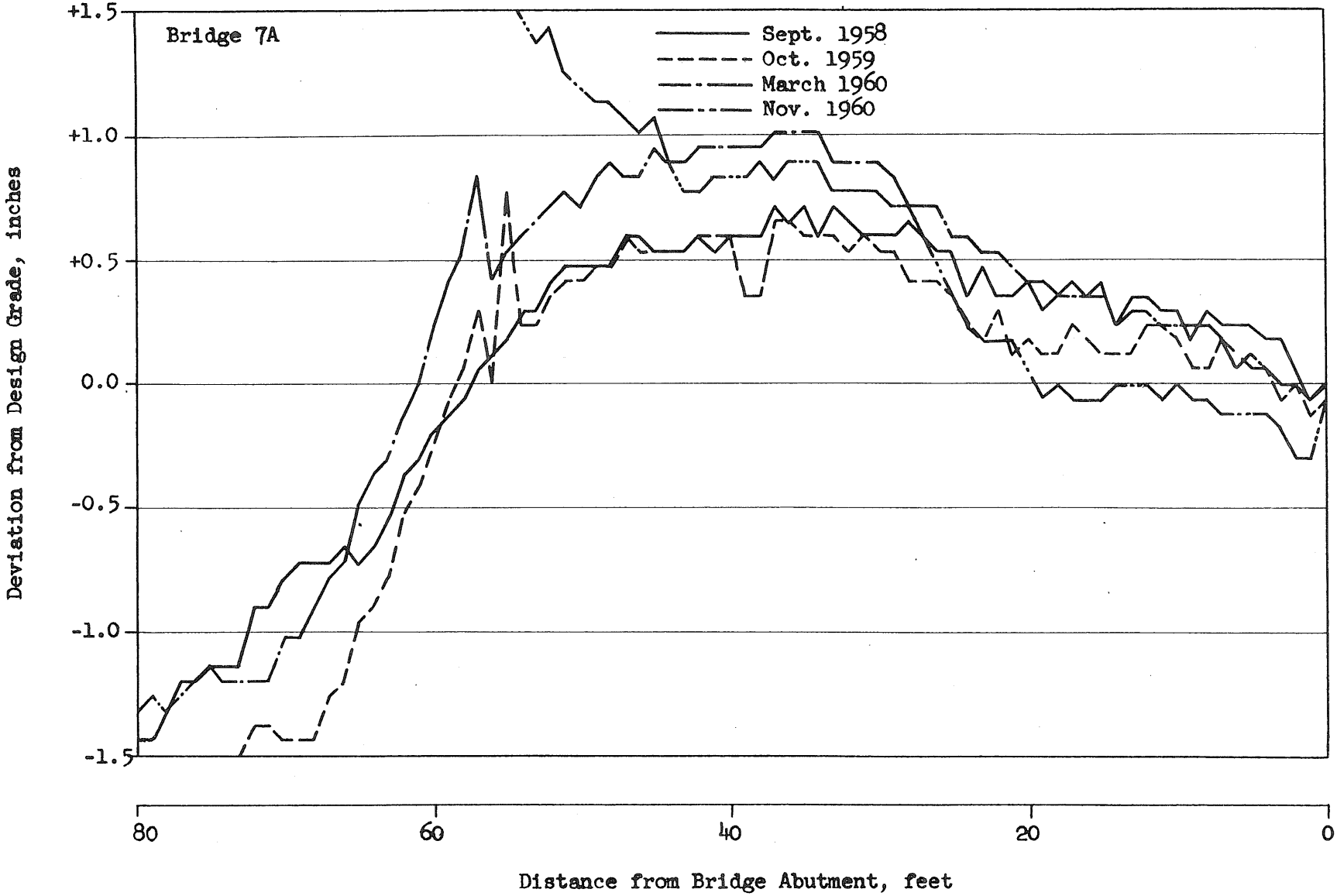

FIG. 12c LONGITUDINAL PROFILE OF APPROACH PAVEMENTS

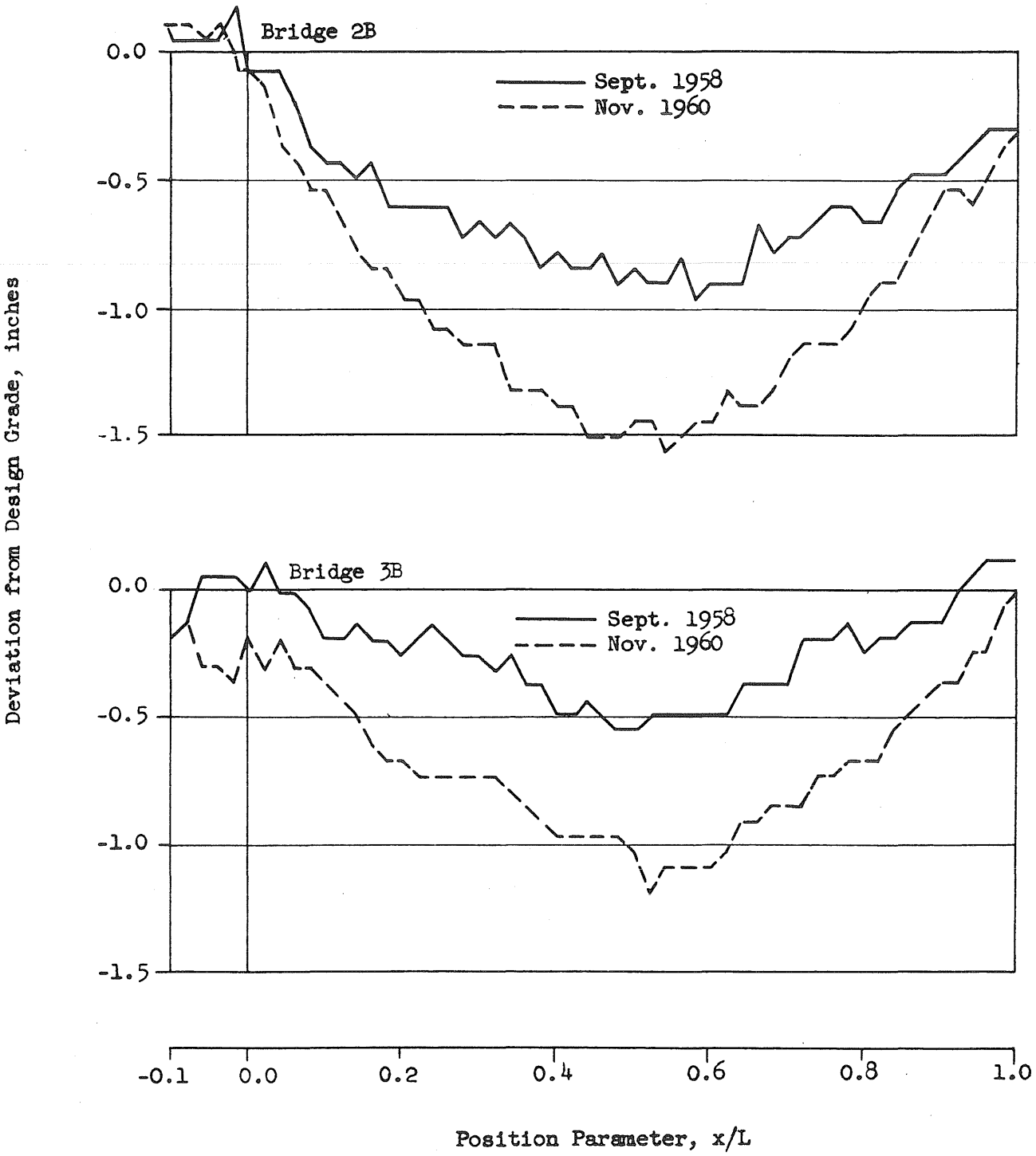

FIG. 13a LONGITUDINAL PROFILE OF BRIDGES

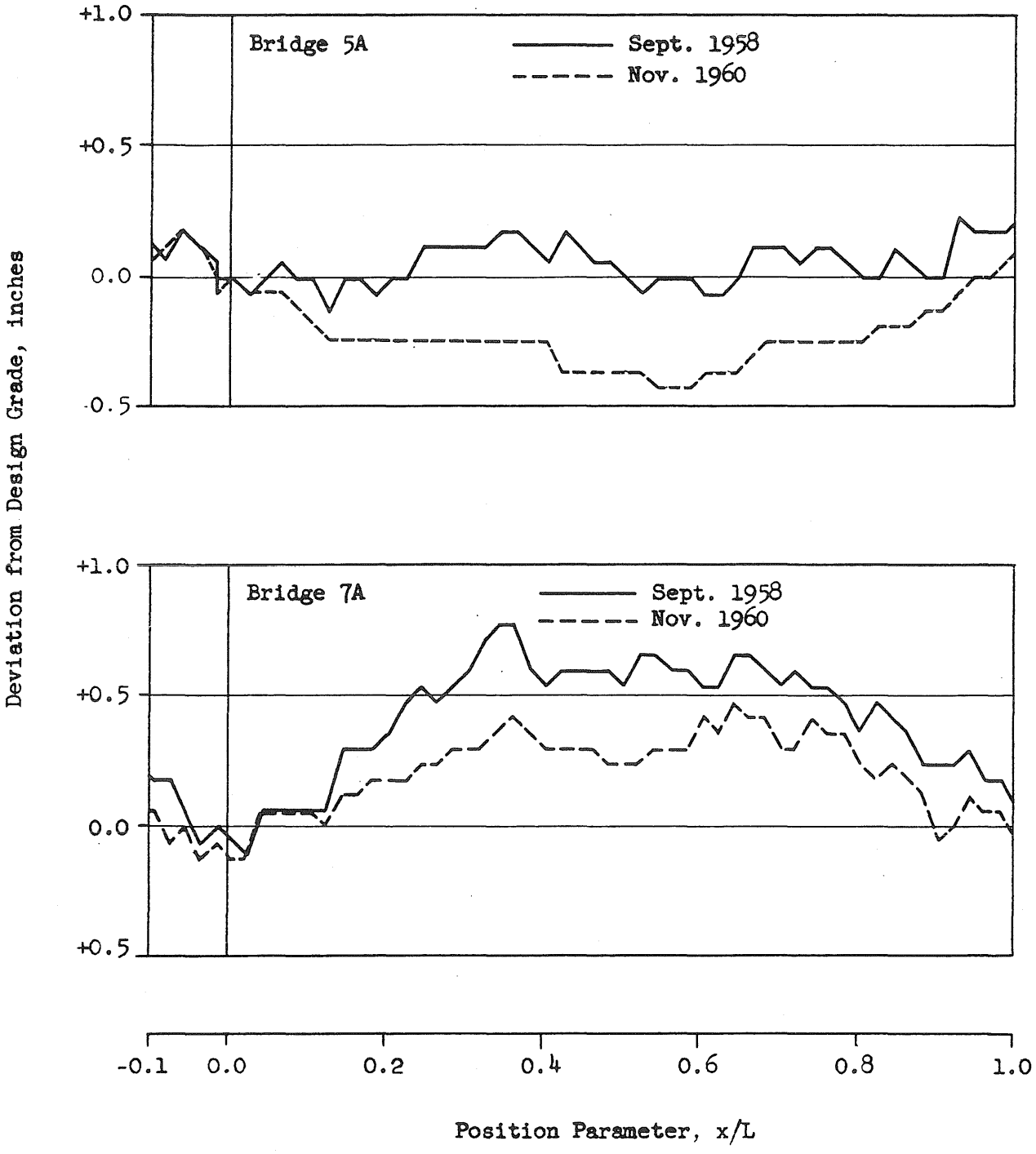

FIG. 13b LONGITUDINAL PROFILE OF BRIDGES

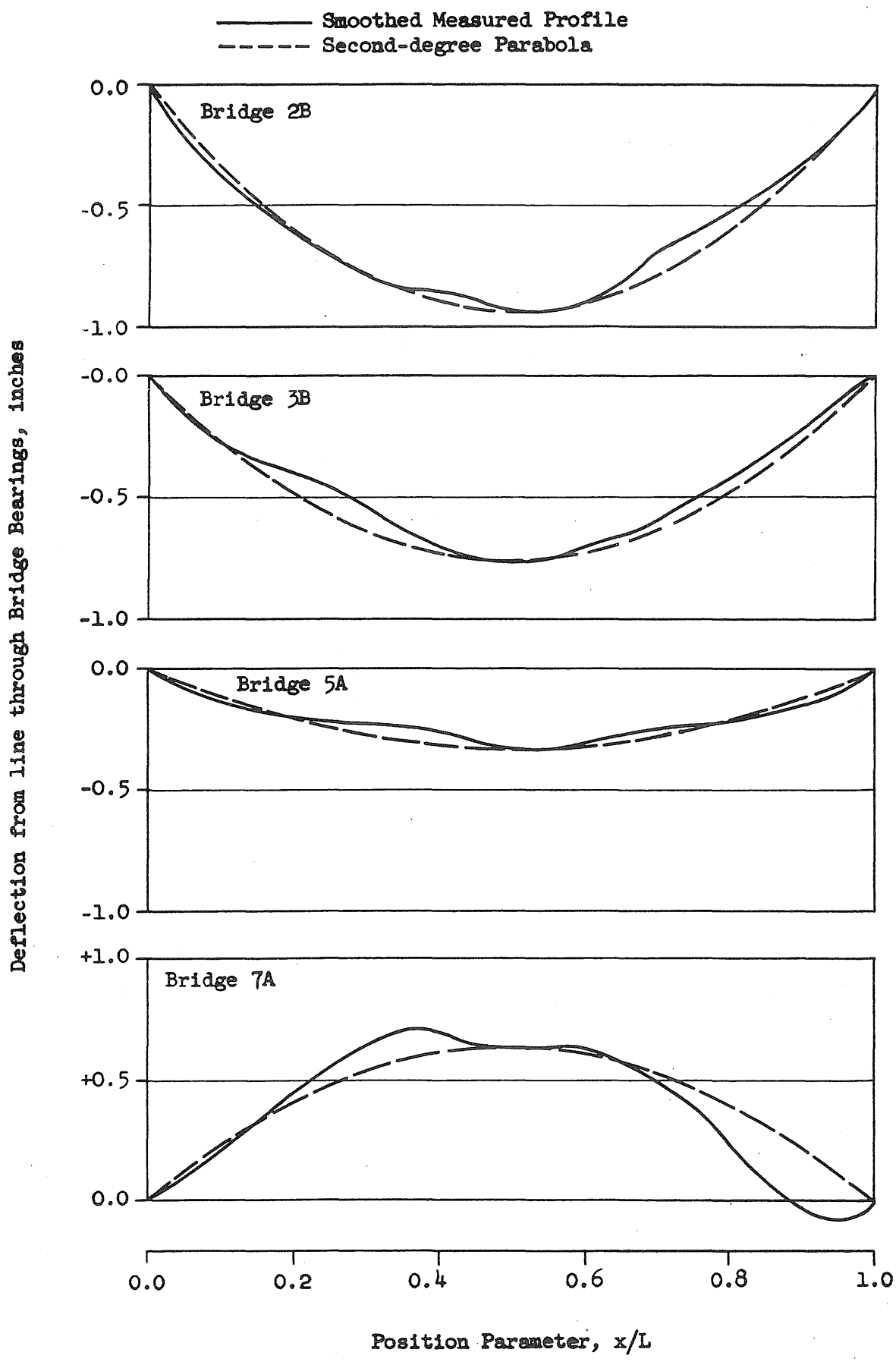

FIG. 14 COMPARISON OF LONGITUDINAL BRIDGE PROFILES
All curves for March, 1960

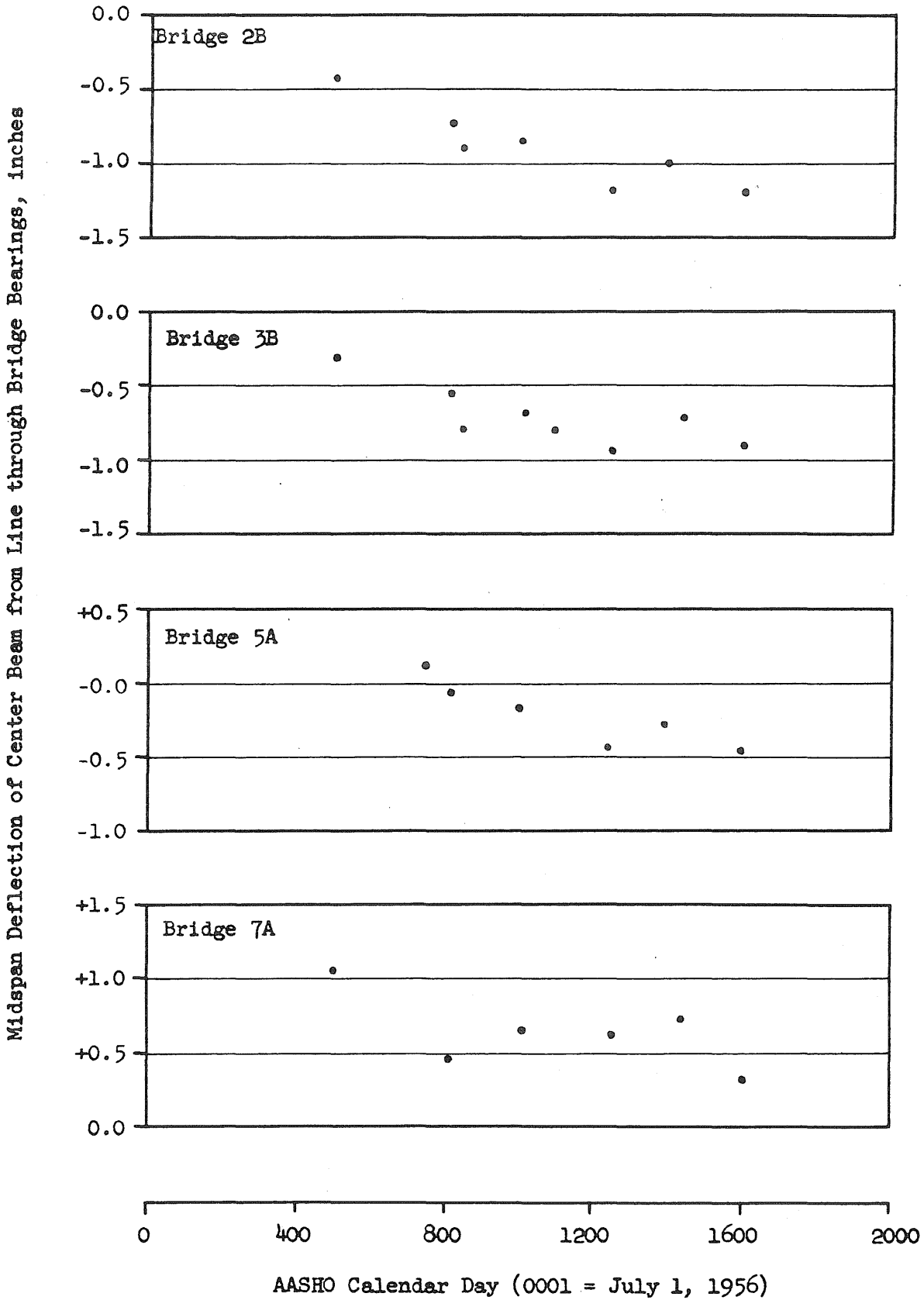

FIG. 15 CHANGE IN BRIDGE DEFLECTION WITH TIME

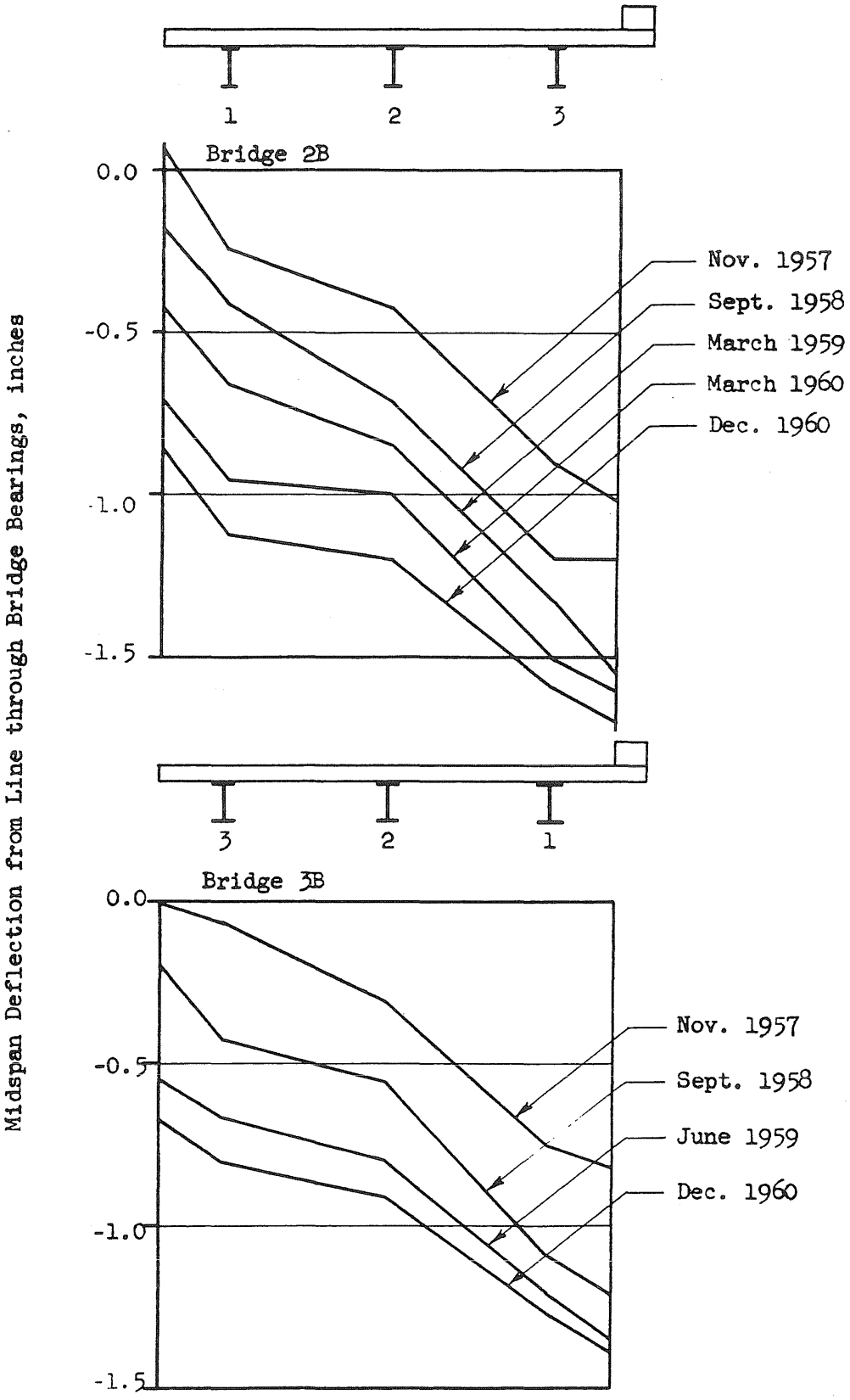

FIG. 16a LATERAL PROFILE OF BRIDGES AT MIDSPAN

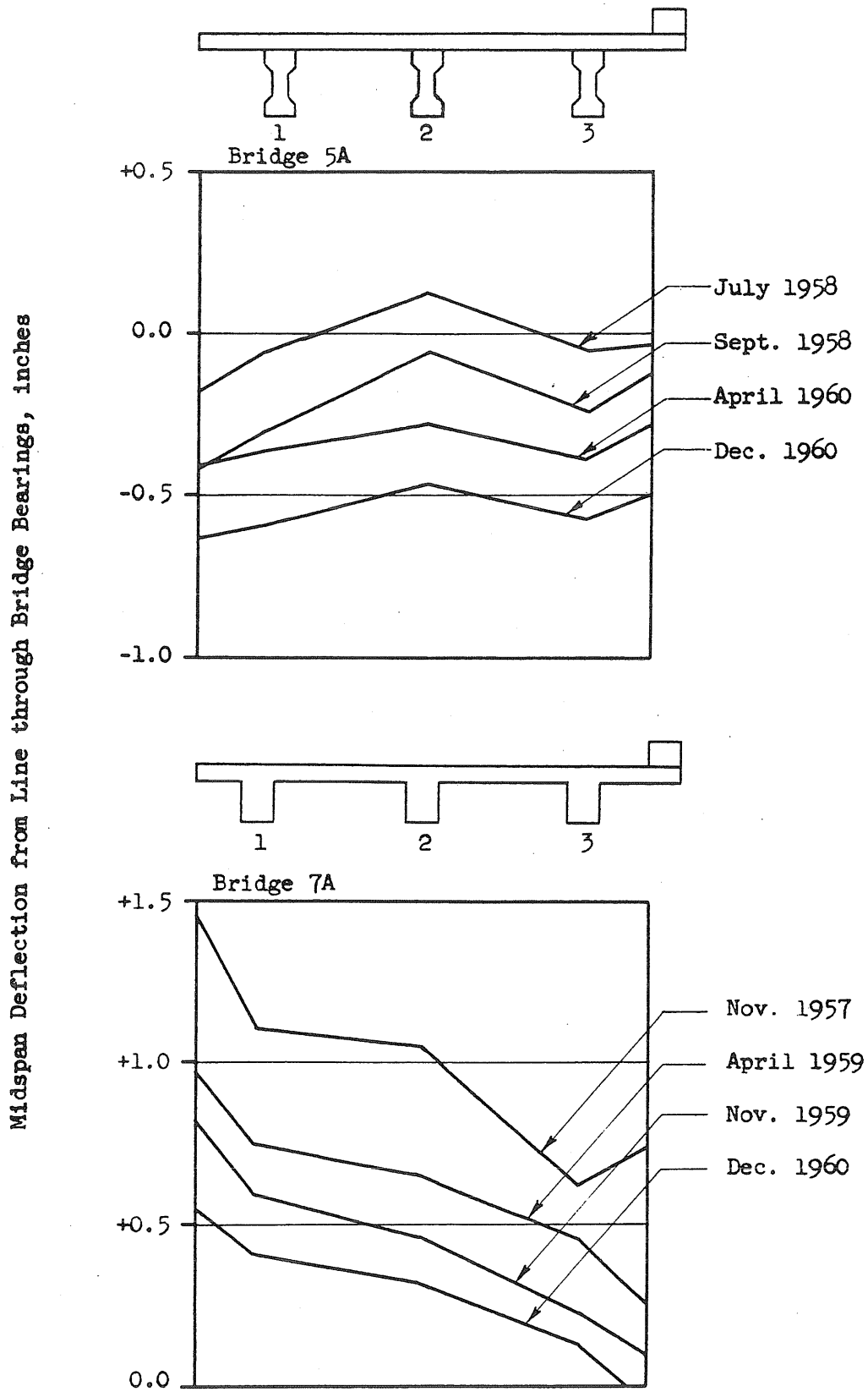

FIG. 16b LATERAL PROFILE OF BRIDGES AT MIDSPAN

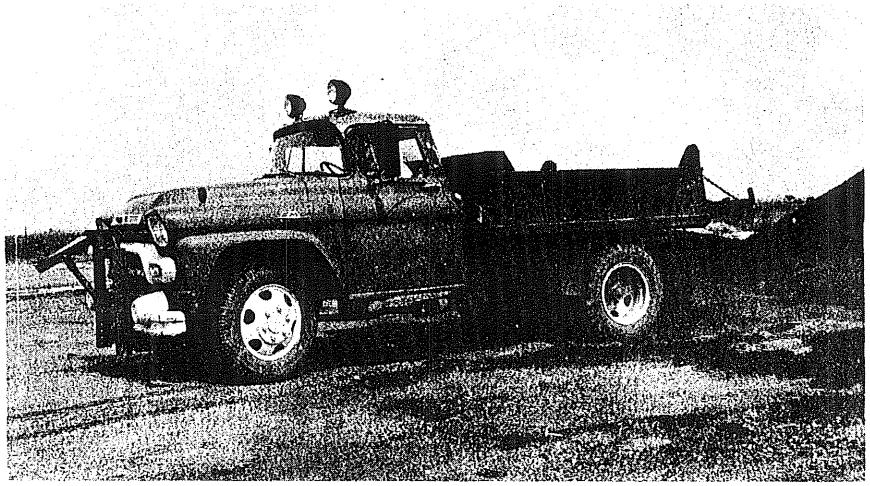

No. 91

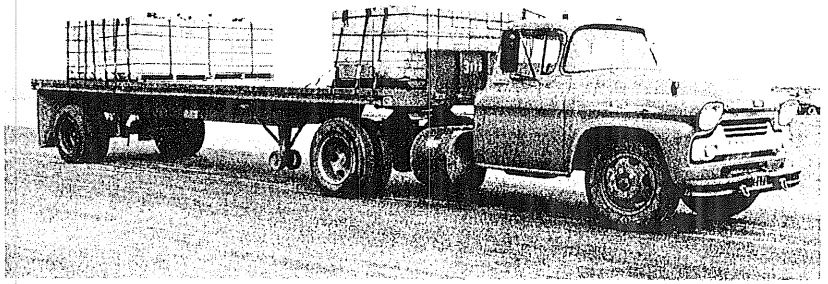

No. 317

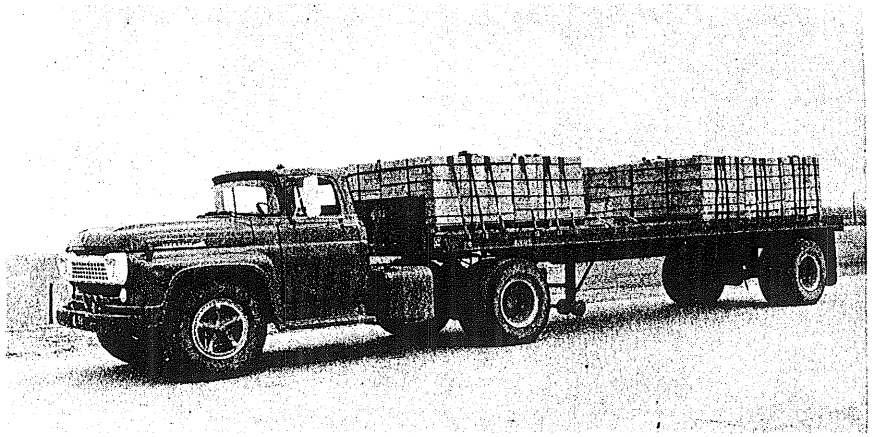

No. 415

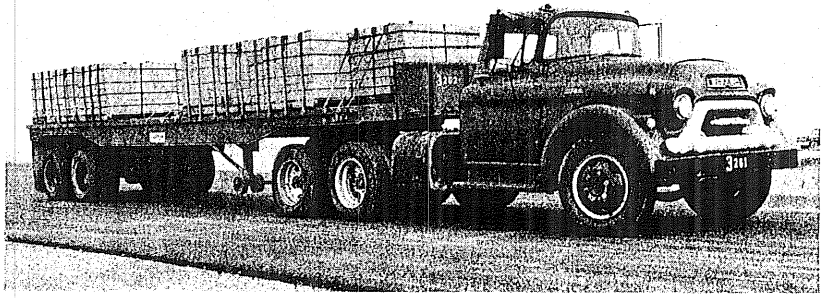

No. 326

FIG. 17 TEST VEHICLES

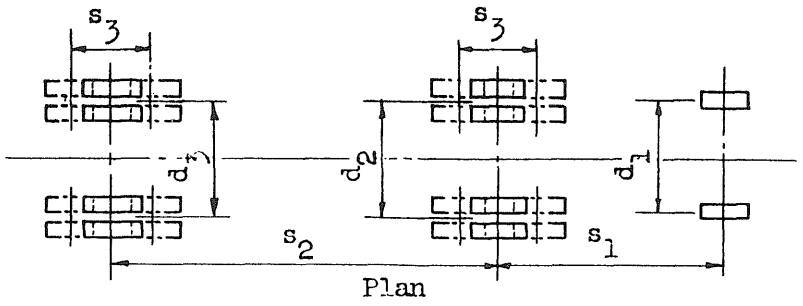

Plan

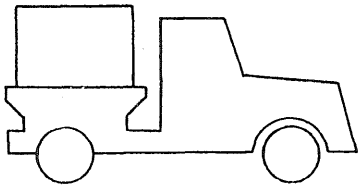

Two-axle Vehicle

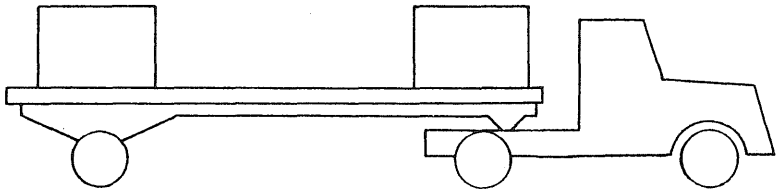

Three-axle Vehicle

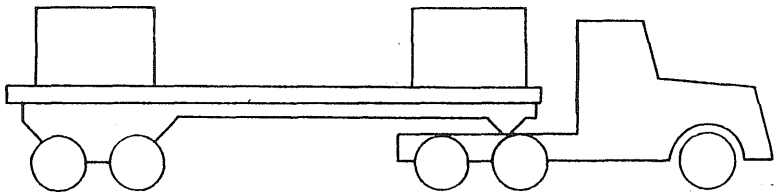

Five-axle Vehicle

Vehicle		Dimensions, inches				
No. of axles	Number	s_1	s_2	d_1	d_2	d_3
2	A	144	-	69	71	-
2	91	133	-	64	69	-
2	94	133	-	64	69	-
2	221	126	-	58	72	-
3	B,C	144	244	69	71	72
3	315	142	241	64	68	69
3	415	143	235	72	71	71
3	417	137	260	68	72	72
3	513	144	244	69	71	72
3	517	137	237	71	72	71
5*	324	154	291	71	68	71
5*	325	156	285	71	68	69
5*	327	156	290	71	71	70

* s_3 = 49 inches for all five-axle vehicles

FIG. 18 DIMENSIONS OF TEST VEHICLES

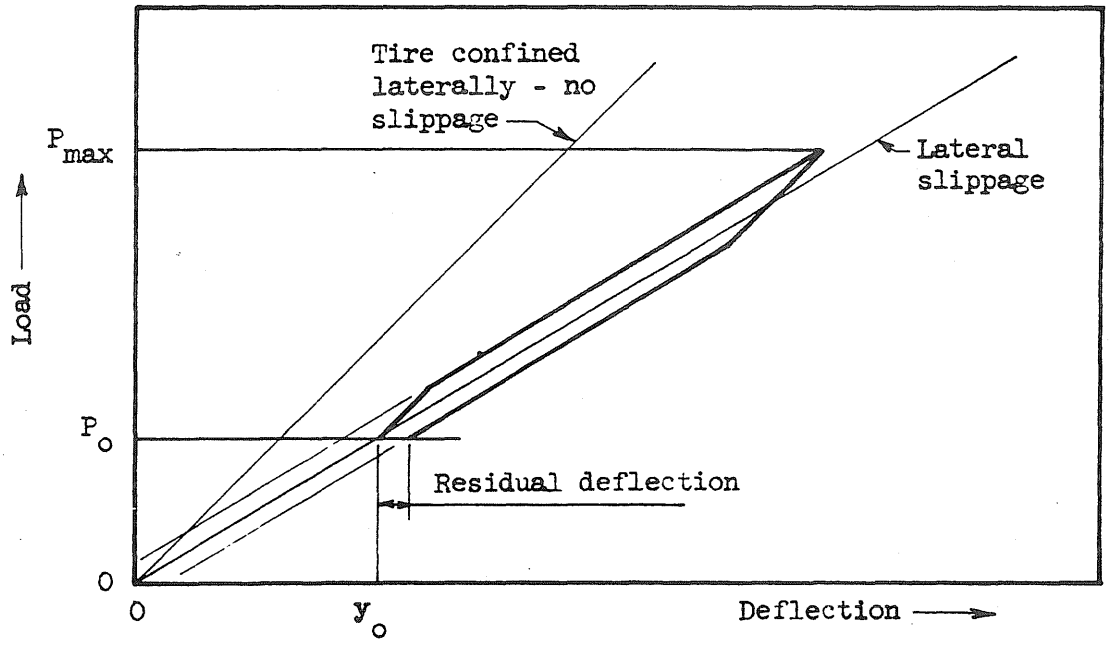

a. Idealized Load - Deflection Curve

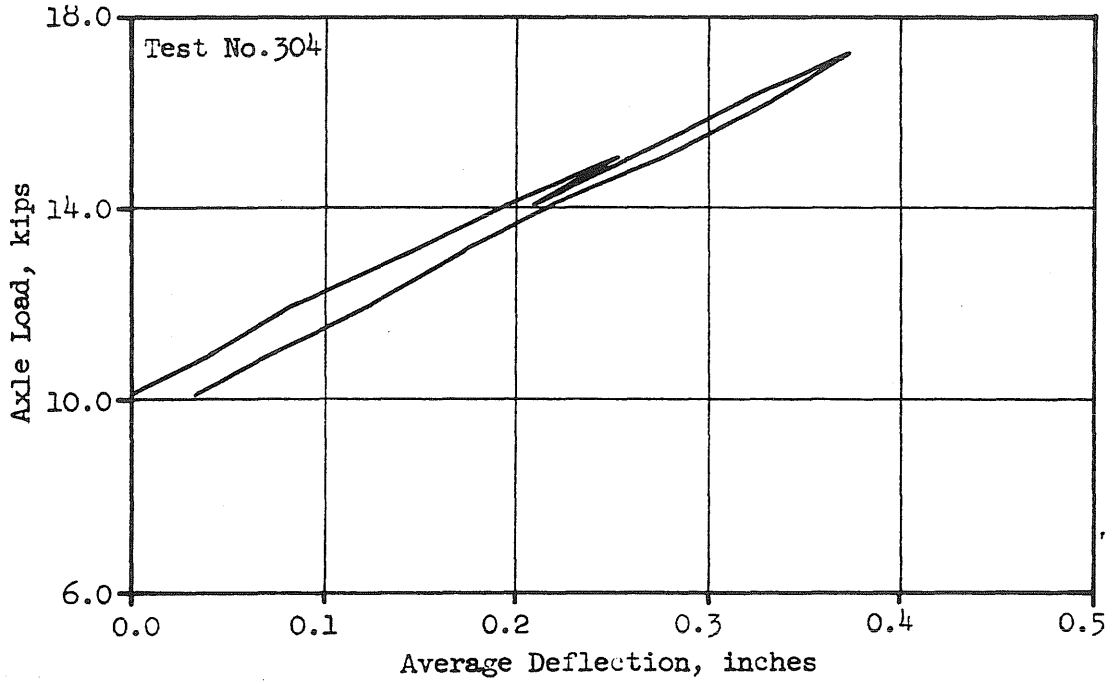

b. Drive Axle, Vehicle No. 91

FIG. 19 LOAD-DEFLECTION CURVES FOR VEHICLE TIRES

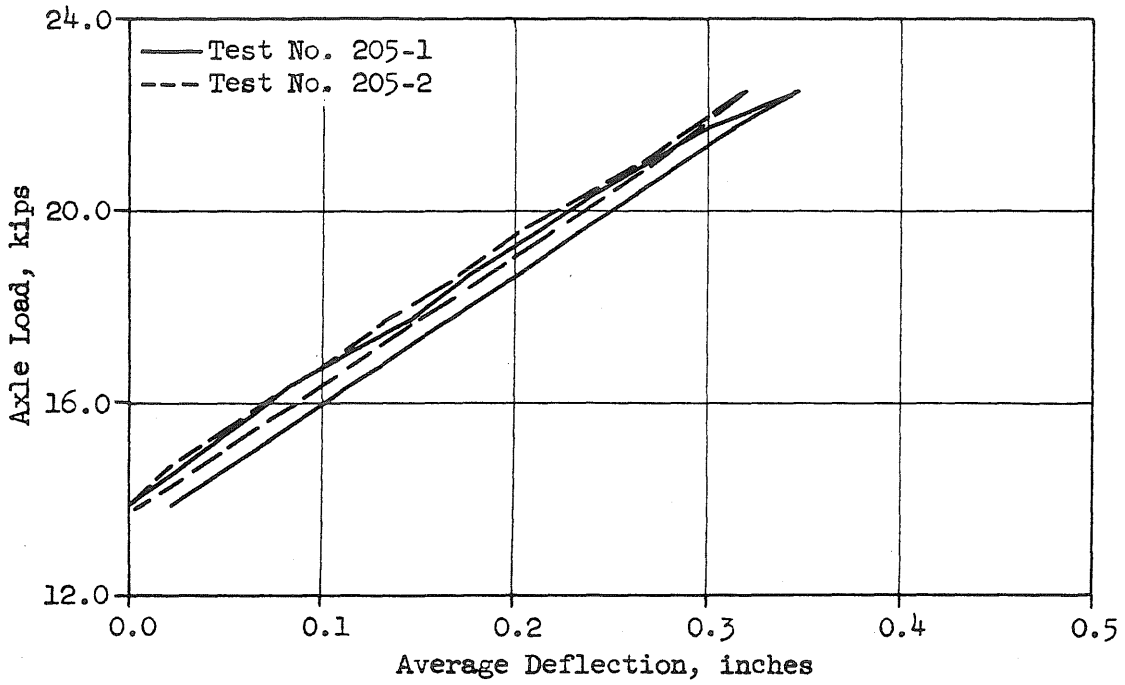

c. Drive Axle, Vehicle No. 415

FIG. 19 LOAD-DEFLECTION CURVES FOR VEHICLE TIRES (Cont'd)

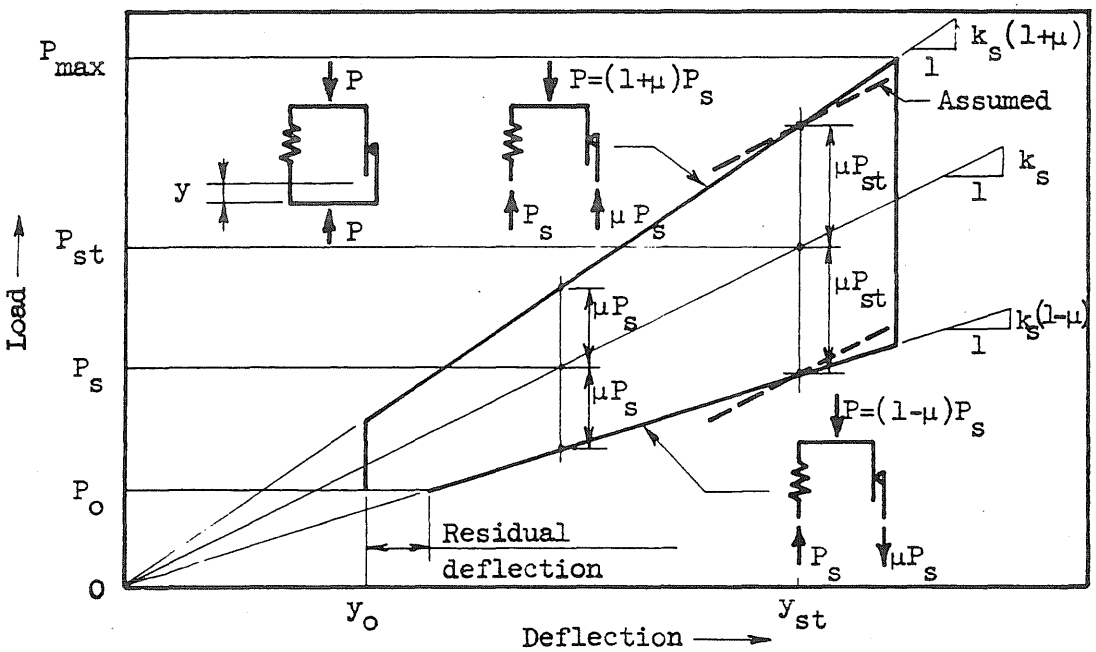

a. Idealized Load-Deflection Curve

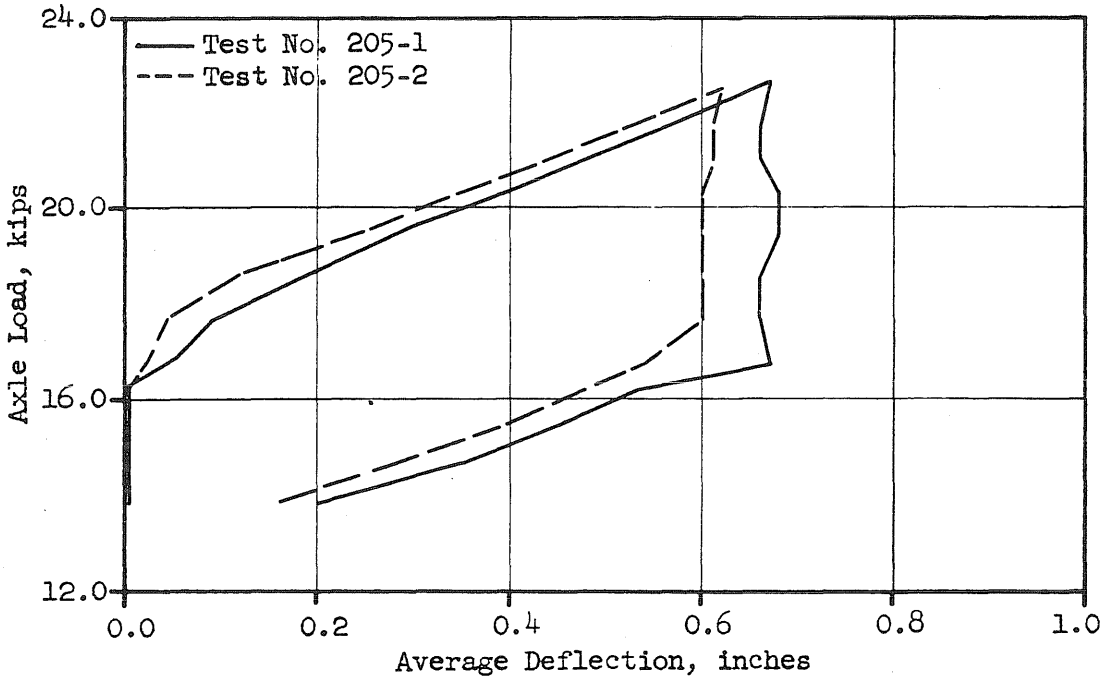

b. Drive Axle, Vehicle No. 415

FIG. 20 LOAD-DEFLECTION CURVES FOR VEHICLE SPRINGS

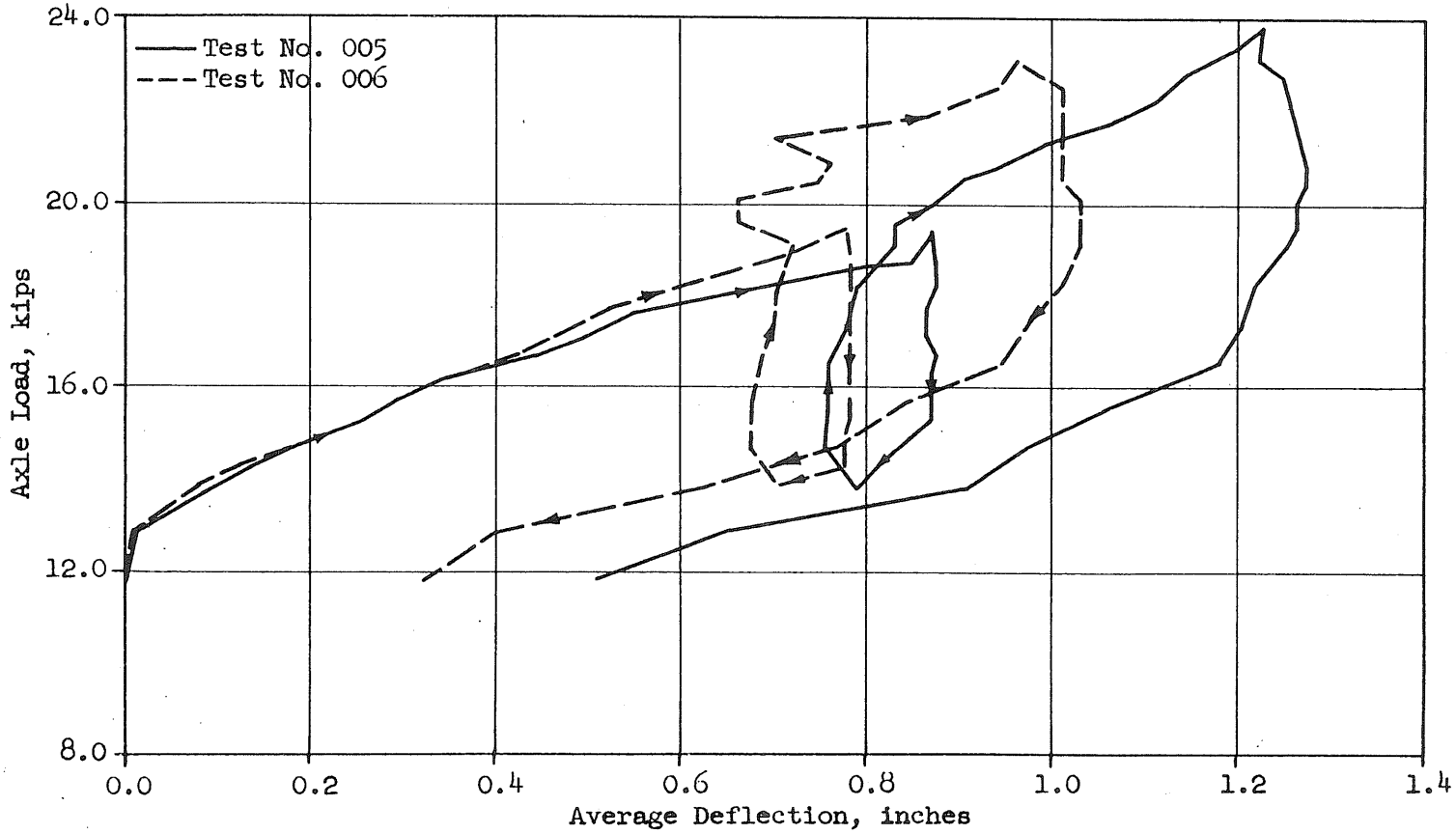

c. Drive Axle, Vehicle No. 511

FIG. 20 LOAD-DEFLECTION CURVES FOR VEHICLE SPRINGS (Contd)

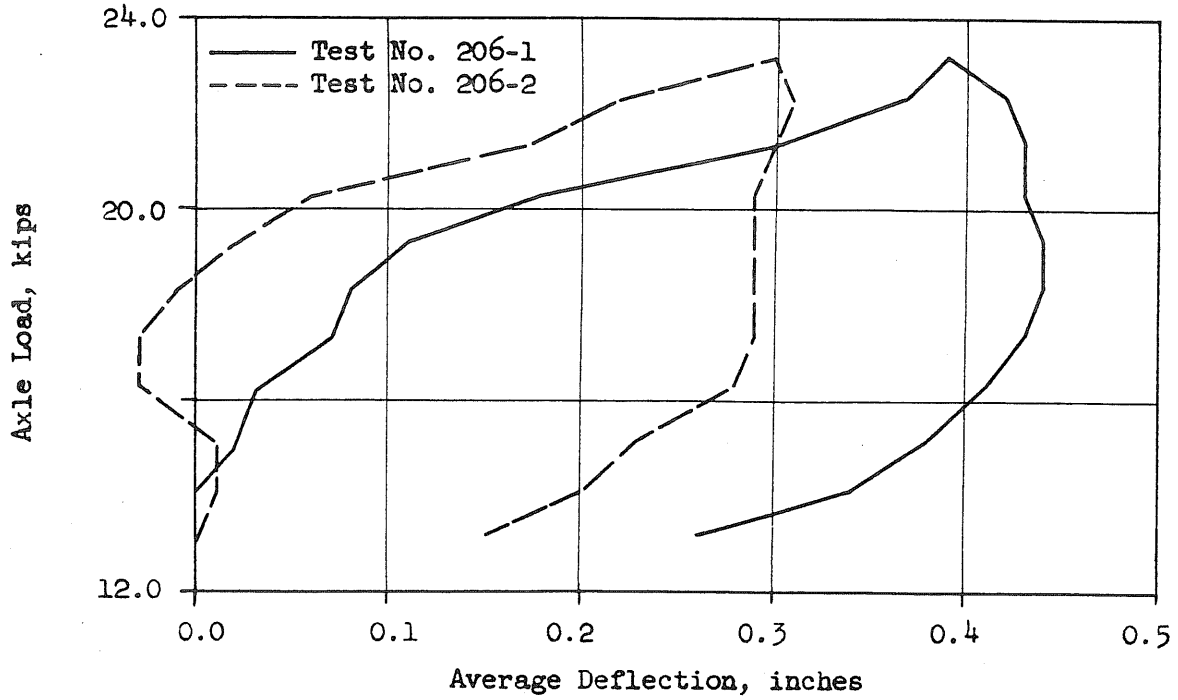

d. Rear Axle, Vehicle No. 415

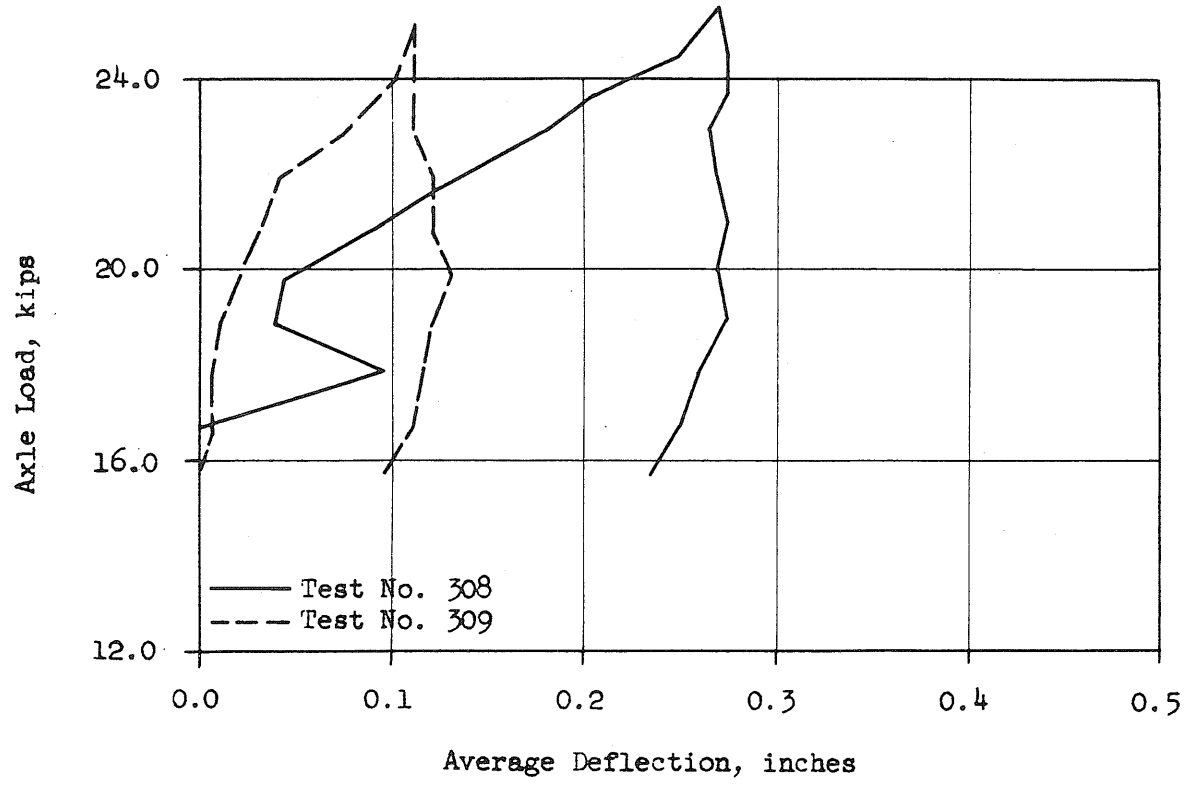

e. Rear Axle, Vehicle No. 513

FIG. 20 LOAD-DEFLECTION CURVES FOR VEHICLE SPRINGS (Cont'd)

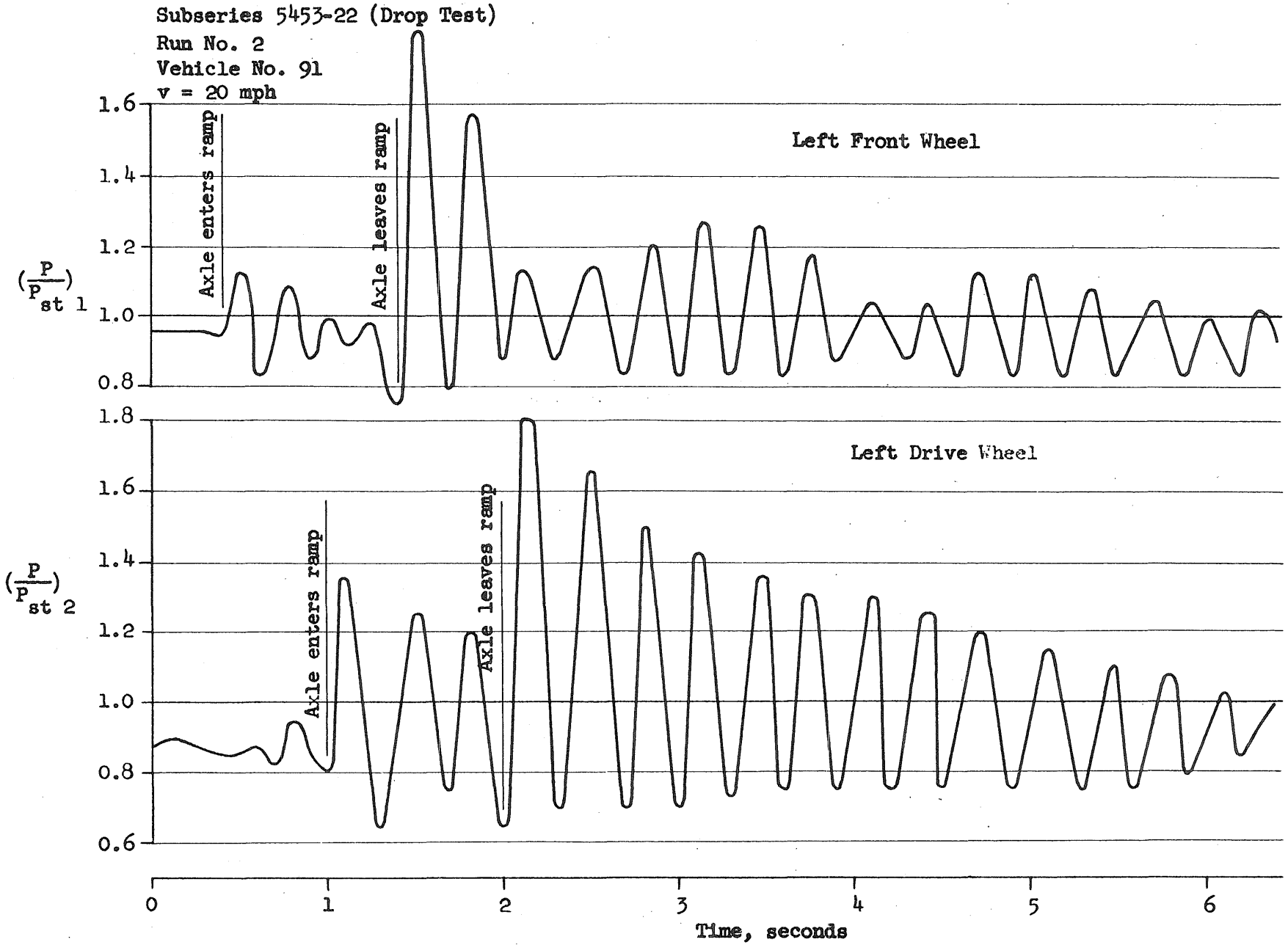

FIG. 21a TYPICAL INTERACTION FORCE DIAGRAMS FOR VEHICLES WITH BLOCKED SPRINGS

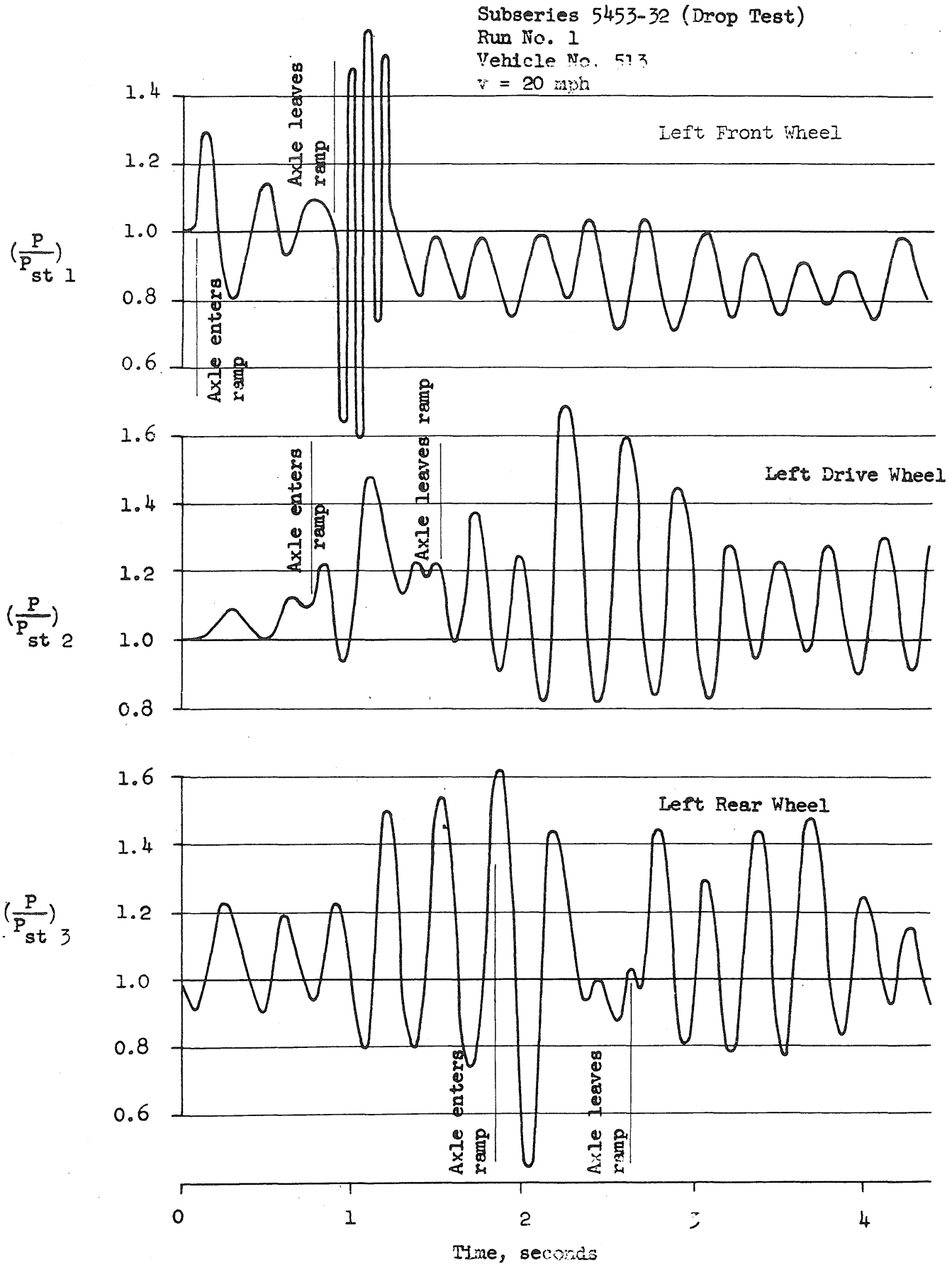

FIG. 21b TYPICAL INTERACTION FORCE DIAGRAMS FOR VEHICLES WITH BLOCKED SPRINGS

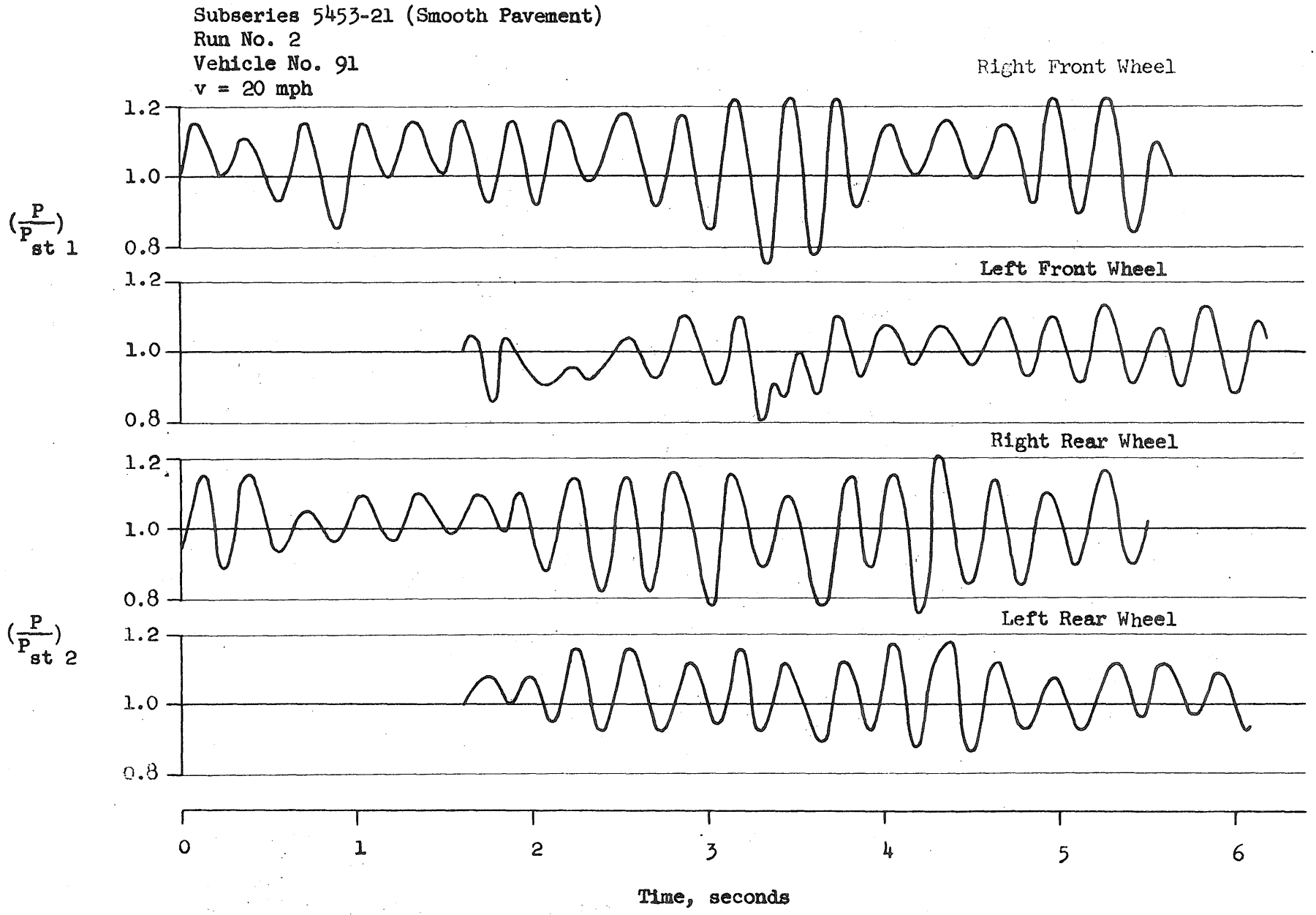

FIG. 21c TYPICAL INTERACTION FORCE DIAGRAMS FOR VEHICLES WITH BLOCKED SPRINGS

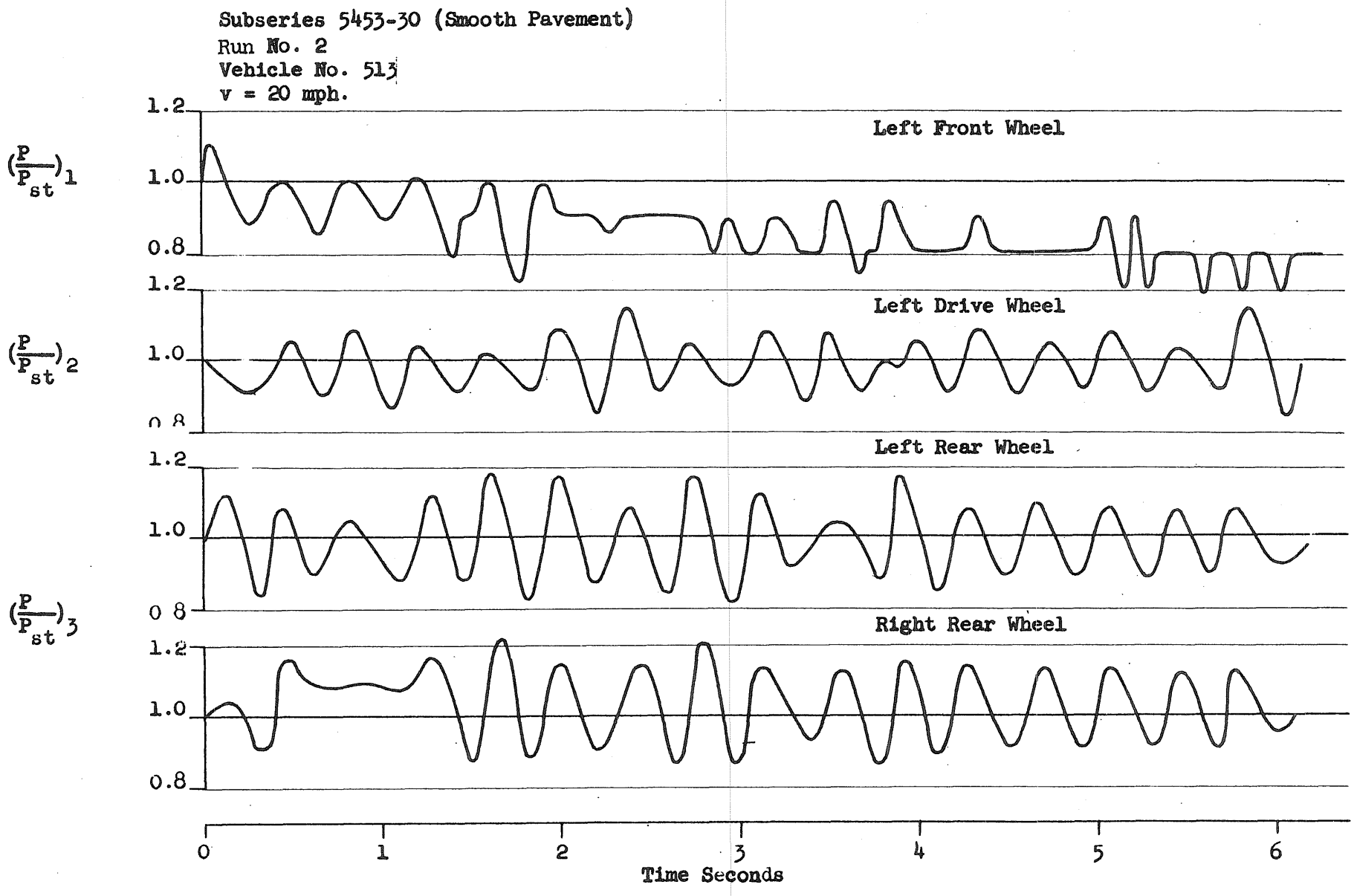

FIG. 21d TYPICAL INTERACTION FORCE DIAGRAMS FOR VEHICLES WITH BLOCKED SPRINGS

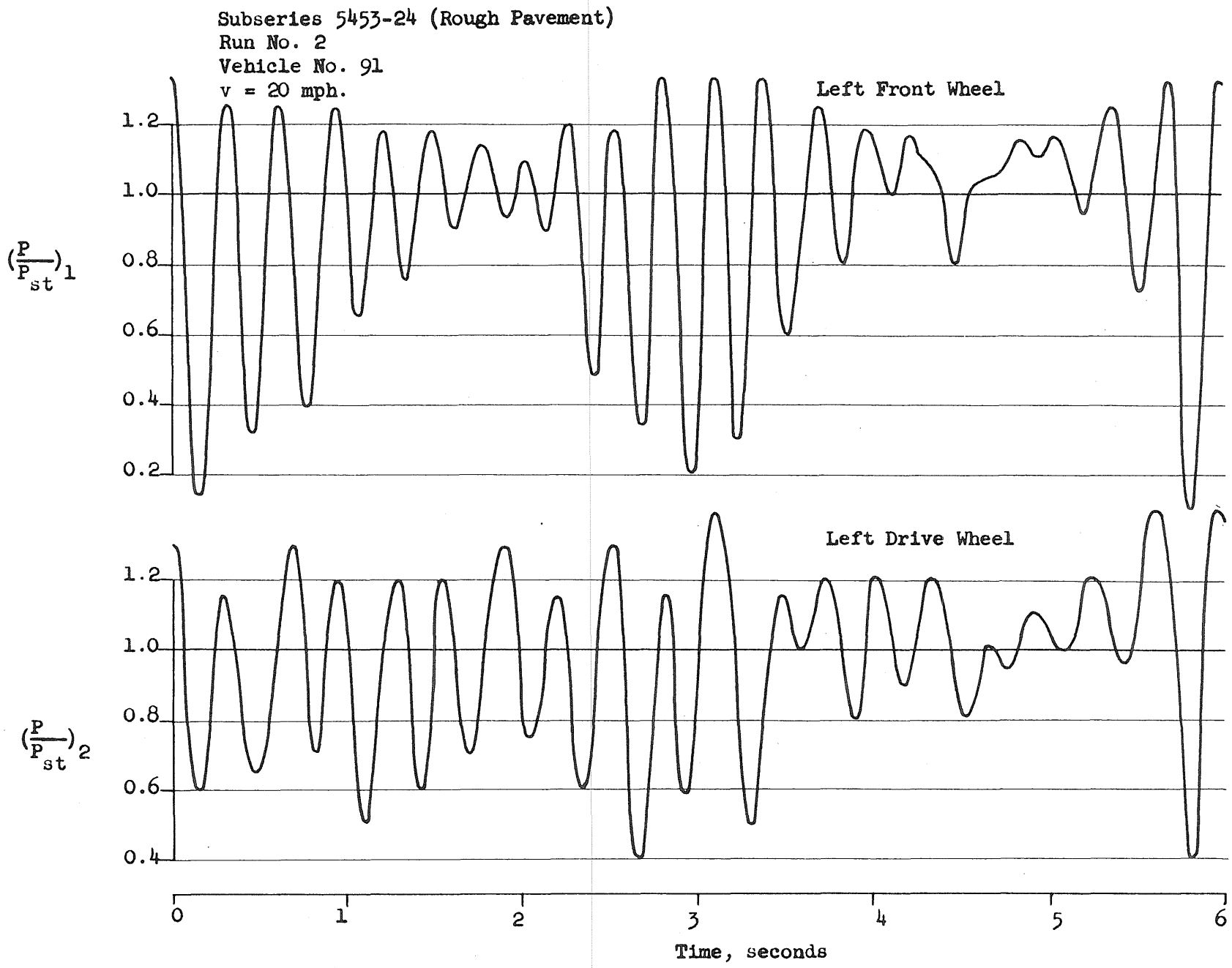

FIG. 21e TYPICAL INTERACTION FORCE DIAGRAMS FOR VEHICLES WITH BLOCKED SPRINGS (Cont'd)

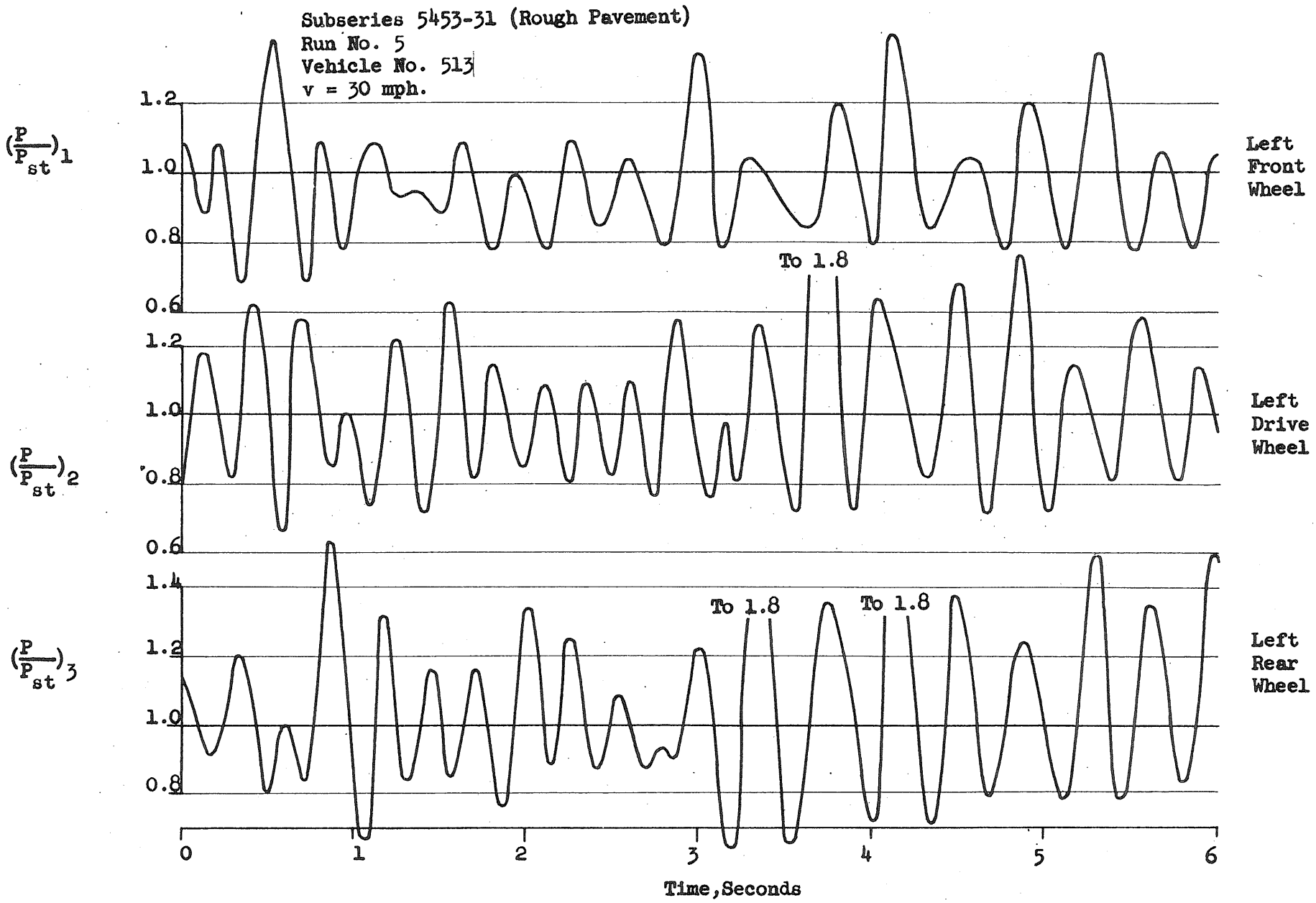

FIG. 21f TYPICAL INTERACTION FORCE DIAGRAMS FOR VEHICLES WITH BLOCKED SPRINGS (Cont'd)

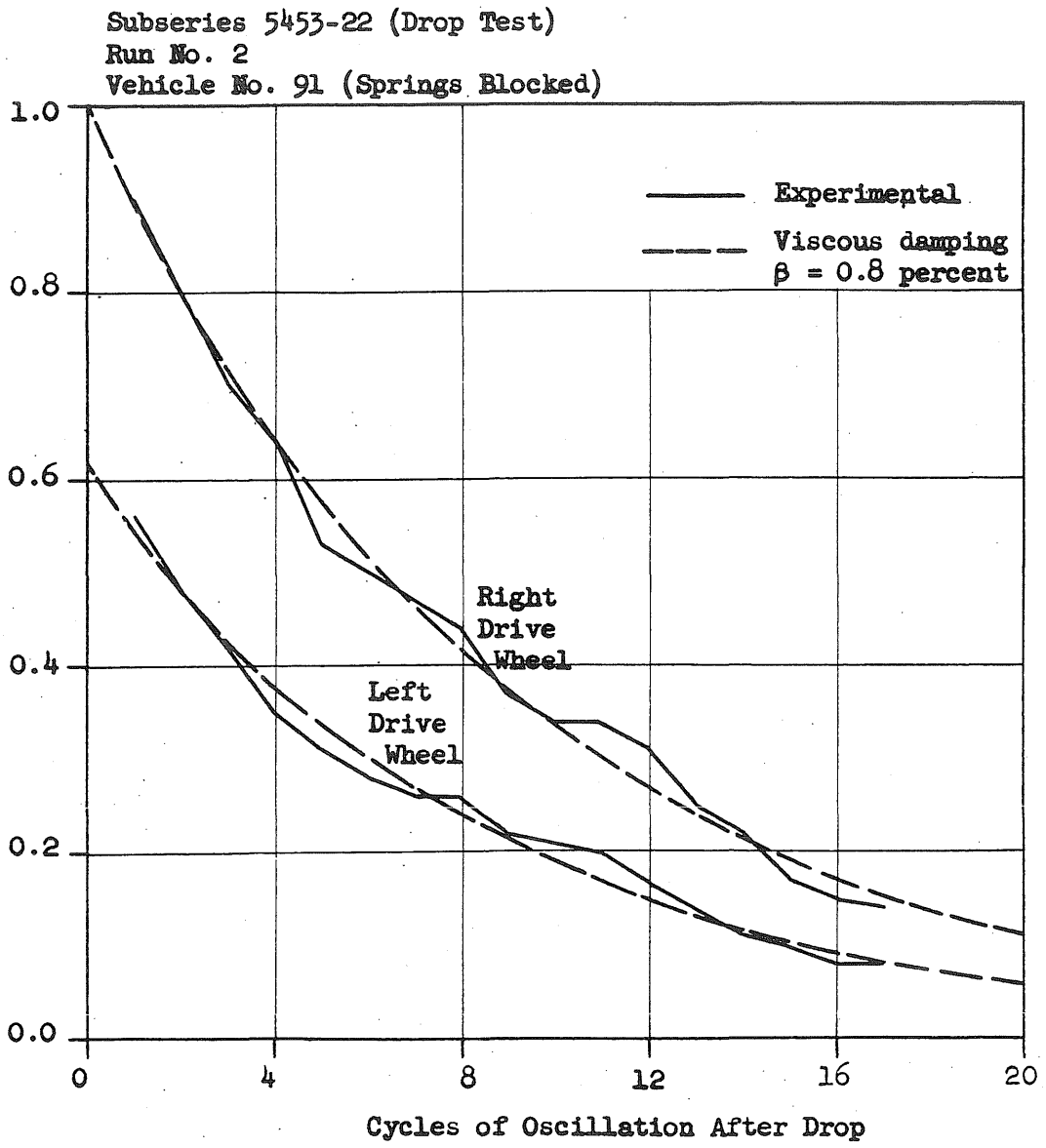

FIG. 22 DECAY OF INTERACTION FORCE

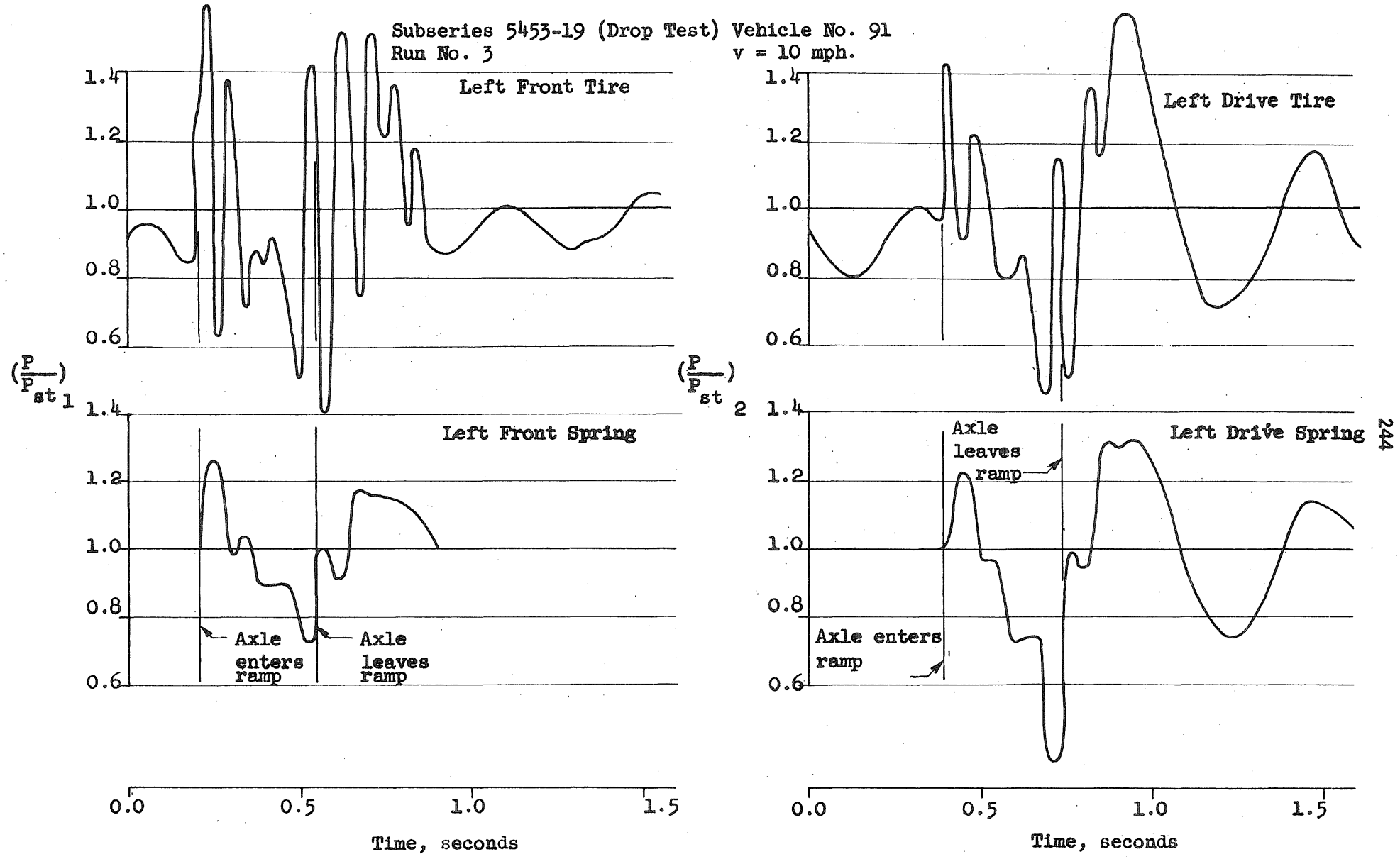

FIG. 23a TYPICAL INTERACTION FORCE DIAGRAMS FOR VEHICLES WITH NORMAL SPRINGS

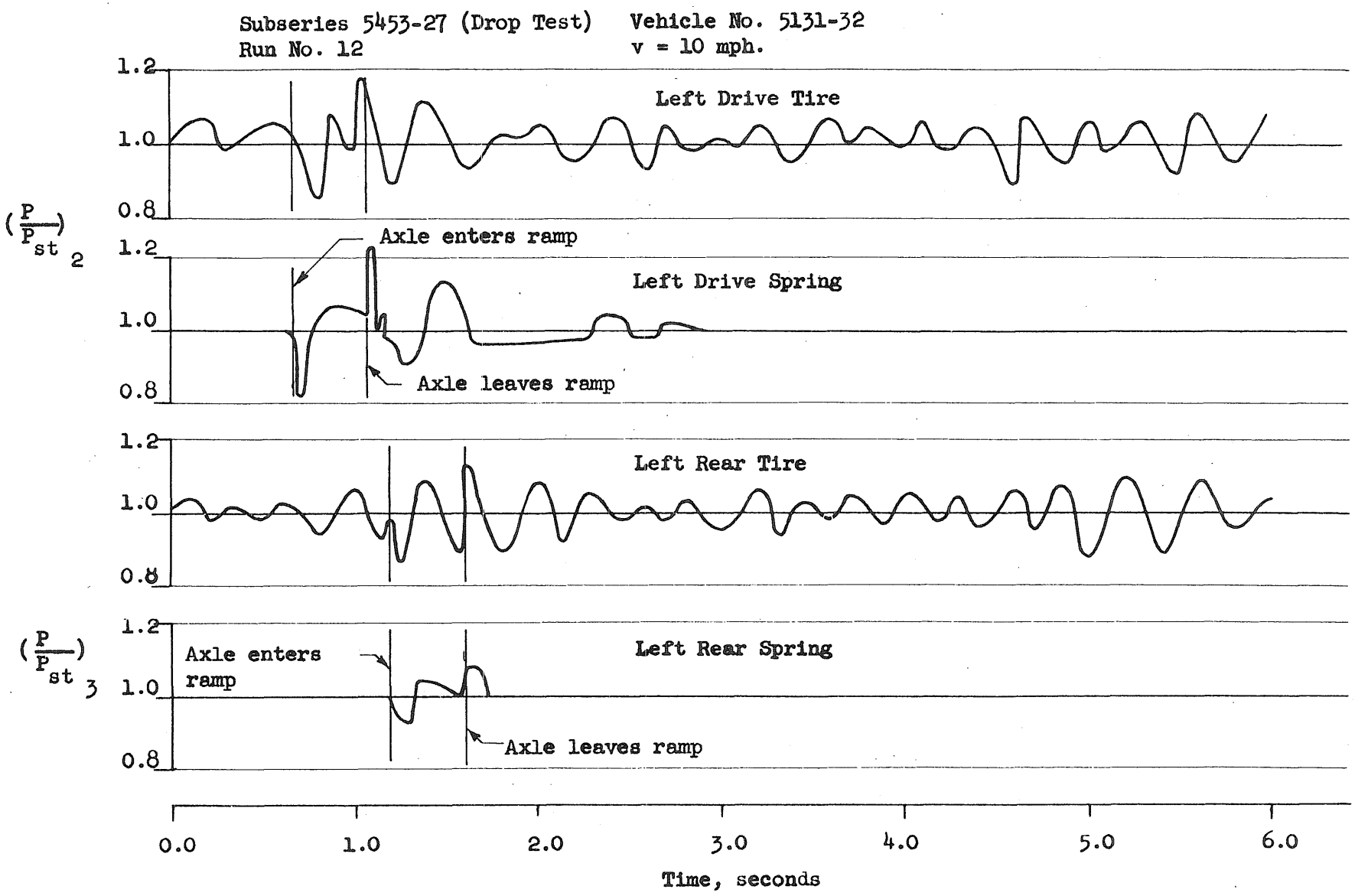

FIG 23b TYPICAL INTERATION FORCE DIAGRAMS FOR VEHICLES WITH NORMAL SPRINGS

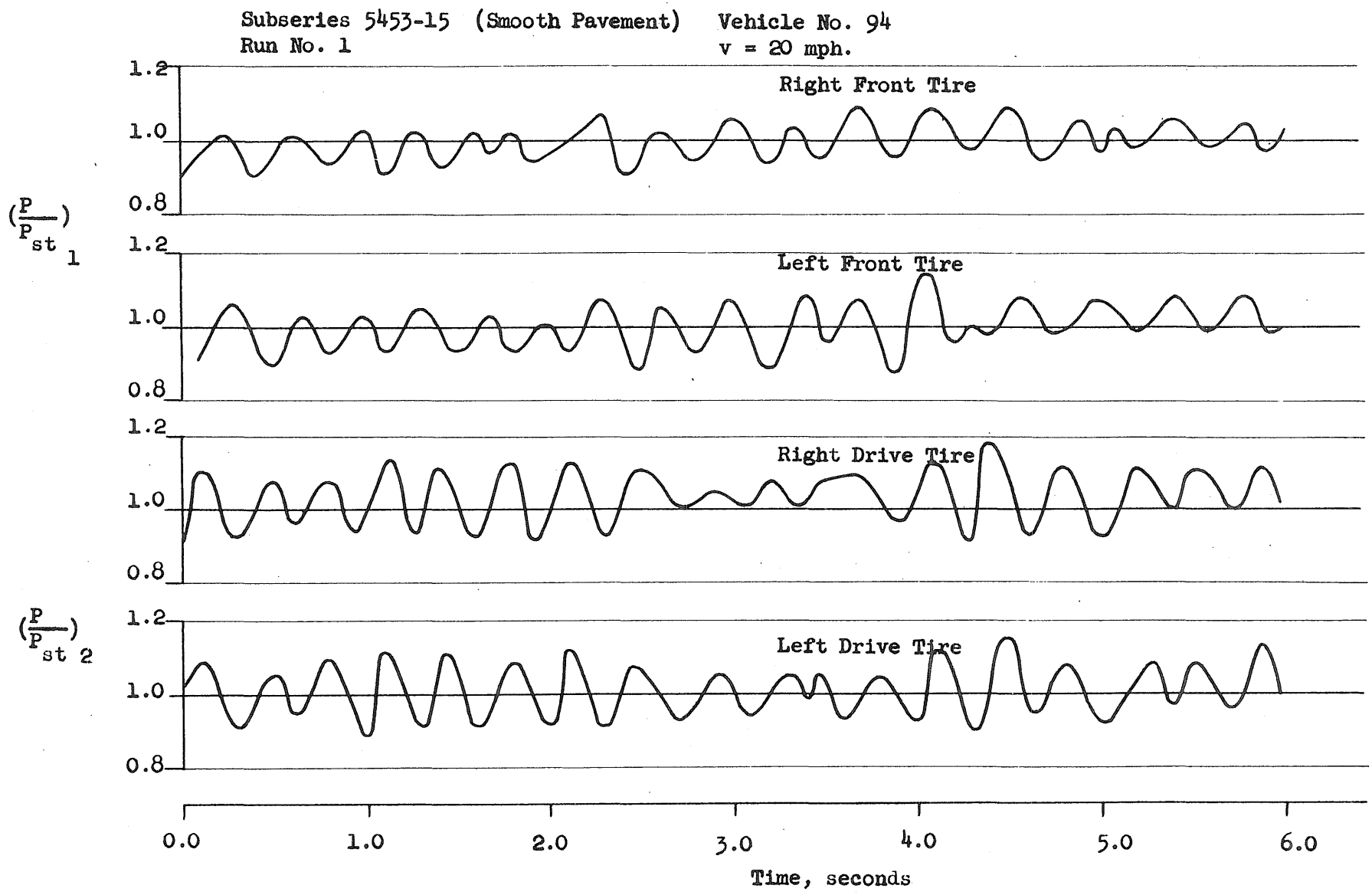

FIG. 23c TYPICAL INTERACTION FORCE DIAGRAMS FOR VEHICLES WITH NORMAL SPRINGS

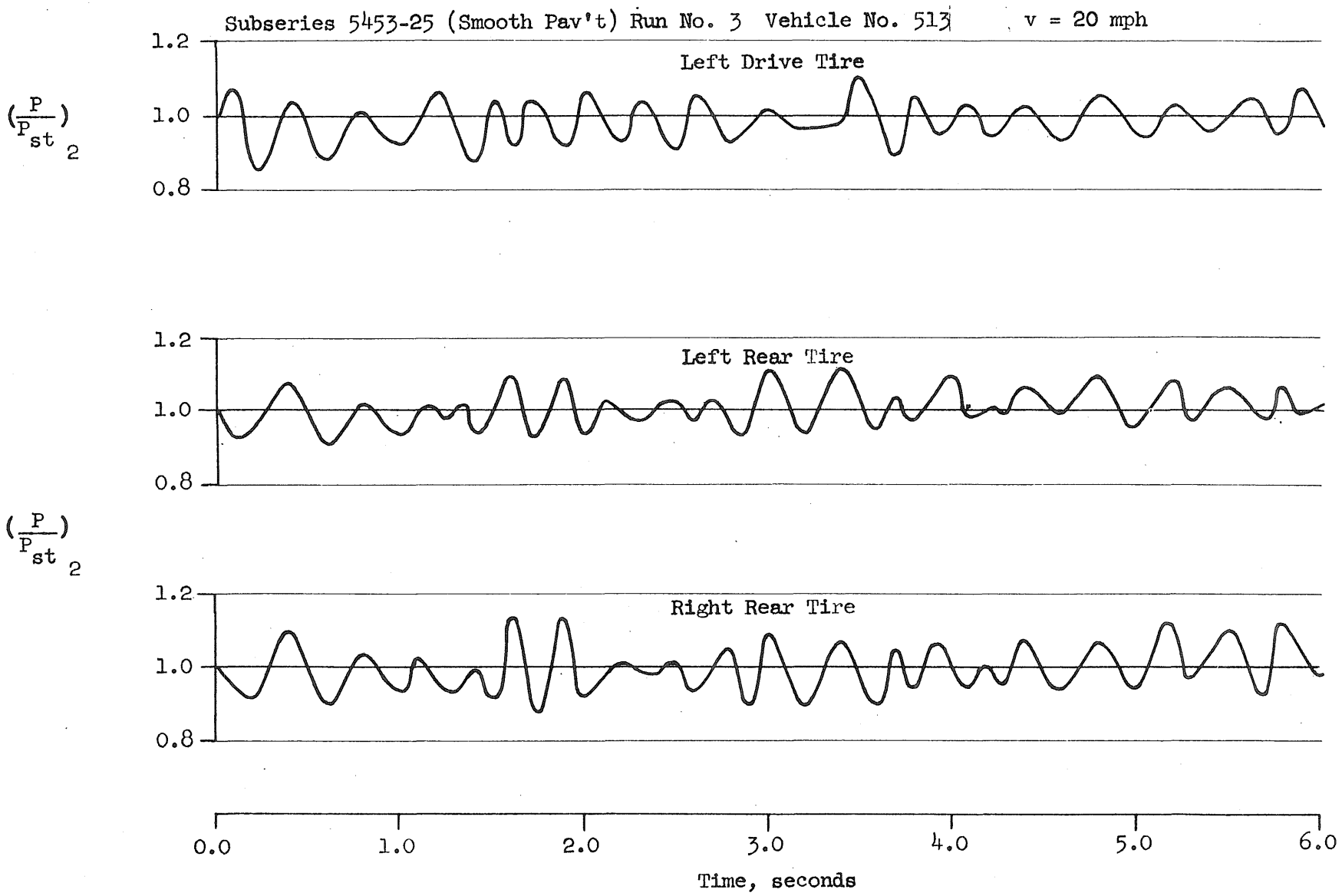

FIG. 23d TYPICAL INTERACTION FORCE DIAGRAMS FOR VEHICLES WITH NORMAL SPRINGS

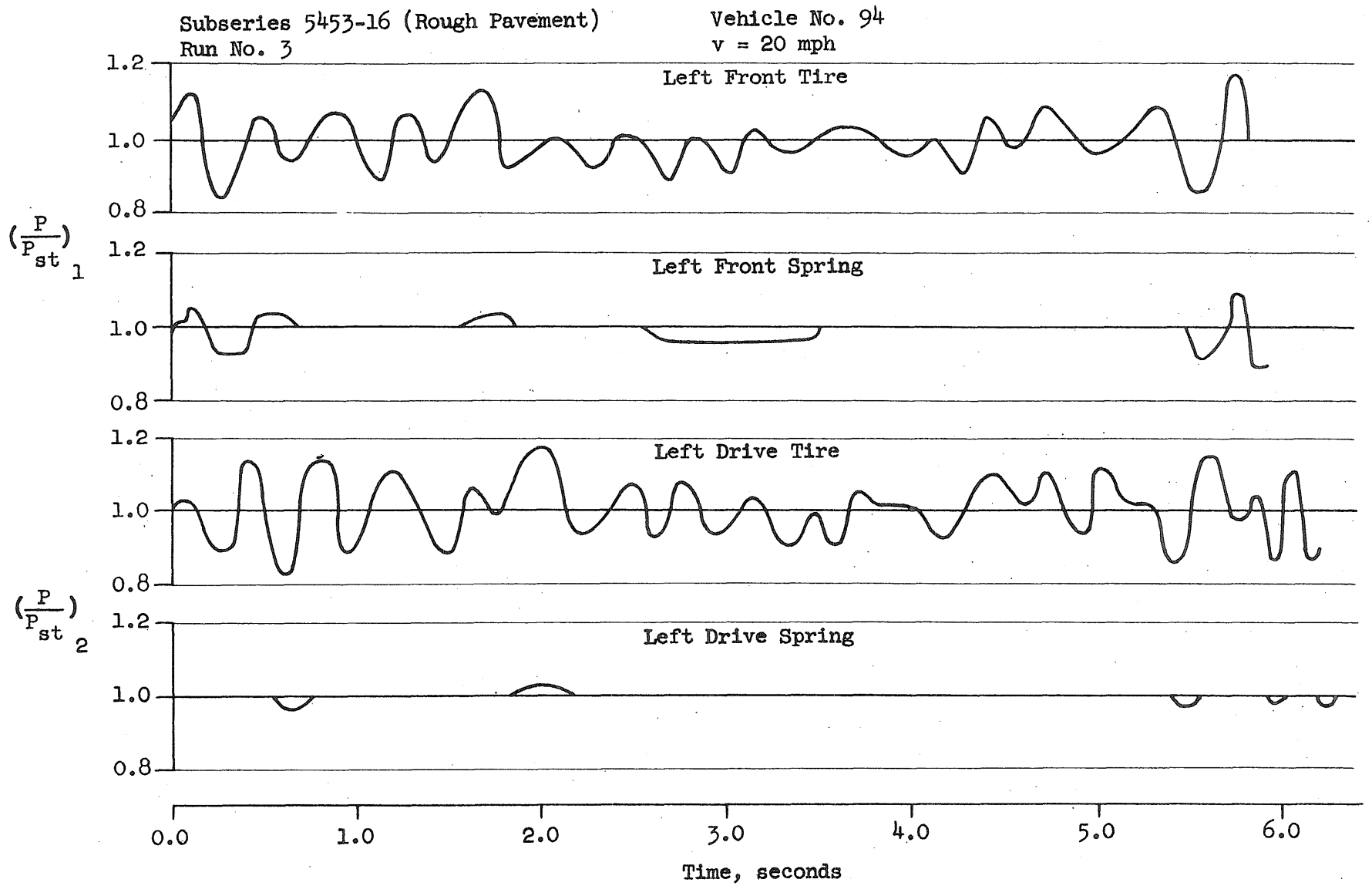

FIG. 23e TYPICAL INTERACTION FORCE DIAGRAMS FOR VEHICLES WITH NORMAL SPRINGS

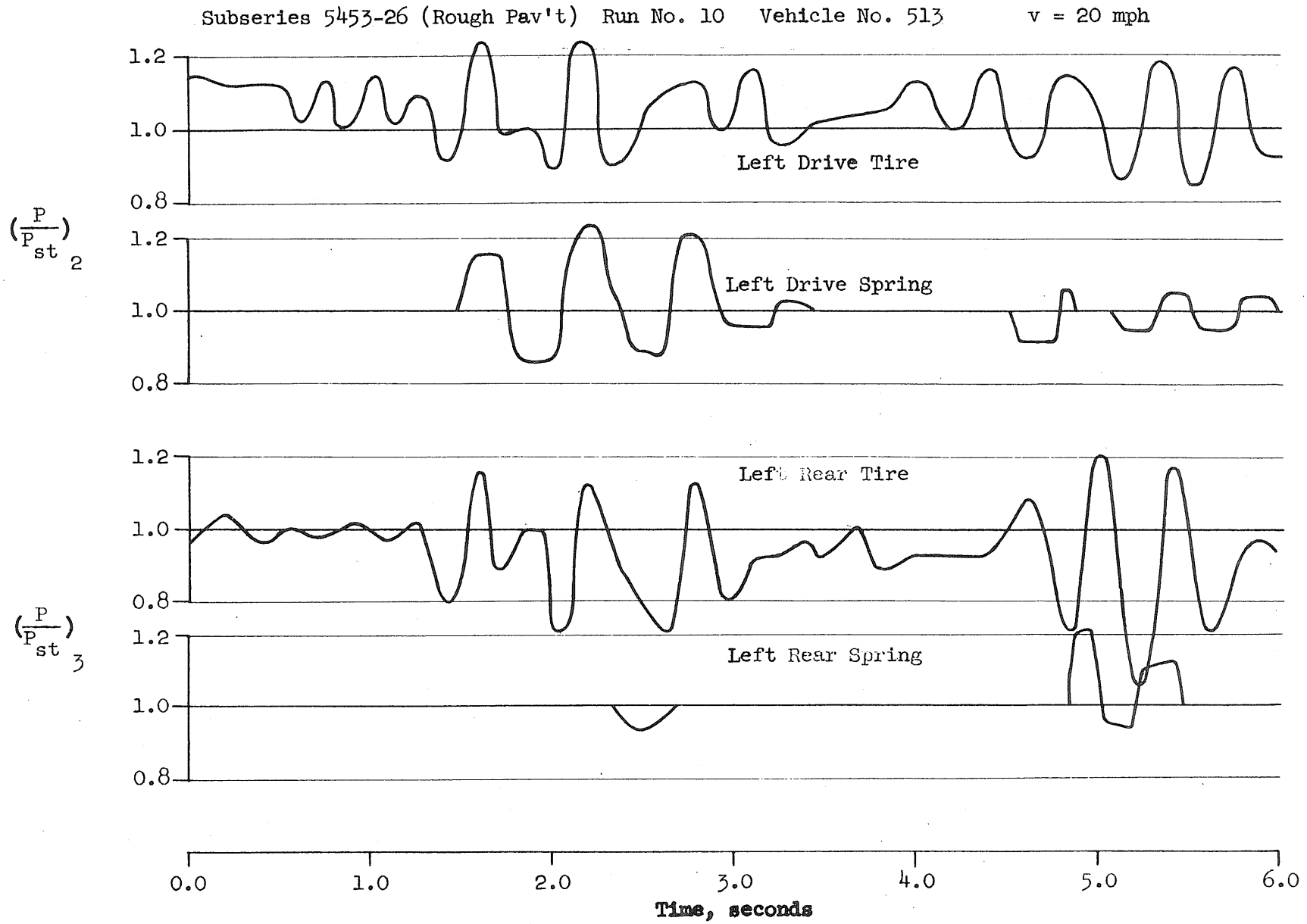

FIG. 23f TYPICAL INTERACTION FORCE DIAGRAMS FOR VEHICLES WITH NORMAL SPRINGS

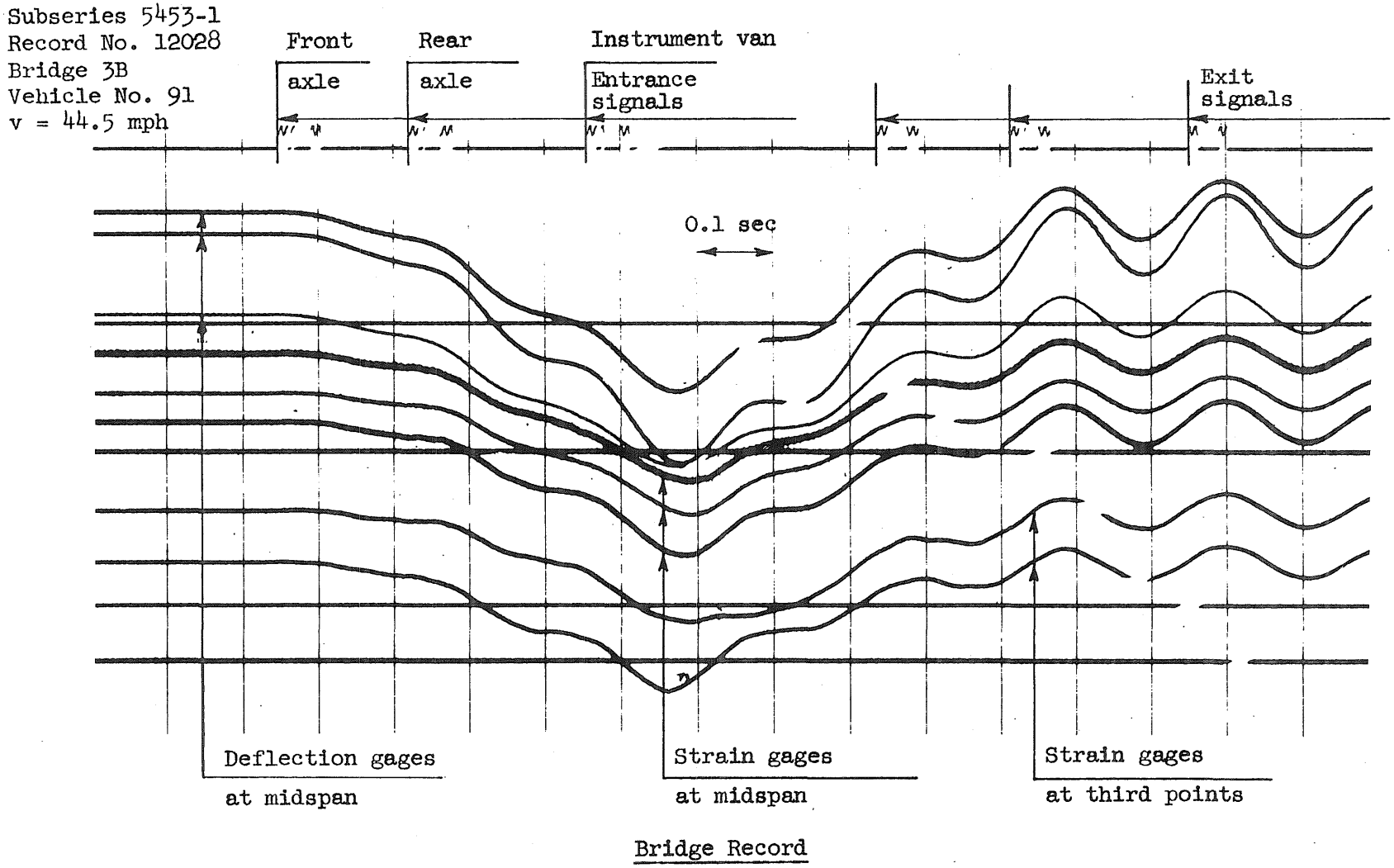

FIG. 24a TYPICAL EXPERIMENTAL RECORDS

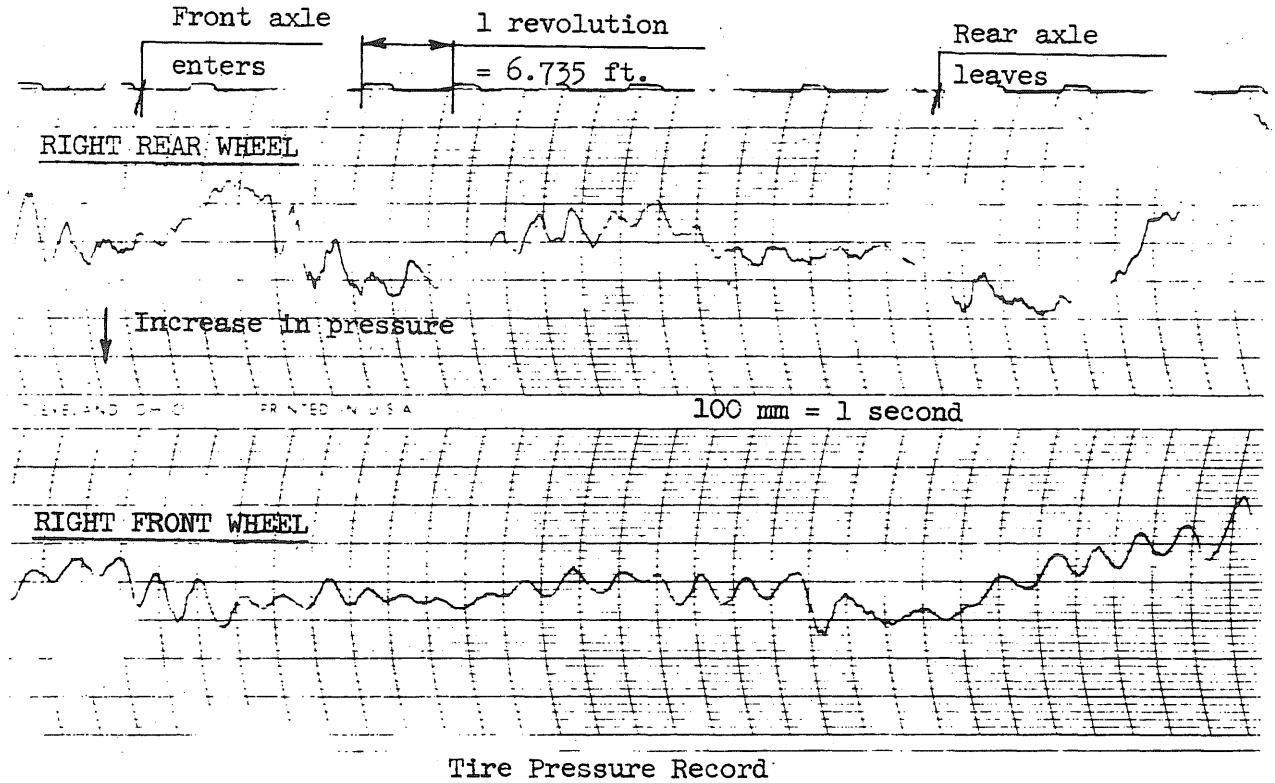

Tire Pressure Record
(Records for left wheels not shown)

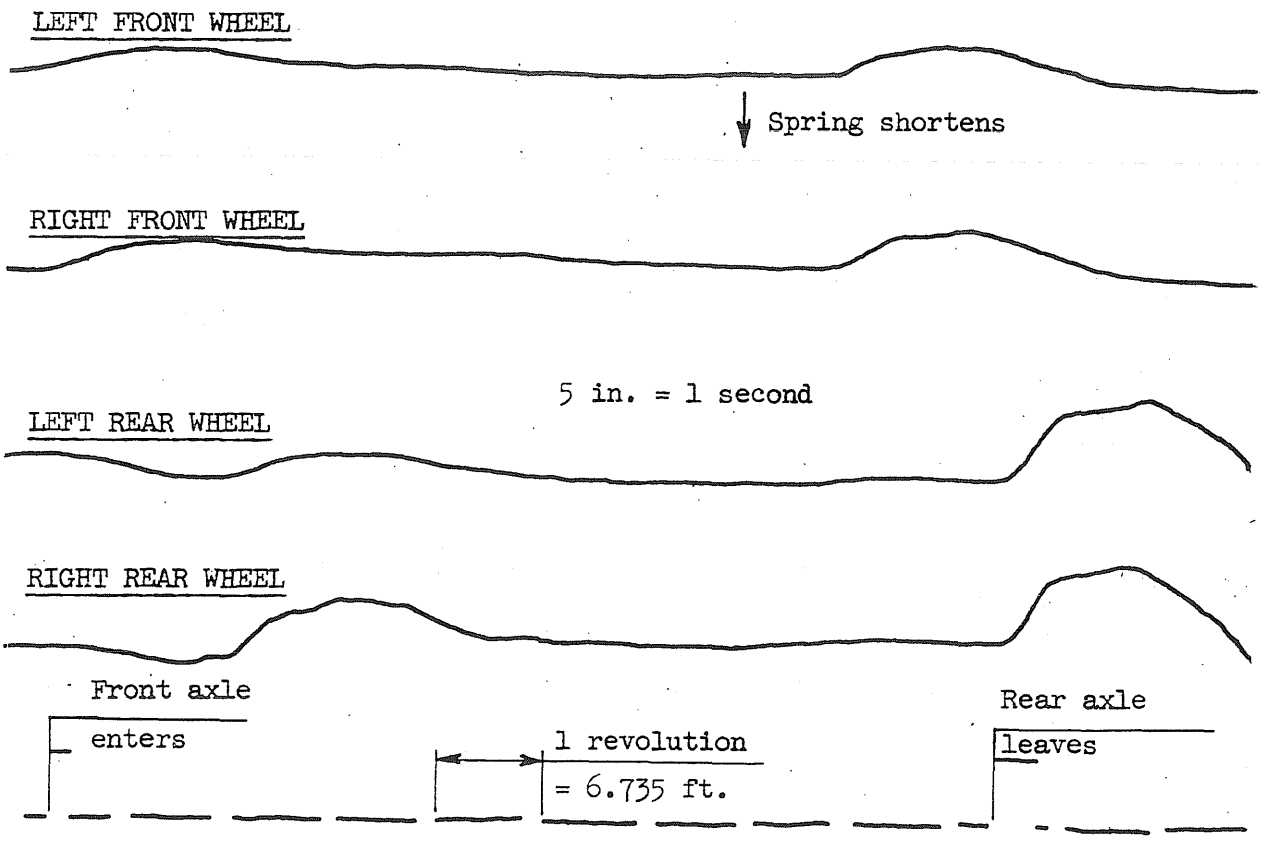

Spring Displacement Record

FIG. 24b TYPICAL EXPERIMENTAL RECORDS

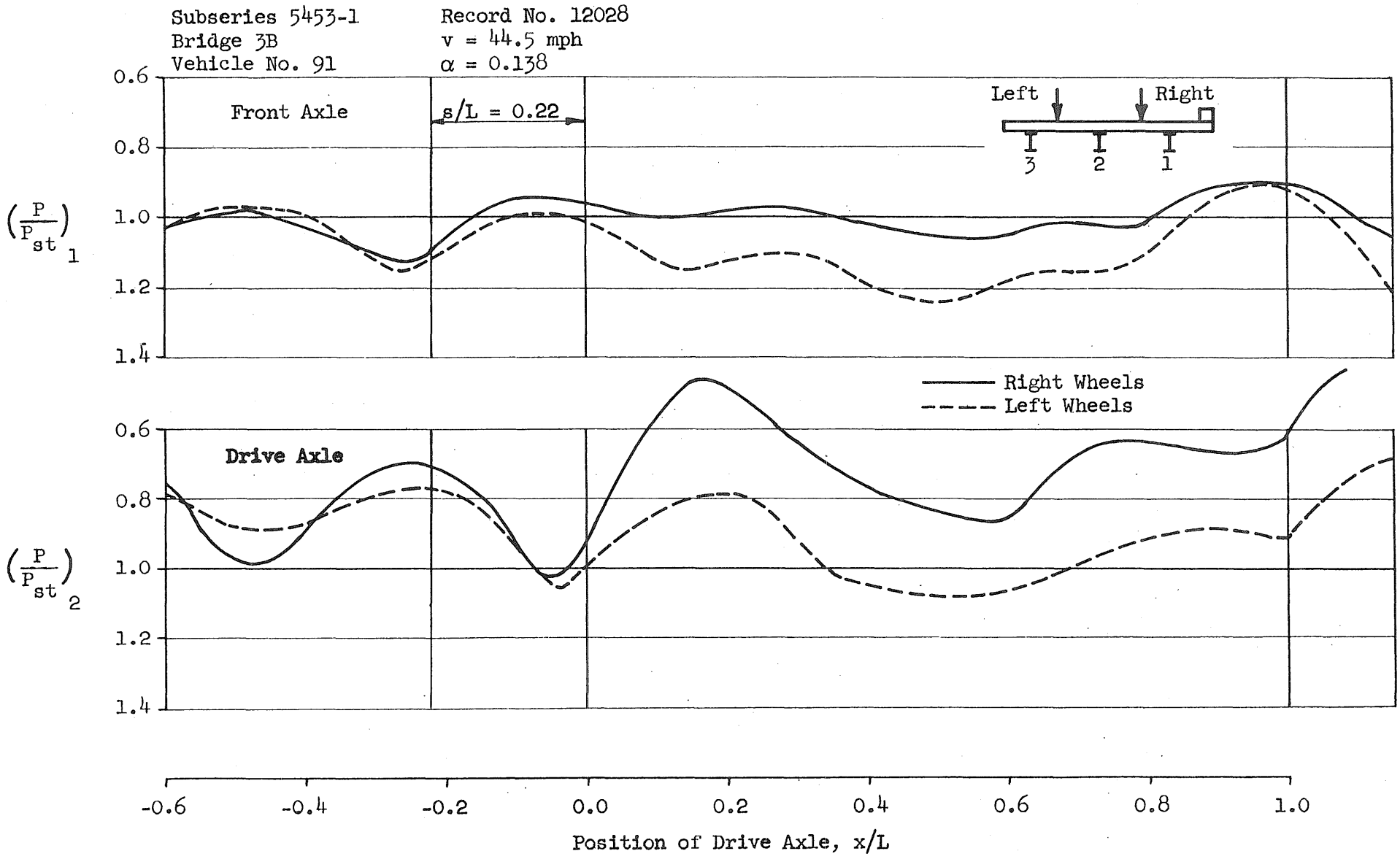

FIG. 25a REPRESENTATIVE RESPONSE CURVES FOR A REGULAR RUN - INTERACTION FORCES

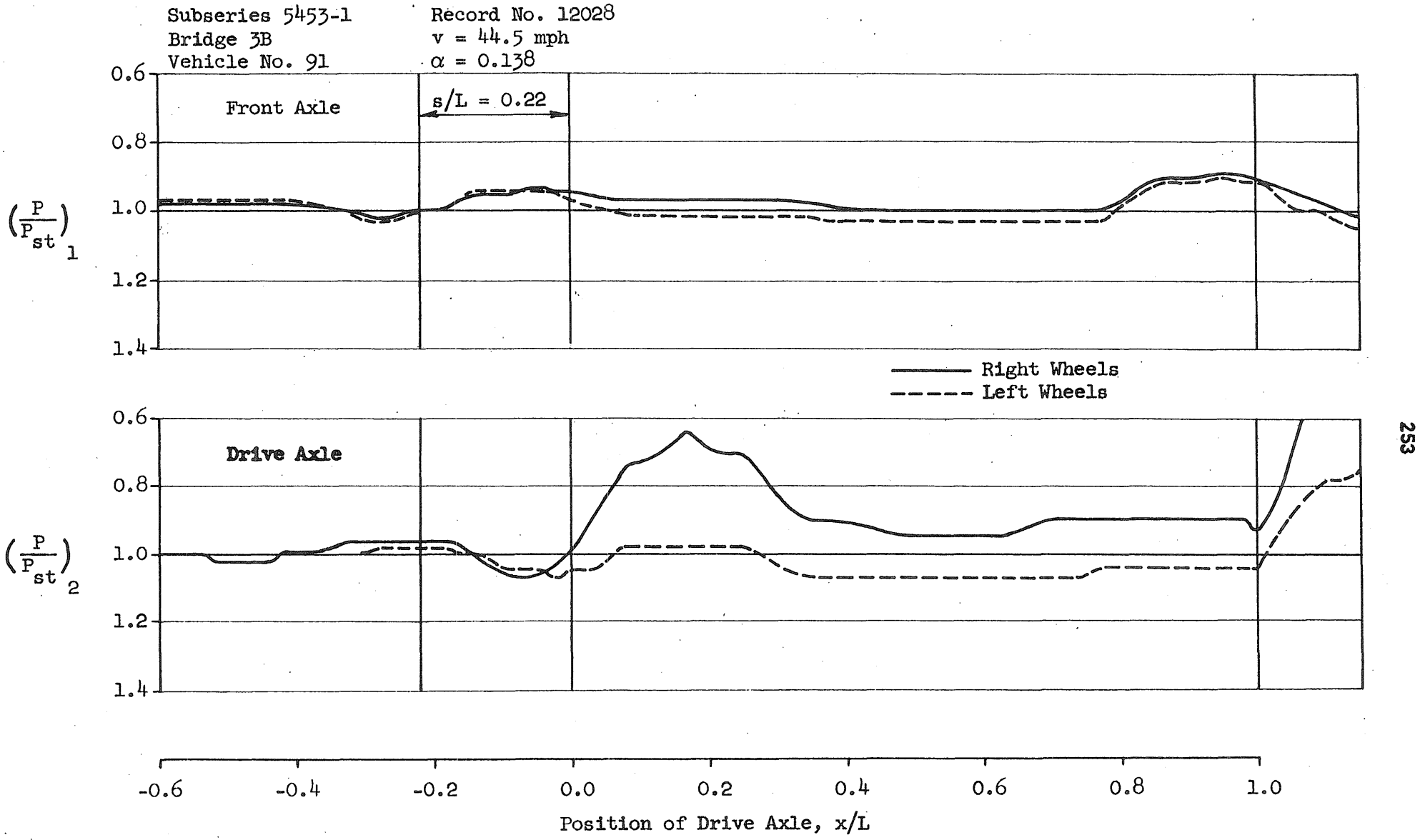

FIG. 25b REPRESENTATIVE RESPONSE CURVES FOR A REGULAR RUN - SPRING RESPONSE

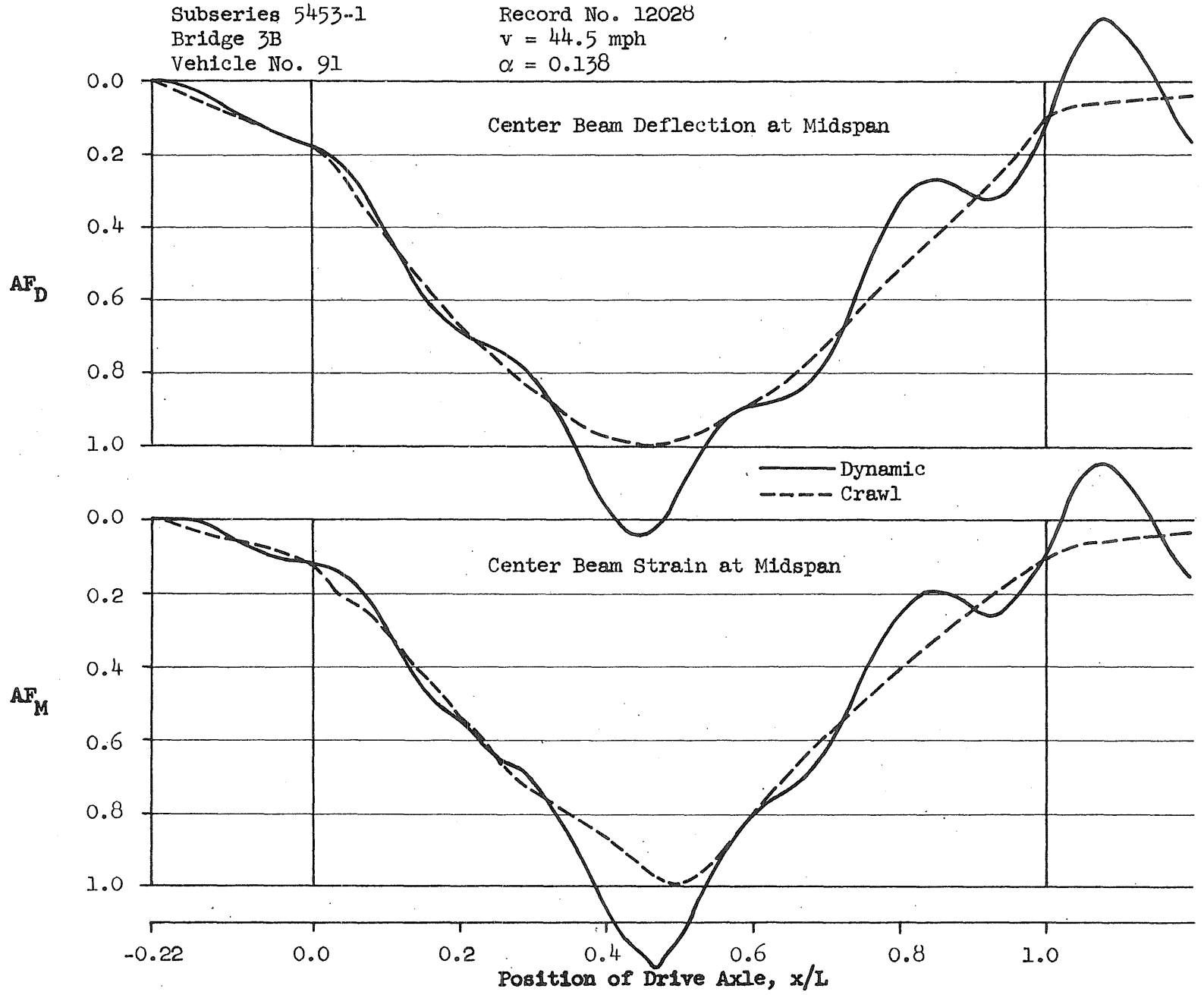

FIG. 25c REPRESENTATIVE RESPONSE CURVES FOR A REGULAR RUN - HISTORY CURVES FOR RESPONSE AT MIDSPAN

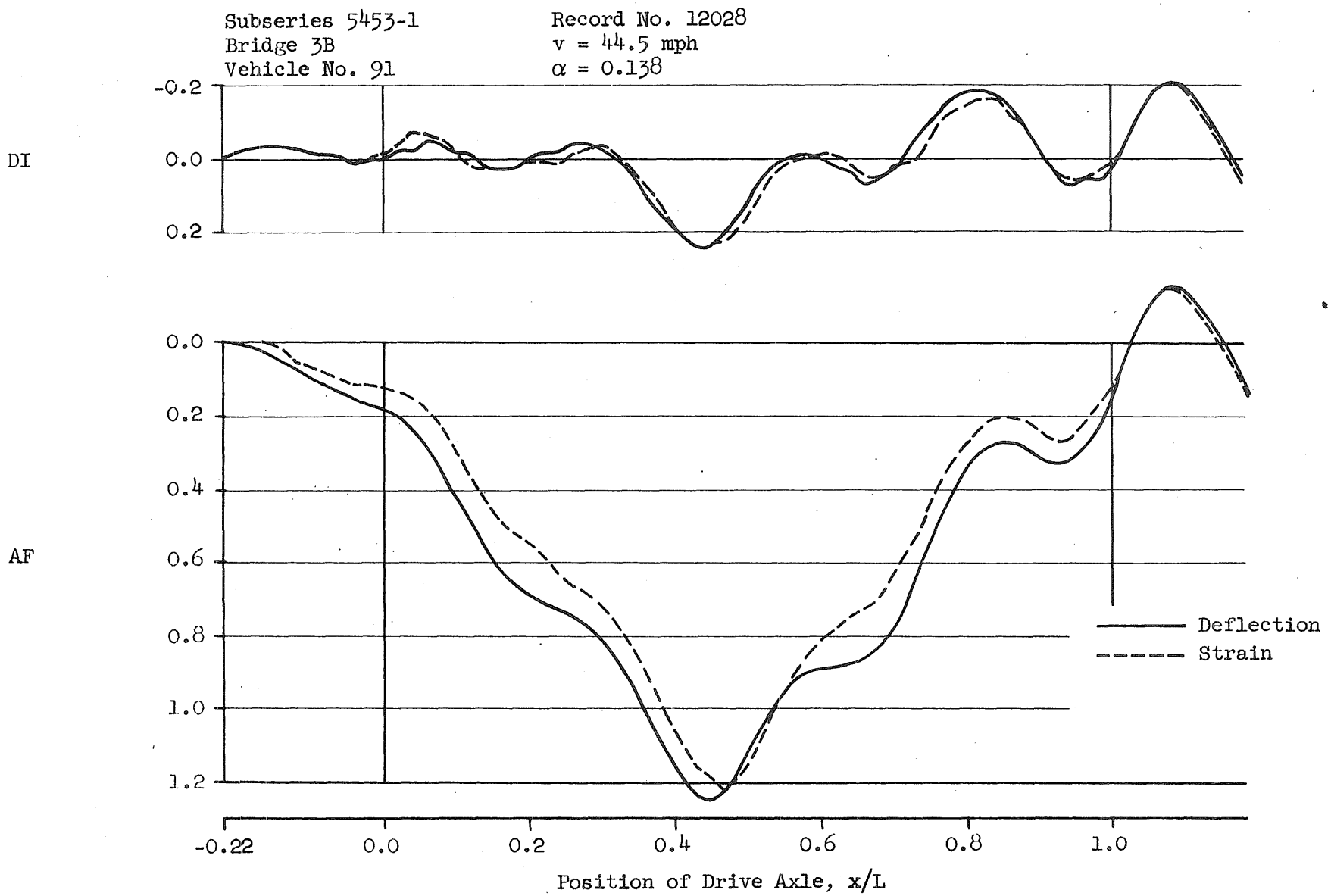

FIG. 25d REPRESENTATIVE RESPONSE CURVES FOR A REGULAR RUN - BRIDGE RESPONSE AT MIDSPAN OF CENTER BEAM

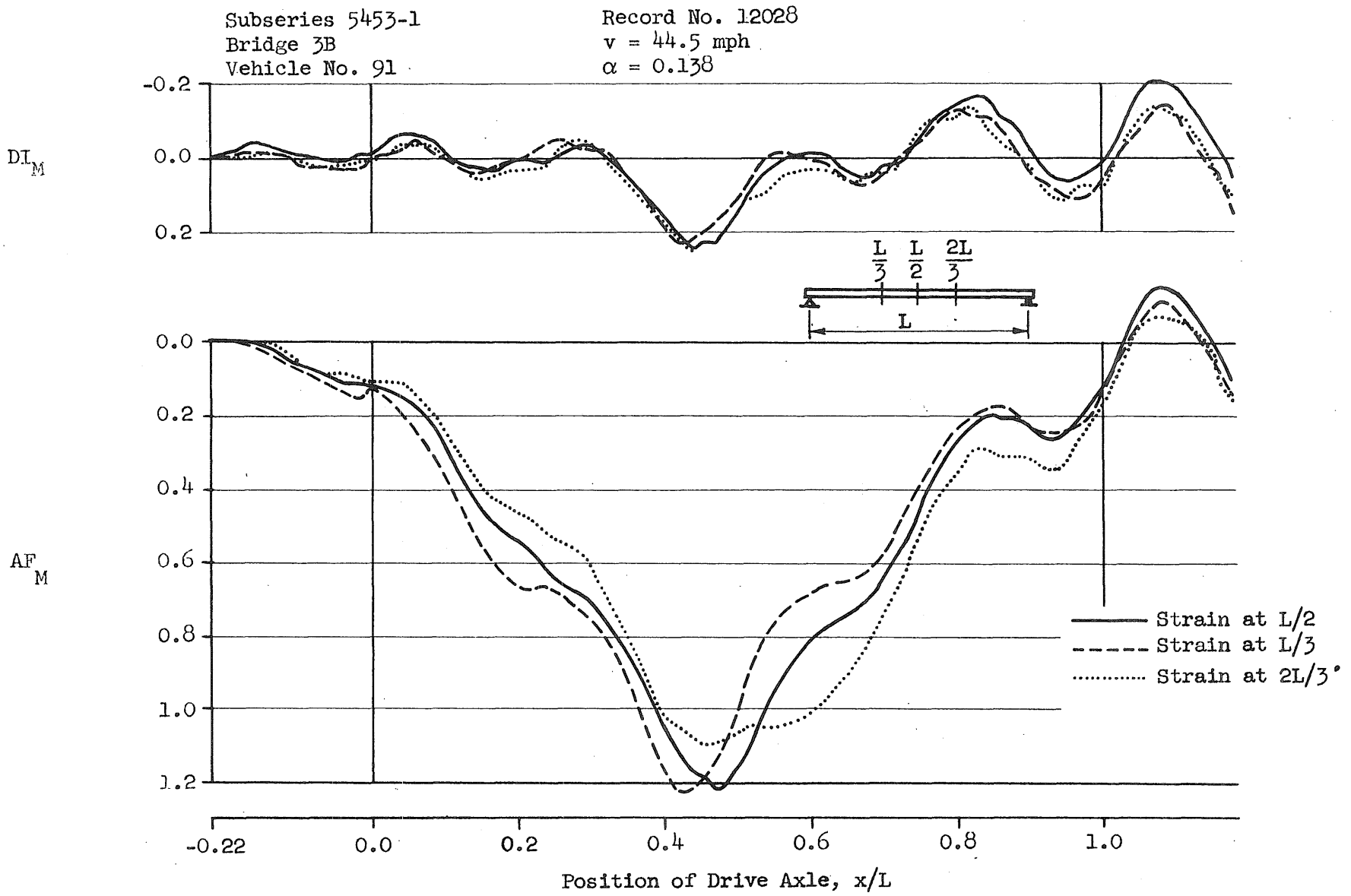

FIG. 25e REPRESENTATIVE RESPONSE CURVES FOR A REGULAR RUN - THIRD-POINT RESPONSE OF CENTER BEAM

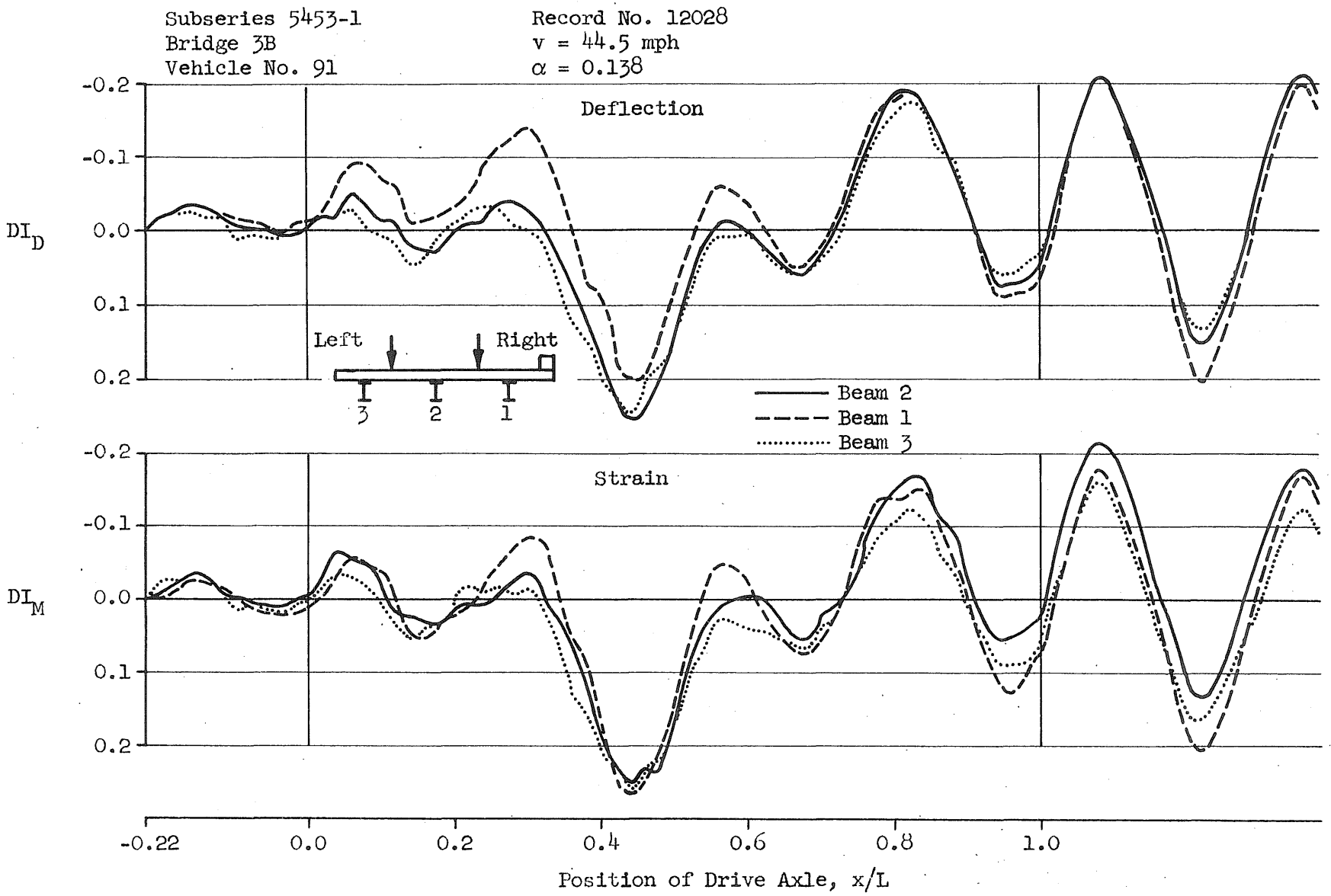

FIG. 25f REPRESENTATIVE RESPONSE CURVES FOR A REGULAR RUN - MIDSPAN RESPONSE OF THREE BEAMS

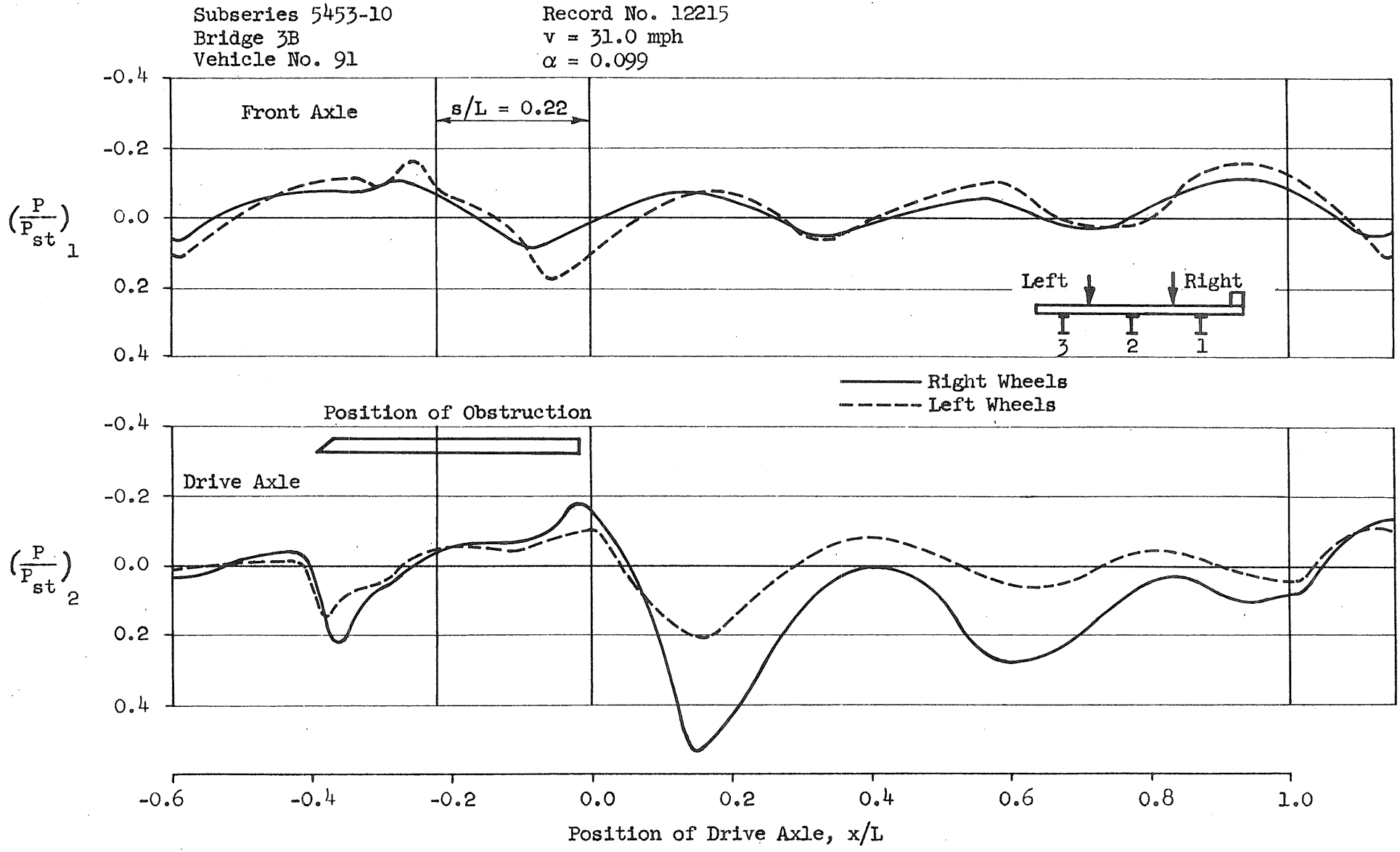

FIG. 26a REPRESENTATIVE RESPONSE CURVES FOR A RUN WITH INDUCED VEHICLE OSCILLATIONS - INTERACTION FORCES

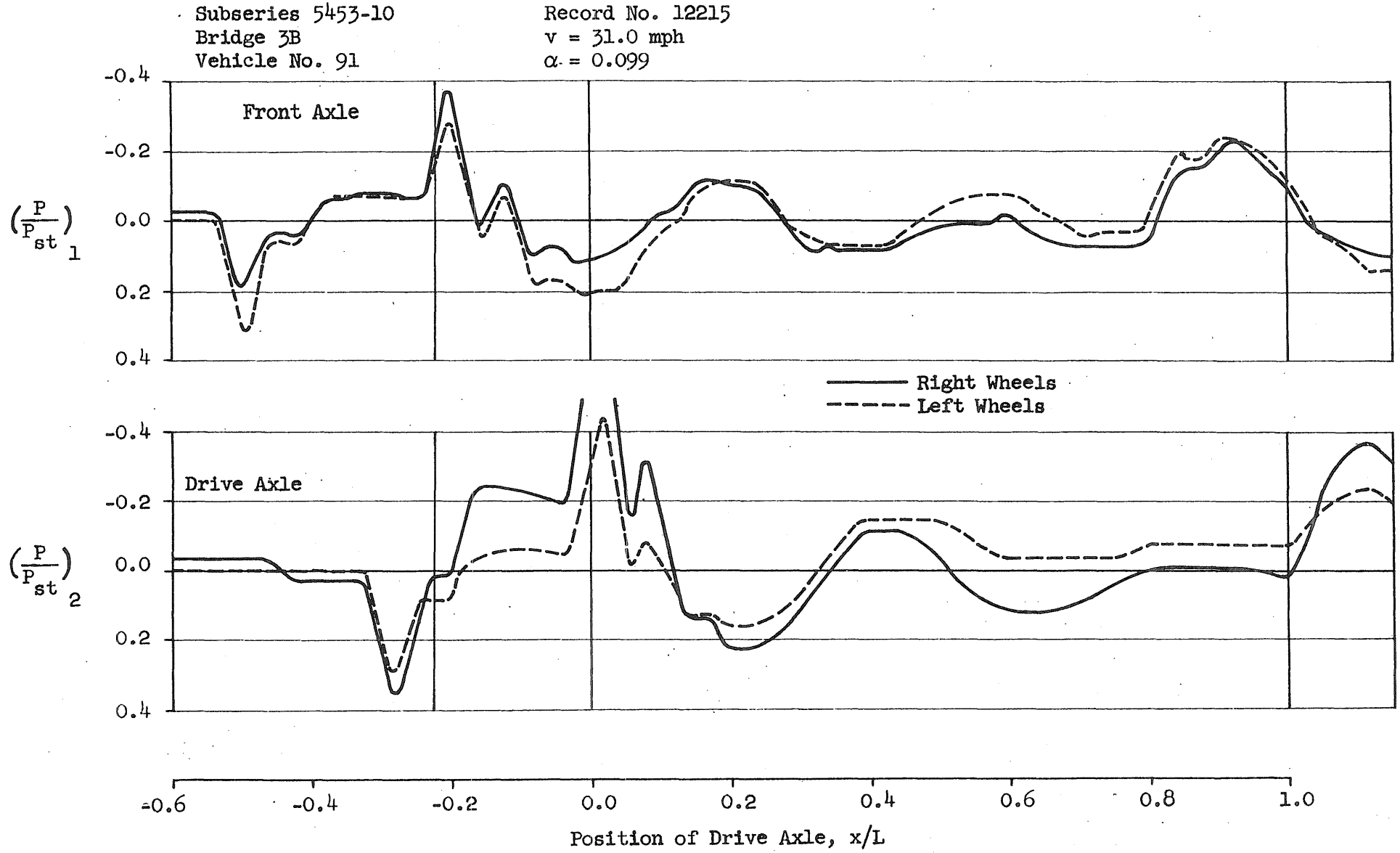

FIG. 26b REPRESENTATIVE RESPONSE CURVES FOR A RUN WITH INDUCED VEHICLE OSCILLATIONS - SPRING RESPONSE

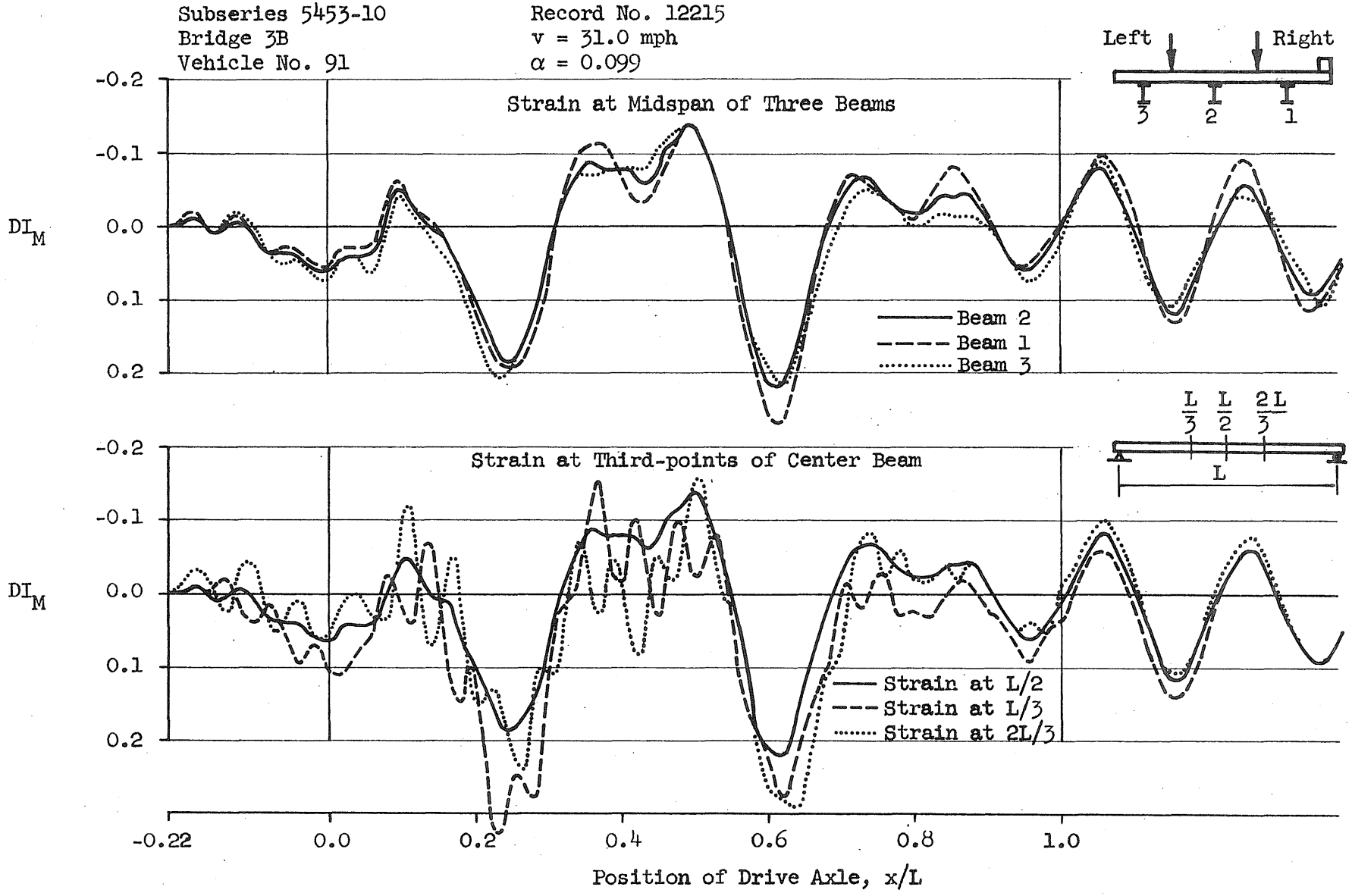

FIG. 26c REPRESENTATIVE RESPONSE CURVES FOR A RUN WITH INDUCED VEHICLE OSCILLATIONS - BRIDGE RESPONSE

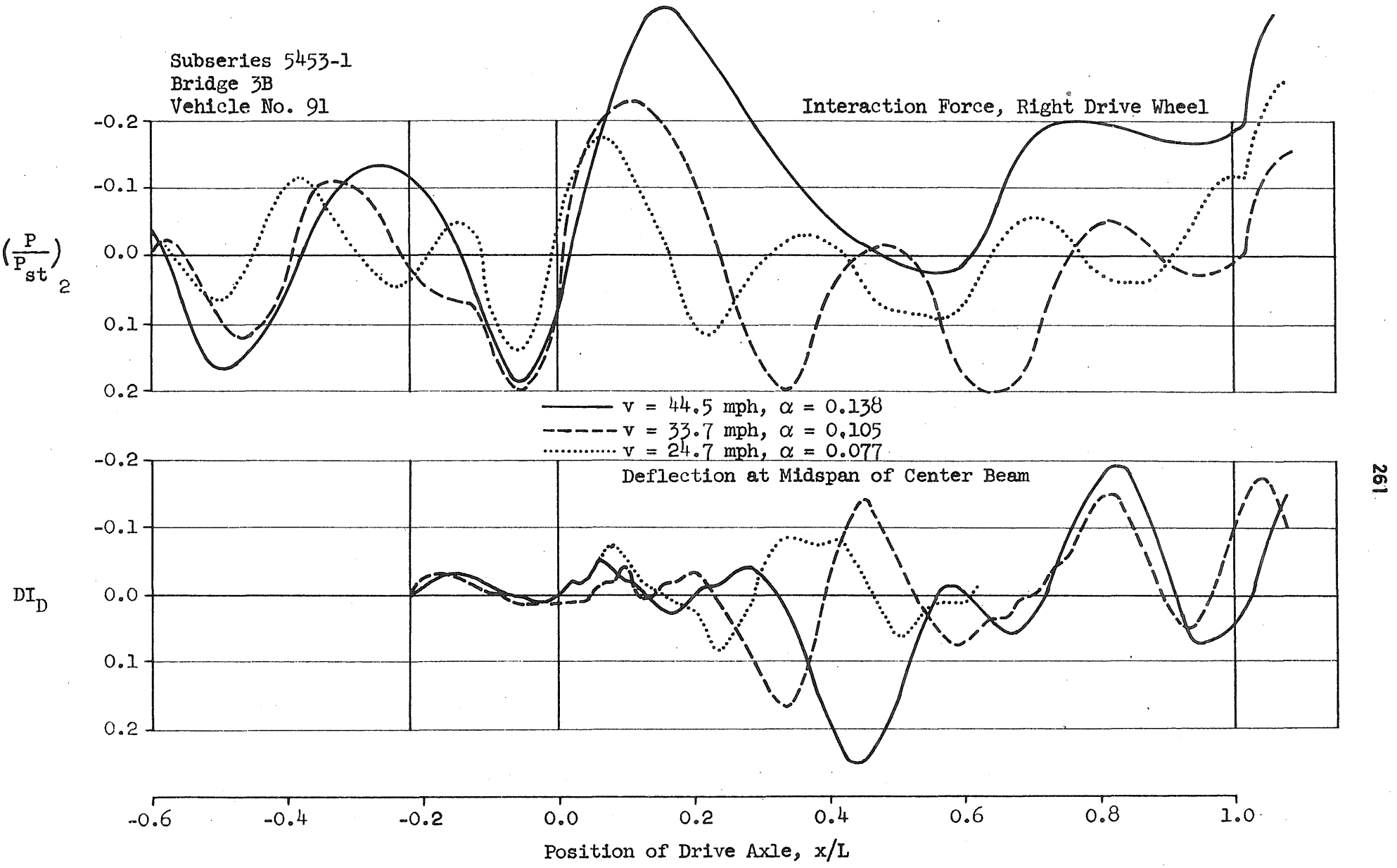

FIG. 27a EFFECT OF SPEED ON BRIDGE AND VEHICLE RESPONSE - REGULAR TESTS

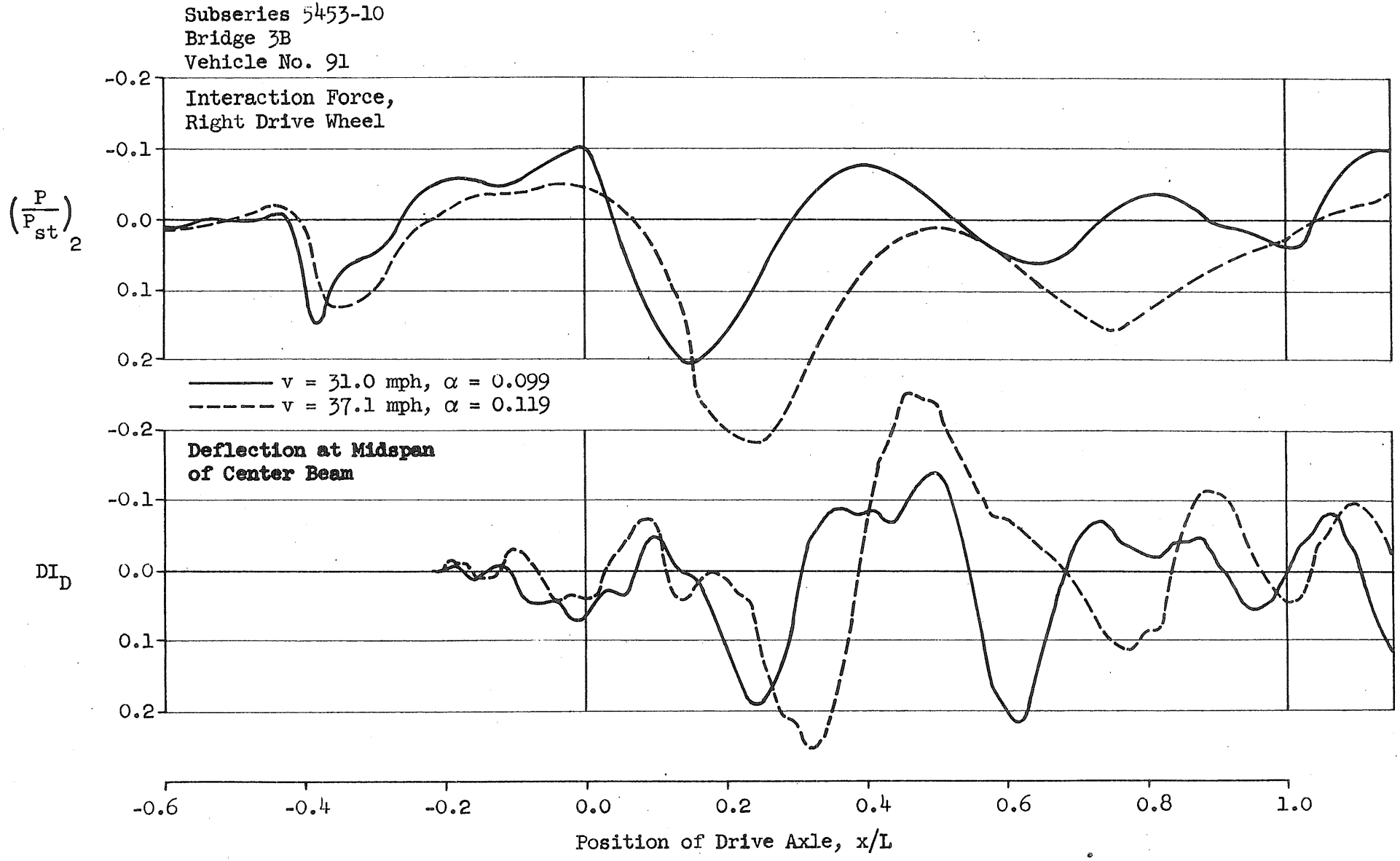

FIG. 27b EFFECT OF SPEED ON BRIDGE AND VEHICLE RESPONSE - TESTS WITH INDUCED VEHICLE OSCILLATIONS

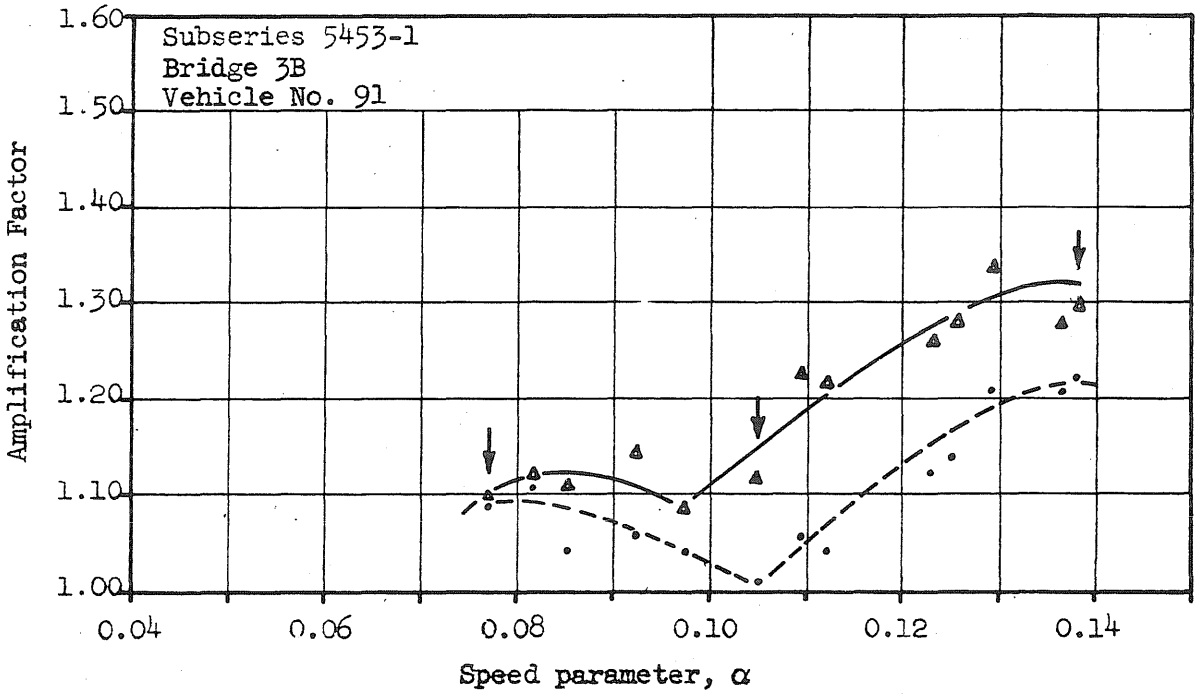

Regular Test Subseries

△ ——— Deflection at Midspan of Center Beam
• – – – – Strain at Midspan of Center Beam

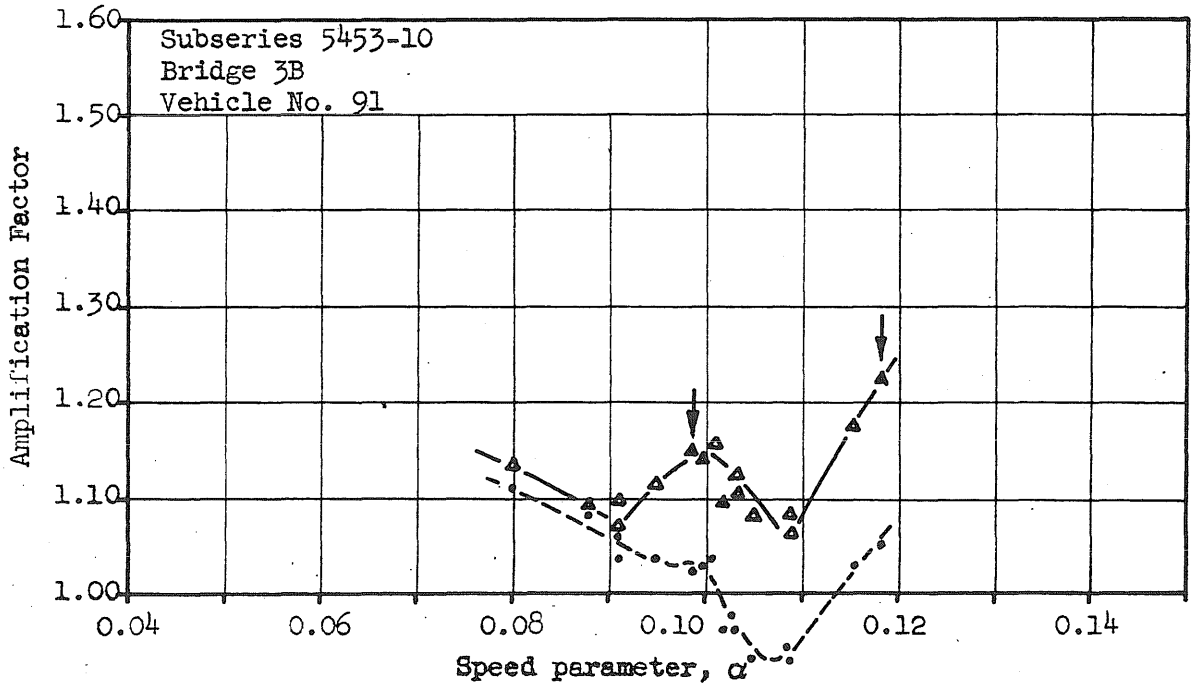

Test Subseries with Induced Vehicle Oscillations

△ ——— Deflection at Midspan of Center Beam
• – – – – Strain at Midspan of Center Beam

FIG. 28 REPRESENTATIVE SPECTRUM CURVES

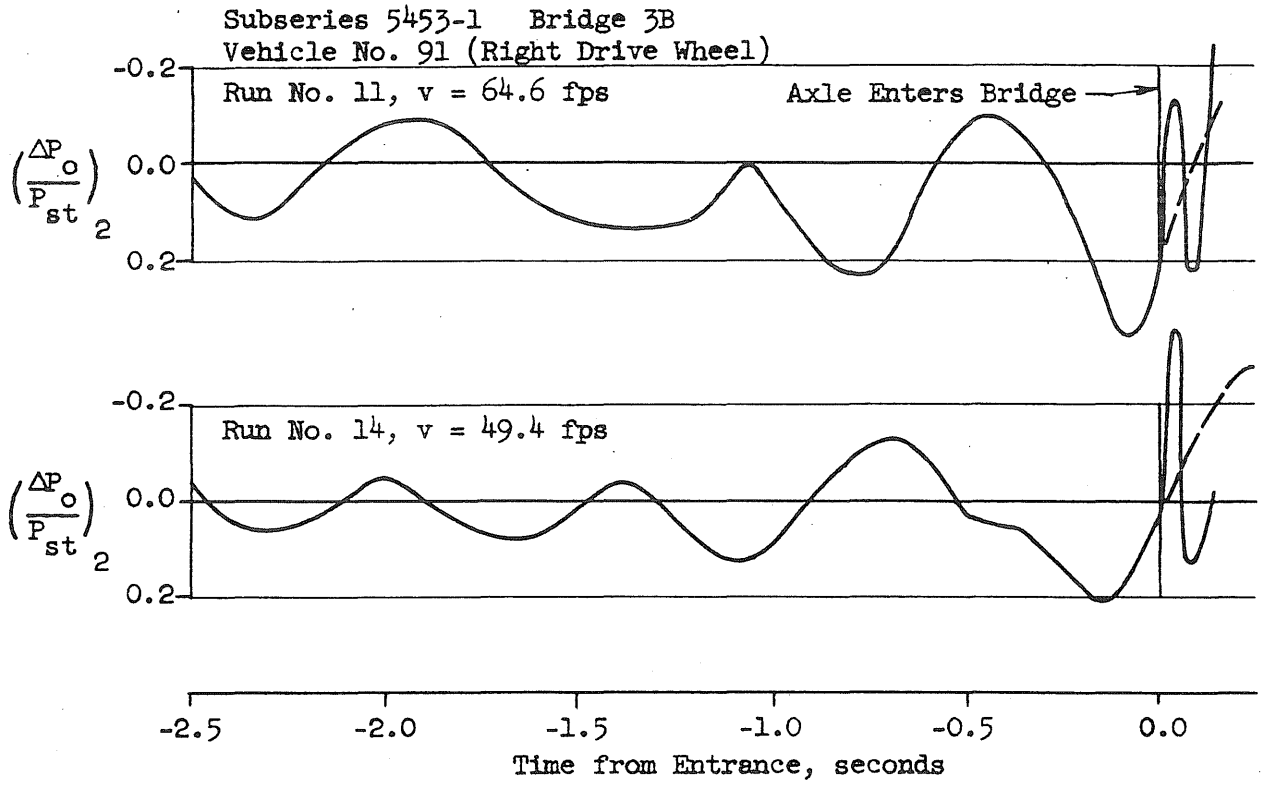

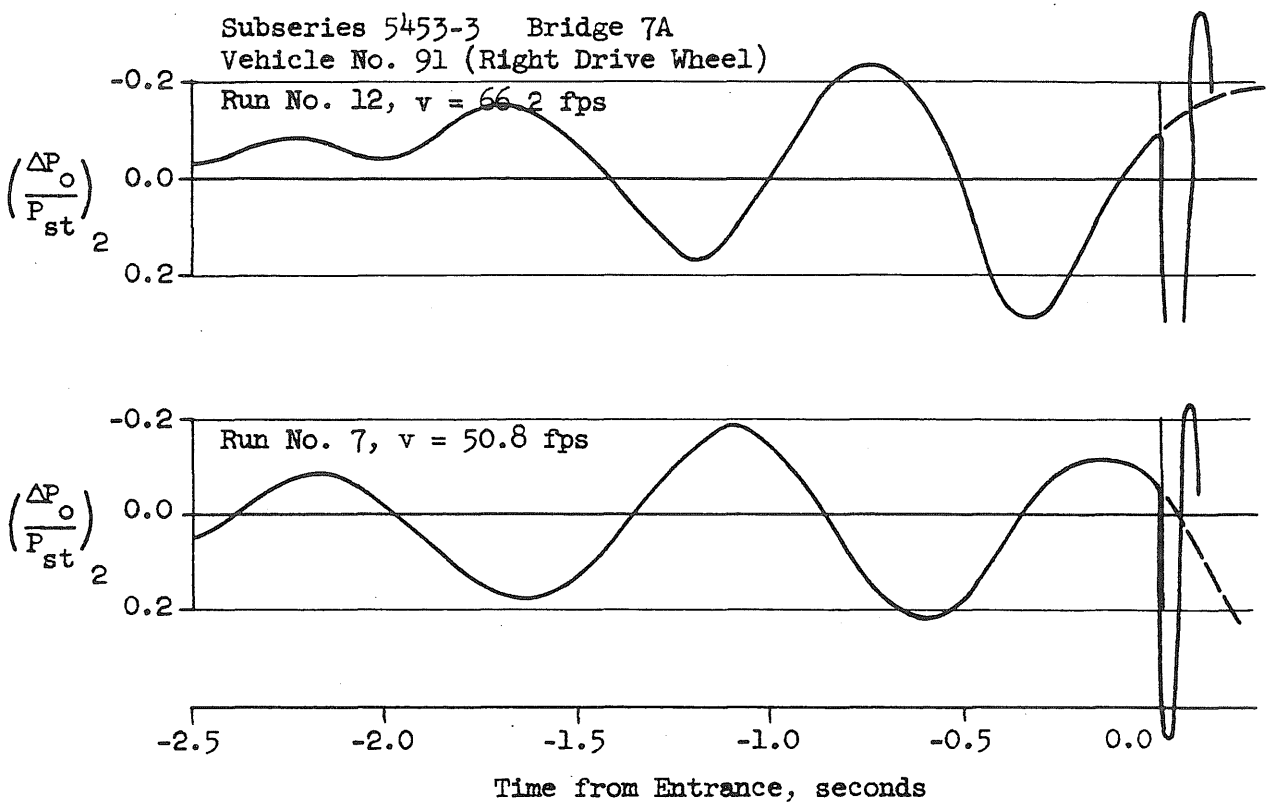

FIG. 29a TYPICAL INTERACTION FORCE PLOTS ON THE APPROACH PAVEMENTS

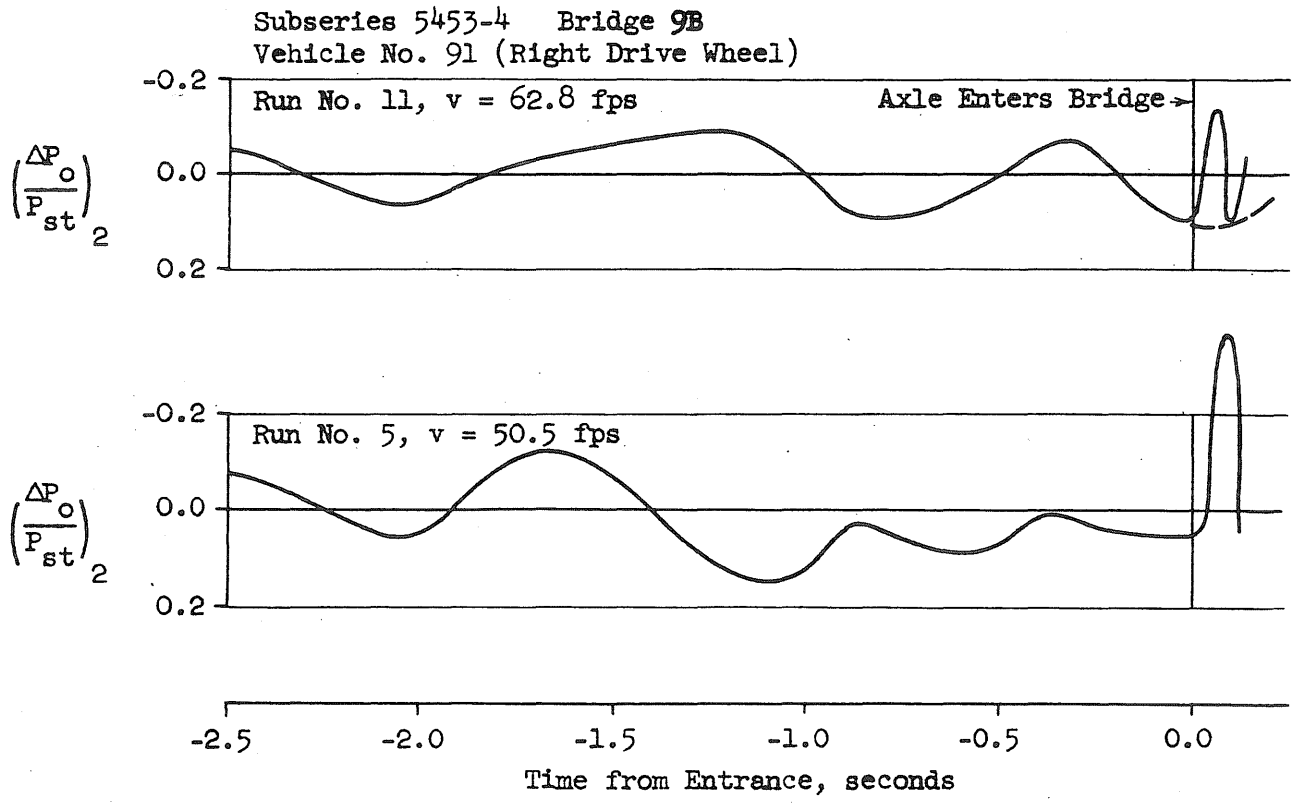

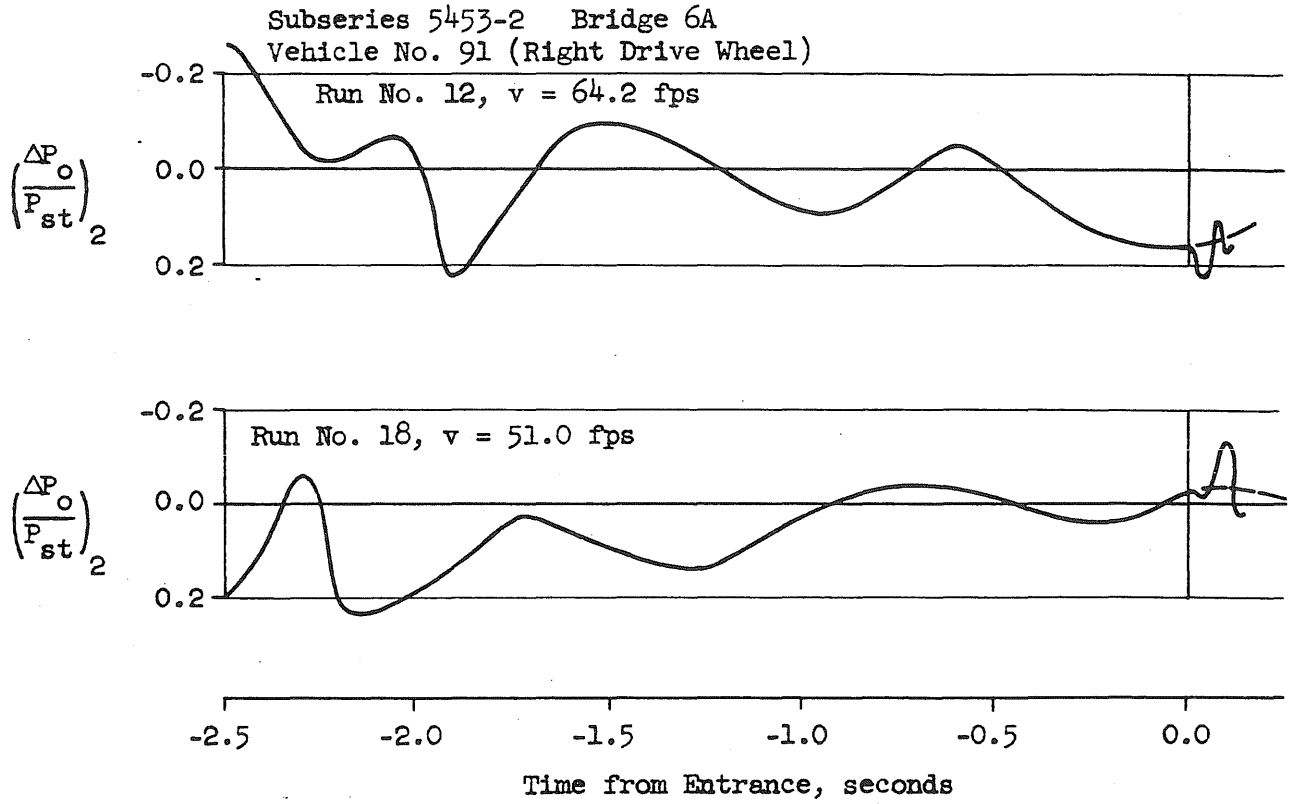

FIG. 29b TYPICAL INTERACTION FORCE PLOTS ON THE APPROACH PAVEMENTS

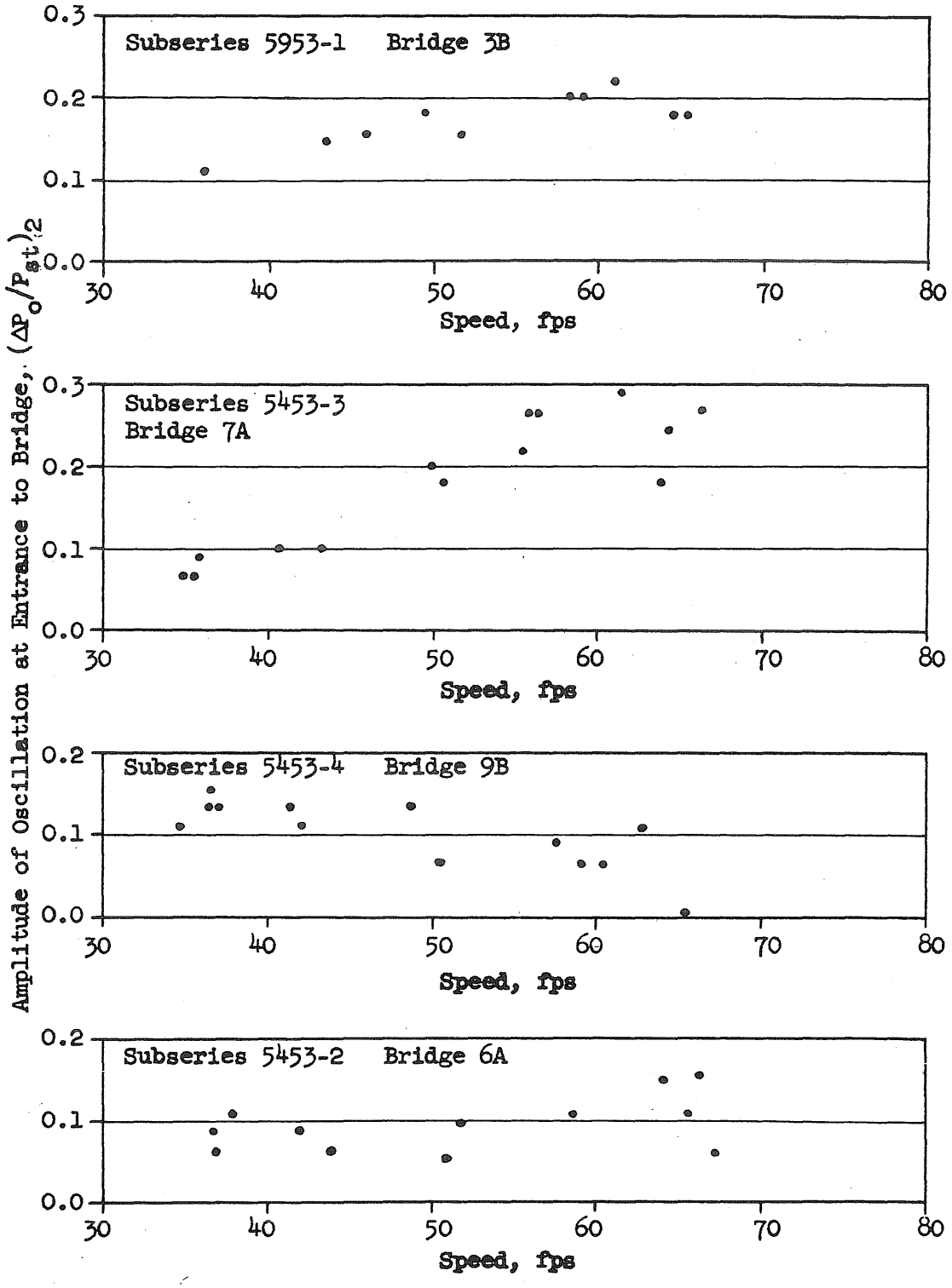

FIG. 30a VARIATION OF MAGNITUDE OF INITIAL OSCILLATIONS WITH SPEED-VEHICLE NO. 91

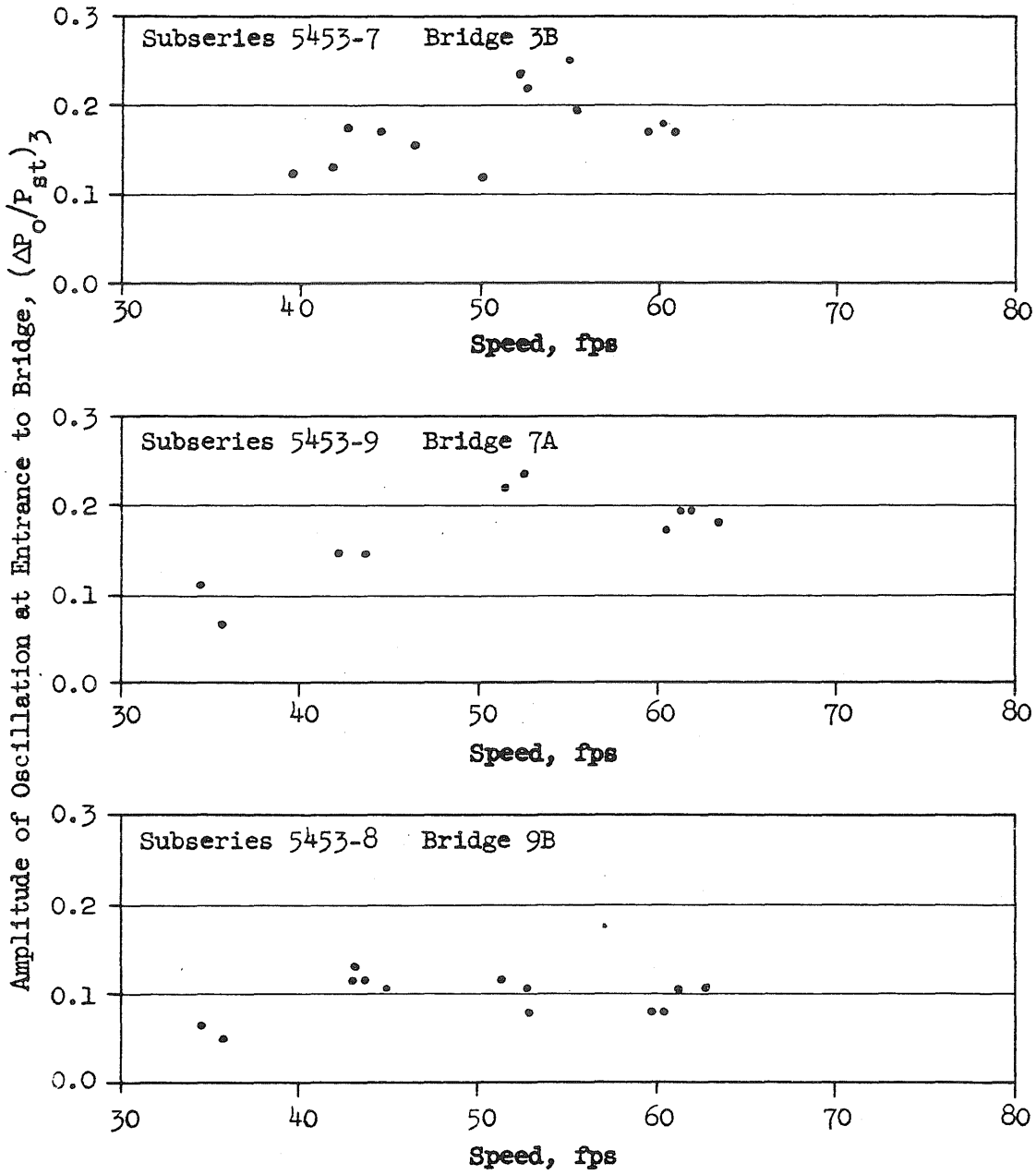

FIG. 30b VARIATION OF MAGNITUDE OF INITIAL OSCILLATIONS WITH SPEED-VEHICLE NO. 513

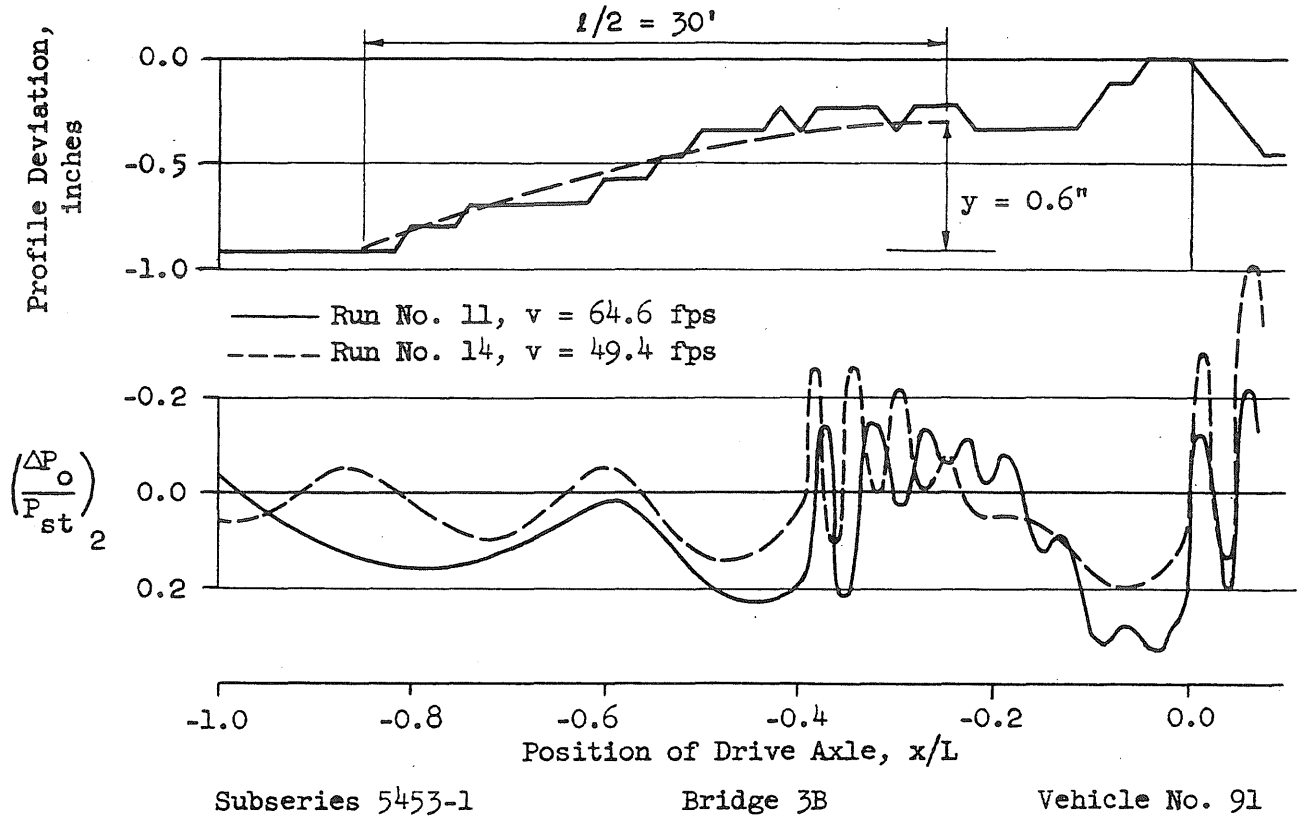

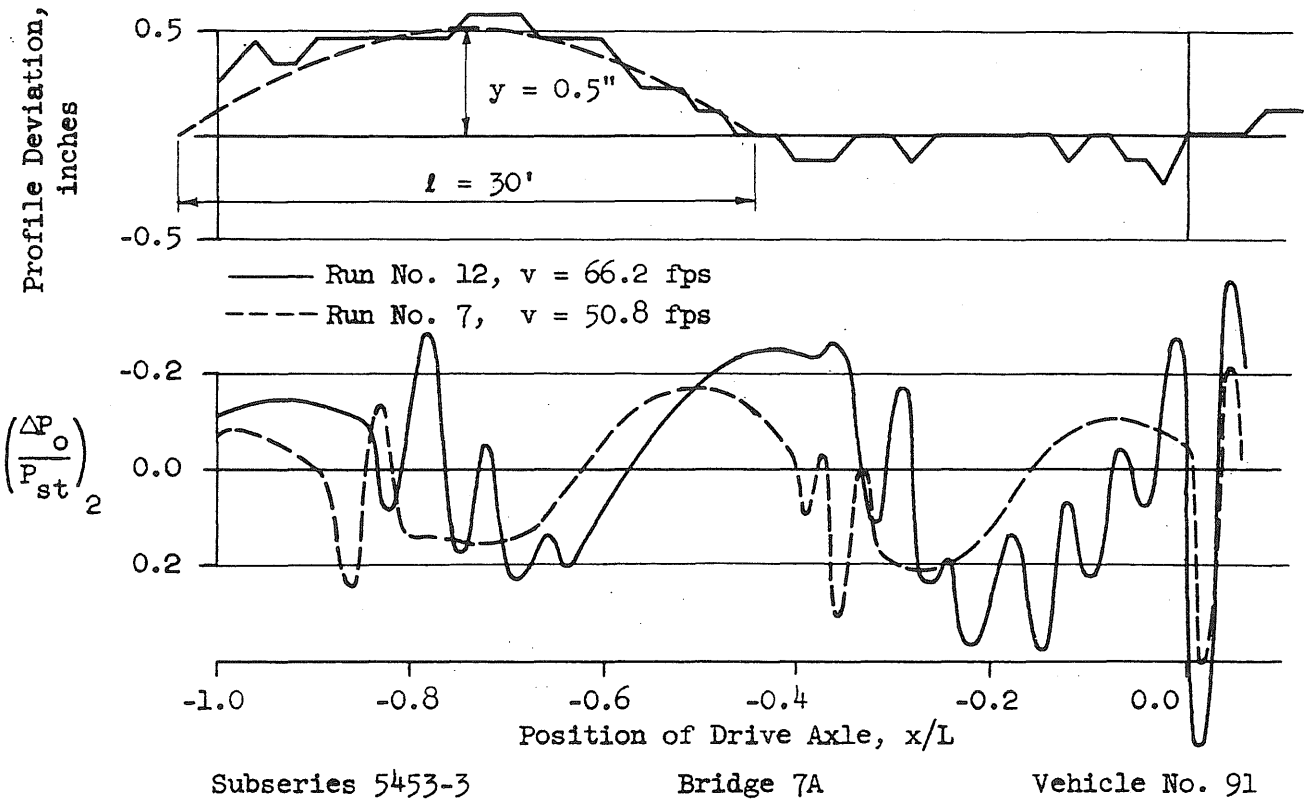

FIG. 31 RELATIONSHIP BETWEEN APPROACH PROFILE AND VEHICLE OSCILLATIONS

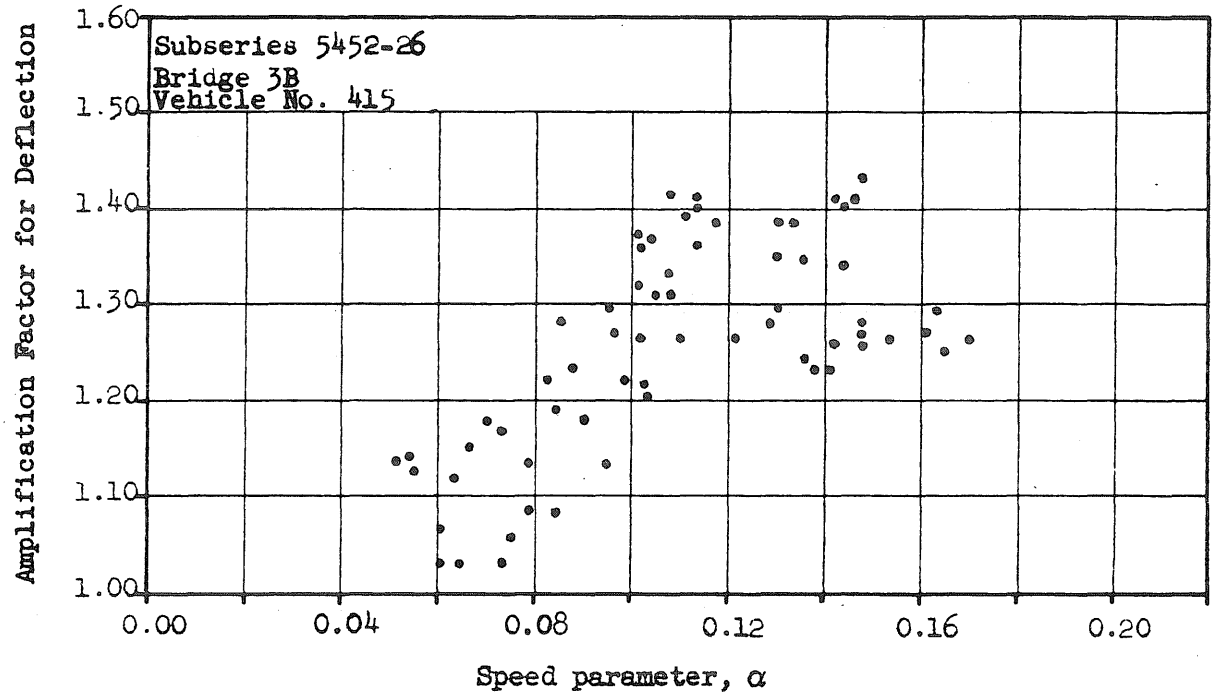

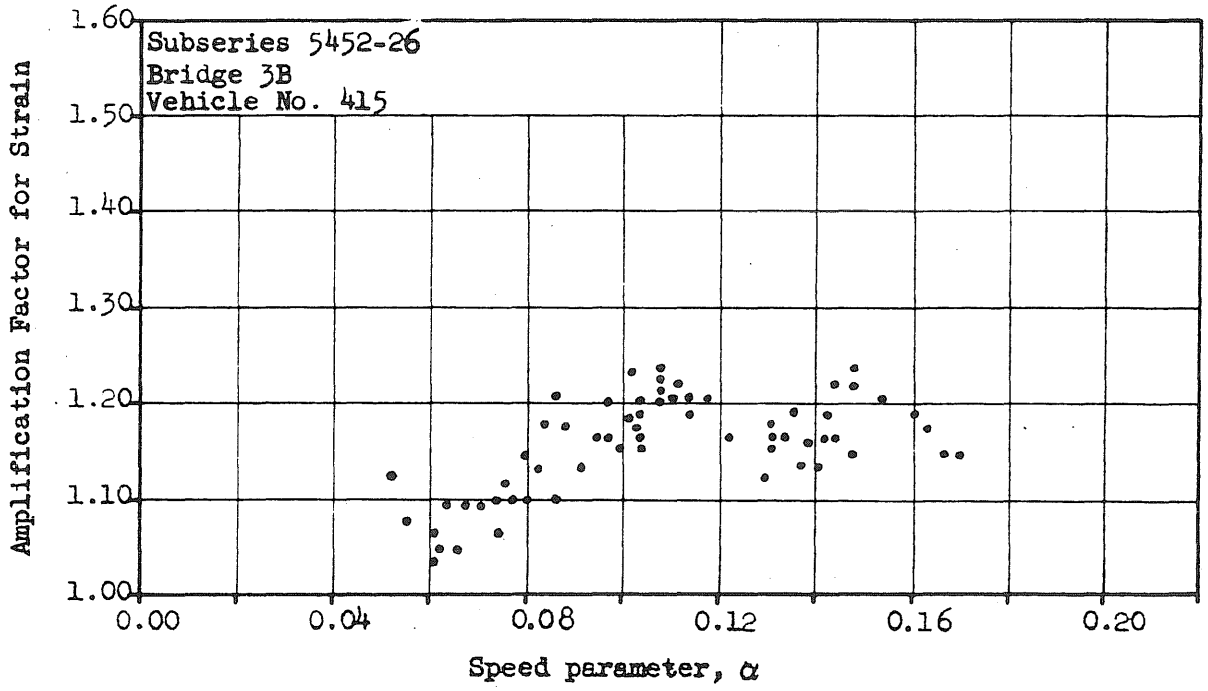

FIG. 32 SPECTRUM CURVES FOR SUBSERIES 5452-26
Center Beam Midspan Response

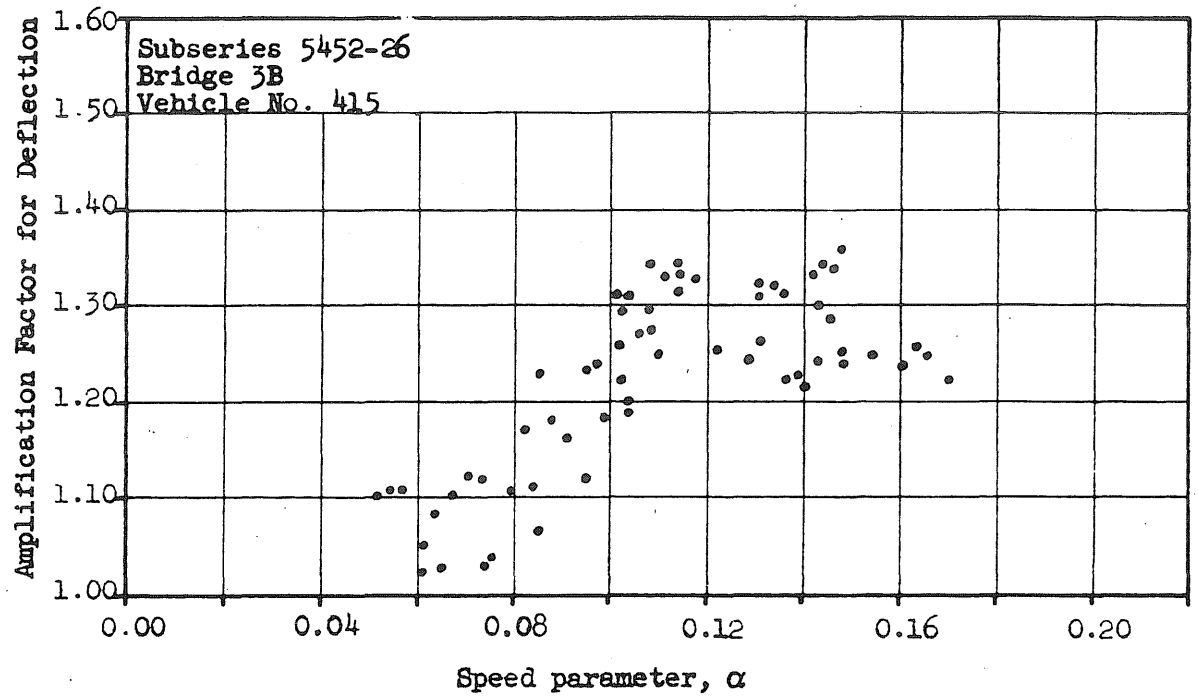

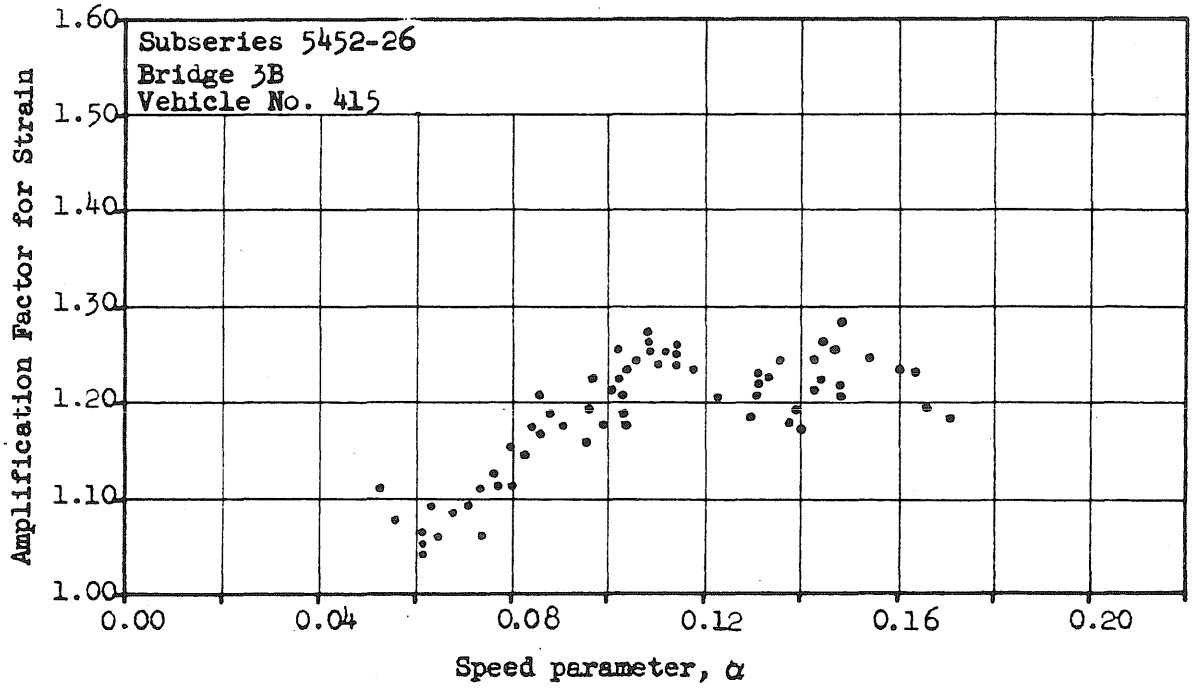

FIG. 33 SPECTRUM CURVES FOR SUBSERIES 5452-26
Average Midspan Response of Three Beams

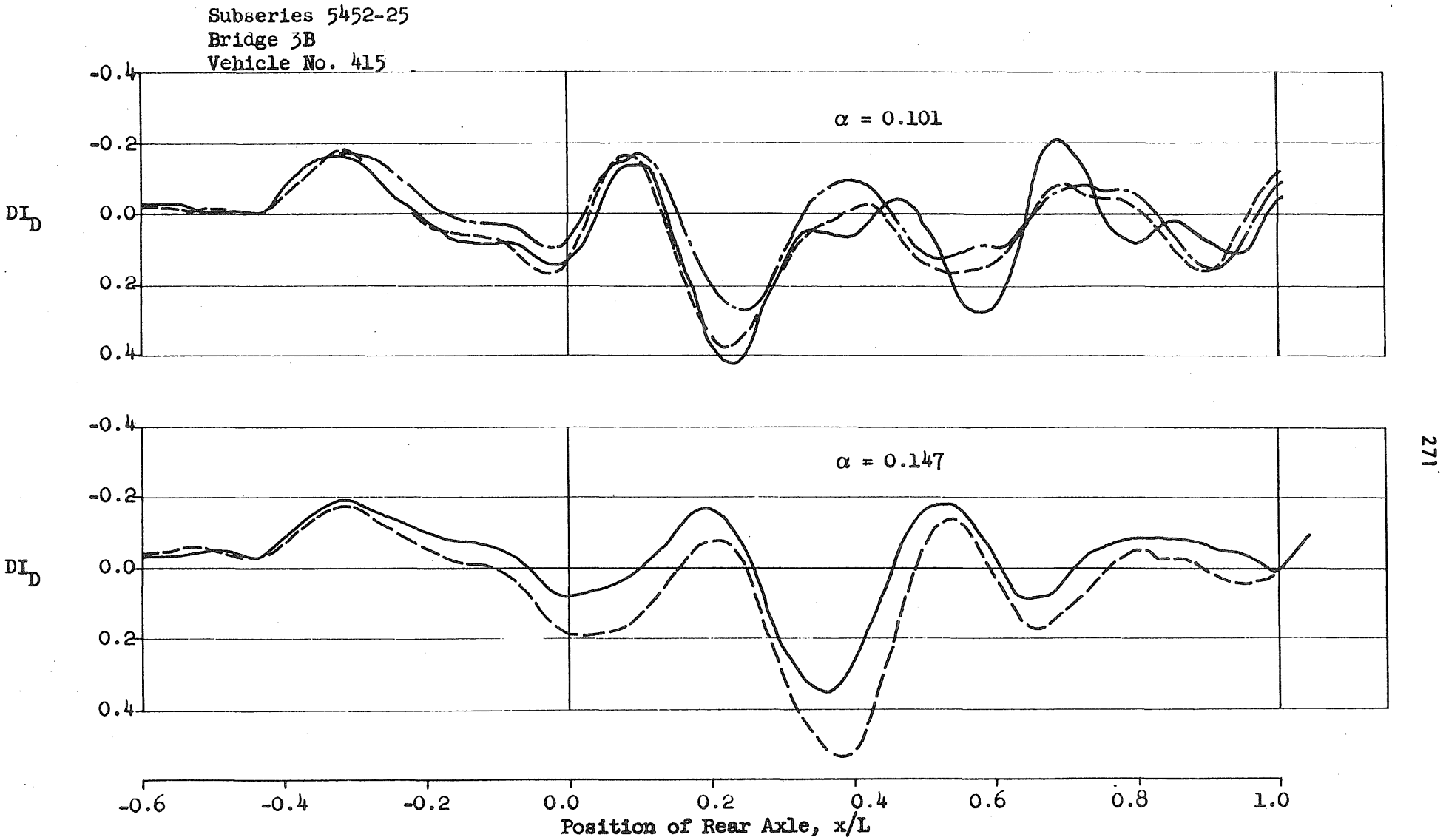

FIG. 34 REPLICATION OF DYNAMIC INCREMENT CURVES

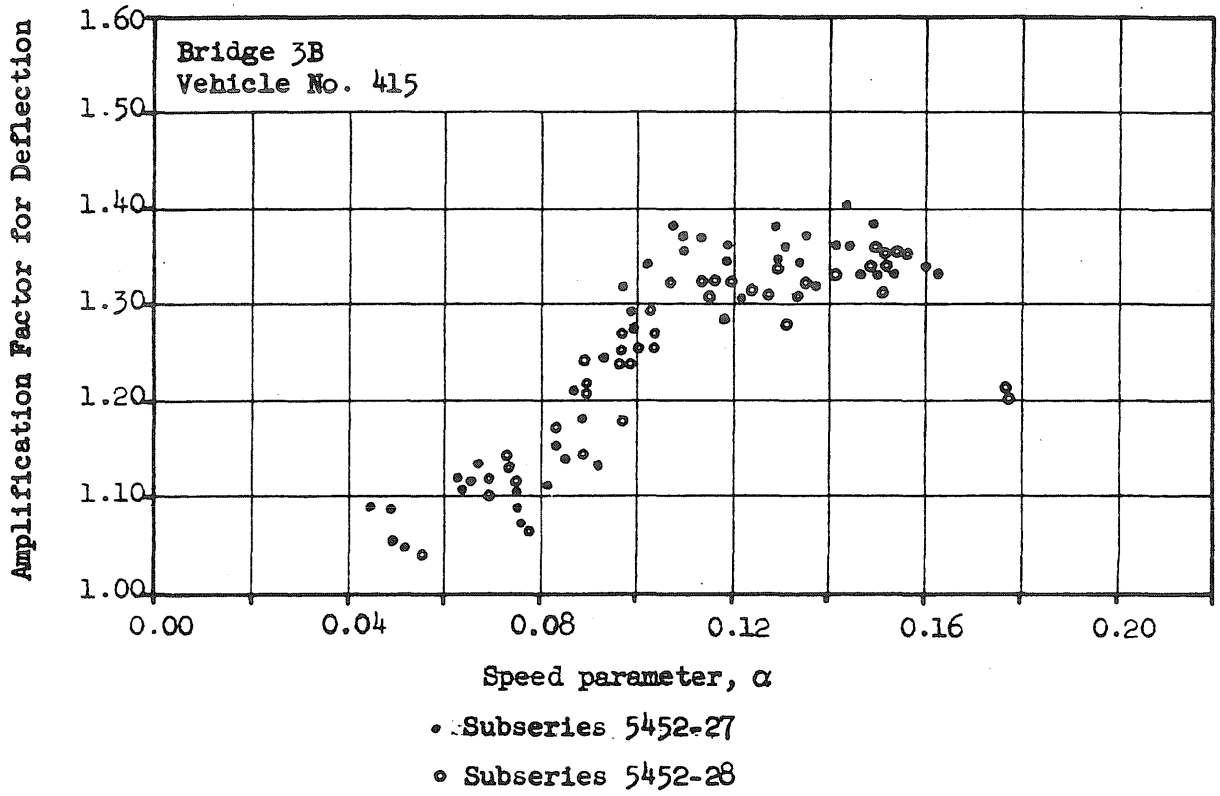

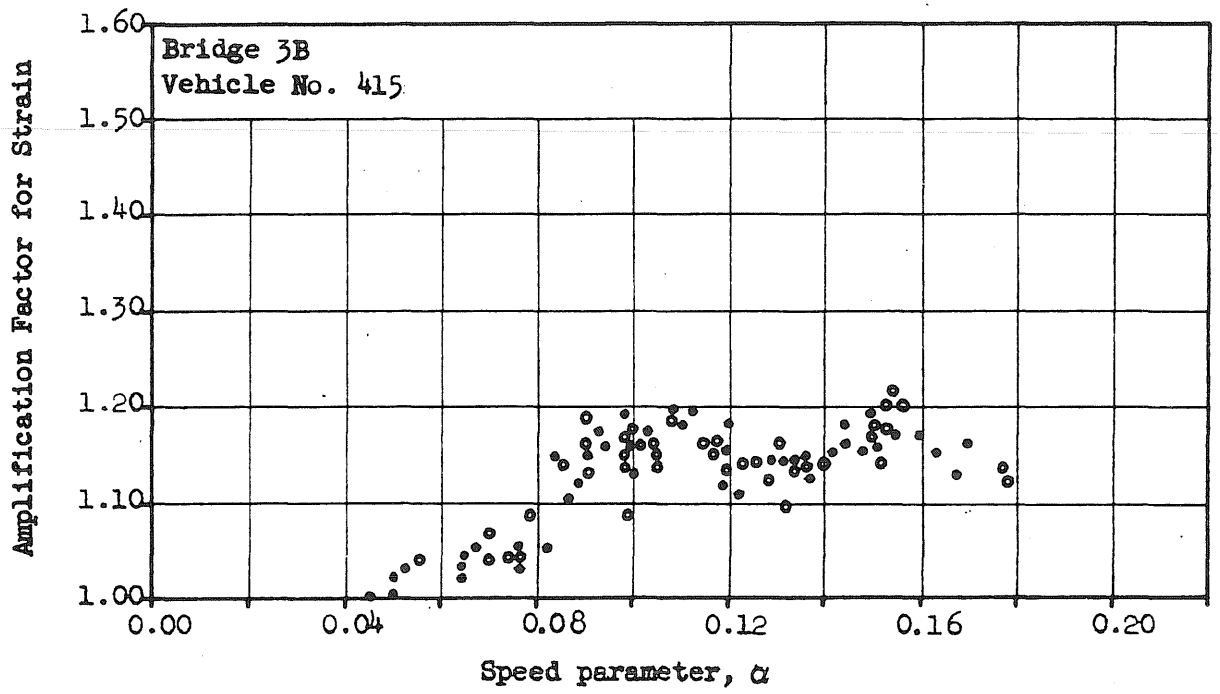

FIG. 35 REPLICATION OF SPECTRUM CURVES

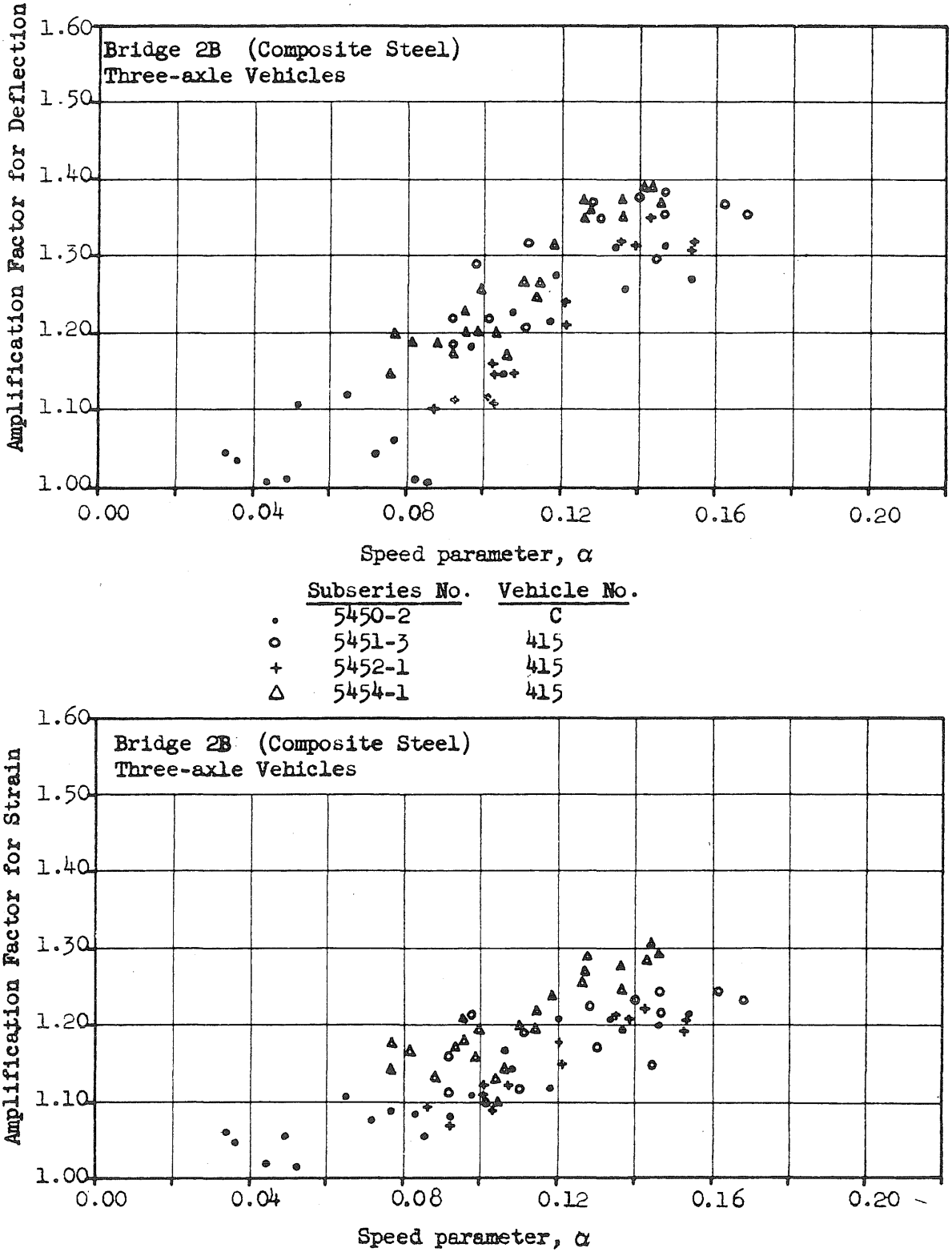

FIG. 36a SPECTRUM CURVES FOR REGULAR TESTS
Bridge 2B - Three-axle Vehicles

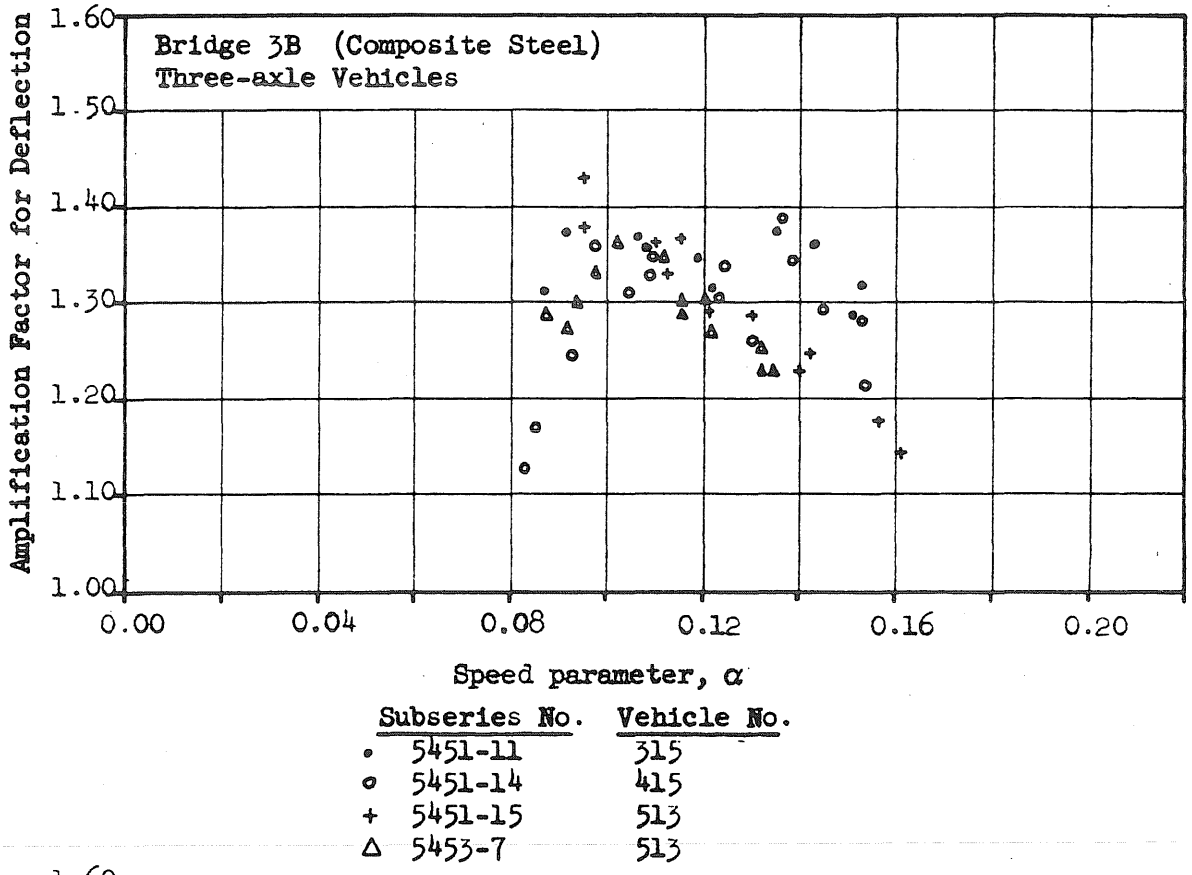

Subseries No.	Vehicle No.
• 5451-11	315
o 5451-14	415
+ 5451-15	513
Δ 5453-7	513

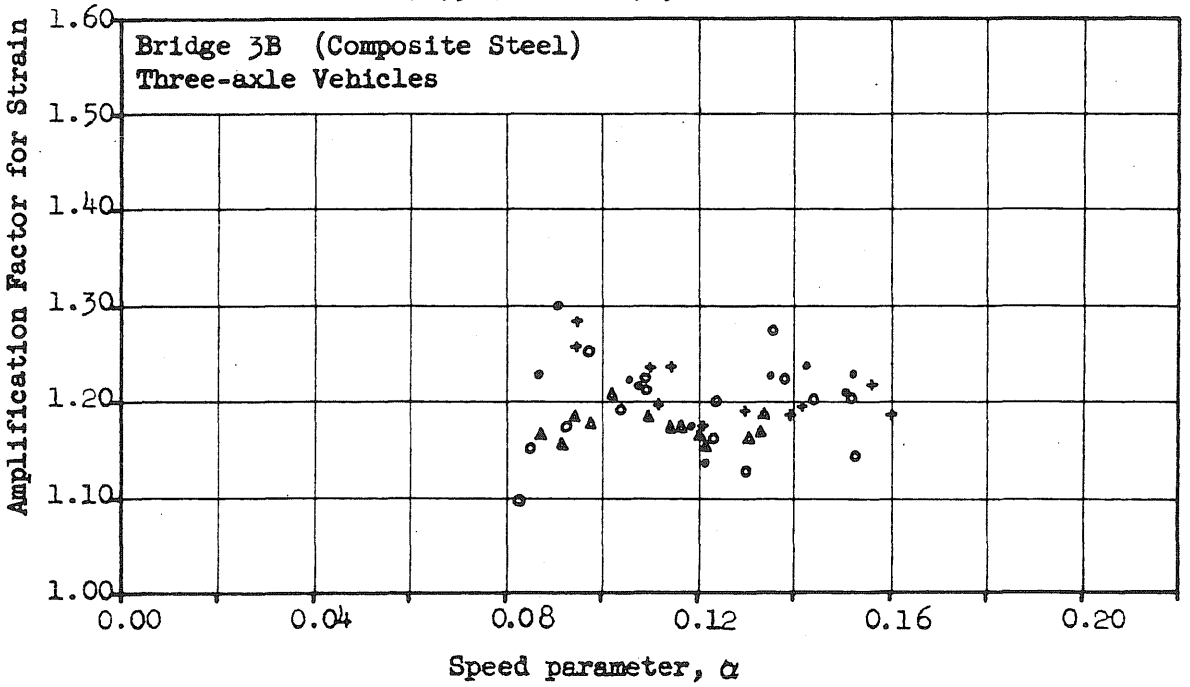

FIG. 36b SPECTRUM CURVES FOR REGULAR TESTS
Bridge 3B - Three-axle Vehicles

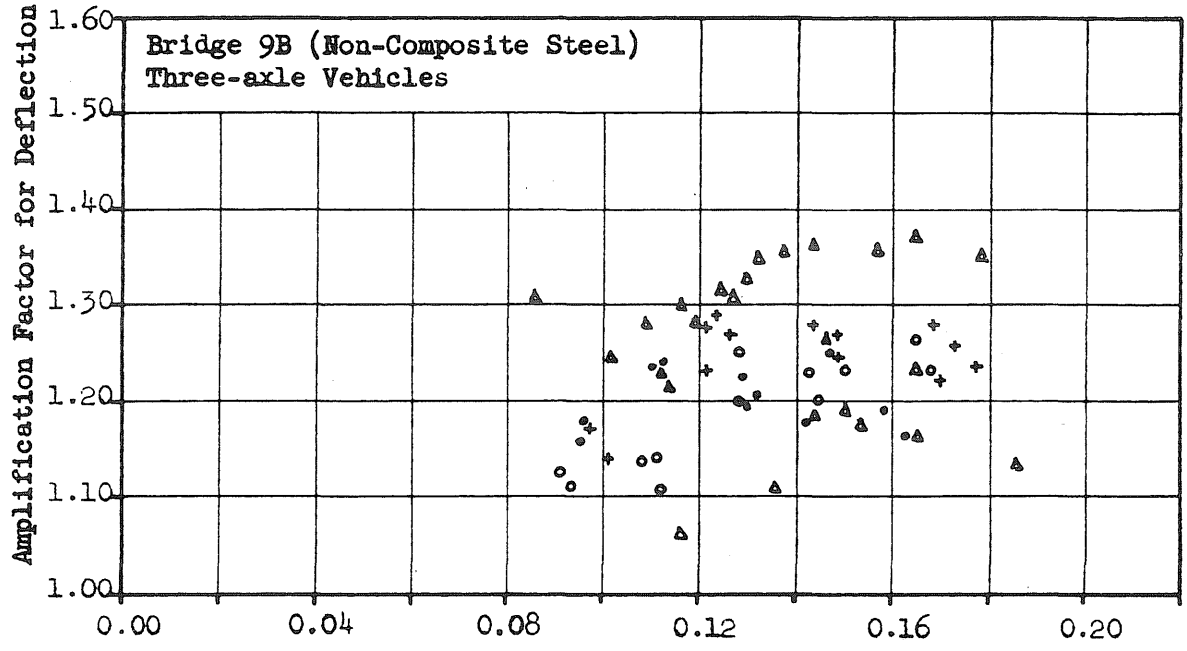

Subseries No.	Vehicle No.
• 5451-6	415
o 5452-3	415
+ 5453-8	513
△ 5454-4	415

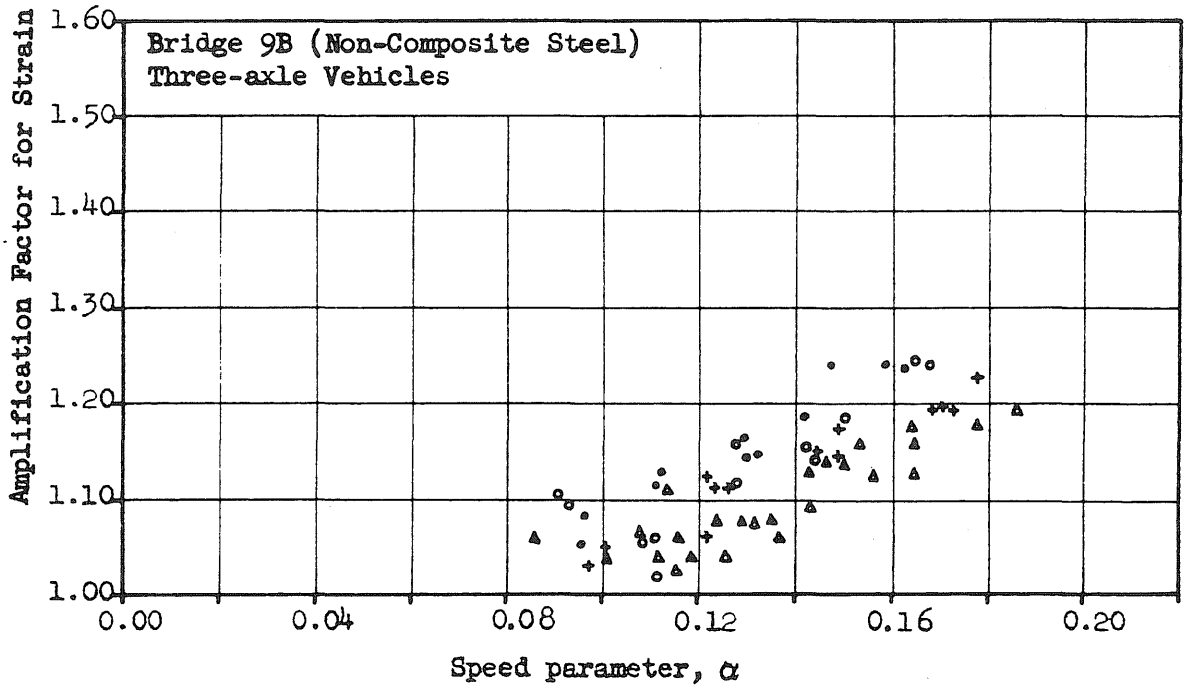

FIG. 36c SPECTRUM CURVES FOR REGULAR TESTS
Bridge 9B - Three-axle Vehicles

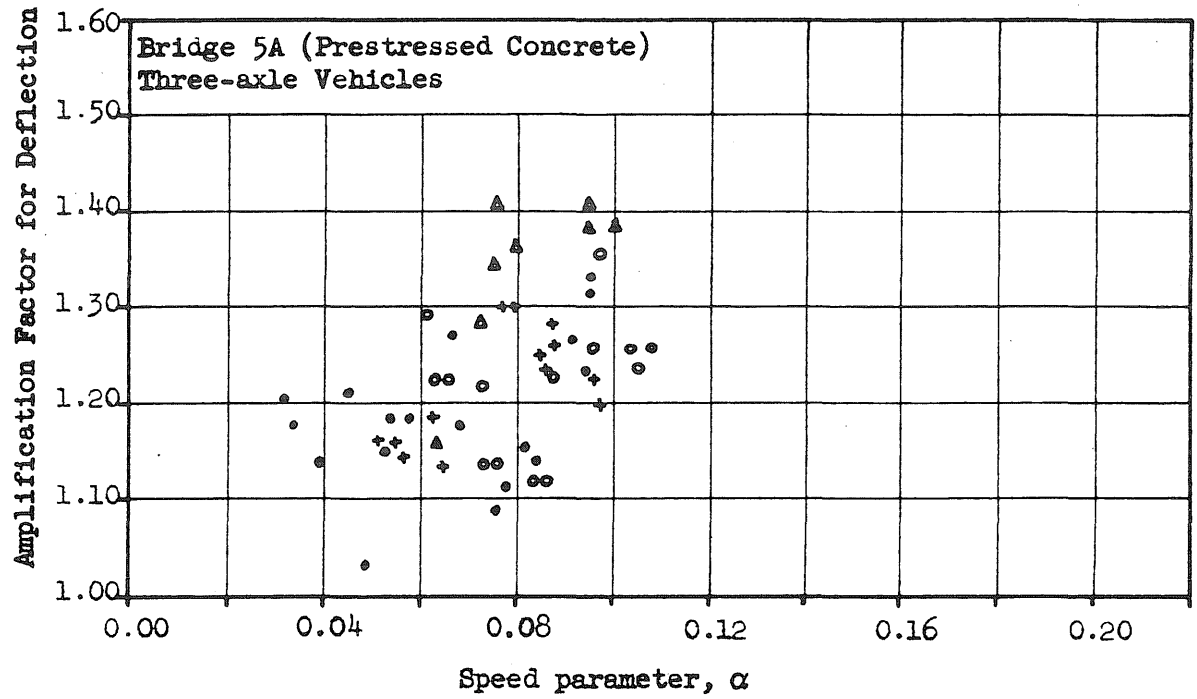

Subseries No.	Vehicle No.
• 5450-3	C
o 5451-12	315
+ 5452-4	415
△ 5454-2	415

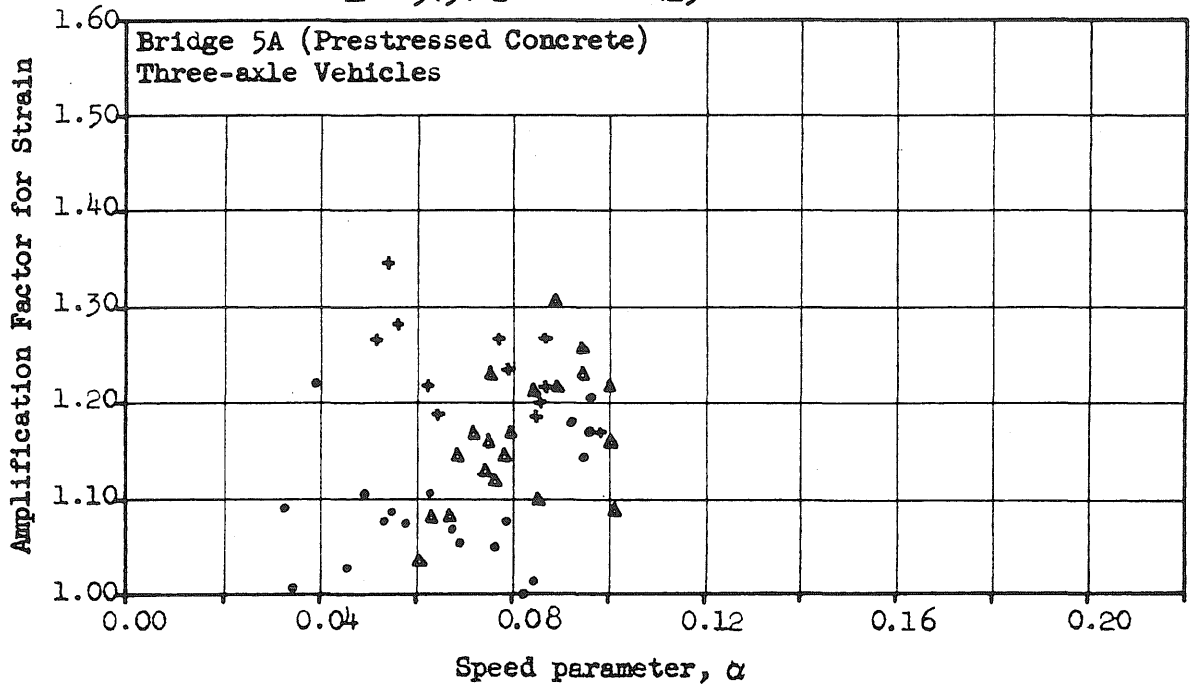

FIG. 36d SPECTRUM CURVES FOR REGULAR TESTS
Bridge 5A - Three Axle Vehicles

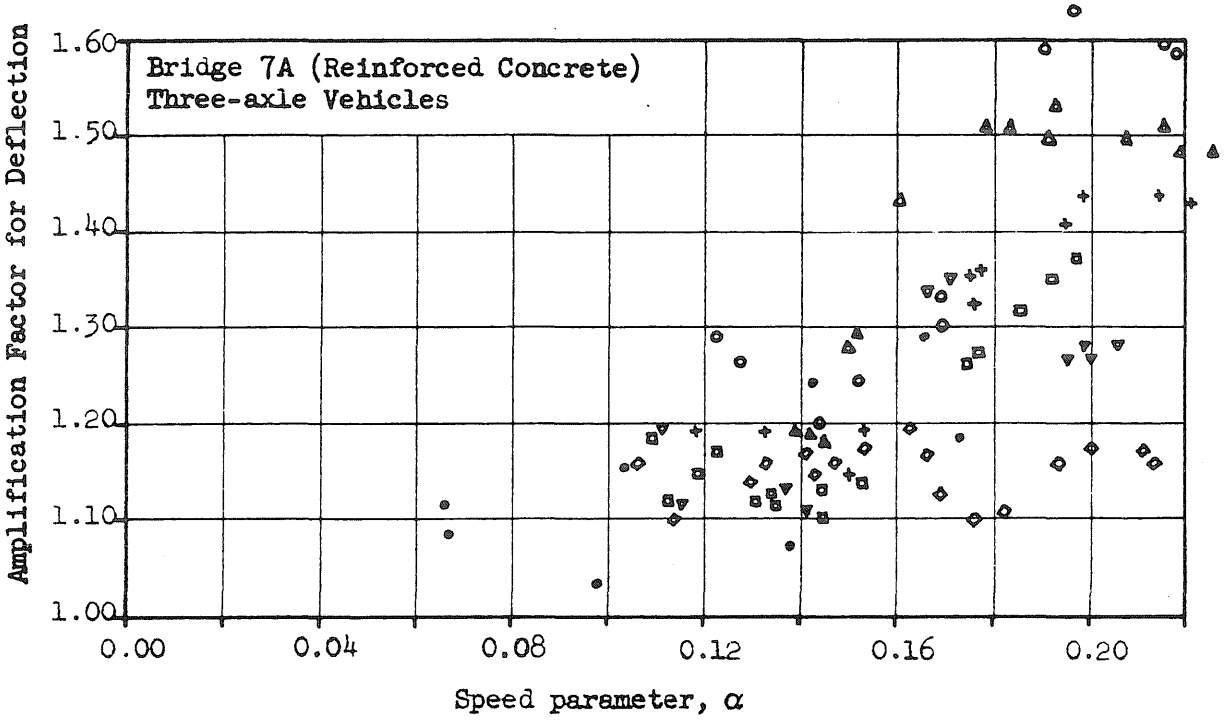

Subseries No.	Vehicle No.	Subseries No.	Vehicle No.
• 5450-5	C	▫ 5452-2	415
○ 5451-13	315	▽ 5453-9	513
+ 5451-5	415	◇ 5454-3	415
△ 5451-16	513		

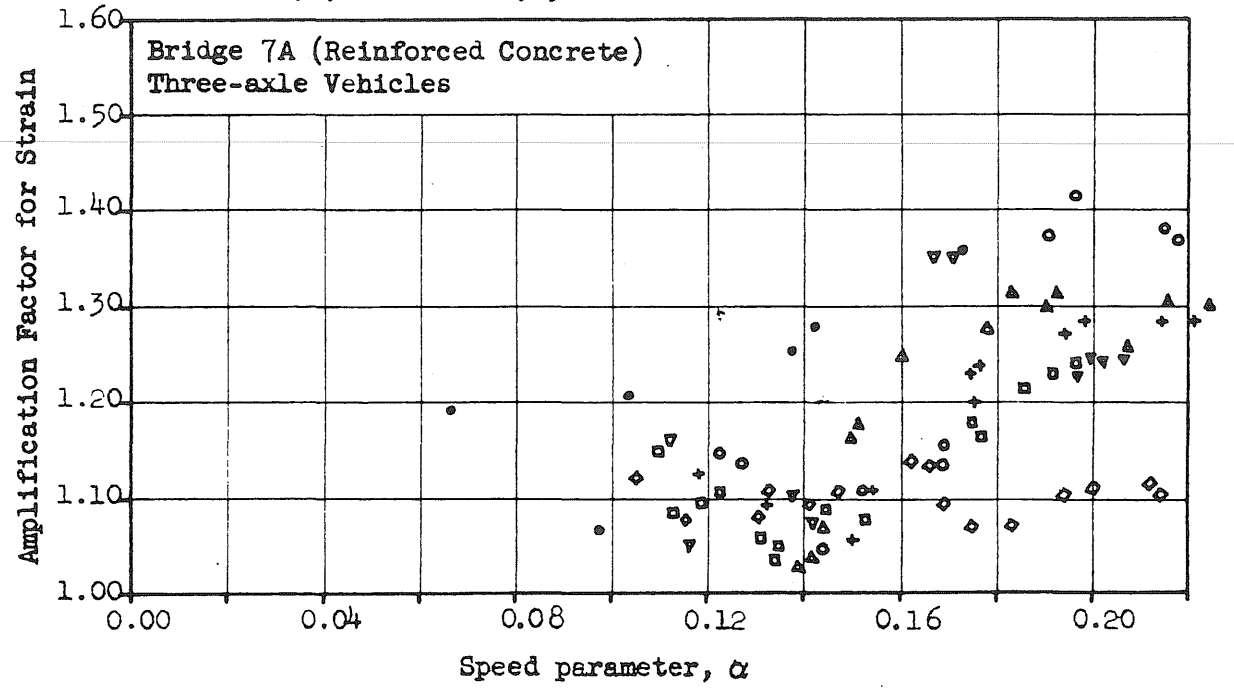

FIG. 36e SPECTRUM CURVES FOR REGULAR TESTS
Bridge 7A - Three-axle Vehicles

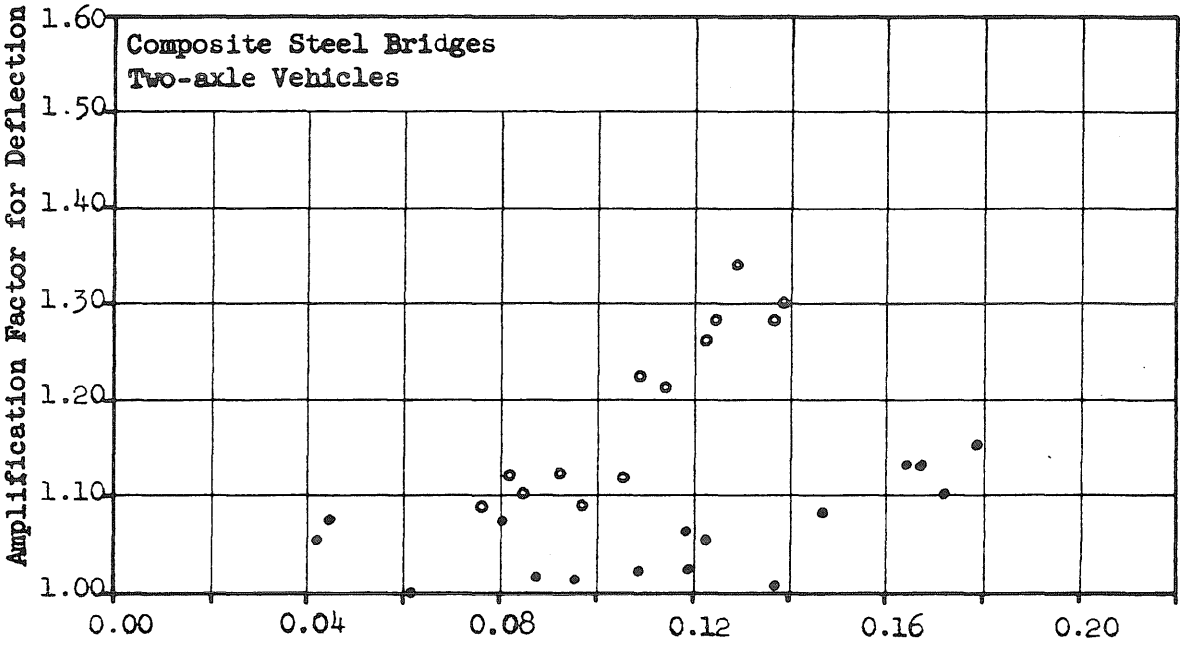

	Subseries No.	Bridge	Vehicle No.
•	5450-1	2B	A
o	5453-1	3B	91

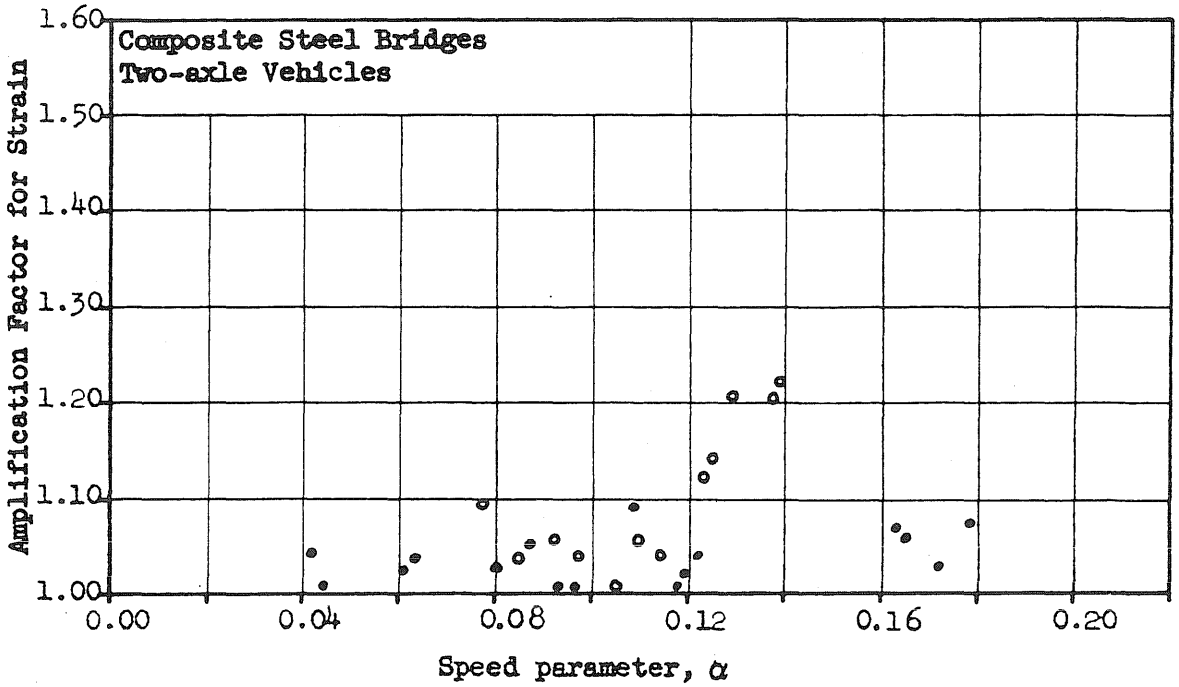

FIG 37a SPECTRUM CURVES FOR REGULAR TESTS
Composite Steel Bridges - Two-axle Vehicles

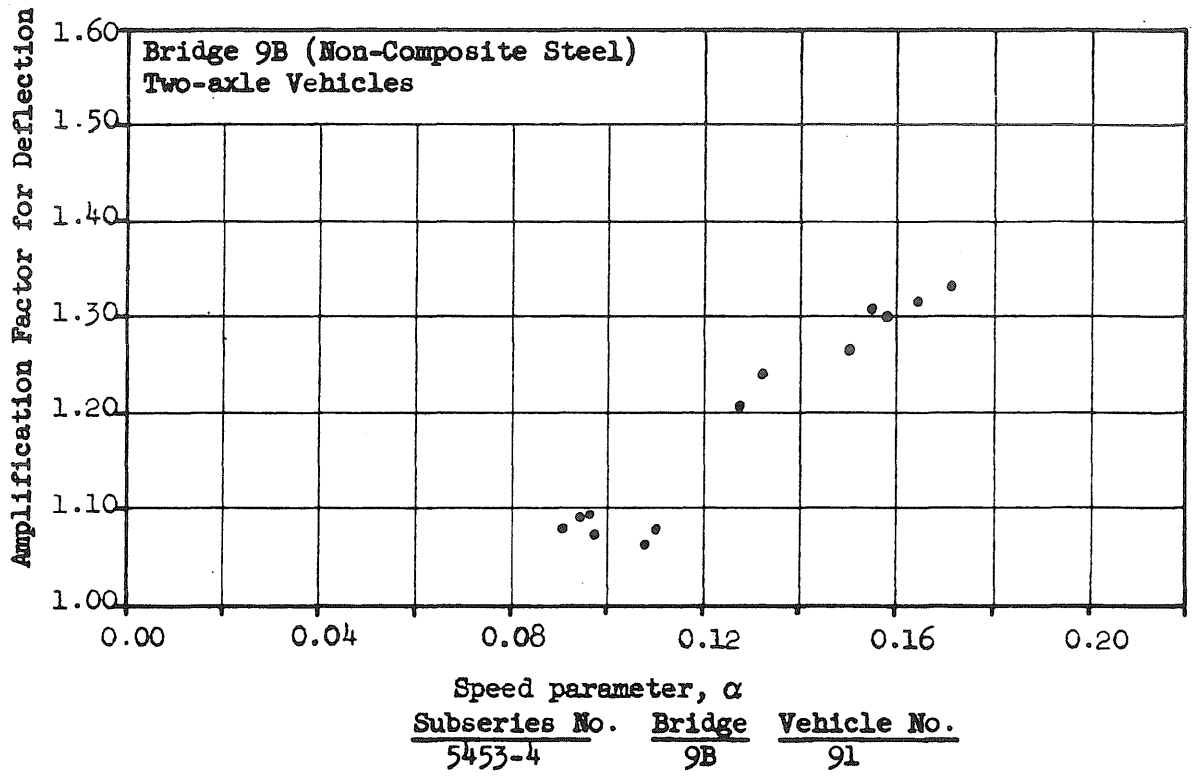

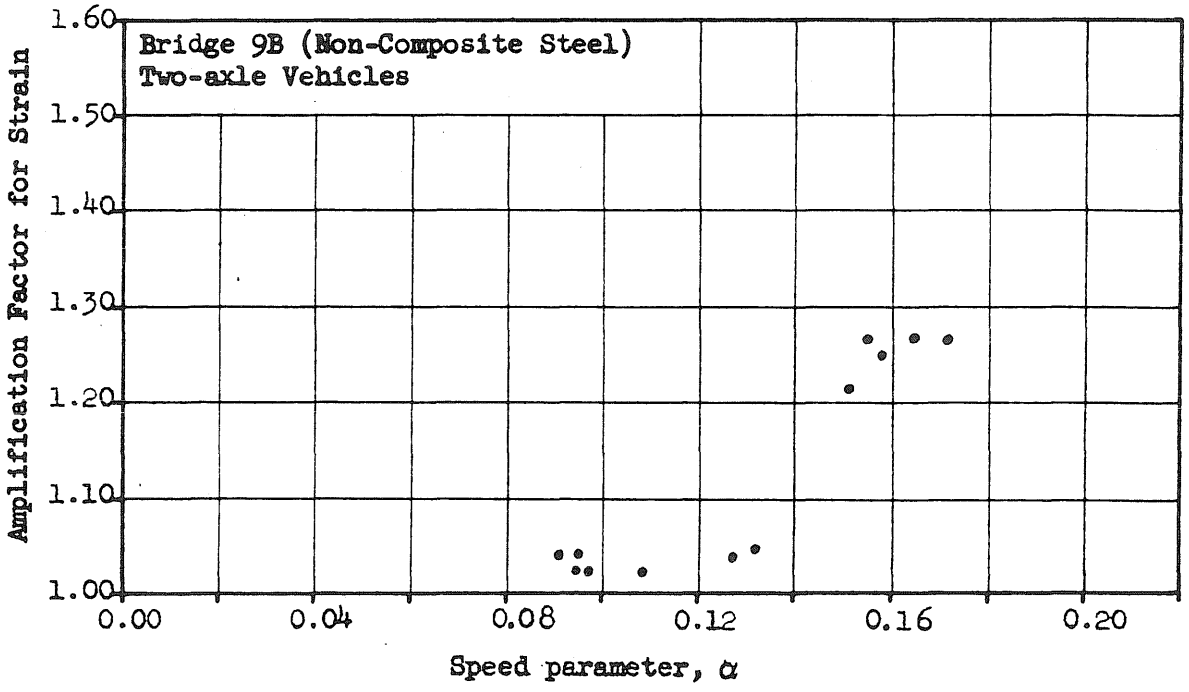

FIG. 37b SPECTRUM CURVES FOR REGULAR TESTS
Non-Composite Steel Bridges - Two-axle Vehicles

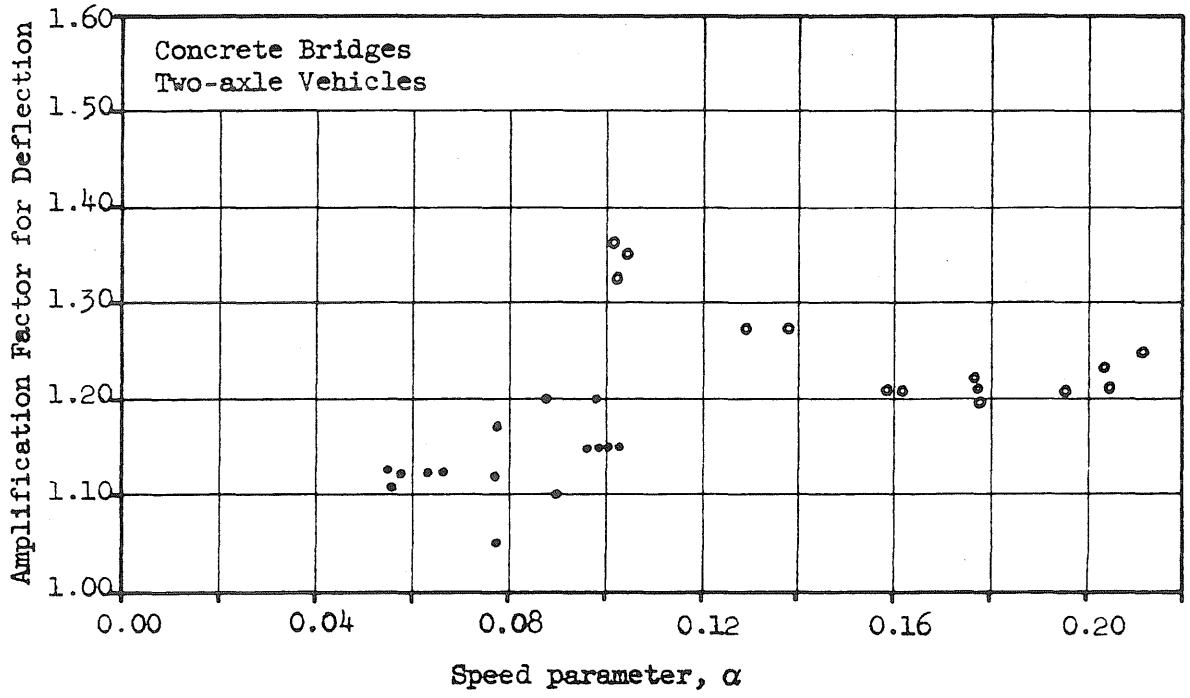

Subseries No.	Bridge	Vehicle No.
• 5453-2	6A	91
o 5453-3	7A	91

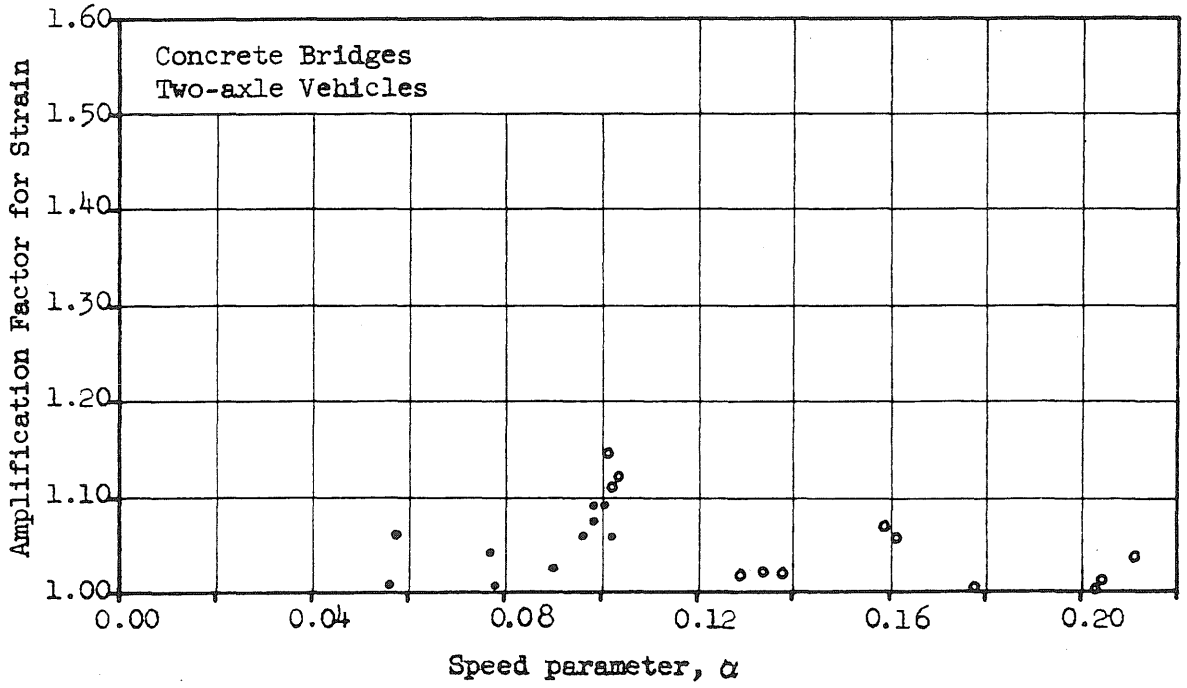

FIG. 37c SPECTRUM CURVES FOR REGULAR TESTS
Concrete Bridges - Two-axle Vehicles

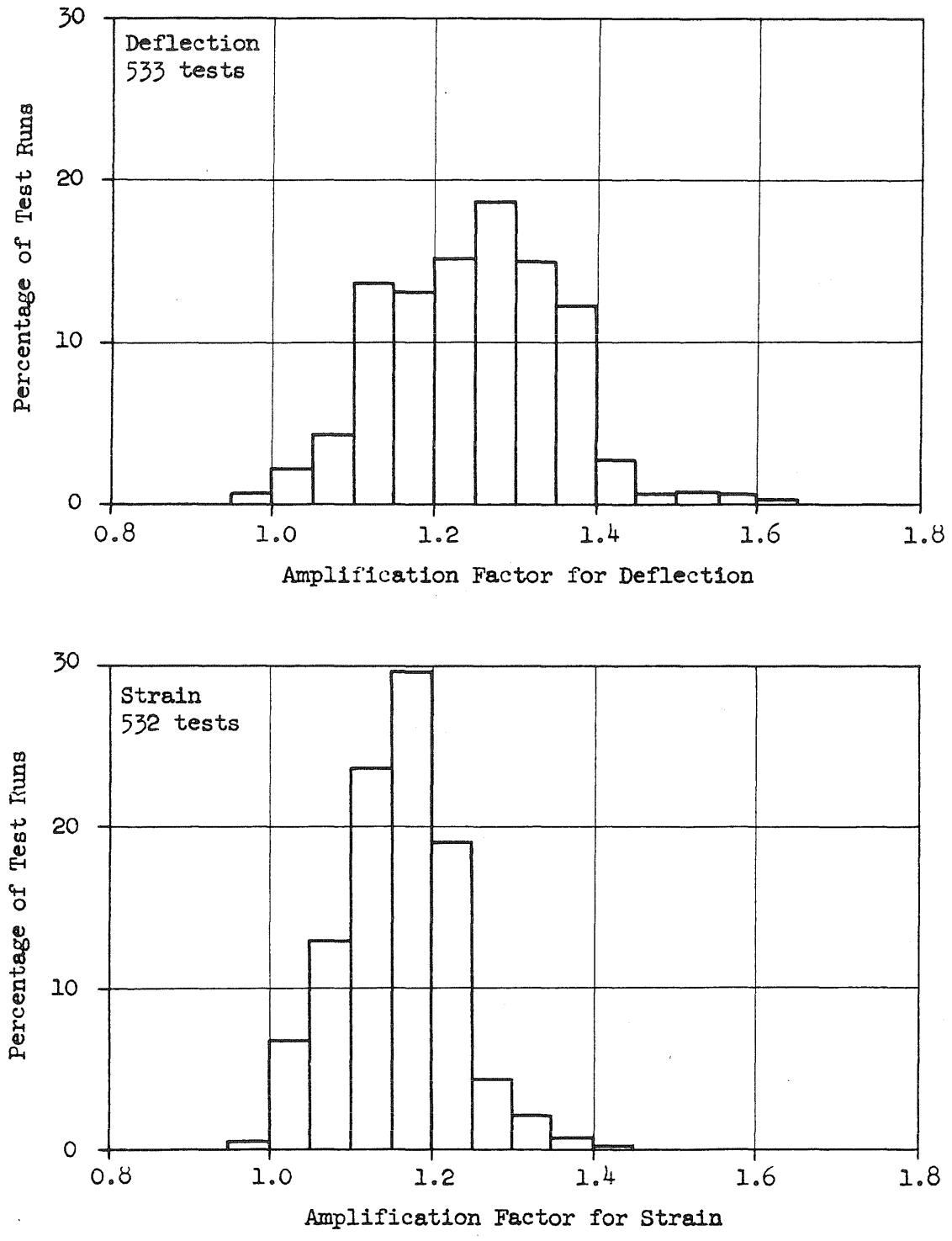

FIG. 38 PERCENTAGE DISTRIBUTION OF AMPLIFICATION FACTORS
Regular Tests - Three-axle Vehicles
Center Beam Midspan Response

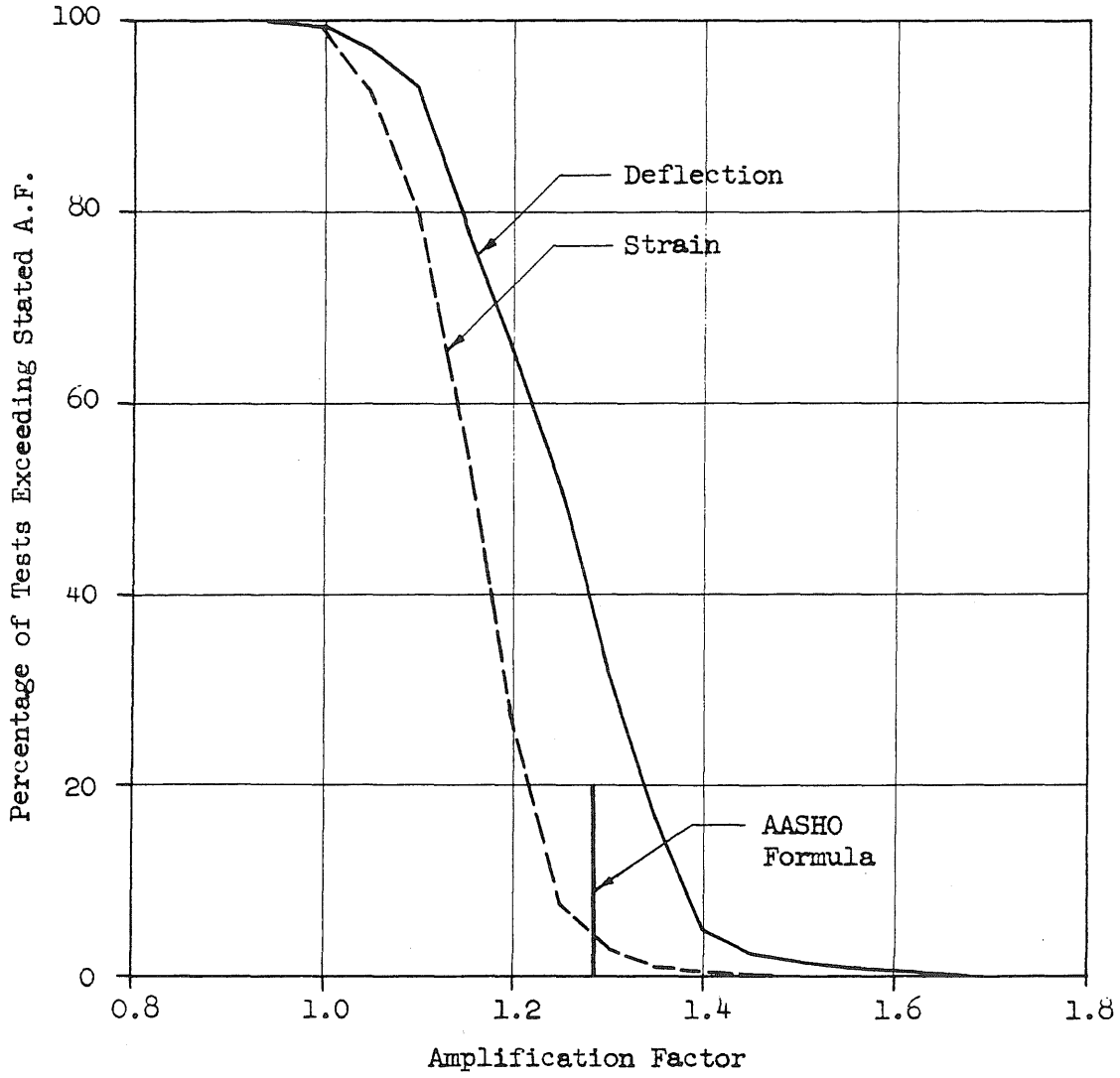

FIG. 39 CUMULATIVE PERCENTAGES OF AMPLIFICATION FACTORS
Regular tests - Three-axle Vehicles
Center Beam Midspan Response

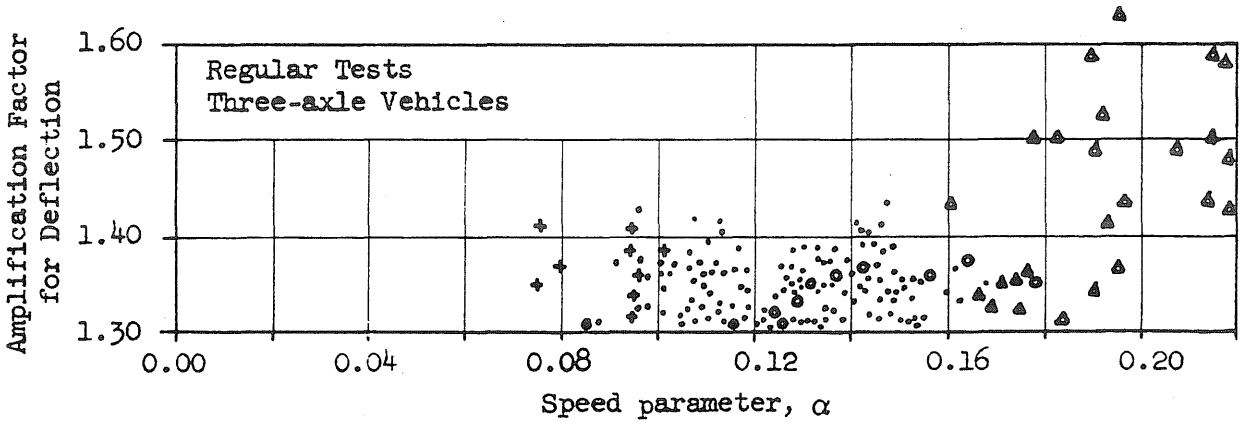

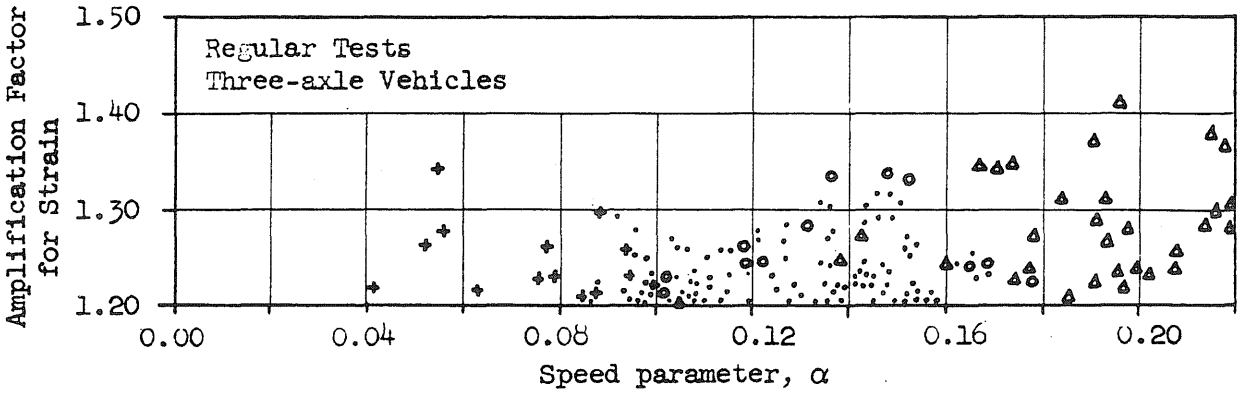

- Composite Steel Bridges 2B and 3B
- Non-composite Steel Bridge 9B
- Prestressed Concrete Bridge 6A
- Reinforced Concrete Bridge 7A

FIG. 40 MAXIMUM AMPLIFICATION FACTORS
Regular Tests - Three-axle Vehicles

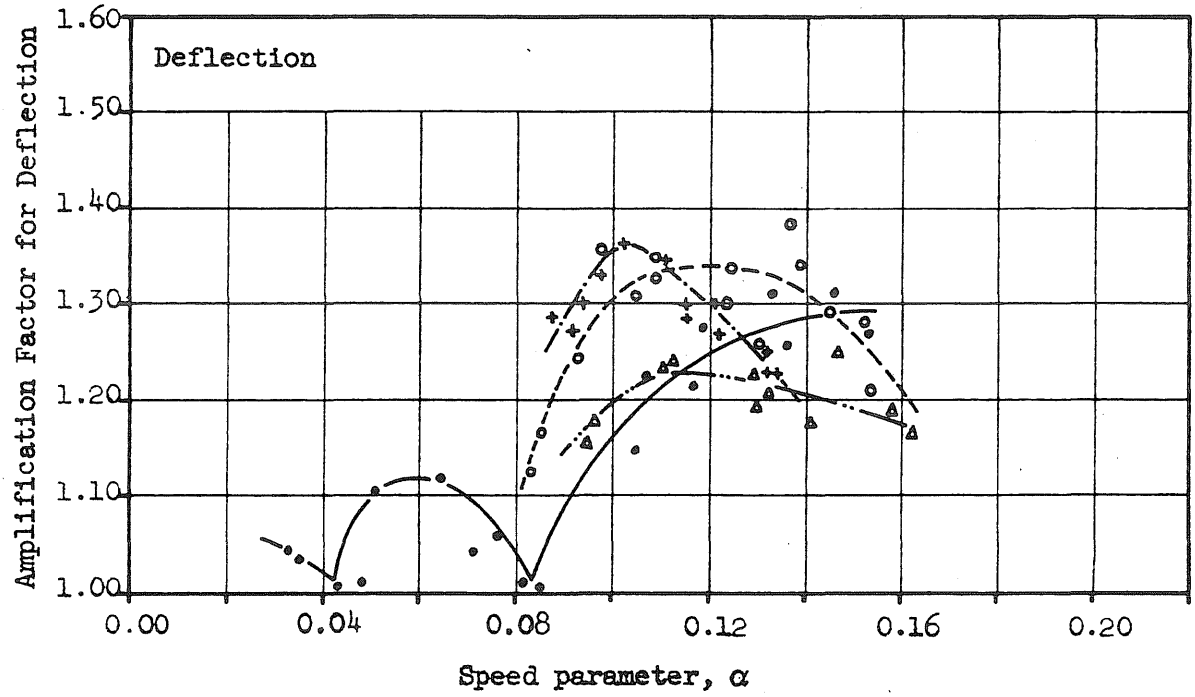

Subseries No.	Bridge	Vehicle No.	R	Φ_t	Δ
5450-2	2B	C	0.62	0.76	0.9
5451-14	3B	415	0.56	0.81	1.0
5453-7	3B	513	0.66	0.66	0.8
5451-6	9B	415	0.52	0.84	0.7

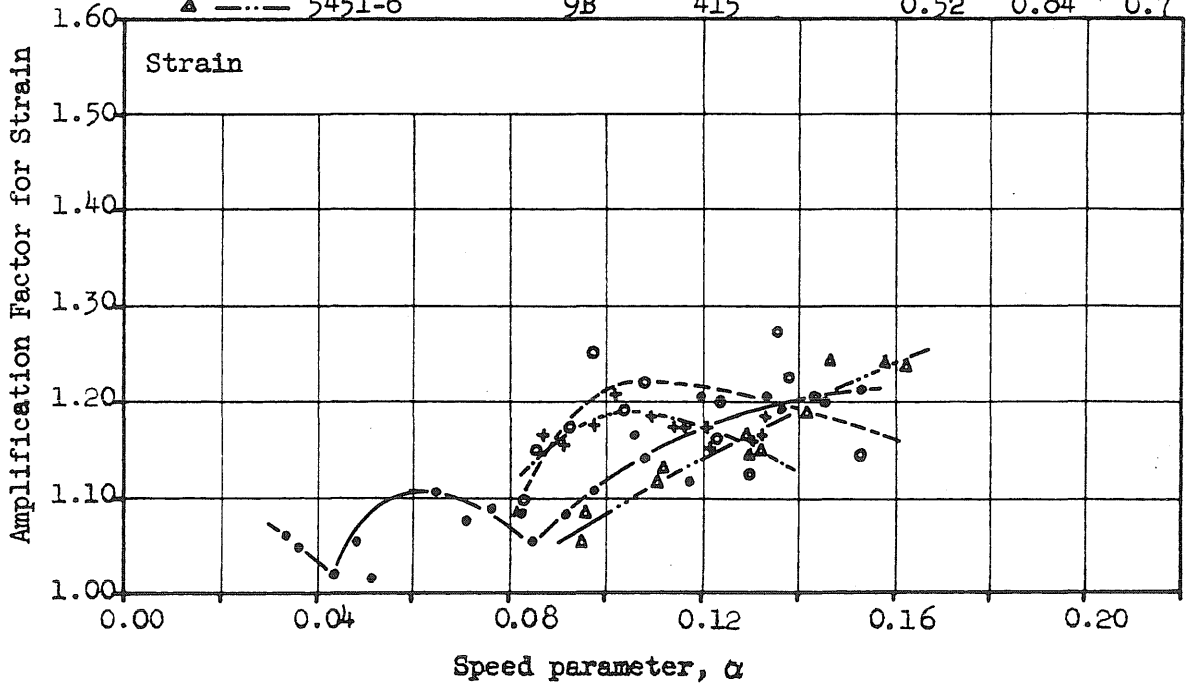

FIG. 41 EFFECT OF SPEED PARAMETER

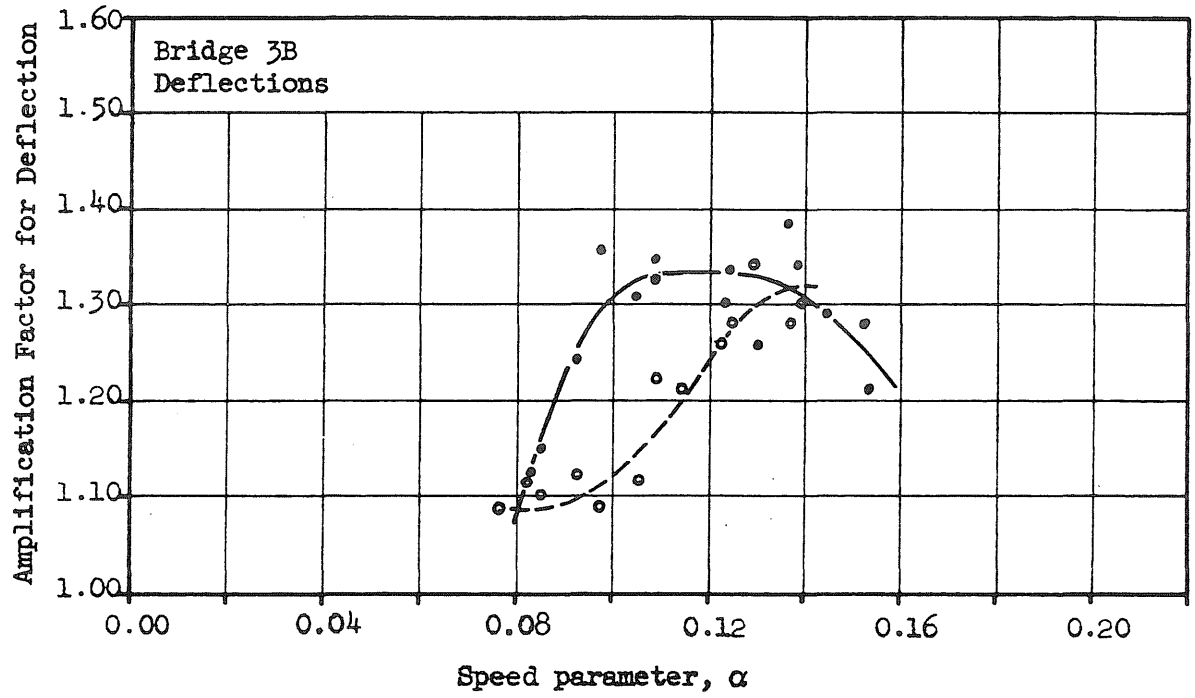

	Subseries No.	Bridge	Vehicle No.	R	φ_t	Δ
• ———	5451-14	3B	415	0.56	0.81	1.0
o - - - -	5453-1	3B	91	0.28	0.78	1.3

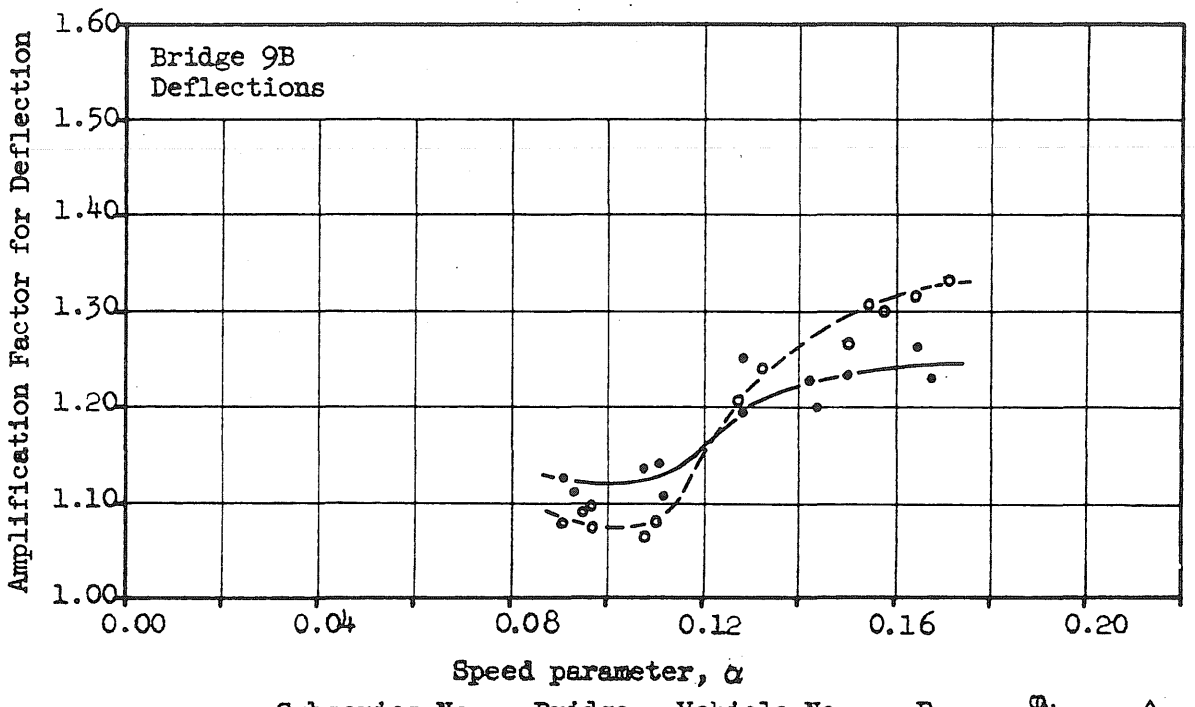

	Subseries No.	Bridge	Vehicle No.	R	φ_t	Δ
• ———	5452-3	9B	415	0.52	0.95	0.9
o - - - -	5453-4	9B	91	0.26	0.97	0.9

FIG. 42 EFFECT OF WEIGHT RATIO

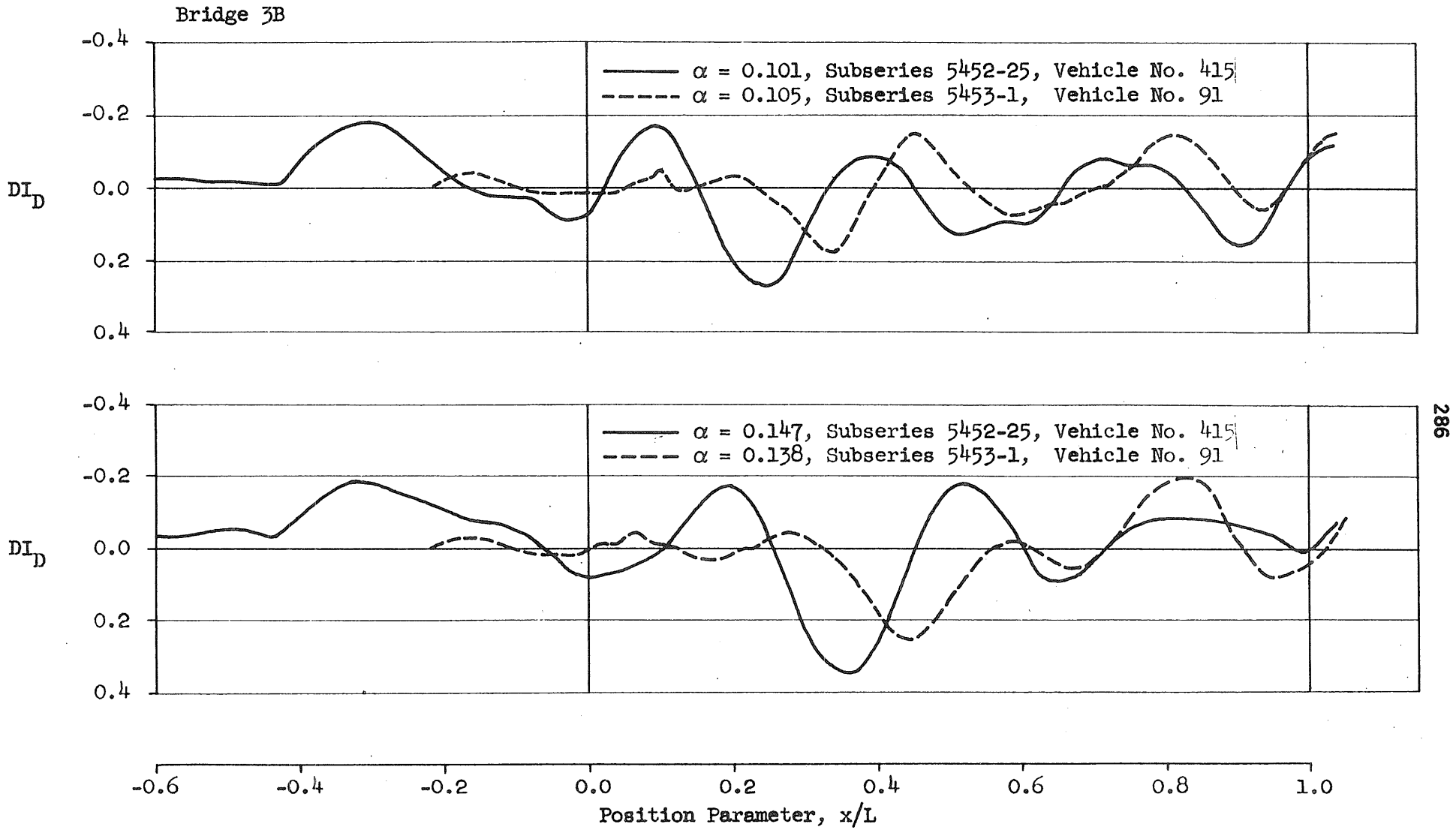

FIG. 43 COMPARISON OF EFFECTS OF TWO- AND THREE-AXLE VEHICLES

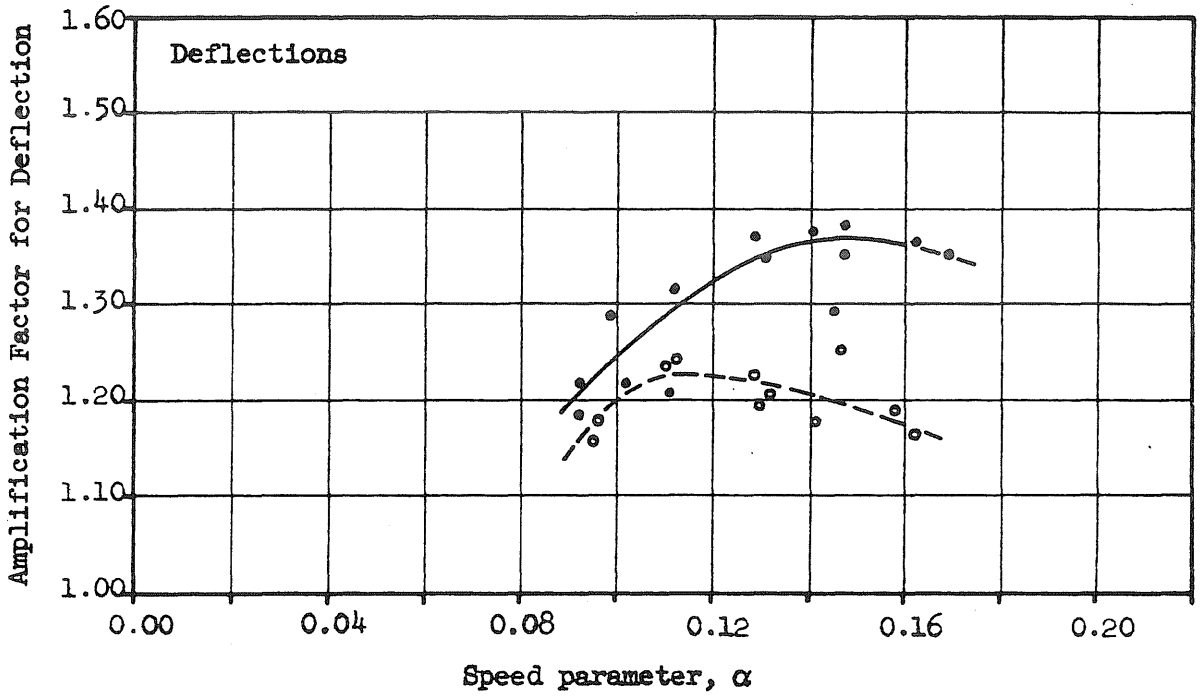

Subseries No.	Bridge	Vehicle No.	R	φ_t	Δ
• ——— 5451-3	2B	415	0.59	0.86	1.3
○ - - - - 5451-6	9B	415	0.52	0.84	0.7

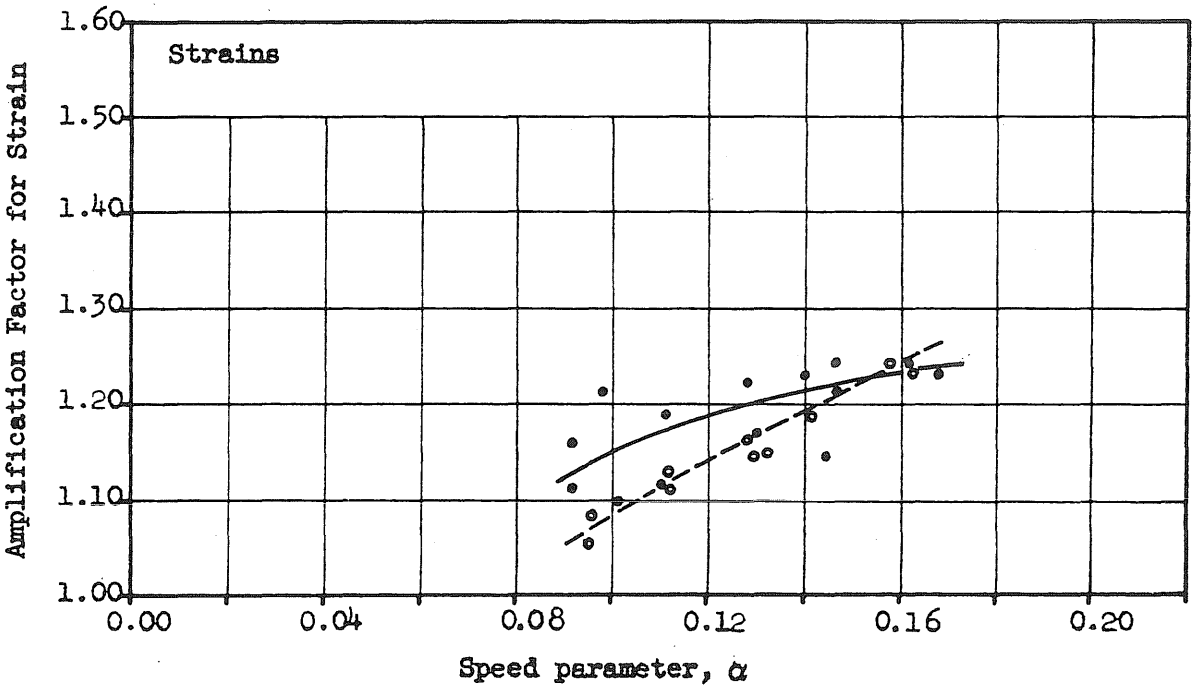

FIG. 44 EFFECT OF PROFILE PARAMETER

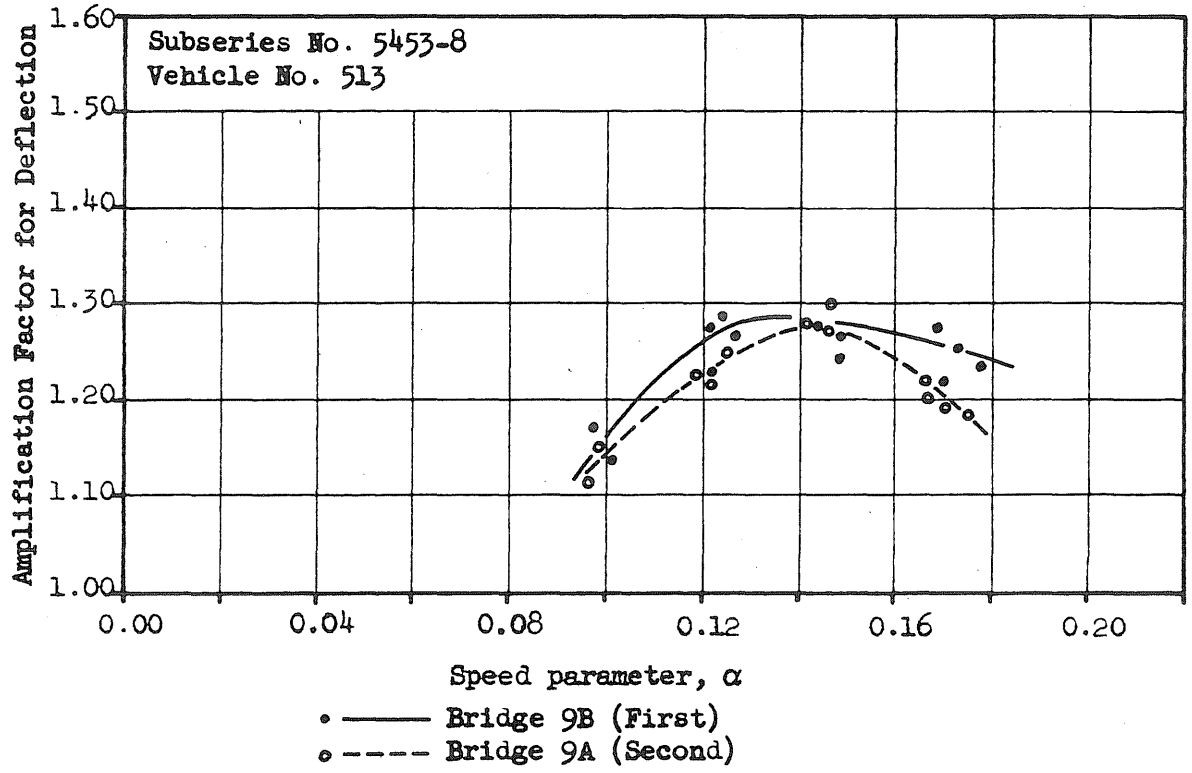

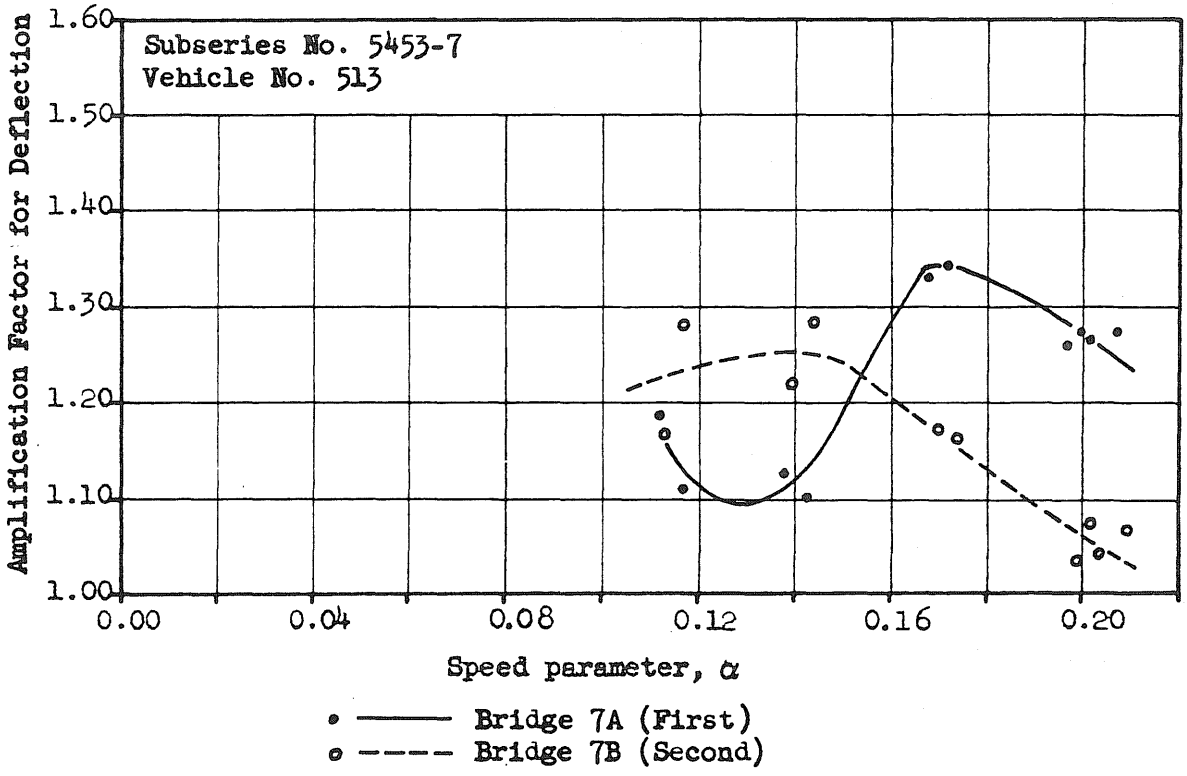

FIG. 45 COMPARISON OF RESPONSES OF FIRST AND SECOND BRIDGES

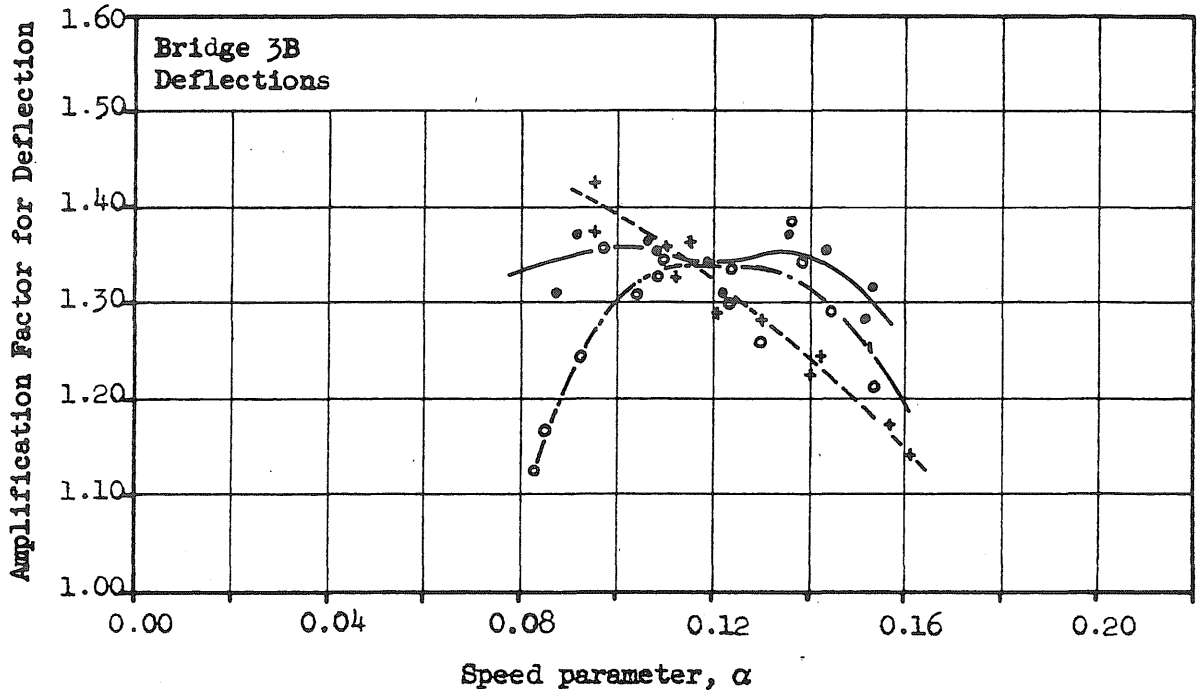

	Subseries No.	Bridge	Vehicle No.	R	φ_t	Δ
• ———	5451-11	3B	315	0.38	0.87	1.2
o —·—	5451-14	3B	415	0.56	0.81	1.0
+ - - - - -	5451-15	3B	513	0.66	0.64	0.6

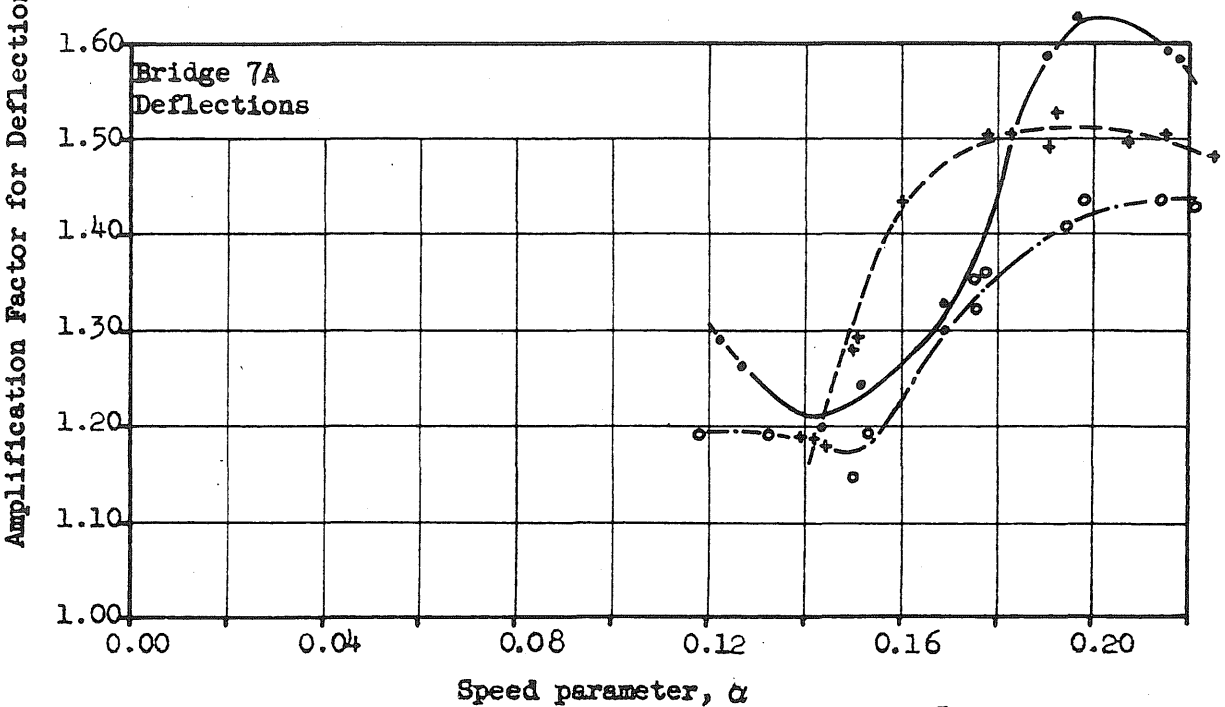

	Subseries No.	Bridge	Vehicle No.	R	φ_t	Δ
• ———	5451-13	7A	315	0.28	1.23	-1.3
o —·—	5451-5	7A	415	0.42	1.15	-1.0
+ - - - -	5451-16	7A	513	0.49	0.90	-0.7

FIG 46 EFFECT OF VEHICLE CHARACTERISTICS

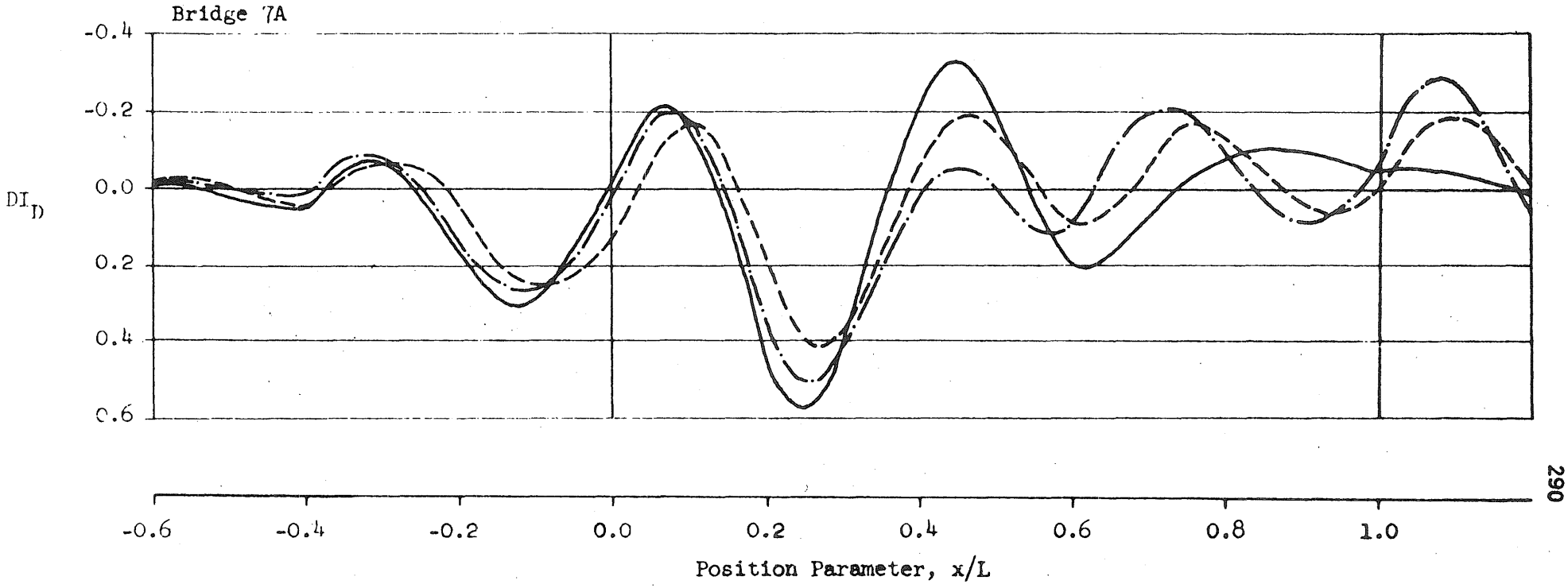

FIG. 47 COMPARISON OF EFFECTS ON BRIDGE 7A

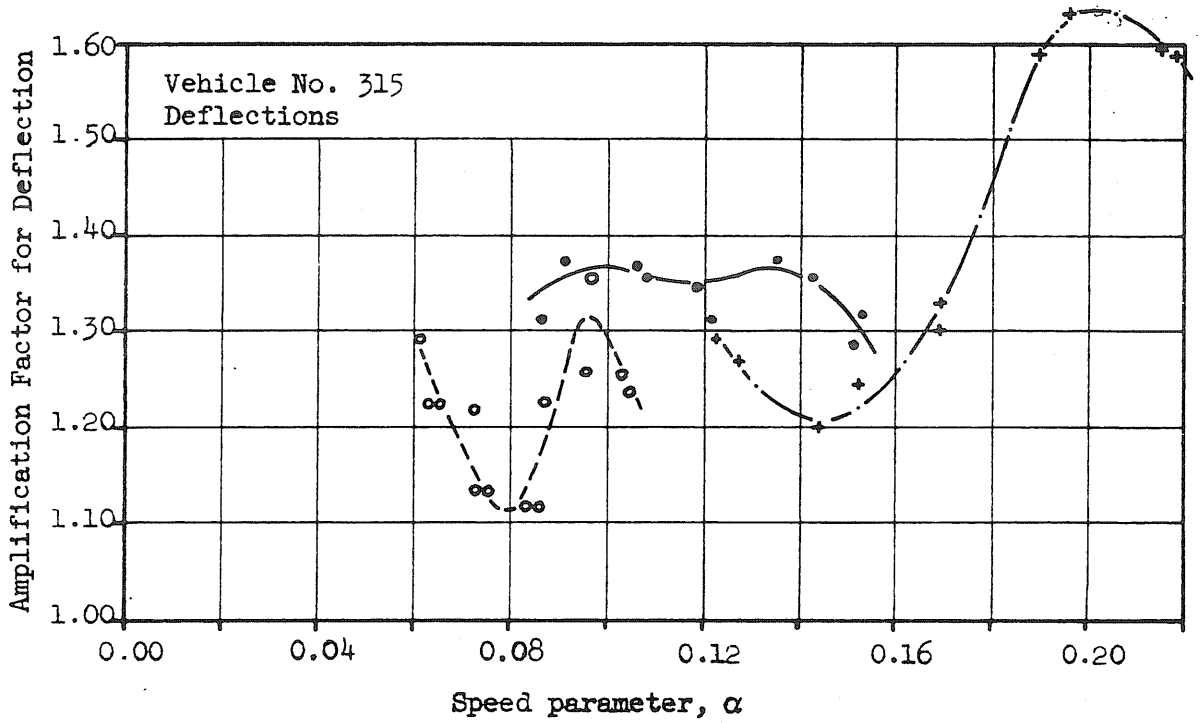

	Subseries	Bridge	R	Φ_t	Δ
• ———	5451-11	3B	0.38	0.87	1.2
o - - - -	5451-12	5A	0.28	0.60	0.2
+ —·—	5451-13	7A	0.28	1.23	-1.2

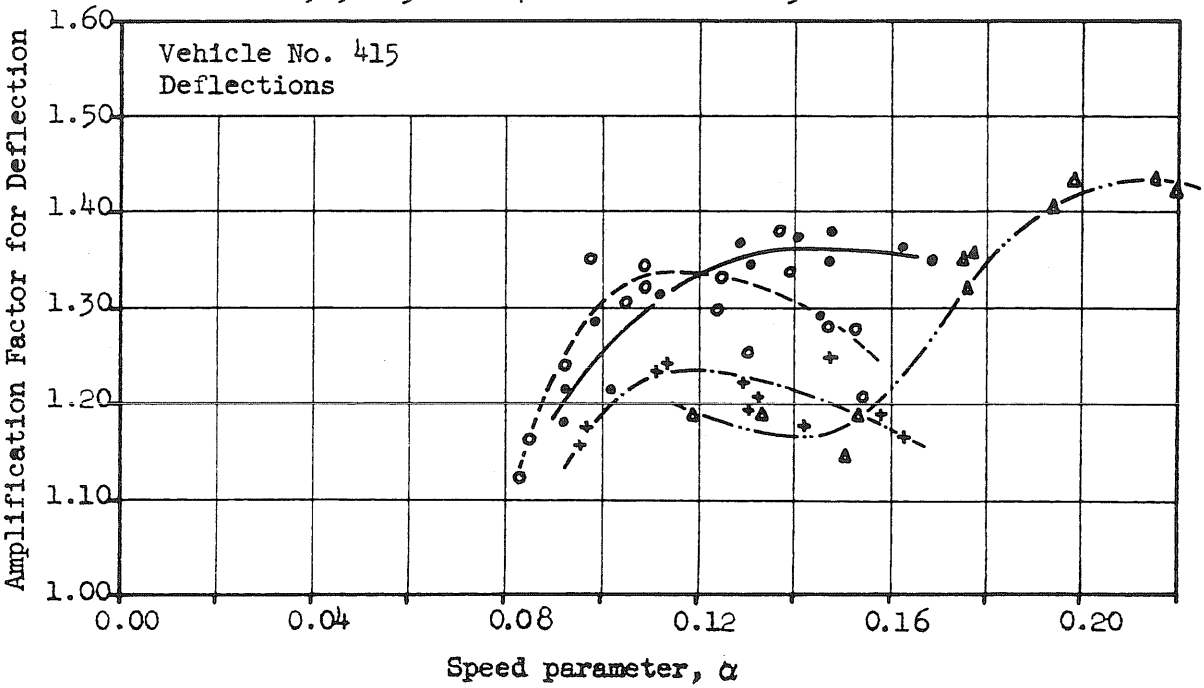

	Subseries	Bridge	R	Φ_t	Δ
• ———	5451-3	2B	0.59	0.85	1.3
o - - - -	5451-14	3B	0.56	0.81	1.0
+ —·—	5451-6	9B	0.52	0.84	0.7
Δ —··—	5451-5	7A	0.42	1.15	-1.0

FIG. 48a EFFECT OF BRIDGE CHARACTERISTICS

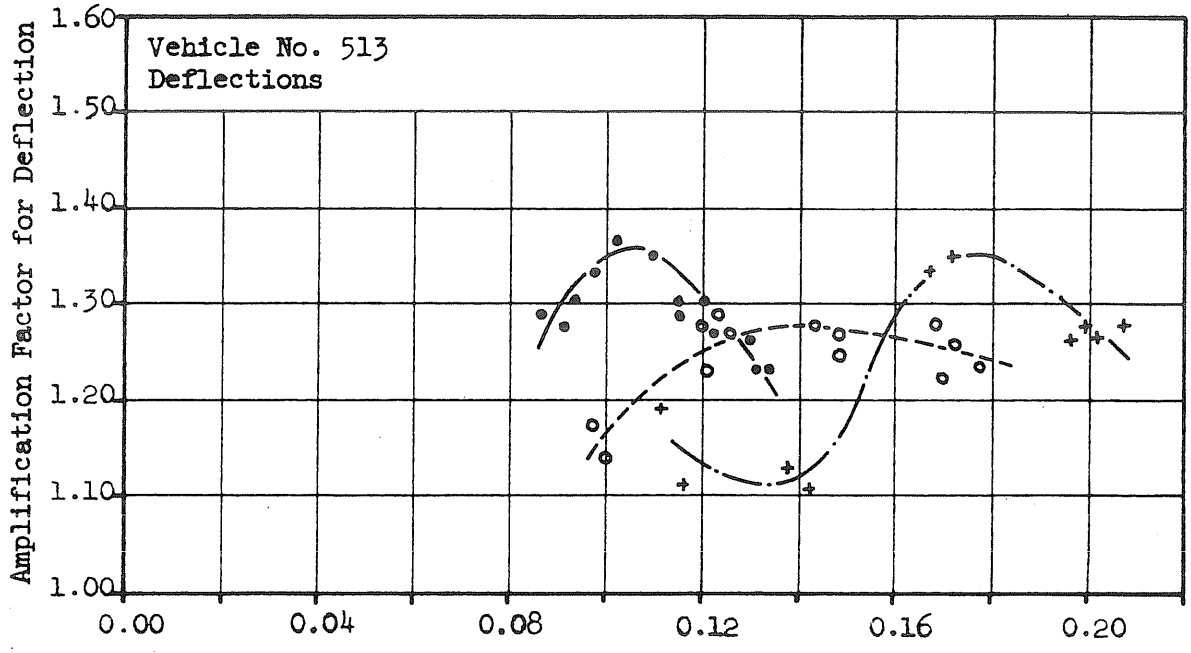

Subseries	Bridge	R	φ_t	Δ
• ——— 5453-7	3B	0.66	0.66	0.8
○ - - - - 5453-8	9B	0.61	0.84	0.6
+ —·— 5453-9	7A	0.49	0.98	-0.4

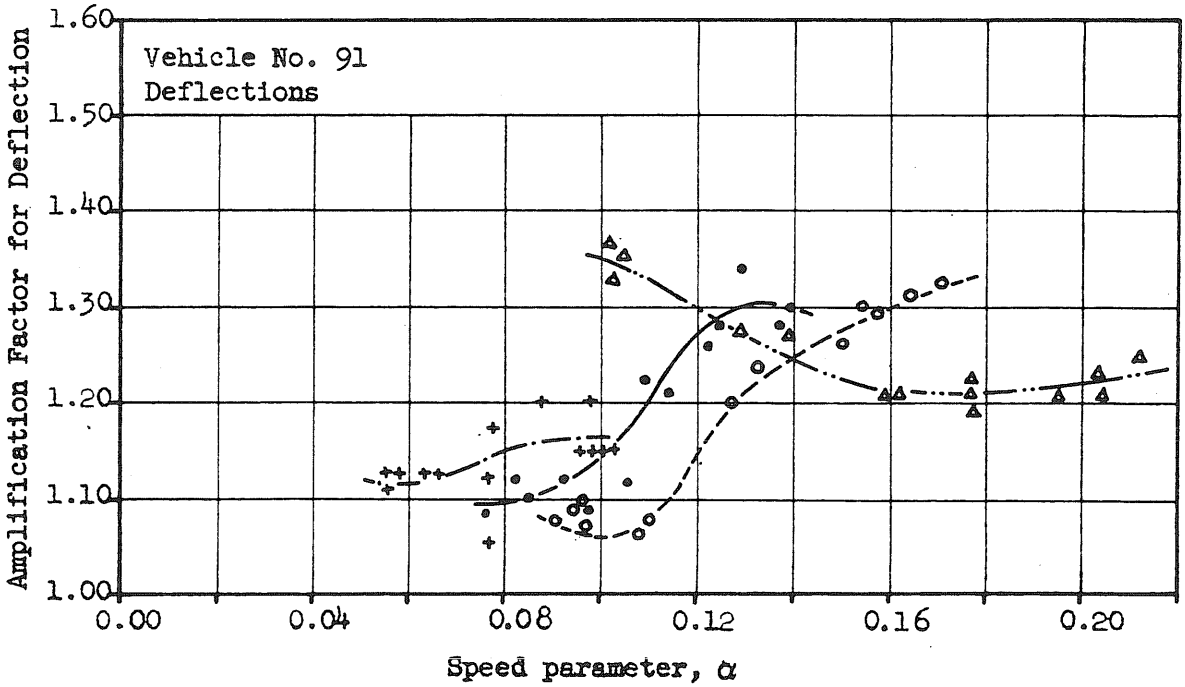

Subseries	Bridge	R	φ_t	Δ
• ——— 5453-1	3B	0.28	0.78	1.3
○ - - - - 5453-4	9B	0.26	0.97	0.9
+ —·— 5453-2	6A	0.21	0.56	0.7
△ —··— 5453-3	7A	0.21	0.56	-0.6

FIG. 48b EFFECT OF BRIDGE CHARACTERISTICS

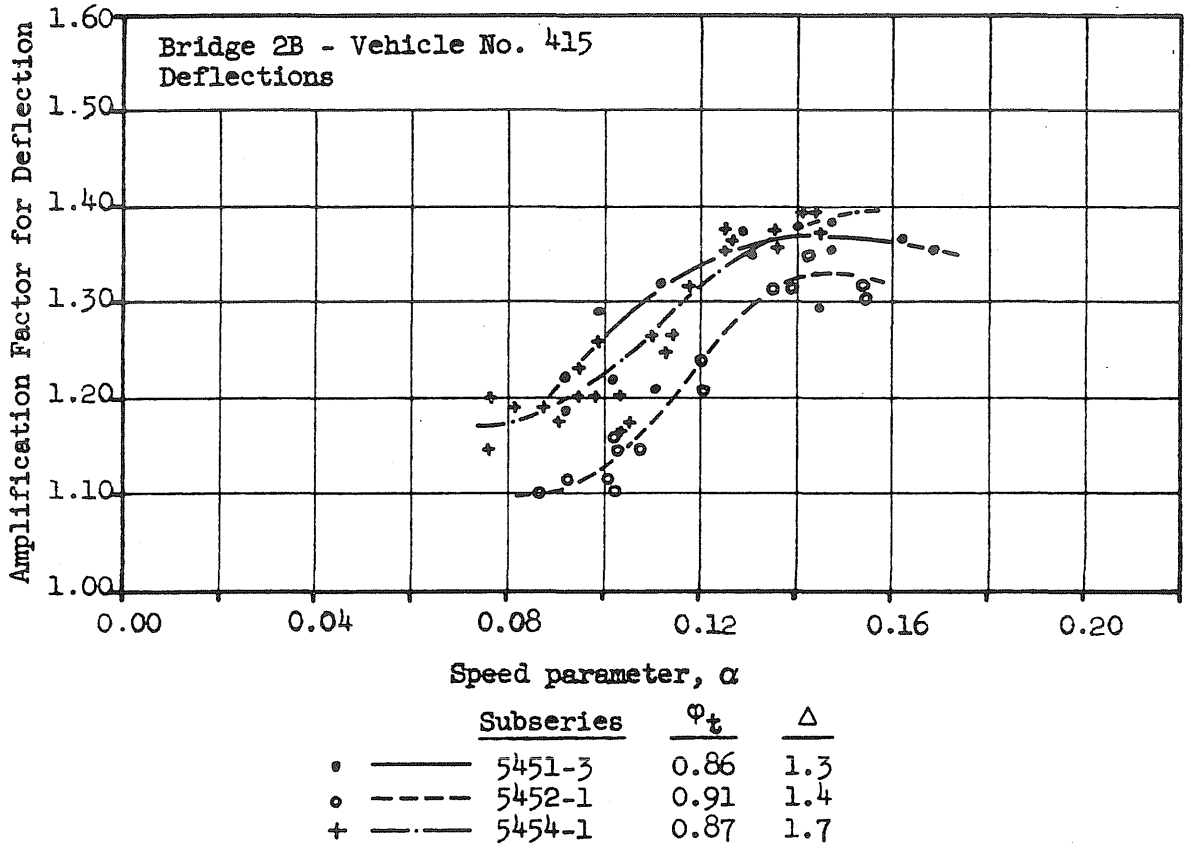

	Subseries	φ_t	Δ
• ———	5451-3	0.86	1.3
o - - - -	5452-1	0.91	1.4
+ —·—	5454-1	0.87	1.7

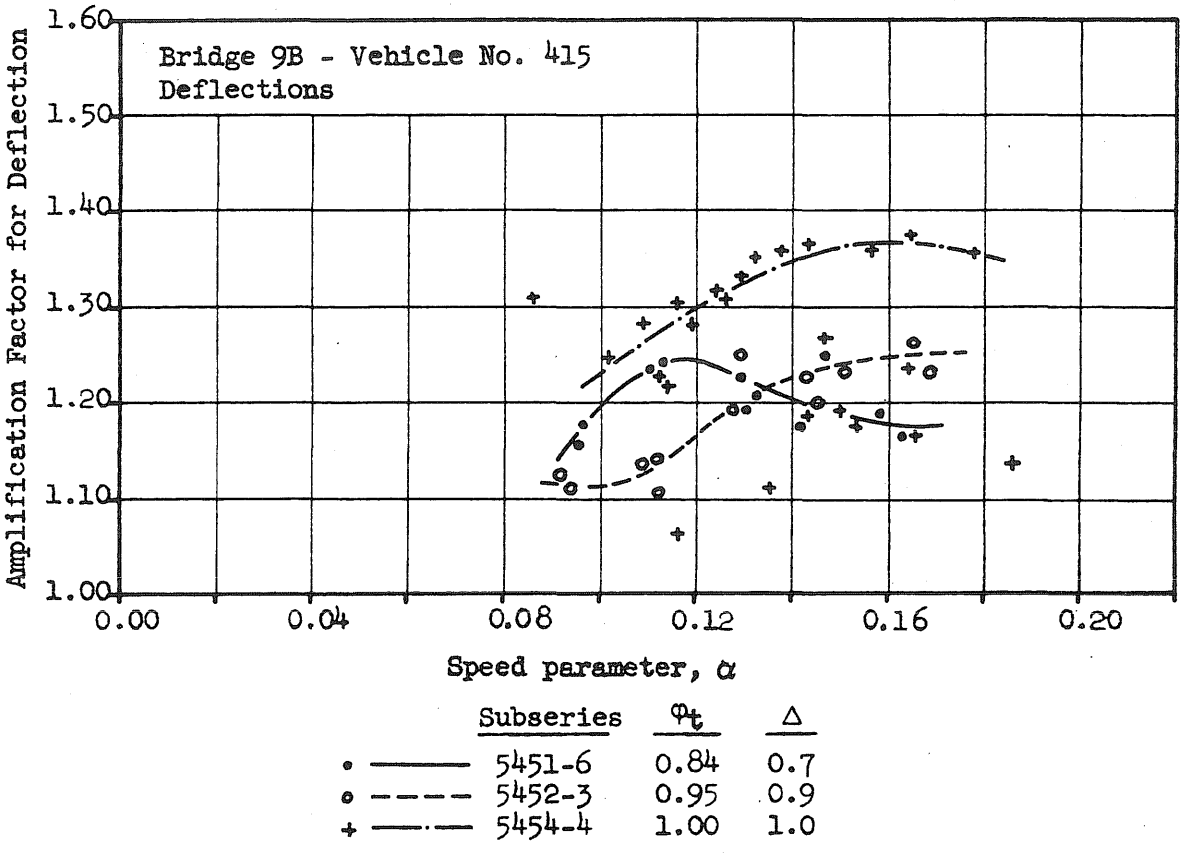

	Subseries	φ_t	Δ
• ———	5451-6	0.84	0.7
o - - - -	5452-3	0.95	0.9
+ —·—	5454-4	1.00	1.0

FIG. 49a EFFECT OF NUMBER OF LOAD APPLICATIONS

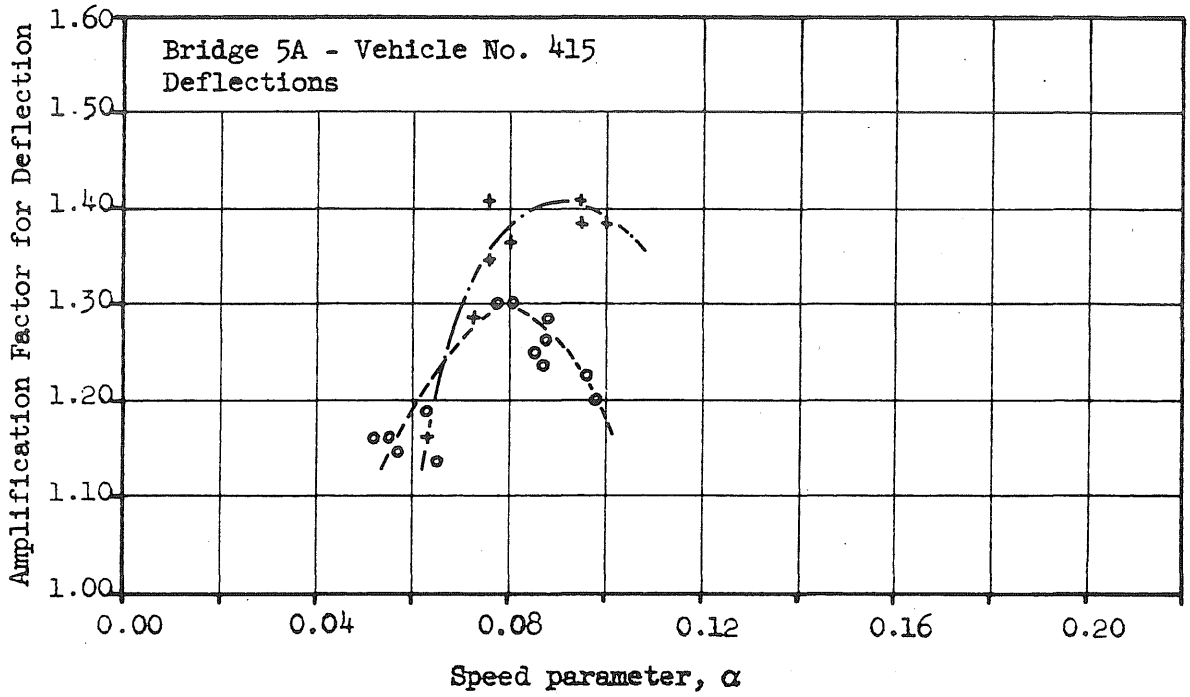

	Subseries	Φ_t	Δ
∘ ----	5452-4	0.42	0.4
+ —·—	5454-2	0.42	0.7

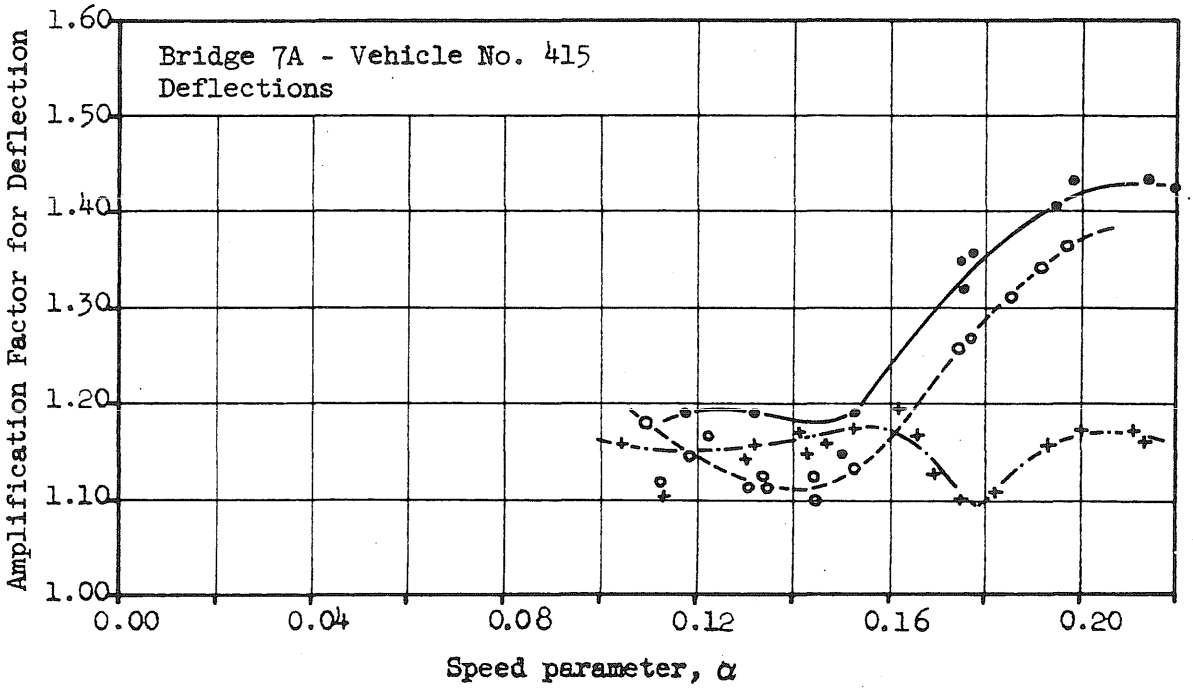

	Subseries	Φ_t	Δ
• ———	5451-5	1.15	-1.1
∘ ----	5452-2	1.10	-0.8
+ —·—	5454-3	1.21	-0.6

FIG. 49b EFFECT OF NUMBER OF LOAD APPLICATIONS

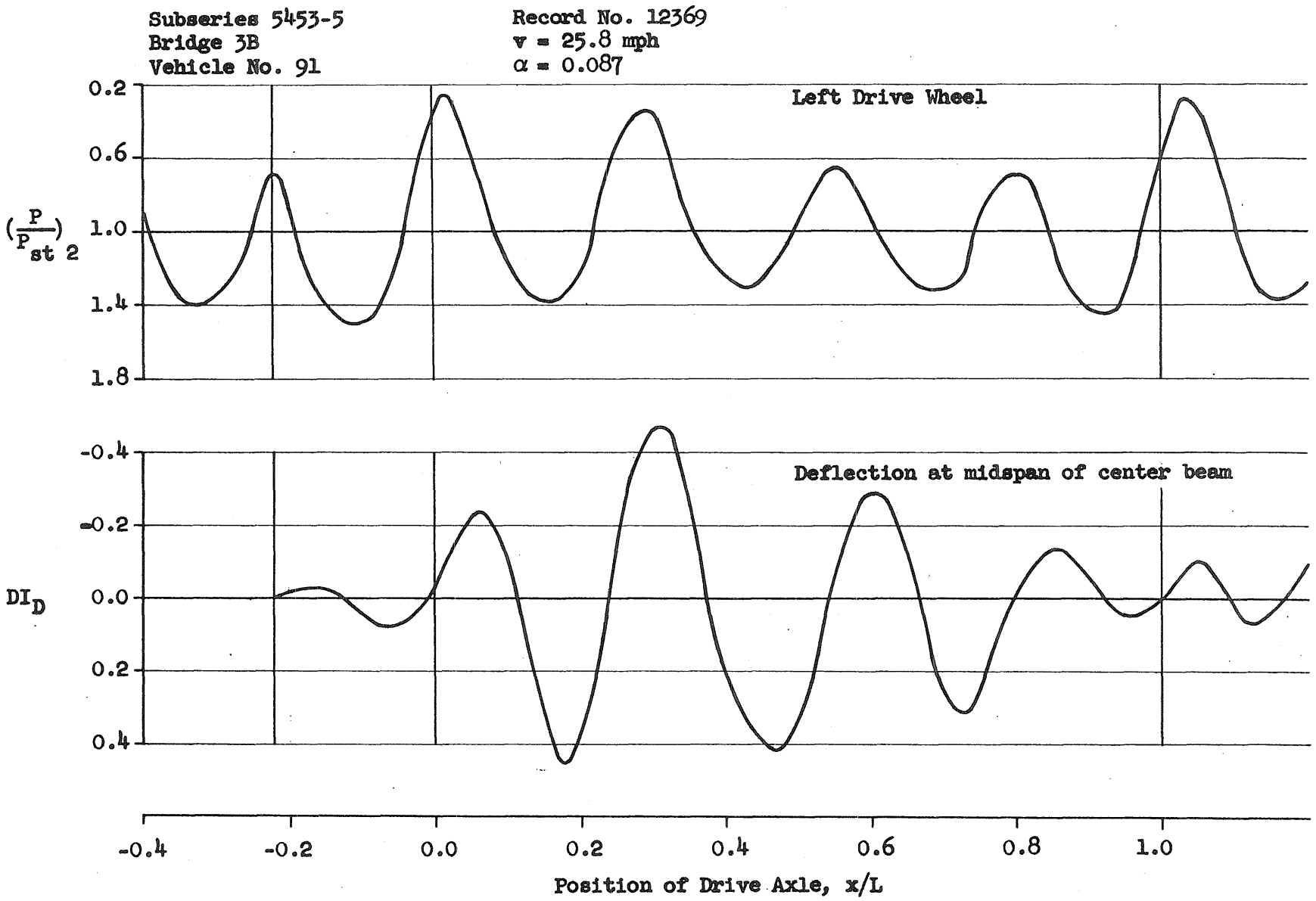

FIG. 50a REPRESENTATIVE RESPONSE CURVES FOR TESTS WITH BLOCKED SPRINGS-TWO AXLE VEHICLE

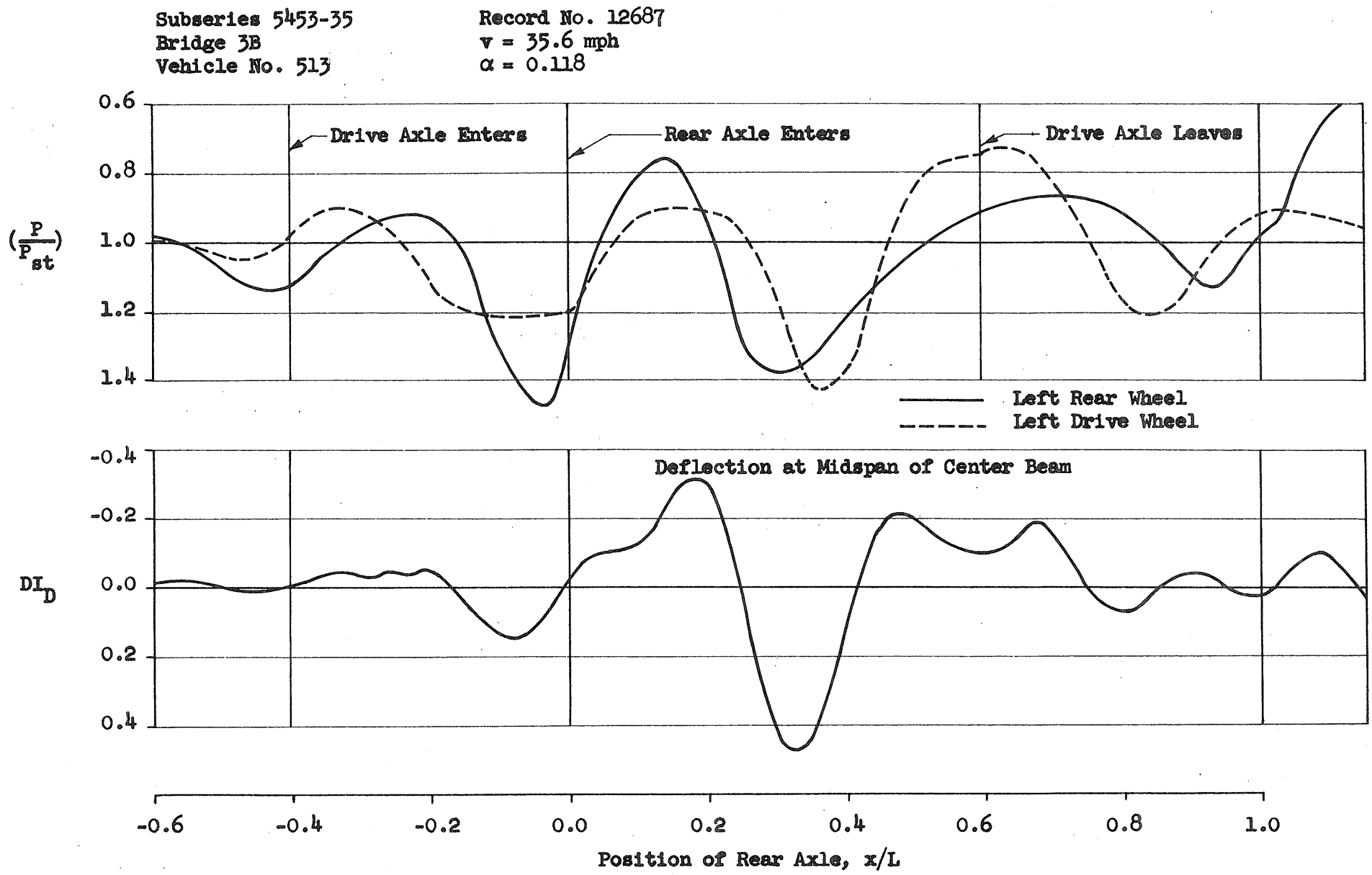

FIG. 50b REPRESENTATIVE RESPONSE CURVES FOR TESTS WITH BLOCKED SPRINGS-THREE-AXLE VEHICLE

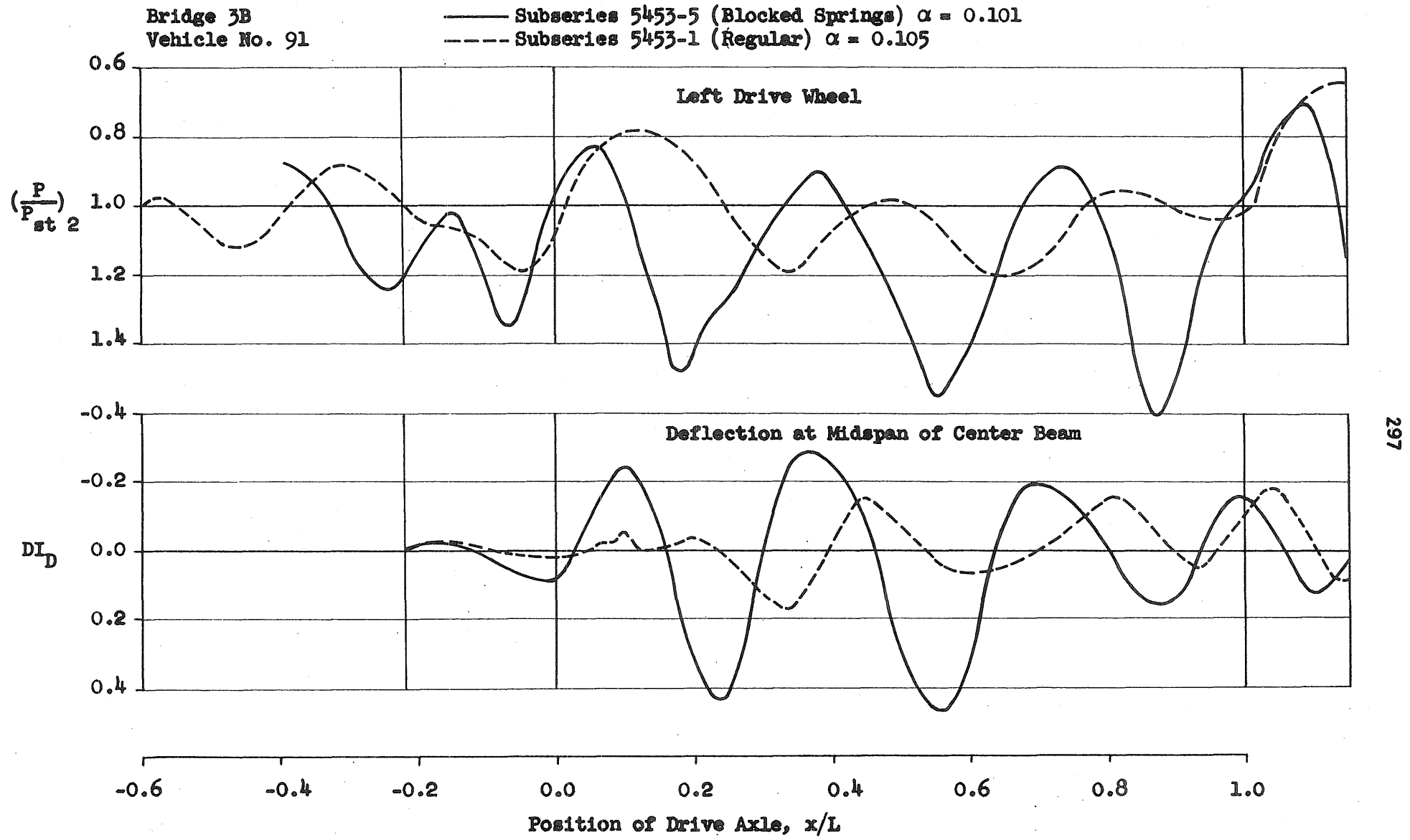

FIG. 51a COMPARISON OF TESTS WITH BLOCKED SPRINGS AND REGULAR TESTS - TWO-AXLE VEHICLE

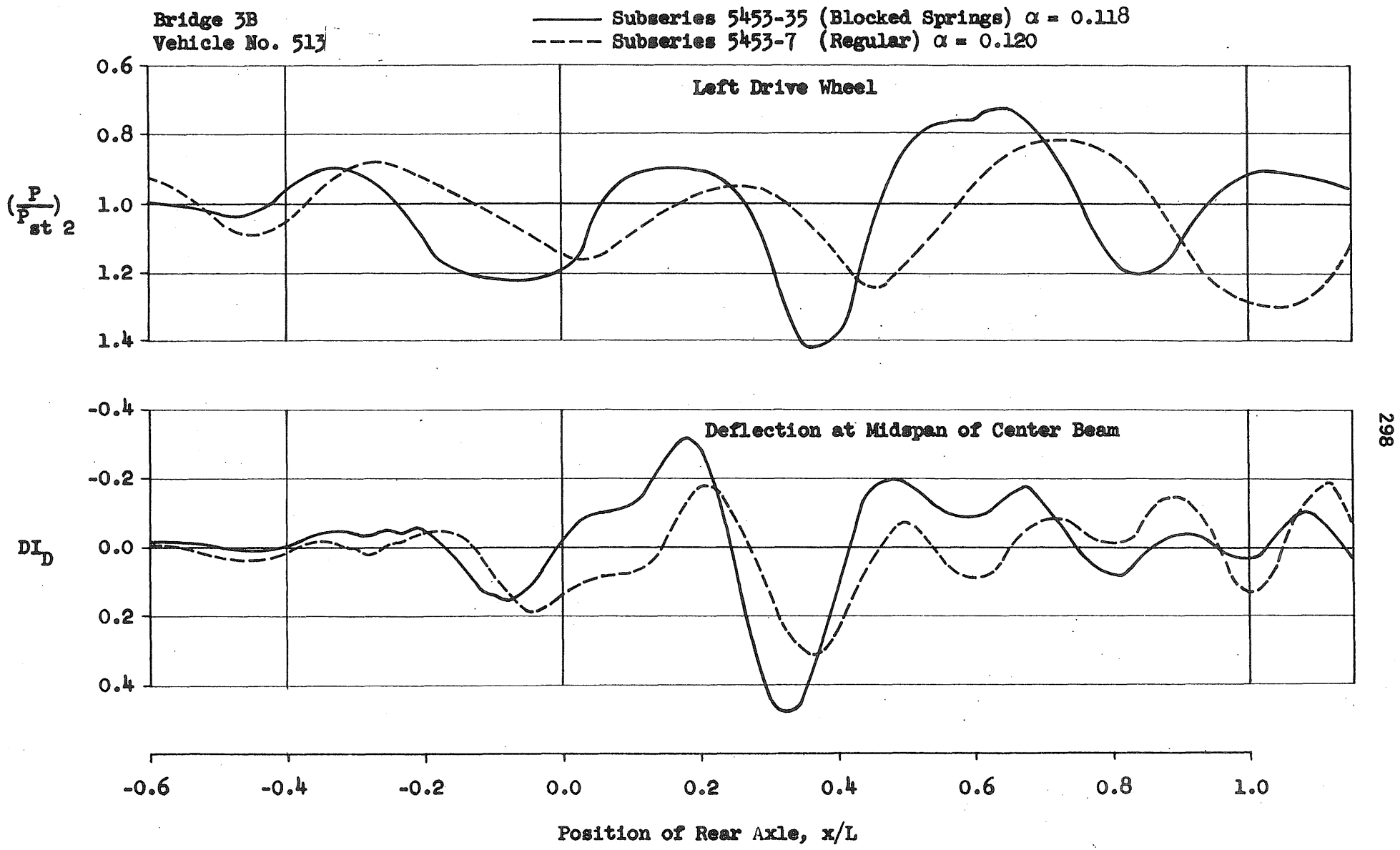

FIG. 51b COMPARISON OF TESTS WITH BLOCKED SPRINGS AND REGULAR TESTS - THREE-AXLE VEHICLE

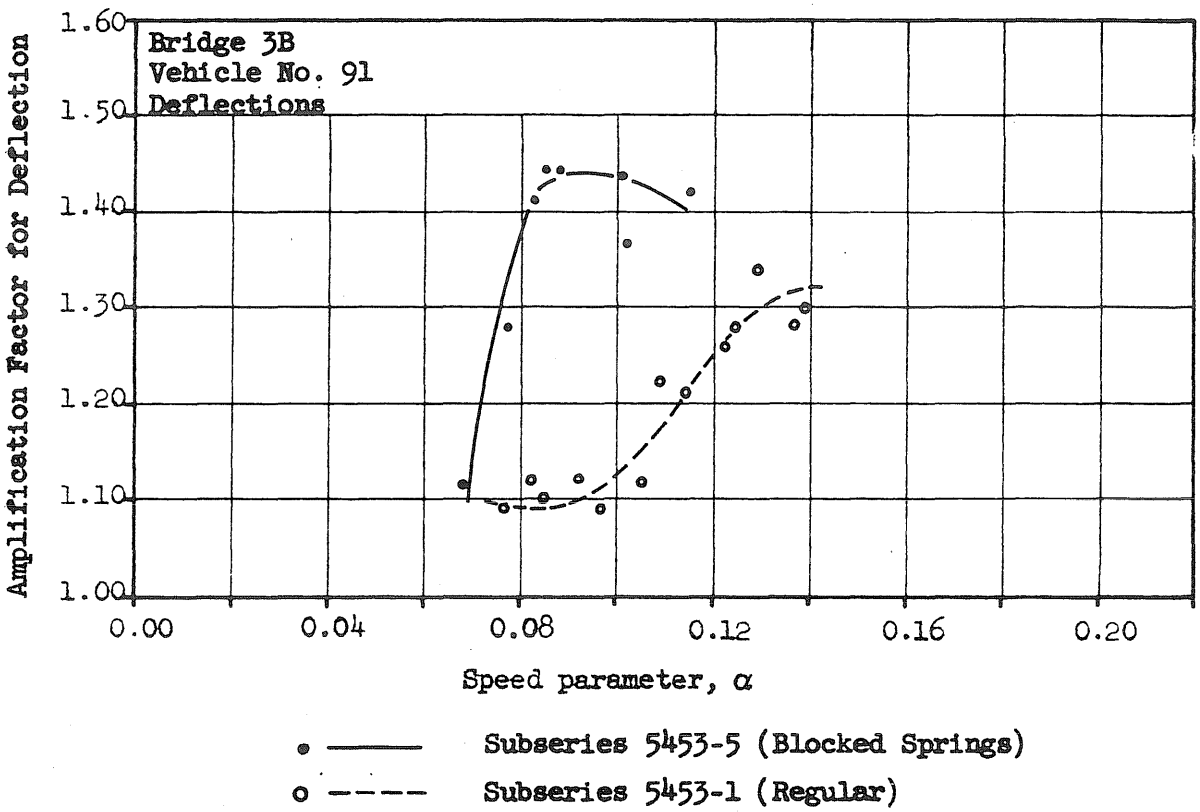

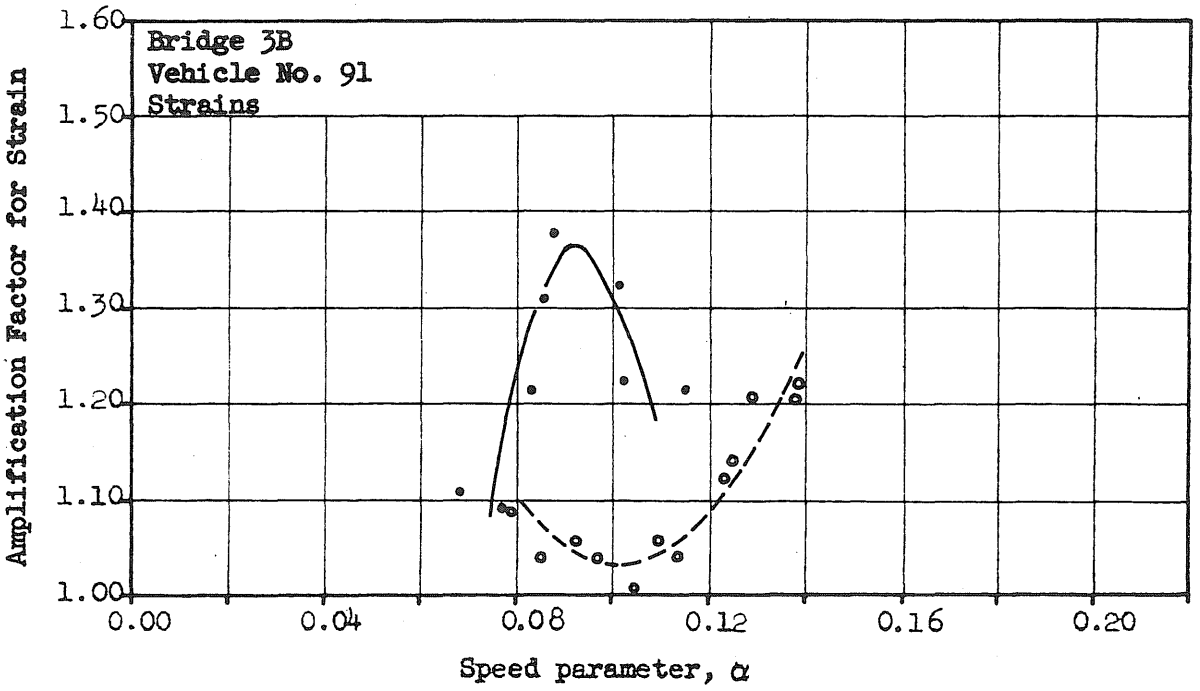

FIG. 52a SPECTRUM CURVES FOR TESTS WITH BLOCKED SPRINGS - TWO-AXLE VEHICLE

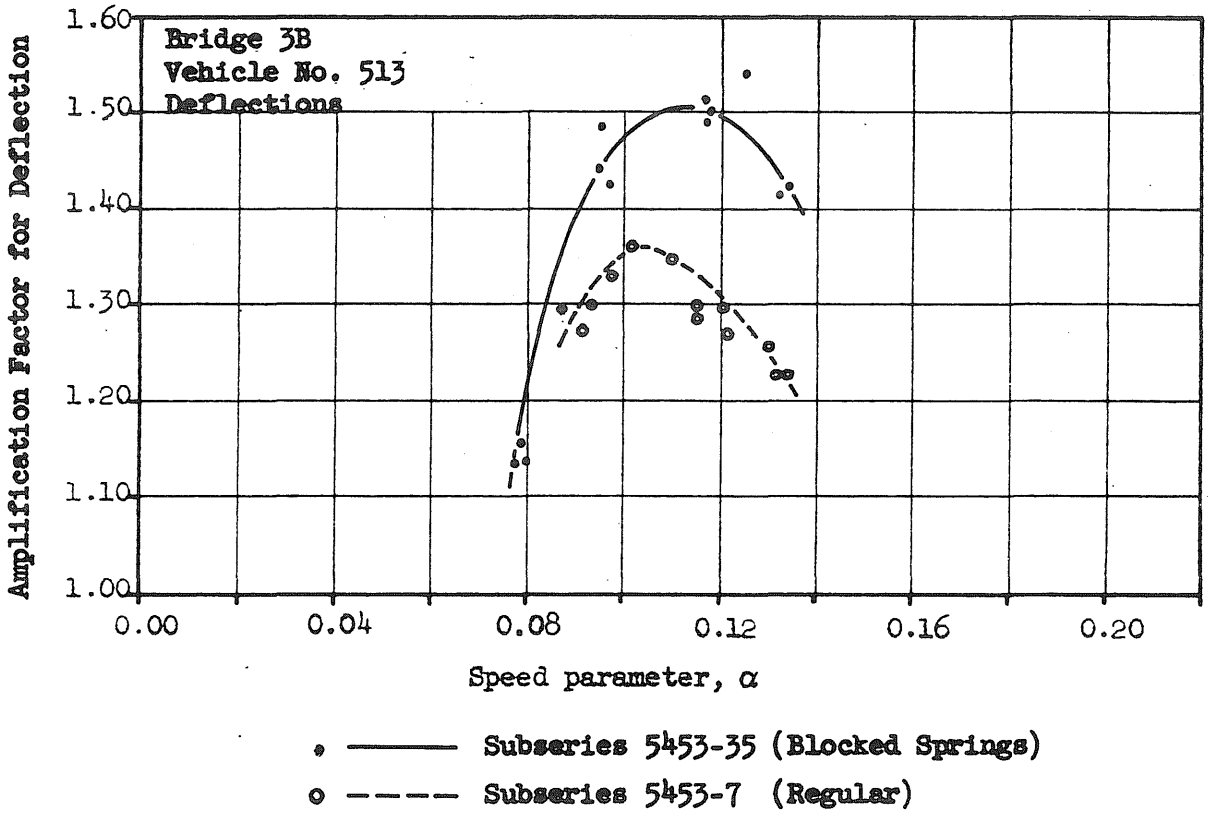

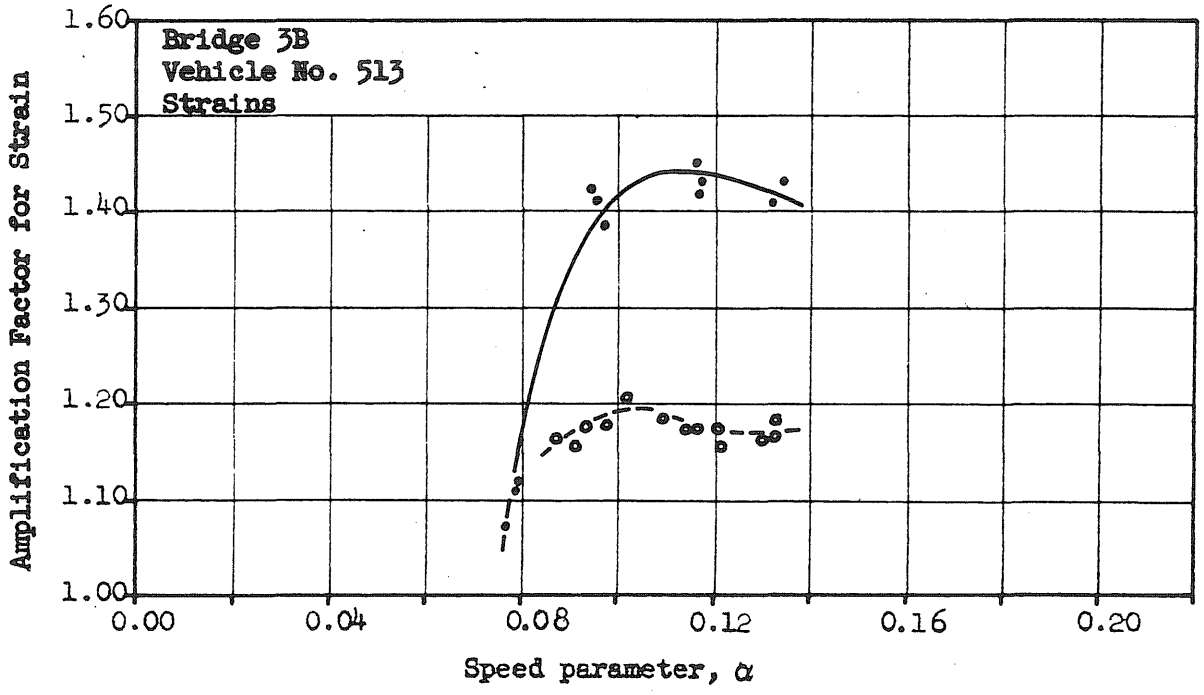

FIG. 52b SPECTRUM CURVES FOR TESTS WITH BLOCKED SPRINGS - THREE-AXLE VEHICLE

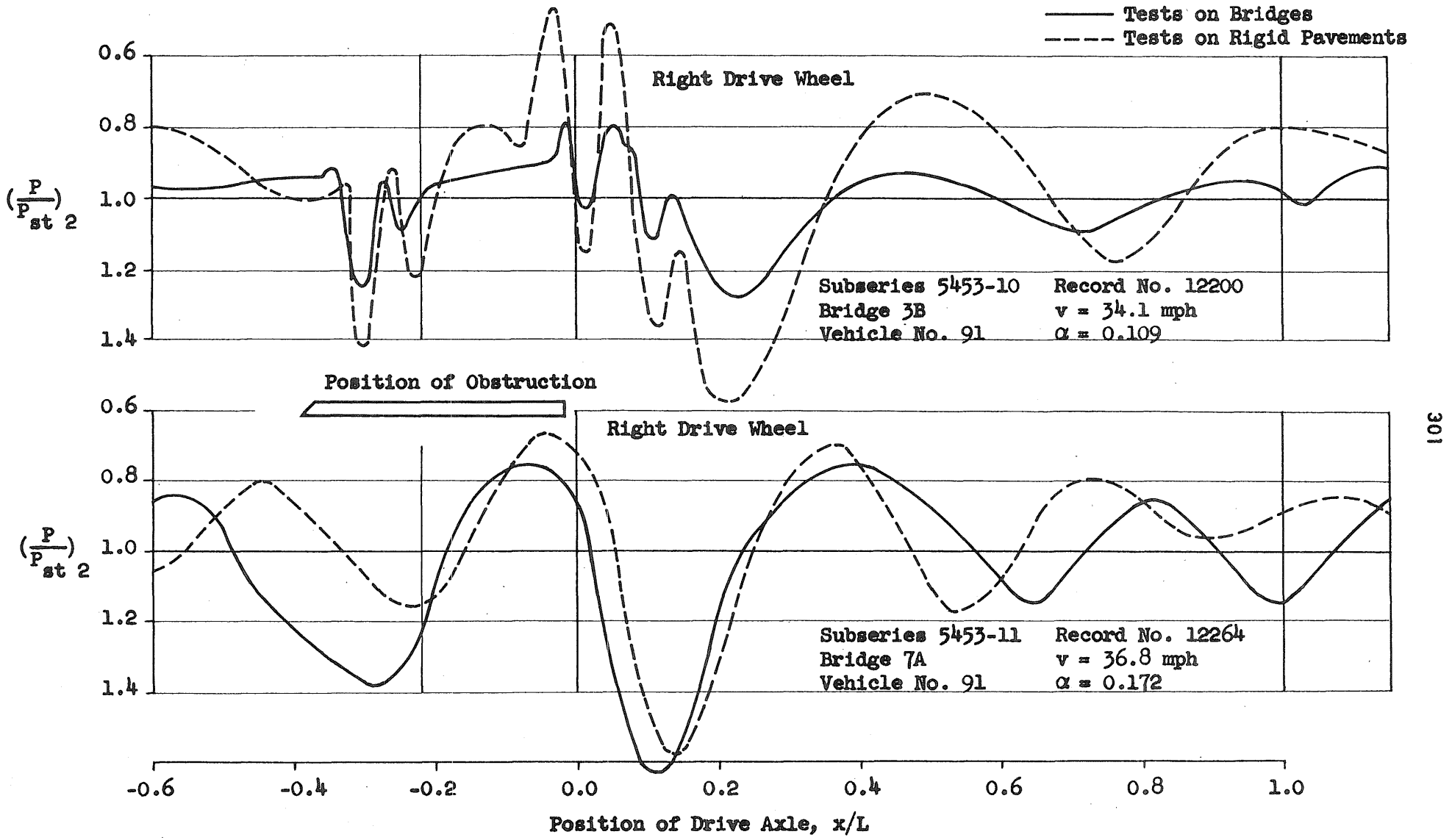

FIG. 53a TESTS WITH INDUCED INITIAL OSCILLATIONS - VEHICLE RESPONSE

Subseries 5453-6
Bridge 3B
Vehicle No. 91 (Springs Blocked)

Record No. 12422
v = 21.0 mph
α = 0.071

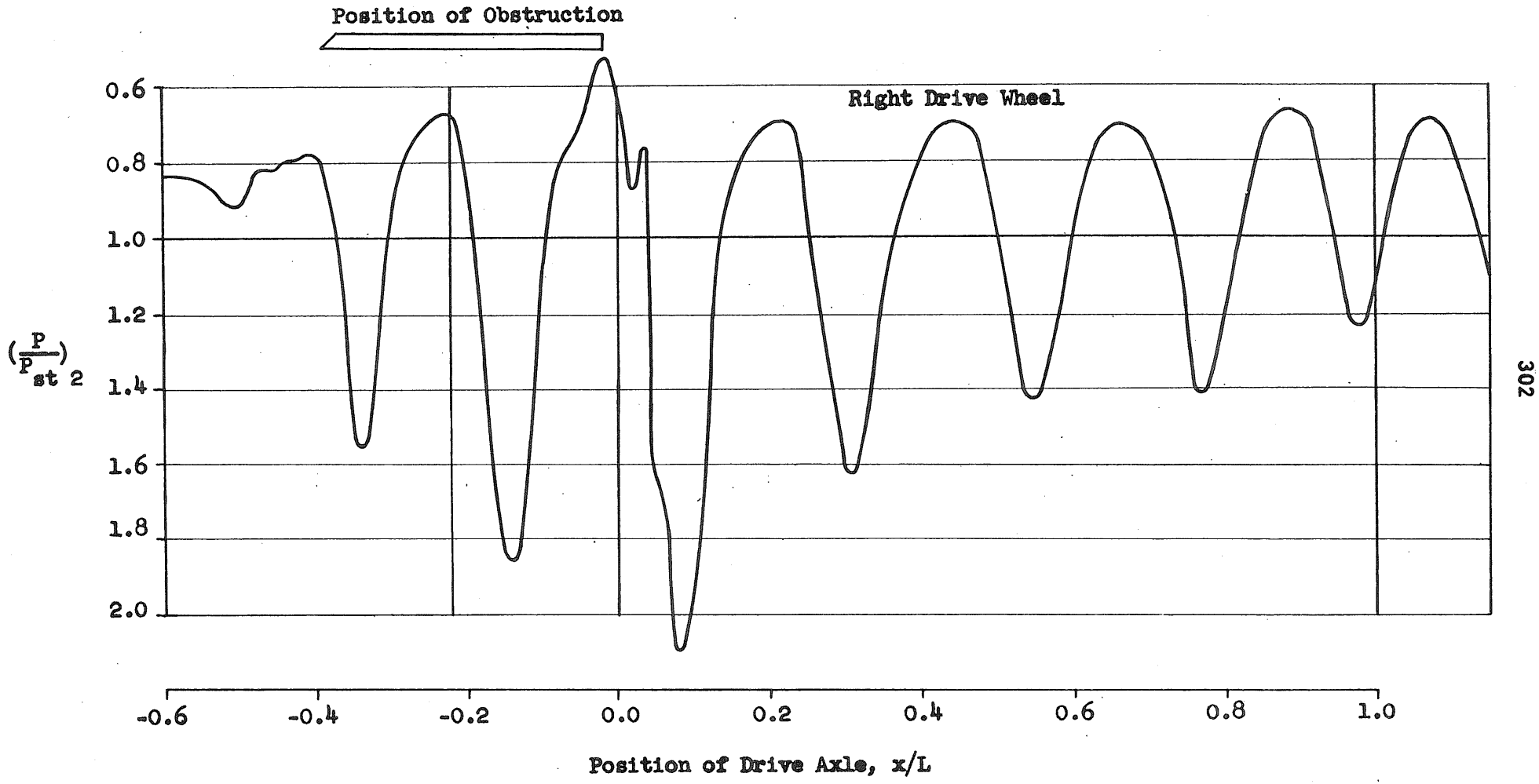

FIG. 53b TESTS WITH INDUCED INITIAL OSCILLATIONS - VEHICLE RESPONSE

Subseries 5453-14
Bridge 7A
Vehicle No. 513

Record No. 12599
v = 19.8 mph
α = 0.096

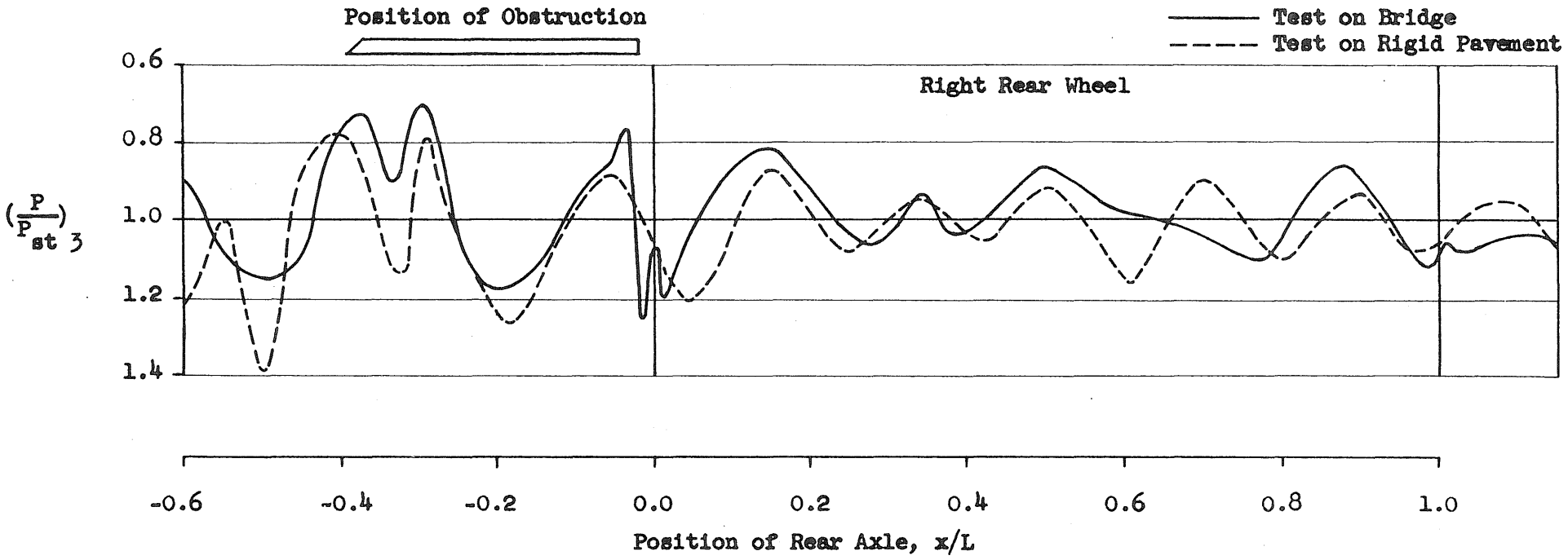

FIG. 53c TESTS WITH INDUCED INITIAL OSCILLATIONS - VEHICLE RESPONSE

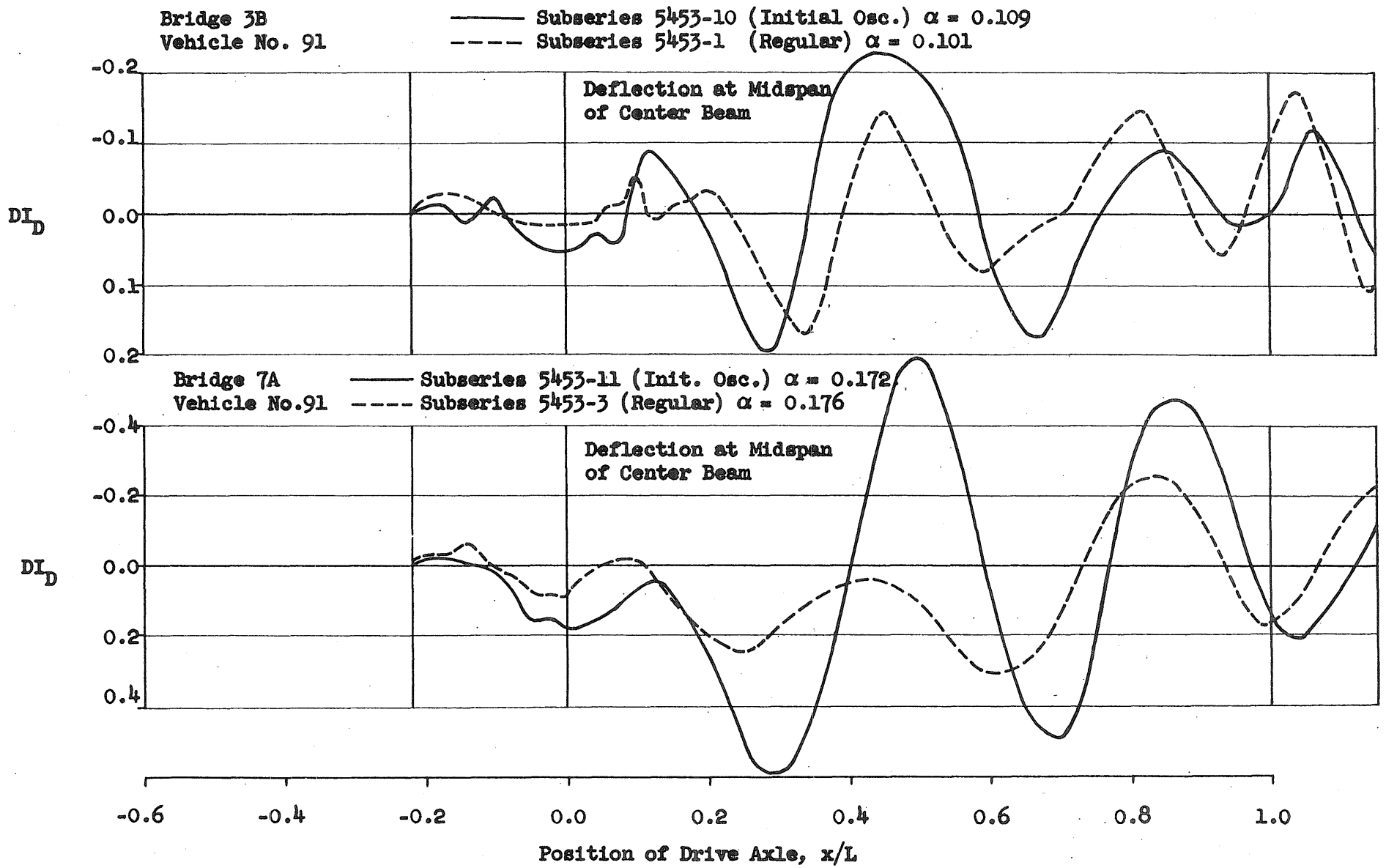

FIG. 54a TESTS WITH INDUCED INITIAL OSCILLATIONS - BRIDGE RESPONSE

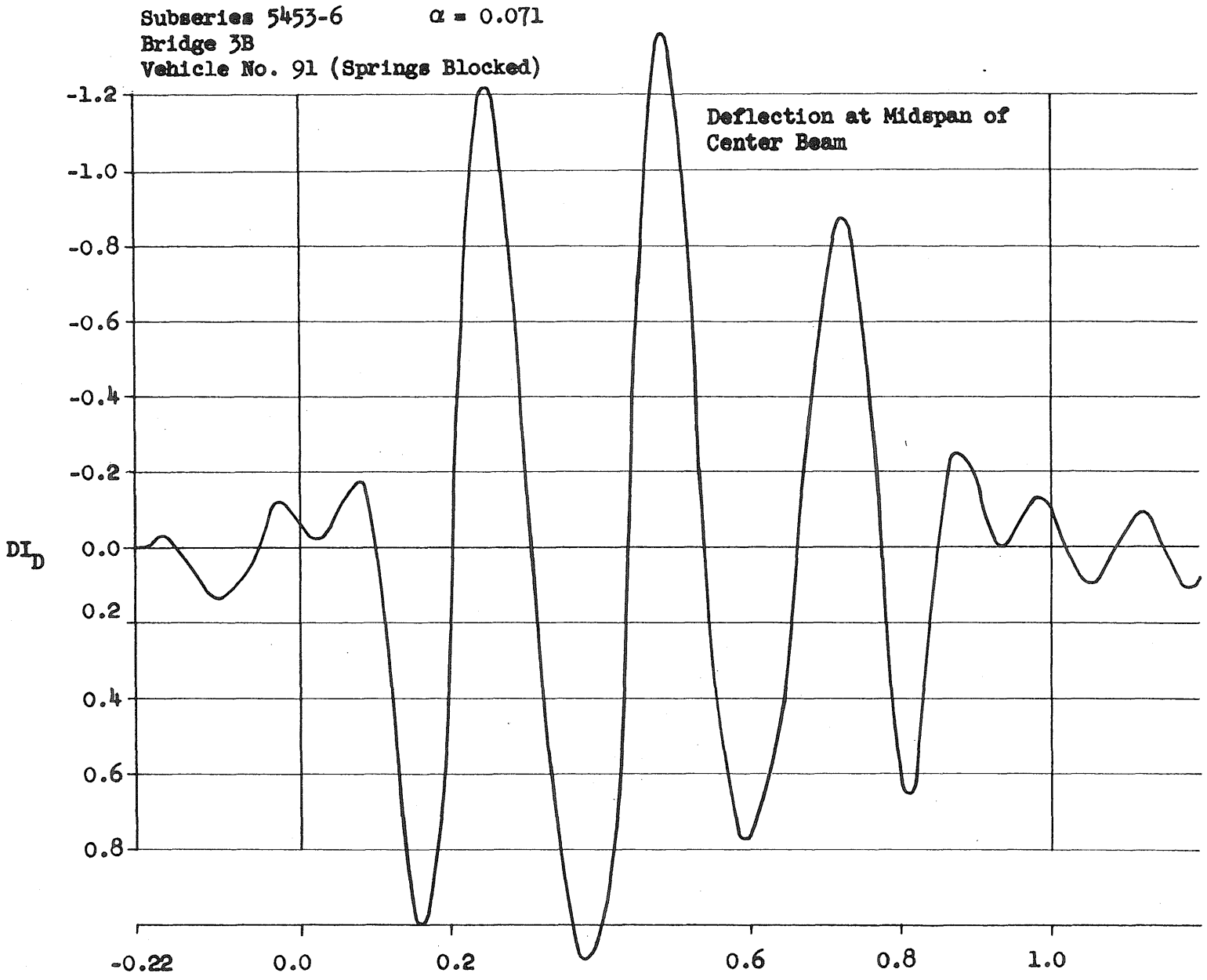

FIG. 54b TESTS WITH INDUCED INITIAL OSCILLATIONS - BRIDGE RESPONSE

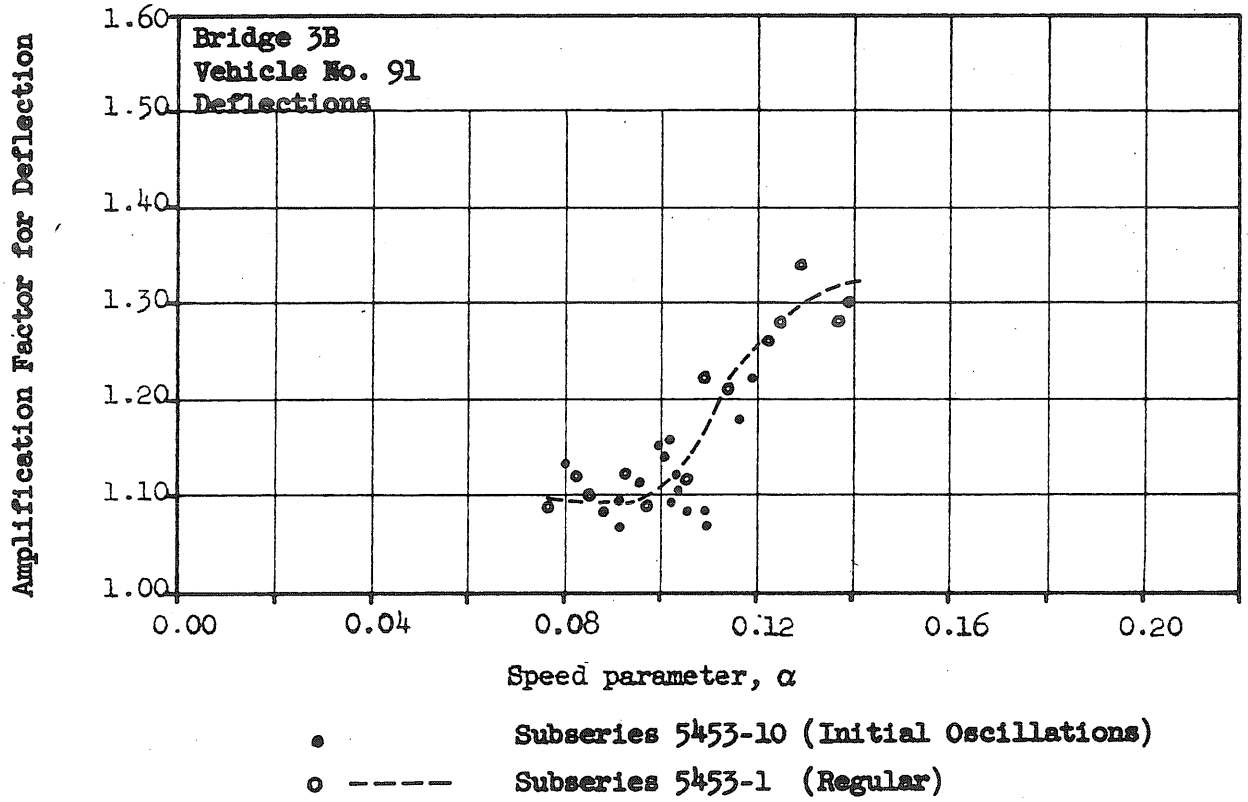

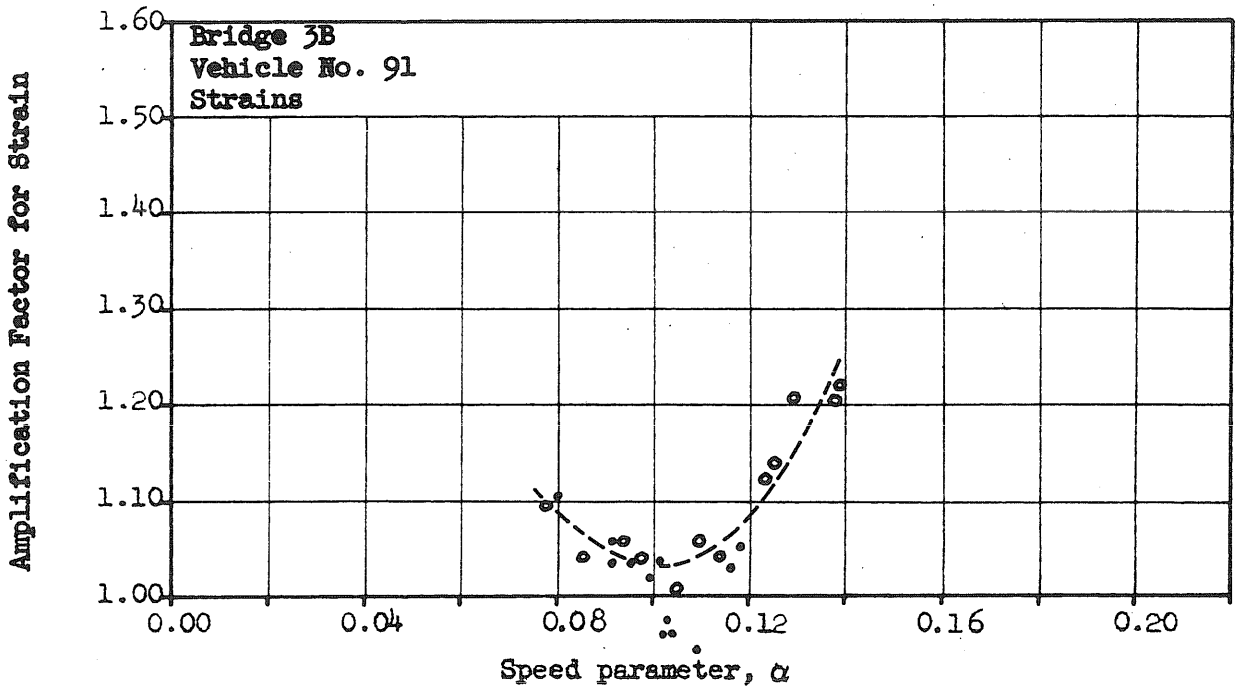

FIG. 55a SPECTRUM CURVES FOR TESTS WITH INITIAL OSCILLATIONS

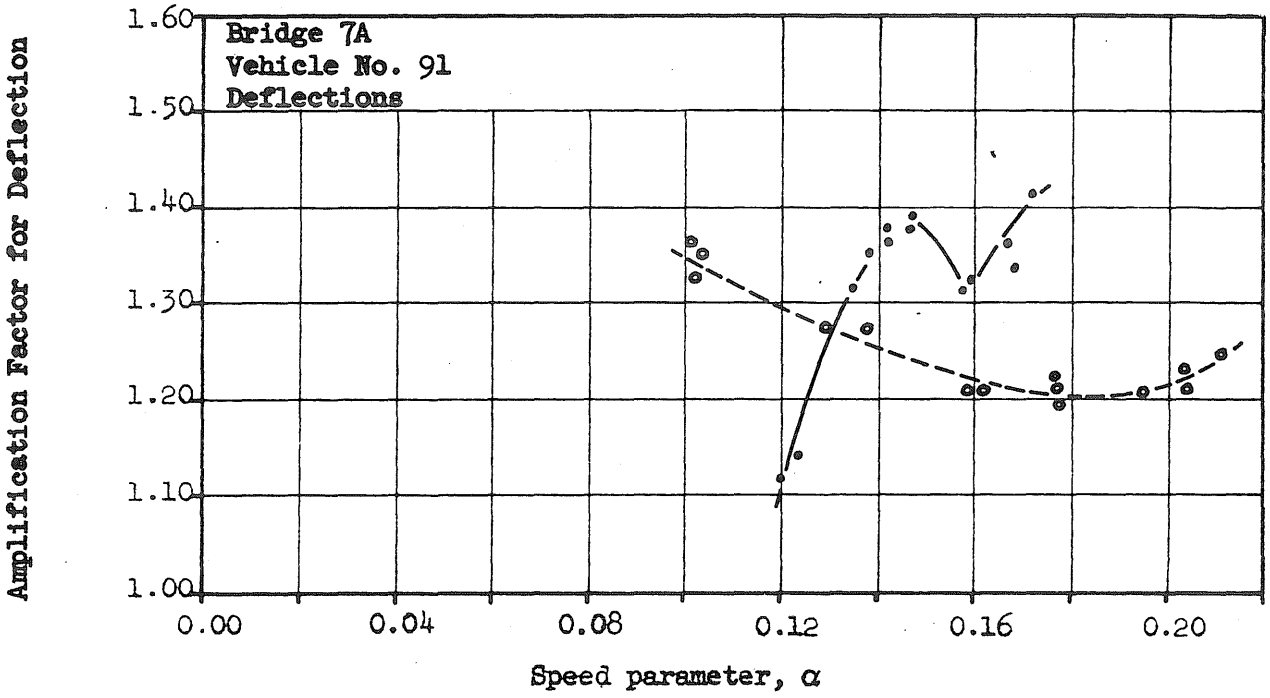

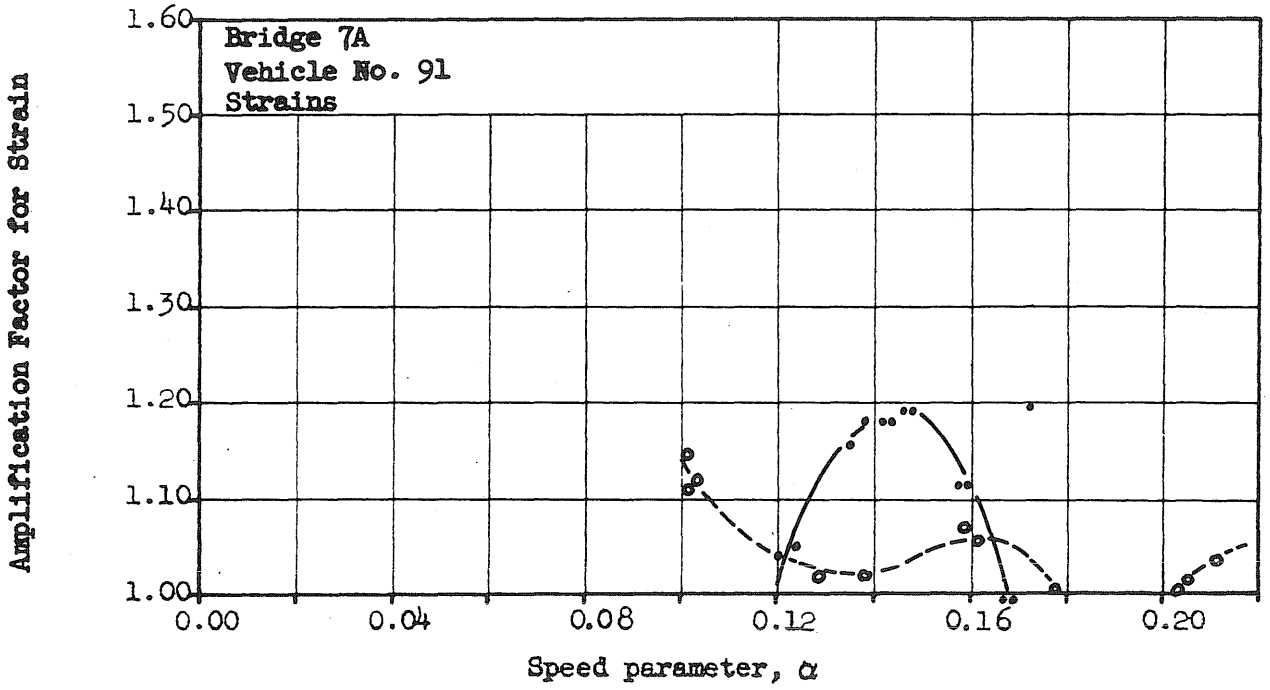

FIG. 55b SPECTRUM CURVES FOR TESTS WITH INITIAL OSCILLATIONS

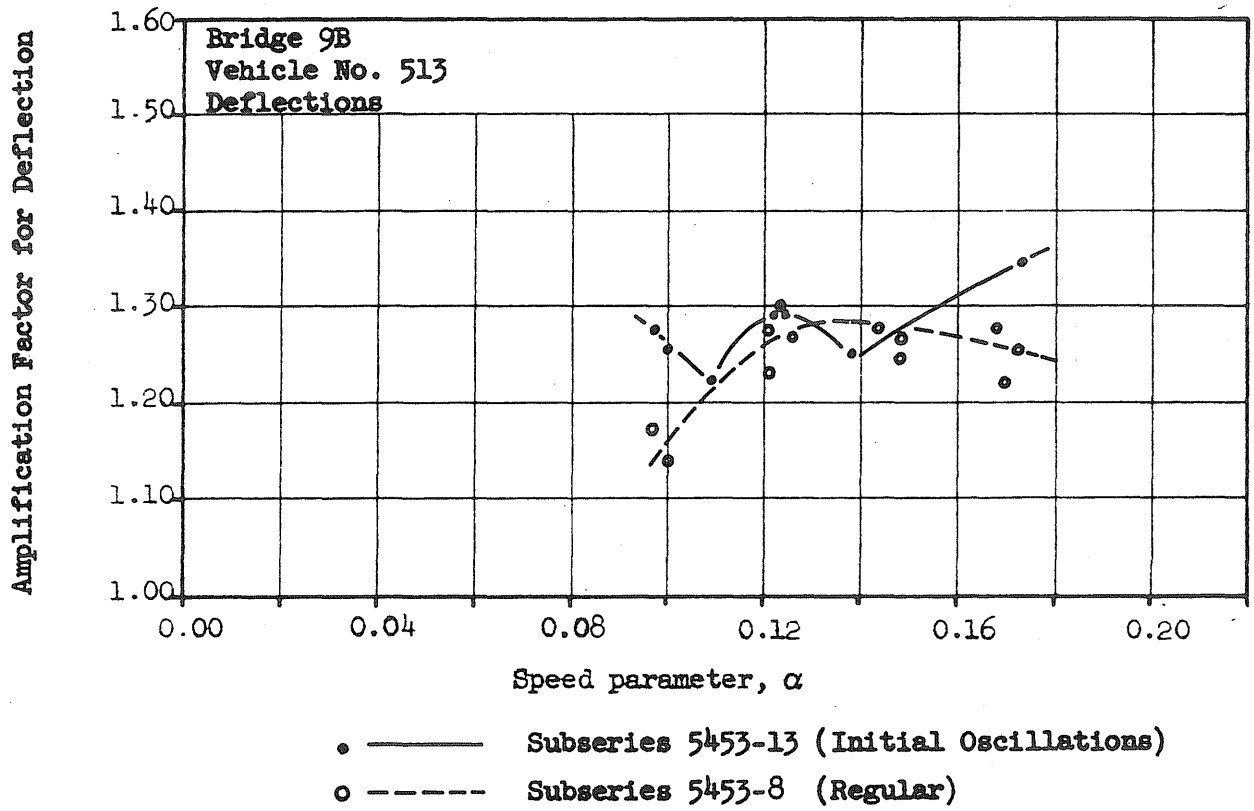

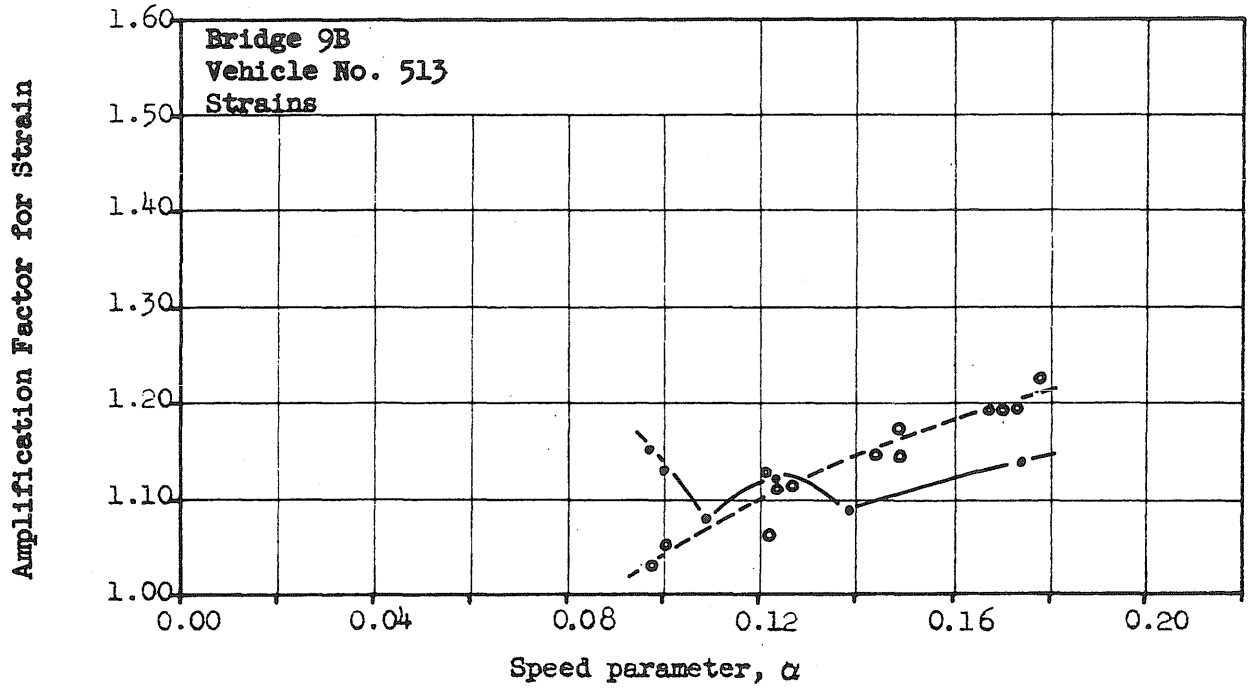

FIG. 55c SPECTRUM CURVES FOR TESTS WITH INITIAL OSCILLATIONS

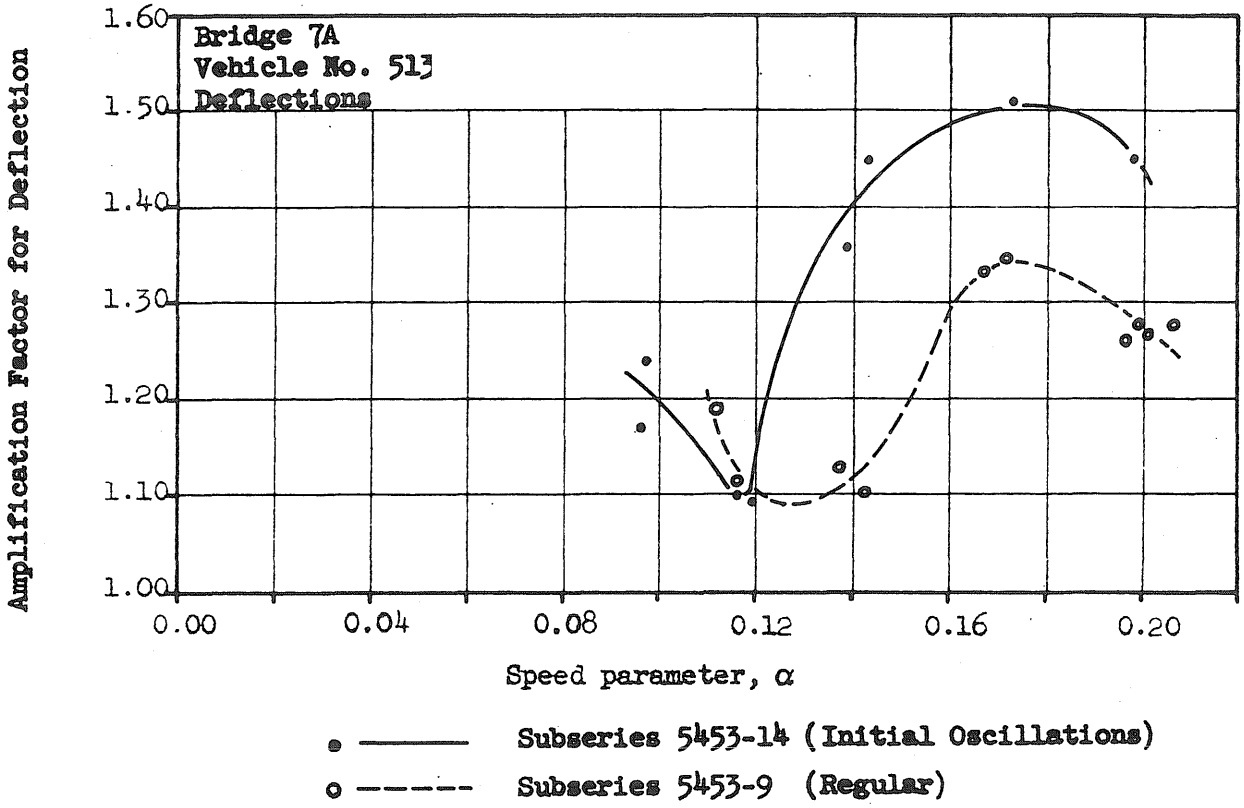

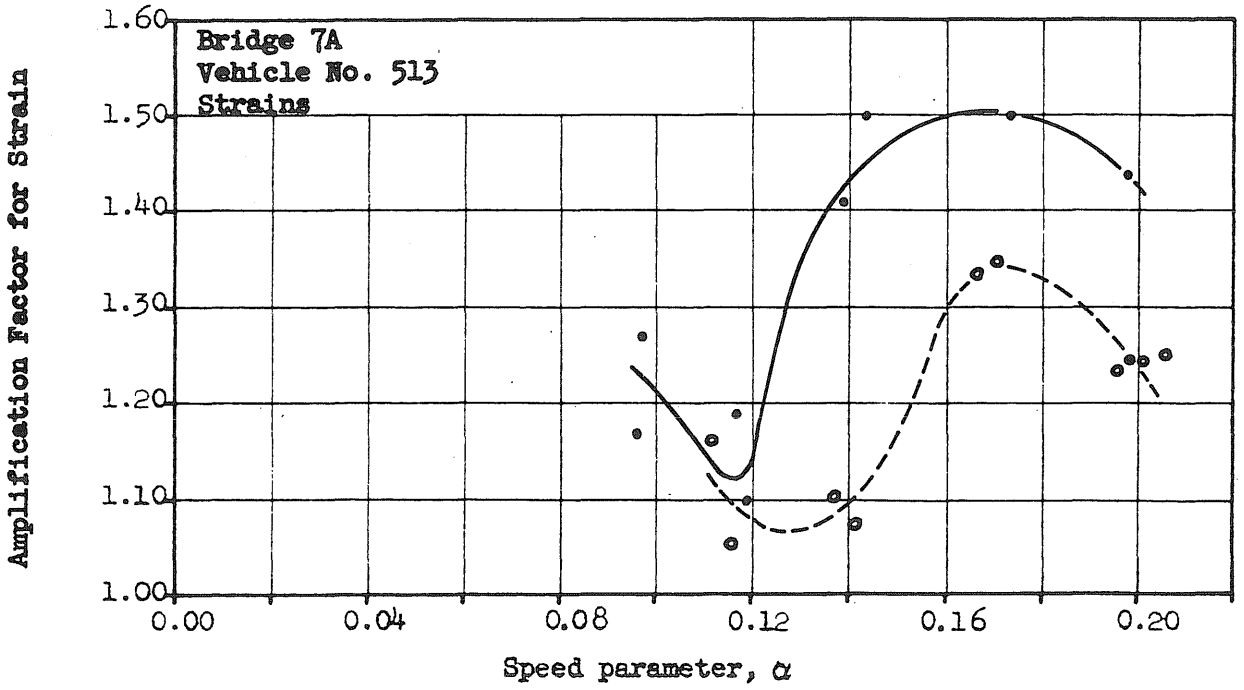

FIG. 55d SPECTRUM CURVES FOR TESTS WITH INITIAL OSCILLATIONS

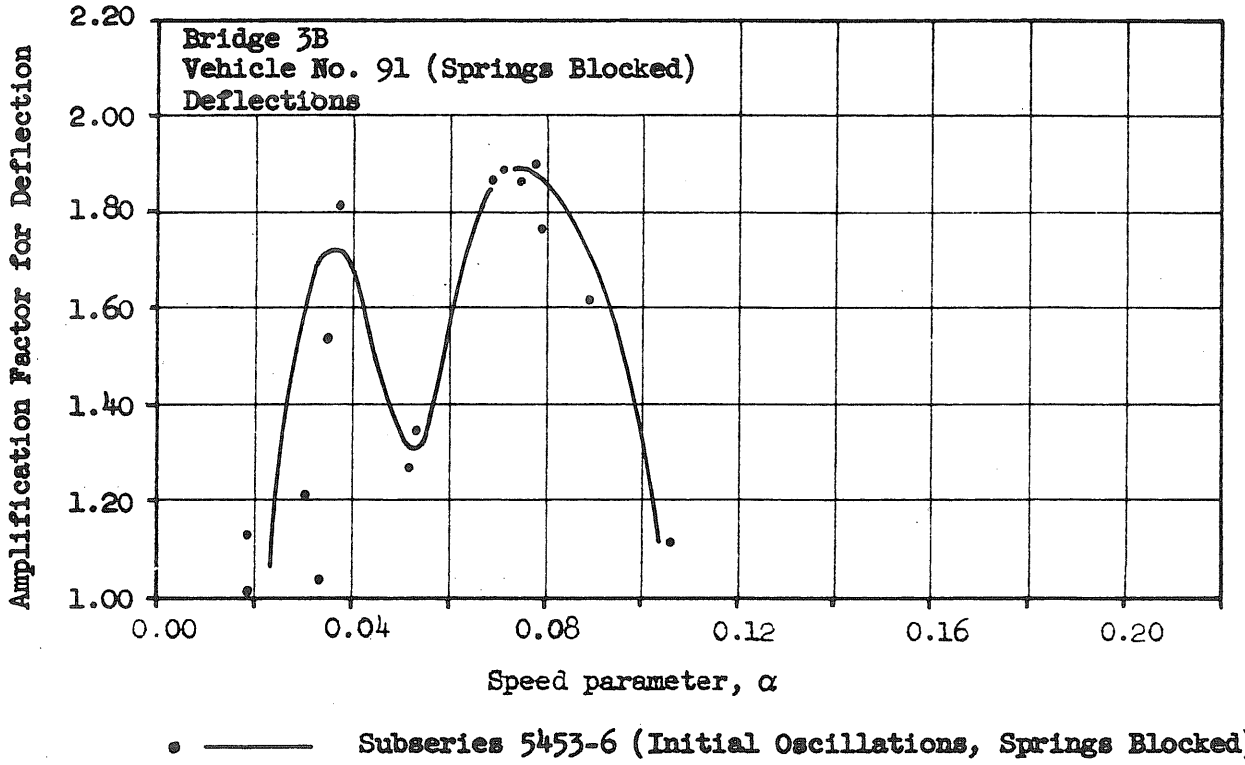

• ——— Subseries 5453-6 (Initial Oscillations, Springs Blocked)

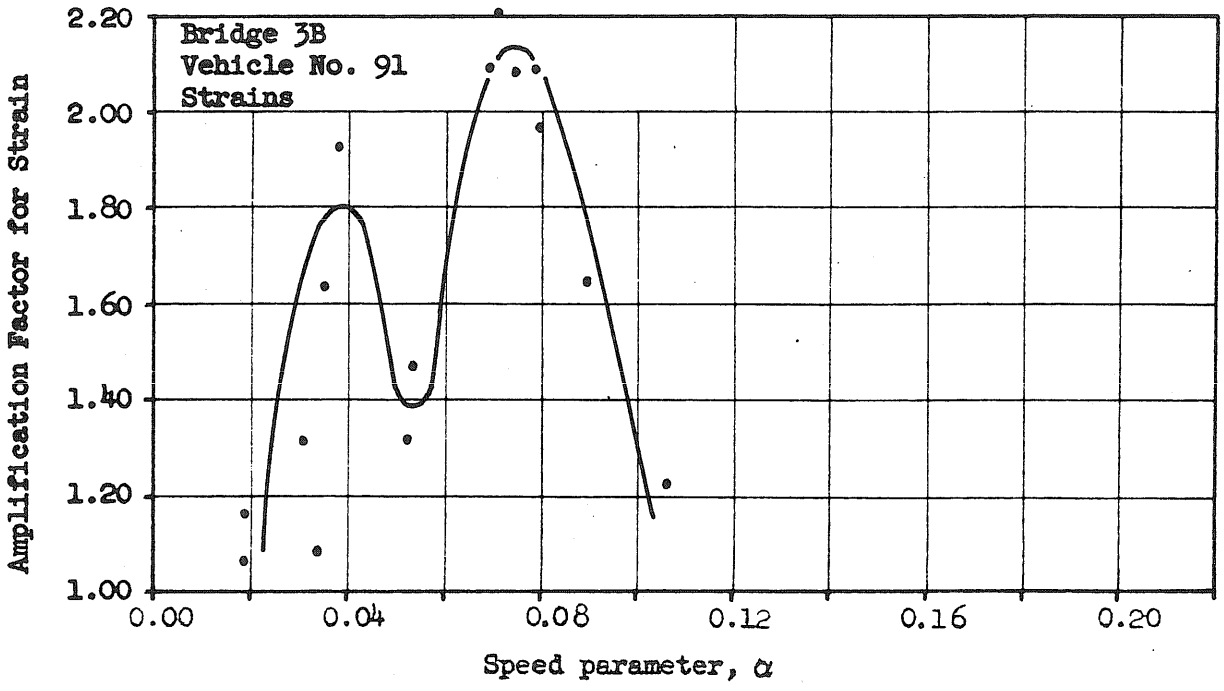

FIG. 55e SPECTRUM CURVES FOR TESTS WITH INITIAL OSCILLATIONS

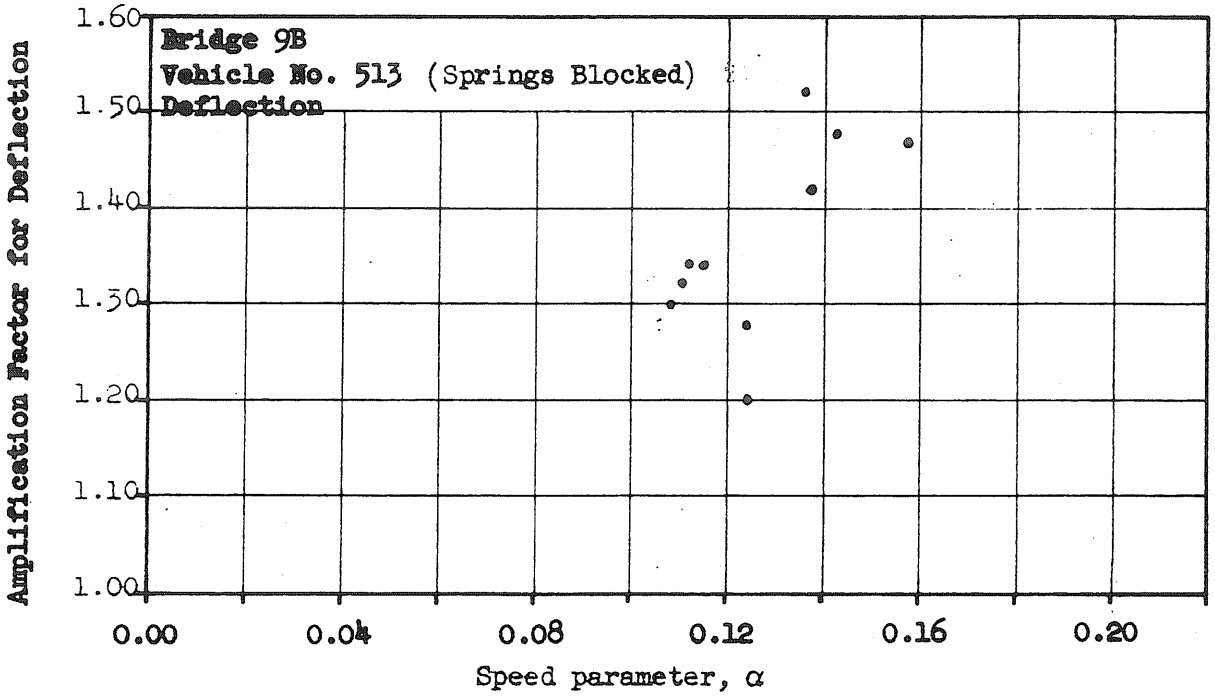

Subseries 5453-36 (Initial Oscillations, Springs Blocked)

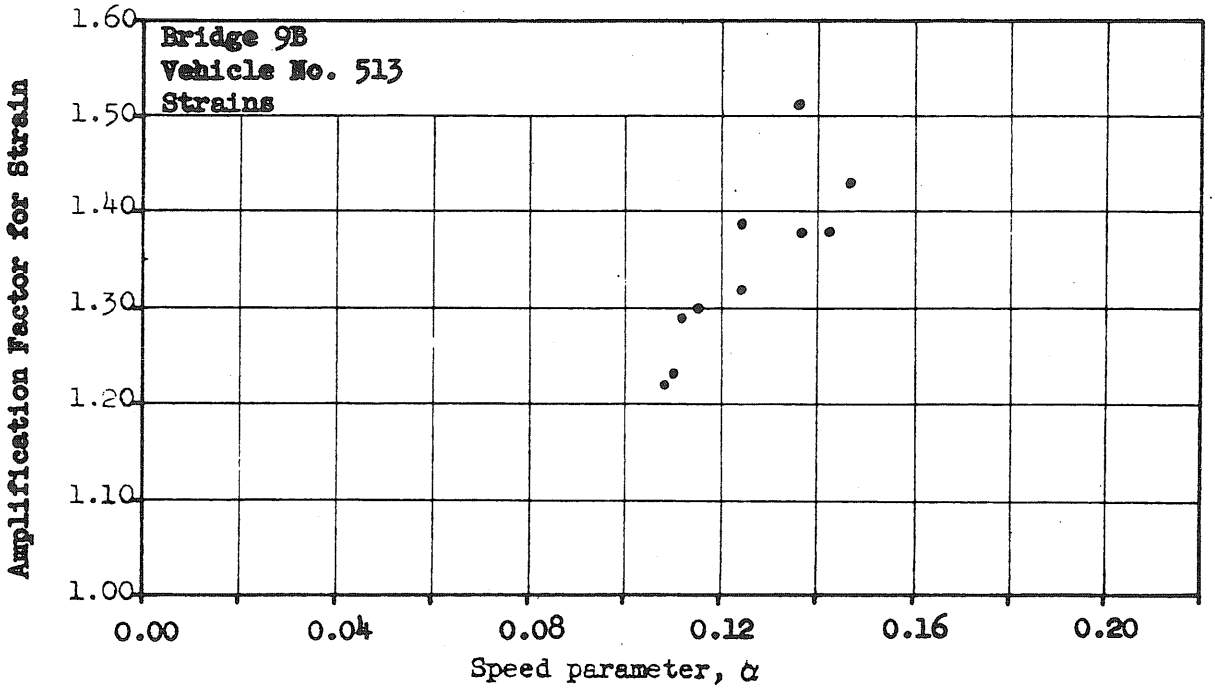

FIG. 55f SPECTRUM CURVES FOR TESTS WITH INITIAL OSCILLATIONS

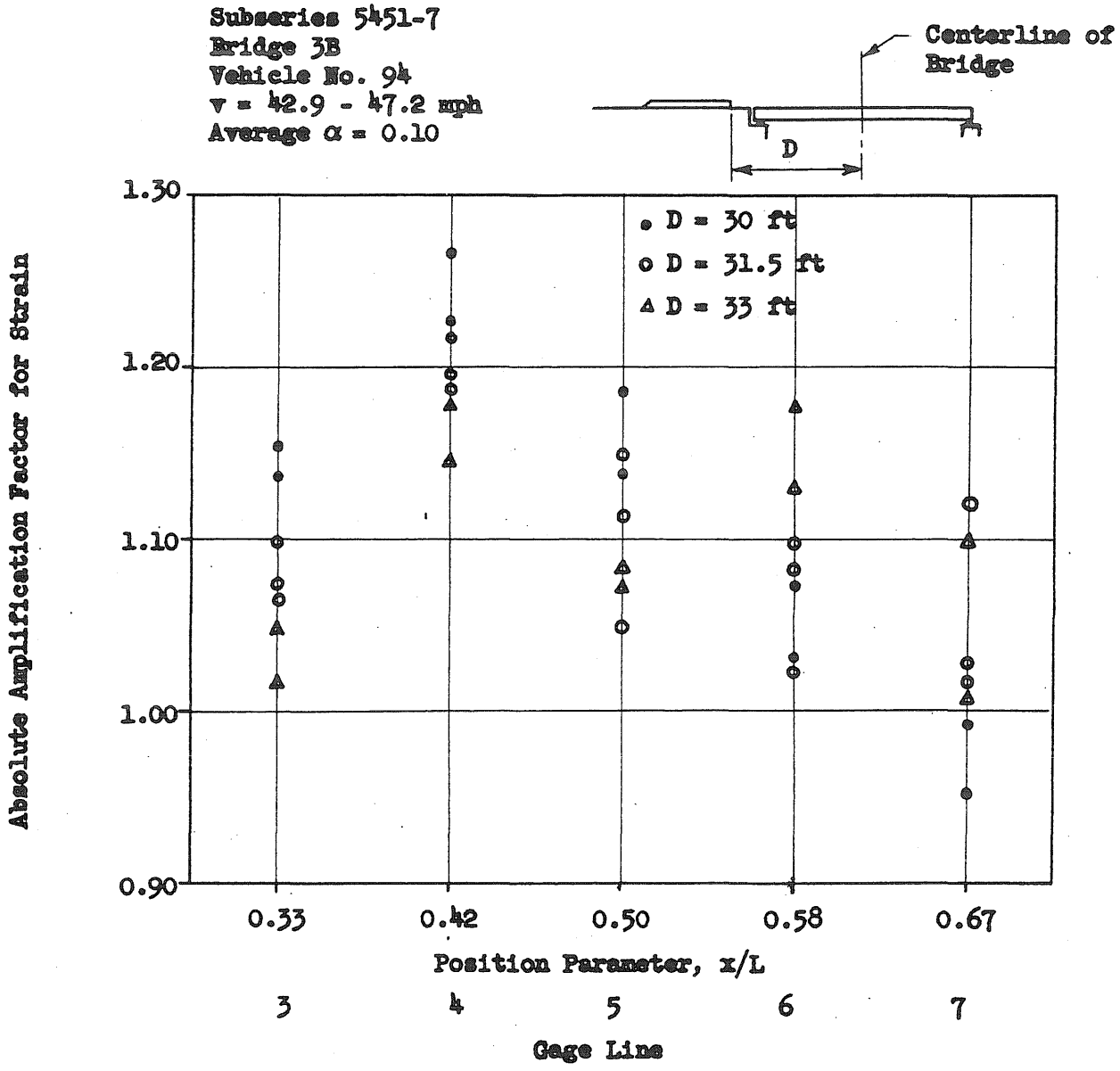

FIG. 56 LONGIDUTINAL DISTRIBUTION OF EFFECTS

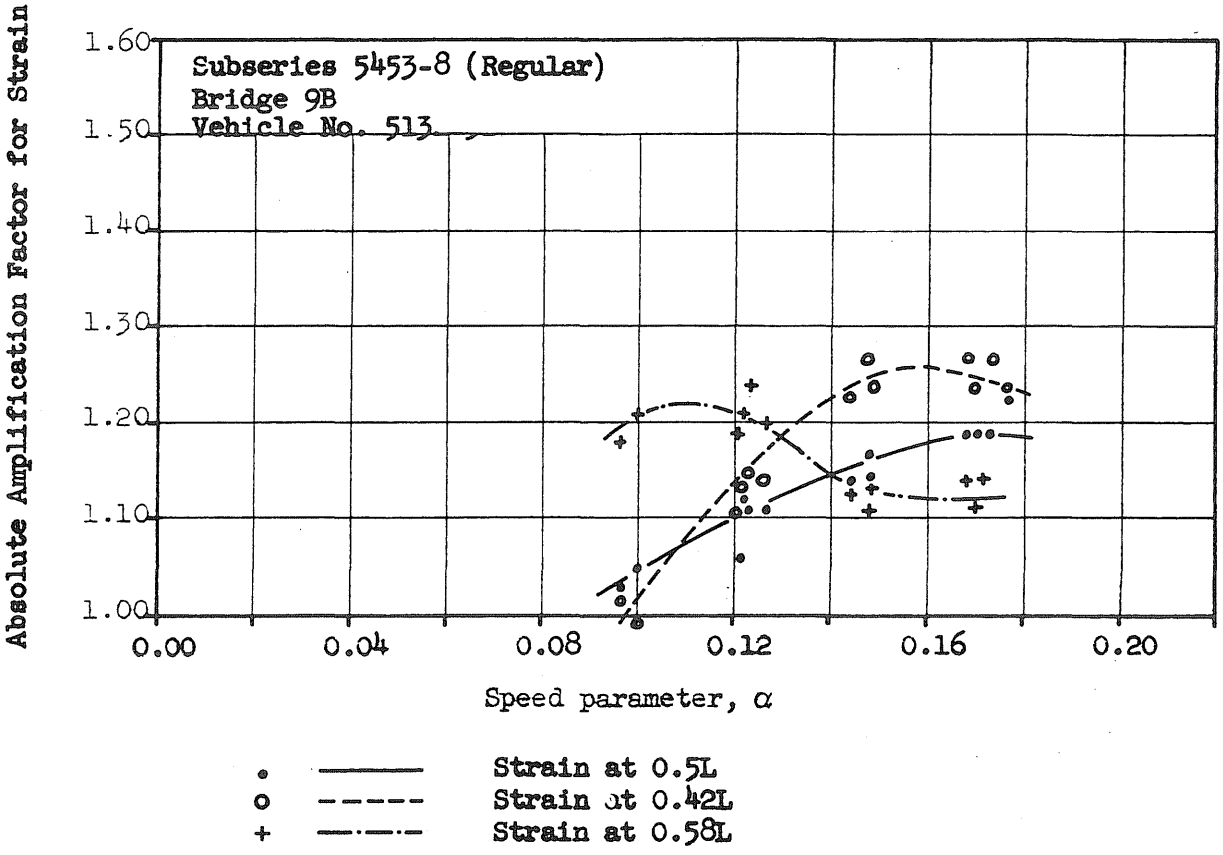

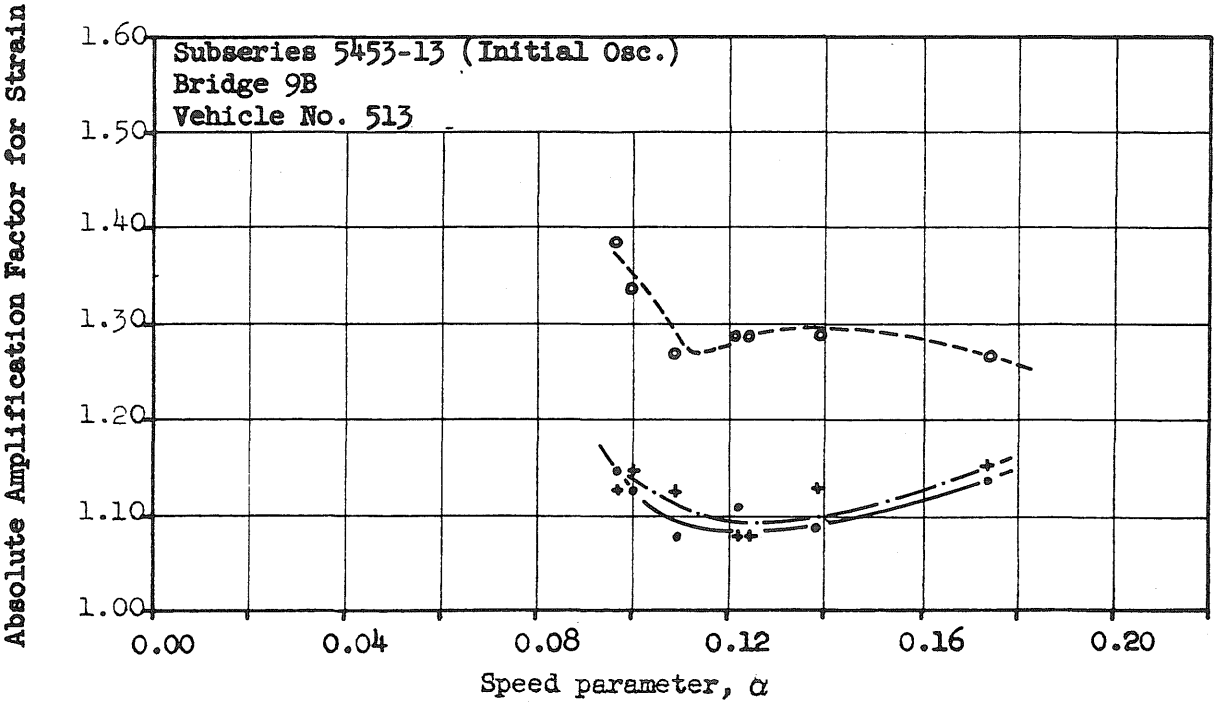

FIG. 57 SPECTRUM CURVES FOR LONGITUDINAL DISTRIBUTION OF EFFECTS

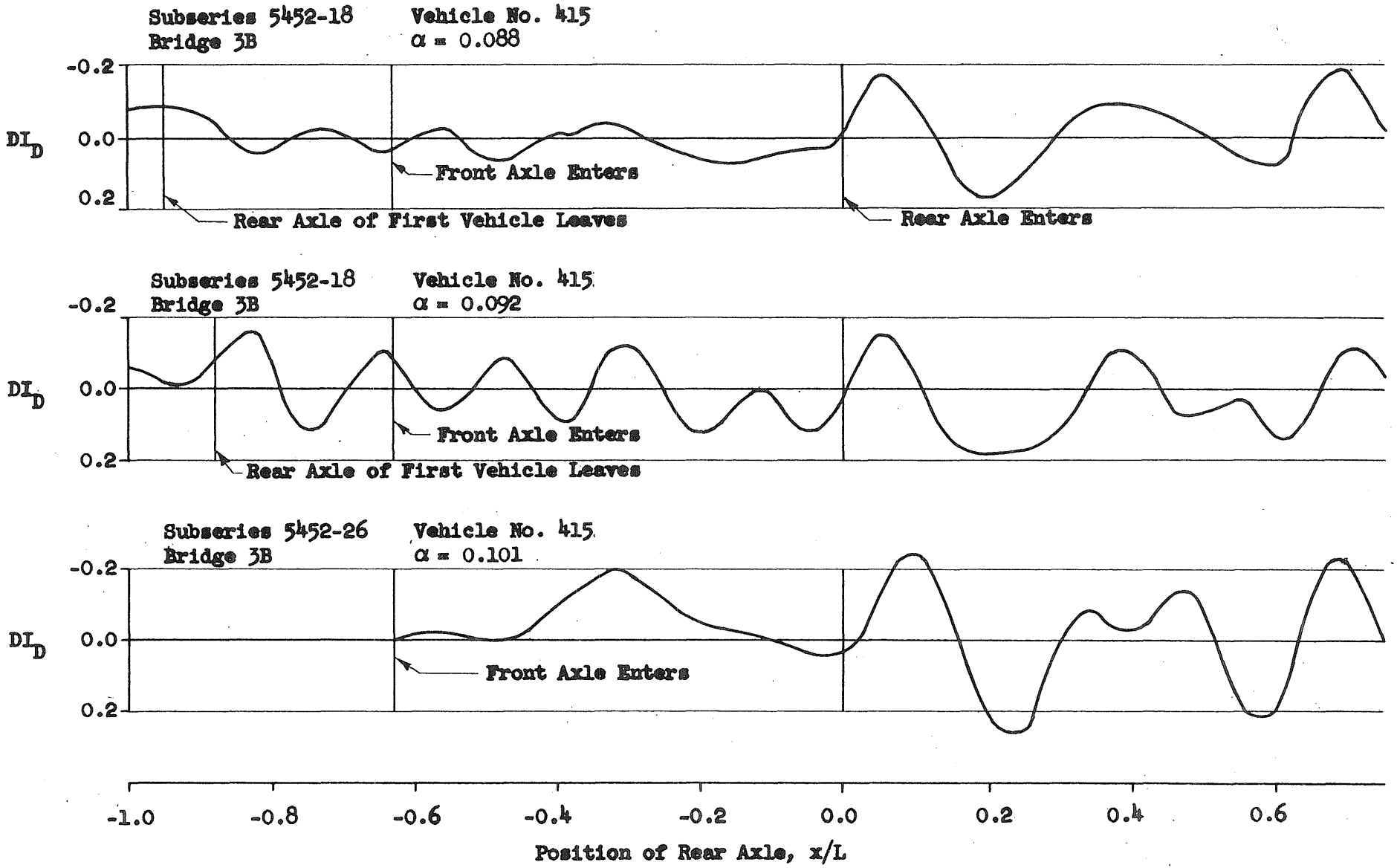

FIG. 58 EFFECT OF INITIAL BRIDGE OSCILLATIONS

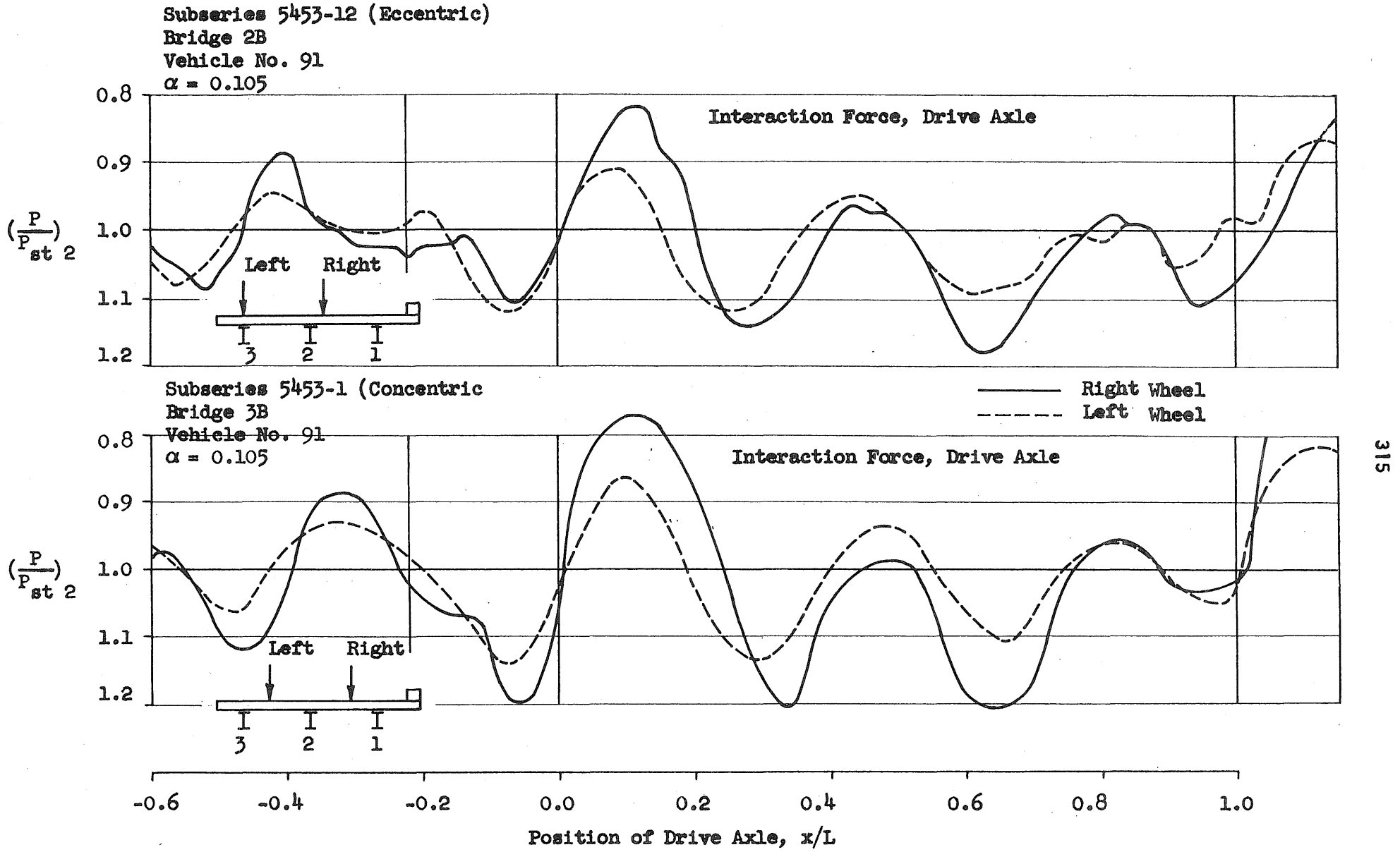

FIG. 59a COMPARISON OF RESPONSE FOR ECCENTRIC AND CONCENTRIC TESTS - Interaction Forces

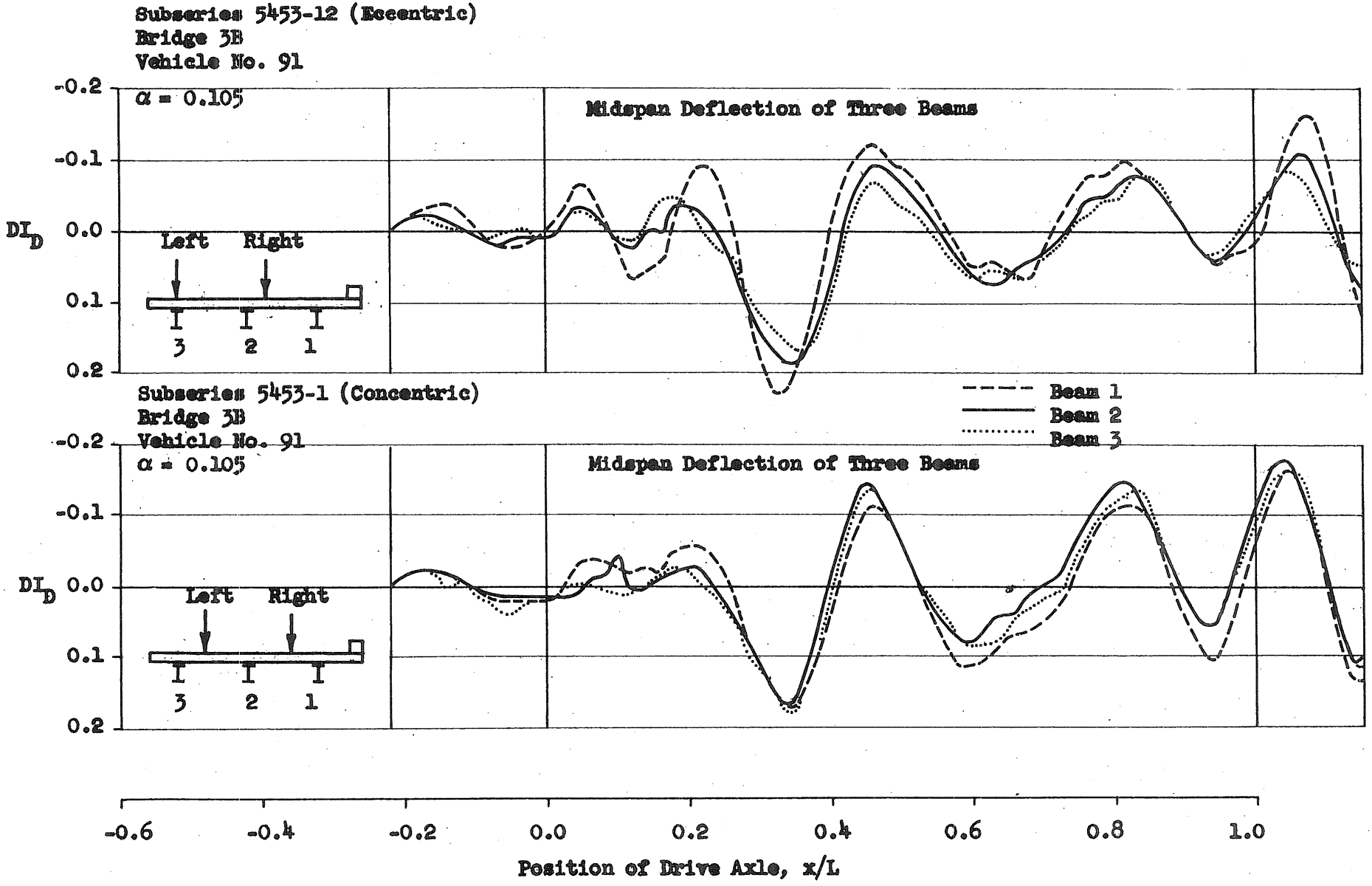

FIG. 59b COMPARISON OF RESPONSE FOR ECCENTRIC AND CONCENTRIC TESTS - BRIDGE RESPONSE, TWO-AXLE VEHICLE

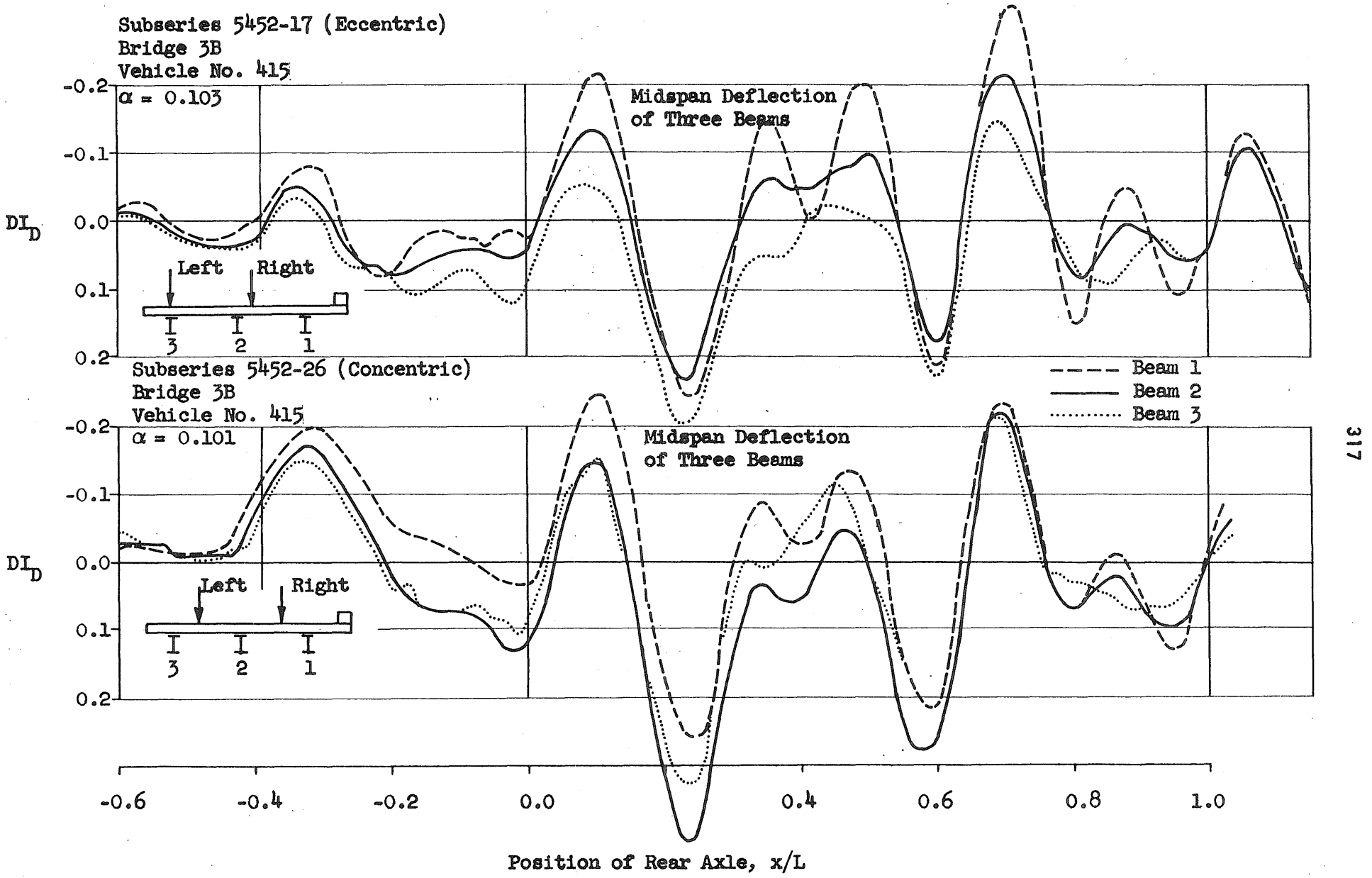

FIG. 59c COMPARISON OF RESPONSE FOR ECCENTRIC AND CONCENTRIC TESTS - BRIDGE RESPONSE, THREE-AXLE VEHICLE

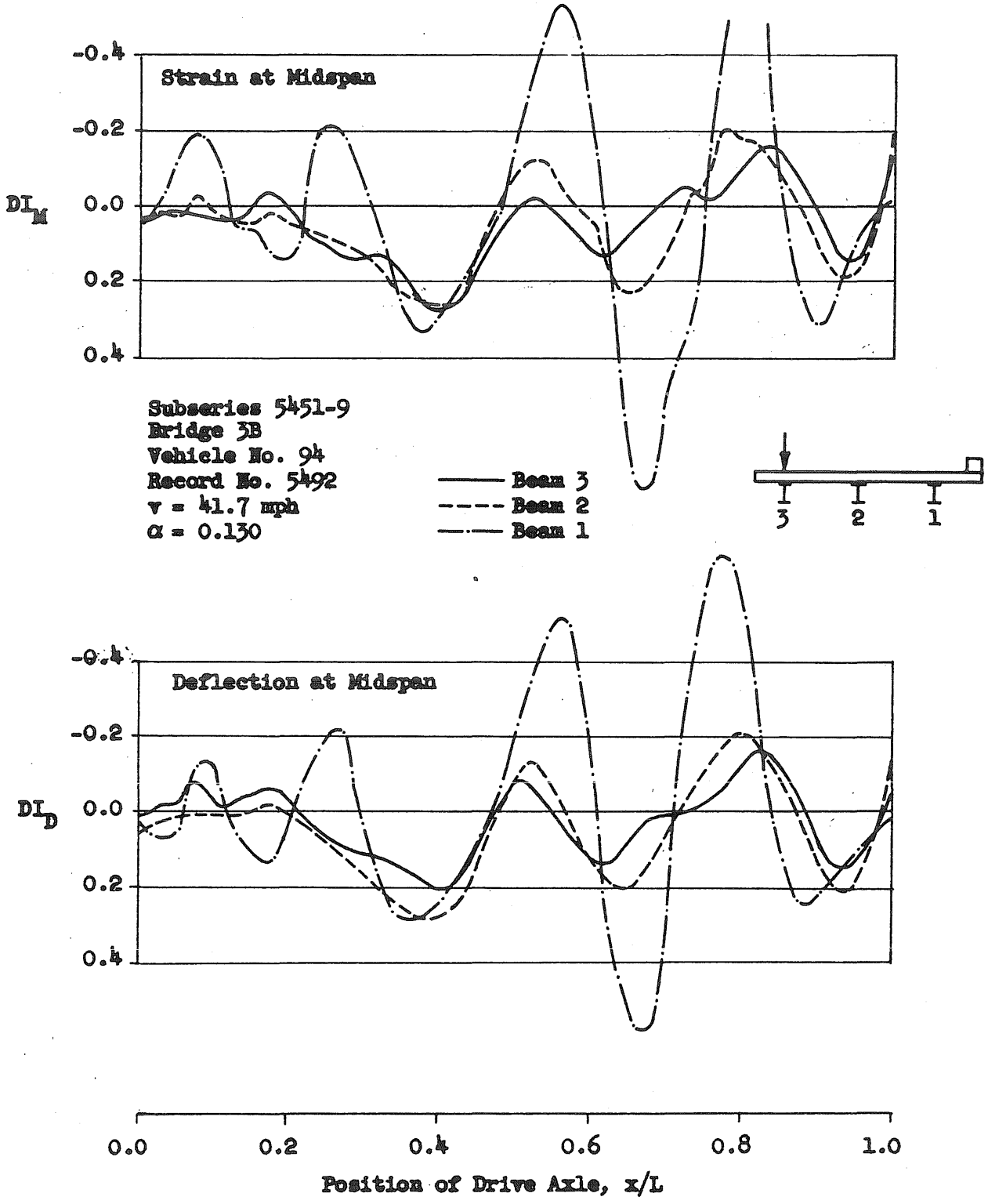

FIG. 60 BRIDGE RESPONSE FOR TEST WITH 60-INCH ECCENTRICITY

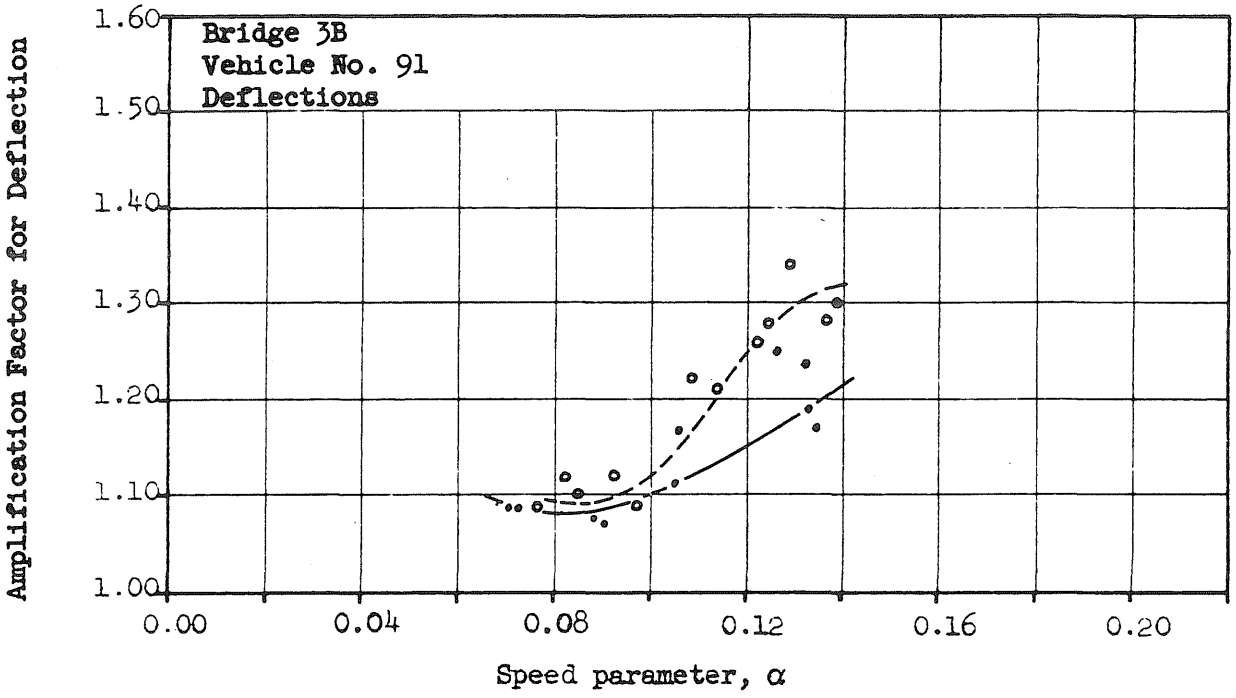

• ——— Subseries 5453-12 Edge Beam, Eccentric Loading

o – – – – Subseries 5453-1 Center Beam, Concentric Loading

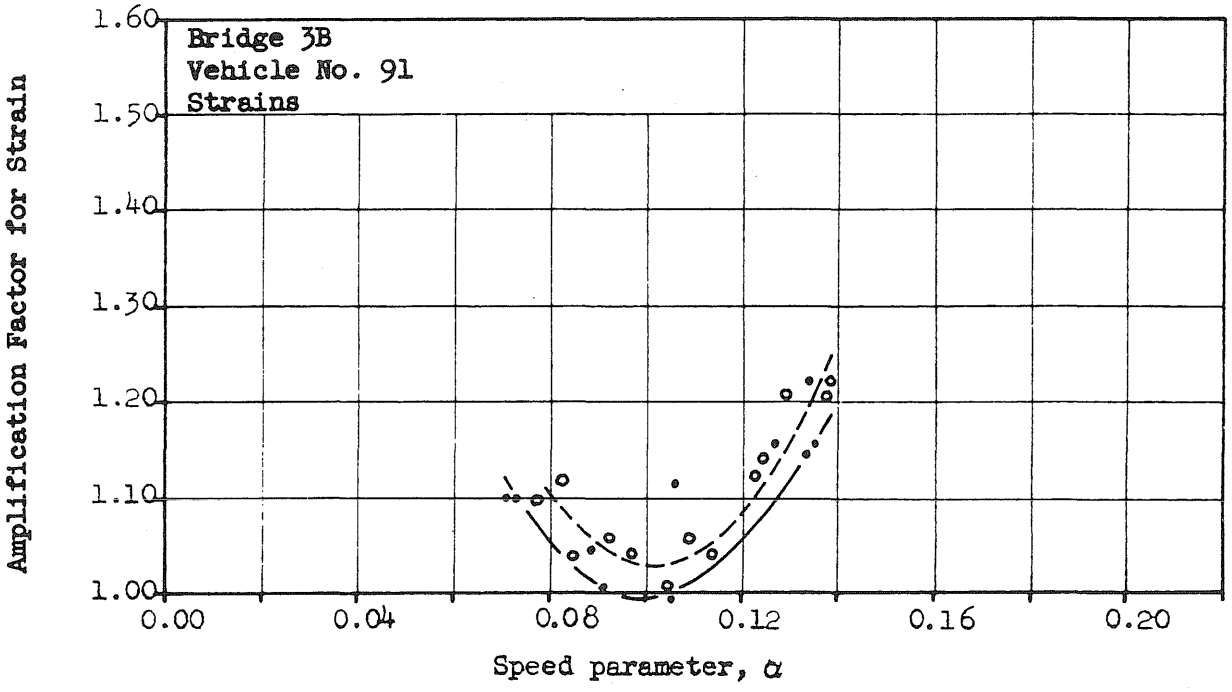

FIG. 61a SPECTRUM CURVES FOR ECCENTRIC TESTS

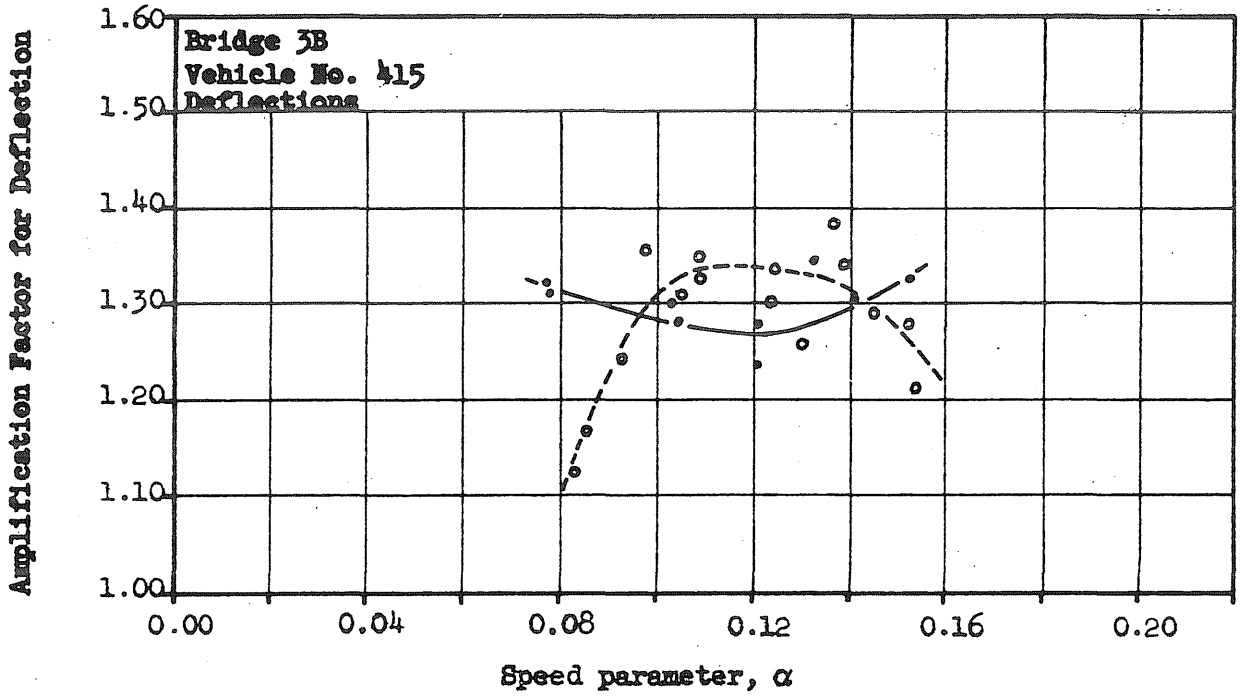

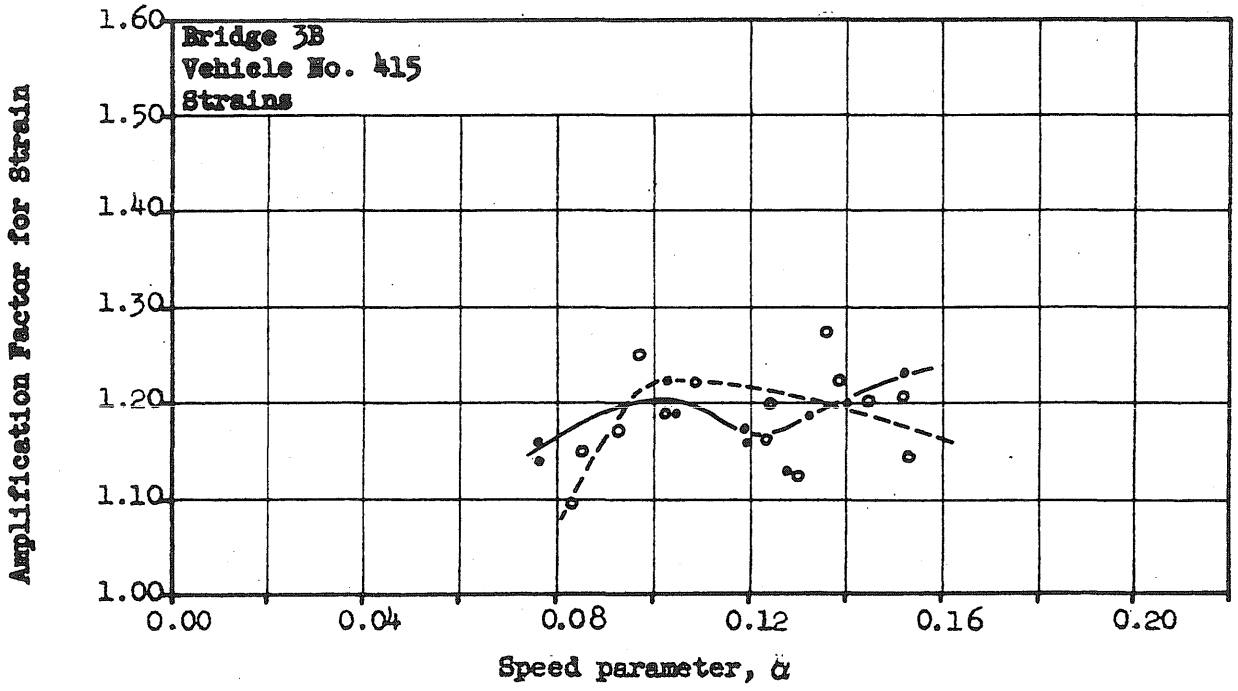

FIG. 61b SPECTRUM CURVES FOR ECCENTRIC TESTS

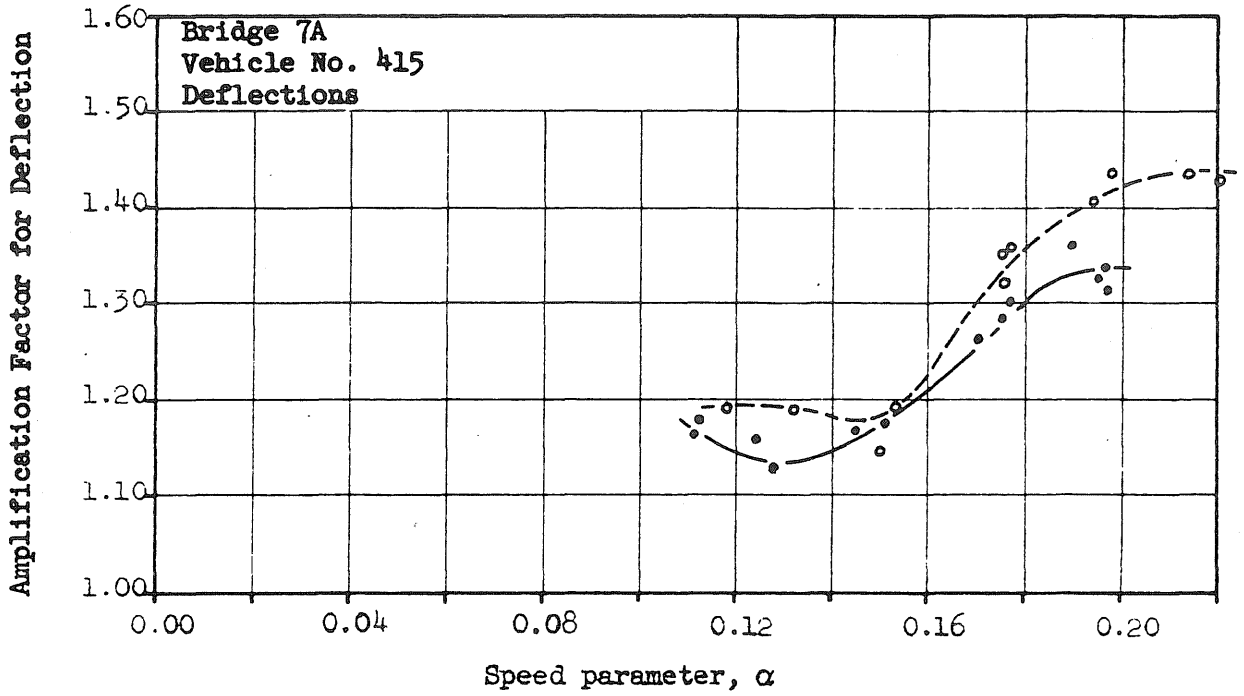

. ——— Subseries 5452-18 Edge Beam, Eccentric Loading

o – – – – Subseries 5451-5 Center Beam, Concentric Loading

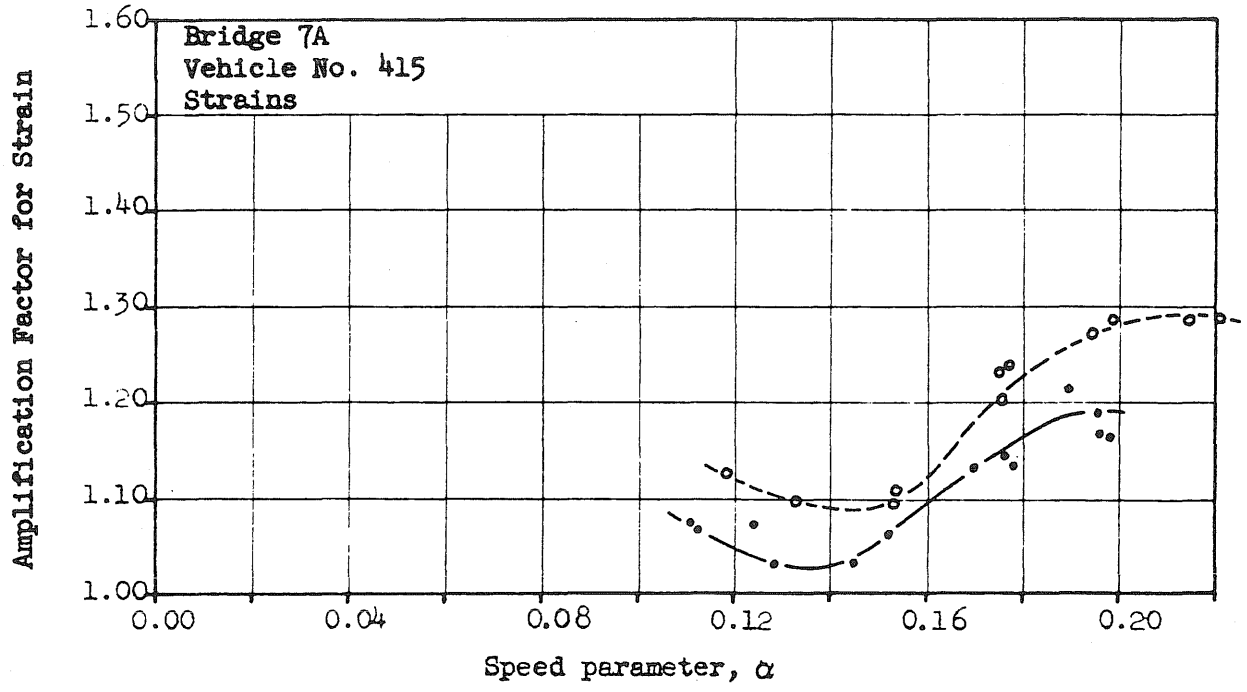

FIG. 61c SPECTRUM CURVES FOR ECCENTRIC TESTS

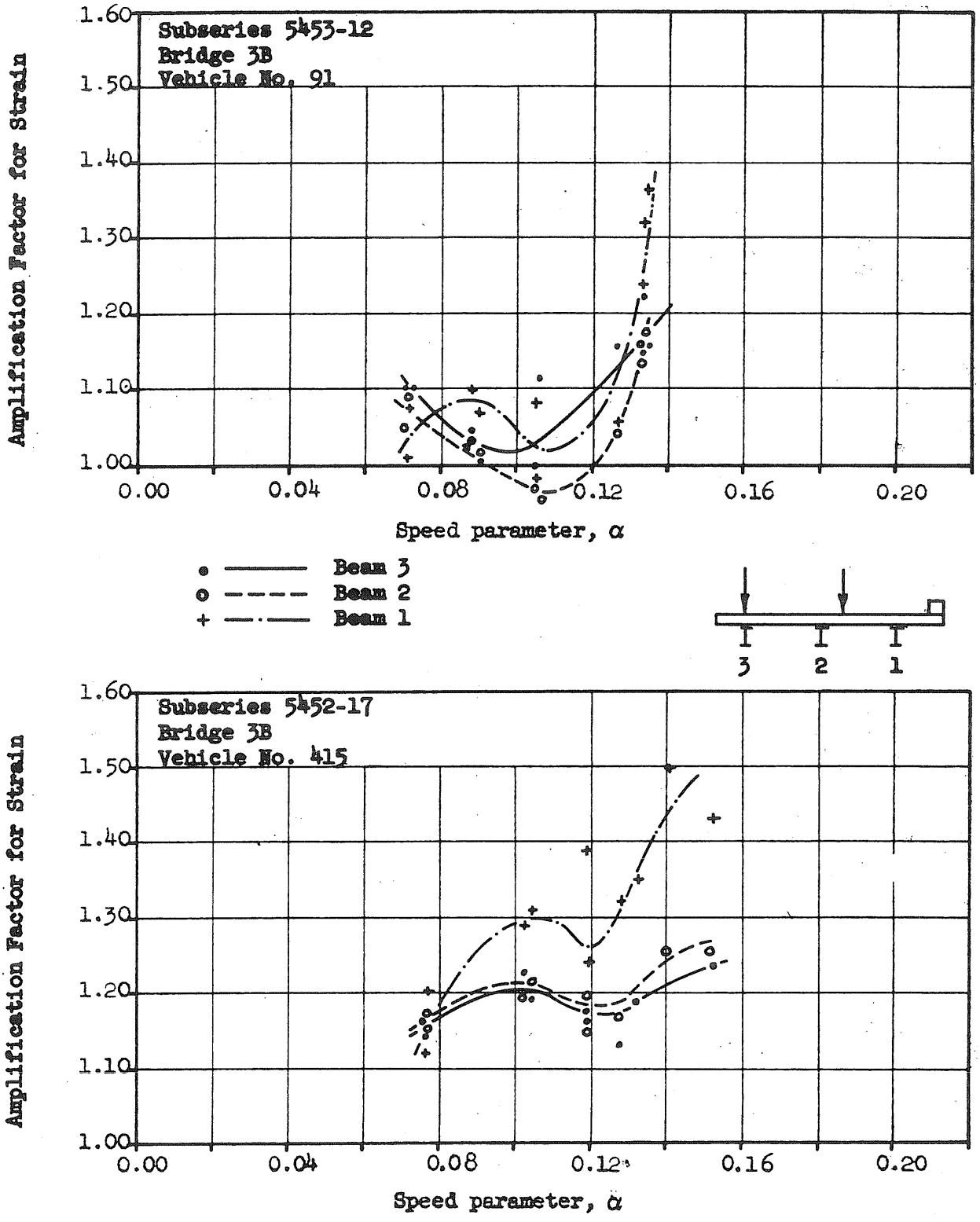

FIG. 62 SPECTRUM CURVES FOR THREE BEAMS-ECCENTRIC TESTS

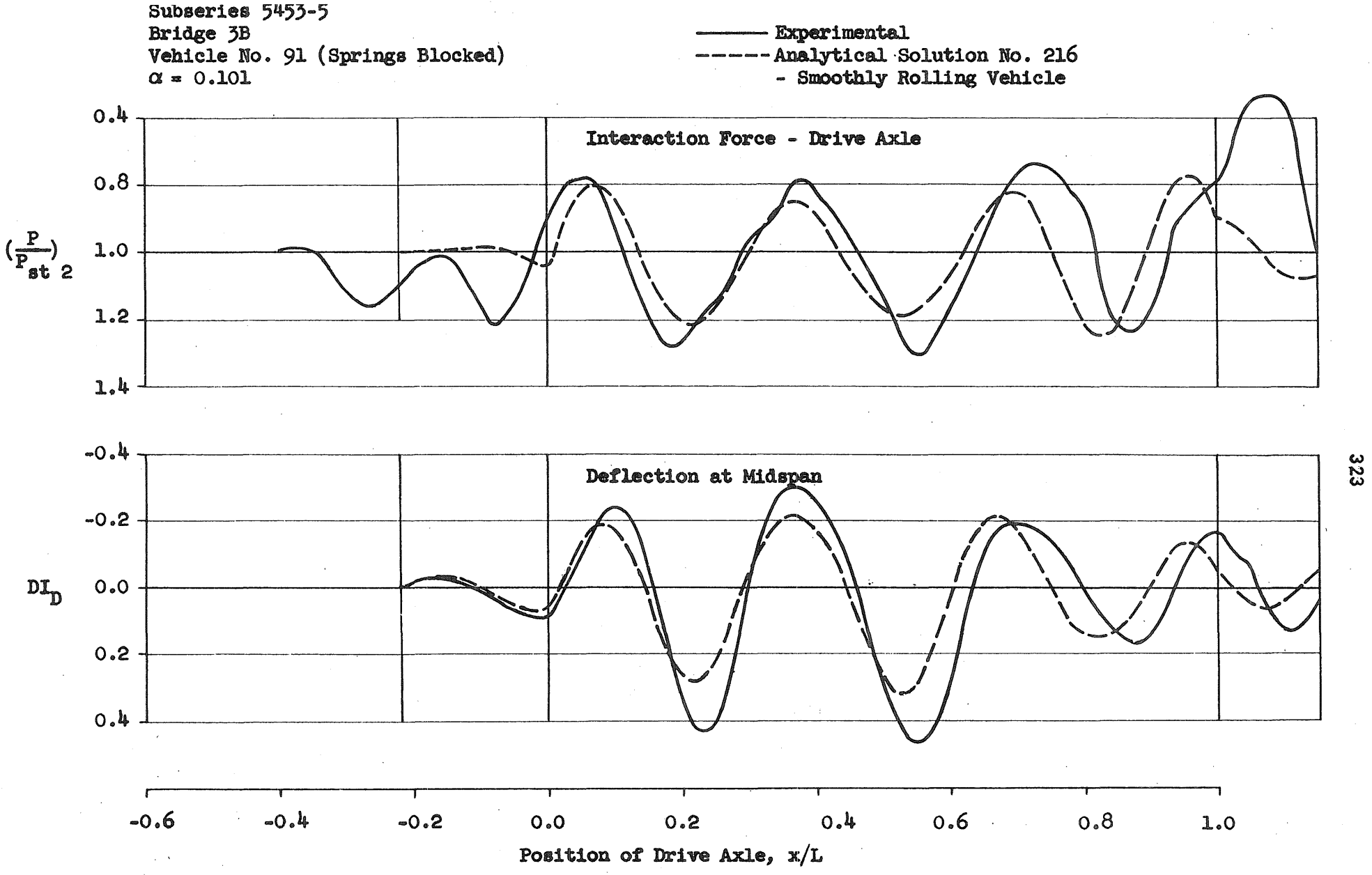

FIG. 63 COMPARISON OF HISTORY CURVES FOR TESTS WITH BLOCKED VEHICLE SPRINGS - Subseries 5453-5, $\alpha = 0.101$

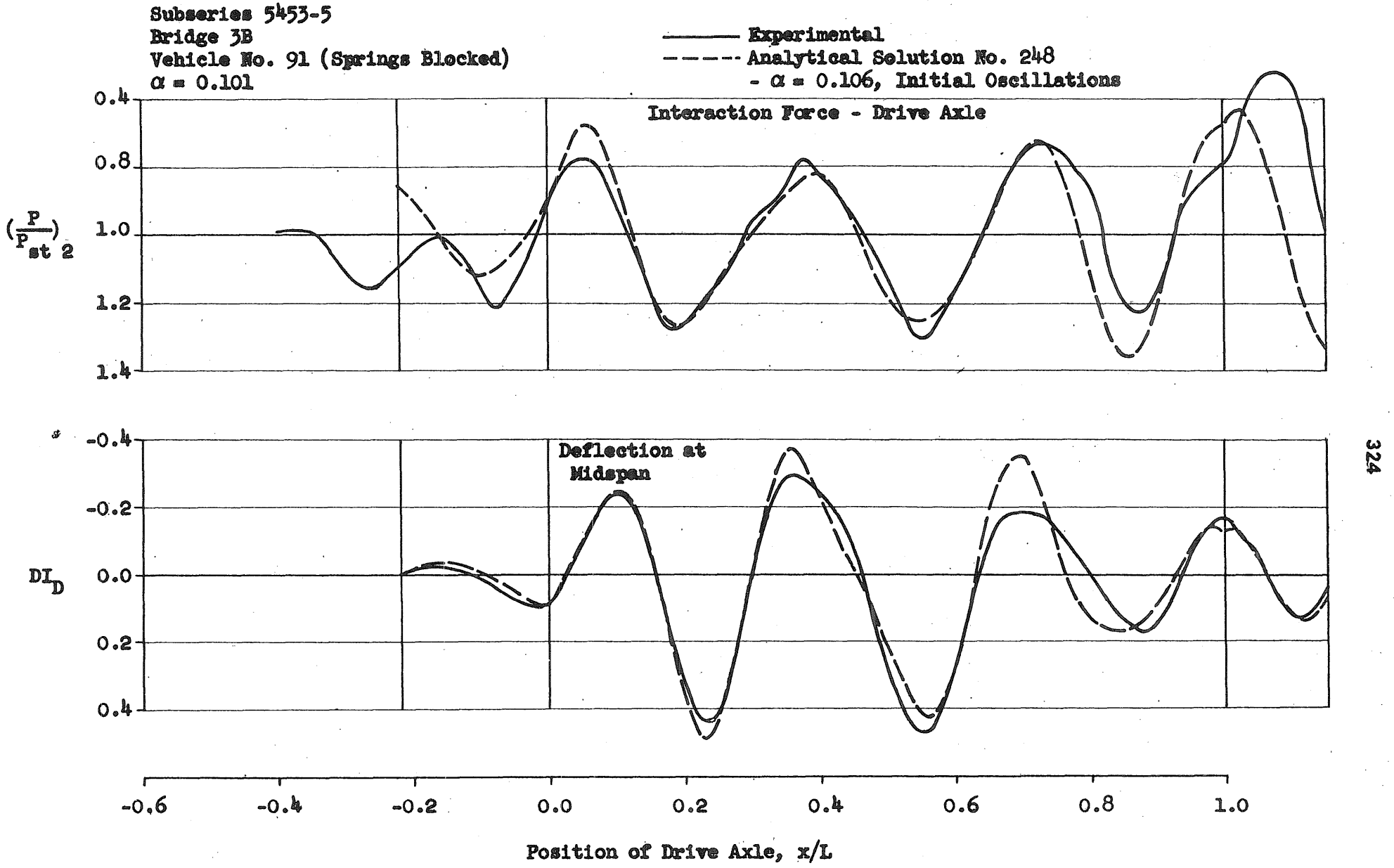

FIG. 64 COMPARISON OF HISTORY CURVES FOR TESTS WITH BLOCKED VEHICLE SPRINGS - Subseries 5453-5, α = 0.101, Second Trial

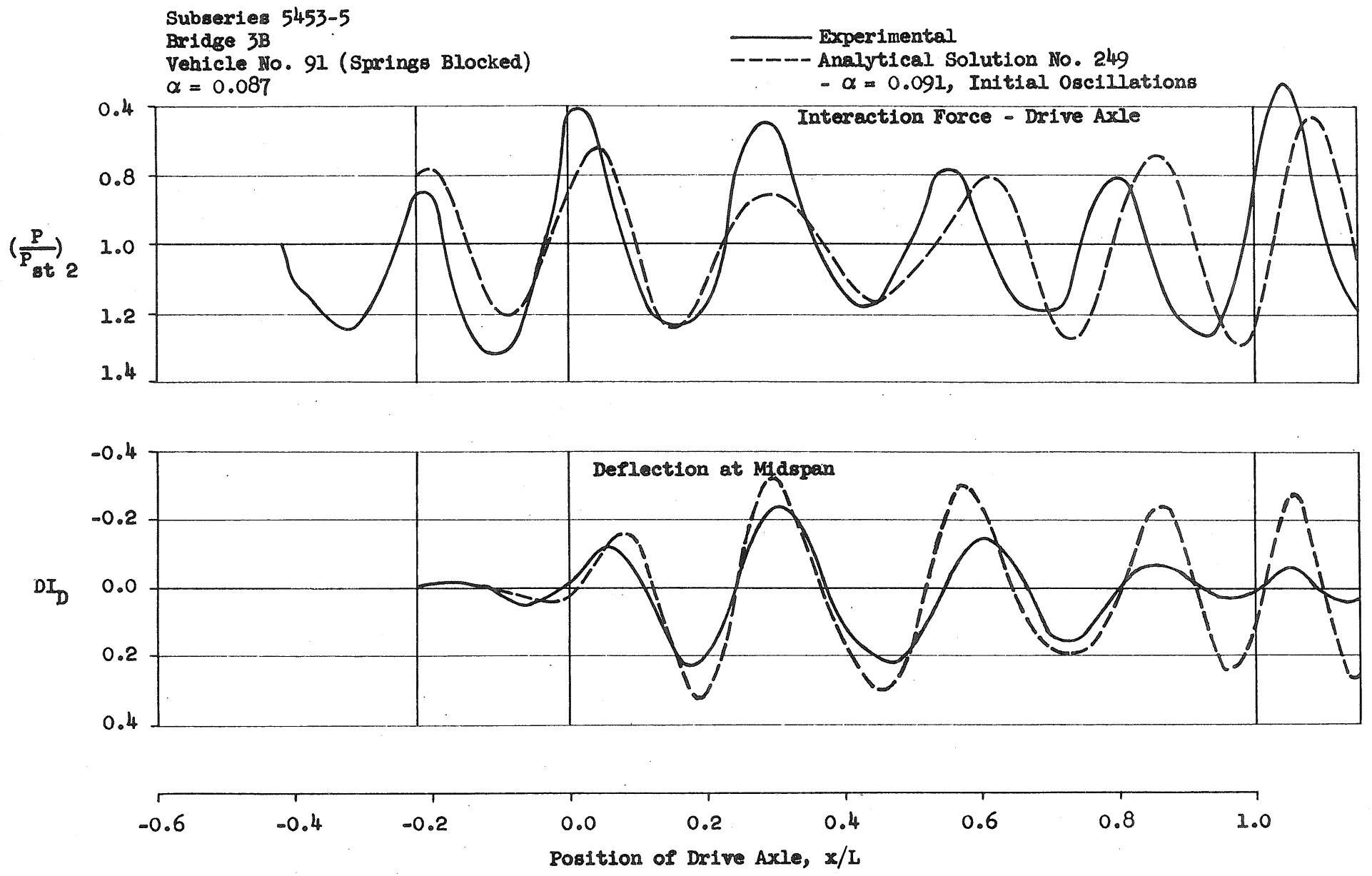

FIG. 65 COMPARISON OF HISTORY CURVES FOR TESTS WITH BLOCKED VEHICLE SPRINGS - Subseries 5453-5, $\alpha = 0.087$

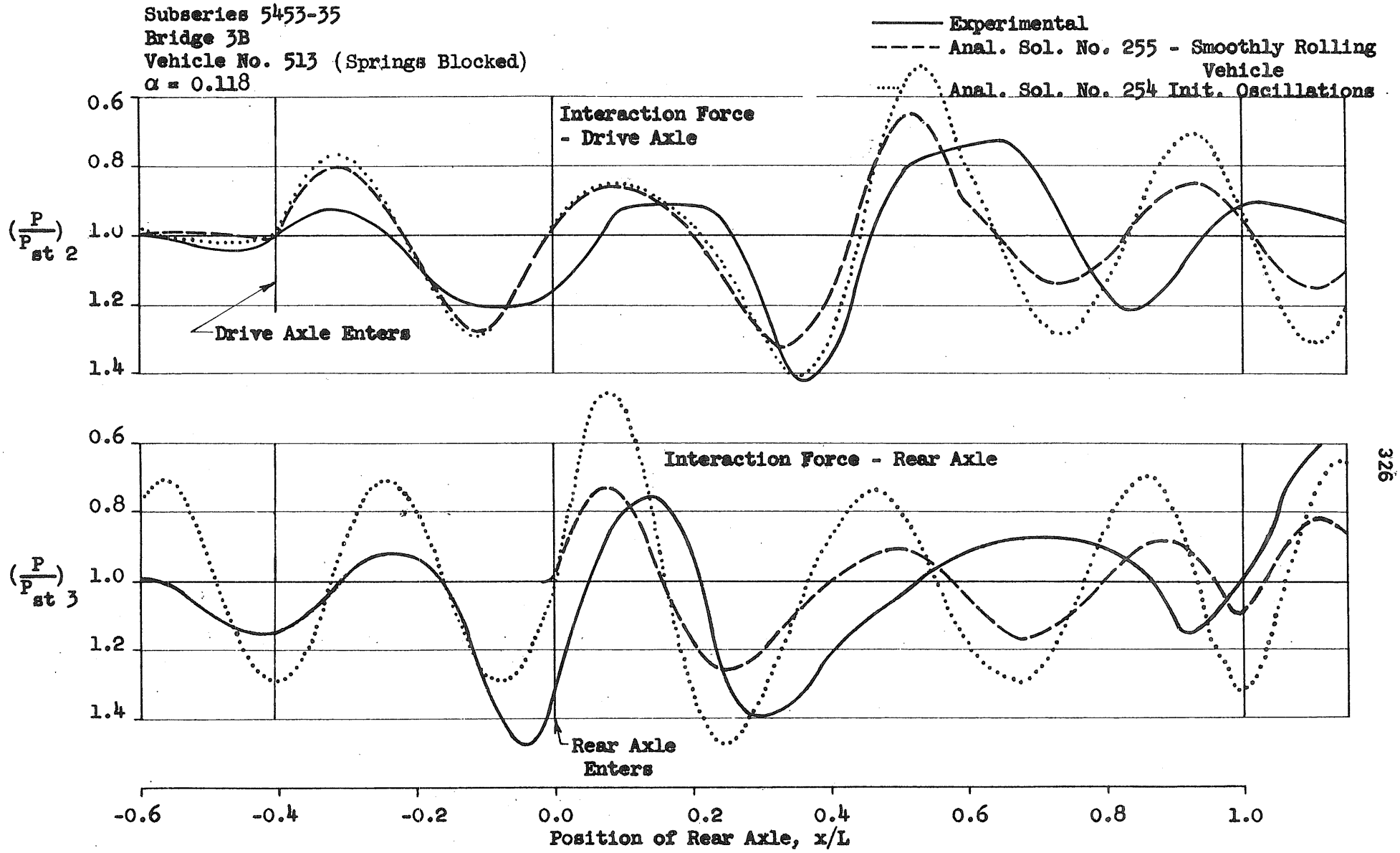

FIG. 66a COMPARISON OF HISTORY CURVES FOR TESTS WITH BLOCKED VEHICLE SPRINGS - Subseries 5453-35, α = 0.118

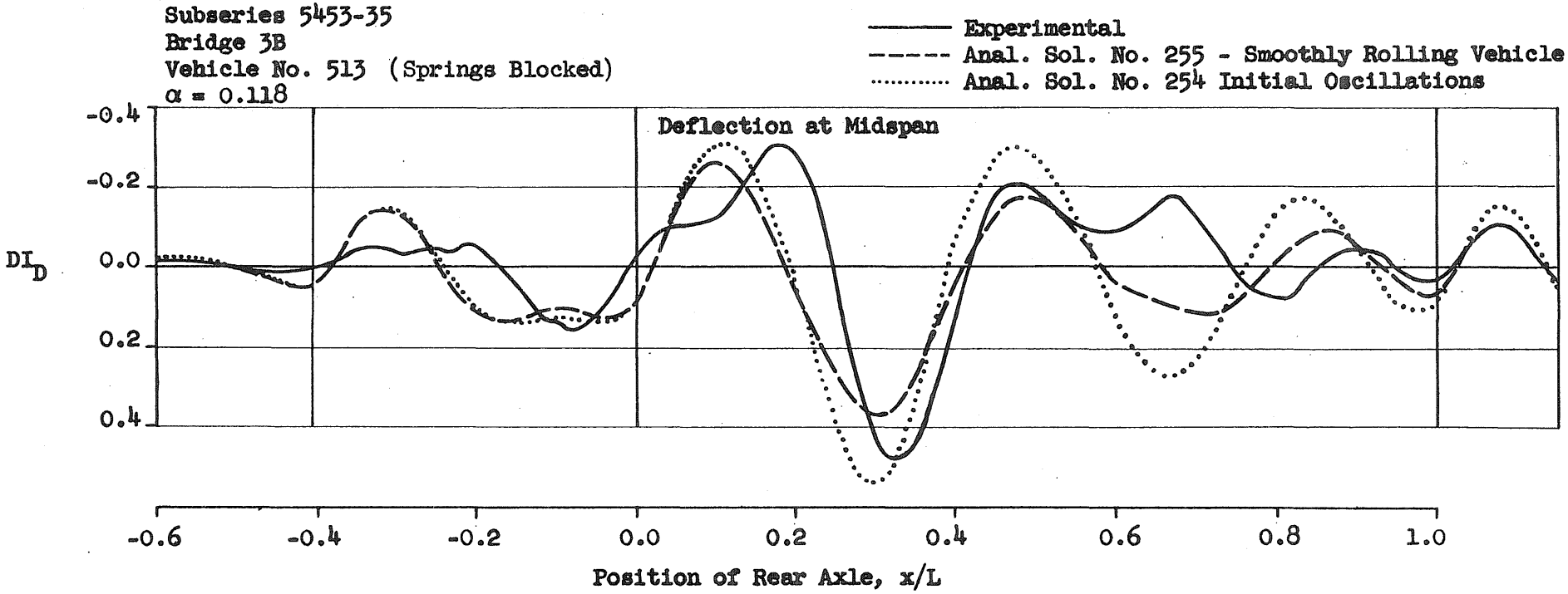

FIG. 66b COMPARISON OF HISTORY CURVES FOR TESTS WITH BLOCKED VEHICLE SPRINGS - Subseries 5453-35, $\alpha = 0.118$

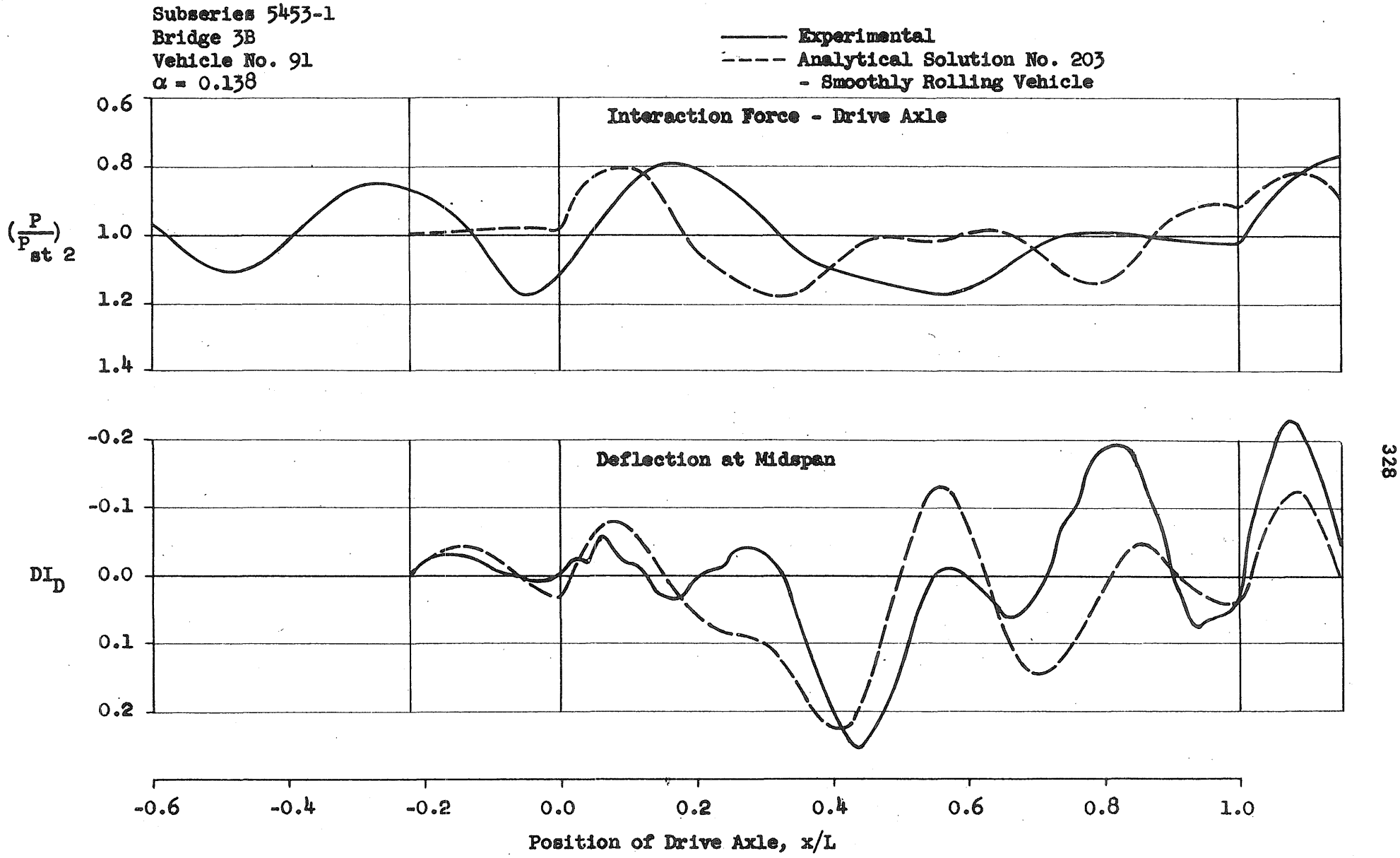

FIG. 67 COMPARISON OF HISTORY CURVES - Subseries 5453-1, $\alpha = 0.138$

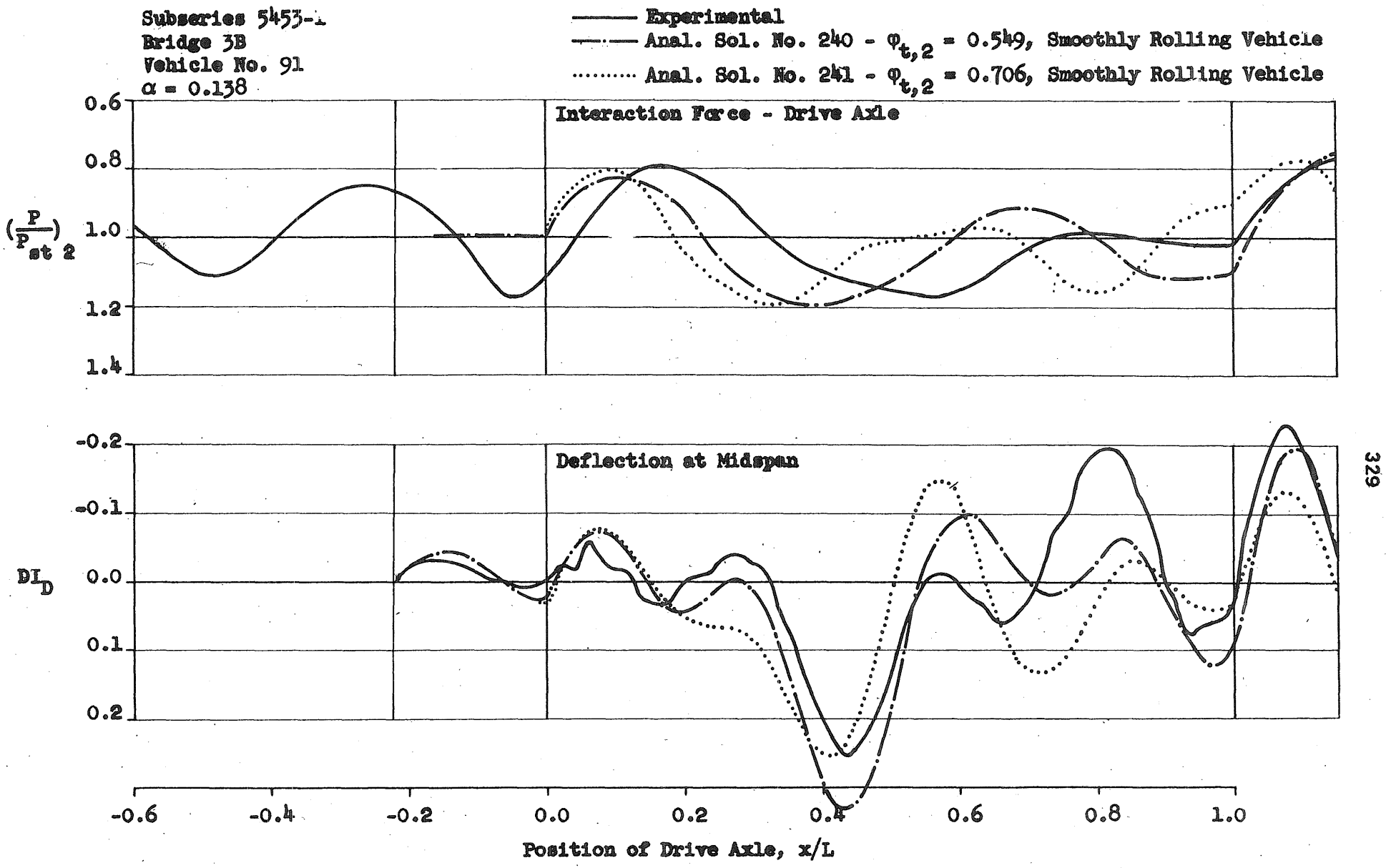

FIG. 68 COMPARISON OF HISTORY CURVES - Effect of Reduced Axle Frequency

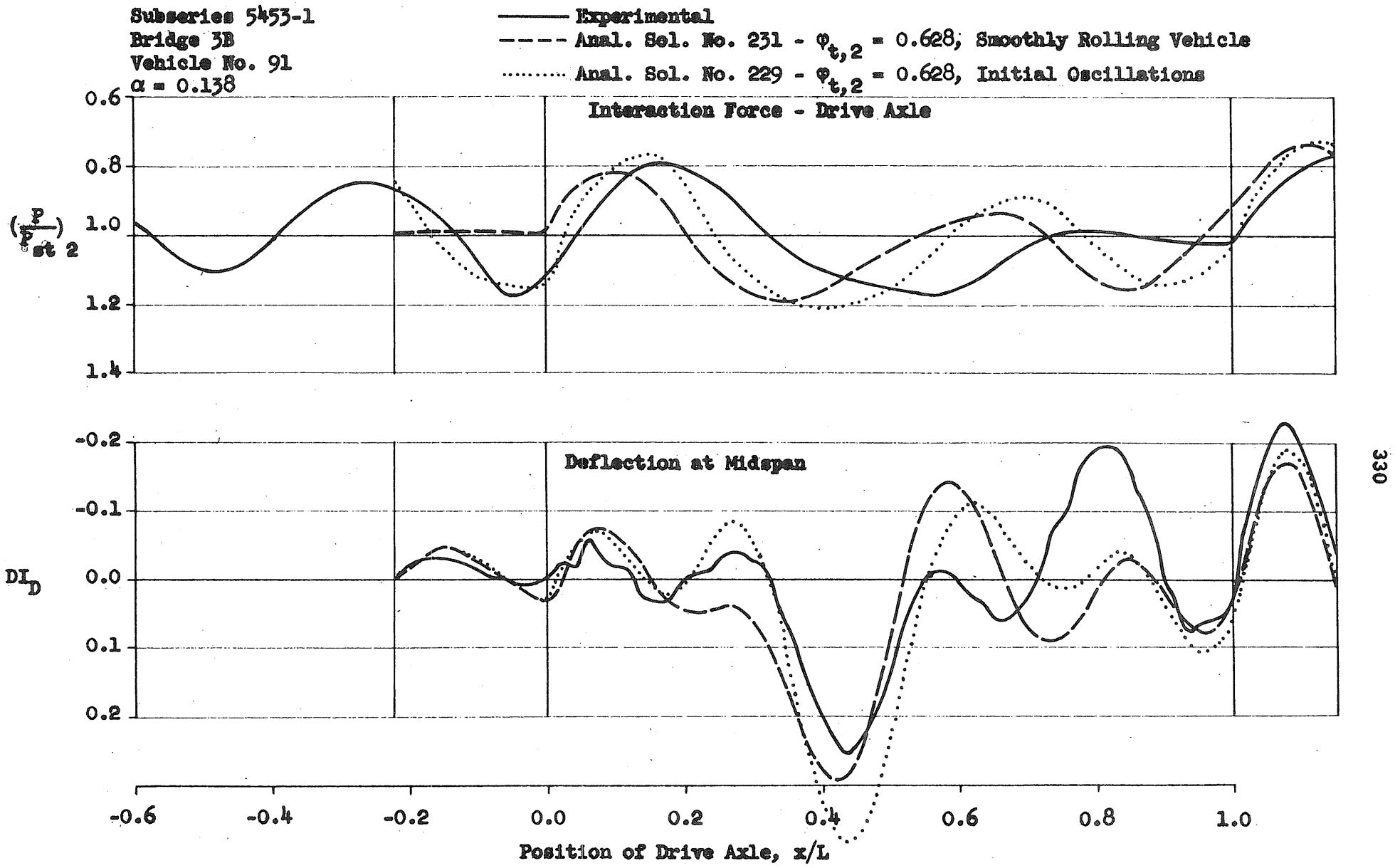

FIG. 69 COMPARISON OF HISTORY CURVES - Effect of Initial Oscillations

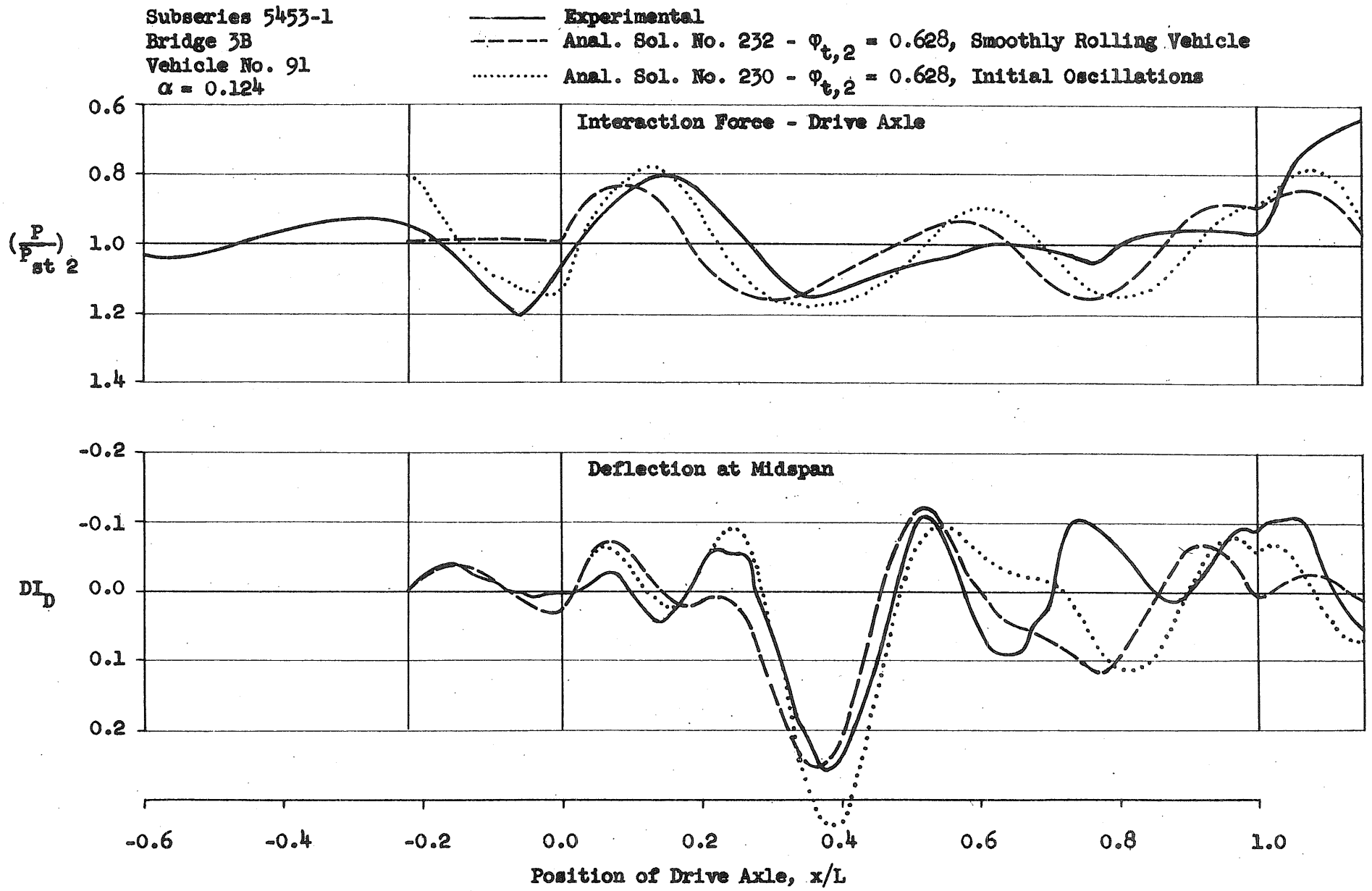

FIG. 70 COMPARISON OF HISTORY CURVES - Subseries 5453-1, $\alpha = 0.124$

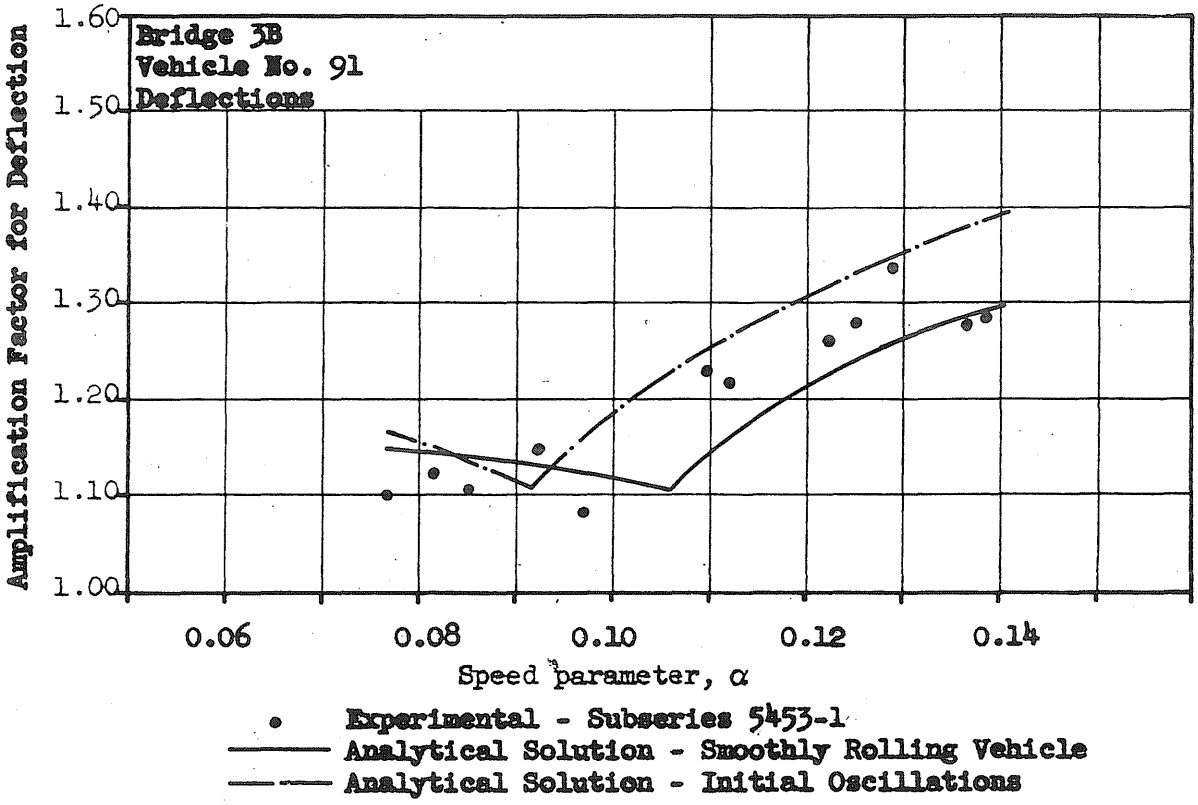

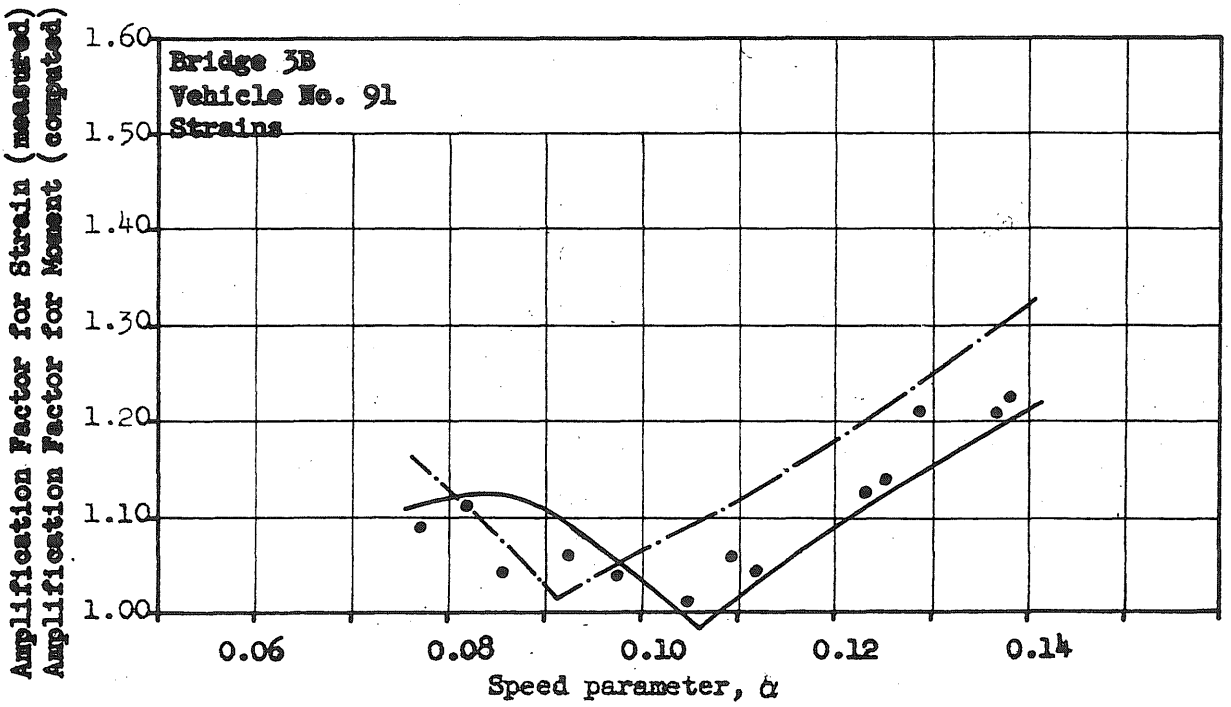

FIG. 71 COMPARISON OF SPECTRUM CURVES - Subseries 5453-1

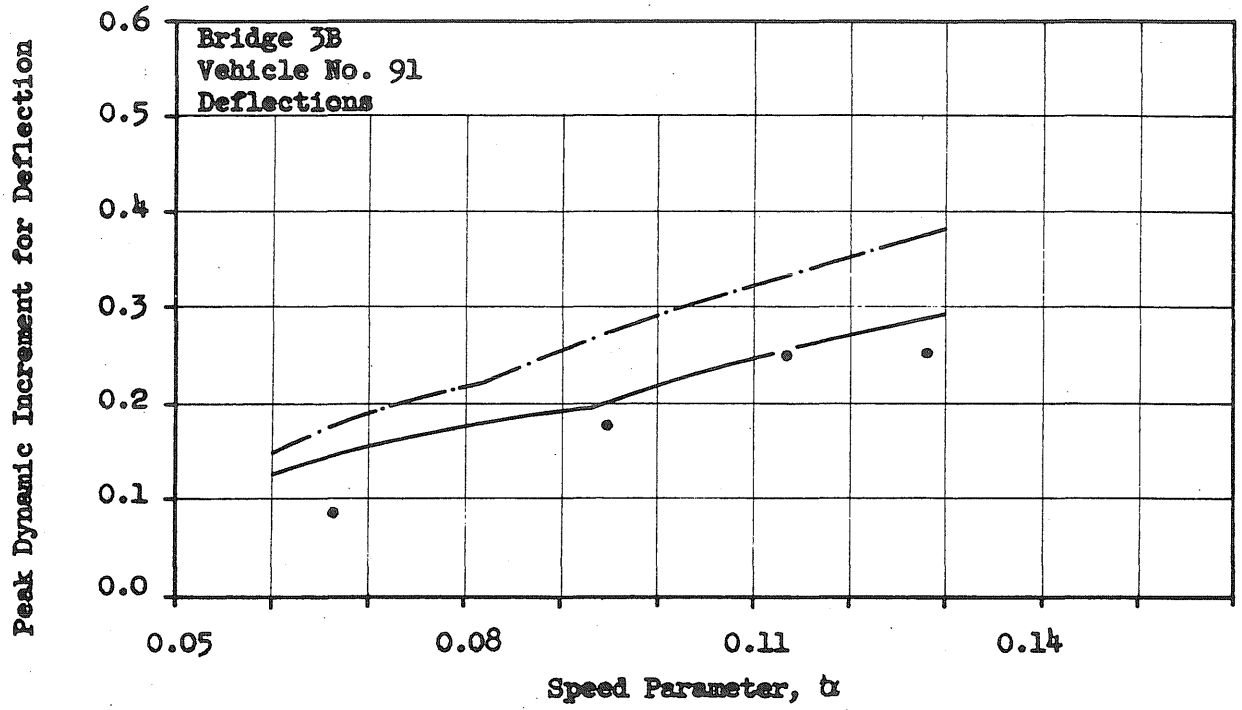

FIG. 72 COMPARISON OF PEAK DYNAMIC INCREMENTS - Subseries 5453-1

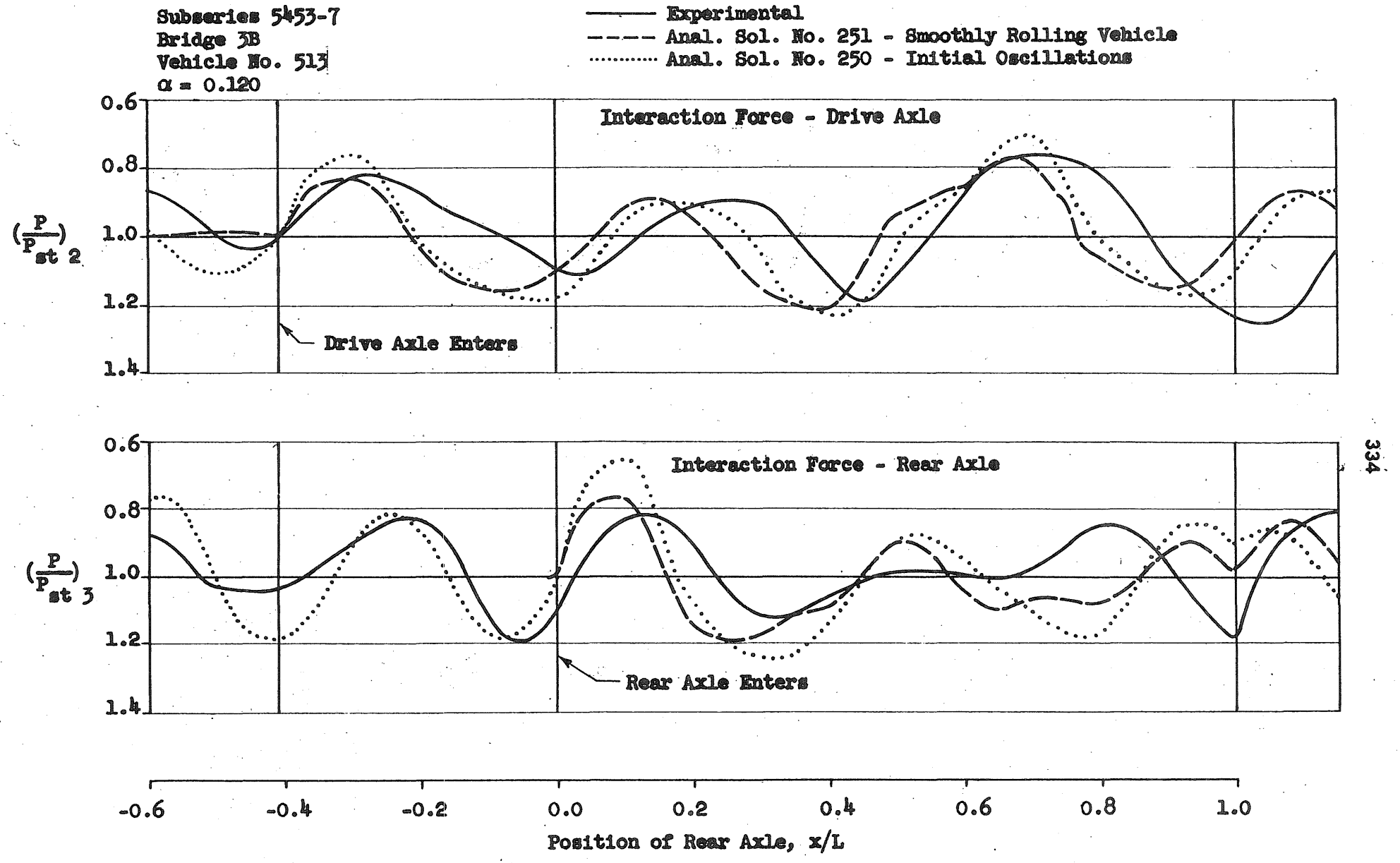

FIG. 73a COMPARISON OF HISTORY CURVES - Subseries 5453, α = 0.120

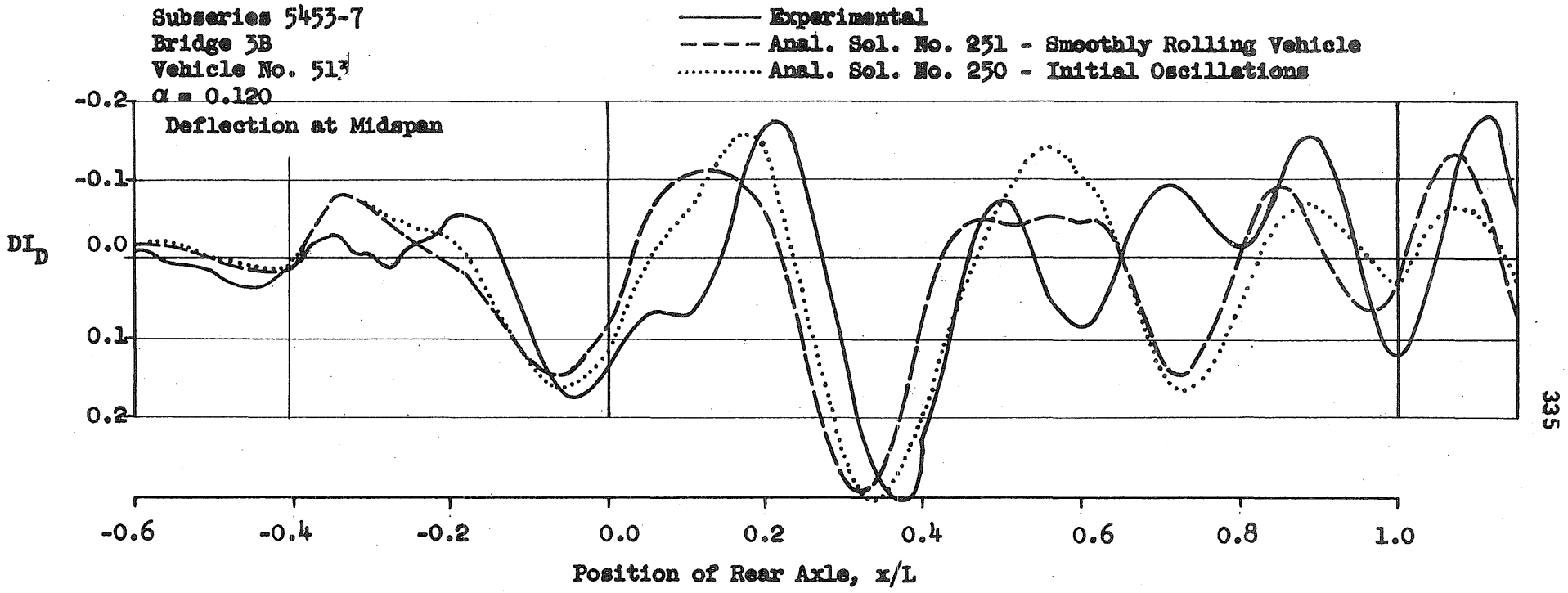

FIG. 73b COMPARISON OF HISTORY CURVES - Subseries 5453, $\alpha = 0.120$

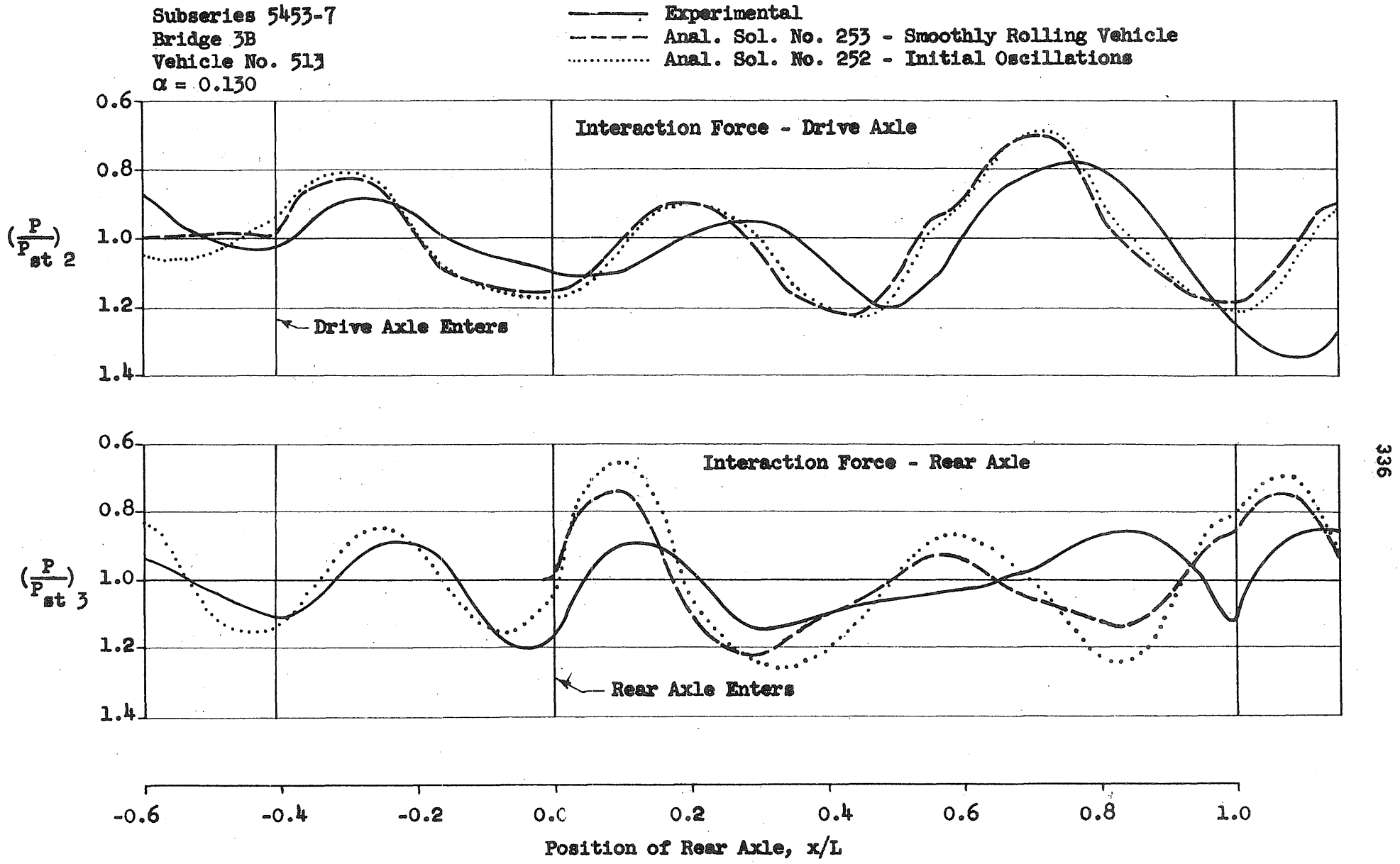

FIG. 74a COMPARISON OF HISTORY CURVES - Subseries 5453-7, α = 0.130

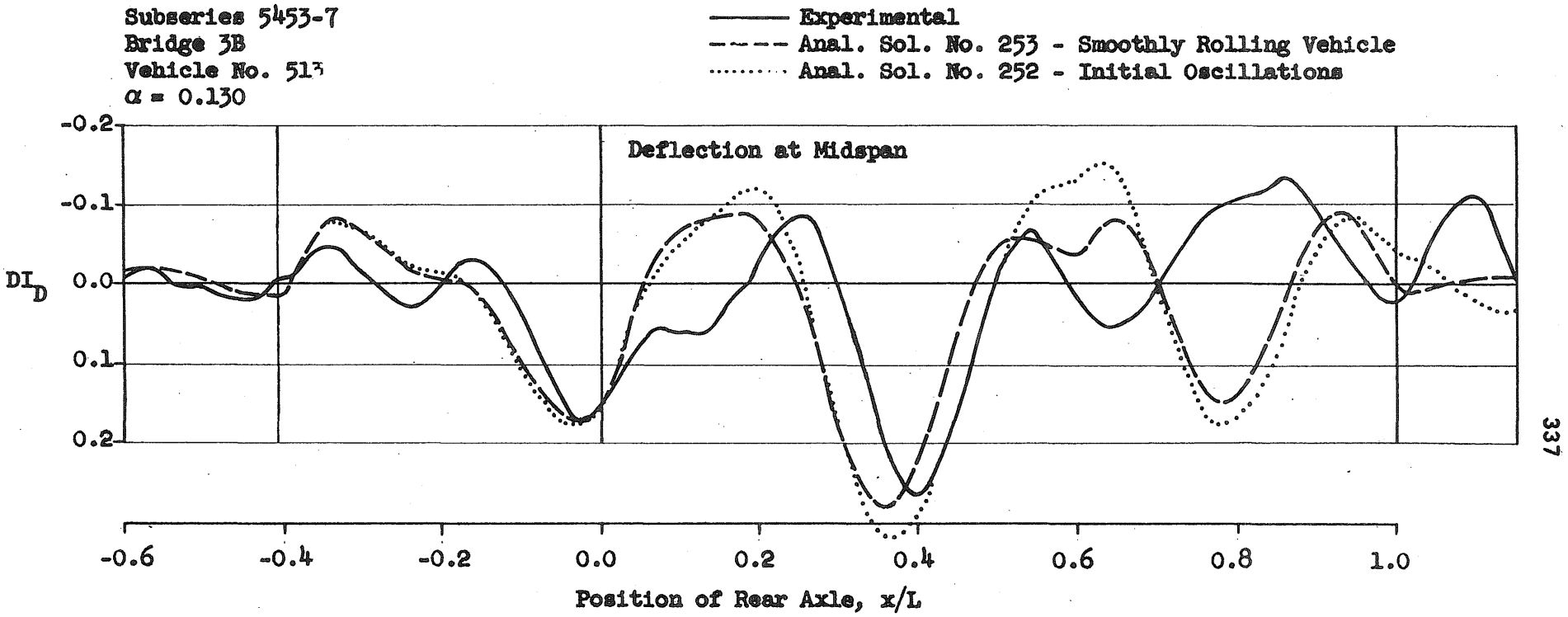

FIG. 74b COMPARISON OF HISTORY CURVES - Subseries 5453-7, $\alpha = 0.130$

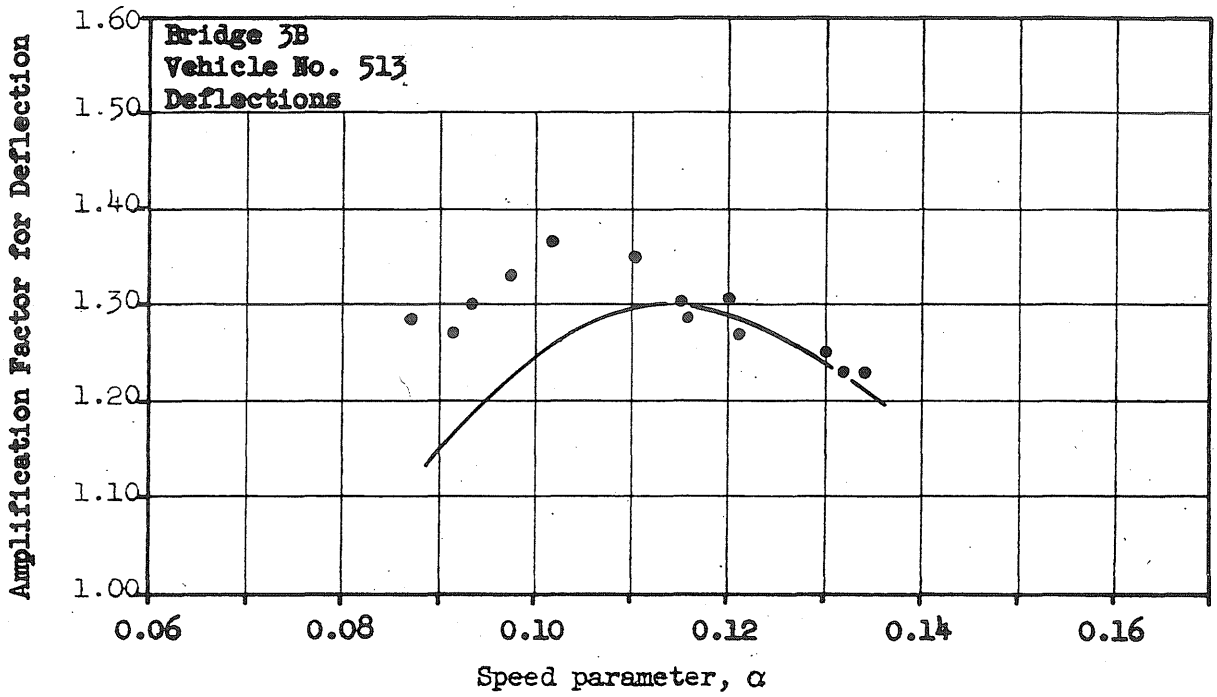

Experimental - Subseries 5453-7

Analytical Solution - Smoothly Rolling Vehicle

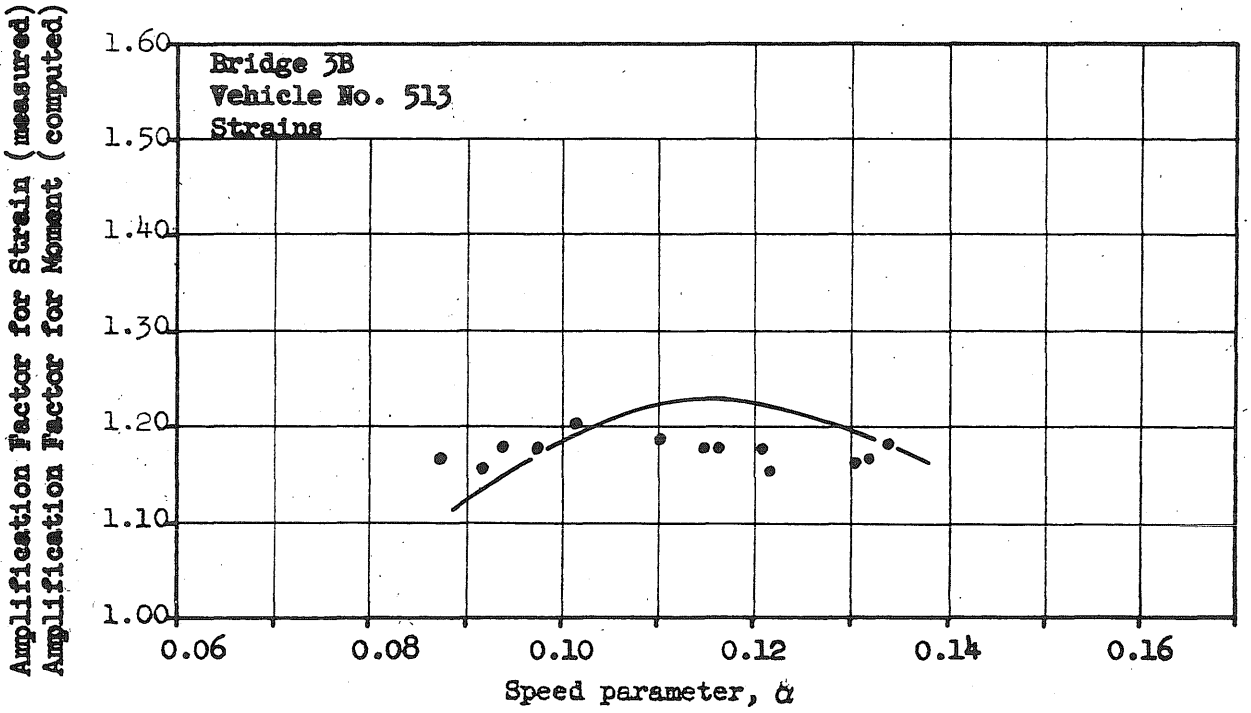

FIG. 75 COMPARISON OF SPECTRUM CURVES - Subseries 5453-7

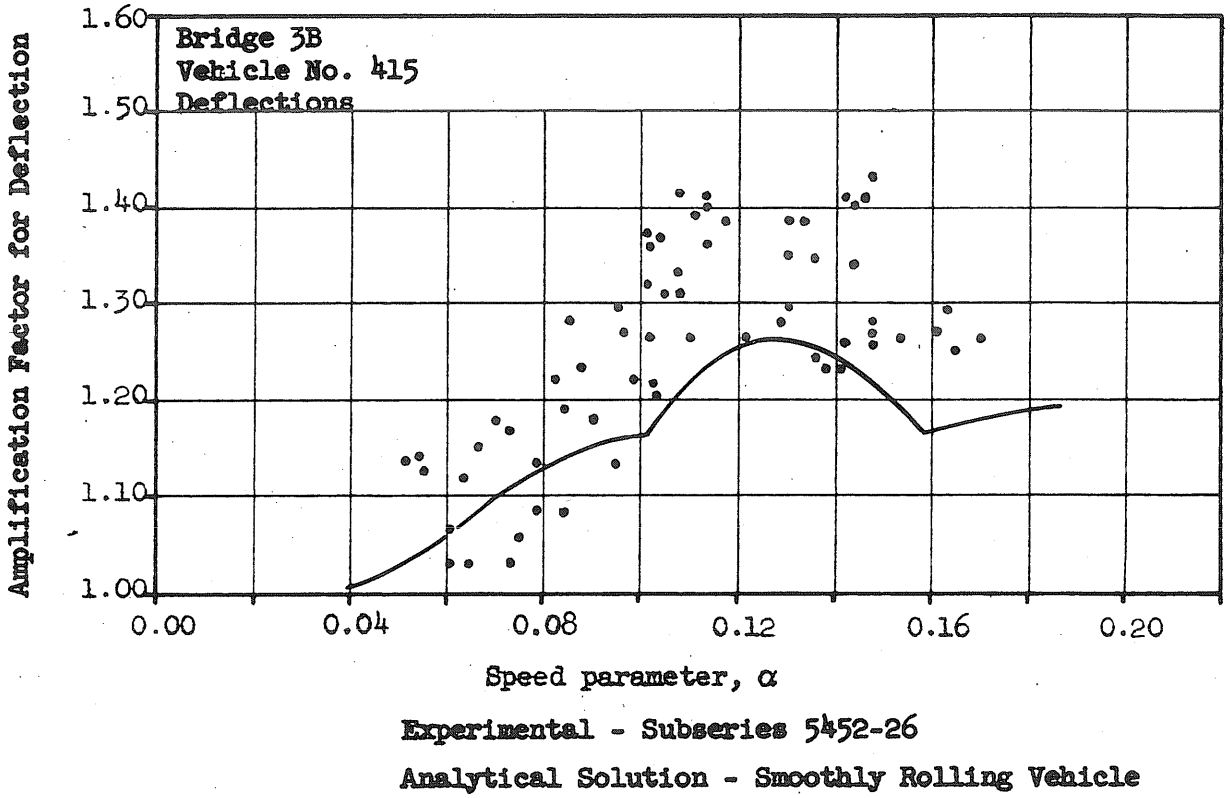

Experimental - Subseries 5452-26

Analytical Solution - Smoothly Rolling Vehicle

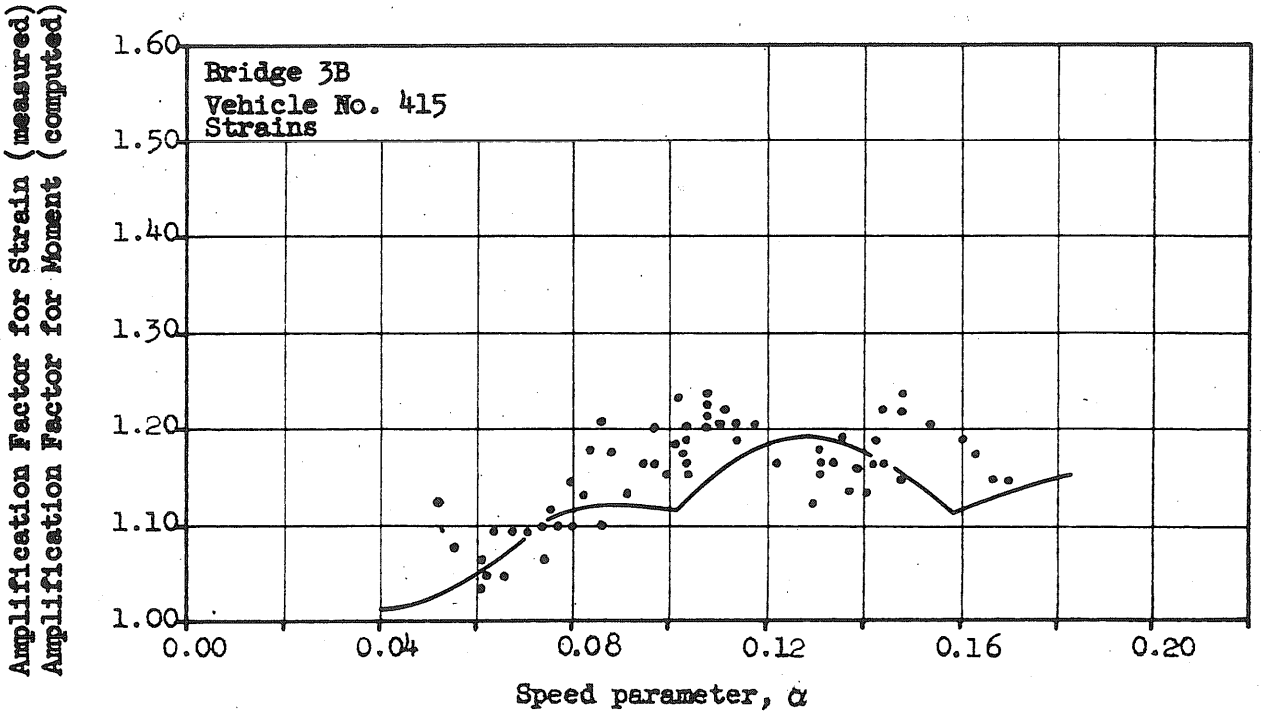

FIG. 76 COMPARISON OF SPECTRUM CURVES - Subseries 5452-26

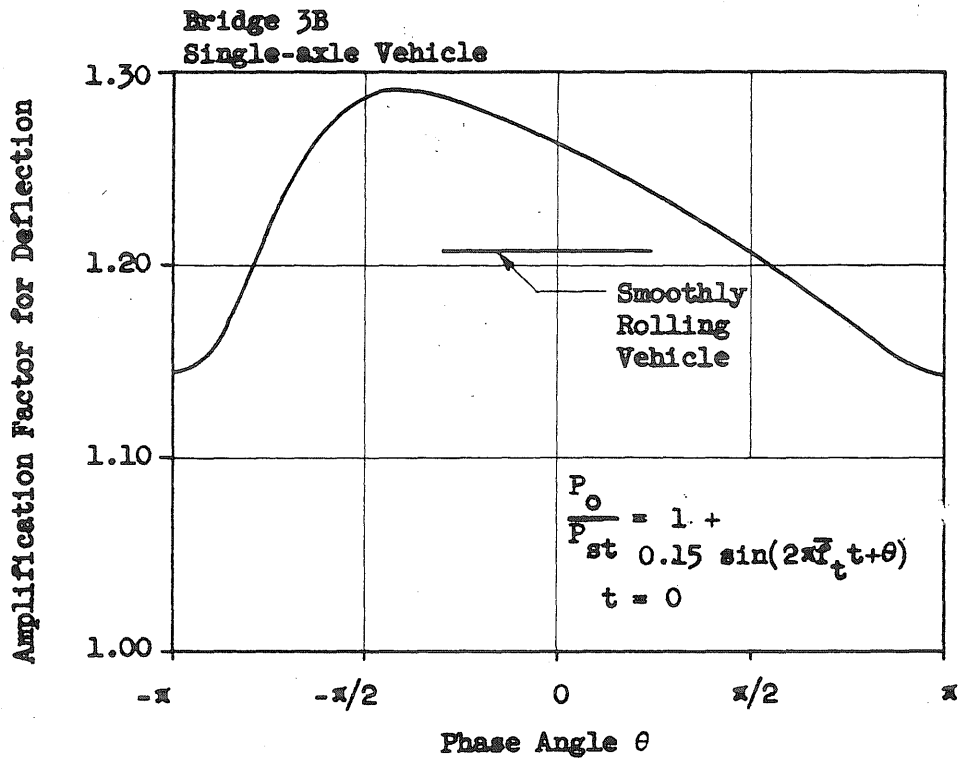

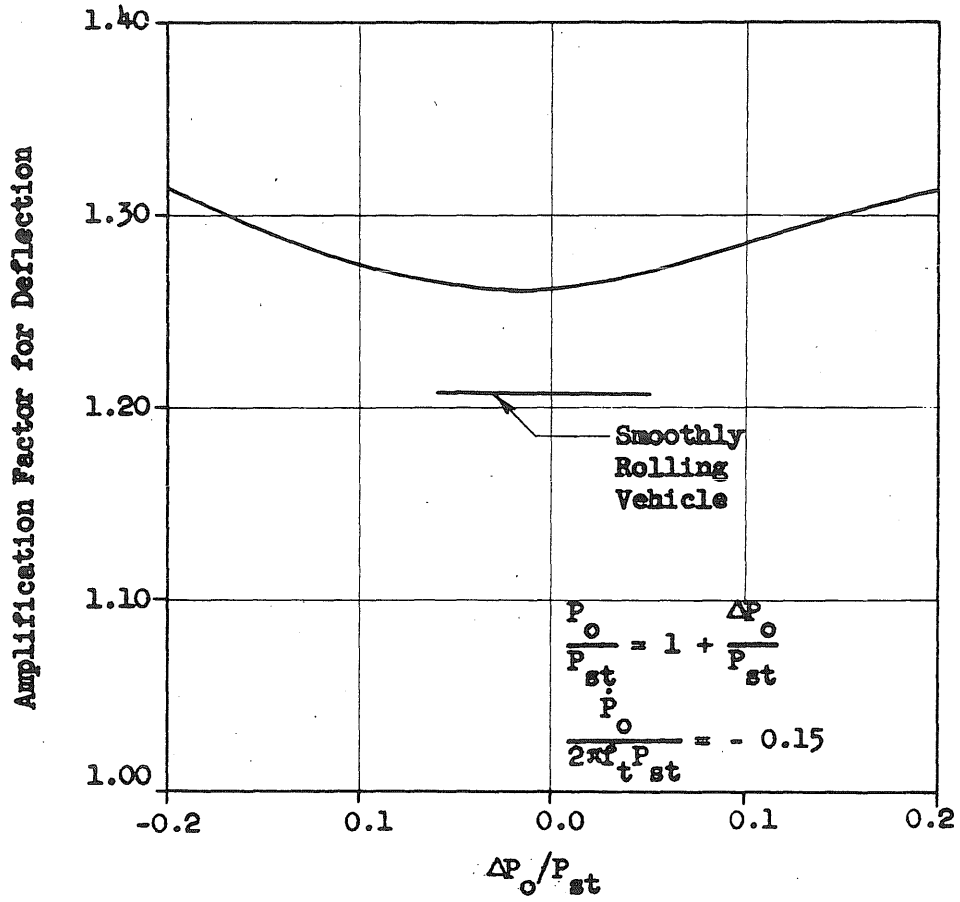

FIG. 77 EFFECT OF UNCERTAINTIES IN INITIAL CONDITIONS OF VEHICLE

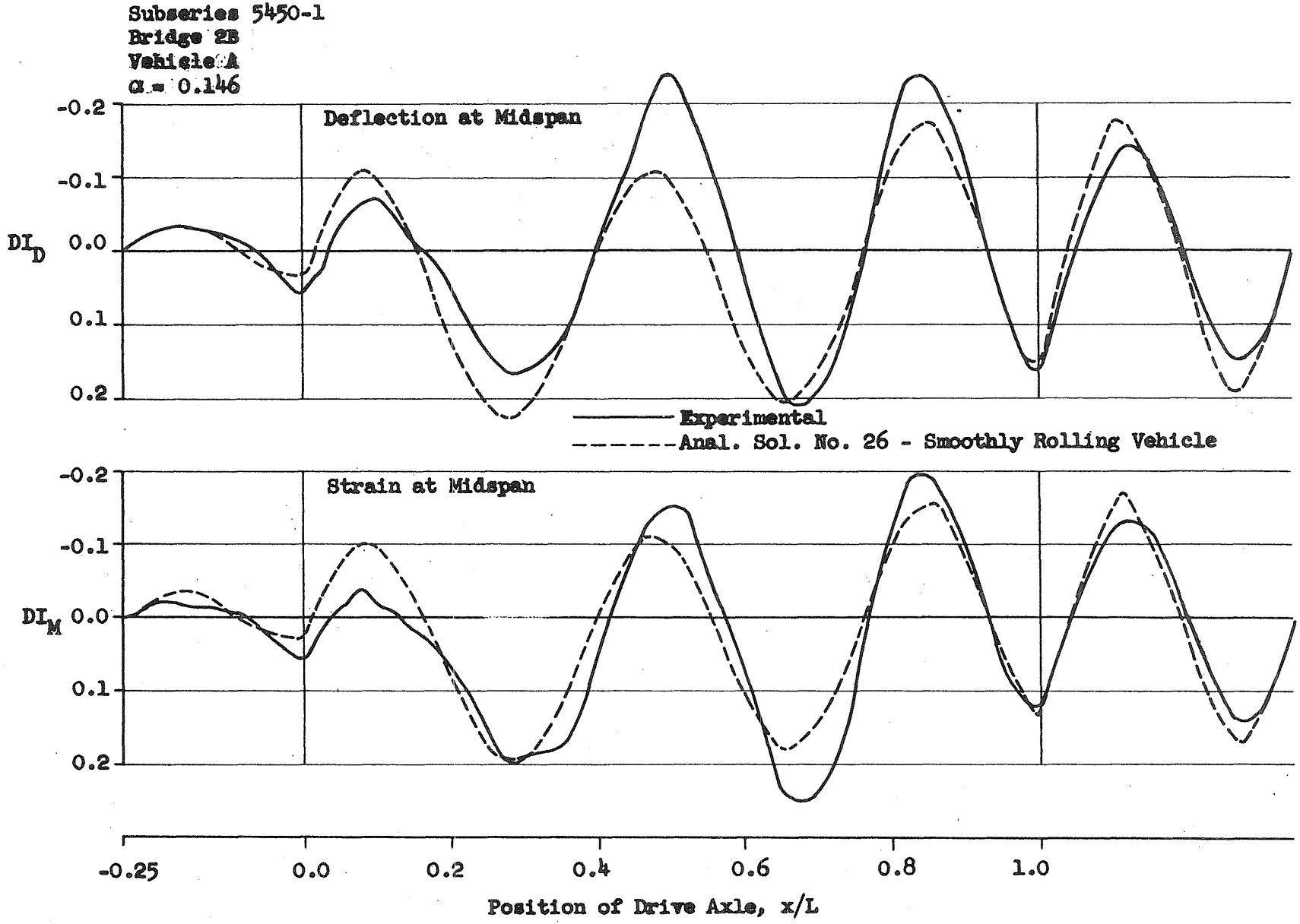

FIG. 78 COMPARISON OF HISTORY CURVES - Subseries 5450-1, $\alpha = 0.146$

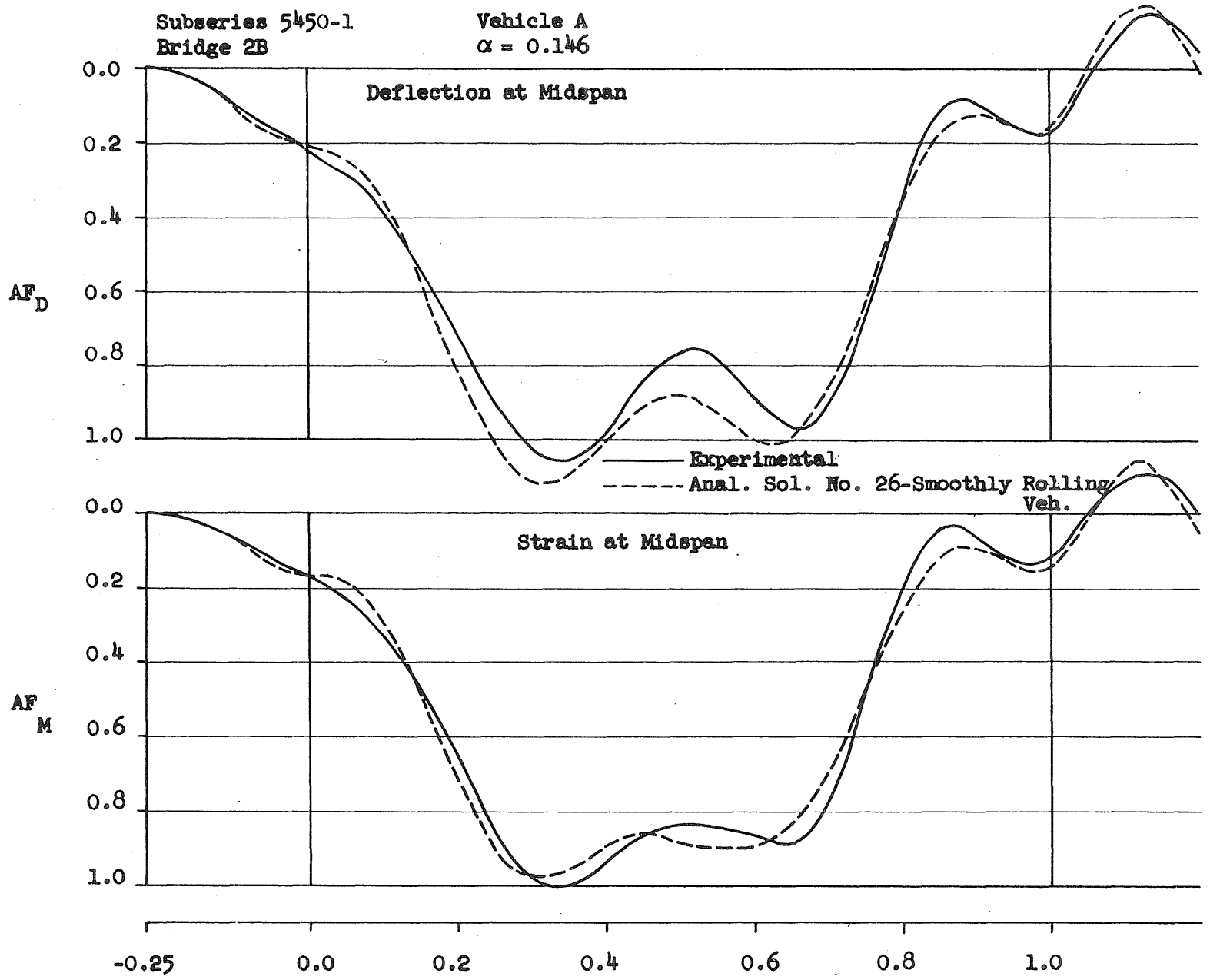

FIG. 79 COMPARISON OF TOTAL EFFECTS - Subseries 5450-1, $\alpha = 0.146$

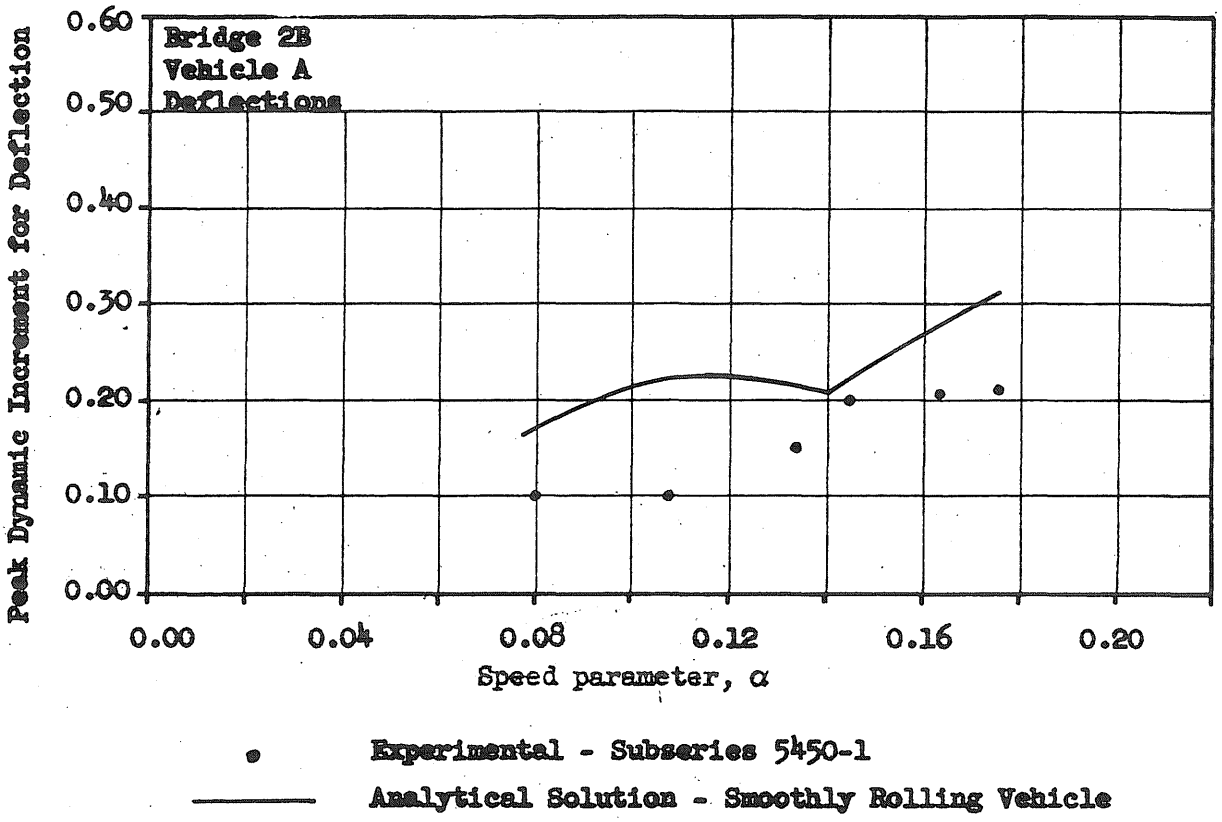

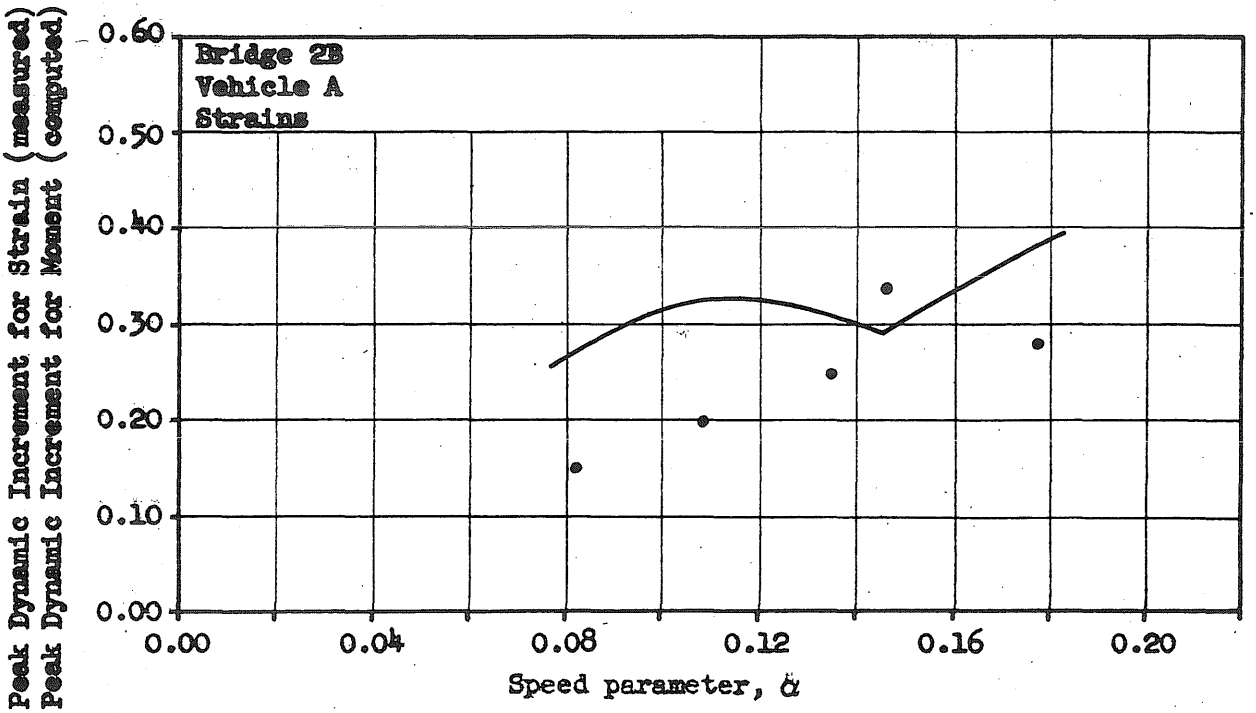

FIG. 80 COMPARISON OF PEAK DYNAMIC INCREMENTS - Subseries 5450-1

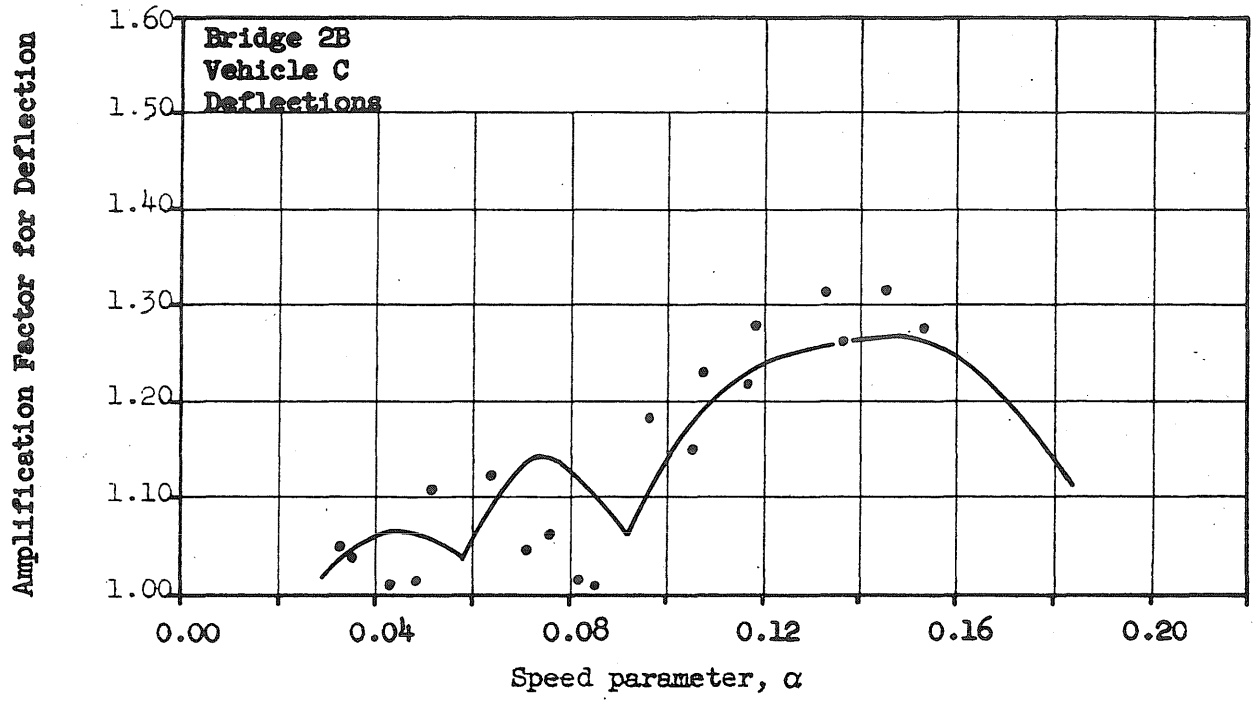

• Experimental - Subseries 5450-2

——— Analytical Solution - Smoothly Rolling Vehicle

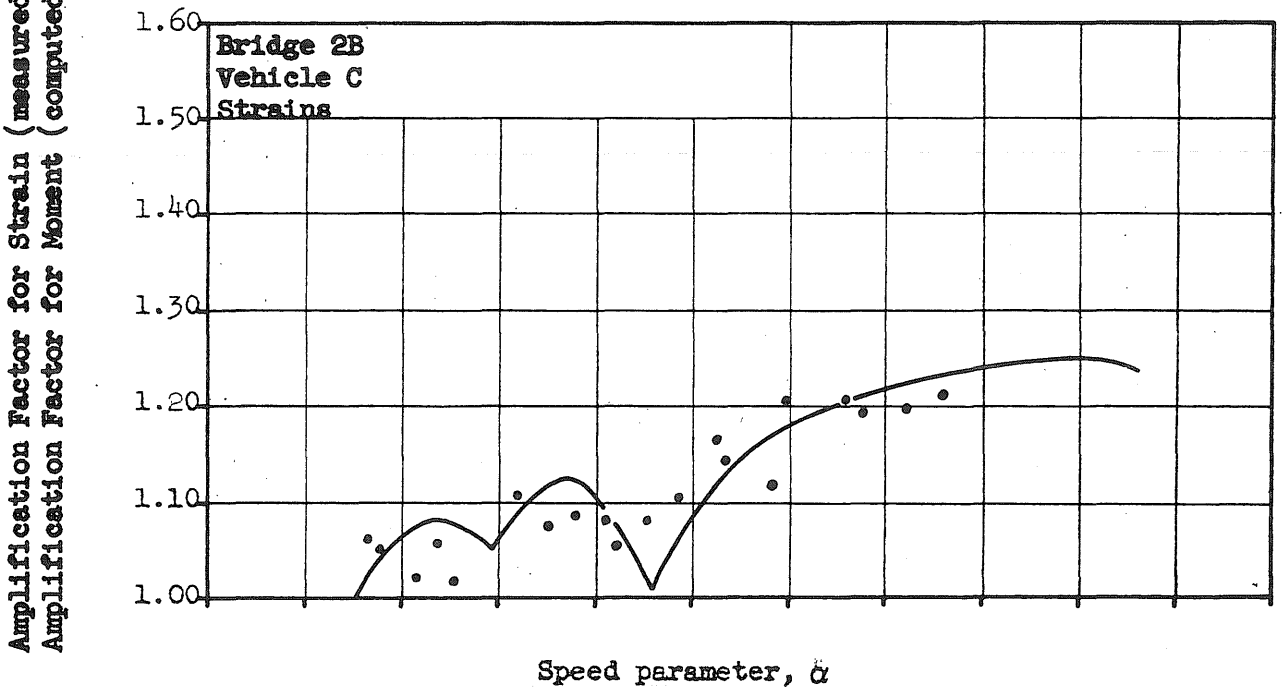

FIG. 81 COMPARISON OF SPECTRUM CURVES - Subseries 5450-2

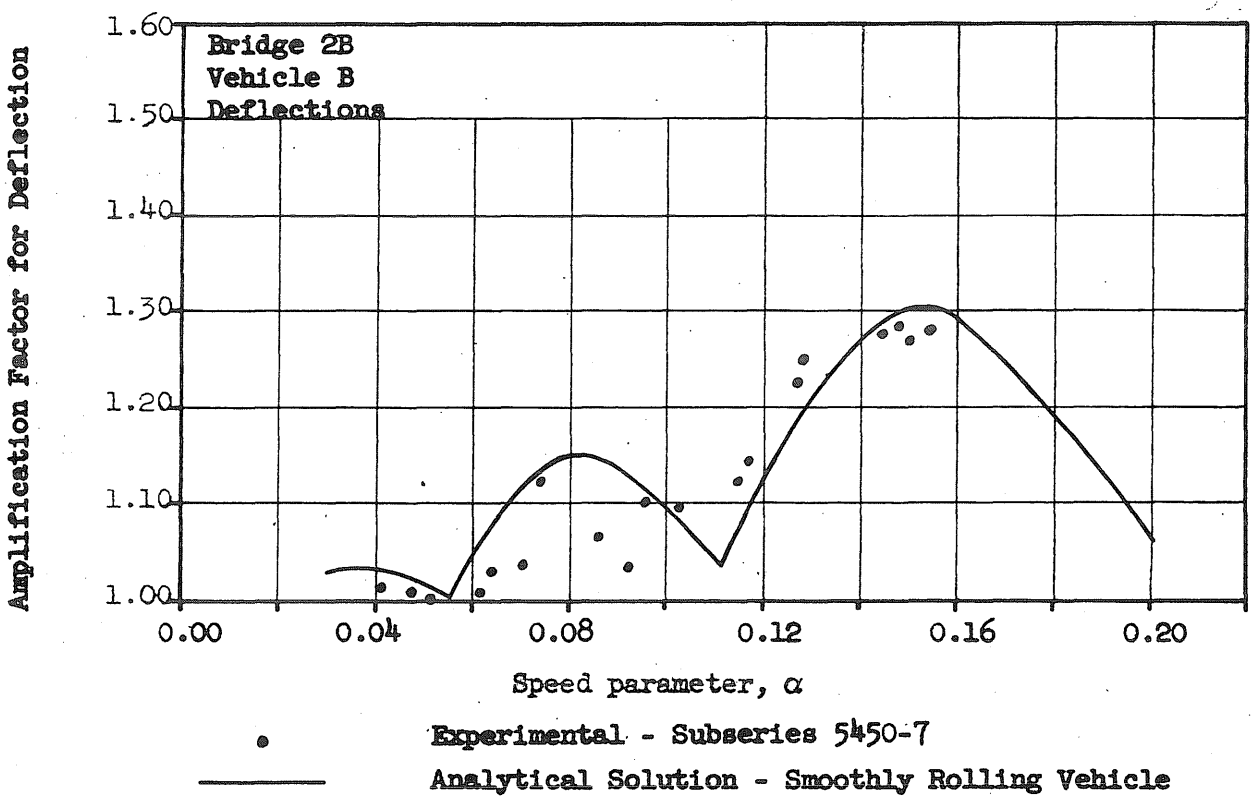

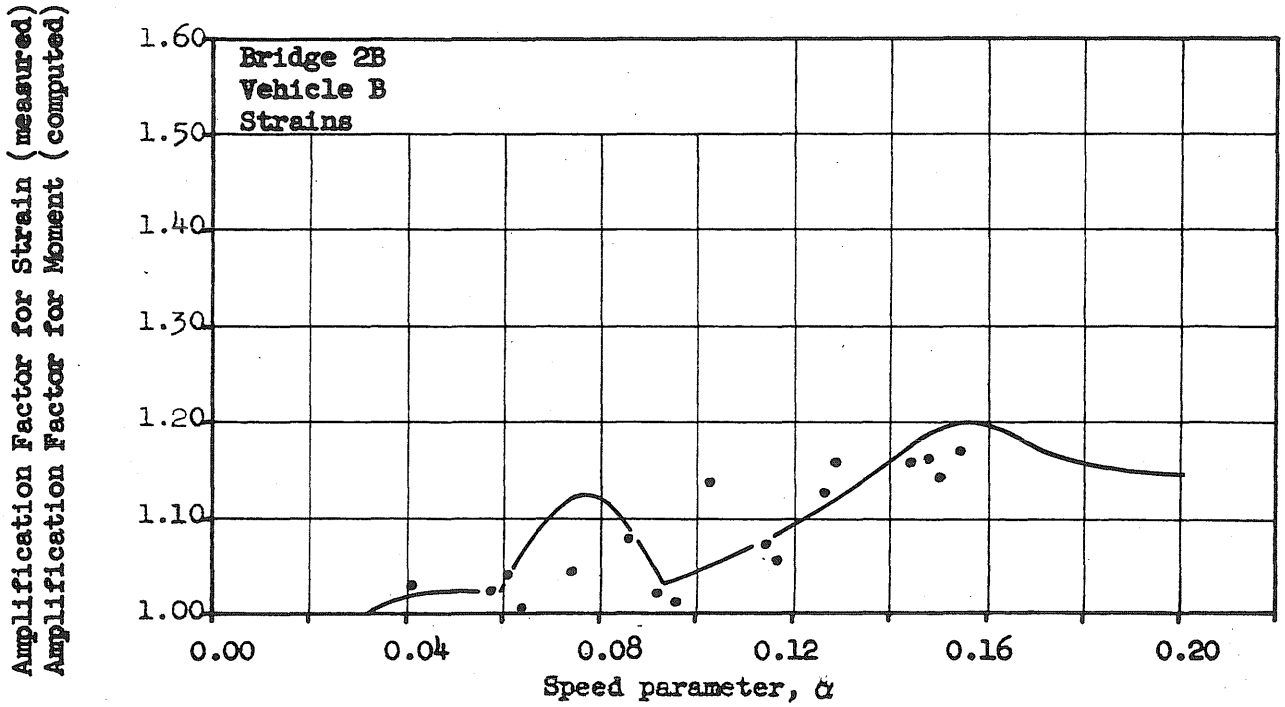

FIG. 82 COMPARISON OF SPECTRUM CURVES - SUBSERIES 5450-7

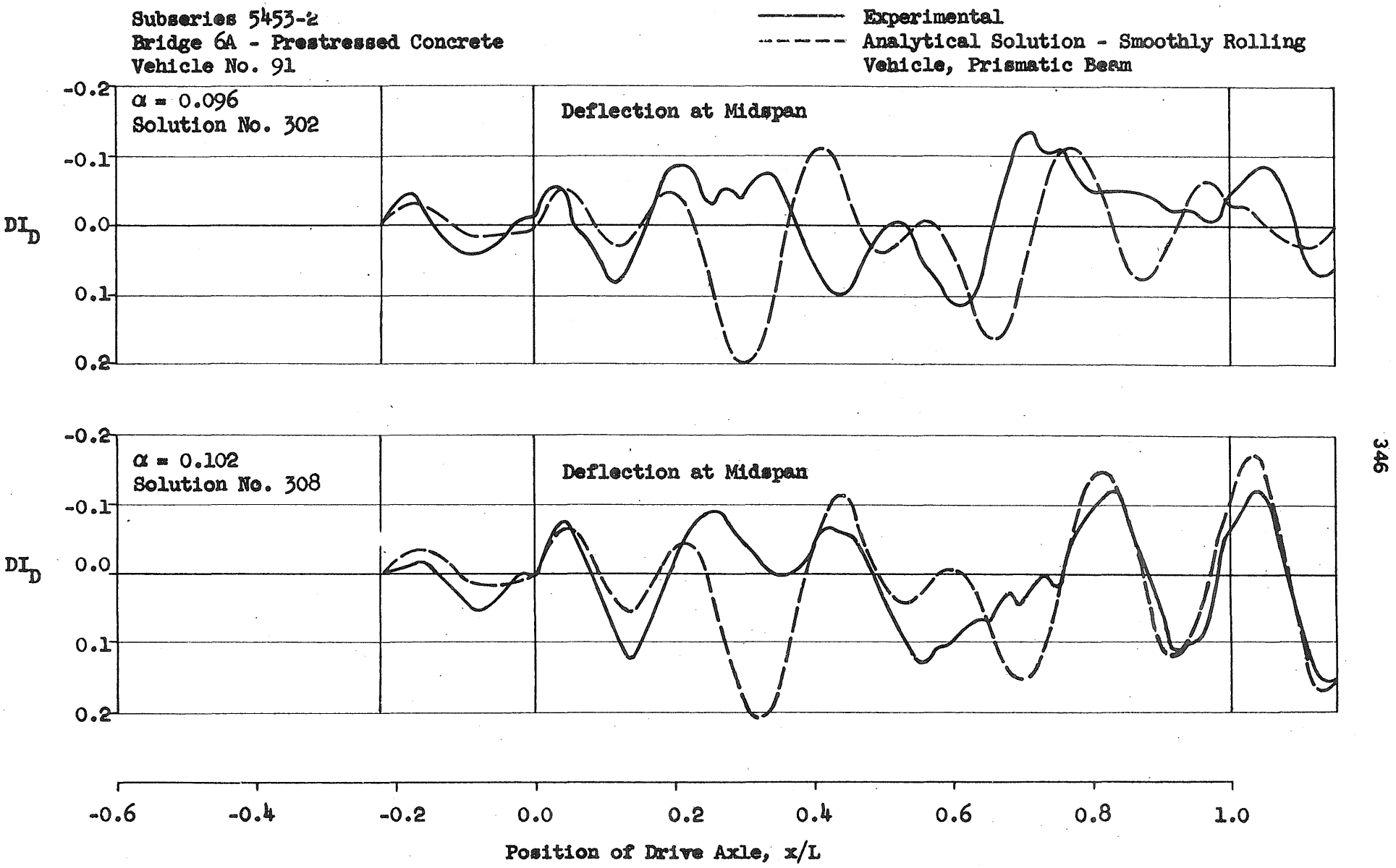

FIG. 83 COMPARISON OF HISTORY CURVES - Subseries 5453-2

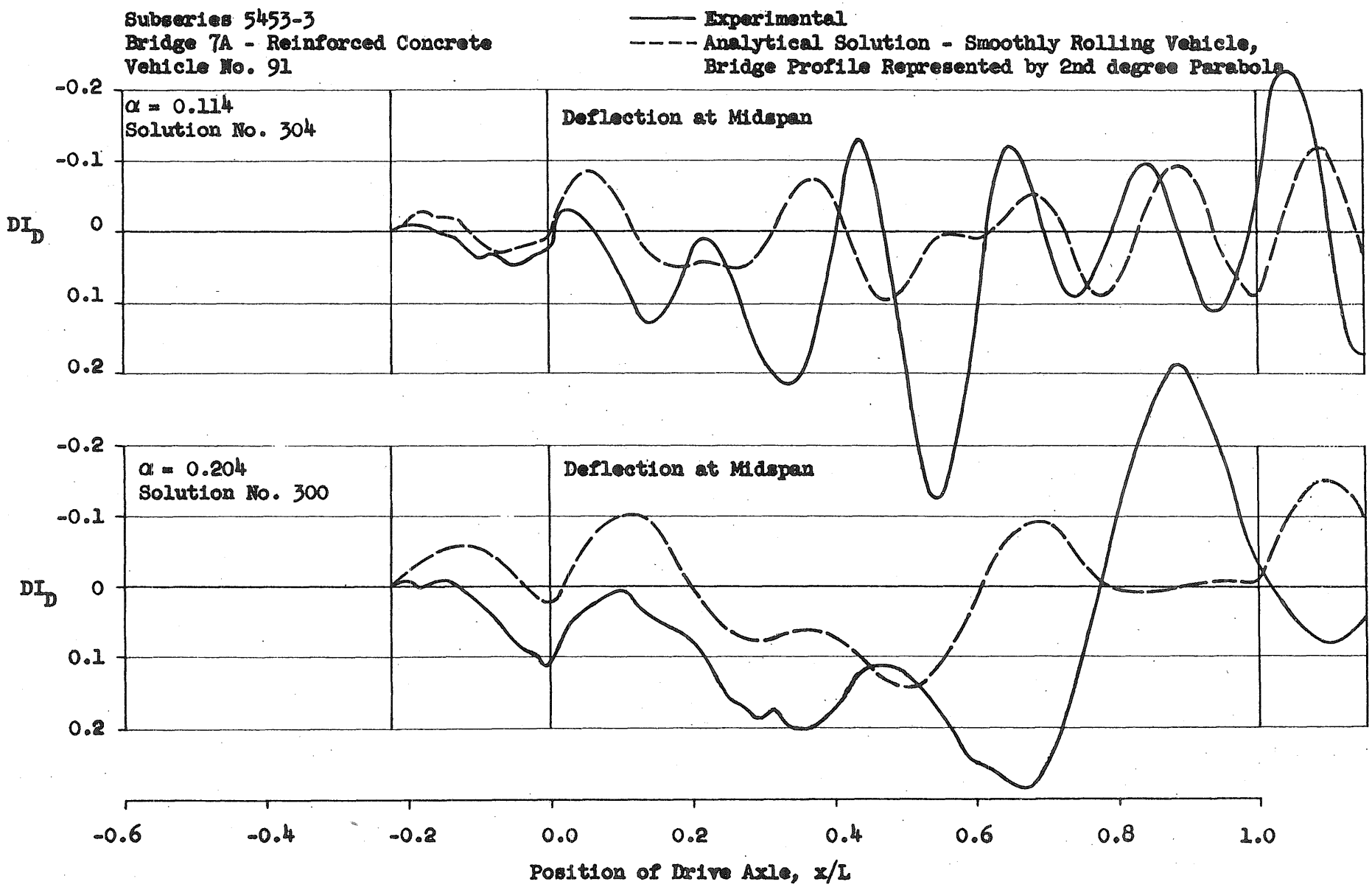

FIG. 84 COMPARISON OF HISTORY CURVES - Subseries 5453-3

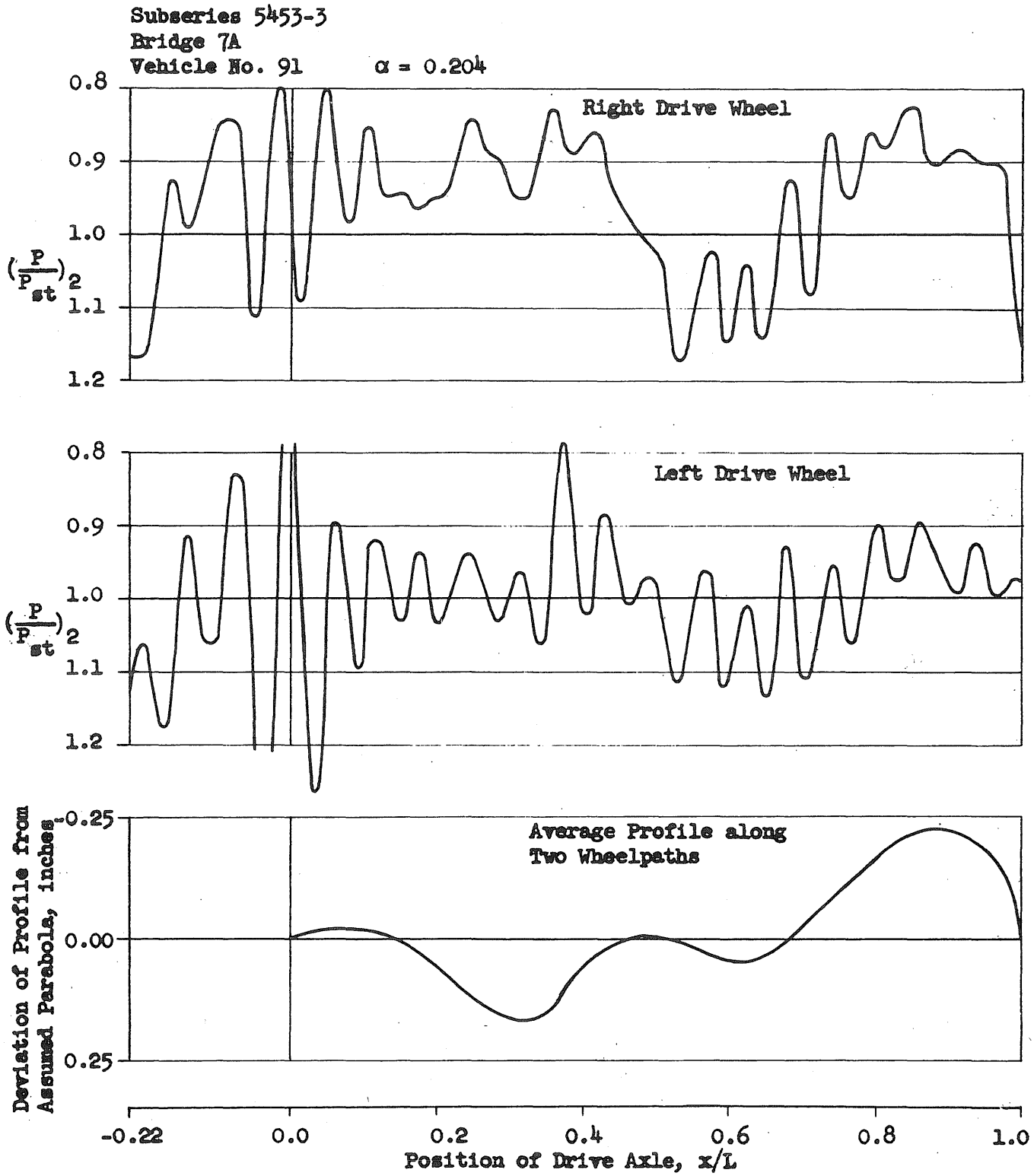

FIG. 85 RELATIONSHIP BETWEEN SURFACE IRREGULARITIES AND INTERACTION FORCE

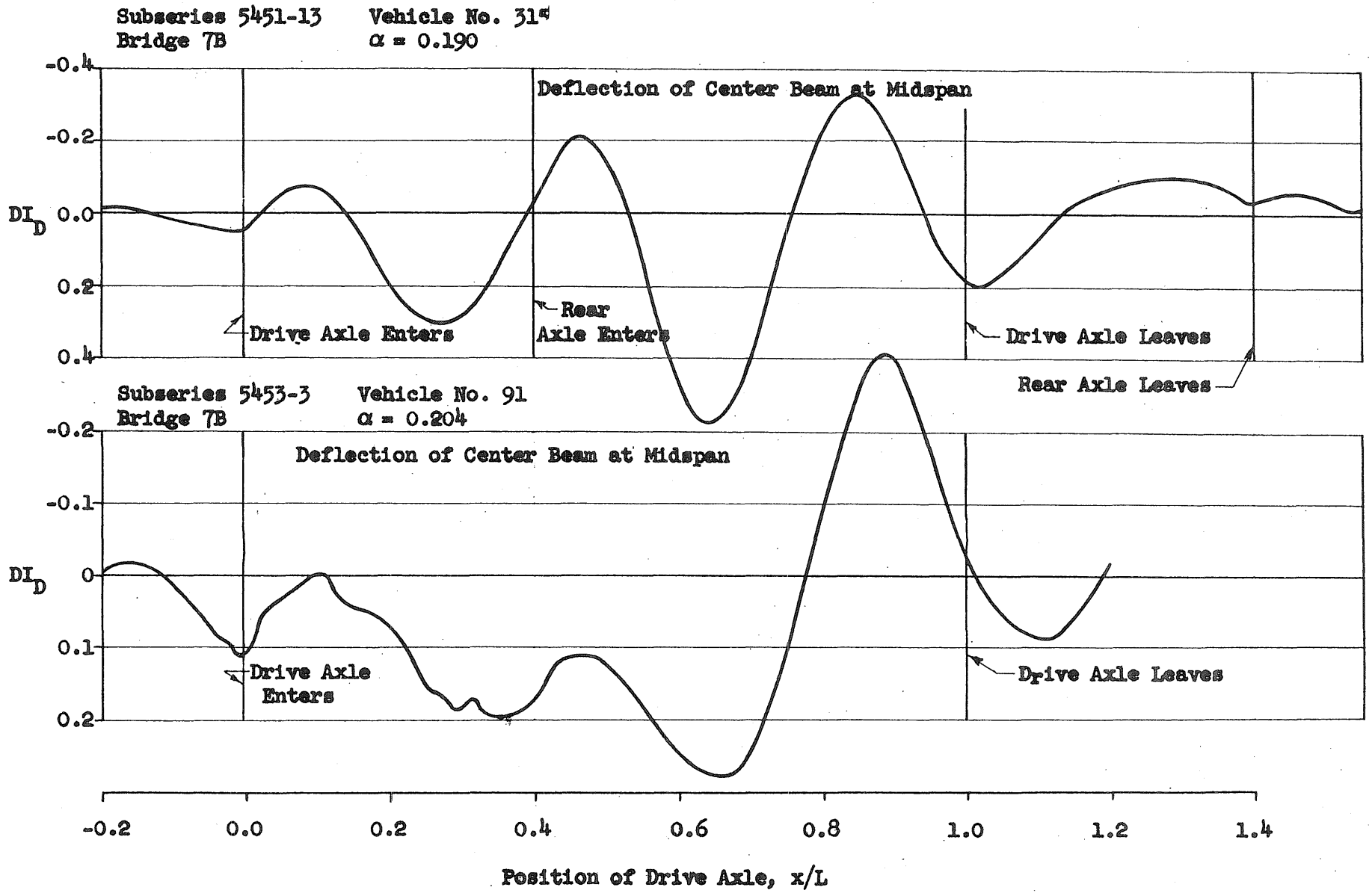

FIG. 86 EFFECT OF SURFACE IRREGULARITIES ON BRIDGE RESPONSE